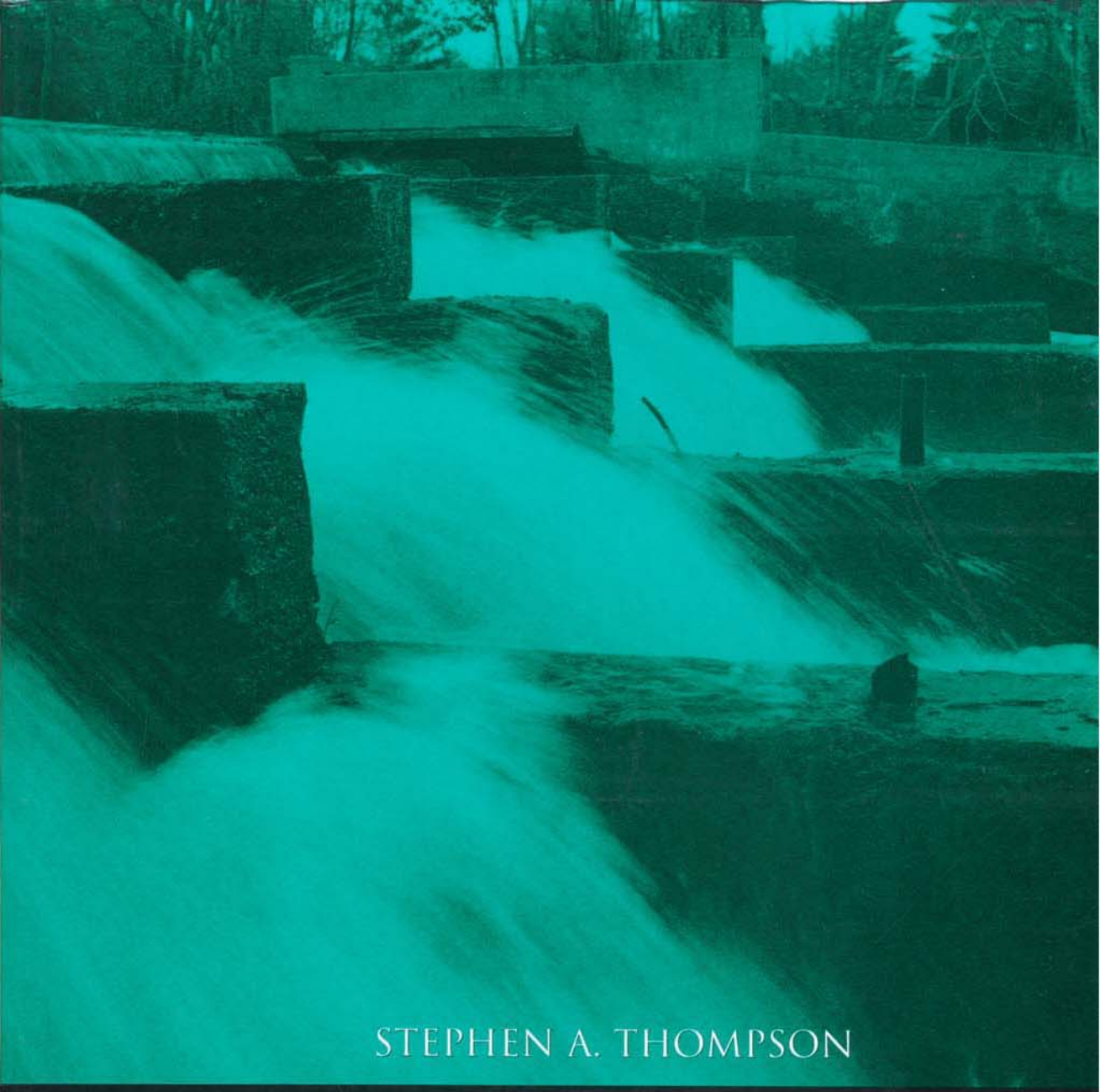

STEPHEN A. THOMPSON

HYDROLOGY FOR WATER MANAGEMENT

HYDROLOGY FOR WATER MANAGEMENT

This Page Intentionally Left Blank

Hydrology for Water Management

STEPHEN A. THOMPSON
Department of Geography, Millersville University, Pennsylvania, USA

A.A. BALKEMA/ROTTERDAM/BROOKFIELD/1999

Published by
A.A. Balkema, P.O. Box 1675, 3000 BR Rotterdam, Netherlands
Fax: +31.10.4135947; E-mail: balkema@balkema.nl; Internet site: http://www.balkema.nl

A.A. Balkema Publishers, Old Post Road, Brookfield, VT 05036-9704, USA
Fax: 802.276.3837; E-mail: info@ashgate.com

ISBN 90 5410 435 X hardbound edition
ISBN 90 5410 436 8 student paper edition

Printed in the Netherlands

This book is dedicated to
my loving wife Marilyn and my wonderful son Benjamin

This Page Intentionally Left Blank

Contents

Preface	XIII
1 THE HYDROLOGIC SYSTEM	1
1.1 System concepts	3
1.1.1 Steady state systems	5
1.2 Modeling hydrologic systems	7
Summary	8
Problem	8
2 DIMENSIONS, DATA AND GRAPHS	10
2.1 Dimensions	10
2.2 Data precision	11
2.3 Continuous and discrete data	12
2.4 Level of measurement	15
2.5 Hydrologic data series	16
2.6 Graphs and graphing	17
Summary	21
Problems	21
Excel Exercise 1	22
3 STATISTICS, PROBABILITY AND PROBABILITY DISTRIBUTIONS	25
3.1 Describing data	25
3.2 Measures of central tendency	26
3.3 Measures of dispersion	27
3.4 Probability functions	32
3.5 Probability and the normal curve	34
3.6 Probability distributions	38
3.7 Fitting probability distributions	38
3.8 Testing goodness-of-fit	40
3.9 Time variations in data	41
Summary	43
Problems	43
4 THE ATMOSPHERIC SUBSYSTEM	44
4.1 Atmospheric water vapor	44

4.1.1 Humidity 46
4.2 Precipitation processes 48
4.3 Weather modification 49
4.4 Adiabatic processes 50
4.5 Precipitation measurement 52
4.5.1 Errors in precipitation measurement 56
4.6 Establishing a precipitation gage 57
4.7 Missing precipitation data 58
4.8 Averaging precipitation over an area 60
4.9 Checking temporal consistency of a precipitation record 62
4.10 Frequency analysis of precipitation 63
4.10.1 The gamma distribution 65
4.11 Intensity-duration-frequency (IDF) 68
4.12 Risk 75
Summary 76
Problems 77
Excel exercise 2 78
Excel exercise 3 79

5 EVAPORATION
5.1 The evaporation process 82
5.1.1 Solar energy 83
5.1.2 Estimating solar radiation 86
5.1.3 Vapor pressure deficit 90
5.1.4 Wind speed 91
5.2 Methods for estimating evaporation 91
5.2.1 Evaporation pans 91
5.2.2 Continuity equations 94
5.2.3 Evaporation equations 95
Summary 99
Problems 100

6 EVAPOTRANSPIRATION 102
6.1 The evapotranspiration process 102
6.1.1 Soil factors 102
6.1.2 Vegetative factors 104
6.2 Methods for estimation evapotranspiration 105
6.2.1 Water balance 105
6.2.2 Lysimeters 105
6.2.3 Potential evapotranspiration equations 106
6.3 Modeling evapotranspiration under limited soil moisture conditions 115
6.3.1 Modeling the soil as one-layer store 116
6.3.2 Modeling the soil as a two-layer store 117
6.4 Vegetation modification 118
Summary 119
Problems 120

7 INFILTRATION AND SOIL MOISTURE 121
7.1 Factors controlling infiltration 122
7.2 Infiltration rate versus cumulative infiltration 125
7.3 Infiltration measurement and estimation 128
7.3.1 Infiltrometers 128
7.3.2 Rainfall simulators 129
7.3.3 Hydrograph analysis 129
7.4 Infiltration models 131
7.4.1 Horton's model 131
7.4.2 Philip's model 132
7.5 Other methods for estimating infiltration 133
7.5.1 The ϕ index 133
7.5.2 Soil classification 134
7.6 Ponding time and runoff 134
7.7 Soil water 135
7.7.1 Porosity 136
7.7.2 Soil water potential 136
7.7.3 Soil water characteristic 138
7.7.4 Water movement in the soil 141
7.7.5 Soil moisture measurement 142
Summary 143
Problems 143

8 GROUNDWATER 144
8.1 Groundwater defined 144
8.2 Aquifers 145
8.2.1 Unconfined aquifers 146
8.2.2 Confined aquifers 147
8.3 Properties of aquifer materials 148
8.3.1 Porosity and water storage 148
8.3.2 Hydraulic conductivity 151
8.4 Groundwater head 153
8.4.1 Hydraulic gradient 155
8.4.2 The three-point method 156
8.5 Groundwater flow 157
8.5.1 Darcy's Law 157
8.5.2 Groundwater discharge 158
8.6 Groundwater and wells 162
8.7 Groundwater flow to wells 164
8.7.1 Steady flow 164
8.7.2 Unsteady flow 166
8.8 Two and three dimensional flow 171
8.9 Groundwater models 173
8.10 Groundwater quality and contaminant transport 175
8.10.1 Multiphase flow 176
8.10.2 Dissolved contaminant transport 176
8.11 Wellhead protection 177

8.12 Groundwater regions in the United States 182
Summary 184
Problems 184

9 THE WATER BALANCE 188
9.1 Components of the water balance 188
9.2 The water balance procedure 189
9.2.1 Steps in calculating an average water balance 189
9.2.2 An example water balance calculation 191
9.2.3 Graphing the water balance 194
9.2.4 Sensitivity of the water balance to AWC 201
9.3 Applications of the water balance 201
Summary 203
Problems 203

10 BASIN MORPHOMETRY AND RUNOFF 205
10.1 Basin morphometry 205
10.1.1 Stream ordering 205
10.1.2 Stream length 207
10.1.3 Basin area 209
10.1.4 Basin relief and slope 210
10.2 Runoff kinematics 212
10.2.1 Continuity 212
10.2.2 Motion: Laminar versus turbulent flow 213
10.3 Timing of runoff 216
10.3.1 Time of concentration 216
10.3.2 Overland flow travel time 217
10.3.3 Channel travel time 220
10.4 Runoff processes 221
10.4.1 Hortonian overland flow 221
10.4.2 Saturation overland flow 223
10.4.3 Human activities affecting runoff 224
Summary 225
Problems 225

11 STREAMFLOW AND FLOODS 226
11.1 Flood waves 228
11.1.1 Hydrographs 230
11.1.2 Hydrograph separation 232
11.2 Runoff volume 233
11.2.1 Infiltration-based approach 233
11.2.2 SCS curve number method 234
11.3 Peak runoff 240
11.3.1 The rational method 240
11.4 Flood frequency analysis 242
11.4.1 The normal distribution 244
11.4.2 The lognormal distribution 245

11.4.3 The Extreme Value I distribution 247
11.4.4 The Pearson Type III distribution 249
11.4.5 The log-Pearson Type III distribution 251
11.4.6 Confidence limits 253
11.4.7 Mixed distributions 254
11.5 Regional analysis 255
11.6 The unit hydrograph 256
11.6.1 Alternate duration unit hydrographs 259
11.6.2 Unit hydrograph convolution 262
11.7 Synthetic unit hydrographs 263
11.7.1 SCS triangular synthetic unit hydrograph 264
11.7.2 Snyder's synthetic unit hydrograph 265
11.7.3 Variations on Snyder's method 267
11.8 Flow routing 268
11.8.1 Reservoir routing 268
11.8.2 Muskingum channel routing 272
11.8.3 Determining K and x 274
11.9 Streamflow measurement 278
11.9.1 Stage-discharge relations 280
Summary 280
Problems 281

12 DROUGHT AND WATER SUPPLY 286
12.1 Defining drought 286
12.2 Runs analysis of drought 288
12.2.1 Analysis of Oklahoma climate division 4 289
12.3 Palmer Drought Severity Index (PDSI) 292
12.3.1 Analysis of Oklahoma climate division 4 294
12.4 Markov chain model of drought 299
12.4.1 Interrelating the Markov chain and runs theory 302
12.5 Water supply 305
12.5.1 Streamflow characteristics 306
12.5.2 Estimating water storage requirements 309
Summary 316
Problems 317

13 HYDROLOGIC MODELS AND GEOGRAPHIC INFORMATION SYSTEMS 318
13.1 Hydrologic models 318
13.1.1 Types of models 318
13.1.2 Deterministic versus stochastic simulation models 319
13.1.3 Classifying deterministic models 320
13.1.4 Steps in using a computer model 321
13.1.5 The HEC-1 simulation model 326
13.1.6 Model components 326
13.1.7 Kinematic wave 328
13.1.8 Input data file and schematic model structure 330

13.1.9 Example simulation using HEC-1 333
13.1.10 Agricultural nonpoint source pollution model (AGNPS) 336
13.2 Geographic Information Systems (GIS) 338
13.2.1 Types of GIS 339
13.2.2 GIS applications to hydrology 341
Summary 345

Appendices 347

References 351

Subject index 359

Preface

As in all areas of environmental science, the science of hydrology is rapidly evolving in the last decade of the twentieth century. Until the 1970s hydrology was a dominated by engineers, both civil and agricultural. They needed to know, for example, how much runoff would be produced from a given storm, or how much water a given type of crop needed so that facilities could be designed. Society was on the move; cities were being built, the desert was being forced to bloom, and forests were being replaced by other land uses. In one way or another all of these development activities had hydrologic impacts. Engineers learned a great deal about hydrology, though much of the knowledge was empirical rather than theoretically based. While a more theoretical foundation is being built, most applications of hydrology today are still for solving day-to-day problems. Hydrology is no longer the sole domain of engineers; it has evolved into a truly interdisciplinary science. According to a report by the National Academy of Science (NAS 1991), understanding the hydrologic system is central to understanding other physical environmental systems, from climate to lithospheric processes.

Human transformation of the Earth continues toady at an ever increasing rate, and there is a growing concern over human alterations of natural systems, particularly the hydrological cycle. One of the most important challenges is understanding better how human activities alter the natural environment so we may design socio-economic systems to work more sensitively with natural systems. For example, understanding how a levee changes both the hydrologic and hydraulic processes of the river, as well as the society situated along its banks, is far more difficult than simply choosing a design flow and building the levee.

I wrote this book to satisfy my need for a text relevant to an introductory hydrology course with a focus on natural resource management. The book covers the basic components and processes of the hydrologic system, and some of the more common methods used to study them. The intended audience is students interested in natural resources and the environment. Environmental geography students in particular comprise a significant percentage of the urban and land use planners working for government agencies. In these positions they encounter water and land resource management problems. This book provides a foundation for understanding the hydrologic components of these problems. If this book happens to inspire a deeper more abiding interest in the subject that would be nice too.

Hydrology is a quantitative interdisciplinary science and my book is mathematically rigorous, but I have tried to provide a balance between quantitative material and

descriptive text. The types of mathematics used are primarily algebra and some statistics. Equations of calculus are used occasionally because calculus describes the true process; however, students are not required to 'do' any calculus. In practice, hydrologic processes are routinely approximated using algebra rather than calculus. This is why I introduce certain topics with calculus, but then explain how the problems are actually solved using algebra.

The book is organized into two sections. The first section (Chapters 1-3) covers properties of systems and systems analysis, characteristics and analysis of environmental data, and probability and statistics. These are fundamental concepts and tools applicable beyond the study of hydrology. The second section (Chapters 4-12) covers hydrology. Chapters in this sections are organized around major components and processes of the hydrologic system, i.e., the atmospheric subsystem, evapotranspiration, infiltration and soil moisture, groundwater, the water balance, surface runoff, streamflow and floods, and droughts and water supply. The topic of the last chapter (Chapter 13) is computer modeling. The two major subtopics in this chapter are deterministic simulation models and Geographical Information Systems (GIS).

In addition to the applied water-management focus, a feature of the text is the repeated use of core concepts. One such concept is the continuity principle – the conservation of mass, energy and momentum. This is perhaps the single-most useful principle in hydrology. Physical quantities can neither be created nor destroyed; they must go somewhere. Many of the analytical techniques used in hydrology are founded on this principle, whether the topic is evaporation or streamflow. Again and again throughout the text the continuity principle is invoked to develop both the approach to understanding the topic, and the equations used for the analysis. Another concept that is repeated throughout the book is the calculus-to-algebra simplification mentioned previously.

The book contains step-by-step spreadsheet (EXCEL®) exercises. Students first do the problem by hand, and then repeat the exercise using the spreadsheet program. I find that by the third exercise many students are comfortable enough to do their assignments using a spreadsheet rather than pencil and paper. I have also included copies of hard-to-find graph papers, BASIC hydrology program listings, and a World Wide Web (WWW) exercise where students follow a step-by-step procedure to use the WWW to retrieve hydrological data for a homework problem.

Finally, I am compelled to say a word about the units used in hydrology. Government agencies in the United States still measure and record hydrologic and meteorologic data in customary English units. Most countries around the world use metric units. Given the book's resource management focus I feel it is appropriate to still include the units that are used day in and day out by water managers across the country. Consequently, you will see both metric and English units. Chapter 2 discusses units in detail and Appendix A includes factors for converting between different unit systems. The problem with units will be with us into the foreseeable future. In closing I thank all of my teachers, because it is to them that any credit should go. I alone take responsibility for the errors.

S.A. Thompson
Conestoga, 1998

CHAPTER 1

The hydrologic system

Hydrology is the science of water. It is the study of the occurrence, character and movement of water within and between the physical and biological components of the environment. The term *water resources* is used to refer to the management and use of water primarily for the benefit of people. Water management involves providing for human uses such as water supply, waste disposal, transportation, recreation, flood control and power generation. Successful management of water resources requires a solid understanding of hydrology. The role of water in the environment is more important than just satisfying human needs. Water is the single most important element of the environment. The availability of water largely determines the spatial pattern of the Earth's terrestrial biomes (forests, grasslands and deserts); it covers 71% of the Earth's surface providing habitat for fresh and saltwater ecosystems; water is a major controlling element of the earth's climate, and it is water that is largely responsible for sculpting the Earth's surface into the infinitely complex associations of erosional and depositional landforms. Water makes life on Earth possible, and, to a large extent, water makes the Earth itself.

Approximately 96.5% of all the water on Earth is stored in the oceans, 1.69% is stored underground and about 1.74% is frozen and stored in ice caps and glaciers (Table 1.1). In just three locations we find 99.93% of the water. Only a minute fraction of the Earth's total water supply comprises all of the water found in rivers, lakes, the soil, and the atmosphere. Water is continuously cycling from the ocean, to the atmosphere, to the land surface, and back again to the ocean in what we call the *hydrologic cycle* (Fig. 1.1). The processes that accomplish this never-ending cycle are *evapotranspiration*, the combination of *evaporation* from water and wet surfaces and *transpiration* from vegetation, which sends water vapor into the atmosphere, *precipitation* which brings water back to the surface in liquid and solid forms, and *runoff* from land to the rivers and streams that ultimately return it to the oceans.

In addition to the amounts of water in storage, Table 1.1 gives approximate *residence times* for water in the various locations. Residence times are calculated by dividing the estimated quantity in storage (L^3) by the estimated flow rate of water (L^3T^{-1}) through that storage location. (Chapter 2 discusses physical dimensions such as *length* (L) and *time* (T) in more detail.) For example, dividing the volume of water in the oceans (1.338×10^9 km^3) by the average annual evaporation rate from the ocean surface (5.05×10^5 km^3 yr^{-1}) gives an average residence time of approximately 2,650 years. Extreme variation exists in residence times for water in the ocean, ranging from a few seconds to thousands of years. The residence time for the

Table 1.1. Storage locations and residence times for water on Earth.

Location	Volume (10^3 km^3)	Percent of total water (%)	Residence time (years)
Ocean	1,338,000	96.5	2650
Ice caps and glaciers	24,064	1.74	100-200,000
Groundwater: – Fresh	10,530	0.76	1-10,000
– Saline	12,870	0.93	1-10,000
Lakes: – Fresh	91	0.007	100
– Saline	85.4	0.006	100
Soil	16.5	0.001	0.25 (2-3 months)
Atmosphere	12.9	0.001	0.022 (8 days)
Rivers	2.12	0.0002	0.05 (20 days)

Sources: Volumes of water come from *World Water Balance and Water Resources of the Earth*, Gidrometeoizdat, Leningrad (in Russian), translated into English by UNESCO 1978, R. Nace (ed.), Paris. Estimates of residence times come from Gardner 1977.

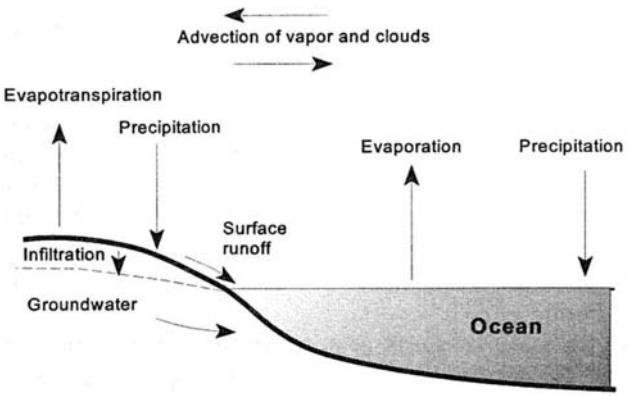

Figure 1.1. A simplified diagram of the global hydrologic cycle.

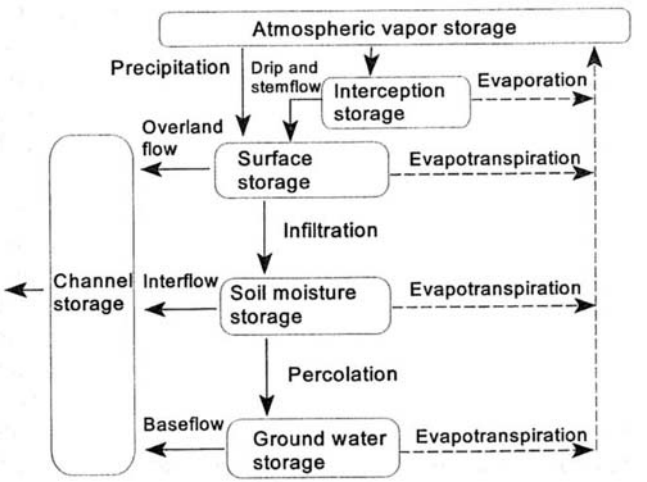

Figure 1.2. The basin-scale hydrologic system (cycle) showing water storages and processes.

ocean is most useful for comparative purposes. For some storage locations, like glaciers and groundwater, a single residence time fails to capture the range that is possible. Recent ice cores from Greenland have yielded dates on basal ice of 200,000 yrs BP. By comparison it may take only decades for ice to flow through a mountain glacier. The very short residence times for water stored in streams, the soil and the atmosphere explain why these locations never 'run out' of water even though they contain such comparatively small quantities.

Moving down in spatial scale from the global to the level of the individual drainage basin brings additional storages and processes into view (Fig. 1.2). A *drainage basin* is an area of land that drains water to a common outlet. Because of this physical continuity the drainage basin scale is extremely useful in many hydrologic investigations. In the United States drainage basins are also called *watersheds*. The topographic line separating adjacent drainage basins is the drainage *divide*. At this scale we see that precipitation may be *intercepted* by vegetation. Intercepted water may evaporate back into the atmosphere, or it may drip or flow down plant stems to the surface. Water reaching the surface may flow across the surface as *overland flow* toward stream channels, it may *infiltrate* the soil, or it may be retained as *depression storage* within surface irregularities. Infiltrated water may move vertically downward eventually reaching the *water table*, which represents the top of the *groundwater zone*. Underground water may move horizontally in the unsaturated zone as *interflow*. Groundwater flow in the saturated (groundwater) zone may eventually reemerge as *baseflow* in streams. Groundwater flow may or may not coincide surface water drainage. Of course at every opportunity water will return to the atmosphere through the process of evapotranspiration.

1.1 SYSTEM CONCEPTS

A *system* is a set of interrelated objects or components. The two key aspects of this simple definition are the *components* and the *processes* that relate them. A group of components with no interaction does not constitute a system. It is only because of mutual interdependence and *feedback* between components that we can say a system exists. The term *systems analysis* is widely used but it often means different things to different people depending on their particular scientific discipline. Here the term systems analysis means a way of looking at the world. It is a way of structuring reality so that we may understand how components of the environment affect, and are affected by, other components. In essence we are creating a simpler *model* of the complex real-world environment. When using a systems approach the challenge is to formulate a (model) system that is simple enough to understand, yet comprehensive enough to adequately capture the relevant interactions and processes observed in the real world.

A physical environmental system describes the flow and storage of the physical quantities of mass, energy and momentum. The hydrologic cycle is an excellent example of a physical environmental system. In terms of mass the components of the system are the locations where water (and chemicals) may be stored, such as the ocean, the atmosphere, lakes, the soil and stream channels. Some of the more familiar processes are the ones that involve either the change of state of water, or that

transfer water from one storage location to another. Condensation, for example, is the process whereby water vapor changes state to become liquid. Precipitation is the process, actually a set of subprocesses as we will see in Chapter 4, that transfers water from the atmosphere to the Earth's surface. There are many other processes at work that are less obvious because they operate at temporal or spatial scales that make them difficult for humans to observe. This book focuses mainly on the flows and storages of mass and energy. While important for theoretical developments and advanced analyses, the flux of momentum is rarely discussed, since it is less central to solving practical hydrologic problems related to water management.

Human activities directly and indirectly alter the natural hydrologic system. Dams create storage reservoirs altering the river's flow regime and evaporation. Aqueducts and diversion channels move water between drainage basins. The transformation of natural land surfaces into streets and parking lots radically changes the partitioning of precipitation between the pathways of infiltration and surface runoff. And of course many human activities change the chemical composition of water.

Most environmental systems, including the hydrologic system, can be reduced to groups of nested and interconnected subsystems. Some examples of the subsystems in the hydrologic system are the soil subsystem, the groundwater subsystem, and the atmospheric subsystem. Whether the components and processes are designated as a system or a subsystem depends entirely upon the needs of the analyst, for it is the analyst who determines the system's boundary (Hugget 1980). Everything inside the boundary is considered part of the system; everything outside the boundary is not. Figure 1.3 is a simple one-component soil system. The soil system receives inputs of water by infiltration and interflow. Water may be stored temporarily in the soil, but it is ultimately transformed by the system into outputs.

One way to classify systems is on the basis of whether mass and energy cross the system's boundary (Bennett & Chorley 1978). An *open* system is one in which both mass and energy are all able to cross the boundary. The soil subsystem in Figure 1.3 is an example of an open system, as are virtually all hydrologic subsystems. A *closed* system allows energy across the boundary, but not mass. For most purposes planet Earth may be considered a closed system.

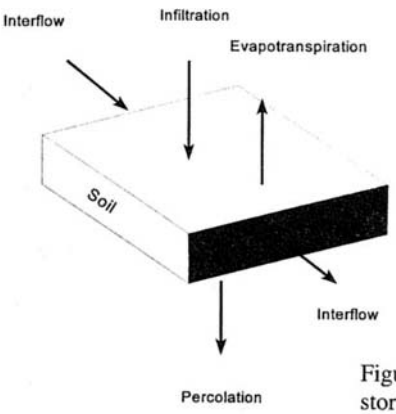

Figure 1.3. Soil system showing inputs and outputs to soil storage.

1.1.1 *Steady state systems*

The term *dynamic equilibrium* or *steady state* describes a certain condition of a system. Dynamic equilibrium is when a system, technically the 'state' of the system, does not change with *time*. In other words, a dynamic-equilibrium system is *time-invariant*, and inputs (I) to the system equal outputs (Q) from the system (Singh 1988). An important result of this condition is that the amount of the physical quantity in storage (S) remains constant. In most hydrologic systems, dynamic equilibrium usually obtains only when inputs and outputs are measured over sufficiently long periods of time so that short-term variations balance out. A simple way to visualize dynamic equilibrium is to imagine a lake with a stream flowing in and a stream flowing out. If you photograph this stream-lake system one day, and then photograph it say a week later, it might look the same in the two pictures (equilibrium), but tremendous quantities of mass and energy have passed through the system (dynamic) during that period. Dynamic equilibrium is easiest to understand, and is often useful as a first approximation of the operation of a complex system. In hydrologic analyses, time-invariance is called a *steady* condition, while a system that changes with time is *non-steady*. We'll consider both time and space domains as a characteristic of hydrologic models in the next section.

The previous discussion of system inputs, outputs and storage introduced perhaps the single-most important principle in hydrology: the conservation of mass, energy and momentum. If we express input and output as functions of time, $I(t)$ and $Q(t)$, respectively, a *continuity equation* describes the principle of conservation:

$$\frac{dS}{dt} = I(t) - Q(t) \tag{1.1}$$

Equation (1.1) says the rate of change of storage with time dS/dt equals the rate of inflow $I(t)$ minus the rate of outflow $Q(t)$. For a system in dynamic equilibrium $I(t) = Q(t)$ and there is no change in storage ($dS/dt = 0$). Equation (1.1) is a *differential* equation. A differential equation gives the *instantaneous rate of change* of storage with time. (In Eq. 1.1, inflow and outflow are also instantaneous values and could have been written as dI/dt and dQ/dt). Figure 1.4 demonstrates these concepts. Figure 1.4a shows inflow and outflow graphs for a hypothetical reservoir, while Figure 1.4b shows the graphs of water storage and the change in storage in the reservoir. We are using a reservoir for our example, but we could just as easily use an entire drainage basin, the soil subsystem, or any hydrologic subsystem. In Figure 1.4a inflow and outflow are equal at time t_0 so there is no change in storage ($dS/dt = 0$). After this time inflow exceeds outlfow, which causes the amount of water in storage S to increase (Fig. 1.4b). Since inflow exceeds outflow the change in storage is positive ($dS/dt > 0$). The change in storage reaches a maximum at t_1 when inflow exceeds outflow by the greatest amount. At time t_2 inflow and outflow are again equal. At this time storage S reaches its maximum value and the change in storage is again zero. After t_2 outflow exceeds inflow, the change in storage becomes negative ($dS/dt < 0$), and storage in the reservoir decreases. Table 1.2 summarizes these relationships between inflow, outflow, storage and the change in storage.

Another important concept shown in Figure 1.4b is the relationship between the incremental change in storage dS and the rate of change in storage dS/dt. The incre-

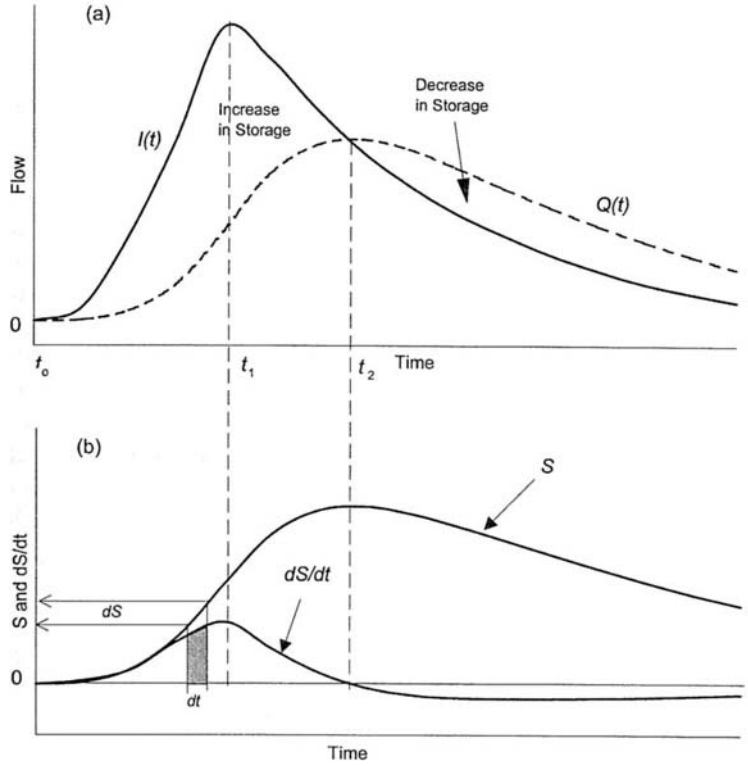

Figure 1.4. a) The input and output curves to a reservoir and the increase and decrease in storage. b) The total storage curve S and the rate of change in storage dS/dt.

Table 1.2. Relationship between inflow, outlfow, storage and change in storage for the reservoir example shown in Figure 1.4.

Time t	Inflow I	Outflow Q	Storage S	Change in storage dS/dt
t_0	$I = Q$	$I = Q$	0	0
$t_0 < t < t_2$	$I > Q$	$Q < I$	Increasing	Positive
t_1	Maximum	$Q < I$	Increasing	Maximum
t_2	$I = Q$	Maximum	Maximum	0
$t > t_2$	$I < Q$	$Q > I$	Decreasing	Negative

mental addition to storage dS in the time increment dt equals the area under the dS/dt curve. This is one of the fundamental theorems of calculus. The procedure of finding the area under the dS/dt curve is called *integration*. The total storage S at time t is equal to the sum of all the incremental storage elements up to that time plus any initial storage. The inverse of integration is *differentiation*. While not shown explicitly on Figure 1.4, differentiating the storage curve gives dS/dt.

The continuity principle and the relationship between the rate-of-change of a quantity (differentiation) and the amount of the quantity (integration) are fundamen-

tal to hydrologic analyses. Equation (1.1) gives the rate-of-change in storage for time measured as a *continuous* variable, which, of course, it is. In Chapter 2, Equation (1.1) is modified for use with time measured in *discrete* intervals (Δt). Discrete approximation of differential equations is a necessary simplifications for many analyses. The assumption is that a continuous, nonlinear process behaves linearly over sufficiently small intervals of time or space. Continuity equations are fundamental to hydrologic models that have a physical basis (Kirkby et al. 1987), and it is to the topic of modeling that we now turn.

1.2 MODELING HYDROLOGIC SYSTEMS

Problems in hydrology are concerned either with issues of water quantity, water quality or both (Singh 1988). Typical of water quantity problems are estimating the water yield from a drainage basin, analyzing the movement of a flood wave in a channel, determining evaporation, or calculating seepage losses from a reservoir. Water quality problems include the migration of pollutants in groundwater or determining the behavior of chemical constituents in a stream. In either case hydrologic problems exhibit characteristics in both time and space. In the previous section the terms steady and non-steady defined a system with respect to variation in time. Similarly, the terms *uniform* and *non-uniform* define the behavior of hydrologic systems in space. A hydrologic system is uniform when there is no change in system variables over space, and non-uniform when there is spatial variation. For example, in developing the theory of groundwater flow to a pumped well, the simplest case is the situation of steady, uniform flow. In this idealized system, the well could pump water indefinitely and there would be no lowering of the water table with time or with distance from the well. The well-aquifer system would be in dynamic equilibrium, with the recharge (input) equal to the discharge (output) from the well, and the amount of water in storage in the aquifer would remain constant. Table 1.3 shows a *space-time domain* matrix for classifying hydrologic systems.

Models can be categorized as physical models or abstract mathematical models (Chow et al. 1988). Physical models are either scaled-down versions of a system constructed of similar materials, e.g., sand and water, or they are analog models. Analog models use different materials to simulate the hydrologic system. The US Army Corps of Engineers (COE) operates complete scale models of hydrologic systems including the Mississippi River and the Chesapeake Bay. The Bureau of Reclamation has built scale models of irrigation projects. A scale model is used when the behavior of the real system is so complex that its operation cannot be adequately represented with abstract models. Scale models also have the advantage of looking like the system they represent. As an example of an analog model, wire mesh networks were once

Table 1.3. Space-time matrix for hydrologic systems.

	Constant	Variable
Space	Uniform	Nonuniform
Time	Steady	Nonsteady

used to simulate groundwater flow; the resistance to flow of electricity through the wire grid being an analog for the resistance to flow of water through an aquifer.

Today the use of abstract mathematical models dominates hydrologic modeling. A simple equation $y = f(x)$ is an abstract model that transforms inputs (x) into outputs (y). But it is the coupling of mathematical equations with computers to create computer models, that has truly revolutionized systems analysis. It is a logical progression from the description of real-world phenomena in systems terms to the development of mathematical/computer model representations, because the system approach provides the structure for model development (Fig. 1.2). The potential of systems analysis for studying complex problems was recognized as early as the 1940s, and became fashionable in the 1960s. Then, however, the tools were not available to implement the approach. The computer revolution in hardware and software during the 1980s has made the earlier promises of systems analysis a reality in the 1990s. The widespread availability of computer models and hardware platforms, ranging from powerful desktop machines to massively parallel supercomputers, has made systems analysis operational. With computer simulation models we can undertake experiments on drainage basins inside the computer. A common experiment is to change land use within the model and observe the resultant changes in water, sediment and chemical transport. Chapter 13 discusses the topic of computer modeling and shows the application of some hydrologic models to water quantity and quality problems.

SUMMARY

This chapter introduced the concept of a system, with the hydrologic cycle being a premiere example of a physical environmental system. Even though a hydrologic system is best defined and understood in terms of the relationships between components, many hydrologic analyses are undertaken on individual components of the system. This approach reflects the history of scientific inquiry in general, and the history of hydrology in particular, i.e. before computer simulation allowed for the integrated study of complex systems. Even today isolated analyses still make sense from a practical point of view. Many problems in applied hydrology can be solved without considering each and every element of the hydrologic cycle. Just because a systems approach is now feasible doesn't mean that it's needed in every instance.

PROBLEM

1.1 The figure below is a portion of a USGS Philipsburg, PA 15-minute quadrangle map. Sixmile Run in the center of the map is tributary to Moshannon Creek running across the top of the map. In this exercise you draw the drainage basin for Sixmile Run. First, outline the stream channel network using a blue pencil and then draw the drainage basin boundary using a red pencil.

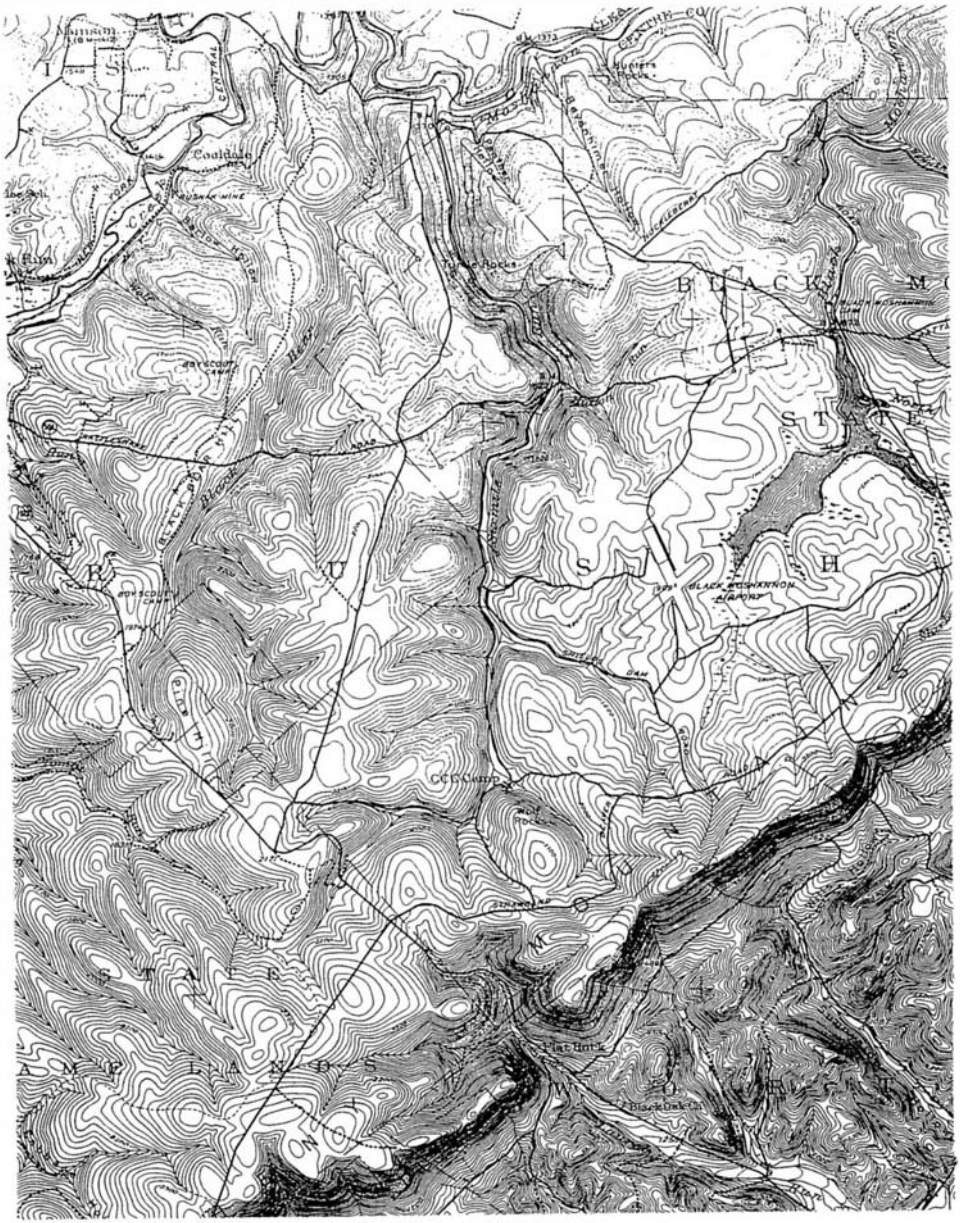
Couldock
Hunters Rock
Three Rocks
BLACK
STATE
SWAMP
BOY SCOUT CAMP
BLACK ARCHANNON CAMP
CCC Camp
Wolf Rock
Flat Rock
Black Oak
AMPLANDS

Problem 1.1.

CHAPTER 2

Dimensions, data and graphs

This chapter presents many topics that are fundamental to the analysis of hydrologic data. While some students may have good preparation in this area, my experience argues that many have not had sufficient exposure to these concepts and techniques. This chapter discusses a variety of characteristics of environmental data, of which hydrologic data are but one example. Topics covered in this chapter include dimensions of physical phenomena, data precision, discrete versus continuous data, data type and quality, and lastly data transformation and graphing.

2.1 DIMENSIONS

To say that physical phenomena exist is to say they have *magnitude* and *dimension*. Magnitude refers to the size of the observed phenomena. Clearly 10 is greater in magnitude than is 5, but the question is, 10 what? The 'what' part is the dimension(s) of the phenomena measured by a system of units. The fundamental dimensions in physical science are length (L), mass (M), time (T) and temperature (Θ). Using these fundamental dimensions, other dimensions are derived such as volume ($L \times L \times L = L^3$) and velocity ($LT^{-1}$). Dimensions can be expressed in any system of units. Time can be measure in seconds, minutes, hours, etc., while length can be measured in the conventional English units of inches, feet or miles, or with the *SI* (*Système International*) unit, the meter, or any of its multiples. *SI* units are used in most nations throughout the world and the United States is conspicuous in its continued use of customary English units – even the English no longer use English units. However, the fact remains that hydrologic data in the United States are frequently reported in English units, and conversion between units is a necessity in hydrologic analyses. Table 2.1 lists fundamental dimensions and three different systems of units. Appendix A contains information for converting between different unit systems.

In hydrologic analyses we encounter equations that are, as well as some that are not, dimensionally homogeneous. An equation is dimensionally homogeneous when the dimensions are the same on each side of the equal sign. The following equation for calculating stream discharge is dimensionally homogeneous:

$$Q = \overline{V}A \tag{2.1a}$$

where Q is discharge (L^3T^{-1}), $\overline{V}$ is average velocity (LT^{-1}) and A is the cross-

Table 2.1. Dimensions and unit systems.

Fundamental dimensions	Système International	Centimeter-gram-second	English
Mass	Kilogram (kg)	Gram (g)	Slug
Length	Meter (m)	Centimeter (cm)	Foot (ft)
Time	Second (s)	Second (s)	Second (s)
Temperature	Kelvin (K)	Deg. (C)	Deg. (F)

sectional area of the channel (L^2). Dimensional analysis shows Equation (2.1a) to be dimensionally homogeneous:

$$L^3T^{-1} = LT^{-1}L^2 \tag{2.1b}$$

By contrast, a widely used equation for calculating average stream velocity is Manning's equation, and it is dimensionally inhomogeneous:

$$\overline{V} = \frac{uR^{2/3}S_0^{1/2}}{n} \tag{2.2}$$

In Equation (2.2), $\overline{V}$ is the average water velocity (LT^{-1}), R is the hydraulic radius (L), a measure of stream depth defined in Chapter 10, S_0 is stream channel slope ($LL^{-1} = 1$), n is Manning's roughness coefficient (1), and u depends upon the system of units used (Dingman 1984). If $\overline{V}$ is in feet per second and R in feet, then $u = 1.49$. For $\overline{V}$ in meters per second and R in meters, $u = 1.0$. The equation is inhomogeneous because the dimensions of the left side are not the same as the dimensions of the right. Physically-based equations that include all relevant physical factors are necessarily dimensionally homogeneous; though it is possible for an equation to be incomplete and still be dimensionally homogeneous. While comprehensiveness is the theoretical ideal, it can pose problems. Including all relevant physical factors in an equation may be difficult, or it may make the equation too cumbersome for practical use. Though empirical equations may not completely describe the physical relationships, they may be sufficiently accurate for everyday application, though realize they will likely be dimensionally inhomogeneous.

2.2 DATA PRECISION

Data precision refers to how accurately we know a measured value. Relative precision indicates the number of significant figures in the measurement. The number of significant figures '...is equal to the number of digits beginning with the left most nonzero digit and extending to the right to include all digits warranted by the measurement precision (Dingman 1984)'. Another way to express precision is to say that we know some number 'to the nearest x.' This is called absolute precision. Precipitation and evaporation data in the United States are measured to the nearest hundredth of an inch, and a precipitation measurement of, say, 2.03 inches has three significant figures. The absolute precision of streamflow data reported by the US Geological Survey decreases with increasing discharge and is never more precise than 0.01 $ft^3\ s^{-3}$ (cfs). Technological advancements have created the potential for misleading

displays of precision. Hand-held calculators can display numbers to as many as nine decimal places; however, we rarely know the displayed value to that many significant figures. This is spurious precision and results simply from the display capability of the device. In some types of analyses, as when working with logarithms of data, keeping four places to the right of the decimal should be considered the minimum level of precision. There are explicit rules for determining data precision following various arithmetic operations. For addition and subtraction absolute precision governs the result. Relative precision controls the results for multiplication and division. The result of a mathematical operation can only be as precise as the least precise number used in the calculation.

Conversion between different systems of units is a good example of the need to monitor data precision. Suppose the distance between two points is 103.5 ft. The absolute precision of this measurement is to the nearest 0.1 ft, and in terms of relative precision there are four significant figures. If we convert this distance into centimeters using the conversion factor of '30.48 cm ft^{-1},' we get (103.5 ft × 30.48 cm ft^{-1}) = 3154.68 cm. The original measurement was precise to the nearest 0.1 ft, whereas the converted distance now appears to a precision of 0.01 cm. Since we multiplied the two numbers, relative precision governs the result. The final answer cannot exceed the least-relatively-precise number in the multiplication. We should therefore round the converted distance to four significant figures, or 3155 cm. Dingman (1984) recommends that unless greater precision is warranted, assume no more than three significant figures for hydrologic measurement and analysis.

2.3 CONTINUOUS AND DISCRETE DATA

Data type can refer to various characteristics of environmental data. One characteristic introduced in Chapter 1 was of the data being either continuous or discrete. Another data characteristic is the level of measurement. First we explore the continuous versus discrete issue in more detail. The issue of continuous versus discrete data was raised with reference to the time variable in Equation (1.1). Continuous means there are an infinite number of data values. Discrete means there are a finite number of data values. Time is a continuous variable because time flows seamlessly from one moment to the next. An analog clock with a sweeping second hand shows time changing continuously. Length is also a continuous variable because a given length can be subdivided into an infinite number of smaller intervals. However, the number of trees on your college campus, or the number of rainy days in a year are discrete phenomena. Continuous time displayed on a digital clock has been 'discretized' into discrete intervals.

For practical purposes, continuous data are often made discrete through either the measurement process, or to simplify an analysis. Methods of measurement create two types of discretized hydrologic data: *sample data* and *pulse data* (Chow et al. 1988). A continuous process sampled at discrete points in time creates a sample data series. Sample data represent the instantaneous value of the variable measured at that moment. In Figure 2.1a we have a record of continuous data as a function of time. These data could be streamflow, air temperature, water level in a reservoir or any continuous process. In Figure 2.1b, sampling at discrete intervals produces a set of sample

data. The magnitude of the sample data point equals is the value of the continuous process at that instant. The dimensions of sample data are the same as the dimensions of the original continuous data. Pulse data are created by accumulating the continuous data over some time interval. The total accumulated value over the interval is the pulse data value. Accumulating the continuous process from time t_1 to t_2 in Figure 2.1c represents the pulse data value for that time period. Precipitation data are pulse data and are recorded as the accumulated depth of water over an interval of time. The dimensions of pulse data are different from the original continuous data. Precipitation pulse data have the dimension length (L), whereas the original continuous data were (LT^{-1}). Precipitation data may be converted back to their original dimension by dividing the pulse value by the time period. The result is the average precipitation intensity over the time interval.

The reason for distinguishing between continuous and discrete data is that different mathematics are used for each type. We analyze continuous variables using differential and integral equations of calculus. Discrete data are analyzed using ordinary difference equations of algebra. Equation (1.1) was given as the basic continuity equation in differential form. However, since hydrologic data are measured at discrete times, Equation (1.1) must be reformulated. We can develop the discrete equivalent of Equation (1.1) by first dividing time into finite intervals of length $\Delta t = (t_2 - t_1)$, where subscripts 1 and 2 mark the beginning and end of each interval. Let I_1, I_2, Q_1, Q_2, and S_1, S_2 represent sample data inflows, outflows and storages at times t_1 and t_2, respectively. The average inflow over the interval Δt is $(I_1 + I_2)/2$, and the average outflow is $(Q_1 + Q_2)/2$. Multiplying the average inflow and outflow by the time interval Δt gives the volume (L^3) of inflow and outflow over the interval:

$$\text{Inflow volume} = \frac{(I_1 + I_2)}{2}\,\Delta t \tag{2.7a}$$

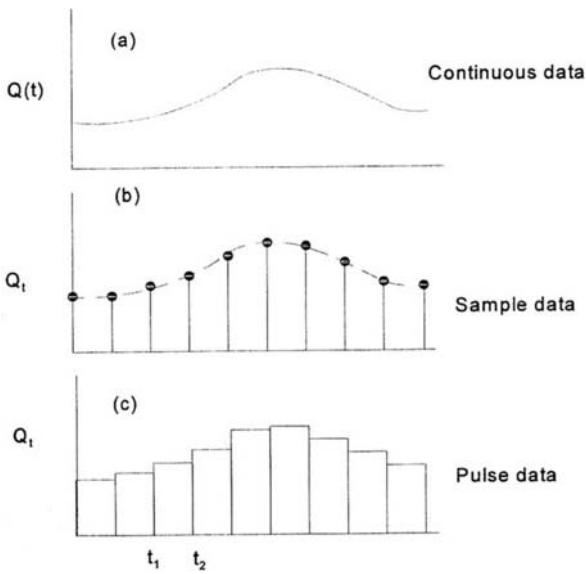

Figure 2.1. The conversion of continuous data (a) into sample data (b) and pulse data (c).

and

$$\text{Outflow volume} = \frac{(Q_1 + Q_2)}{2}\,\Delta t \tag{2.7b}$$

The volumetric change in water storage over the interval is:

$$\Delta S = (S_2 - S_1) = \frac{(I_1 + I_2}{2}\,\Delta t - \frac{(Q_1 + Q_2)}{2}\,\Delta t \tag{2.8}$$

The change in storage (ΔS) is either positive or negative depending upon the relative magnitudes of the inflow and outflow. The average rate of change in storage for the interval is found by dividing both sides of Equation (2.8) by Δt:

$$\frac{\Delta S}{\Delta t} = \frac{(I_1 + I_2)}{2} - \frac{(Q_1 + Q_2)}{2} \tag{2.9}$$

Equation (2.9) is the discrete-time approximation of Equation (1.1). Equation (1.1) gives the true instantaneous change in storage, but it is impractical, if not impossible, to use. On the other hand, Equation (2.9) is easy to use even though it is only an approximation of the true (continuous) process. Notice that as the time interval Δt becomes smaller and smaller, Equation (2.9) will come closer and closer to Equation (1.1). Using the concept of the limit from calculus, as Δt becomes smaller and smaller (written $\Delta t \rightarrow 0$), it is called dt, and Equation (2.9) actually becomes Equation (1.1).

Observe that Equation (2.9) gives the change in storage from one time period to the next. To find the quantity in storage at the end of the interval S_2, we must know the initial quantity in storage at the beginning of the time interval S_1. The quantity in storage at the end of the interval is then calculated as:

$$S_2 = S_1 + \Delta S \tag{2.10}$$

Example 2.1

This example re-examines the data graphed in Figure 1.4 using discrete time. Table 2.2 gives the hypothetical data used to create the inflow-outflow reservoir example in Chapter 1. Time is discretized to an interval of $\Delta t = 2$ hours, and average inflows, outflows and change in storage have been calculated.

For example, the average rate of change in storage (Eq. 2.9) for the interval $t = 4$ to $t = 6$ is:

$$\Delta S/\Delta t = (450 + 845)/2 - (142 + 250)/2$$

$$\Delta S/\Delta t = 648 - 196$$

$$\Delta S/\Delta t = 452 \text{ ft}^3 \text{ s}^{-1}$$

The incremental increase in storage over this interval is:

$$\Delta S = (452 \text{ ft}^3 \text{ s}^{-1})(7200 \text{ s}) = 3{,}250{,}800 \text{ ft}^3$$

If we assume no water in the reservoir at $t = 0$, then the total storage at the end of time interval $t = 6$ is $S = 4{,}726{,}800$ ft^3. Total storage is the sum of the individual storage increments from $t = 0$ to $t = 6$ plus the initial storage which is zero.

As long as inflow exceeds outflow storage increases (Fig. 2.2a). Maximum storage occurs during the 2–hour interval ending at hour 14. Because of averaging over discrete intervals the exact instant of maximum storage cannot be identified.

As in the continuous variable case (Fig. 1.4b), the discrete change in storage ΔS in Figure 2.2b is equal to the area under the rate curve $\Delta S/\Delta t$ for the period Δt. Figure 2.2b shows that storage increases when $\Delta S/\Delta t > 0$. Maximum storage is reached when $\Delta S/\Delta t = 0$, and storage decreases when $\Delta S/\Delta t < 0$. This is directly analogous to the continuous case of dS/dt in Figure 1.4b.

2.4 LEVEL OF MEASUREMENT

A second characteristic of data type is the level of measurement. Hydrologic data are almost always either *interval-level* or *ratio-level*. Interval-level data have constant increments between successive values, but the measurement scale does not have a true zero value. Air temperature measured on the Celsius scale is interval-level data. An air temperature of 21°C is exactly one degree higher than 20°C, which is exactly one degree higher than 19°C. But a temperature of 20°C does not mean the air is twice as hot as air at a temperature of 10°C. The reason is that 0°C is not a true zero; it does not represent the condition of zero energy stored in a substance. 0°C is not a

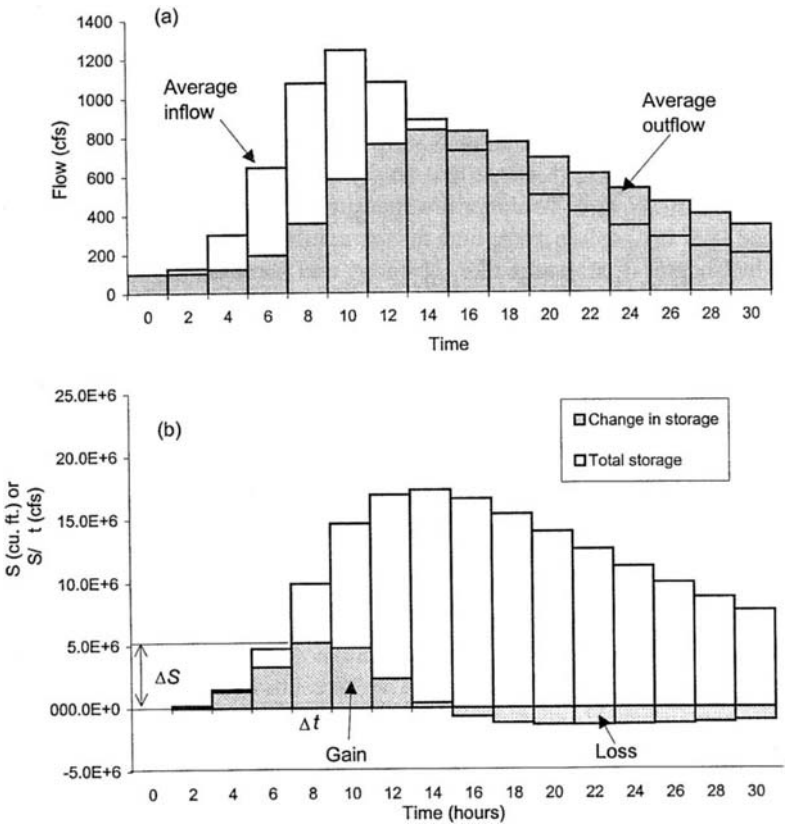

Figure 2.2. a) Reservoir inflow and outflow using discrete time, and b) Storage and change in storage. Values are given in Table 2.2.

Table 2.2. Example of input, output and change in storage using the discrete time continuity equation.

Time t (h)	Inflow I_t (cfs)	Average inflow $(I_1 + I_2)/2$ (cfs)	Outflow Q_t (cfs)	Average outflow $(Q_1 + Q_2)/2$ (cfs)	Change in storage ΔS_t (cfs)	Storage S_t (ft^3)
0	100	100	100	–	–	–
2	155	128	104	102	183600	183600
4	450	303	142	123	1292400	1476000
6	845	648	250	196	3250800	4726800
8	1310	1078	465	358	5184000	9910800
10	1185	1248	705	585	4770000	14680800
12	980	1083	825	765	2286000	16966800
14	800	890	850	838	378000	17344800
16	660	730	810	830	–720000	16624800
18	545	603	735	773	–1224000	15400800
20	455	500	650	693	–1386000	14014800
22	375	415	570	610	–1404000	12610800
24	310	343	495	533	–1368000	11242800
26	255	283	430	463	–1296000	9946800
28	215	235	370	400	–1188000	8758800
30	180	198	315	343	–1044000	7714800

physically-based zero, but rather an arbitrary zero. Ratio-level data have a true, physically-based zero value. Solar radiation is ratio-level data because zero radiation means no energy flux. Therefore, it is true that an energy flux of 500 W m^{-2} is twice as much radiation as 250 W m^{-2}. Temperature measured on the Kelvin scale (K) is ratio level because 0°K is absolute zero, and means a substance is totally devoid of thermal energy. In Chapter 3, statistics like the mean and standard deviation will be discussed. These statistics should be calculated only for interval- or ratio-level data. Statistics for interval- or ratio-level data are called parametric statistics.

2.5 HYDROLOGIC DATA SERIES

Hydrologic data can be selectively sampled to create different data series (Fig. 2.3). The *complete duration series* includes every observation from a hydrologic record. In Figure 2.3 there are 17 years of record with two observations on the variable X in each year. The complete duration series includes all 34 observations. The *partial duration series* is a subset of the complete duration series. For the partial duration series only observations greater than some arbitrary threshold are selected for analysis. In Figure 2.3b seven observations do not exceed the threshold so the partial duration series includes the remaining 27 observations. Note that the time sequence is irrelevant and some years might not be represented because they did not have any observations above the threshold. The *extreme value series* is a third category of hydrologic data series. There are different types of extreme value series, but the most widely used is the annual maximum series. This series is constructed by selecting the single largest observation from each year of record. For n years of record the annual

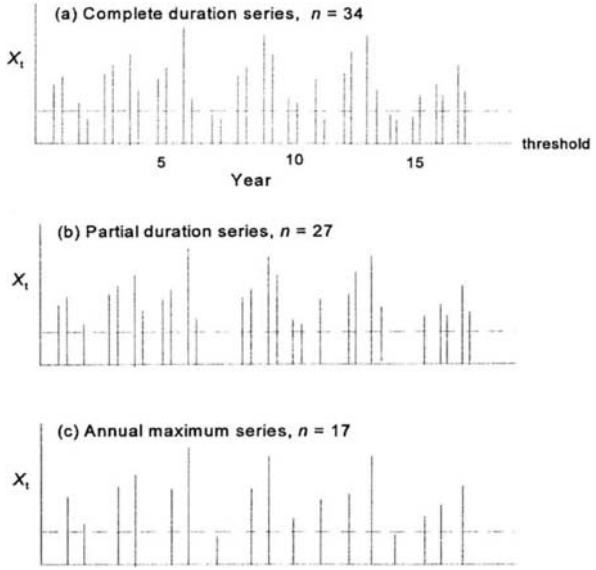

Figure 2.3. The complete duration series (a) is composed of every observation in the sample. The partial duration series (b) is every value above some threshold. The annual maximum series (c) includes only the single largest value from each year.

maximum series will contain n observations. In Figure 2.3c the annual maximum series has 17 observations.

The complete duration series is used to develop flow-duration curves for rivers. Flow-duration curves show discharge versus the percentage of time the river is above (below) that discharge level. These curves are useful in water supply planning, hydroelectric power generation studies and pollution damage analysis. Partial duration series and annual maximum (minimum) series are used in frequency analysis. Frequency analysis is the procedure whereby a probability of exceedence is assigned to an event of a certain magnitude. In practice, the annual maximum series is used for the analysis and the results are converted into partial duration series using conversion factors (see Appendix B). The partial duration series gives better probability estimates for high-frequency events. For exceedence probabilities less than 10%, the two series are essentially identical. Frequency analysis is discussed in Chapter 3, and the technique is demonstrated in Chapter 4 using precipitation data, and in Chapter 9 for floods.

2.6 GRAPHS AND GRAPHING

Computer-based graphing software is now widely available and most computer spreadsheet programs have excellent graphing capability. Computer programs have removed much of the tedium of pencil and paper graphing and have vastly improved the speed and efficiency of graphical exploration and data presentation. Graphs are simple but powerful methods for representing data because they are visual. An '*X Y*'

graph shows the relationship between two variables, and an '*X, Y, Z*' graph shows the relationship between three variables. The two variable case is called *bivariate*; more than two variables is called *multivariate*. The three variable relationship graphs as a surface, whereas the bivariate relationship graphs as a line. Relationships among more than three variables are possible but cannot be represented in graphical form. The following discussion is limited to the bivariate case.

If there is a causal relationship between two different variables, then a change in the independent variable *X* causes a change in the dependent variable *Y*. The strength of the relationship between two or more variables is called correlation. The correlation coefficient ranges from +1 to –1, where +1 means a perfect direct relationship, and –1 means a perfect inverse relationship. A value of 0 means no correlation – the observations are independent. Figure 2.4 is a graph of average annual precipitation and temperature versus elevation along a transect through the Front Range of the Rocky Mountains in Colorado. The transect runs from the City of Longmont on the Piedmont to the tundra environment of Niwot Ridge high in the mountains. The two left-most points on the graph are precipitation and temperature for Longmont. The two right-most points are precipitation and temperature for the Niwot Ridge station. It is apparent that temperature and precipitation are causally related to elevation. Precipitation is directly related to elevation whereas temperature is inversely related. Another way of saying this is that precipitation is 'positively correlated' with elevation, and temperature is 'negatively correlated' with elevation. We could actually calculate the correlation coefficients, but with so few observations we could not have much confidence in the result. In Figure 2.4 which do you think is the independent variable and which are dependent? The causal structure in this example is fairly obvious: changing elevation causes the change in precipitation and temperature. Causal structure between variables may not always be so obvious, and with multivariate relationships discerning causality can be quite difficult. Both axes on Figure 2.4 are scaled arithmetically. This means the magnitude of the intervals between successive tick marks on the axes is constant. This is the standard type of graph with which students are undoubtedly familiar. Arithmetic scaling for a graph is appropriate when all

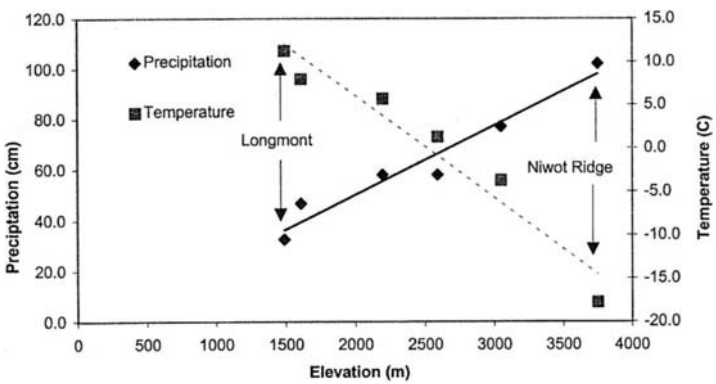

Figure 2.4. The spatial variation in annual average precipitation and temperature along a transect from the City of Longmont, Colorado on the plains to Niwot Ridge in the Rocky Mountains (source: University of Colorado, Geography Department).

data are within one or two orders-of-magnitude. However, it is common in hydrology to encounter data that span many orders-of-magnitude. Pollutant concentrations in a stream may vary from parts per billion (ppb) to parts per thousand. (This is a range of six orders-of-magnitude (10^{-9} to 10^{-3}). Standard arithmetically-scaled graph paper is inadequate for graphing data that span many orders-of-magnitude because it is difficult to accommodate the full range of the data. There are two ways to deal with this problem: either transform the axes of the graph paper or transform the data themselves. Whenever data range through more than two orders-of-magnitude, it is easier to plot and work with the data if they are logarithmically transformed. The easiest way to make such a transformation is to plot the data on log paper. Log paper is either semilog (arithmetic-log), which means one axis is a standard arithmetic axis and the other is a logarithmic axis, or log-log (double log) where both axes are logarithmic. Axes on log paper typically range from one to four cycles (orders-of-magnitude) (See Figs 2.5 and 2.6). Take the data in Table 2.3 as an example. The data range over three orders-of-magnitude – 'tens,' 'hundreds,' and 'thousands.' If you plot these data on arithmetically-scaled paper, it's difficult to plot and see the very small and very large values, and the data plot as an extreme curve (Fig. 2.7). How-

Table 2.3. Example data for demonstrating logarithmic transformation.

X	Y	$\ln X$	$\ln Y$
10	3000	2.3026	8.0064
30	1000	3.4012	6.9078
100	300	4.6052	5.7038
300	100	5.7038	4.6052
1000	30	6.9078	3.4012
3000	10	8.0064	2.3026

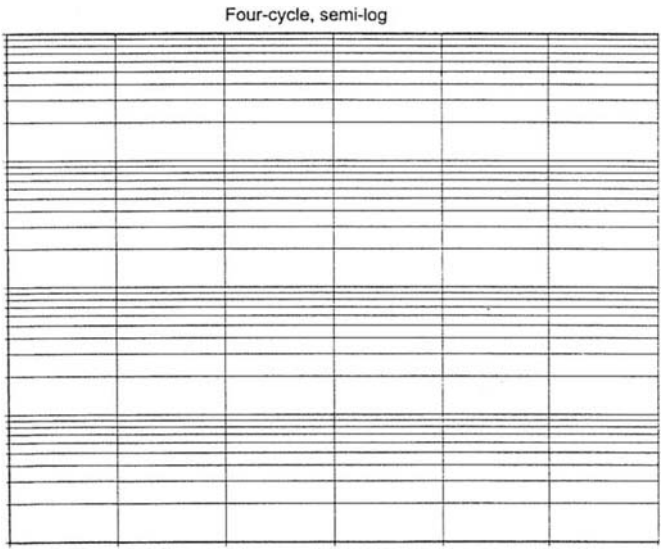

Figure 2.5 Semi-log (arithmetic-logarithmic) graph paper.

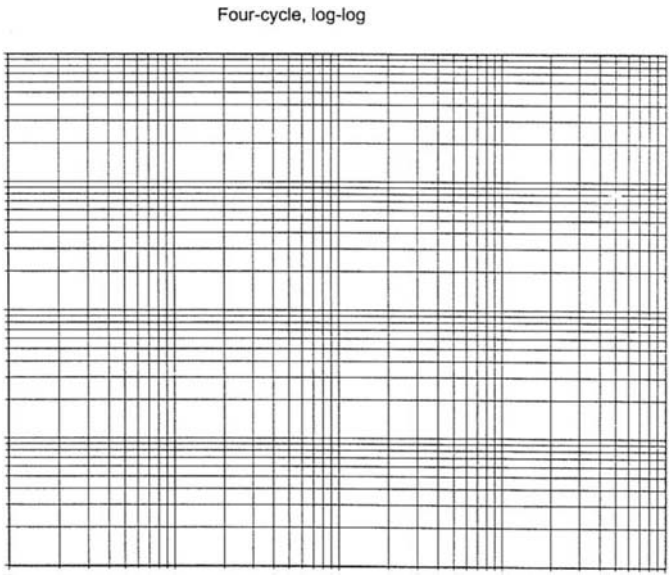

Figure 2.6. Logarithmic-logarithmic graph paper. This is an example four cycle log-log paper.

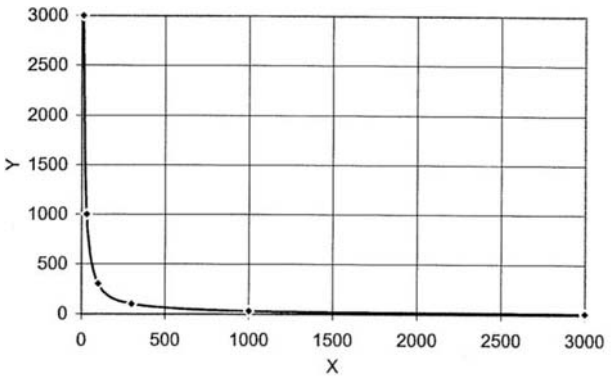

Figure 2.7. Exponential data from Table 2.3 plotted on arithmetic graph paper. It is difficult to see the data because of the range in magnitude between the largest and smallest values.

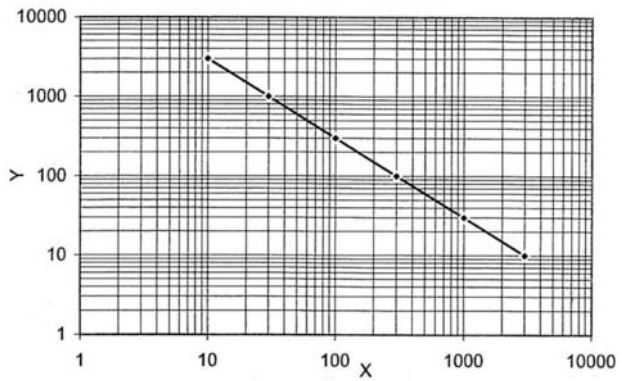

Figure 2.8. Data from Table 2.3 plotted on log-log graph paper makes it much easier to see the data.

ever, when plotted on log-log paper (use double log because both the X and Y data are exponential) the data are linearly transformed and much easier to see and work with (Fig. 2.8).

The second way to transform data is to take the logarithm of each datum (Table 2.3) and plot the log-transformed values on arithmetically-scaled paper. Logarithms of base 10 and base e (natural logs) are commonly used. (Accepted notation is to use the term 'log' to refer to logarithms of base 10 and 'ln' to refer to logarithms of base e.) Regardless of the method of transformation used the same goal is accomplished; however, using log paper may somewhat easier. Most spreadsheet programs and graphing software have built-in functions that allow either approach.

SUMMARY

This chapter has presented some basic issues concerning environmental data. Environmental data have both magnitude and dimension: magnitude refers to 'how much?' while dimension indicates 'of what?'. Dimensions may be expressed by any unit system. While the system of conventional English units is widely used in the United States for hydrologic data, students should be equally familiar with *SI* units. Because of the variety of units in use, it is often necessary to convert between different systems. In some areas of hydrology like soil moisture measurement, the lack of consensus on units and terminology can be both frustration and confusing.

The topic of continuous versus discrete data is of more than theoretical interest. Most hydrologic processes and variables are continuous in time and/or space, and, therefore, are truly described by differential and integral equations of calculus. For reasons of practicality, most of our data gathering and analytical procedures transform continuous data into discrete approximations. While discretation is often necessary for the analysis, the results are correspondingly less accurate. Graphing is widely used in hydrologic analyses for data exploration, representation, and interpolation. Graphing software and multifunction spreadsheet programs provide fast and efficient means for examining data.

An extremely important topic in hydrology is that of probability and statistics. This is such an important topic that it could not be treated adequately as a subsection within this chapter, and is the subject of Chapter 3. We shall see that there are continuous and discrete probability distributions for use with continuous and discrete data.

PROBLEMS

2.1 Over a long time a lake is in dynamic equilibrium with respect to water inflow and outlfow. Long-term annual average hydrologic values for the lake are given below.
   a) Find the average stream outflow from the lake in cfs.
   b) Find the average residence time of water in the lake.
   Lake surface area = 59 acres.
   Volume of water stored in the lake = 886 acre-feet.
   Streamflow input = 3.00 cfs.
   Precipitation onto the lake = 33 in yr^{-1}.

Evaporation from the lake = 27 in yr^{-1}.

2.2 Given below are the average monthly water balance variables for a drainage basin. Create a table and graph similar to text Table 2.2 and text Figure 2.2b and answer the following questions.

a) Which two months have the most rapid change (increase or decrease) in storage? Why?

b) Which months have almost no change in storage. Even though storage barely changed, what were magnitudes of the inputs and outputs.

Month (mm)	Streamflow (mm)	Precipitation (mm)	Evaporation (mm)	End of month soil storage (mm)
Jan	39	71	–	250
Feb	57	61	–	
Mar	98	99	16	
Apr	94	134	43	
May	52	96	86	
Jun	26	99	123	
Jul	13	83	132	
Aug	7	103	121	
Sep	3	79	84	
Oct	2	100	48	
Nov	25	109	18	
Dec	78	131	–	
Total	494	1165	671	

2.3 Given below are two sets of data. The *X* values are storm duration (hours) and the *Y* values are rainfall depth (mm) for '10-year' recurrence interval storms.

a) Transform the *X* and *Y* data by plotting on log-log paper.

b) Transform the *X* and *Y* data by taking the natural logs of the data and plotting on arithmetic paper.

X (hours)	*Y* (mm)
0.5	49
1.0	56
6.0	85
24.1	114

c) What would be the rainfall depth for a 10-year storm of 3.5 hours duration?

Log paper Answer .....

Arithmetic paper Answer .....

d) What is the average rainfall intensity (mm hr^{-1}) for a 10-year storm of 3.5 hours duration?

Log paper Answer .....

Arithmetic paper Answer .....

EXCEL EXERCISE 1

In this exercise use EXCEL to transform and plot the rainfall depth and duration data from the previous problem. 'LB' refers to the left button on the mouse.

Titles, column headings, data entry and formulas

1. Go to cell A1 and type 'Graphics Exercise'. (Do not include the quote marks.) Now you will

change the format of the text. Click (LB) on **Format** on the upper menu bar. This opens a drop down menu with more choices. Click (LB) **Cells**. This opens a final box with font choices. Click **MS Sans Serif / Bold / 12**.

You could also change fonts by selecting the cell and clicking the RB. This produces a 'short cut' menu to commonly used commands.

2. Go to cell G1 and type your name.
3. Go to A3 and enter the data from homework problem 2.3. Enter the hour values in A3:A6 and the precipitation values in B3:B6.
4. Go back to cell A2 and insert a row above it. Select cell A2 and click RB. Choose **Insert / Entire Row / OK**.
5. Make sure you are in cell A3 and type 'Hours.' Move to cell B3 and type 'PPT.' Let's reformat the text. Select A3:B3 and then click (LB) the Centertext button on the toolbar; it looks like a series of horizontally-stacked long and short lines centered on a page. Go back to cell A1 and select cells A1:E1. Now click the Center Across Columns button on the toolbar. This button will center your title over the selected columns.
6. Select (move to) cell A23. You are now going to calculate the natural logarithm of the data in the range A4:B7. EXCEL has a built-in function for natural logs. In cell A23 type '=LN(A4)' (without quotes) and press Enter. Cell A23 should now display the natural log of 0.5 which is –0.693. Rather than enter the formula in every cell separately, you can copy the formula to the other cells. With A23 selected press the RB on the mouse and choose **Copy** from the menu. Move to cell B23 and press Enter. You will now copy cells A23:B23 to the range A24:B26 using the click and drag. First copy A23:B23 then move to A24 and click and drag to B26. Release the LB and press Enter. EXCEL has an even faster way of entering a formula into a range of cells but we won't do it here.

Graphing data

1. You are now going to graph the two sets of data. Select the range A3:B7. Choose the ChartWizard tool (a wand leaning over a chart) from the toolbar. The selected data are now marqueed and at the bottom of the screen in the status bar it says 'drag in document.' Move the cursor (which is now a crosshair) to the lower right corner of C2. Click LB and drag to the lower right corner of I17. As you drag you will see a window open; this is where your chart will be drawn. As you can see, you can make it any size you want, but the range C2:I17 should be sufficient. Release the LB.
2. Now you see a dialogue box stating ChartWizard Step 1 of 5. Choose **Next**. Step 2 of 5 gives you choices for the chart; choose 'XY (Scatter)' and **Next**. Step 3 of 5 show you types of scatter charts; choose number 2 and **Next**. Step 4 of 5 shows you what your chart will look like and allows you to make corrections. If all looks well choose **Next**.

   Finally, Step 5 asks for the title of the chart and the name for the axes. Click on the space for the title and you will see a blinking vertical bar. When you enter text into these spaces do not press Enter at the end of the line. Use the mouse to move to the next text box and click. Only press Enter after you have entered your final axis title. Title your chart 'Original Data' and call the X axis 'Hours' and the Y axis 'PPT'; choose **Finish** or press Enter.
3. Now your 'embedded' chart will be plotted on your worksheet. If you change the data in the worksheet the changes will automatically be reflected on the graph. You can move the chart or change its size by selecting it. A chart is selected if little black boxes can be seen along the margin. Select the chart by placing the cursor anywhere on the chart and click the LB. To move the chart, first select it and then click and drag the chart. To change its size, first select it, place the cursor on one of the little black squares, and then click and drag the square.
4. Make a second chart for your logarithm data in the space to the right of the log data in the same manner as above. Call this chart 'Log Values,' the X axes 'Log Hours,' and the Y axis 'Log PPT.'

Printing and saving your worksheet

1. When you have finished creating two charts to go with the two data tables, you may print your graph. To print the graph choose **File** from the top menu (upper left). Next choose **Print Preview**. This will allow you to see your entire worksheet before you print it. Select **Print** if you are satisfied with your worksheet.
2. Save your worksheet to your diskette. First, make sure you have a formatted 3.5 inch diskette in drive A. Ask for assistance if you do not know which drive is A and which direction to insert your disk. Choose **File** and **Save** from the menu. Enter a name for your worksheet like 'EXER_1.XLS' (without quotes) and then click on the **Drive** button and choose Drive A. Choose **OK** to save your file.

CHAPTER 3

Statistics, probability and probability distributions

This is not an exhaustive discussion of probability and statistics, and students should consult a text on statistics for detailed treatment on topics introduced here. This chapter covers some basic concepts and techniques, and, while some examples are given, applications of certain techniques are deferred until Chapters 4 and 11. Statistics and probability come up frequently in analyzing hydrologic data, and they are useful in two ways:

1. *Description.* Statistics summarize and describe temporal and spatial data. Statistics such as the *mean* and *standard deviation* are commonly used to summarize a sample of data. *Histograms* are used to visually summarize the distribution of a set of data. Since the occurrence and magnitude of hydrologic phenomena are largely random, they are described probabilistically.

2. *Inference.* Statistics are used to infer characteristics about a larger population based on a random sample from that population. Hypothesis testing is an example of inferential statistics.

3.1 DESCRIBING DATA

Let us call a random hydrologic variable X. Each individual measurement on a variable is an *observation*, and x_1, x_2, and x_3 represent three separate observations on the variable. The variable X might be monthly precipitation or daily evaporation. Since X is a variable, by definition it takes on different values at different times and/or locations. The condition of randomness means that we cannot know with certainty what those values will be; we can only specify the probability that the variable will fall within a certain magnitude range. *Probability distributions assign probabilities to random variables.*

When a random variable is (self) *independent* the occurrence of the variable at one point in time (place) does not influence the occurrence or magnitude of the variable at any other time (place). When the occurrence of the variable influences its occurrence elsewhere or at some other point time it is (self) *dependent.* Correlation describes the strength of the relationship between variables. When describing the correlation between the same variable at different points in time, the term is *serial correlation.* For spatially-dependent data the term *autocorrelation* is often preferred.

A time sequence of observations of a variable make up a *time series.* Serial correlation decreases as the length of time between individual observations increases. Sta-

tistical analyses on time-series data where serial correlation is important are *stochastic* analyses. Serial correlation and time dependence is discussed further in Chapter 4. The concepts and techniques discussed in this chapter assume the data are random and independent.

To make the notation for a sequence of data more compact, call the variable x_i and let the *index variable i* assume the appropriate sequential value. The summation operator Σ is frequently used in statistical formulae. A compact formula to add up three observations of the x_i variable is:

$$\sum_{i=1}^{3} x_i = (x_1 + x_2 + x_3) \tag{3.1}$$

A formula to add up n observations is:

$$\sum_{i=1}^{n} x_i = (x_1 + x_2 + \ldots + x_{n-1} + x_n) \tag{3.2}$$

Just as the capital Greek letter sigma (Σ) is the summation operator, the capital letter pi (Π) denotes the multiplication operator.

3.2 MEASURES OF CENTRAL TENDENCY

Central tendency refers to 'where' in a sample the data are most concentrated. There are several different measures of central tendency, though some are used more frequently than others. The *arithmetic mean,* the *median*, the *mode*, the *geometric mean* and the *harmonic mean* are all encountered in hydrology. The arithmetic mean, also called the average, is the most widely used:

$$\bar{x} = \frac{\sum_{i=1}^{n} x_i}{n} \tag{3.3}$$

where n is the number of observations in the sample, and $\bar{x}$ is the mean of the *sample*. When describing the mean of a *population*, the symbol μ is used. The population consists of all the possible observations of a variable; the sample is a randomly selected subset of the larger population. In hydrology we will always be working with a small sample from a much larger hydroclimatological population. Most instrumental records of streamflow in the United States are less than 100 years. The same is true of most climatological records. When one considers that the present hydroclimatological regime may have existed for thousands of years, our instrumental records are pitifully short. Statisticians distinguish between *statistics*, which are values calculated from a sample of data, and *parameters*, which are values calculated from the entire population. Following this notation $\bar{x}$ is a statistic, whereas μ is a parameter.

The median is the observation located in the middle of a set of data. If a sample of n observations is ranked from the largest to the smallest, and if n is odd, the median

is the middle observation, with half the observations above and half below. The median is also called the 50th percentile. If n is even, the median is the average of the two most centrally-located observations.

The mode is the value of the variable, or interval for classified data (explained below), that contains the most observations. In a sample of data there are more observations of the modal value than any other. The last two measures, the geometric mean and the harmonic mean, are less frequently used. The geometric mean is the nth root of the product of n observations:

$$G = \sqrt[n]{\prod_{i=1}^{n} x_i} \tag{3.4}$$

The geometric mean is useful when working with highly skewed data. The harmonic mean is calculated as:

$$H = \frac{n}{\sum_{i=1}^{n} (1/x_i)} \tag{3.5}$$

An example of the use of the harmonic mean arises in the study of aquifer properties in Chapter 8.

Measures of central tendency all indicate, albeit in different ways, the middle of a set of data, but they do not indicate how the data distribute around this central location. Statistics (parameters) discussed in Section 3.3 provide information on the spread or dispersion of the data about the central location.

3.3 MEASURES OF DISPERSION

Dispersion refers to how data are distributed around their central location. One way to measure the spread of the data is the *range*. The range is the simply the difference between the largest and smallest observation in the sample. The range provides limited information about the distribution because it uses only two of the n observations. A more powerful measure of dispersion is the *variance*. As with the mean, the symbol differs for the population (σ^2) and the sample (s^2). The formula for the sample variance is:

$$s^2 = \frac{\sum_{i=1}^{n} (x_i - \bar{x})^2}{(n-1)} \tag{3.6}$$

The denominator in Equation (3.6) is n–1 rather than n to correct for a downward bias introduced by using the mean in the calculation. The formula says first subtract the sample mean ($\bar{x}$) from each observation (x_i). This difference measures how far the observation is from the center of the distribution. Next, square the difference to eliminate negative values; sum the squared values, and then divide the total by n–1. The result is the average squared distance (deviation) from the mean. The problem

with the variance is that it is in 'squared' units. To get back to the original units of the data, take the square root. The square root of the variance is the *standard deviation* (s), and has the formula:

$$s = \sqrt{s^2} = \sqrt{\frac{\sum_{i=1}^{n}(x_i - \bar{x})^2}{(n-1)}} \tag{3.7}$$

Example 3.1 below explains the calculation of the various measures of central tendency and dispersion. While Equation (3.6) may be used, a more efficient formula for the variance is:

$$s^2 = \frac{\sum_{i=1}^{n} x_i^2 - \left[\left(\sum_{i=1}^{n}(x_i)^2\right)/n\right]}{n-1} \tag{3.8}$$

These two statistics, the mean and standard deviation, describe the location and dispersion in a sample of data. The *coefficient of variation* $CV = \sigma/\mu$ is a dimensionless measure of variability and is useful in comparing different samples or types of data. Again, because we work with samples and not populations, the coefficient of variation is estimated as $CV = s/\bar{x}$.

Another important characteristic of hydrologic data is *skewness*. Skewness describes the degree of symmetry in the data about the mean. Many hydrologic data exhibit positive skewness; they are bounded by zero on the left (since it is impossible to have a negative value for hydrologic quantities), but occasionally very large-magnitude (positive axes direction) events occur. Figure 3.1 shows distributions with different types of skewness. Annual maximum series data are positively skewed. Streamflow, for example, can never be less than zero, but very large flood discharges occasionally occur. The sample-based estimate of the coefficient of skewness C_s is:

$$C_s = \frac{\sum_{i=1}^{n}(x_i - \bar{x})^3}{(n-1)(n-2)s^3} \tag{3.9}$$

Sample skewness calculated by Equation (3.9) is considered unreliable for $n \leq 50$, and it is recommended that the value be adjusted. Hazen (cited in Kottegoda 1980) suggested a correction factor of $(1 + 8.5/n)$. The adjusted skewness (C_s') is determined as:

$$C_s' = \left(1 + \frac{8.5}{n}\right) C_s \tag{3.10}$$

Figures 3.1a-c are examples of three different probability distributions. Figure 3.1b shows a distribution with no skewness, or more accurately, the skewness is equal to zero. Data with negligible skewness are *normally* distributed. Figure 3.1b is an example of a normal distribution, while Figures 3.1a and 3.1c are other probability dis-

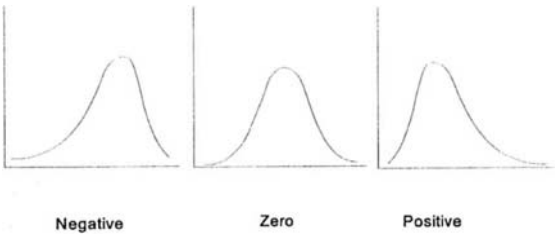

Figure 3.1. Three distributions showing positive, negative and zero skewness.

tributions. The term normal is used to describe symmetrical, bell-shaped distributions, and does not mean that the other distributions are somehow abnormal, though they certainly are non-normal. One way to eliminate skewness is to logarithmically transform the data as done in Section 2.6. The reason for normalizing data is so that we can use normal-distribution statistical techniques. We will see in Chapter 11 that certain methods of flood frequency analysis use logarithmically-transformed data.

Example 3.1

In this example the data in Table 3.1 are used to demonstrate the calculation of different measures of central tendency and dispersion. Values are rounded to three significant figures.

a) The arithmetic mean is:

$$\bar{x} = (2 + 3 + 4 + 3 + 5 + 3 + 4 + 8) / 8 = 4.0$$

b) To find the median, rearrange the data in ascending order and find the middle value, 2, 3, 3, 3, 4, 4, 5, 8. Since n is even, the median is determined as $(3 + 4) / 2 = 3.5$, with half of the data below and half above.

c) The mode is 3. There are more '3s' than any other value.

d) The geometric mean is:

$$G = \sqrt[8]{2 \cdot 3 \cdot 4 \cdot 3 \cdot 5 \cdot 3 \cdot 4 \cdot 8} = 3.69$$

e) The harmonic mean is:

$$H = 8 / (1/2 + 1/3 + 1/4 + 1/3 + 1/5 + 1/3 + 1/4 + 1/8) = 3.44$$

The calculated values are all close to 3.5. The mean is higher because the data are positively skewed and observation eight, $x_8 = 8$, 'drags' the mean up to 4.

The range, variance and standard deviation are calculated as follows. The range is $(8 - 2) = 6$. In order to use Equation (3.6), find the sum of the squared deviations as follows:

i	$(x_i - \bar{x})$	$(x_i - \bar{x})^2$	i	$(x_i - \bar{x})$	$(x_i - \bar{x})^2$
1	$(2 - 4) = -2$	4	5	$(5 - 4) = 1$	1
2	$(3 - 4) = -1$	1	6	$(3 - 4) = -1$	1
3	$(4 - 4) = 0$	0	0	$(4 - 4) = 0$	0
4	$(3 - 4) = -1$	1	8	$(8 - 4) = 4$	16
					Σ 24

The variance and standard deviation are calculated using Equation (3.6) as:

$$s^2 = 24/7 = 3.43$$

$$s = \sqrt{3.43} = 1.85$$

Again, the extreme influence of observation x_8 is apparent in the calculation of both the range and the standard deviation.

Using Equation (3.8), the variance is:

$$s^2 = [152 - (32)^2 / 8] / 7 = 24/7 = 3.43$$

A *histogram* is a convenient way to organize and display data. A histogram shows data *classified* into groups. It is up to the analyst to decide how many classes to use and the class boundaries. There is no rule for determining the number of class intervals, but there are some guides available. Two equations for estimating the number of class intervals are:

$$m = \sqrt{n} \tag{3.11a}$$

or

$$m = 5 (\log n) \tag{3.11b}$$

where m is the number of class intervals rounded to the nearest whole number. Equation (3.11a) is used by the EXCEL spreadsheet program and determines the number of intervals as the square root of the number of observations. Equation (3.11b) is from Panofsky & Brier (1968) and uses a logarithmic approach. The boundaries between intervals should be chosen such that each observation falls unambiguously into one and only one class.

Table 3.2 gives 38 observations of annual precipitation for Philadelphia, Pennsylvania from 1950 to 1987. Figure 3.2a is a histogram of the Philadelphia data displaying the number of observations by class interval. Histograms are useful for qualita-

Table 3.1. Hypothetical data.

$x_1 = 2$	$x_5 = 5$
$x_2 = 3$	$x_6 = 3$
$x_3 = 4$	$x_7 = 4$
$x_4 = 3$	$x_8 = 8$

Table 3.2. Annual total precipitation (inches) for Philadelphia, PA, 1950–1987.

Year	Precip.	Year	Precip.	Year	Precip.	Year	Precip.
1950	40.47	1960	41.15	1970	39.14	1980	38.80
	42.06		41.05		47.79		37.38
	45.84		42.63		49.63		40.43
	48.13		34.95		46.06		54.41
	34.04		29.88		37.78		43.66
1955	33.03	1965	29.34	1975	52.13	1985	35.20
	45.90		40.00		33.27		40.42
	32.20		44.82		49.42		33.40
	47.87		35.45		45.95		
	38.37		43.36		52.79		

Mean $\bar{x} = 41.28$. Standard deviation $s = 6.49$.

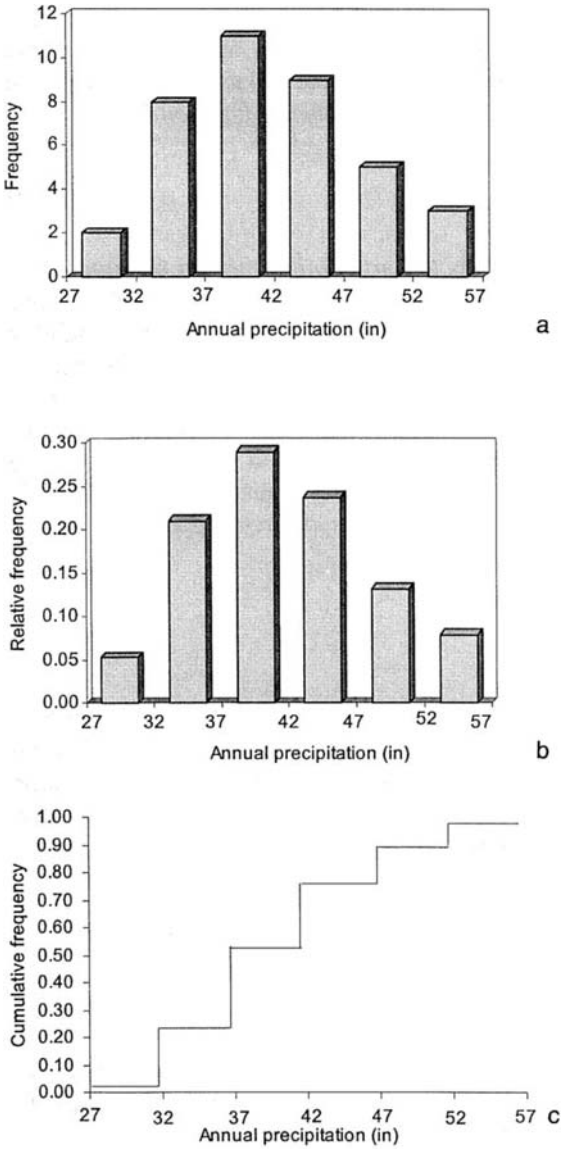

Figure 3.2. Histogram, relative frequency function and cumulative frequency function for the Philadephia precipitation data.

tively examining the distribution of a sample of data. Dividing the number of observations (n_i) in each class interval (i), by the total number of observations in the sample (n) we obtain the sample *relative frequency function* $f_s(x)$:

$$f_s(x_i) = \frac{n_i}{n} \tag{3.12}$$

Figure 3.2b is the relative frequency histogram for the Philadelphia data. *The relative frequency histogram provides sample estimates of the probability that an observation of annual precipitation will fall within a given interval.* For example, based on

the sample, the probability of getting between 37 and 42 inches in any given year is 0.29 (29%). These sample-based estimates of probability only approximate the true population-based probabilities. The sum of the sample relative frequencies up through any particular interval yields the *cumulative frequency function* $F_s(x)$:

$$F_s(x_i) = \sum_{j=1}^{i} f_s(x_j) \tag{3.13}$$

The cumulative frequency function estimates the probability that an observation is less than some value of X. Figure 3.2c is the $F_s(x)$ for the Philadelphia data. Notice that the sum of all of the relative frequencies equals 1. An axiom of probability theory states that probability ranges from 0 (impossible) to 1 (absolute certainty).

For classified data, each observation falling within a given class interval is assigned the same relative frequency. A technique called frequency analysis is introduced in Chapter 4. With frequency analysis each observation is assigned a unique probability. Section 3.4 shows that the relative frequency function and the cumulative frequency function for classified sample data are discrete approximations of continuous probability functions for populations.

3.4 PROBABILITY FUNCTIONS

The relative frequency and cumulative frequency functions provide probability estimates for classified sample data. The relative frequency function $f_s(x)$ is a discrete sample approximation of a continuous probability function for the entire population called a *probability density function f(x)* (PDF). There are some important differences between the PDF and the relative frequency function. Whereas the relative frequency function gives probability estimates for intervals of the variable X, the PDF shows the probability 'concentration' or 'density' for intervals of X along the abscissa (Chow et al. 1988). The relative frequency function gives probability and ranges between (0,1), but the probability density function ranges from (0,∞). A third difference is that the relative frequency function is dimensionless, whereas the probability density function has dimensions of $(X)^{-1}$. The sample cumulative frequency function $F_s(x)$ has a continuous counterpart for the population called the *cumulative distribution function F(x)* (CDF). Both functions give probabilities; therefore, both range from (0,1), and both are dimensionless.

The PDF and the CDF can be derived from their discrete sample counterparts by using the concept of the limit introduced in Chapter 2 (Fig. 3.3). If the interval for X on the relative frequency histogram approaches zero ($\Delta x \to 0$), while n becomes infinitely large ($n \to \infty$), then $f_s(x) \to f(x)$, and $F_s(x) \to F(x)$. Mathematically this is expressed as:

$$f(x) = \lim_{\substack{n \to \infty \\ \Delta x \to 0}} f_s(x) \tag{3.14}$$

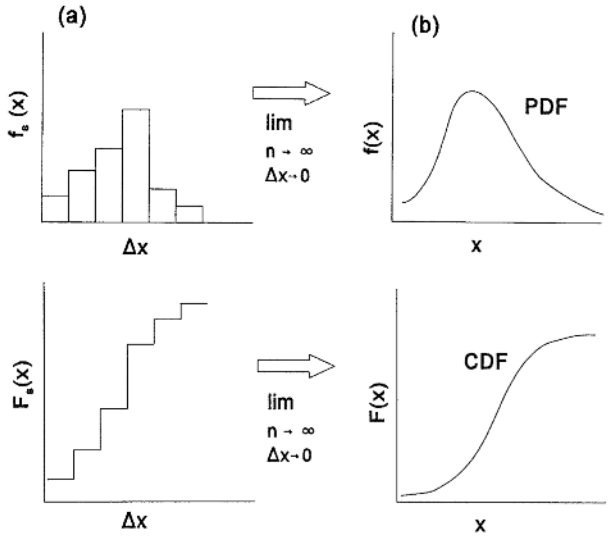

Figure 3.3. This figure shows the transformation of the (a) sample functions $f_s(x)$ and $F_s(x)$ into their (b) continuous counterparts $f(x)$ and $F(x)$.

and

$$F(x) = \lim_{\substack{n \to \infty \\ \Delta x \to 0}} F_s(x) \tag{3.15}$$

Just as Equation (3.13) shows the relationship between the discrete sample functions $F_s(x)$ and $f_s(x)$, the continuous functions $F(x)$ and $f(x)$ are mathematical inverses of each other. $F(x)$ is the integral of $f(x)$:

$$F(x) = \int_{-\infty}^{x} f(u)\mathrm{d}u \tag{3.16}$$

and $f(x)$ is the derivative of $F(x)$:

$$f(x) = \frac{\mathrm{d}F(x)}{\mathrm{d}x} \tag{3.17}$$

The letter u in Equation (3.16) is a dummy variable needed for the integration. Equation (3.16) is an integral equation and Equation (3.17) is a differential equation. Note the similarity between Equations (3.13) and (3.16). Though in its present form Equation (3.13) is not a direct analog of Equation (3.16), the integral operation on a continuous variable (Eq. 3.16) can be thought of as being similar to the summation operation on a discrete variable (Eq. 3.13). Integral and differential equations come up again in Chapter 7 when we describe the infiltration of water into the soil.

We shall see later that there are a half dozen or so probability distributions widely employed in hydrology. Probability distributions are 'fit' to a sample of data. Section 3.5 discusses some probability concepts and shows how to use the normal distribution to assign probability to annual precipitation data. Later we discuss fitting a sample of data to a theoretical probability distribution.

3.5 PROBABILITY AND THE NORMAL CURVE

This section demonstrates how to use the normal distribution to estimate probability, though the techniques apply to any probability distribution. The key concept in using a probability distribution to estimate probability is to *equate the area under the probability density function curve with the quantitative estimate of probability*. We know that probability ranges from 0 to 1. A probability of 0.5 means that there is a '50% chance' of an event either occurring or not occurring. Let the letter p represent the probability of an event occurring, and the letter q the probability of the event *not* occurring. By the *Law of Total Probability*, $(p + q) = 1$, and it follows that $q = (p - 1)$ and $p = (q - 1)$.

A more compact way of saying 'what is the probability of the variable X being less than some value x?' is to write $P(X < x)$. Likewise the probability that X is greater than some value can be written $P(X > x)$. Finally, the probability of X falling between the values x_1 and x_2 is written $P(x_1 < X < x_2)$. It can be shown that for a continuous distribution $P(X \geq x) = P(X > x)$, and $P(X \leq x) = P(X < x)$.

The normal distribution is a symmetrical theoretical distribution for use with continuous variables. Because the distribution asymptotically approaches $-\infty$ and $+\infty$, probability density is greatest near the mean and diminishes in the 'tails' of the distribution. As a result, more area under the PDF curve is found close to the mean. Since probability is equal to the area under the PDF curve, the probability of getting a value near the mean is greater than the probability of getting values far from the mean.

The total area under the normal probability density function from $-\infty$ to $+\infty$ is equal to 1 (100%). Figures 3.4a and 3.4b show the percentage of area under the normal curve between values of the standard deviation. Figure 3.4a shows that half the area under the PDF curve (50%) is less than the mean and half is above the mean. This should be obvious since the mean is the center of the distribution, and a normal distribution is symmetrical about the mean. Figure 3.4b shows that 0.6826 (68.26%) of the area under the curve lies within one standard deviation of the mean. The normal distribution is appropriate for assigning probabilities to data that are (at least approximately) normally distributed. Hydrologic and climatologic variables measured

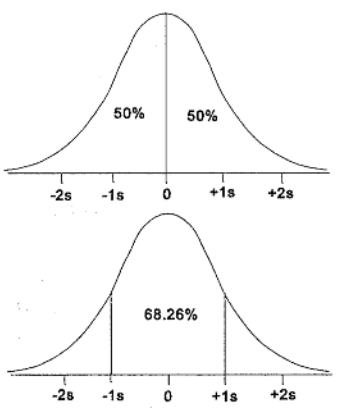

Figure 3.4. Area under the normal distribution PDF curve.

on an annual basis, such as total annual precipitation, average annual temperature, annual evaporation and annual streamflow volume are usually approximately normal in their distribution. This is true because the *central limit theorem* in statistics says variables that are the sum of many independent random events assume a normal distribution regardless of the underlying distribution of the individual events. Hydroclimatological variables for other time periods, e.g., monthly, weekly or daily, can also be fitted to a normal distribution as long as the sample is chosen correctly. For example, suppose you wanted to estimate precipitation probabilities for the month of March and you had 50-years of monthly precipitation data ($n = 600$). The correct sample would be just the March observations ($n = 50$) (see Fig. 3.5). The primary disadvantage of the normal distribution for hydrology is that it is bounded on the left by $-\infty$ and not 0.

What is the probability that an observation on a normally-distributed variable will be less than the mean? Recalling the key concept the answer is equal to the area under the PDF curve less than the mean, or 0.50 (50%). What is the probability that the variable will have a value between –1 and +1 standard deviations of the mean? Again the answer is the area under the PDF curve between these two values, or 0.6826 (68.26%). Probability is equal to the area under the PDF curve between the two limiting values. This is the solution of Equation (3.16). In other words, probability can be obtained directly from the CDF.

The PDF curve is scaled to the mean and standard deviation of the particular sample of data. This raises the question of how to generalize the technique of assigning probability to any sample of normally-distributed data. Such a generalization is accomplished through a transformation variously called *normalization*, *standardization*, or the *z transform*. Standardized z scores are calculated as:

$$z = \frac{(x_i - \bar{x})}{s} \tag{3.18}$$

The z transform standardizes the scale of any normal distribution so that it has a mean of 0 and a standard deviation of 1. The cumulative distribution function $F(z)$ for the transformed z variable is:

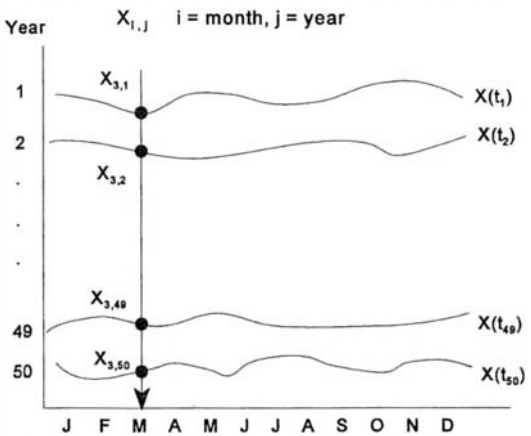

Figure 3.5. Selection of 50 monthly precipitation values from a time series of 50 years.

$$F(z) = \int_{-\infty}^{z} f(u)\mathrm{d}u \tag{3.19}$$

Equation (3.19) is the z-transformed equivalent of Equation (3.16). Table 3.3 gives the area under the standardized normal PDF curve from $-\infty$ to z. In other words, Table 3.3 is the solution of Equation (3.19) for discrete values of z. Because the normal distribution is symmetrical, only the area for $z \geq 0.00$ is given in Table 3.3. The area for $z \leq 0.00$ can be found as one minus the area for $z \geq 0.00$. The following example uses the Philadelphia precipitation data to show the calculation of z scores and the use of Table 3.3 to solve Equation (3.19) and estimate probability.

Table 3.3. Cumulative probability of the standard normal distribution.

z	0	0.01	0.02	0.03	0.04	0.05	0.06	0.07	0.08	0.09
0.00	0.5000	0.5040	0.5080	0.5120	0.5160	0.5199	0.5239	0.5279	0.5319	0.5359
0.10	0.5398	0.5438	0.5478	0.5517	0.5557	0.5596	0.5636	0.5675	0.5714	0.5753
0.20	0.5793	0.5832	0.5871	0.5910	0.5948	0.5987	0.6026	0.6064	0.6103	0.6141
0.30	0.6179	0.6217	0.6255	0.6293	0.6331	0.6368	0.6406	0.6443	0.6480	0.6517
0.40	0.6554	0.6591	0.6628	0.6664	0.6700	0.6736	0.6772	0.6808	0.6844	0.6879
0.50	0.6915	0.6950	0.6985	0.7019	0.7054	0.7088	0.7123	0.7157	0.7190	0.7224
0.60	0.7257	0.7291	0.7324	0.7357	0.7389	0.7422	0.7454	0.7486	0.7517	0.7549
0.70	0.7580	0.7611	0.7642	0.7673	0.7704	0.7734	0.7764	0.7794	0.7823	0.7852
0.80	0.7881	0.7910	0.7939	0.7967	0.7995	0.8023	0.8051	0.8078	0.8106	0.8133
0.90	0.8159	0.8186	0.8212	0.8238	0.8264	0.8289	0.8315	0.8340	0.8365	0.8389
1.00	0.8413	0.8438	0.8461	0.8485	0.8508	0.8531	0.8554	0.8577	0.8599	0.8621
1.10	0.8643	0.8665	0.8686	0.8708	0.8729	0.8749	0.8770	0.8790	0.8810	0.8830
1.20	0.8849	0.8869	0.8888	0.8907	0.8925	0.8944	0.8962	0.8980	0.8997	0.9015
1.30	0.9032	0.9049	0.9066	0.9082	0.9099	0.9115	0.9131	0.9147	0.9162	0.9177
1.40	0.9192	0.9207	0.9222	0.9236	0.9251	0.9265	0.9279	0.9292	0.9306	0.9319
1.50	0.9332	0.9345	0.9357	0.9370	0.9382	0.9394	0.9406	0.9418	0.9429	0.9441
1.60	0.9452	0.9463	0.9474	0.9484	0.9495	0.9505	0.9515	0.9525	0.9535	0.9545
1.70	0.9554	0.9564	0.9573	0.9582	0.9591	0.9599	0.9608	0.9616	0.9625	0.9633
1.80	0.9641	0.9649	0.9656	0.9664	0.9671	0.9678	0.9686	0.9693	0.9699	0.9706
1.90	0.9713	0.9719	0.9726	0.9732	0.9738	0.9744	0.9750	0.9756	0.9761	0.9767
2.00	0.9772	0.9778	0.9783	0.9788	0.9793	0.9798	0.9803	0.9808	0.9812	0.9817
2.10	0.9821	0.9826	0.9830	0.9834	0.9838	0.9842	0.9846	0.9850	0.9854	0.9857
2.20	0.9861	0.9864	0.9868	0.9871	0.9875	0.9878	0.9881	0.9884	0.9887	0.9890
2.30	0.9893	0.9896	0.9898	0.9901	0.9904	0.9906	0.9909	0.9911	0.9913	0.9916
2.40	0.9918	0.9920	0.9922	0.9925	0.9927	0.9929	0.9931	0.9932	0.9934	0.9936
2.50	0.9938	0.9940	0.9941	0.9943	0.9945	0.9946	0.9948	0.9949	0.9951	0.9952
2.60	0.9953	0.9955	0.9956	0.9957	0.9959	0.9960	0.9961	0.9962	0.9963	0.9964
2.70	0.9965	0.9966	0.9967	0.9968	0.9969	0.9970	0.9971	0.9972	0.9973	0.9974
2.80	0.9974	0.9975	0.9976	0.9977	0.9977	0.9978	0.9979	0.9979	0.9980	0.9981
2.90	0.9981	0.9982	0.9982	0.9983	0.9984	0.9984	0.9985	0.9985	0.9986	0.9986
3.00	0.9987	0.9987	0.9987	0.9988	0.9988	0.9989	0.9989	0.9989	0.9990	0.9990
3.10	0.9990	0.9991	0.9991	0.9991	0.9992	0.9992	0.9992	0.9992	0.9993	0.9993
3.20	0.9993	0.9993	0.9994	0.9994	0.9994	0.9994	0.9994	0.9995	0.9995	0.9995
3.30	0.9995	0.9995	0.9995	0.9996	0.9996	0.9996	0.9996	0.9996	0.9996	0.9997
3.40	0.9997	0.9997	0.9997	0.9997	0.9997	0.9997	0.9997	0.9997	0.9997	0.9998

Example 3.2

The mean and standard deviation for the Philadelphia data are 41.28 and 6.49 inches, respectively. Assume the data are approximately normally distributed and determine the following four probabilities:

1. The probability of getting less than 45 inches of precipitation in any given year, $P(X < 45.00)$.
2. The probability of getting between 43 and 45 inches of precipitation in any given year, $P(43.00 < X < 45.00)$.
3. The probability of getting less than 35 inches of precipitation in any given year, $P(X < 35.00)$.
4. The probability of getting exactly 35 inches of precipitation in any given year, $P(X = 35.00)$.

Solutions:

1. Find $P(X < 45.00)$? The z score for 45.00 inches is $z = (45.00 - 41.28) / 6.49 = 0.57$ so $P(X < 45.00) = P(Z < 0.57)$. From Table 3.3 the area from $z = -\infty$ to $z = 0.57$ is 0.7157. Based on our sample there is an 71.57% chance of getting less than 45 inches in any given year. And conversely, from Law of Total Probability, the probability of getting *more* than 45 inches is $(1.0 - 0.7157) = 0.2843$.
2. Find $P(43 < X < 45)$? The equivalent z-transformed expression is $P(43 < X < 45) = P(0.27 < Z < 0.57)$. The area from $z = -\infty$ to $z = 0.27$ is 0.6064, and from $z = -\infty$ to $z = 0.57$ is 0.7157. The net area is $(0.7157 - 0.6064) = 0.109$. The probability of getting between 43 and 45 inches is approximately 10.9%.

   As demonstrated in these two examples, the answer is found by subtracting the CDF (Eq. 3.19) evaluated at the two limiting z scores:

   $$P(z_1 < Z < z_2) = F(z_2) - F(z_1)$$

   Repeating the first example:

   $$P(-\infty < Z < 0.57) = F(0.57) - F(-\infty)$$

   $$P(-\infty < Z < 0.57) = 0.7157 - 0 = 0.7157$$

   For the second example:

   $$P(0.27 < Z < 0.57) = F(0.57) - F(0.27)$$

   $$P(0.27 < Z < 0.57) = 0.7157 - 0.6064 = 0.109$$

3. Find $P(X < 35.00)$? The z value is $z = -0.97$. Since this value is less than zero:

   $$P(-0.97) = 1 - 0.8340 = 0.1660$$

   $$P(-\infty < Z < -0.97\ ) = F(-0.97) - F(-\infty) = 0.1660$$

4. Find $P(X = 35.00)$? Following the procedure as before, $P(X = 35) = P(Z = -0.97)$. The answer is:

   $$P(Z = -0.97) = F(-0.97) - F(-0.97)$$

   $$P(Z = -0.97) = 0.1660 - 0.1660 = 0$$

   For a continuous distribution the probability of getting *exactly* some value is zero.

The probabilities in Example 3.2 are the theoretical probabilities for a continuous normal distribution fit to the Philadelphia data using the sample mean and standard deviation. In Chapter 4 we will see that probabilities based on sample data differ from the theoretical values. As the size of the sample increases, the difference between the theoretical probability estimates and the sample estimates should decrease.

3.6 PROBABILITY DISTRIBUTIONS

There are a half dozen or so probability distributions commonly used in hydrology. Six continuous distributions that are widely applied are the normal, lognormal, gamma, Pearson Type III, log-Pearson Type III, and Extreme Value Type I. The PDFs for these distributions are given in Table 3.4. The choice of which distribution to use in a particular situation depends upon the type of problem, the characteristics of the data and the researcher's preference. Of the six distributions, five are (or can be made) positively skewed; only the normal distribution is symmetrical. The positively skewed distributions find their widest application in precipitation and flood frequency analysis where the objective is to determine the probability of different rainfall or discharge events. In the United States, it has been recommended that federal agencies use the log-Pearson Type III distribution for the analysis of flood discharges (US Water Resources Council 1981). On the other hand, the Extreme Value I (EVI) distribution is often preferred for assigning probabilities to extreme precipitation events. In the United Kingdom it is just the opposite, the EVI is often the distribution of choice for the analysis of flood data. Two discrete distributions that have important hydrologic applications are the binomial distribution and the exponential distribution. The objective in discrete analyses is usually to determine the probability of a sequence of discrete events. The exponential distribution can be use to estimate the probability of different time intervals between a sequence of independent events. For example, it is used to estimate the probability that the interval of time between storms will be greater than t hours. The binomial distribution is used in the assessment of risk and is demonstrated in Chapter 4.

3.7 FITTING PROBABILITY DISTRIBUTIONS

A theoretical probability distribution must be fit to a sample of data. There are three ways to fit a theoretical distribution to a sample. The most fundamental method is to estimate the parameters of the distribution using the sample statistics. Two methods for doing this are the *method of moments* and the *method of maximum likelihood*. The method of moments is generally easier but the resulting parameter estimates are less accurate, especially for small samples. The moments for the normal distribution are the mean μ and variance σ^2 (see Table 3.4). The maximum likelihood parameter estimation is a more accurate, but a more complex method. In practice simplicity often triumphs over accuracy and the method of moments is more often used. With the parameters in hand probability is estimated using the either PDF or CDF. The PDF was used in Example 3.2. In Chapter 4 the technique is demonstrated using the CDF for both the normal and gamma distributions.

The second way to fit a distribution is by *frequency factors* (Chow 1951). Frequency factors (K) depend upon the parameters of a distribution, and so this is a variation of the parameter-based approach. Frequency factors take the general form:

$$K = \frac{(x - \bar{x})}{s} \tag{3.20}$$

Table 3.4. Probability distributions for fitting hydrological data. (Source: Chow et al. 1988, used by permission).

Distribution PDF	Equations for parameters (methods of moments)
Normal $f(x) = \frac{1}{\sigma\sqrt{2\pi}} \exp\left(-\frac{\left(x-\mu^2\right)}{2\sigma^2}\right)$	$\mu = \bar{x}, \sigma = s_x$
Lognormal $f(x) = \frac{1}{x\sigma\sqrt{2\pi}} \exp\left(-\frac{\left(y-\mu_y^2\right)}{2\sigma^2}\right)$ where $y = \log x$	$\mu_y = \bar{y}, \sigma_y = s_y$
Exponential $f(x) = \lambda e^{-\lambda x}$	$\lambda = (1/x)$
Gamma $f(x) = \frac{\lambda^\beta x^{\beta-1} e^{-\lambda x}}{\Gamma(\beta)}$ where Γ = gamma function	$\lambda = \frac{\bar{x}}{s_x^2}, \beta = \frac{\bar{x}^2}{s_x^2} = \frac{1}{CV^2}$
Pearson Type III $f(x) = \frac{\lambda^\beta (x-\varepsilon)^{\beta-1} e^{-\lambda(x-\varepsilon)}}{x\Gamma(\beta)}$	$\lambda = \frac{s_x}{\sqrt{\beta}}, \beta = \left(\frac{2}{C_s}\right)^2, \varepsilon = \bar{x} - s_x\sqrt{\beta}$
Log-Pearson Type III $f(x) = \frac{\lambda^\beta (y-\varepsilon)^{\beta-1} e^{-\lambda(y-\varepsilon)}}{x\Gamma(\beta)}$ where $y = \log x$	$\lambda = \frac{s_y}{\sqrt{\beta}}, \beta = \left(\frac{2}{C_s(y)}\right)^2, \varepsilon = y - s_y\sqrt{\beta}$
Extreme Value Type 1 $f(x) = \frac{1}{\alpha} \exp\left[-\frac{x-u}{\alpha} - \exp\left(-\frac{x-u}{\alpha}\right)\right]$	$\alpha = \frac{\sqrt{6s_x}}{\pi}, u = \bar{x} - 0.5772\alpha$

Rearranging Equation (3.20) gives:

$$x = \bar{x} + Ks \tag{3.21}$$

Equation (3.21) calculates a value for the variable X as a function of the sample mean, standard deviation and a frequency factor. The form of Equations (3.20) and (3.18) are identical, which means that the frequency factors for the normal distribution are the z scores. Frequency factors are used to fit the lognormal, the Pearson Type III, log-Pearson Type III and the Extreme Value distributions to flood discharges in Chapter 11.

A third way to fit a sample of data to a theoretical distribution is graphically – by plotting the data on special graph paper scaled to that particular distribution. The normal, lognormal and Extreme Value distributions have dedicated graph paper. A theoretical distribution plots as a straight line on its special graph paper. The fit is accomplished by assigning a 'plotting position' estimate of frequency to each observation and plotting the observation versus frequency. If the data follow that particular distribution, they plot as a straight line. As with the logarithmic transformation (Chapter 2) where plotting on log paper was easier than taking logarithms of the data, plotting on graph paper is easier than calculating the parameters of the distribution. The plotting position approach should accompany the parameter-based methods so the sample distribution can be directly compared against the assumed theoretical distribution. Visual comparison shows how well the data follow the presumed theoretical distribution, and is especially important for the identification of 'outliers.' Outliers are observations that have sample frequencies significantly different from their corresponding theoretical probability value.

3.8 TESTING GOODNESS-OF-FIT

Classifying data as a histogram qualitatively shows the distribution of the data. Similarly, plotting a sample against a theoretical distribution qualitatively shows how well the sample follows the theoretical distribution. Neither method objectively assesses how well the sample fits the theoretical distribution. There are two common goodness-of-fit tests for checking how well a sample of data fit a distribution. One is the X^2 (Chi square) test, the other is the Kolmogorov-Smirnov (K-S) test. The K-S test is the simpler of the two and is described here.

The first step is to formulate the null hypothesis (H_0). The null hypothesis states: 'There is not a significant difference between the sample distribution $F_s(x)$ and the theoretical distribution $F(x)$.' Next, a significance level α is chosen for the test. A significance level of $\alpha = 0.05$ means that the test is expected to be wrong 5% of the time and right 95% of the time.

For each of the n observations in the sample, subtract the sample frequency estimate from the corresponding theoretical probability estimate. The objective is to find the single largest difference D_{max} between the two distributions regardless of the sign:

$$D_{max} = \max \left| F_s(x) - F(x) \right| \tag{3.22}$$

Table 3.5. Critical D values for the Kolmogorov-Smirnov goodness-of-fit test. For use when $\bar{x}$ and s are estimated from a sample (H.W. Lilliefors 1967).

Sample size (n)	$\alpha =$ 0.15	0.10	0.05	0.01
4	0.319	0.352	0.381	0.417
5	0.299	0.315	0.337	0.405
6	0.277	0.294	0.319	0.364
7	0.258	0.276	0.300	0.348
8	0.244	0.261	0.285	0.331
9	0.233	0.249	0.271	0.311
10	0.224	0.239	0.258	0.294
11	0.217	0.230	0.249	0.284
12	0.212	0.223	0.242	0.275
13	0.202	0.214	0.234	0.268
14	0.194	0.207	0.227	0.261
15	0.187	0.201	0.220	0.257
16	0.182	0.195	0.213	0.250
17	0.177	0.189	0.206	0.245
18	0.173	0.184	0.200	0.239
19	0.169	0.179	0.195	0.235
20	0.166	0.174	0.190	0.231
25	0.153	0.165	0.180	0.203
30	0.136	0.144	0.161	0.187
over 30	$0.768/\sqrt{n}$	$0.805/\sqrt{n}$	$0.886/\sqrt{n}$	$1.031/\sqrt{n}$

This maximum difference D_{max} is then compared to a 'critical difference' value $D_{n,\alpha}$ found in Table 3.5. The critical difference value depends upon the sample size n and significance level α. If the maximum difference is less than the critical value, $D_{max} < D_{n,\alpha}$, then accept the null hypothesis that there is not a significant difference between the two distributions. If $D_{max} > D_{n,\alpha}$ then reject the null hypothesis. Rejection of H_0 means that, with 95% certainty, the sample does not come from that theoretical distribution. The test is not very powerful. Acceptance of H_0 means only that the sample *could* come from that distribution; it does not mean that it does. The *K-S* test is demonstrated with precipitation data in Chapter 4.

3.9 TIME VARIATIONS IN DATA

The last topic in this chapter touches on the question of the constancy of the statistical properties of a hydrologic process over time. Two terms are used in the hydrologic literature to describe constancy over time – *stationary* and *homogeneous*. While there are subtle differences between the terms (see Chow 1964), many authors appear to use the two interchangeably. We will use the term stationary here and reserve the term homogeneity for a discussion in Chapter 4.

Chow (1964, p. 8-9) defines stationary as follows: 'The random variable $X(t)$ has a certain probability distribution. If this distribution remains constant throughout the process, the process and time series are said to be *stationary*. Otherwise, they are *nonstationary*.'

In other words, if the probability distribution describing X remains constant over time, the probability of a specific event is the same at different points in time. This necessarily means that the parameters of the distribution are also constant through time. Say we have a time series such as the Philadelphia precipitation data. If you calculate a mean and standard deviation for different subperiods within the time series, the statistics (parameters) would be the same for each subperiod if the data are stationary. There would likely be small differences due to sampling variability, but they would not be *significantly* different in a statistical sense. If the statistics (parameters) are significantly different for different time periods, the data are nonstationary. Figure 3.6 shows the difference between stationary and nonstationary data. Only Figure 3.6a is a stationary time series. The data vary randomly over time but the mean and variation remain constant over time. In Figure 3.6b the data are nonstationary since they display a trend over time. Trends in hydrologic data might be caused by a change in climate or by human activities such as urbanization. Figure 3.6c displays a 'step function' where the data change abruptly from one regime to another, and the probability distribution in the earlier period is different from that in the later period. Step functions might result from catastrophic geophysical events such as landslides and volcanic eruptions. Clear cutting of a forest might be a cause of either a trend or a step function response in streamflow depending upon how rapidly the forest was cleared. Periodicity due to annual cycles is another cause of nonstationarity (Fig. 3.6d). We encountered this in Section 3.5 on probability and the normal curve when discussing how to correctly choose a sample of monthly precipitation data.

Anthropogenically-induced climate change poses a potentially serious problem in this regard. By changing climate, existing hydroclimatological records become nonstationary. If that happens we will have difficulty using existing historical records to assess the likelihood of future events, because the future will not resemble the past. This could have serious consequences for society in terms of planning for future hydrologic events.

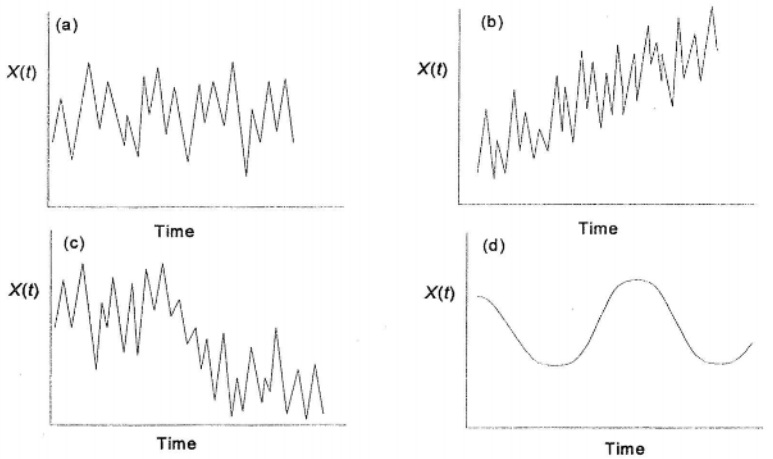

Figure 3.6 Temporal variations in time series data. The series in: a) Random and stationary, and b-d) All nonstationary.

SUMMARY

The topics covered in this chapter play a very important role in hydrology because they represent basic techniques, skills and concepts that are used again and again in analyzing hydrologic phenomena. Demonstrations of many techniques has been deferred until Chapters 4, 11 and 12. This decision was based on a pedagogical view that it is better to demonstrate a technique later in a relevant context, than discuss it in abstract terms now. When you encounter the techniques in latter chapters, come back to this chapter to review.

There are many important topics that were not covered here but will be introduced in Chapters 4, 11 and 12. Chapter 4 on atmospheric water vapor and precipitation begins our examination of the hydrologic system. The hydrologic cycle really starts with evaporation and transpiration, because solar energy drives the cycle. If the sun were turned off, the cycle would stop. However, from a systems point of view, it is convenient to begin the analysis with inputs, and precipitation is a major input to the drainage basin system.

PROBLEMS

3.1 Given below are annual total precipitation values (inches) for Raleigh, North Carolina from 1955 to 1984.

1955	40.88	1965	34.42	1975	46.83
1956	39.89	1966	39.60	1976	33.71
1957	46.26	1967	39.58	1977	37.10
1958	45.57	1968	35.60	1978	42.97
1959	48.95	1969	41.52	1979	45.37
1960	48.00	1970	36.01	1980	35.64
1961	41.11	1971	45.64	1981	36.38
1962	48.27	1972	51.74	1982	44.35
1963	36.91	1973	46.44	1983	47.23
1964	42.91	1974	40.74	1984	46.27

a) Calculate the median for the sample.
b) Calculate the arithmetic mean and standard deviation for the sample. Show your work.
c) Create a histogram, a relative frequency function and a cumulative frequency function.
d) What can you say about the apparent distribution of the data? Do they appear to be normally distributed?

3.2 Using the Raleigh precipitation data and statistics, answer the following questions.

a) What rainfall values are located +1 and −1 standard deviation from the sample mean?
b) Assuming a normal distribution, statistical theory predicts that approximately 68% of the observations should be within 1 standard deviation of the mean. What is your observed percentage?
c) What are the 'Z scores' for the following years?
1969 ..... 1972 ..... 1976 .....
d) Use Z scores and estimate probabilities for the following values. (Show your work.)
1. Greater than 35.50 inches?
2. Between 35.50 and 45.50 inches?
3. Greater than 48.00 inches?
4. Between 30.30 and 40.80 inches?

CHAPTER 4

The atmospheric subsystem

The amount of water stored in the atmosphere is 0.001% of the total water on Earth. The residence time of atmospheric water vapor is quite short, on the order of 8-10 days (Table 1.1). This makes the atmosphere one of the smallest but most active storage locations for water. Figure 4.1 is a diagram of the atmospheric subsystem over a drainage basin. The atmospheric subsystem is idealized as a control volume with dimensions x, y, and z. The arrows represent fluxes of vapor in and out of the control volume. Since most of the water vapor is found in the troposphere, the volume in Figure 4.1 is assumed to extend through the troposphere with negligible vapor flux across the tropopause.

As with any physical system a continuity equation (Eq. 1.1) describes the status of water vapor in the control volume. The continuity equation states that the change in the vapor content of the volume equals the inputs of vapor as evapotranspiration from the surface and horizontal advection into the volume, minus the outputs of vapor by advection, precipitation and condensation to the surface. Benton & Estoque (1954) applied this type of mass balancing to the entire North American continent to determine the net flux of vapor across the coastlines and from the surface. Satellite observations show water vapor is highly variable in both time and space, with 'atmospheric rivers' of vapor advecting around the Earth. In this chapter we briefly examine atmospheric water vapor and the different measures of humidity. Following this is a discussion of precipitation processes, measurement and analysis.

4.1 ATMOSPHERIC WATER VAPOR

Water vapor enters the atmosphere from the surface by changing from the liquid state (evapotranspiration) or the solid state (sublimation). The states, processes, and energy requirements are given in Table 4.1. Changing state requires energy to break the bonds of attraction between water molecules. This energy is called *latent heat* and only changes the state of water; it does not change the amount of energy stored in the water; therefore, it does not change the water's internal temperature. This same quantity of energy is released back into the environment as sensible heat when these bonds reform during sublimation, condensation and fusion. *Vaporization* from liquid to gas requires a tremendous amount of latent-heat energy, approximately 590 calories per gram of water evaporated. The latent heat of vaporization depends upon the temperature of the water and is approximated by the empirical formula:

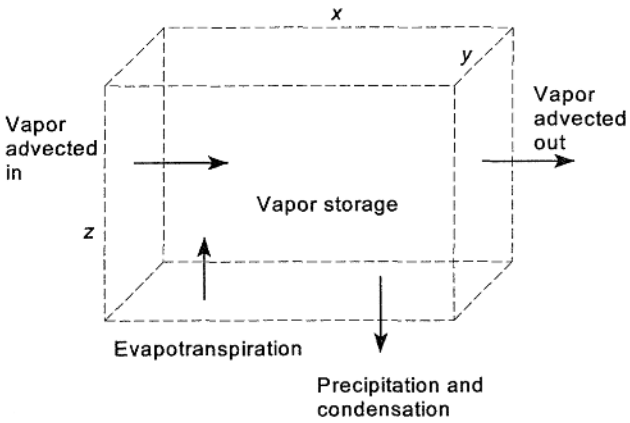

Figure 4.1. The atmosphere subsystem over a drainage basin idealized as a control volume with inputs, outputs and storage.

Table 4.1. Approximate latent heats associated with state changes of water.

State change	Latent heat of	Approximate quantity (cal g^{-1})
Ice to water	Fusion	79
Water to ice	Fusion	
Water to vapor	Vaporization	590
Vapor to water	Condensation	
Ice to vapor	Sublimation	669
Vapor to ice	Sublimation	

$$L_v = 597.3 - 0.564T \tag{4.1}$$

where L_v is the latent heat of vaporization in calories per gram, and T is temperature in °C (Linsley et al. 1982). On average, most of the solar energy absorbed at the Earth's surface returns to the atmosphere in the form of latent heat. The movement of vapor in the atmosphere thus has important implications for the storage and transfer of energy as well. Latent heat is the primary energy source for thunderstorms and hurricanes.

The atmosphere is a mechanical mixture of gases and each gas exerts a *partial pressure* independent of every other gas. The sum of the partial pressures of the individual gases equals the total pressure p of the atmosphere. The unit used by meteorologists for measuring atmospheric pressure is the millibar (mb), but pascals (Pa) are the preferred *SI* unit (1 mb equals 100 Pa). Standard sea level pressure is 1013.25 mb (101.3 kPa). The *vapor pressure* e is the partial pressure due to water vapor. The vapor pressure is given by the ideal gas law as:

$$e = \rho_v R_v T \tag{4.2}$$

where ρ_v is the density of water vapor in g m^{-3}, R_v is the gas constant for water vapor, and T is absolute temperature in °K. The gas constant for water vapor is R_v =

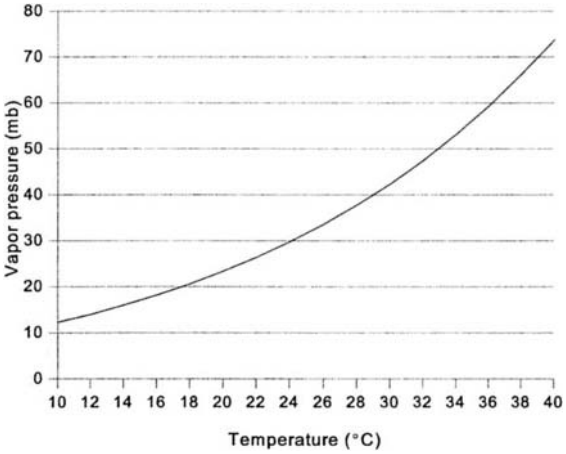

Figure 4.2. Saturation vapor pressure over water versus air temperature.

$R_d/0.622$, where R_d, the gas constant for dry air, equals 2.87×10^3 cm^2 s^{-2} K^{-1} for vapor pressure in millibars. The *saturation vapor pressure* e_s is the vapor pressure of a parcel of air when it is holding all the water vapor it can hold at a given temperature. When this condition obtains the parcel is *saturated*. The capacity of the air to hold vapor is a function of its temperature. The temperature at which a mass of air becomes saturated is the *dew point temperature*. Figure 4.2 is a graph of saturation vapor pressure versus air temperature over water. The figure shows that the vapor-holding capacity of the air increases at an increasing rate with temperature. The vapor pressure over ice is less than the vapor pressure over water at the same temperature. The difference in vapor pressure over ice and water is thought to be important in the growth of cloud droplets. Since the molecular weight of water is only 0.622 times the molecular weight of dry air at the same temperature and pressure, moist air is less dense than dry air. This means moist air rises over dry air at the same temperature. The following formula from Bosen (1960) approximates the saturation vapor pressure over water when air temperature is between –50 and 55°C:

$$e_s \approx 33.8639\,[(0.00738T + 0.8072)^8 - 0.000019|8T + 48| + 0.001316] \qquad (4.3)$$

where e_s is in millibars and T is in °C. Equation (4.2) can be differentiated to get the rate of change in saturation vapor pressure with temperature (Δ):

$$\Delta = \frac{de_s}{dT} \approx (0.00815T + 0.8912)^7 \qquad (4.4)$$

4.1.1 *Humidity*

There are different ways to measure humidity, and each has advantages and disadvantages depending upon the situation. Three different measures of humidity are *specific humidity*, *mixing ratio*, and *relative humidity*. The specific humidity (q_h) is the mass of water vapor per unit mass of *moist* air. Specific humidity is defined using the densities of water vapor (ρ_v) and moist air (ρ_a) as:

$$q_h = \frac{\rho_v}{\rho_a} \tag{4.5}$$

The typical units for specific humidity are grams per kilogram. While Equation (4.5) defines specific humidity, it is often approximated as:

$$q_h \approx 622\left(\frac{e}{p}\right) \tag{4.6}$$

where q_h is in grams per kilogram and e and p are in millibars. The mixing ratio (w_r) is the mass of water vapor per unit mass of *dry* air:

$$w_r = \frac{\rho_v}{\rho_d} \tag{4.7}$$

As with specific humidity, mixing ratio is approximated as:

$$w_r = 622\left(\frac{e}{p-e}\right) \tag{4.8}$$

Unlike the previous measures relative humidity (f) does not indicate the actual amount of water in the air. Relative humidity is the percentage ratio of the vapor content of the air to the vapor content of the air at saturation. Relative humidity can be calculated by any of the previous measures of humidity:

$$f = \frac{e}{e_s}100 = \frac{q_h}{q_{hs}}100 = \frac{w_r}{w_{rs}}100 \tag{4.9}$$

where the additional subscript s in the denominators indicates the condition of saturation.

Example 4.1
Assume a climatological station has an air pressure of 1010 mb, an air temperature (T) of 22°C and a dew point temperature (T_d) of 15°C. Find the relative humidity, the specific humidity and the mixing ratio? Using Equation (4.3), the saturation vapor pressure at 22°C is 26.43 mb, and the saturation vapor pressure at 15°C is 17.06 mb. The relative humidity is:

$$f = (17.06/26.43)100 = 64.5\%$$

The specific humidity is approximated by Equation (4.6) as:

$$q_h \approx (17.06 / 1010)\ 622 \approx 10.51 \text{ g kg}^{-1}$$

From Equation (4.8) the mixing ratio is:

$$w_r \approx [17.06 / (1010 - 17.06)]\ 622 \approx 10.68 \text{ g kg}^{-1}$$

The *precipitable water* is the total amount of water vapor in a layer of air. Even though there is no natural mechanism to precipitate all the vapor from a column of air, the concept is useful in estimating the *probable maximum precipitation* (PMP) for rainfall-runoff studies. While the precipitable water provides an upper limit for precipitation, the amount of precipitation from a given storm depends upon the efficiency of the entire precipitation-generation process.

4.2 PRECIPITATION PROCESSES

Water vapor in the atmosphere is the source for precipitation, but how does the vapor become measurable precipitation at the Earth's surface? Four factors are required to generate measurable precipitation. First, there must be a continuous influx of moisture into the control volume. A continuous influx of vapor is required to support the continuous formation of precipitation. At any given time the vapor in the control volume amounts to only a few centimeters depth of water. Only a fraction of this vapor may fall as precipitation because some vapor simply advects directly through the volume. A typical thunderstorm of 10 km^2 may scavenge and concentrate atmospheric vapor from a surrounding area 1000 km^2 in size (Miller 1977).

The second requirement is a mechanism to lift the air mass. When air rises it cools by *adiabatic* expansion. Conversely, descending air warms by adiabatic compression. The adiabatic process is discussed in more detail below. As Figure 4.2 shows, cool air can hold less water vapor than warm air. If the rising air mass is cooled to its dew point temperature, it becomes saturated and vapor changes state to liquid and/or solid forms. There are 4 major lifting mechanisms to cool a parcel of air:

1. *Convective* lifting occurs when solar energy absorbed by the ground heats the overlying air. The warmer air expands, becomes less dense than the surrounding cooler air, and rises in a convective stream. This type of lifting produces convective thunderstorms year round in the equatorial regions. During the summer in the mid-latitudes convection generates air mass thunderstorms and is important in the creation of 'mesoscale convective complexes'.

2. *Orographic* lifting occurs when air is forced up and over a topographic barrier such as a mountain or a plateau. In regions with persistent winds orographic lifting and cooling produces wetter climate conditions on the windward side of the barrier, while the leeward side may be a rainshadow desert.

3. *Frontal* lifting occurs along frontal boundaries between air masses with different temperature and moisture characteristics (Fig. 4.3). Cold, dry air is denser than warm, moist air. When air masses collide along a frontal boundary, the warmer, moister air masses are lifted over cooler, drier ones. The boundary between air masses is called a *front*. A *cold front* is when cold air moves into a region of warm air, and a *warm front* is when cold air exists a region which is then occupied by warm air. In either case the warmer air is lifted and cooled.

4. A final lifting mechanism is *convergence*. When air streams converge the excess of mass in the zone of convergence forces air rise. Convergence plays an im-

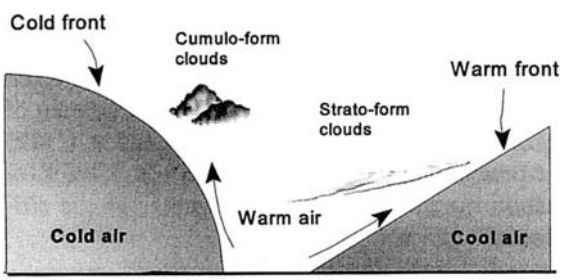

Figure 4.3. Cross-sectional view of a cold front and a warm front.

portant – some say dominant – role in each of the previous lifting mechanisms (Gilman 1964).

The third requirement for precipitation formation is *condensation* or *freezing nuclei*. These nuclei are small *hygroscopic* particles 10^{-3} to 10 μm in diameter and they come from a variety of natural and anthropocentric sources. Nuclei may be small dust particles blown up from the surface, sulfur and nitrogen compounds from combustion, or salt particles from evaporated sea spray. When a parcel of air reaches its dew point temperature, vapor changes state only when sufficient and suitable nucleation sites are available.

The fourth and final requirement for measurable precipitation is cloud droplet growth. Cloud droplets have extremely small diameters, generally less than 700 μm. In order for measurable precipitation to occur, droplets must grow large enough to overcome any ascensional air currents that can keep the small droplets aloft, and they must be large enough so that they do not evaporate before reaching the ground. The latter phenomena is called *verga*. Raindrops are normally between 0.1 and 4 mm in diameter, with 7 mm the upper limit of droplet size. Drops larger than 7 mm lack sufficient internal cohesion to remain whole and are torn apart by shearing winds as they fall through the air.

Cloud droplets grow by vapor diffusion and by the collision and coalescence of droplets. Because the vapor pressure over ice is lower than the vapor pressure over water at the same temperature, if a cloud contains both water droplets and ice crystals, vapor diffuses from the water droplets (higher pressure) to the ice crystal surfaces (lower pressure), causing growth of the ice crystals. This is the essence of the Bergeron-Findeisen Process of cloud droplet growth (Henderson-Sellers & Robinson 1991). Vapor diffusion from water to ice is thought to be an important mechanism for cloud droplet growth in midlatitude clouds where both ice and water droplets coexist. Collision and coalescence of smaller drops creating larger drops occurs in midlatitude clouds; however, coalescence is thought to be the primary mechanism for cloud droplet growth in warm tropical clouds that are composed primarily of water.

4.3 WEATHER MODIFICATION

Cloud seeding to generate precipitation is one type of weather modification. Other types of modification include fog dispersal, hail suppression and frost prevention. In economic terms, fog dispersal around airports is one of the most cost-effective types of weather modification. Cloud seeding experiments to generate precipitation have been undertaken in a number of countries around the world including the former USSR, Australia, Zimbabwe and Israel. In the United States both private and public agencies have tried cloud seeding. The largest experimental programs in the United States have been carried out in the West by the US Bureau of Reclamation. The primarily objective being to increase the water supply for urban and agricultural users. The results of these experiments are mixed because they often lacked sufficient and satisfactory control. In all fairness we should recognized that it is extremely difficult to 'experiment' on the atmosphere because so many variables are beyond our control. Some of the factors that appear to influence the efficacy of cloud seeding include

cloud temperature and height, cloud type, and the number and location of artificial nuclei introduced into the cloud.

The challenge for cloud seeding is to prove that precipitation actually increased above the level which might have occurred naturally. Under ideal conditions the evidence suggests an increase of 10 to 15% is possible. Along with the potential benefits of increased water supply are some potential ecological and economic costs. Costs include the detrimental effects on wildlife from a deeper and longer-lasting snowpack, the fate of the chemicals, i.e. silver iodide, that comprise the artificial nuclei, the increased cost of snow removal and the potential for greater avalanche hazard. The issue also has great potential for sparking interstate conflict. If the state of Colorado seeds clouds over the Rocky Mountains is it stealing water that might otherwise have become precipitation over Kansas? The Bureau of Reclamation announced in 1994 that it will no longer sponsor weather modification research. The feeling is that weather modification research is not in keeping with the Bureau's emerging focus on water management in the 1990s.

4.4 ADIABATIC PROCESSES

Air temperature normally decreases with altitude. The rate of air temperature change through the troposphere is the *environmental lapse rate* (ELR), and averages 6.4C°/1000 m change in altitude. Figure 4.4 shows the ELR under normal conditions and under the condition of a surface *inversion*, where temperature increases with altitude from the surface. When a distinct parcel of air rises (subsides) *through* the surrounding atmosphere, its temperature decreases (increases) adiabatically. Adiabatic temperature change is due to the expansion (compression) of the parcel by the surrounding air, and does not change the heat energy content of the parcel. When a parcel rises it expands, expansion is work, and the energy for that work comes from within the parcel causing its temperature to decrease. When the parcel descends through the atmosphere, it moves into a region of higher air pressure and is compressed by the surrounding air. Compression is work done on the parcel, adding energy to it, thereby increasing its temperature.

If a parcel is not at its dew point temperature and it is lifted, it expands and cools at the *dry adiabatic lapse rate* (DALR). The DALR is 9.81C°/1000 m. A subsiding parcel always compresses and warms at the DALR. The DALR is numerically equal to the acceleration of gravity given in *SI* units because it is derived from the hydro-

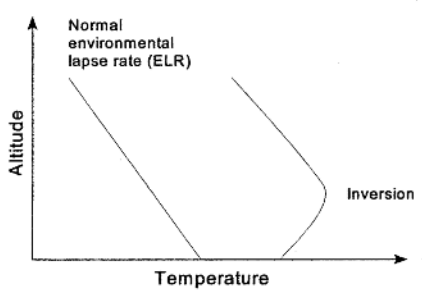

Figure 4.4. Environmental lapse rate curves under normal conditions and under the condition of a surface inversion.

static pressure law for the atmosphere. The hydrostatic pressure law equates the change-in-pressure-with-altitude to the force of gravity times the mass of the air. If a rising parcel is at its dew point temperature, it is, by definition, saturated and when lifted cools at a *saturated adiabatic lapse rate* (SALR). The SALR is not a constant; the rate depends upon the amount of water vapor in the air. The SALR is usually between 4 and 6C°/1000 m. All parcels actually cool at the DALR, but when the parcel is saturated, adiabatic cooling releases latent heat of condensation. The *net* effect is that the parcel cools less than the DALR, i.e. it cools at a SALR.

Figure 4.5 shows an adiabatic lapse rate diagram for a parcel lifted and then returned to the same elevation. The unsaturated parcel starts at altitude z_1 with a temperature T_1. Being unsaturated the parcel initially cools at the DALR. The parcel eventually reaches its dew point temperature T_d and becomes saturated. The altitude where saturation occurs is called the *lifting condensation level* (LCL). Beyond the LCL, the parcel cools at the SALR reaching a temperature of T_2 at altitude z_2. If the parcel then descends back to its original altitude (z_1), it warms at the DALR and its temperature rises to T_3. The increase in temperature ($T_3 > T_1$) at altitude z_1 is equal to the latent heat of condensation transformed into sensible heat between the LCL and z_2.

The relative magnitude of the ELR compared to the DALR and SALR is important in determining atmospheric *stability*. If the ELR is less than the SALR (Fig. 4.6a), the atmosphere is stable. A parcel forced to rise under stable conditions becomes colder and denser than the surrounding air and will try to return to its initial position if the lifting mechanism ceases. If the ELR is greater than the DALR, the air is unstable (Fig. 4.6b). In an unstable atmosphere, as the parcel rises it becomes pro-

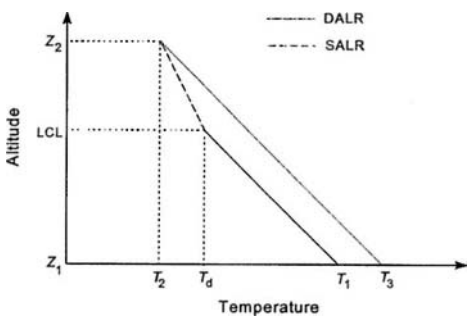

Figure 4.5. Adiabatic diagram showing the temperature of a parcel cooling at the DALR up to the lifting condensation level (LCL). The parcel cools at the SALR up to elevation z_2 and descends again at the DALR.

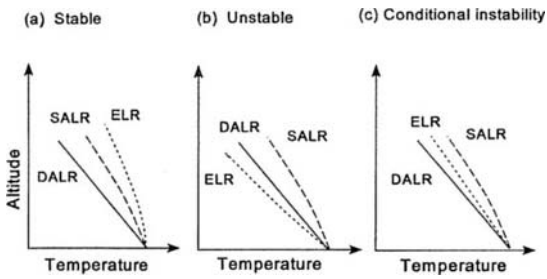

Figure 4.6. The conditions of stability, instability and conditional instability are defined by the relative magnitudes of the ELR, DALR and SALR.

gressively warmer than the surrounding air, making the parcel rise even more rapidly. Instability is an excellent example of positive feedback in the atmospheric system, and can lead temporarily to the explosive growth of thunderstorms. A stable atmosphere is not conducive to lifting and precipitation, while an unstable atmosphere is likely to produce significant lifting and precipitation. An inversion layer (Fig. 4.4) tends to promote stability, since warmer air overlies colder, denser air and lifting is suppressed at the surface. Figure 4.6c shows conditional instability where the parcel may be stable below some level and unstable beyond. When the ELR equals the DALR the atmosphere has *neutral* stability.

4.5 PRECIPITATION MEASUREMENT

Point measurements of precipitation are made with nonrecording and recording rain gages. Precipitation can be measured over an area with radar. Nonrecording precipitation gages are open containers that catch and accumulate the total precipitation. While any open receptacle is a potential gage, only gages of similar design and exposure provide data that are directly comparable. The standard US Weather Bureau nonrecording gage is a cylinder 8 inches in diameter (Fig. 4.7a). A removable funnel-shaped orifice channels water into an inner cylinder $^1/_{10}$ the diameter of the outer cylinder. This 10-fold reduction in diameter creates a 10-fold magnification in precipitation depth within the inner cylinder. A measuring stick, incremented in tenths of an inch, is inserted into the inner cylinder allowing measurement to the nearest $^1/_{100}$ of an inch. If snow is expected, the funnel and inner cylinder are removed. The snow is subsequently melted and measured as before.

In the United States, approximately 8000 volunteer stations and 278 governmental stations collect and report daily precipitation data. These data are used for determining climatological statistics such as *normal annual precipitation*. The normal annual precipitation is a running 30-year average value. Through the decade of the 1990s, normal annual precipitation is calculated using the period 1961 to 1990. In the year 2001, a new normal will be calculated by dropping the decade of the 1960s and adding the decade of the 1990s. The term normal is misleading since it implies that this is the value that should be observed. But climate is naturally variable, and variation is quite normal. Figure 4.8 is a map showing mean annual precipitation for the United States. The map displays two important patterns. One is the greater spatial vari-

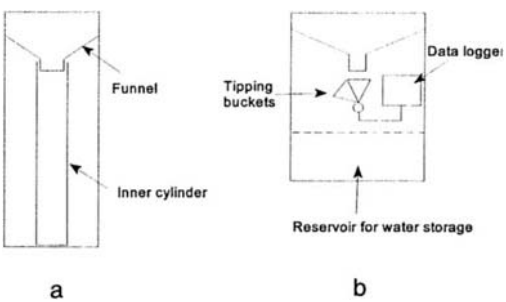

Figure 4.7. Simplified sketches of: a) Standard non-recording precipitation gage, and b) Tipping-bucket recording gage.

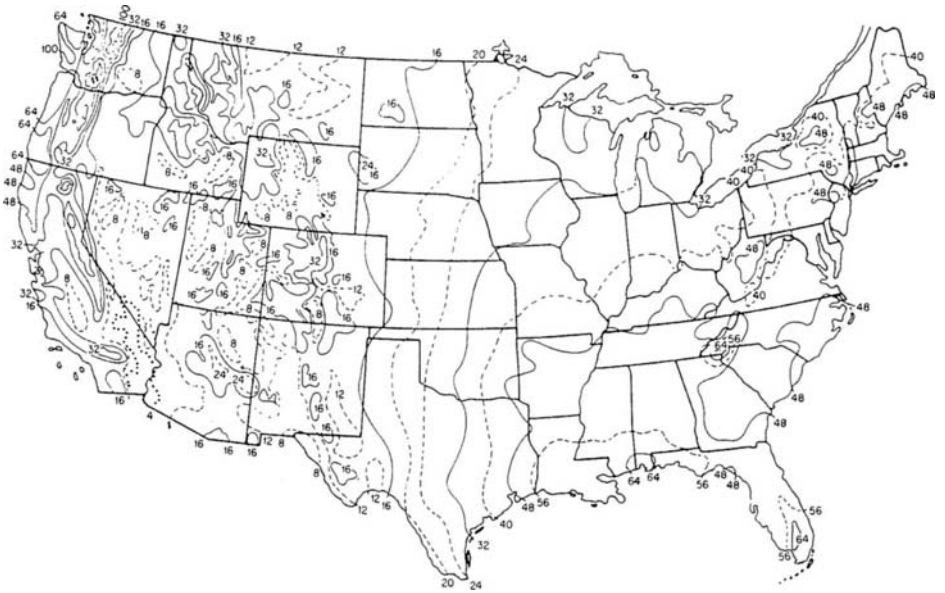

Figure 4.8. Mean annual precipitation in the United States (source: Linsley et al. 1982, used by permission).

ability in precipitation in the West as compared to the East. The greater variability in the West is largely the result of the more rugged topography. The second pattern is the larger precipitation values in East versus the West. The 20-inch isohyet, usually located near the 98th meridian, is conventionally taken to separate the humid East from the semi-arid and arid West. The National Weather Service (NWS), a subdivision of the National Oceanographic and Atmospheric Administration (NOAA), collects and publishes these data. Climatological data are also available on diskette and CD-ROM through both public and private vendors. Appendix C lists some public sources of climatological data.

Recording precipitation gages record the time distribution of rainfall through a storm. Recording-gage data are used primarily for rainfall-runoff studies. Recording gages use either a tipping bucket mechanism, a float mechanism, or some type of weighing mechanism to record the accumulated rainfall through time. A tipping bucket gage is shown in Figure 4.7b. The rain enters the gage and is directed into a small bucket that holds 0.01 inch of water. When the bucket fills, it over tips bringing the second bucket under the funnel. Each tip generates an electrical pulse which is recorded to give a record of the rainfall rate in discrete increments of 0.01 inch. Float gages and weighing gages measure accumulated precipitation by continuously recording the change in the height of the float, or the accumulated weight of water, on a strip chart recorder. Figure 4.9 is *hyetograph* made from a recording gage showing the distribution of a rain at 5-minute intervals through a storm. Figure 4.10 shows the same data accumulated through the storm. The overall pattern is '*S*-shaped' indicating low rainfall intensity (LT^{-1}) at the beginning of the storm, intensity increasing to a peak around the time 22:10, and then decreasing as the storm

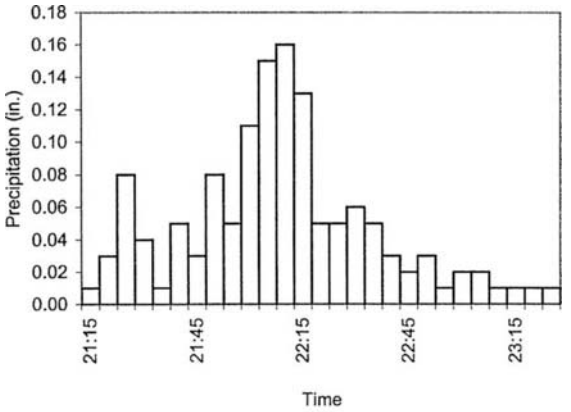

Figure 4.9. Hyetograph of precipitation at 5-minute intervals for Swarr Run, Pennsylvania.

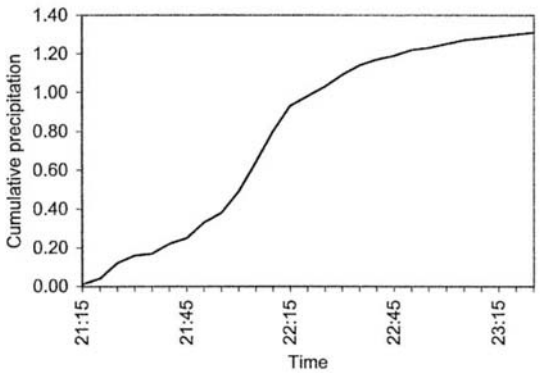

Figure 4.10. Hyetograph of accumulated precipitation for the same gage and storm as in Figure 4.9.

passes. The peak average intensity for the 5-minute interval ending at 22:10 hours was (0.16 in./0.0833 hrs) = 1.92 in hr^{-1}. This *S*-shaped pattern is typical and results from two interrelated processes. One is the evolutionary development of the storm itself. As a storm develops, matures and dissolves, the precipitation intensity varies accordingly. The other process at work is the fact that storms are in motion relative to the stationary gage. The precipitation intensity measured at a stationary point on the ground will vary as the center of the storm (which is typically the most intense region) approaches and passes the gage. This will be true even for a storm of constant intensity through time. Since there are far fewer recording gages than nonrecording gages, the Soil Conservation Service (SCS 1986) has developed four generalized precipitation intensity curves for a 24-hour-duration storm (Fig. 4.11). The four curves cover different regions of the United States (Fig. 4.12).

Example 4.2
Assume for a location near Atlanta, Georgia a total daily (24-hour) rainfall of 3.5 inches. Generate the rainfall intensity for the 30-minute period from time interval 8 to 9. The Type II SCS curve is appropriate for this region. The intensity of precipitation for any interval in the 24-hour period is found by multiplying 3.5 inches by the appropriate 30-minute increment from Table 4.2

and dividing by the interval duration. For the interval from 8 to 9 the fractional value is (0.0555 – 0.0483) = 0.0072. The incremental precipitation for the 30-minute interval is (3.5 inches × 0.0072) = 0.025 inches. The average intensity for the interval is (0.025/0.5) = 0.05 in hr^{-1}.

The SCS curves distribute a 24-hour rainfall into 30-minute intervals of varying intensity. These curves are helpful for planning purposes when recording gage data are unavailable, but generating precipitation intensity from these curves should be considered a *very* approximate technique.

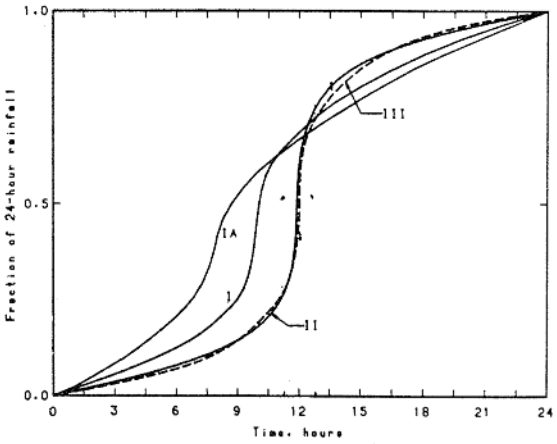

Figure 4.11. Four SCS standardized rainfall intensity curves for a 24-hour storm (source: SCS 1986).

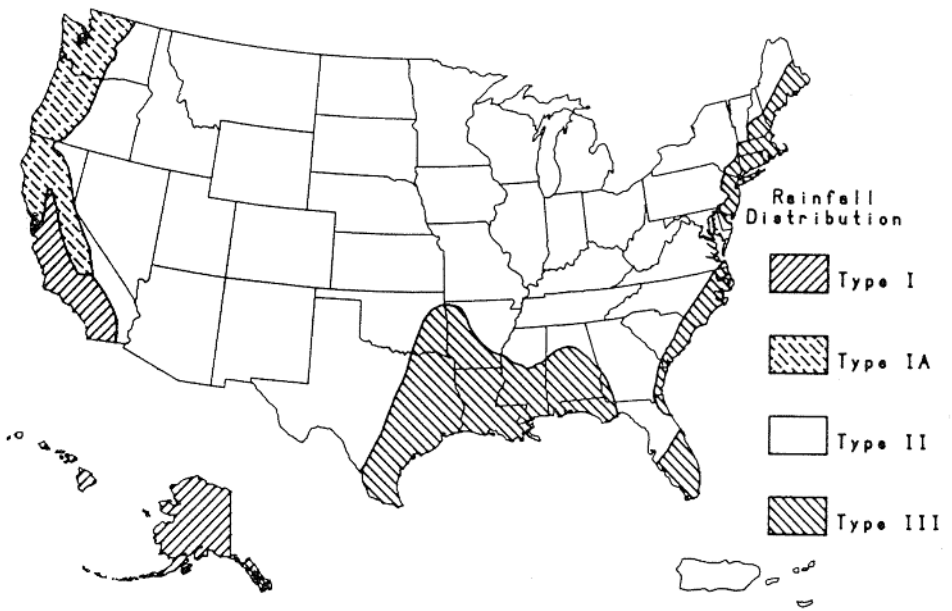

Figure 4.12. Regions in the United States where the four standardized SCS curves are applicable (source: SCS 1986).

Table 4.2. Cumulative 30-minute fractional increments for the SCS Type II curve (source: SCS 1986).

Interval	Fraction	Interval	Fraction	Interval	Fraction	Interval	Fraction
0	0.0000	13	0.0887	26	0.7724	39	0.9446
1	0.0053	14	0.0984	27	0.7989	40	0.9519
2	0.0108	15	0.1089	28	0.8197	41	0.9588
3	0.0164	16	0.1203	29	0.8380	42	0.9653
4	0.0223	17	0.1328	30	0.8538	43	0.9717
5	0.0284	18	0.1467	31	0.8676	44	0.9777
6	0.0347	19	0.1625	32	0.8801	45	0.9836
7	0.0414	20	0.1808	33	0.8914	46	0.9892
8	0.0483	21	0.2042	34	0.9019	47	0.9947
9	0.0555	22	0.2351	35	0.9115	48	1.0000
10	0.0632	23	0.2833	36	0.9206		
11	0.0712	24	0.6632	37	0.9291		
12	0.0797	25	0.7351	38	0.9371		

In mountainous regions much of the annual precipitation comes as snow in the winter. Snow can measured with a yardstick, a snowboard or snow pillows. Using a yardstick snow depth is measured at three locations and the recorded depth is taken as the average of the three measurements. A snow board is a level board at the same temperature as the surrounding air. At hourly intervals through the storm, accumulated snow depth on the board is recorded and the board is then wiped clean. This procedure minimizes the potential under-recording of snowfall due to compression of the underlying snow. In remote areas of heavy snowfall it is impractical to use standard precipitation gages, and snowfall must be measured in other ways. Throughout the western United States the SCS operates the SNOTEL system. There are currently around 500 SNOTEL sites in eleven western states. The system combines automated ground sensors with a satellite relay system to automatically record snowfall. Snow pillows on the ground are compressed by the weight of the overlying snow. The information is sent via satellite link to a data recording center.

As an approximation, fresh snow has a density of about 0.10 g cm^{-3}, or about 10 cm (inches) of snow represents 1 cm (inches) of liquid water. Compression of the underlying snow causes the density to increase with depth through the snowpack. The snowpack also becomes denser with age through the process of melting and refreezing. Estimates of snow water content are crucial for runoff and water supply forecasting. Based on estimates of snowpack water content the Bureau of Reclamation and hundreds of irrigation districts and cities throughout the West plan for the allocation of scarce water supplies. The Corps of Engineers, regional, state and local water management agencies also plan the operation of flood control facilities to safely store and pass the water downstream when it melts in the spring.

4.5.1 *Errors in precipitation measurement*

Precipitation gage records contain many sources of error. Errors can be considered *random* or *systematic*. The most frequent source of random errors is misreading the gage. By their nature random errors are compensating so that average values are un-

affected. Systematic errors on the other hand are cumulative and produce a biased record. Sources of systematic errors include the effects of wind, ignoring trace amounts, evaporation from the gage, water adhering to the sides of the gage, and poor gage exposure. All of these errors systematically reduce the recorded catch, yielding measurements that are consistently too low. Of all the sources of error those caused by wind are the largest. The effect of wind is to systematically reduce the catch in the gage. The influence is greatest on small rain droplets and snow, since these are more easily accelerated than large droplets. In an effort to minimize the effect of wind researchers have developed different types of gage shields. In a recent study, Groisman & Legates (1994) estimate that the United States actually receives about 9% more precipitation than is officially recorded because of systematic errors.

4.6 ESTABLISHING A PRECIPITATION GAGE

For many studies the data published by the NWS may be sufficient. But for specific projects or small-scale applications it may be necessary to establish a new gage or network of gages. For example, in Albuquerque, New Mexico the NWS and the Albuquerque Metropolitan Arroyo Flood Control Authority (AMAFCA) operate a network of approximately 40 backyard rain gages in the metropolitan area. During the summer monsoon season volunteers monitor and report rainfall events that might cause local flooding on arroyos.

When selecting a site for a precipitation gage a location near the ground and protected from the wind is ideal. Gages should be close to the ground because wind speed increases with height in a nonlinear fashion. Under neutral atmospheric conditions, the wind profile can be described as a *logarithmic velocity profile*:

$$u_z = \frac{u^*}{k} \ln\left(\frac{z}{z_0}\right) \tag{4.10}$$

where u_z is wind speed at height z, k is the von Karman constant ($k \approx 0.4$), u^* is the friction velocity, and z_0 is the *roughness length* of the surface. The roughness length is the height above the surface where the wind speed is assumed to go to zero and depends upon the roughness of the surface (Table 4.3). If measured values are not

Table 4.3. Roughness lengths (z_0) for different surfaces.

Surface	Height (cm)	z_0 (cm)
Large City	198	
Trees	1000-1500	20
Corn	220	74-84
Wheat	60	22-23
Grass	10-50	2-5
Grass	≤ 10	0.1-2.0
Water		0.01-0.06
Dry lake bed		0.003
Mud flats		0.001

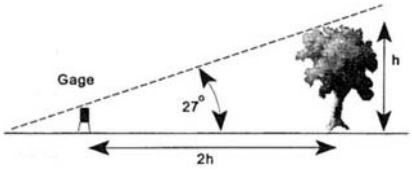

Figure 4.13. Recommended positioning of a precipitation gage.

available the roughness length can be approximated as 1/10 the height of the vegetation. The rapid increase in wind speed with height means gages should not be installed more than a few feet above the ground. Protecting the gage behind trees or buildings lowers wind velocities, but the barriers should not be so close as to cause turbulent eddies that may influence the catch of the gage. A guideline is that the distance from the gage to the barrier be approximately twice the height of the barrier. This translates into an angle of approximately 27° from the gage to the top of the barrier (Fig. 4.13).

4.7 MISSING PRECIPITATION DATA

Sometimes you'll find that data for a given event at a given station are missing. Three techniques are described below for estimating missing data. In the following discussion station X is the station for which the data are missing data. The first technique is simply to assign station X a value equal to the *arithmetic average* (Eq. 3.3) of the values at the three surrounding stations. This method is acceptable if the normal annual precipitation at each surrounding station is within 10% of the normal annual precipitation at station X.

A second method is the *normal ratio method.* With this method the observed precipitation at each surrounding station is weighted by the ratio of the normal annual precipitation at station X to the normal annual precipitation at that station. The estimated value at X is the sum of the weighted values. The formula for the normal ratio method is:

$$P_x = \frac{1}{n}\left(\sum_{i=1}^{n} P_i \frac{N_x}{N_i}\right) \tag{4.11}$$

where P_x is the estimated precipitation at station X, and N_x and N_i are normal annual precipitation at station X and at the ith surrounding station. Typically, three stations ($n = 3$) are deemed sufficient.

A third method for estimating data is the *inverse distance squared* method. This technique is called the *quadrant method* when four surrounding stations are used (US National Weather Service 1972). With this method, the inverse of the squared distance between station X and a neighboring station is used as the weighting factor. The closer a station is to station X, the greater the weight assigned to that station's precipitation. The formula for this method is:

$$P_x = \frac{\sum_{i=1}^{n}\left[\left(1/d_i^2\right)P_i\right]}{\sum_{i=1}^{n}\left(1/d_i^2\right)} \tag{4.12}$$

where d_i is the distance from station X to station i. It is reasonable to expect the inverse distance squared method to be *less* reliable in mountainous areas where large variations in precipitation occur over relatively short distances.

Example 4.3
To illustrate the three techniques for calculating missing data, assume there are four stations as shown in Figure 4.14. Table 4.4 lists the various data required for the different techniques.

Since the normal annual precipitation at each surrounding station is within 10% of station X the arithmetic average is acceptable. The estimated value at station X by this method is:

$$P_x = (200 + 150 + 170) / 3 = 173 \text{ mm}$$

For comparative purposes, the normal ratio method gives:

$$P_x = [(1180/1090)200 + (1180/1205)150 + (1180/1117)170] / 3 = 181 \text{ mm}$$

The answer for the inverse distance method is:

$$P_x = (200/30.25 + 150/49 + 170/144) / 0.0604 = 180 \text{ mm}$$

There are many other methods available for estimating missing data. Isohyetal interpolation is another alternative. The analyst draws isohyets using observed precipitation at the nearby stations, and interpolates a value to station X from the isohyetal pattern. This method is time-consuming because it requires constructing the isohyetal map.

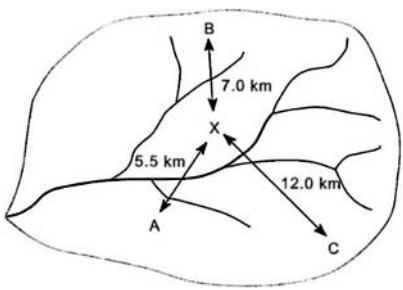

Figure 4.14. Location of stations in a hypothetical drainage basin for calculating missing data.

Table 4.4. Data for calculating missing precipitation values.

Station	Observed precipitation (mm)	Normal annual precipitation (mm)	Distance from X (km)
A	200.0	1090.0	5.5
B	150.0	1205.0	7.0
C	170.0	1117.0	12.0
X		1180.0	

4.8 AVERAGING PRECIPITATION OVER AN AREA

Precipitation gage data are point measurements of precipitation. Many hydrologic analyses require that point precipitation measurements be converted into an areal average. Rainfall-runoff simulation models often require basin or subbasin average precipitation as an input (see Chapter 13). The three most common techniques for spatial averaging are the *arithmetic average*, *Thiessen polygons* and the *isohyetal* method. As with the methods for missing data, each spatial averaging technique determines the average precipitation as the sum of weighted precipitation values. The techniques differ mainly in how they determine the weights assigned to the precipitation values.

The *arithmetic average* calculates the average value using Equation (3.3). We can rewrite Equation (3.3) in terms of individual weighting factors as:

$$P = \left(\frac{1}{n}(P_1) + \frac{1}{n}(P_2) + \ldots + \frac{1}{n}(P_n) \right) \tag{4.13}$$

where $1/n$ is the weighting factor, and P_i is the precipitation at station i. The weighting factors are identical for each station. The arithmetic average is acceptable in relatively flat areas where rainfall does not vary drastically with distance.

The Thiessen method weights each observed precipitation value by the proportional size of the *Thiessen polygon* drawn around the station and contained within the basin. Polygons are constructed by first drawing lines connecting each station. Next, the perpendicular bisectors of these connecting lines are drawn. The perpendicular bisectors are then joined to form the polygons boundaries. The area of the polygons are found with a planimeter or by digitizing the map. A drawback of this method is that a new polygon network must be drawn when a station is added or deleted from the network. While the method assigns weights based on the location of the station in the basin and the relative density of the station network, it cannot account for the effects of elevation on precipitation. The ability to account for elevation is why the isohyetal method can, at least potentially, produce the most accurate results.

The isohyetal method involves drawing isohyets using observed precipitation data and any other information available to aid in the interpolation of precipitation values between stations. An important additional piece of information is elevation data, since elevation and precipitation are causally related (Fig. 2.4). The area between the isohyets is used to weight a representative precipitation value for the area enclosed by the isohyets. The method is similar to the Thiessen method in using areas as weights, but differs in that the isohyetal method does not weight the observed values, but rather a representative value chosen by the analyst. Example 4.4 demonstrates the application of the three techniques.

Example 4.4

This example demonstrates the three techniques for spatial averaging precipitation data. Figure 4.15 shows five meteorological stations A through E, four of which are in the drainage basin. The observed precipitation values are as follows:

Station	Precipitation (mm)
A	22
B	35
C	57
D	42
E	77

The arithmetic average uses only the four stations within the basin (A, B, C, D) to calculate the basin average precipitation.

$$P = (22 + 35 + 57 + 42) / 4 = 39 \text{ mm}$$

The Thiessen method uses all five stations and weights the observed value at each station by the area of the polygon as a percentage of the total basin area (Table 4.5). The polygons are created by first connecting the stations (dashed lines) and then drawing the perpendicular bisectors of those lines (solid).

The isohyetal method (Table 4.6) requires more judgement than the other two by requiring the analyst to interpolate the isohyets, and assign representative values of precipitation to the area between isohyets.

Singh (1989) lists fifteen different methods for areal averaging precipitation data, including the three discussed here. Comparative evaluation of the different methods shows that as the precipitation measurement period increases, from daily through annual precipitation, the differences between techniques decreases (Singh & Chowdhury 1986). According to one investigator, 'The simpler methods were practically as good as somewhat more complex ones.' (Singh 1989, p. 104).

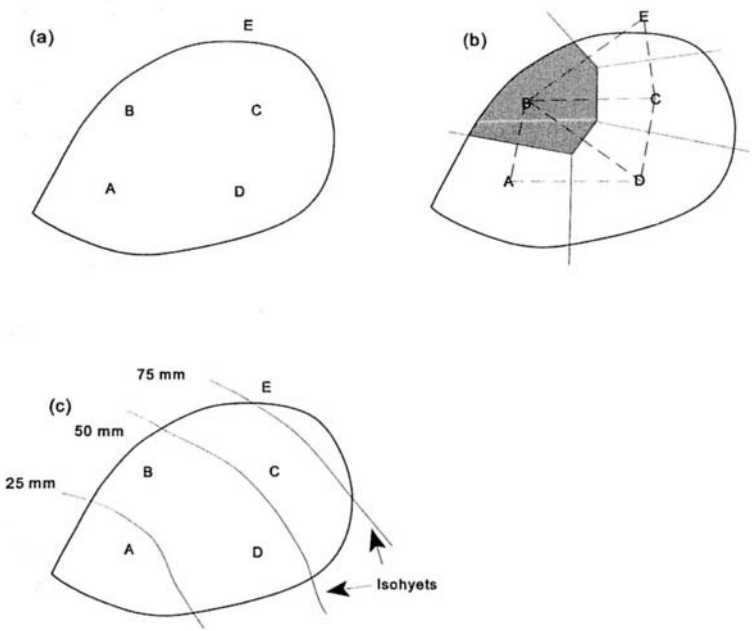

Figure 4.15. a) Four stations used for the arithmetic average, b) Construction of the Thiessen polygons, and c) Isohyets for the isohyetal method.

Table 4.5. Spatial averaging of precipitation using the Thiessen method.

(1) Station	(2) Observed ppt. (mm)	(3) Polygon area within basin (km^2)	(4) Fraction of total area	(5) Weighted ppt. (mm)
A	22	18.0	0.200	4
B	35	16.0	0.177	6
C	57	22.0	0.244	14
D	42	27.0	0.300	13
E	77	7.0	0.077	6
		Σ 90.0	Σ 1.000	Σ 43

Table 4.6. Spatial averaging of precipitation using the isohyetal method.

(1) Isohyet (mm)	(2) Area enclosed (km^2)	(3) Fraction of total area	(4) Average ppt. (mm)	(5) Weighted ppt. (mm)
≥ 75	3.0	0.033	78	3
51-75	24.0	0.266	64	17
25-50	43.0	0.477	38	18
< 25	20.0	0.222	13	3
	Σ 90.0	Σ 1.000		Σ 41

4.9 CHECKING TEMPORAL CONSISTENCY OF A PRECIPITATION RECORD

Precipitation records at a particular station may change over time relative to neighboring stations if the gage is moved, if the exposure changes, or if observational methods change. It is recommended a gage be given a new name if it is moved more than 8 km (5 mi) horizontally or 30 m (100 ft) vertically. When analyzing inconsistencies in the record of an individual station due to gage changes, the term *homogeneity* is generally used rather than the term stationarity (see Chapter 3). A station record with no inconsistencies is *homogeneous* in time, whereas a record with inconsistencies is *heterogeneous*. A heterogeneous record can be adjusted to re-establish homogeneity because the change occurred only at that station. Adjustment would be impossible if the change affected all the gages in a region, as would happen with changing climate.

A graphical technique known as *double-mass analysis* can be used to adjust a heterogeneous record. The procedure can be applied to annual, seasonal or monthly data. The accumulated precipitation at the gage in question (station *X*) is plotted against the mean of the accumulated precipitation at a group of surrounding stations. If the change at station *X* was due to natural causes, e.g. climate variation, then all stations in the region would be similarly affected, and the plotted relationship would remain the same. If the change occurred only at station *X*, a deviation in the relationship would occur and would be identified by a change in the slope of the line. Figure 4.16 shows a double-mass analysis for a hypothetical station. Realize the points will always deviate around the line by chance, and a change in slope should be accepted

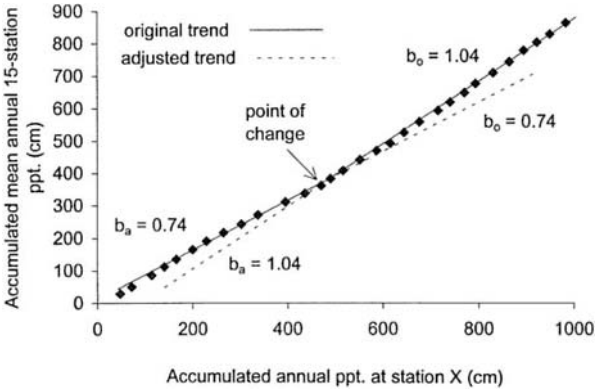

Figure 4.16. Curves for a double-mass analysis. Solid line represents the original relationship, the dashed line represents the adjusted relationship.

as real only if verified through other independent evidence, or if it persists for a long period of time. The record at station X can be made homogeneous by adjusting the values after the change so that they conform to the old slope, or by adjusting the older precipitation data to conform to the new slope. In either case the formula is (Singh 1989):

$$P_a = \frac{b_a}{b_o} P_o \tag{4.14}$$

where P_a is the adjusted precipitation value, P_o is the observed value, b_a is the slope of the line to which the records are adjusted, and b_o is the slope of the graph at which time P_o was observed. Heterogeneity can also be detected through statistical tests.

4.10 FREQUENCY ANALYSIS OF PRECIPITATION

When a time-random process shows significant serial correlation it is a stochastic process. Serial correlation describes the degree to which events sequenced in time are dependent upon previous events, resulting in non-pure-randomness. Another term to describe time dependence is *persistence*. As discussed at the beginning of Chapter 3, the strength of the dependence is a function of the length of time separating the individual events. Daily rainfall values can show strong serial correlation, though the strength may also depend upon the season. For example, if it rained one day there might be a high probability of rain the next day because the synoptic-scale rainfall generating processes may still exist in the region one day later. As the period of time increases, serial correlation decreases. Whether or not it rained last Tuesday has no significant influence on rainfall occurring many months later. Persistence tends to be stronger in streamflow data than precipitation data.

Annual total precipitation values are often assumed to be independent for frequency analysis, but the assumption may not be completely valid. There is abundant evidence of persistence in hydrometeorological phenomena over inter-annual time scales. Droughts and wet years are excellent examples of multiyear persistence. The old adage 'wet years follow wet years and dry years follow dry years' is folk evi-

dence of hydrometeorological persistence. For reasons not completely understood, the atmosphere may set up in a flow pattern that produces low or high rainfall conditions, and the pattern can persist for months to years. The El Niño/Southern Oscillation (ENSO) phenomena is now recognized as a major mechanism forcing persistent variations in atmospheric circulation patterns from the tropics to the midlatitudes. Exactly how an ENSO event causes floods or droughts months later and thousands of kilometers downstream is not completely understood. The effect of persistence in the data is to increases the variability of the data, reducing the accuracy of statistical estimates derived from frequency analyses (Chow 1964). The correct application of frequency analysis requires the data be random, independent and stationary. In practice these conditions are met with varying degrees of fidelity. The problem is that we must work with very short historical records, and we cannot afford to discard any data even if it means violating the prerequisite assumptions.

The data for frequency analysis are either annual maximum (minimum) series, partial duration series, or a series composed of a sum of values such as total annual precipitation. The *return period* or *recurrence interval* T is the reciprocal of the exceedence probability:

$$T = \frac{1}{p} \tag{4.15}$$

where T is the return period in years and p the exceedence probability. An event with an exceedence probability of 0.01 (1%) has an average return period of 100 years. Said another way, the 100-year event, whether a storm, flood, or whatever, has an average probability of occurrence of 1% each and every year. The perception that if the 100-year event occurred this year and therefore will not occur for another 100 years is wrong. There is a slight difference in the meaning of return period and exceedence probability between the annual maximum series and the partial duration series. If the partial duration series is used for the analysis, the interpretation of the T–year return period means an event of that magnitude will occur once every T years, on the average. If the annual maximum series is used, the interpretation is that the event will occur once every T years on average as an *annual maximum* (Dunne & Leopold 1978). The distinction is subtle but real. Frequency analysis assigns exceedence probabilities to individual hydrologic observations using the sample cumulative distribution function (F_s). In the following discussion the terms exceedence probability and frequency are used interchangeably. The following procedure creates the sample CDF for a frequency analysis.

1. Collect the appropriate data.
2. Rank the n observations from largest to smallest to generate sample estimates of exceedence probabilities. Ranking the data from smallest to largest generates non-exceedence probabilities.
3. Assign a rank number m to each observation. Assign a rank of $m = 1$ to the first ranked observation and $m = n$ to the last ranked observation.
4. Assign a sample-based frequency F_s to each observation using a plotting position formula. A common plotting position formula is Weibull's formula , $F_s = m / (n + 1)$.
5. Graph the observation magnitude versus the frequency (exceedence probability).

The sample CDF created here differs from the sample CDF for classified data in

Chapter 3. For classified data the same probability is assigned to every observation in a class. Here the data are not classified so each observation is assigned its own probability. If you think of classification as ranking the data by groups, the two methods are similar.

Observations are assigned exceedence probability estimates based solely on the sample size, rank position and the plotting position formula. This type of frequency analysis is 'distribution free'; it does not assume *a priori* that the data follow any particular probability distribution. A more sophisticated analysis combines this approach with a parameter-based fit of the data to a theoretical distribution as recommended in Chapter 3. An example of frequency analysis is demonstrated in Example 4.5.

Example 4.5

This example is a frequency analysis of the annual precipitation data for Philadelphia, PA (Table 3.2). The steps in the analysis outlined above are shown in Table 4.7. The observations are ranked from largest to smallest (column 2) and assigned a rank (m). Column 4 are the sample exceedence probabilities calculated by the Weibull formula.

Figure 4.17 is a plot of the sample exceedence probabilities along with the theoretical normal CDF for the Philadelphia data. The data are plotted on arithmetic normal probability paper. The theoretical normal CDF plots as a straight line on this paper. Once you have the CDF, it's easy to answer probability-related questions. For example, find $P(X \geq 45.0)$? Assuming the sample follows the normal distribution, the answer is around 28%, or an average return period of 3.6 years.

4.10.1 *The gamma distribution*

Total annual precipitation tends to follow a normal distribution, particularly in humid climates. In arid and semiarid climates the proximity of zero (as the left boundary) produces a positively-skewed distribution. This raises the question of whether there might be a more robust theoretical distribution capable of handling both normal and

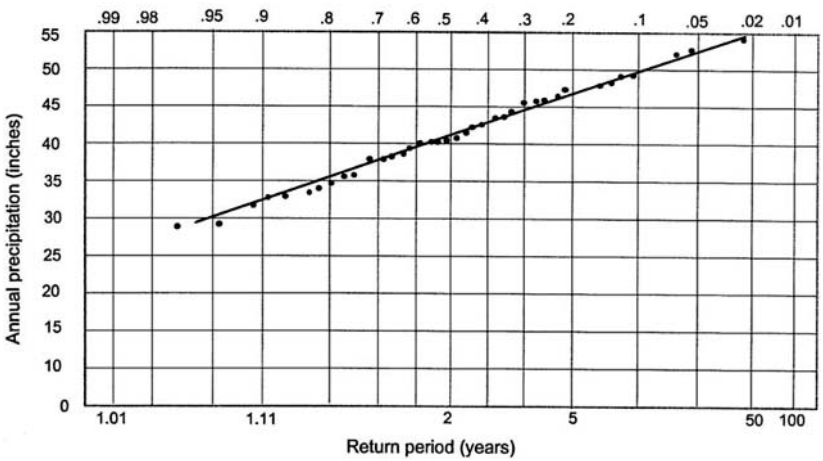

Figure 4.17. Plot of the sample CDF and the theoretical normal CDF for the Philadelphia annual precipitation data.

Table 4.7. Frequency analysis of Philadelphia, PA annual precipitation data.

Year	Ranked precipitation (inches)	Rank (m)	Sample frequency $F_s = [m / (n + 1)]$
1983	54.41	1	0.026
1979	52.79	2	0.051
1975	52.13	3	0.077
1972	49.63	4	0.103
1977	49.42	5	0.128
1953	48.13	6	0.154
1958	47.87	7	0.179
1971	47.79	8	0.205
1973	46.06	9	0.231
1978	45.95	10	0.256
1956	45.90	11	0.282
1952	45.84	12	0.308
1967	44.82	13	0.333
1984	43.66	14	0.359
1969	43.36	15	0.385
1962	42.63	16	0.410
1951	42.06	17	0.436
1960	41.15	18	0.462
1961	41.05	19	0.487
1950	40.47	20	0.513
1982	40.43	21	0.538
1986	40.42	22	0.564
1966	40.00	23	0.590
1970	39.14	24	0.615
1980	38.80	25	0.641
1959	38.37	26	0.667
1981	37.83	27	0.692
1974	37.78	28	0.718
1968	35.45	29	0.744
1985	35.20	30	0.769
1963	34.95	31	0.795
1954	34.04	32	0.821
1987	33.40	33	0.846
1976	33.27	34	0.872
1955	33.03	35	0.897
1957	32.20	36	0.923
1964	29.88	37	0.949
1965	29.34	38	0.974

positively-skewed data? One such distribution is the two-parameter gamma distribution (Table 3.4). The National Weather Service uses the gamma distribution to estimate annual precipitation probabilities. It is bounded by zero on the left and is unbounded on the right. The gamma distribution is defined by two parameters: a shape parameter (λ) and a scale parameter (β). The gamma PDF can vary from being *J*-shaped, to bell-shaped, to positively-skewed depending upon the values of the parameters. This makes the gamma more versatile than the normal distribution for modeling data. As with the normal distribution, the gamma can be evaluated by the use of

tables. The EXCEL program has a wide variety of theoretical PDF and CDF distributions available as built-in functions including the normal and gamma. This is an extremely easy way to evaluate a distribution.

As demonstrated in Example 4.5, the sample CDF and the theoretical CDF do not necessarily give the same probability estimate for the same magnitude event. Remember the sample CDF is only an estimate of the theoretical distribution. In Figure 4.17 the sample function deviates around the theoretical curve. The maximum deviation between the sample CDF and the theoretical CDF is the basis of the *K-S* goodness-of-fit test. Recall that the *K-S* test compares the absolute value of the maximum difference between the sample distribution and a theoretical distribution against some critical difference value (students should review the description of the *K-S* test in Chapter 3.) The logic of the test is that the farther a sample value is from its corresponding theoretical value, the less likely the sample comes from that particular theoretical distribution. If the absolute value of the maximum of these differences is less than a critical difference value, then the null hypothesis is accepted, and the sample data are judged not significantly different from the theoretical distribution. Example 4.6 demonstrates the *K-S* test.

Example 4.6

In this example we will test the goodness-of-fit of the Philadelphia precipitation data to both the normal and the gamma distributions. The test was performed in EXCEL using the program's normal and gamma CDF functions. The null hypothesis H_0 is that there is not a significant difference between the observed sample distribution and the theoretical distribution. Rejection of the null hypothesis means the data come from some distribution other than the one being tested. A significance level of $\alpha = 0.05$ will be used.

The parameters of the normal distribution are the sample-estimated mean $\bar{x}$ and standard deviation s. For the gamma distribution, moment-based estimators for the shape and scale parameters are found using the equations from Table 3.4:

$$\lambda = \frac{\bar{x}}{s^2} = 0.98, \quad \beta = \frac{\bar{x}^2}{s^2} = 40.45$$

Table 4.8 gives the sample CDF, and the CDF for each of the two theoretical distributions. The D columns are the differences between the sample and the respective theoretical distributions.

The maximum difference between the sample distribution and the gamma distribution occurs at rank item 12 (1952) with a value of $D_{max} = 0.075$. The maximum difference between the sample and the normal distribution occurs for rank item 29 (1968) with a value of $D_{max} = 0.071$. From Table 3.5 the critical difference value for the test with $\alpha = 0.05$ and $n = 38$ is 0.14. Since D_{max} is less than the critical value for both theoretical distributions, the null hypothesis is accepted in both cases. In other words, the sample data *could* come from *either* distribution. Note that the test does not say the data actually come from either distribution, only that they could.

Whether the data fit one distribution better than the other is a separate question. If you calculate the *average* difference between the sample and the theoretical distributions by summing the values in the D column and dividing by n, the average difference between the normal and the sample is 0.023, while it is 0.024 for the gamma and the sample. Overall, the normal distribution fits the data slightly better.

Table 4.8. Kolmogorov-Smirnov goodness-of-fit test for the Philadelphia, PA annual precipitation.

Year	Rank	PPT	Sample frequency	Normal Distribution	*D*	Gamma Distribution	*D*
1983	1	54.41	0.026	0.022	0.004	0.029	0.004
1979	2	52.79	0.051	0.038	0.013	0.046	0.005
1975	3	52.13	0.077	0.048	0.029	0.056	0.021
1972	4	49.63	0.103	0.099	0.003	0.104	0.001
1977	5	49.42	0.128	0.105	0.023	0.109	0.019
1953	6	48.13	0.154	0.146	0.008	0.146	0.008
1958	7	47.87	0.179	0.155	0.024	0.155	0.025
1971	8	47.79	0.205	0.158	0.047	0.157	0.048
1973	9	46.06	0.231	0.231	0.000	0.223	0.008
1978	10	45.95	0.256	0.236	0.020	0.228	0.028
1956	11	45.90	0.282	0.238	0.044	0.230	0.052
1952	12	45.84	0.308	0.241	0.066	0.233	0.075
1967	13	44.82	0.333	0.293	0.041	0.280	0.053
1984	14	43.66	0.359	0.357	0.002	0.340	0.019
1969	15	43.36	0.385	0.374	0.010	0.357	0.028
1962	16	42.63	0.410	0.417	0.007	0.398	0.012
1951	17	42.06	0.436	0.452	0.016	0.432	0.004
1960	18	41.15	0.462	0.508	0.046	0.487	0.025
1961	19	41.05	0.487	0.514	0.027	0.493	0.006
1950	20	40.47	0.513	0.549	0.036	0.529	0.016
1982	21	40.43	0.538	0.552	0.013	0.531	0.007
1986	22	40.42	0.564	0.552	0.012	0.532	0.032
1966	23	40.00	0.590	0.578	0.012	0.558	0.032
1970	24	39.14	0.615	0.629	0.013	0.611	0.005
1980	25	38.80	0.641	0.648	0.007	0.631	0.010
1959	26	38.37	0.667	0.672	0.006	0.657	0.009
1981	27	37.83	0.692	0.712	0.020	0.700	0.008
1974	28	37.78	0.718	0.705	0.013	0.692	0.026
1968	29	35.45	0.744	0.815	0.071	0.813	0.069
1985	30	35.20	0.769	0.825	0.056	0.824	0.055
1963	31	34.95	0.795	0.835	0.040	0.835	0.040
1954	32	34.04	0.821	0.867	0.047	0.871	0.051
1987	33	33.40	0.846	0.887	0.041	0.893	0.047
1976	34	33.27	0.872	0.891	0.019	0.898	0.026
1955	35	33.03	0.897	0.898	0.000	0.905	0.008
1957	36	32.20	0.923	0.919	0.004	0.928	0.005
1964	37	29.88	0.949	0.960	0.011	0.971	0.022
1965	38	29.34	0.974	0.967	0.008	0.977	0.003

4.11 INTENSITY-DURATION-FREQUENCY (IDF)

Hydrologic planning often requires combining the concepts of probability with measurements of precipitation intensity and duration. Average precipitation intensity is the recorded precipitation depth (pulse data) divided by the duration of the collection period. Precipitation intensity is an important determinant of surface runoff. If the rate of precipitation reaching the surface exceeds the rate that water can infiltrate

into the soil, then surface runoff occurs. Excessive surface runoff moving rapidly into stream channels causes downstream flooding. High intensity rainfall also dislodges soil particles and washes nutrients and chemicals from the land surface. When these materials enter the waterways they become pollutants detrimental to humans and aquatic ecosystems. Additionally, sediment clogs river channels and shortens the useful life of reservoirs by reducing storage capacity.

Intensity-frequency analysis assigns a probability of occurrence to storms of different depths and durations. The US Weather Bureau published a series of studies during the 1950s defining intensity-frequency characteristics for precipitation in the eastern United States. Hershfield (1961) synthesized the results from these studies into one rainfall frequency atlas that included values for the western United States between 90 and 105°W longitude. The values for the western United States were not very good because topographic influences were only general considered. *Technical Paper No. 40* (Hershfield 1961) is still considered the standard source for intensity-frequency data east of the Rocky Mountains, though recent studies have updated the information for selected areas (see Sheaffer et al. 1982). Figure 4.18 shows the IDF curves for Boston, MA and Figure 4.20 shows IDF isopluvial maps for the United States. Reliable maps and techniques for IDF calculations for the western United States became available in 1973 with the publication of the *Precipitation-Frequency Atlas for the Western United States, NOAA Atlas No. 2* (NOAA 1973).

The IDF curves and maps were constructed by piecing together data from different storms. The durations, therefore, are not total storm durations, but rather durations for subintervals within a storm. Also, the curves are average intensities and do not represent actual time histories of storms (Bedient & Huber 1992). Graphical interpolation can determine IDF values for durations and return periods other than those given in Figures 4.18 and 4.19. The technique of graphical interpolation is demonstrated in Example 4.7.

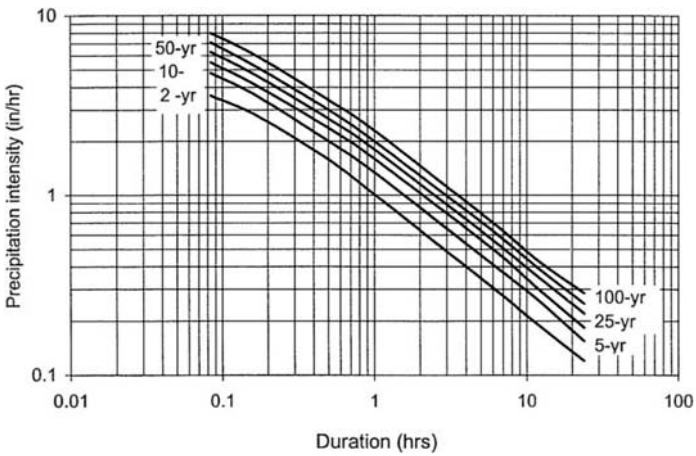

Figure 4.18. Precipitation-intensity-duration graph for Boston, MA. Durations are for 5, 10, 30, 60 minutes and 6, 12 and 24 hours. Return periods are 2, 5, 10, 25, 50 and 100 years (source: Hersfield 1961).

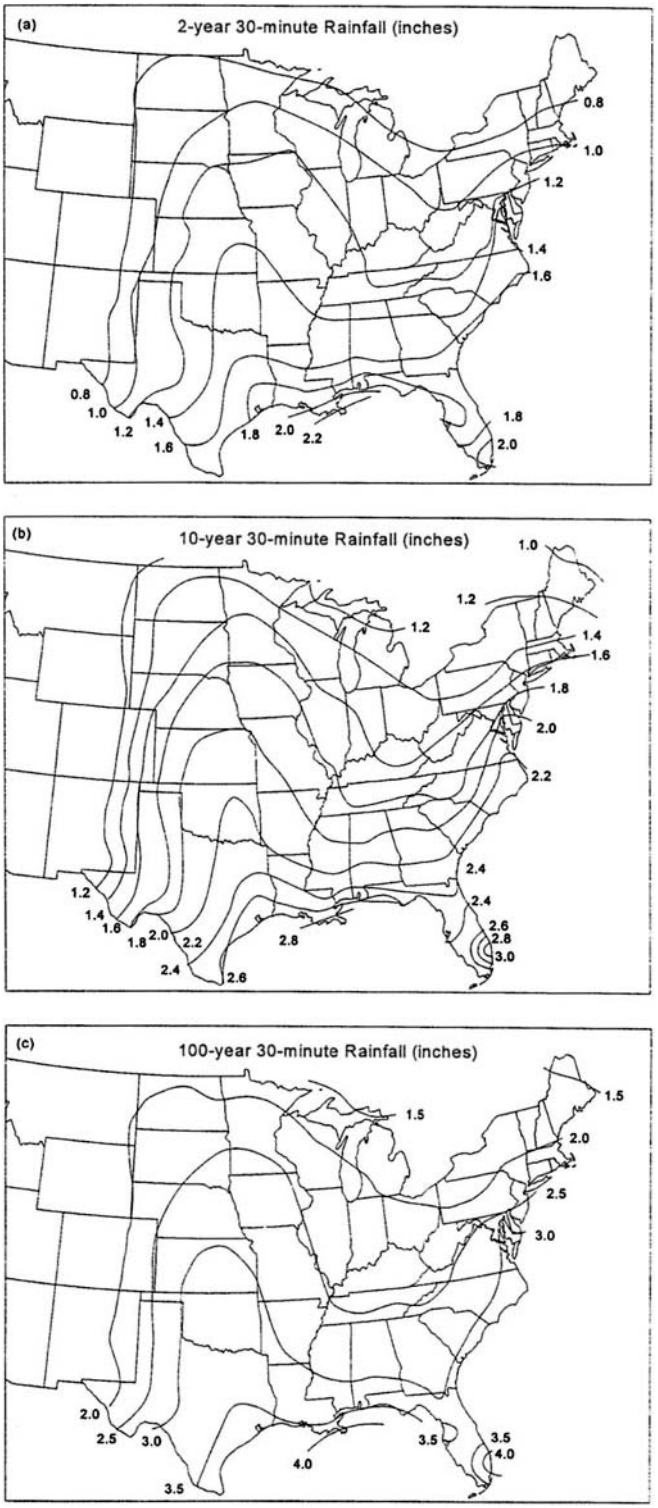

Figure 4.19. Precipitation depth (inches) for storms of varying recurrence interval and duration (redrawn from Hershfield 1961).

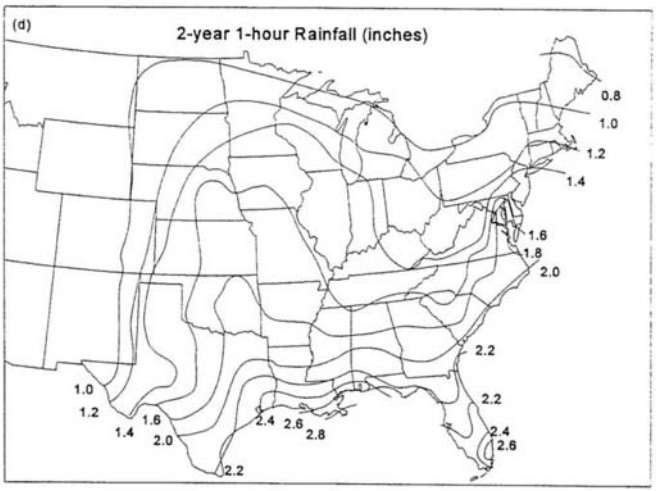

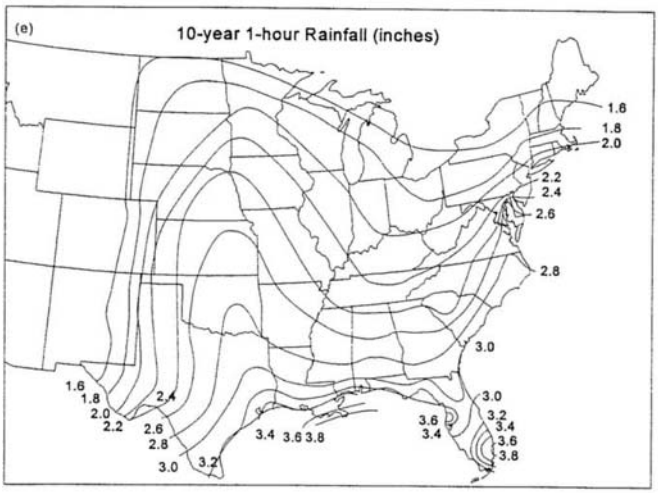

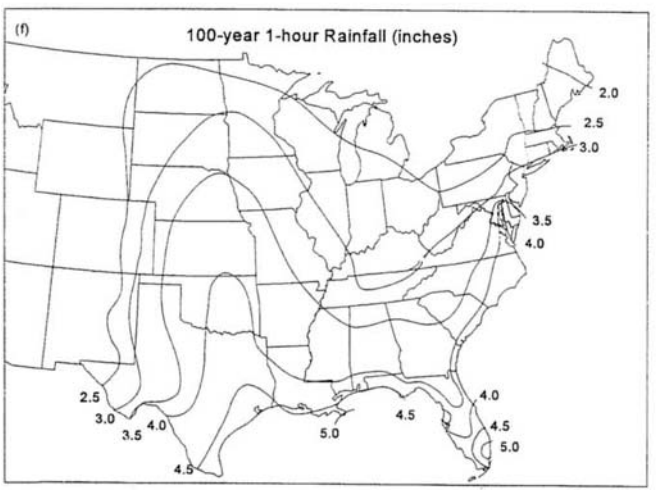

Figure 4.19. Continued.

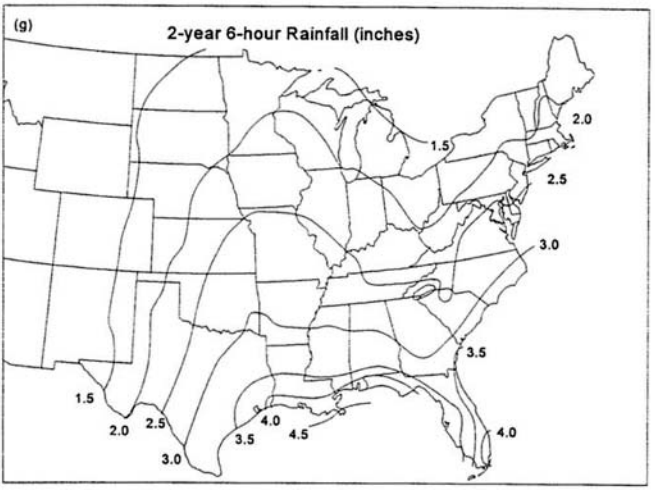

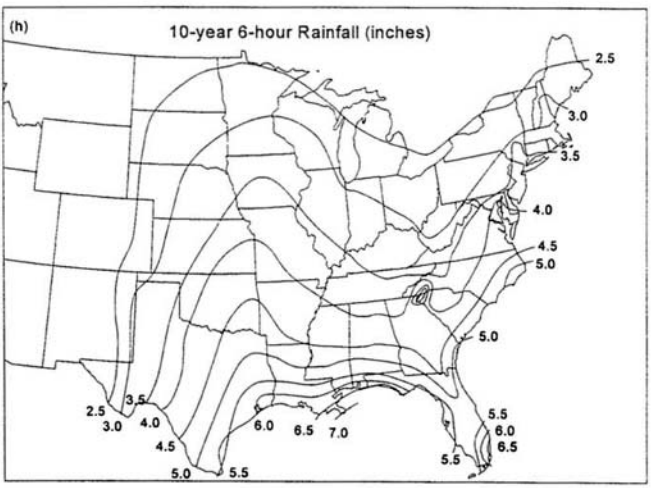

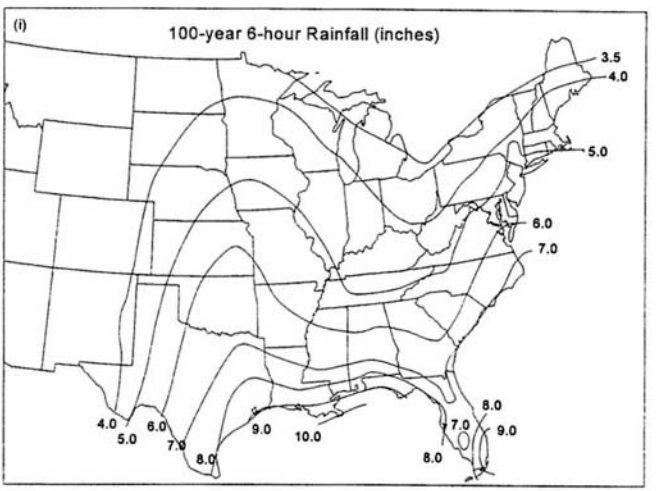

Figure 4.19. Continued.

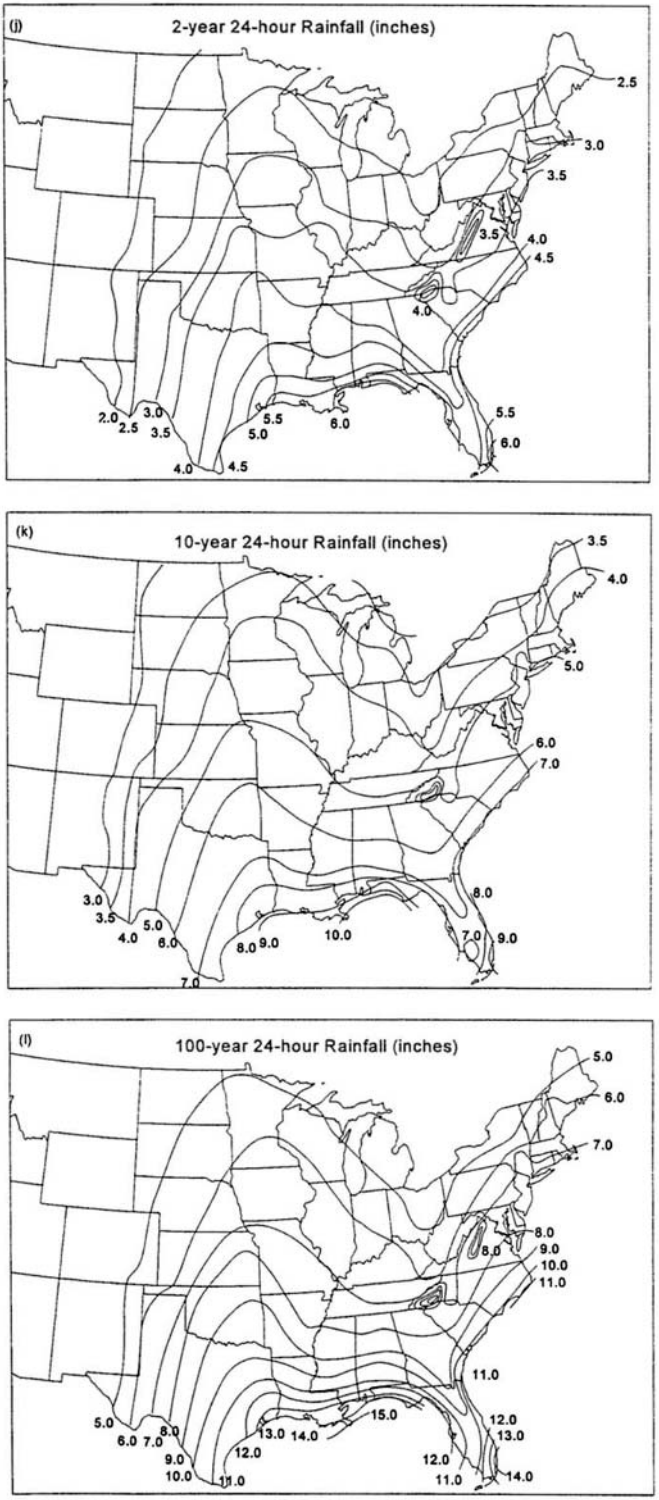

Figure 4.19. Continued.

Example 4.7
Find the precipitation intensity for a 10-year, 4-hour duration event near Tulsa, OK. From either the IDF maps or graphs find the 10-year 30-minute, 1-hour and 6-hour precipitation depths or intensities.

	0.5 hour	1 hour	6-hours
Precipitation (in)	2.19	2.72	4.30
Intensity (in hr^{-1})	4.38	2.72	0.72

Plot either intensity or depth and interpolate the 4-hour event as shown on Figure 4.20. From Figure 4.20, the interpolated precipitation intensity is 0.95 inches per hour, for a total depth of 3.80 inches.

Storms do not have uniform intensity over time (Fig. 4.10) or space. Rainfall intensity is greatest near the storm's center and decreases towards the edges. One way to incorporate the spatial variation in intensity is with Figure 4.21, which gives average depth-area relationships as a percentage of point values for areas up to 400 mi^2. For example, if a point observation for a 10-year return period, 6-hour duration event along the southern boundary between Colorado and Kansas is 3 inches (see Fig. 4.19), then the areal average depth for a 200 mi^2 area is approximately 85% of the point values, or 0.85 (3.00 inches) = 2.55 inches.

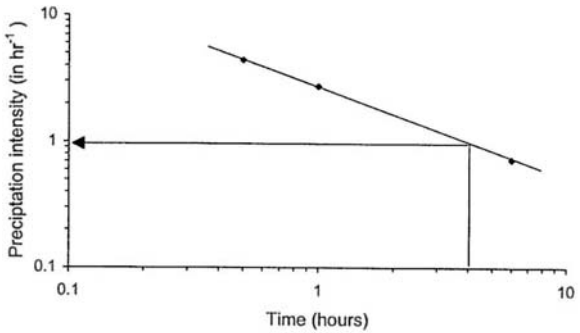

Figure 4.20. Graphical interpolation of the 10-year, 4-hour precipitation event for Tulsa, Oklahoma.

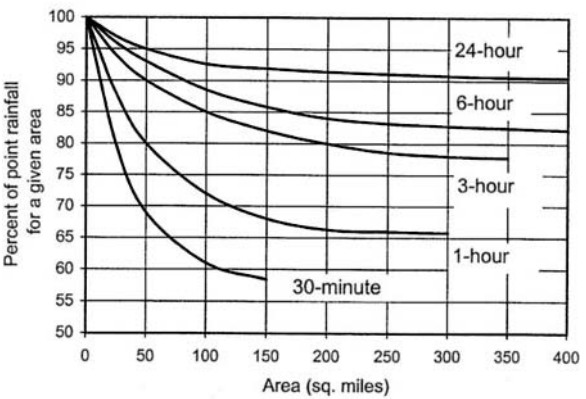

Figure 4.21. Relation of point rainfall to average rainfall over an area for various durations (source: US Weather Bureau 1958).

4.12 RISK

The final topic of this chapter is *risk*. The term risk used in hydrology means *the probability of an event occurring within a specified period of time*. For example, what is the risk of having a 100-year precipitation event as an annual maximum in the next 5 years? Recall from the discussion of frequency analysis that an event with an average return period of 100 years has an average probability of exceedence of $p = 0.01$, or 1%, each and every year as an annual maximum. From the Law of Total Probability, if p is the probability that an event will occur (exceedence), then the probability that it will *not* occur is $(1 - p)$. The probability that the event will not occur for two years is:

$$(1-p)\,(1-p) = (1-p)^2 \tag{4.16}$$

Equation (4.16) is an example of the *multiplication rule* for independent events, i.e. when the occurrence of the event at one time has no influence on the occurrence at some other time. Equation (4.16) expresses the *conditional probability* of nonoccurrence of the event this year *and* nonoccurrence the year after. Therefore, the probability that an event will not occur in the next n years is:

$$(1-p)^n \tag{4.17}$$

Equation (4.17) says apply the multiplication rule as many times (n) as is necessary. If Equation (4.17) gives the probability of an event not occurring in the next n years, what is the probability that the event *will* occur in the next n years? By the Law of Total Probability, it equals one minus the probability of the event not occurring in the next n years, or:

$$J = 1 - (1-p)^n \tag{4.18}$$

Equation (4.18) is used for estimating the risk J that *at least* one occurrence of an event, having an average probability of occurrence in any given year of p, will occur in the next n years. The formula above is from the binomial distribution, a discrete theoretical distribution useful in describing the occurrence of discrete events (Chapter 3). A formal derivation of Equation (4.18) comes from Linsley et al. (1982):

$$J_k = \frac{n!}{k!(n-k)!}(1-p)^{n-k}\,p^k \tag{4.19}$$

Equation (4.19) gives the risk J that an event with an average probability of occurrence p will be exceeded exactly k times during an n-year period. The ! sign means factorial. For example, $3! = 3 \times 2 \times 1$, and $0! = 1$. The probability of one or more exceedences in n years is found by setting $k = 0$ and noting that the probability of exceedence is one minus the probability of nonexceedence, or:

$$J_{1 \text{ or more}} = 1 - (1-p)^n \tag{4.20}$$

Figure 4.22 shows risk J as a function of different exceedence probabilities and time intervals.

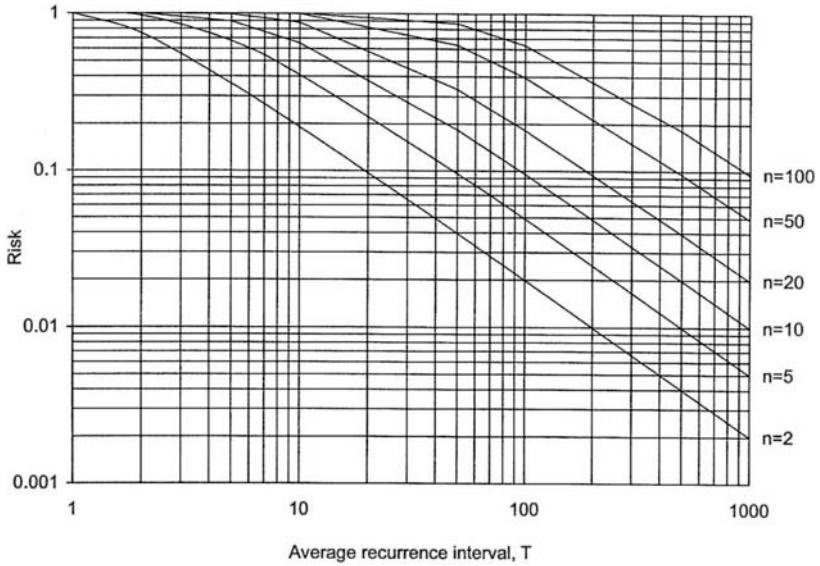

Figure 4.22. Risk as a function of the average recurrence interval (T) and time periods (n).

Example 4.8
Find the risk of experiencing the 20-year event in the next 3 years?

$p = 1/T = 0.05$

$n = 3$

$J = 1 - (1 - 0.05)^3$

$J = 1 - 0.857$

$J = 0.143 = 14.3\%$

There is slightly greater than 14% chance that the 20-year event will occur during the 3-year period. Is this risk acceptable? That is a question for decision makers to answer. The estimate of risk assumes you know p exactly.

If you calculate the probability of the 100-year event occurring in a 100-year period, it equals 63%. In other words, the chance that the return period of the 100-year event will be less than the 'average' value of 100 years is 63%.

SUMMARY

Precipitation is a major input to the land phase of the hydrologic system. It is one of the most basic of natural resources for human and ecological systems by replenishing the storage of water in the soil, streams, lakes and groundwater. But a resource at one level of availability may become a natural hazard at a different level. High intensity precipitation may lead to surface runoff and flooding, while a lack of precipitation results in drought. Under some range of expected or 'normal' conditions precipitation is a resource; when that range is exceeded the results may be disastrous.

As with all hydrologic phenomena, the occurrence and distribution of precipitation can only be described in probabilistic terms, hence the importance of understanding concepts of statistics and probability. The techniques of measurement and analysis described in this chapter are only the most basic. More advanced topics can be explored in advanced hydrology texts and hydrologic research journals.

Another important input to the hydrologic system is energy. Solar energy drives the hydrologic system by transforming precipitation into water vapor. While water vapor was covered in this chapter as a prerequisite to the formation of clouds, in Chapters 5 and 6 we turn our attention to how water moves from the surface to the atmosphere by evaporation and evapotranspiration.

PROBLEMS

4.1 Calculate the specific humidity, mixing ratio and relative humidity for the following situation. Assume standard sea level pressure.
Air temperature = 82.5°F
Dew point temperature = 58.7°F
Relative humidity = ...
Specific humidity = ...
Mixing ratio = ...

4.2 The precipitation gage at station X was inoperative for part of a month during which a storm occurred. The respective storm totals at three surrounding stations, A, B, and C, their normal annual precipitation values, and their distance from station X are given below. Estimate the storm precipitation for station X two different ways.

Station	Normal annual ppt (mm)	Storm total (mm)	Distance from station X (km)
A	1008	115	4
B	842	90	2
C	1080	120	5
X	880		

Answer ....., using the ..... method.
Answer ....., using the ..... method.

4.3 Using the map below, determine the areal average precipitation using the arithmetic, Thiessen, and isohyetal methods. Make copies of the basin map so you can show the Thiessen and isohyetal methods separately. For the isohyetal analysis use a one-inch isohyetal interval. Note: To calculate area you need a planimeter.

Map scale 1:40,000

Observed precipitation
Station A 1.00 inches
Station B 3.00 inches
Station C 4.50 inches

	Arithmetic	Thiessen	Isohyetal
Average precipitation (inches)	.....	.....	.....
Acre-feet equivalent	.....	.....	.....

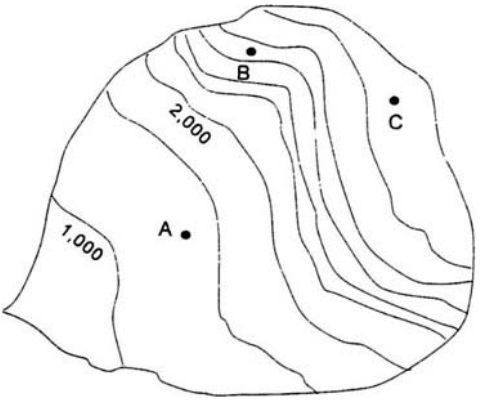

4.4 In this problem you will do a frequency analysis of total annual precipitation data.

a) Rank the Raleigh precipitation data and determine the sample cumulative probability distribution F_s. If you rank from smallest to largest you create non-exceedence probability estimates (q); if you rank from largest to smallest you create exceedence probability estimates (p). Use the Weibull plotting position formula to assign sample frequencies.

b) Plot your data on normal probability paper as shown in Figure 4.17. Draw the line representing the theoretical normal distribution through the data points. Clearly mark the +1 and −1 standard deviation limits and the mean on your graph.

c) Assuming the data fit a normal distribution, use the line to estimate the following annual probabilities:

1. $P(X > 35.50)$ inches?
2. $P(X < 35.50)$ inches?
3. $P(X > 45.00)$ inches?
4. $P(36.00 < X < 42.80)$ inches?

You can see that, if the data fit an assumed distribution, once you have the CDF, it is much easier to estimate probabilities than using Z scores.

d) Use the Kolmogorov-Smirnov test to test whether the data could come from the normal distribution.

Test the sample data for goodness-of-fit using the K-S test and a significance level of 0.05.

D_{max} = ... $D_{n,\,0.05}$ = ...

What can you say about the distribution based on the K-S test? (You should include the level of significance (α) and the null hypothesis in your answer.)

EXCEL EXERCISE 2

In this exercise you duplicate the precipitation homework exercise on calculating statistics and creating a histogram.

1. As with your first EXCEL exercise, enter a title, your name and the course number at the top of your worksheet. Give this worksheet the title 'Precipitation Statistics.' Format these cells the same as in EXCEL Exercise 1.
2. Before you go any further save your worksheet to your diskette; however, don't save it as a worksheet file but as a template file. Saving it as a template means you can use it over and over as a template for future exercises and you won't have to do the formatting in step 1 above.
3. Starting in cell A4 and ending in cell A33 enter the 30 years 1955 to 1984. Rather than entering one year moving down one row and entering the next year use the following approach. Move to

cell A5 and type ' = A4+1 ' (without quotes). Now select A5, press the RB, choose **Copy**, move to cell A6 and copy to the range A6:A33. To copy to A6:A33 click and drag. You should have the sequence 1955 to 1984 in column A. Change these formula-based dates into real numbers by selecting the dates and using **Copy / Paste Special / Values**.

EXCEL has an even faster way to do this operation. Type 1955 in A4 and 1956 in A5. Now select A4:A5. Place the cursor on that little dot in the lower-right-hand corner of the box outlining the selected cells. The cursor turns into a cross. Click the LB and drag down to cell A33.

4. In column B enter the annual precipitation data for each year.
5. You are now going to rank the data to find the median. Select the full range of the data (A4:B33). It is important that you select from column B to column A so that the active cell is in column B. Click on **Data** on the top menu. From the pull down menu choose **Sort**. Alternatively, from the utility toolbar click the 'sort in ascending order' button. This button has the letter A over the letter Z with an arrow pointing down. After you click the button you may be asked to choose a 'sort key.' The sort key is the column with the active cell. You are using precipitation as the sort key (column B) and your active cell should already be in that column. If you are not asked to choose a sort key then the data are ranked immediately. Notice that by having column A selected along with column B, the values in column A (years) are sorted along with the precipitation values. Had you not selected column A also, the years would have remained in place. Sorting in ascending order generates the probability of *nonexceedence*.
6. Now calculate the mean and standard deviation. Move to cell A36 and type Mean and in cell A37 type SD. Select cell B36 and click on **Insert / Function** on the upper menu. From the dialog box select **Statistical** function. Click on the function **AVERAGE** then **Next**. You now move to Step 2 to edit the formula you chose. Edit number 1 so that it says B4:B33 and click **Finish** when you are done. Paste the standard deviation function into cell A37 the same way by choosing the function **STDEV**.
7. The last step is to plot the histogram for data. For this step you must have the Analysis Toolpak Add-in installed. You can't go directly into the ChartWizard program. First you have to classify the data into intervals by frequency.

   Click on **Tools** from the menu and then **Data Analysis**. From the dialog box choose **HISTOGRAM** and then OK. Next will appear another dialog box which asks for the **Input Range**, the **Bin Range,** and the **Output Range**.

   The Input Range is the data you want to analyze – B4:B33.

   The Bin Range is the 'bins' or intervals you want to use to classify the data. You have to create this range and the bin values. In the range C8:C15 type the numbers 33, 36, 39, 42, 45, 48, 51, 54. So your Bin Range is C8:C15 and the class intervals used to group the data are the numbers in that range. (Note: the Bin Range numbers must always be in ascending order.)

   The Output Range tells EXCEL where to print the results. All you need do is designate the cell in the upper left corner of this range. Use the cell E5.

   Click on the box that says Pareto and the box that says Cumulative. This should remove the check which means you do not want these options. You do want the chart option so leave the check in that box. Press Enter or click on the OK button to generate the histogram.

   The chart is created not as an embedded chart but as a separate chart file in earlier versions of EXCEL. To see your chart in this case click the minimize button in the upper right corner of your worksheet; *not* the upper right corner of the screen. The button has an arrow pointing down. To restore your worksheet click on the maximize button.

EXCEL EXERCISE 3

In this exercise you duplicate your precipitation frequency analysis. The exercise is designed to

create nonexceedence probabilities, but you can easily change the steps to generate exceedence probabilities.

1. You want to replicate the first two columns of EXCEL Exercise 2. There are different ways to do this. You could copy all of the information from the 'Precipitation Statistics' worksheet (Exercise 2) to another empty worksheet on the screen. Probably the easiest way, however, is just to save Exercise 2 with a new filename. From **File** on the top menu select **Open**. From the dialog box select drive A and then click on your second exercise filename. Now again from the menu **File / Save As..** and save the worksheet under a new filename (e.g. EXER_3.XLS). This duplicates a copy of Exercise 2 on your diskette with the new filename. From the menu **File / Close** Exercise 2, and **File / Open** your new Exercise 3 worksheet.
2. Delete all of the cells used for the histogram. This leaves years in column A and ranked precipitation data in column 2. Place the active cell anywhere in column B and press the RB on the mouse. Choose **Insert** from the drop down menu and from the dialog box select **Entire Column** with the LB. This will move the precipitation data to column C and insert a new blank column B. In cell B3 type 'Rank' (without quotes) and fill this cell with rank values. Place a number 1 in cell B4, number 2 in cell B5 etc. Do this by copying the same way you created the sequence of years in Exercise 2.
3. Now enter the headings for the rest of the columns. In cell D3 type 'Frequency,' in Cell E3 type 'Normal,' and in cell F3 type *D*. Column D cells will hold the frequency formula $m/(n+1)$; cells in column E will hold the normal probability estimates for the precipitation data using a built-in EXCEL function; and column F will give the results (difference values) for the Kolmogorov-Smirnov goodness-of-fit test.

   In cell D4 type the formula '=(B4/31)' (without quotes). Now copy this formula to the range D5:D33. The values are the frequency formula estimates for the probability that annual precipitation is less than or equal to the value in the corresponding cell in column C.

   Move to cell E4. From the top menu select **Insert / Function**. From the dialog box select **Statistical / NORMDIST / Next**. This pastes the normal distribution function into cell E4 and places you (cursor) in the function wizard. The normal distribution function calculates either the PDF or the CDF. You need to supply three things to calculate a probability estimate: the X value (from column B) for which the probability is being estimated, and the mean and standard deviation. You should have the mean and standard deviation already in cells C36 and C37, respectively. The syntax for the function is this:

   =NORMDIST(X,MEAN,STANDARD_DEV,CUMULATIVE)

   Edit the function wizard using cell C4 for X, C36 for the mean, C37 for the standard deviation, and TRUE for cumulative.

   The TRUE statement gives you the CDF, a FALSE would give you the PDF. Now copy cell E4 to the range E5:E33. Column E now contains the normal distribution estimates for the probability that annual precipitation is less than or equal to the value in the corresponding cell in column C. Look at your normal distribution CDF values. Do they look correct? Do they look like the sample frequency estimates? The EXCEL function NORMDIST gives the nonexceedence probability, not the exceedence probability. How would you fix it so you have exceedence probability in column E?
4. Now you will perform the *K-S* test by subtracting the values in column E from the values in column D. Move to cell F4 and enter the formula =ABS(E4-D4). ABS means take the absolute value of the difference between the numbers in the two cells because we are not interested in the sign just the magnitude of their difference. Now copy cell F4 to the range F5:F33. In column F you now have the 'D' values for the *K-S* test. Scan down column F and find the largest D value and see if it exceeds the appropriate critical D value from Table 3.5. If not, then the data are not significantly different from a normal distribution. If it does exceed the critical value, the data are significantly different from the normal distribution and we need to try another distribution.

5. You can graph your data if you want to but it is not required. EXCEL does not have a built in normal distribution graph, so the data plot as a curve.
6. When you are finished print your worksheet and save it to your disk. But before you do, are there some things you could do to make your worksheet look better? How about removing the gridlines around the cells. Try changing the format of the cells so that data in the same column, e.g. precipitation, all have the same number of decimal places.

CHAPTER 5

Evaporation

The hydrologic cycle starts when solar energy changes water from the liquid or solid state to the gaseous state. Evaporation is the change from liquid to gas. Sublimation occurs when ice becomes vapor directly without passing through the liquid state. The latent heats required for the state changes were given in Table 4.1, and Equation (4.1) showed the latent heat of vaporization is inversely related to water temperature. The Earth's surface is 71% water; consequently, most of the solar energy reaching the Earth's surface evaporates water and returns to the atmosphere as latent heat (Fig. 5.1). Winds carry water vapor thousands of feet vertically and thousands of miles horizontally from its source. The Pacific Ocean and the Gulf of Mexico are the major sources of vapor for North America. On average, 70% of the precipitation over the United States returns to the atmosphere in vapor form. When this vapor condenses or sublimates, the latent heat is transformed again into sensible heat. These fluxes of mass (water) and energy (latent heat) are major components of the Earth's climate system.

From a water management perspective evaporation is tremendously important. Evaporation is a major water 'loss' from reservoirs, especially in arid and semi-arid climates like those of the western United States. The single largest 'use' of water in the entire state of New Mexico is evaporation from Elephant Butte Reservoir on the Rio Grande. Evaporation from reservoirs in the Colorado River Basin amounts to millions of acre-feet annually. Water resource development in the Colorado Basin long ago reached the level where any additional storage of water in reservoirs results in a net reduction in water availability because of increased evaporation. This chapter first identifies the meteorological factors that control evaporation, and then discusses several methods for measuring and estimating evaporation.

5.1 THE EVAPORATION PROCESS

Assume we have a shallow lake. Solar radiation is absorbed by the lake and winds blow across the surface. Evaporation from shallow lakes follows meteorological conditions more closely than evaporation rates from deep lakes because of energy storage in deep lakes. Individual water molecules are attracted to each other because of the molecule's unique structure. The water molecule, with two hydrogen atoms covalently bonded to one atom of oxygen, is polarized – it is positively charged on one end and negatively charged on the other. The positive ends (hydrogen atoms) are

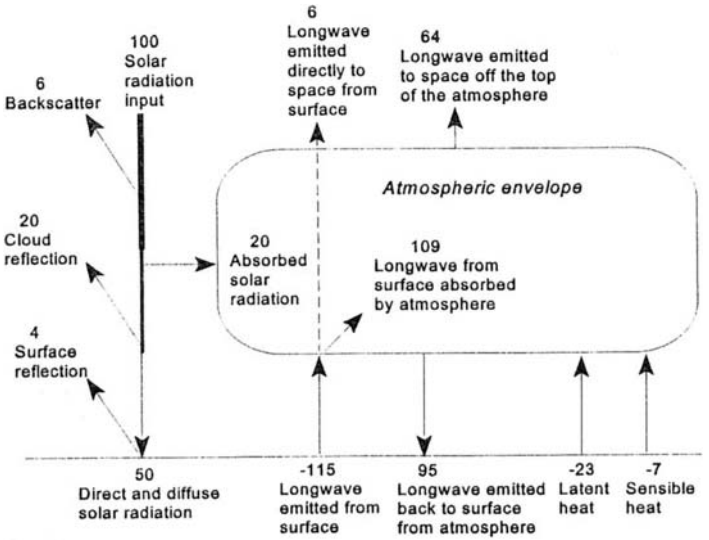

Figure 5.1. Global average input and output of radiant energy. Values are percent of the solar constant (Henderson-Sellers & Robinson 1986).

attracted to the negative ends (oxygen atoms) forming *hydrogen bonds*. These hydrogen bonds provide the force holding the molecules together as a coherent liquid mass which we know as water. For water to evaporate, the molecule must acquire sufficient kinetic energy to overcome the attractive forces of the hydrogen bonds. There are three sources of energy available to a water molecule: solar radiation, sensible heat energy in the overlying air, and heat energy stored in the lake. Of the three, solar radiation is the most important in providing the energy for evaporation. Utilizing energy stored in the water or in the overlying air results in a net cooling of the water or the air. The meteorological variables responsible for controlling the rate of evaporation are solar energy, the vapor pressure deficit between the water surface and the overlying air, and the wind speed. Each of these factors is discussed below; however, because of its dominance, solar energy receives considerably more attention than the other two.

5.1.1 *Solar energy*

Evaporation requires energy to break the hydrogen bonds between water molecules, and solar radiation is the primary source. Solar energy is a form of electromagnetic radiation (EMR). EMR is classified by wavelength (λ) along the EMR spectrum (Fig. 5.2). The *ultraviolet* spectral region is that portion of the spectrum with wavelengths slightly shorter than 0.40 μm. Radiation with wavelengths between 1 and 100 μm is *infrared*. Between these two regions is the visible spectrum (0.40 to 0.70 μm). Incoming solar energy Q_s is called *insolation*. It is composed of relatively short wavelength energy, with approximately 9% being ultraviolet, 41% visible light, and 50% infrared energy of wavelengths less than 5 μm. Most of the ultraviolet radiation is absorbed in the stratospheric ozone layer and never reaches the surface. Solar radiation absorbed at the Earth's surface is transformed and reradiated back to the at-

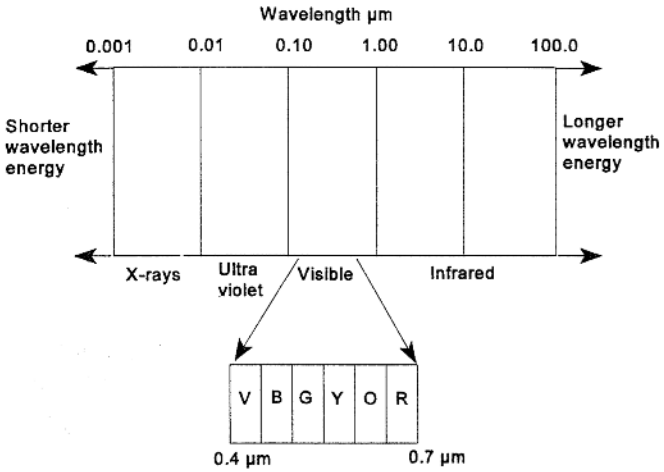

Figure 5.2. A portion of the electromagnetic spectrum. Spectral regions are classified by wavelength (λ).

mosphere as relatively long wavelength infrared radiation between the wavelengths 3 and 80 μm. Much of this outgoing infrared energy is absorbed by water vapor and carbon dioxide in the lower troposphere, and heats the atmosphere close to the Earth's surface (Fig. 5.1). This is the so-called greenhouse effect and it keeps the environment near the surface warm enough to support life. In the discussion that follows we use energy-balance equations to analyze energy input, output and storage. Radiant energy is measured as pulse data, e.g. as the total (accumulated) energy per unit area per day.

The energy for evaporation is part of the *net allwave* radiation Q_n at the surface. Net allwave radiation is the difference between the incoming solar radiation Q_s, the amount of Q_s reflected by the surface Q_{rs}, and the *net* longwave energy Q_{lw}:

$$Q_n = Q_s - Q_{rs} - Q_{lw} \tag{5.1}$$

where Q_{rs} is equal to:

$$Q_{rs} = Q_s(\alpha) \tag{5.2}$$

and Q_{lw} is equal to the difference between the incoming longwave radiation Q_a, the reflected longwave radiation Q_{ar}, and the emitted outgoing longwave radiation Q_b:

$$Q_{lw} = Q_a - Q_{ar} - Q_b \tag{5.3}$$

Net longwave radiation is discussed below. Rearranging Equation (5.2) shows *albedo* (α) is the ratio of the solar radiation reflected by a surface to the amount of solar energy incident upon the surface ($\alpha = Q_{rs}/Q_s$). The higher the albedo, the more energy reflected back to space, and the lower the available net energy. Table 5.1 gives albedos for some natural surfaces and vegetation types. Water is somewhat unique in that its albedo depends on the angle of incidence of the radiation. For high sun angles the albedo is usually between 0.05 and 0.10, but when sun angles are low albedo increases due to *specular reflection* off the water surface. This is apparent to anyone watching the sun set over a body of water. Alternatively, Equation (5.1) may be written:

$$Q_n = Q_s(1 - \alpha) - Q_{lw} \tag{5.4}$$

Equations (5.1)-(5.4) all describe *energy flux. Flux* describes the *flow of a quantity per unit area per unit time.* Energy flux is the flow of energy per unit area per unit time. Units for radiant energy flux are calories per square centimeter per day (cal cm^{-2} d^{-1}) or watts per square meter (W m^{-2}). (One watt is equal to one joule per second, and one calorie is equal to 4.186 joules.) The *solar constant* I_0 is the flux of insolation measured at the outer edge of the Earth's atmosphere, perpendicular to the Sun's rays, at the mean distance between the Earth and the Sun. The current estimated value for the solar constant is 1.97 cal cm^{-2} min^{-1} (1372 W m^{-2}). The term solar constant is misleading as the flux varies by as much as 0.5% around this value. Averaged over the entire Earth, only about 50% of the solar constant reaches the Earth's surface. The remainder is scattered, absorbed or reflected by the atmosphere and the surface (Fig. 5.1). Table 5.2 gives average values for I_o in cal cm^{-2} d^{-1} for various latitudes. The values in Table 5.2 are based on an earlier (lower) estimate of

Table 5.1. Albedo and emmissivity for natural surface materials (source: Henderson-Sellers & Robinson 1986, used by permission).

Material	Albedo	Emissivity
Tropical forest	0.13	0.99
Woodland	0.14	0.98
Farmland/grassland	0.20	0.95
Semi desert	0.25	0.92
Dry sandy desert	0.37	0.89
Water (0-60°)*	<0.08	0.96
Water (60-90°)*	<0.10	0.96
Snow covered ice	0.80	0.92
Sea ice	0.90	0.90

*Zenith angle.

Table 5.2. Average values for the solar constant I_o (cal cm^{-2} d^{-1}) (source: Dunne & Leopold 1978).

Latitude	Jan	Feb	Mar	Apr	May	Jun	Jul	Aug	Sep	Oct	Nov	Dec
90°N	–	–	–	465	880	1070	930	660	155	–	–	–
80	–	–	105	460	860	1050	970	625	235	10	–	–
70	–	65	255	540	800	1000	870	670	400	140	5	–
60	75	205	400	655	860	975	925	750	500	275	110	55
50	200	350	540	750	910	985	950	820	620	430	155	175
40	355	490	650	820	880	985	960	870	740	550	395	325
30	500	620	750	870	945	975	955	900	795	670	540	465
20	640	725	820	895	930	930	930	900	850	760	660	610
10	755	820	870	895	885	870	870	885	880	830	770	730
0	855	885	895	870	820	790	795	840	880	885	860	840
10	930	930	885	810	730	685	705	770	845	900	920	930
20	985	940	855	740	630	570	595	680	790	900	965	990
30	1015	930	800	640	505	445	465	575	725	870	985	1030
40	1020	895	715	525	375	305	335	450	630	810	960	1045
50°S	1000	835	620	400	240	175	200	315	505	735	950	1040

the solar constant and should be increased by 2% (Frohlich 1977), but only if such precision is warranted.

Obtaining data on Q_s and Q_{lw} can be difficult. There are relatively few stations in the United States that measure and report radiation data on a regular basis, and they typically record only incoming radiation. Data for outgoing longwave radiation is virtually nonexistent. To overcome this paucity of data various empirical equations have been developed to estimate both incoming and outgoing radiation.

5.1.2 *Estimating solar radiation*

Regression relationships have been developed between measured Q_s and available meteorological variables such as the fraction of cloud cover and the observed duration of sunshine. Observations of cloud cover and sunshine are routinely made at most weather stations, and are readily available in published climatological reports. Black's equation (quoted in Chang 1968) calculates mean daily solar radiation for a given month as:

$$Q_s = I_o(0.803 - 0.340C - 0.458C^2) \tag{5.5}$$

In Equation (5.5) Q_s is mean daily solar radiation for the month in the units of I_o, I_o is the mean daily solar constant for the month (Table 5.2), and C is the mean monthly cloudiness as a decimal fraction. Equation (5.5) says that on a cloudless day ($C = 0$) Q_s is 80.3% of the solar constant. The nearly 20% loss of incoming energy is due to the combination of back-scattering and direct absorption of the solar beam by atmospheric gases and particulate matter.

For stations that record the observed duration of sunshine, an equation originally proposed by Ångstrom (1924) (quoted in Chang 1968) is:

$$Q_s = I_o\,[a + b\,(n/N)] \tag{5.6}$$

where a and b are empirically-determined constants (see Table 5.3), n is the observed duration of sunshine (hours) for the month, and N is the maximum possible duration of sunshine (hours) at that latitude (Table 5.4). Regression equations like Equations(5.5) and (5.6) summarize the results of many individual observations (Fig. 5.3). While they are easy to use for predicting the Q_s from a single variable, the user must recognize their limited accuracy. List (1966) provides a more detailed method for estimating Q_s. The method calculates direct and diffuse (forward-scattered) radiation separately (see Bedient & Huber 1992).

Longwave infrared radiation is emitted and absorbed by all matter. The basic law governing the emittance of longwave radiation from a body is *Stefan's Law*, also called the *Stefan-Boltzman Law*:

Table 5.3. Empirical coefficients for Equation (5.6).

Location	a	b	Source
World	0.23	0.48	Black et al. (1954)
Virginia (USA)	0.22	0.54	Penman (1948)

Table 5.4. Maximum possible duration of sunshine (hours) (source: Dunne & Leopold 1978, used by permission).

Lat	Jan	Feb	Mar	Apr	May	Jun	Jul	Aug	Sep	Oct	Nov	Dec
50°N	265	280	366	415	480	490	495	450	380	330	274	252
40	303	300	370	400	445	450	455	425	375	345	300	290
30	324	314	370	388	425	420	430	410	370	353	320	316
20	341	324	370	378	407	400	410	400	366	360	335	338
10	360	327	370	370	390	380	390	385	366	366	352	356
0	375	340	375	363	375	363	375	375	363	375	363	375
10	388	350	378	355	363	346	360	364	360	380	378	396
20	410	360	378	350	346	328	340	344	360	388	393	414
30	430	370	380	342	330	306	328	345	360	404	410	435
40	466	380	385	334	310	280	302	330	360	415	432	463
50°S	490	403	387	320	276	242	266	315	356	427	465	508

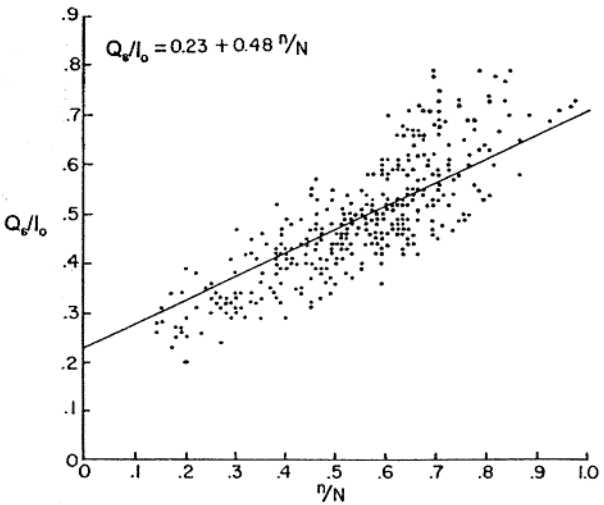

Figure 5.3. Relationship between monthly solar radiation and the percentage of possible sunshine for 32 stations (after Black et al. 1954, used by permission).

Example 5.1

Calculate Q_s and Q_{rs} over a lake on August 8 at 40°N. Do the problem first with clear skies and then assume 40% cloud cover.

For clear skies, obtain I_o from Table 5.2 and $C = 0$:

$$Q_s = I_o(0.803 - 0.340C - 0.458C^2) \qquad \text{(Eq. 5.5)}$$

$$Q_s = 870(0.803)$$

$$Q_s = 698.6 \text{ cal cm}^{-2} \text{ d}^{-1}$$

Assuming 0.07 for water albedo, the reflected energy is:

$$Q_{rs} = 698.6(0.07) = 48.9 \text{ cal cm}^{-2} \text{ d}^{-1} \qquad \text{(Eq. 5.2)}$$

For the condition of 40% cloud cover:

$$Q_s = I_o(0.803 - 0.340C - 0.458\ C^2)$$

$$Q_s = 870\ [0.803 - 0.340(0.40) - 0.458(0.16)]$$

$$Q_s = 516.5 \text{ cal cm}^{-2} \text{ d}^{-1}$$

And reflected energy is:

$$Q_{rs} = 516.5(0.07) = 36.2 \text{ cal cm}^{-2} \text{ d}^{-1}$$

This example uses the same conditions as an example in Bedient & Huber (1992, p. 653). Using List's (1966) method they calculate direct and diffuse radiation separately. Their value for clear skies is Q_s = 728 cal cm^{-2} d^{-1}, which is agreeably close to the value here. For the 40% cloud cover condition, they calculate 652 cal cm^{-2} d^{-1}, which is significantly different from the value calculated here.

$$Q_b = \varepsilon \sigma T^4 \tag{5.7}$$

where Q_b is the total emitted longwave radiation cal cm^{-2} d^{-1}, T is the absolute temperature of the body (°K), σ is the Stefan-Boltzman constant (1.17×10^{-7} cal cm^{-2} °K^{-4} d^{-1}), and ε is the emissivity of the material.

Stefan's Law states that the total radiation emitted by a body is directly proportional to the fourth power of its absolute temperature. This means small changes in temperature produce large changes in the total emitted radiation. A *blackbody* is a theoretical material that is both a perfect absorber and emitter of radiation; however, true blackbodies do not exist. (The term does not refer to the color of the substance.) Emissivity ε ($0 < \varepsilon < 1$) is the ratio of the emittance of a material to the emittance of a blackbody at the same temperature. The emissivity of a blackbody is $\varepsilon = 1.0$. Emissivities of some natural materials are given in Table 5.1. The emissivity of the atmosphere depends upon the amount of water vapor in the air. An equation by Brunt (Hatfield et al. 1983) approximates atmospheric emissivity ε_a as:

$$\varepsilon_a = c + d\sqrt{e_a} \tag{5.8}$$

where the vapor pressure of the air e_a is measured in mb and c and d are empirical constants. Hatfield et al. (1983) found Brunt's values of c = 0.51 and d = 0.066 to work well. Other values for c and d were complied by Anderson (1954) and given in Dunne & Leopold (1978) (see Table 5.5).

Net longwave radiation Q_{lw} was defined in Equation (5.1). Brunt developed empirical equations to estimate net longwave radiation. The first (quoted in Anderson1954) combines Equations (5.7) and (5.8) with a factor that incorporates cloud cover:

Table 5.5. Empirical values for constants in the Brunt equation (source: Dunne & Leopold 1978, Hatfield et al. 1983).

Location	c	d
Sweden	0.43	0.082
Washington, D.C.	0.44	0.061
California	0.50	0.032
England	0.53	0.065
World (Hatfield et al. 1983)	0.51	0.066

$$Q_{lw} = \sigma\left[T_s^4 - \left(c + d\sqrt{e_2}\right)T_2^4\right](1 - aC) \tag{5.9}$$

where T_s is the temperature of the surface (°K), T_2 is air temperature at the 2-meter level (°K), e_2 is the vapor pressure at the 2-meter level (mb), and a is a constant dependent upon cloud type and equals 0.25, 0.60, and 0.90 for high, medium and low clouds, respectively.

A second equation (quoted Chang 1968) is simpler in that it uses only a single temperature measurement at the 2-meter level:

$$Q_{lw} = \sigma T_2^4\left(0.56 - 0.08\sqrt{e_2}\right)(1 - aC) \tag{5.10}$$

If data on cloud type are not available, the factor $(1 - aC)$ may be replaced by either $(0.10 + 0.9C)$ or $(0.10 + 0.90\ n/N)$ (Chang 1968). Equations (5.9) and (5.10) are both fairly crude approximations of net longwave radiation and may only be within 15 to 20% of the actual value over long periods of time (Chang 1968). For example, both equations ignore the emissivity of the water surface and reflected longwave energy (Q_{ar}). The longwave albedo for water and snow is $(1 - \varepsilon)$.

Example 5.2

Calculate the net allwave radiation Q_n for the following conditions.

- Date: August 8
- Latitude: 40°N
- Cloudiness: 40%
- Air temperature at 2 m: 30°C
- Relative humidity: 60%
- Water surface temperature: 20°C.

From Example 5.1:

$$Q_s = 516.5 \text{ cal cm}^{-2} \text{ d}^{-1}$$

$$Q_{rs} = 516.5(0.07) = 36.2 \text{ cal cm}^{-2} \text{ d}^{-1}$$

We use Equation (5.9) with $c = 0.51$ and $d = 0.066$. Since there is no information on cloud type, use $(0.10 + 0.9C)$. Equation (4.3) gives $e_s = 42.4$ mb, and from Equation (4.9), $e_a = 0.6(42.4) = 25.4$ mb. Using these variables, Q_{lw} is calculated as:

$$Q_{lw} = \sigma\ [293^4 - (0.51 + 0.066\sqrt{25.4})303^4]\ [0.10 + 0.90(0.40)]$$

$$Q_{lw} = 14.4 \text{ cal cm}^{-2} \text{ d}^{-1}$$

And net allwave radiation is:

$$Q_n = Q_s - Q_{rs} - Q_{lw}$$

$$Q_n = 516.5 - 36.2 - 14.4 = 465.9 \text{ cal cm}^{-2} \text{ d}^{-1}$$

This example uses the same data as an example in Bedient & Huber (1992, p. 660). In addition to calculating direct and diffuse incoming solar radiation, they determine net longwave radiation by calculating Q_a, Q_{ar} and Q_b separately rather than using Equations (5.9) or (5.10). Bedient and Huber calculate:

$$Q_{lw} = 30 \text{ cal cm}^{-2} \text{ d}^{-1}$$

and

$$Q_n = 576 \text{ cal cm}^{-2} \text{ d}^{-1}$$

Since evaporation is measured and recorded as a depth of water, just like precipitation, we convert net allwave energy into an equivalent depth of water (LT^{-1}). This is done by dividing energy flux by the latent heat of vaporization and water density:

$$E_n = \frac{Q_n}{\rho L_v} \tag{5.11}$$

where E_n is the net energy-based evaporation (cm d^{-1}), Q_n is net allwave energy flux (cal cm^{-2} d^{-1}), ρ is the density of water (g cm^{-3}), and L_v is the latent heat of vaporization (cal g^{-1}).

Example 5.3

A lake has a surface temperature of 10°C, a mass density of 1 g cm^{-3}, and a net allwave energy flux to the surface of Q_n = 465.9 cal cm^{-2} d^{-1} (from Example 5.2). How much water evaporates from the lake per day assuming all the solar radiation is used for evaporation and no other sources of energy are involved?

The latent heat of vaporization L_v is:

$$L_v = 597.3 - 0.564(10) = 591.6 \text{ cal g}^{-1} \qquad \text{(Eq. 4.1)}$$

Equation (5.11) gives energy-based evaporation E_n as:

$$E_n = \frac{\left(465.9 \text{ cal cm}^{-2} \text{ d}^{-1}\right)}{\left(591.6 \text{ cal g}^{-1}\right)\left(1 \text{ g cm}^{-3}\right)}$$

$$E_n = 0.79 \text{ cm d}^{-1}$$

Dimensional analysis shows Equation (5.11) to be dimensionally homogeneous.

$$E_n\left(LT^{-1}\right) = \frac{Q_n\left(MT^{-3}\right)}{L_v\left(L^2T^{-2}\right)\rho\left(ML^{-3}\right)}$$

5.1.3 *Vapor pressure deficit*

Atmospheric vapor pressure is directly proportional to the mass of vapor in the air. Figure 4.2 shows the atmosphere's capacity to hold vapor is a function of its temperature. Water molecules escaping from the water surface into the overlying air produce a vapor pressure proportional to the rate they leave the surface, and the rate is a function of the water's temperature. At the same time the molecules are leaving the surface, vapor in the air re-enters the lake by condensation. Evaporation is thus a *net* mass transfer process; if more molecules leave the water than re-enter, we say evaporation is occurring. If molecules re-enter at the same rate they are leaving, then no (net) evaporation occurs. The difference between the vapor pressure of the atmosphere (e_a) and the vapor pressure of the water surface (e_o) is the vapor pressure deficit ($e_o - e_a$). Evaporation is directly proportional to the vapor pressure deficit – the greater the deficit the greater the rate of evaporation.

5.1.4 *Wind speed*

The third meteorological variable controlling the rate and amount of evaporation is wind speed. Imagine a layer of air over a lake on a calm day. With continued evaporation the air near the surface becomes more humid causing the vapor pressure deficit to decrease. Eventually, dynamic equilibrium is achieved when the air becomes saturated and water molecules leave and re-enter the water surface at the same rate. Wind is important in promoting evaporation by moving the saturated air away from the surface and replacing it with drier air. The importance of wind is obvious to anyone who has used an electric hair drier.

5.2 METHODS FOR ESTIMATING EVAPORATION

Evaporation is not measured directly though new technologies are emerging that allow the direct measurement of vapor flux from the surface. For now we rely primarily on three approaches to estimate evaporation – evaporation pans, continuity equations, and empirical formulae.

5.2.1 *Evaporation pans*

In the United States, the US Weather Bureau Class A evaporation pan is the most widely used. The pan is 4 ft in diameter and 10 inches deep, and is exposed on a wooden platform so that air may freely circulate beneath the pan (Fig. 5.4). Other pan exposures are possible, e.g. sunk in the ground or floating in a lake, but the

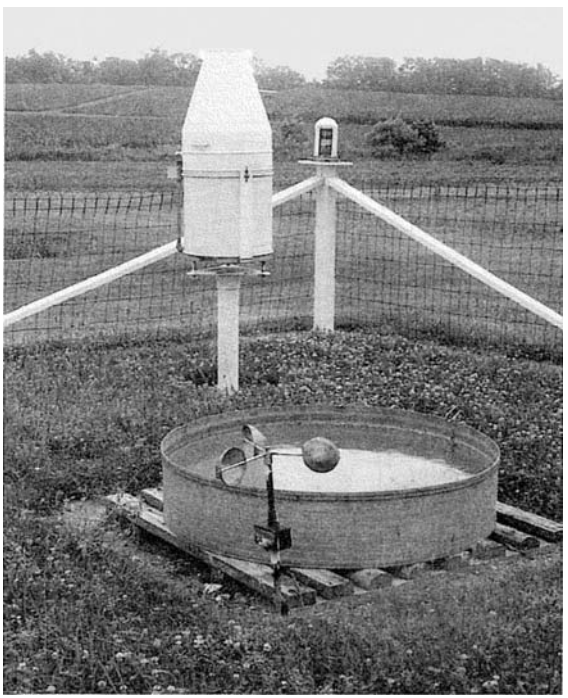

Figure 5.4. A Class A evaporation pan exposed on a platform allowing air to pass beneath the pan. Next to the pan is an anemometer to measure wind speed. In the background are a recording rain gage (inside the large white conical container), and a pyranometer (mounted on the fence post) to measure hemispherical direct and diffuse solar radiation.

platform exposure is the easiest and most trouble free. One method of operation is to fill the pan to a depth of 8 inches and then refill the pan when the water level falls to 7 inches. Measurements are made in a small stilling well located inside the pan. There are other evaporation pans in use in the United States and throughout the world, and each pan has its own characteristic evaporative response. This means that under similar conditions, different pans can evaporate different amounts of water.

When exposed on a platform the Class A pan tends to evaporate more water than a nearby shallow lake. The reason is that energy is conducted through the walls and the bottom of the pan. The smaller volume of water in the pan becomes warmer than the lake, and the warmer water results in increased pan evaporation. A pan coefficient is used to correct for this upward bias in pan evaporation. Evaporation from a lake can be estimated from the pan as:

$$E_o = cE_p \tag{5.12}$$

where E_o is lake evaporation, c is the pan coefficient, and E_p is the measured pan evaporation. The pan coefficient varies by season and location. A widely used value for the *annual* pan coefficient is 0.70. Figure 5.5 was adapted from Farnsworth et al. (1982) and shows isolines for the annual Class A pan coefficient. The coefficient ranges from 0.64 in the hot, dry interior valleys of the Southwest, to greater than 0.80 around the Great Lakes. Figure 5.6 is a map of shallow-lake evaporation in the United States.

Lake evaporation exceeds 100 inches per year in the deserts of southeastern Cali-

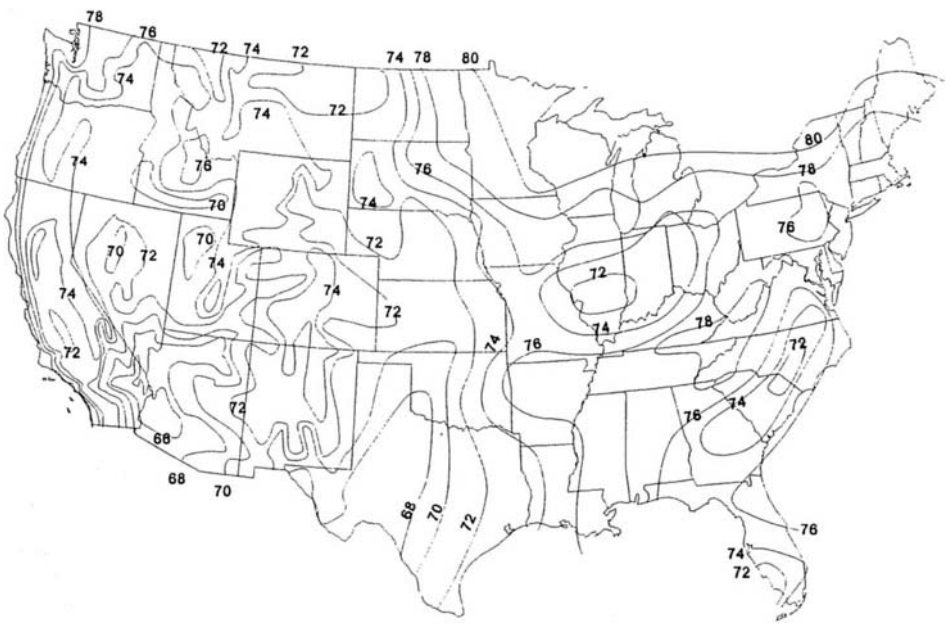

Figure 5.5. Generalized isolines for the annual Class A pan coefficient (adapted from Farnsworth et al. 1982).

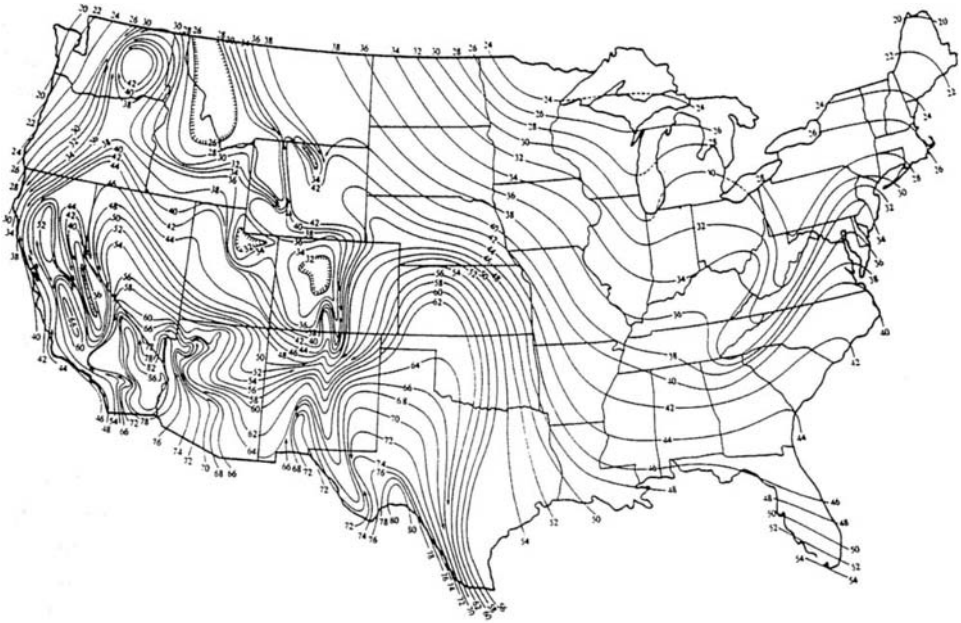

Figure 5.6. Annual average shallow lake evaporation in the United States for the period 1949-1955 (source: Kohler et al. 1959).

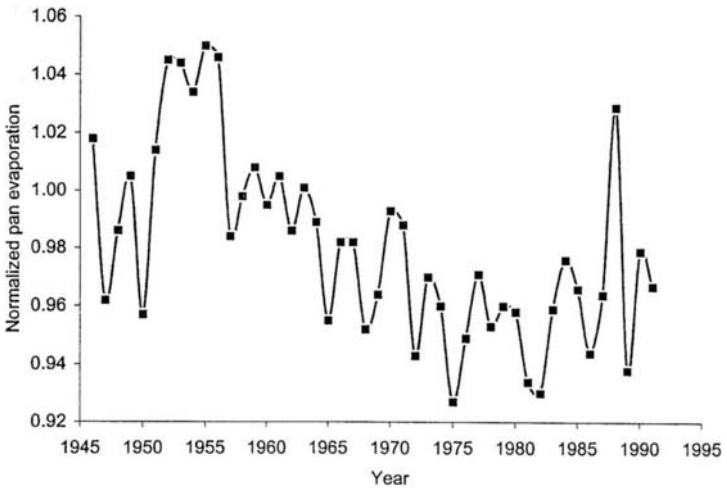

Figure 5.7. Variation in normalized pan evaporation in the United States for the period 1946-1991. Normalized values are values relative to the mean value for the period 1955-1964.

fornia. The pattern is highly variable in the mountain states, but evaporation changes fairly regularly from west to east across the Great Plains. In the eastern United States, evaporation decreases with latitude, with the highest values along the lower Mississippi River and the lowest values following the spine of the Appalachian Mountains into the Northeast. In a study of pan evaporation data for the period 1945

to 1991, the author found pan evaporation in the United States exhibited long-term variation (Fig. 5.7). Pan evaporation reached a maximum during the severe drought of the 1950s, and then decreased for 30 years. Pan evaporation began to increase again in the decade of the 1980s.

5.2.2 *Continuity equations*

5.2.2.1 *Water balance*

Recall that a continuity equation relates inputs, outputs and the amount of the quantity in storage (Eq. 1.1). Lake evaporation can be estimated using either a continuity equation in water (mass balance) or a continuity equation in energy (energy balance). A mass balance equation written for a lake over a given period of time is:

$$(P + I_s + I_g) = (E_o + O_s + O_g) + (S_2 - S_1) \tag{5.13}$$

The terms on the left-hand side represent all of the inputs to the lake – precipitation (P), surface inflows (I_s) and groundwater inflows (I_g). The first set of terms on the right-hand side represent all of the outflow components – evaporation (E_o), surface outflows (O_s) and subsurface outflows (O_g). The term ($S_2 - S_1$) is the change in storage. Equation (5.13) can be rearranged and solved for E_o by measuring all of the inputs, outputs and storage terms. Evaporation is calculated as the residual quantity needed to balance the equation. Equation (5.13) is good in theory but limited in its real-world applicability. The problem is that all measurement errors on the individual components end up in the final estimate of evaporation. Also, some components like subsurface inflows and outflows are difficult to measure. In the United States the most comprehensive set of experiments utilizing this approach were undertaken in the late 1940s and early 1950s at Lake Hefner in Oklahoma. The results of the experiments indicated that the water balance approach was within 5% of actual evaporation one-third of the time, and within 10% two-thirds of the time (Harbeck et al. 1951). While not particularly outstanding, these results are likely to be *better* than expected for most lakes. Lake Hefner was selected from over 100 lakes based on the feasibility of measuring the various water balance components.

5.2.2.2 *Energy balance*

Since evaporation is an energy conversion process, it can be estimated using an energy balance equation. In this case, inputs, outputs and storage of energy are measured, and the energy used for evaporation is the residual energy quantity needed to balance the equation. The energy balance equation is:

$$Q_e = Q_n - Q_h - Q_\theta + Q_v - Q_{ve} \tag{5.14}$$

In Equation (5.14): Q_e is the energy used for evaporation, Q_n is the net allwave radiation, Q_h is sensible heat transferred by conduction and convection to the atmosphere, Q_θ is the change in energy storage within the lake, Q_v is the *net* energy advected into the lake with inflows and outflows of water, and Q_{ve} is the energy that is advected out of the lake along with the evaporated water.

All values in Equation (5.14) are in units of energy flux, e.g. cal cm^{-2} d^{-1}, and are converted into a depth of water using Equation (5.11). A water balance is necessary

with this method also in order to obtain estimates of Q_θ and Q_v. The two terms Q_h and Q_{ve} cannot be measured directly, and must be reformulated in terms of measurable quantities. Like the water balance, the energy balance is good in theory by impractical for everyday use. It suffers the same limitations as the water balance method in that all measurement errors end up in the estimated value of evaporation, and measurement of some components may be even more uncertain than with the water balance.

5.2.3 *Evaporation equations*

Evaporation equations use combinations of the three meteorological factors – solar energy, vapor pressure deficit and wind speed. Two basic approaches are discussed here – the mass transfer/aerodynamic approach, which uses vapor pressure deficit and wind speed, and the so-called 'combination method' which combines solar energy with the mass transfer/aerodynamic method.

5.2.3.1 *Mass transfer/aerodynamic approach*

The mass transfer/aerodynamic approach uses the vapor pressure deficit and wind speed as the two variables for determining evaporation. The method is based on theories of turbulent flux of mass (water vapor) and momentum (wind) from the water surface to the overlying air. Both turbulent fluxes can be described using diffusion-type equations of the general form:

$$\frac{\text{flux of quantity } x}{\text{unit horizontal area}} = \rho K \frac{dx}{dz} \tag{5.15}$$

where ρ is the density of the material x (ML^{-3}), K is a diffusivity constant, and dx/dz is the gradient in the quantity x with altitude z.

Following the discussion of Chow et al. (1988), a diffusion equation for water vapor can be written:

$$m_v = -\rho_a K_w \frac{dq_h}{dz} \tag{5.16}$$

where m_v is the flux of water mass (vapor) per unit horizontal area ($ML^{-2}T^{-1}$), ρ_a is the density of moist air (ML^{-3}), K_w is the eddy diffusivity for vapor (L^2T^{-1}), dq_h/dz is the gradient of specific humidity q_h with altitude z (L^{-1}).

Equation (5.16) says that water vapor diffuses into the overlying air at a rate directly proportional to the gradient in the concentration of water vapor. This is precisely the concept of the vapor pressure deficit discussed earlier. The gradient in specific humidity with altitude is a continuous function. Over short distances it may be approximated as a linear function, $dq_h/dz \approx \Delta q_h/\Delta z \approx (q_{h2} - q_{h1})/(z_2 - z_1)$. The subscripts represent two altitudes where location 2 is higher than location 1. Equation (5.16) has a minus sign because the concentration of water vapor decreases with increasing altitude.

In a similar manner the upward flux of momentum is given by an equation where momentum flux is proportional to the gradient in wind velocity:

$$\tau = \rho_a K_m \frac{du}{dz} \tag{5.17}$$

where τ is the upward momentum flux per unit horizontal area ($ML^{-1}T^{-2}$), K_m is the momentum diffusivity (L^2T^{-1}), du/dz is the wind velocity gradient (T^{-1}).

Again, the true continuous wind velocity profile can be approximated as a linear ratio of the difference between wind speed measured at two altitudes, $du/dz \approx \Delta u/\Delta z \approx (u_2 - u_1)/(z_2 - z_1)$. Dividing Equation (5.16) by Equation (5.17), substituting in the logarithmic velocity profile for wind (Eq. 4.10), and rearranging yields:

$$m_v = \frac{K_w k^2 \rho_a (q_{h1} - q_{h2})(u_2 - u_1)}{K_m \left[\ln(z_2 / z_1)\right]^2} \tag{5.18}$$

where $k \approx 0.40$ is the von Karman constant from the logarithmic wind velocity profile law (Eq. 4.10). Equation (5.18) is the *Thornthwaite-Holzman equation* for vapor transport (Thornthwaite & Holzman 1939). The equation says evaporation can be estimated by measuring specific humidity and wind speed at two heights (z_1 and z_2). While this equation is suitable for scientific research, it is not practical for general application. The equation can be simplified by substituting the roughness length (z_0) for z_1, assuming $K_w/K_m \approx 1.0$, $q_h \approx 622$ (e/p), and that the saturation vapor pressure of the air (e_s) at the ambient air temperature approximates the vapor pressure of the water surface (e_o). Equation (5.19) (Chow et al. 1988) is a simplified version of Equation (5.18):

$$m_v = \frac{0.622 k^2 \rho_a}{p \left[\ln(z_2 / z_0)\right]^2} (e_s - e_a) u_2 \tag{5.19}$$

Mass flux per unit area (m_v) is converted into evaporation (LT^{-1}) by dividing both sides of Equation (5.19) by the density of water (ρ_w). This gives the basic form of the mass transfer/aerodynamic evaporation equation:

$$E_a = b u_2 (e_s - e_a) \tag{5.20}$$

where

$$b = \frac{0.622 k^2 \rho_a}{p \rho_w \left[\ln(z_2 / z_0)\right]^2} \tag{5.21}$$

The constant b has the dimensions of (pressure^{-1}) or ($M^{-1}LT^2$), with time in seconds. The particular form and value of b varies from location to location. The Lake Hefner studies produced a number of empirical equations of the form of Equation (5.20). One such equation with $b = 0.122$ is:

$$E_a = 0.122 u_4 (e_s - e_2) \tag{5.22}$$

where evaporation is in millimeters per day, wind speed is in meters per second, and vapor pressure is in mb. Wind speed is measured at the 4-meter level, and both vapor pressure and wind speed are measured over the lake (Linsley et al. 1982). A more generalized version of the mass transfer/aerodynamic equation is:

$$E_a = (a + bu)(e_s - e_a) \tag{5.23}$$

Example 5.4
Find the value of b and calculate evaporation for the following conditions:
- Height 1 (z_0) = 0.03 cm
- Height 2 (z_2) = 2 m
- Von Karman constant k = 0.40
- Water temperature = 25°C, thus ρ_w = 997 kg m^{-3}
- Air temperature = 25°C, thus ρ_a = 1.19 kg m^{-3}
- Atmospheric pressure (p) = 1013 mb
- Wind speed (u) = 1.8 m s^{-1}
- Relative humidity = 40%

First, calculate b as:

$$b = \frac{0.622(0.4)^2\,1.19}{997(1013)\left[\ln(2/0.0003)\right]^2} \qquad \text{(Eq. 5.21)}$$

$$b = 1.512 \times 10^{-9}$$

To facilitate direct comparison with Equation (5.22), convert b from the current units of meters and seconds to units of millimeters and days:

$$b = 1.512 \times 10^{-9} \times \frac{1000\text{ mm}}{1\text{ m}} \times \frac{86400\text{ s}}{1\text{ d}}$$

$$b = 0.131$$

Assuming the saturation vapor pressure of the air at 25°C closely approximates the saturation vapor pressure of the water surface at the same temperature ($e_s = e_o$), then:

$$e_s = 31.66 \qquad \text{(Eq. 4.3)}$$

$$e_a = 0.4(31.66) = 12.66 \qquad \text{(Eq. 4.9)}$$

and

$$E_o = 0.131(1.8)(19.00) \qquad \text{(Eq. 5.20)}$$

$$E_o = 4.5 \text{ mm d}^{-1}$$

5.2.3.2 *Combination approach*

Combination equations combine net energy (Eq. 5.11) and the mass transfer/aerodynamic approach (Eq. 5.23) into a single equation. The most popular combination equation is Penman's equation (1948). Penman was trying to predict *evapotranspiration* using a small sunken pan. Starting with Equation (5.14), $Q_e = Q_n - Q_h - Q_\theta + Q_v - Q_{ve}$, the last three terms ($Q_\theta$, Q_v, Q_{ve}) were either equal to zero or were small enough to be ignored for a sunken pan. The remaining energy terms are restated as:

$$Q_n = Q_e + Q_h \tag{5.24}$$

In other words, net allwave radiation either goes to evaporate water (latent heat), or it goes to heat the overlying air (sensible heat). Equation (5.24) ignores energy used to heat the soil. This omission is acceptable over a period of a day, since the energy that

goes into the soil during the daytime hours is radiated back to the atmosphere at night. Converting the terms in Equation (5.24) into equivalent depths of water yields:

$$E_n = E_o + K \tag{5.25}$$

By rearranging Equation (5.25), adding the mass transfer/aerodynamic component (E_a), and 'fixing up' the K term, the Penman equation may be written:

$$E_o = \frac{\Delta}{\Delta+\gamma} E_n + \frac{\gamma}{\Delta+\gamma} E_a \tag{5.26}$$

where E_o is lake evaporation in cm d^{-1}, E_n is net allwave radiation expressed in units of cm d^{-1} (Eq. 5.11), E_a is mass transfer/aerodynamic evaporation in cm d^{-1} (Eq. 5.23), Δ is the slope of the e_s versus temperature curve (Eq. 4.4), and γ is the *psychometric constant* (assumed to be 0.66 mb°C^{-1}).

Dunne & Leopold (1978) give one form of the mass transfer/aerodynamic component as:

$$E_a = (0.013 + 0.00016u_2)(e_s - e_a) \tag{5.27}$$

where E_a is evaporation in cm d^{-1}, u_2 is wind speed in kilometers per day at the 2–meter level, e_s and e_a are in mb (where again e_s approximates e_o).

The coefficients in Equation (5.27) are generic, and local calibration is recommended for improved accuracy. The Penman equation consists of two parts: the energy term and the mass transfer/aerodynamic term. The relative importance of each term depends upon the values of the dimensionless weighting factors $\Delta / (\Delta + \gamma)$ and $\gamma / (\Delta + \gamma)$. The sum of these two weighting factors is 1.0. As air temperature rises, the increase in Δ (see Fig. 4.2) increases the relative importance of the energy term (E_n) by more rapidly increasing the weighting factor $\Delta / (\Delta + \gamma)$.

Example 5.5

Calculate evaporation using the Penman equation for the following conditions:

- Net allwave radiation = 465.9 cal cm^{-2} d^{-1}
- Air temperature = 25°C
- Relative humidity = 40%
- Wind speed (u) = 110 km d^{-1}

The weighting factors are:

$\Delta = (0.00815T + 0.8912)^7$ (Eq. 4.4)

$\Delta = 1.88$

$\Delta / (\Delta + \gamma) = 1.88 / (1.88 + 0.66) = 0.74$

$\gamma / (\Delta + \gamma) = 0.66 / (1.88 + 0.66) = 0.26$

(Note $0.74 + 0.26 = 1.0$)

From Example 5.3, the equivalent depth of evaporation from net allwave radiation is:

$E_n = 0.79$ cm d^{-1}

The mass transfer/aerodynamic contribution is:

$E_a = (0.013 + 0.00016u_2)(e_s - e_a)$ (Eq. 5.27)

$E_a = [0.013 + 0.00016(110)](18.99)$

$$E_a = 0.58 \text{ cm d}^{-1}$$

And, finally, from the Penman equation:

$$E_o = \frac{\Delta}{\Delta + \gamma} E_n + \frac{\gamma}{\Delta + \gamma} E_a$$

$$E_o = 0.74(0.79) + 0.26(0.58)$$

$$E_o = 0.73 \text{ cm d}^{-1}$$

Dunne & Leopold (1978) give an alternate form of the Penman equation that combines the two weighting factors into a single factor, thus offering a slight computational advantage:

$$E_o = \frac{(\Delta/\gamma)E_n + E_a}{(\Delta/\gamma) + 1} \tag{5.28}$$

The Penman method is one of the most accurate of the meteorologically-based formulas. The equation is largely based on physical principles, and, according to Chang (1968), should not be regarded as an empirical formula. It is, however, data intensive and few areas have all the necessary input data. Priestley & Taylor (1972) found that the second term $E_a(\gamma / (\Delta + \gamma)$ is approximately 30% of the first term (in Example 5.5 the second term is 26% of the first). Taking 30% as the average value they developed the *Priestley-Taylor* equation:

$$E_o = \alpha \frac{\Delta}{\Delta + \gamma} E_n \tag{5.29}$$

where $\alpha = 1.3$. Using the Priestley-Taylor equation with the data from Example 5.5, $E_o = 1.3(0.74)(0.79) = 0.75$ cm d^{-1}. The Priestley-Taylor equation is more applicable to humid environments than arid environments.

The coaxial relationship in Figure 5.8 was developed by correlating pan evaporation data and the Penman equation. To use the figure first determine the aerodynamic component E_a by using the small figure in the upper left corner of the diagram. Enter the small figure with mean daily temperature and proceed to the right until you reach the curve for the mean daily dew point temperature. Turn down at the dew point curve and go until you intersect the appropriate wind movement curve. Turn right and exit the figure with a value for E_a. Now enter the main diagram on the right side with mean daily air temperature, and proceed in the same manner.

SUMMARY

Evaporation drives the hydrologic cycle. In this chapter we examined the meteorological variables that control evaporation from shallow lakes. Evaporation is not measured directly as is precipitation, but we rely instead on evaporation pans and meterologically-based equations to estimate evaporation. The two basic approaches of the meteorologically-based equations are the mass transfer/aerodynamic approach and the combination approach, which combines an energy term with a mass transfer term. The Penman equation is the best known of the combination equations and is one of the most accurate methods of estimating evaporation. In Chapter 6 we look at

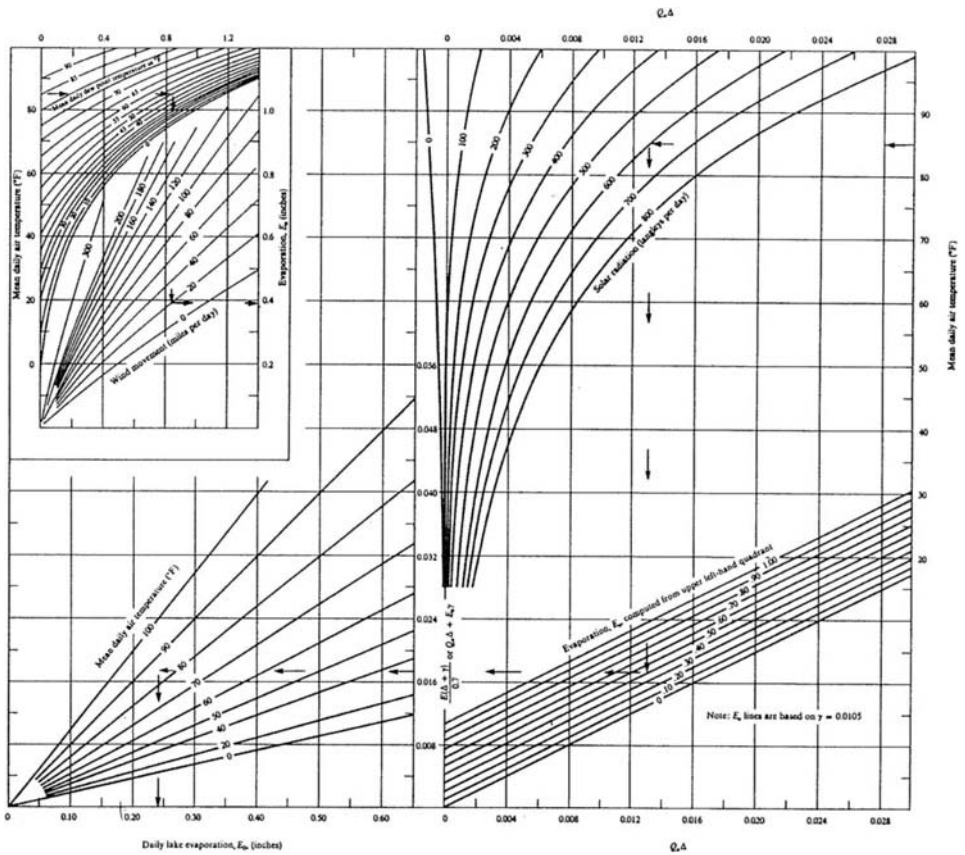

Figure 5.8. Coaxial relationship for solving the Penman equation (source: Kohler et al. 1955).

evapotranspiration. We will see the Penman equation again as one of the methods used to estimate evapotranspiration.

PROBLEMS

5.1 Given below are mean values for the Little Rock, Arkansas station located at 34°44′N.

Month	Cloud cover (decimal fraction)	Possible sunshine (%)	Air temperature (°F)	Relative humidity (%)
Jan.	0.65	46	39.9	70
Feb.	0.60	54	44.0	67
Mar.	0.62	57	52.2	65
Apr.	0.61	62	62.4	67
May	0.60	68	70.5	71
Jun.	0.54	73	78.5	70

Month	Cloud cover (decimal fraction)	Possible sunshine (%)	Air temperature (°F)	Relative humidity (%)
Jul.	0.55	71	82.1	72
Aug.	0.50	73	81.0	71
Sep.	0.52	68	74.3	74
Oct.	0.45	69	63.1	71
Nov.	0.55	56	51.2	71
Dec.	0.62	48	43.2	71

Calculate Q_s, Q_{lw}, Q_n over water for January and June. Do the calculations using both Equation (5.5) and (5.6).
(For your information, the mean measured value for Q_s for the month January is 198 cal cm^{-2} d^{-1}, and for June Q_s = 568 cal cm^{-2} d^{-1})

5.2 Use the data below and calculate average daily evaporation for June at Little Rock, Arkansas by the Penman method. Calculate evaporation first with Q_n estimated from Equation (5.5) and then with Q_n estimated from Equation (5.6).
(For your information, the average daily pan evaporation at Hope, Arkansas is 0.22 in d^{-1})

June data:
Q_n using Equation (5.5) = 346 cal cm^{-2} d^{-1}
Q_n using Equation (5.6) = 462 cal cm^{-2} d^{-1}

2-meter wind speed = 7.4 mph
monthly temperature 78.5°F
humidity = 70%

What does the Priestly-Taylor equation give for this same problem?

5.3 Use the following data and determine daily lake evaporation from text Figure 5-8.
Mean daily air temperature 25°C
Mean daily dew point temperature 13°C
Mean daily wind speed 100 km d^{-1}
Mean daily solar radiation 470 langleys d^{-1}

5.4 At a consumption rate of 150 gallons per person per day, how large a population could be supplied from the *net* annual loss (evaporation – precipitation) from a 150,000 acre reservoir located in the Four Corners area of the United States.

CHAPTER 6

Evapotranspiration

Evaporation from wet leaves and soil, water ponded on the surface, and transpiration from vegetation are combined as the single process of evapotranspiration. Evapotranspiration is a major component of the water balance of a drainage basin. Transpiration is the process whereby soil water, absorbed through plant roots, flows up through the vascular channels (xylem cells), and escapes to the atmosphere through stomata on the leaf surface. Irrigation planning and management historically has been concerned with estimating and meeting the evapotranspiration requirements (consumptive use) of different crops. In this chapter we discuss the factors that control evapotranspiration, some of the methods used for its estimation, and modeling evapotranspiration under conditions of limited soil moisture.

6.1 THE EVAPOTRANSPIRATION PROCESS

As with evaporation, evapotranspiration is strongly related to climatic conditions. Transpiration increases primarily with increasing net allwave energy and secondarily with air temperature when soil moisture is not limiting and the vegetation completely covers the ground. As discussed below, when these conditions exist it is sometimes assumed that evapotranspiration proceeds at a rate indistinguishable from the rate of evaporation from a free-water surface. However, there are factors that change the rate of evapotranspiration relative to the rate of evaporation. These factors fall into 2 groups:

1. Soil-related factors, and
2. Vegetation-related factors.

Soil factors include soil moisture content and soil texture. Vegetation factors are related to the type and age of the vegetation.

6.1.1 *Soil factors*

To understand how soil factors affect evapotranspiration we can distinguish the concepts of *potential evapotranspiration* and *actual evapotranspiration*. The concept of potential evapotranspiration E_{tp} was first proposed by the geographer C.W. Thornthwaite (1948). He defined potential evapotranspiration as the rate of evapotranspiration from a spatially-extensive vegetated surface having uniform physiological and structural characteristics, given the condition of unlimited soil moisture. Defined in

this way potential evapotranspiration minimizes the role of the vegetation and is essentially an energy-based concept. Potential evapotranspiration has often been considered identical to evaporation from a free-water surface. However, as the soil dries plants must exert a greater suctional force through their roots in order to extract soil moisture. The generally accepted upper limit for the suctional force exerted by plants is a pressure of around 15 bars (1 bar equals 1000 mb). The logical conclusion is that evapotranspiration decreases as the soil dries, and the actual evapotranspiration rate E_t falls below the potential rate E_{tp}. While this is generally true, the process is complex, and exactly how evapotranspiration changes as a function of soil moisture is still subject to debate. One view is that evapotranspiration and soil moisture are linearly related with evapotranspiration decreasing (increasing) in direct proportion to decreasing (increasing) soil moisture (Fig. 6.1). In Figure 6.1 *AW* represents the available water in the soil. The *AWC* is the available water capacity of the soil – the maximum amount of water the soil can hold. These are discussed in more detail later in the chapter. An alternate view is that evapotranspiration continues at or near the potential rate as the soil dries, and it is not until soil moisture approaches the *permanent wilting point* (also explained later) that actual evapotranspiration begins to fall below the potential rate. These two views most likely define boundaries within which E_t falls depending upon the type of soil and vegetation involved.

Soil texture influences E_t through its affect on the strength of the attractive force between soil particles and soil water. The strength of attraction depends upon the size of the soil pores and the curvature of the soil-water interface (Skaggs 1980). For a given soil moisture content, fine-texture (clay) soils with small pores hold water with a stronger 'tensional force' than coarse-texture (sand) soils with larger pores. Plants in clayey soils must work harder to extract water. To the extent that soil moisture is a controlling factor, E_t drops below E_{tp} sooner for plants rooted in clayey soils than for plants rooted in sandy soils (Fig. 6.2).

In a recent study using data from the First ISLSCP Field Experiment (FIFI), Chen & Brutsaert (1994) examined soil moisture and vegetative cover as controls on latent heat flux. (ISLSCP stands for the International Satellite Land Surface Climatology Program.) They found that the relative strength of vegetation versus soil moisture in

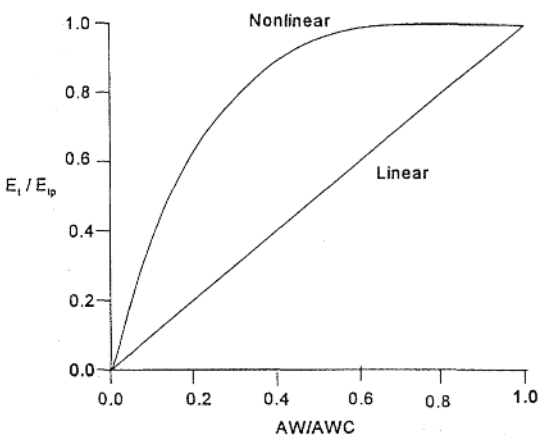

Figure 6.1. Curves showing the possible changes in evapotranspiration as a function of soil moisture (after Dunne & Leopold 1978).

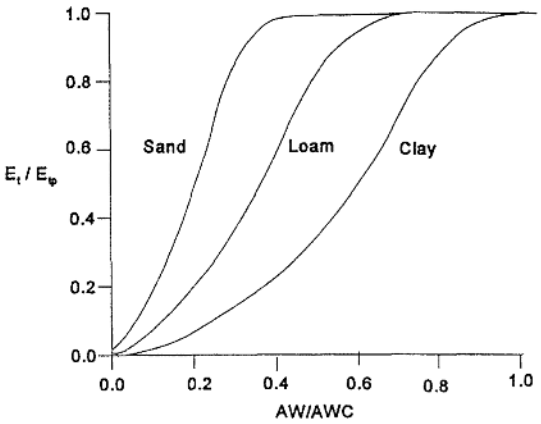

Figure 6.2. Possible relationship between evapotranspiration and soil texture. Evapotranspiration decreases more quickly with finer texture soils (after Dunne & Leopold 1978).

controlling latent heat flux depended upon soil moisture content and its distribution. When average soil moisture was high, defined as greater than 27%, evaporation was uniform over the region regardless of the uniformity of vegetation. For intermediate soil moisture conditions, between 20 and 27%, vegetation and soil moisture alternated as the primary control: vegetation played the dominant role if moisture was uniformly distributed, and soil moisture exerted the dominant control when it was not. For moisture conditions of less than 20%, soil moisture was usually nonuniform and was the primary factor controlling latent heat flux.

6.1.2 *Vegetative factors*

Plant-related factors that influence E_t include the density and depth of the root system, differential stomatal resistance, plant age, height and color. Plant root density is typically greatest near the surface with perhaps 40% of the total root system found in the upper 25% of the root zone. Plants with dense root systems extract moisture more efficiently since water does not have to travel as far to reach the roots. Because the upper soil zone is depleted of water sooner than lower zones, shallow-rooted plants may experience water stress and a reduction in E_t sooner than deep-rooted plants.

Water molecules exiting the moist cell walls inside the leaf do not exit directly to the atmosphere; rather, they enter intercellular spaces within the leaf. It is from within these intercellular spaces that vapor diffuses to the atmosphere. This additional step whereby water molecules move from the plant cells to the intercellular spaces is called stomatal resistance (r_s). Stomatal resistance differs with the type of plant as well as with soil moisture levels. The movement of vapor from the intercellular spaces to the atmosphere is called aerodynamic resistance (r_a), and is governed mainly by wind speed and turbulence. Plants are able to control transpiration to some extent by opening and closing stomata. During periods of extreme transpiration demand, and/or when soil moisture becomes low, leaf dehydration reduces turgor pressure, and stomatal apertures close in an effort to limit transpiration. Plant color also plays a role – dark plants absorb more energy resulting in higher leaf temperatures and increased transpiration.

Plant-related factors differ between different types of plants, and they can change

over time for the same plant. This is especially true of annual crops that change leaf area, height, root density, albedo, and respiration rate throughout the growing season. Accounting for intraseasonal changes in crop plants is done with the use of crop coefficients. The use of crop coefficients is explained in the section on estimating evapotranspiration.

One other factor that can greatly affect E_t is the advection of warm air into the vegetation. This is important in arid and semi-arid environments where a relatively small area of well-watered vegetation is surrounded by hot, dry desert conditions. Examples would be natural riparian communities and irrigated fields in dry climates. Large quantities of sensible heat are advected from the hot, upwind desert into the vegetation. This additional sensible heat can drive E_t values *above* E_{tp} levels determined solely by net allwave energy. This is the 'oasis' effect.

6.2 METHODS FOR ESTIMATION EVAPOTRANSPIRATION

Methods for determining evapotranspiration include a water balance, lysimeters and meteorologically-based equations. Evapotranspiration equations range from the completely empirical to more physically-based approaches.

6.2.1 *Water balance*

As with evaporation, a continuity equation in water can be written for a specific volume over a specified period of time. For evaporation the volume was a shallow lake. By measuring inflows, outflows and storage, evaporation was determined as the residual quantity needed to balance the continuity equation. Evapotranspiration can be determined using the same approach. In this case the volume might be a drainage basin or an agricultural field. For a drainage basin, precipitation, streamflow and groundwater flows would be measured. Groundwater flows in or out of the basin beneath the surface divide must to be estimated, along with the amount of water stored in the soil, lakes and as groundwater. The major problem with this approach again is that all measurement errors accumulate in the final estimate of E_t. Over a sufficiently long period of time, the change in storage terms balance to zero, and for basins where cross-divide flows of groundwater are unimportant, reasonably accurate estimates of annual evapotranspiration can be obtained by subtracting annual streamflow volumes from annual precipitation.

6.2.2 *Lysimeters*

Lysimeters are soil-filled tanks buried flush with the ground. They should be planted to the same type of vegetation as that found in the surrounding area. Lysimeters operate on the continuity principle but they provide considerably more control over the measurement of inputs, outputs and storage. The two basic types are the nonweighing and weighing lysimeter. The nonweighing lysimeter evaluates evapotranspiration as the difference between inputs (precipitation and irrigation) and output (drainage water). This device does not measure soil moisture and should only be used in situations where the change in soil moisture storage is negligible. The weighing lysimeter

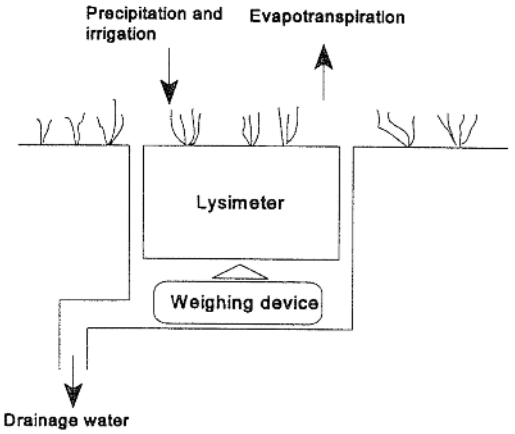

Figure 6.3. A simplified diagram of a weighing lysimeter for measuring evapotranspiration.

uses either some type of scale or manometers to weigh the soil, allowing the determination of the change in soil moisture storage from the change in the weight of the device (Fig. 6.3). The weighing lysimeter thus allows evaluation of all the water balance components. Lysimeters can be operated to give estimates of either E_{tp} or E_t, depending upon whether they are irrigated. If the lysimeter is irrigated so that soil moisture is always sufficient, it yields estimates of E_{tp}. If it is not irrigated, then soil moisture follows the natural wetting and drying regime and the lysimeter evaluates E_t.

6.2.3 *Potential evapotranspiration equations*

Numerous equations have been developed to estimate potential evapotranspiration. These equations use combinations of meteorologic variables in addition to plant information to estimate E_{tp}. The following 5 methods, roughly listed in order of increasing complexity, are discussed here:

1. Thornthwaite,
2. Blaney-Criddle,
3. Modified Jensen-Haise,
4. Penman, and
5. Penman-Monteith.

The Thornthwaite and the Blaney-Criddle methods are the simplest and use air temperature as the primary independent variable for determining E_{tp}. The Modified Jensen-Haise method is more sophisticated; in addition to air temperature, it uses solar energy and an approximate measure of vapor pressure deficit. The most comprehensive methods are based on the Penman equation. However, as we have already seen, the more sophisticated the method the more data required. The user must weigh the benefits of increased accuracy against the costs of gathering the requisite data. For the best results, these equations, with the exception of the Thornthwaite method, should be calibrated for local conditions.

6.2.3.1 *The Thornthwaite method*

The Thornthwaite method uses average monthly air temperature as the primary vari-

able for estimating potential evapotranspiration. This is the basis for its widespread appeal as well as its major criticism. Because average monthly temperature data are widely available, the method is easily applied to many areas. But using air temperature alone to estimate evapotranspiration has a tradeoff in accuracy. One of the assumptions of the method is that Q_n is partitioned in constant proportion between sensible heat and latent heat (Eq. 5.24). Another criticism of the method is that it assumes no E_{tp} for temperatures at or below 0°C, which is not true. Finally, there is no adjustment made for different plant types. The Thornthwaite equation gives monthly E_{tp} estimates, though these monthly values are sometimes subdivided into crude estimates of weekly or daily E_{tp}. Thornthwaite's empirical equation is:

$$E'_{tp} = 1.6\left(\frac{10T_a}{I}\right)^a \tag{6.1}$$

where E'_{tp} = *unadjusted* potential evapotranspiration (cm mo^{-1}), T_a = mean monthly temperature (°C), and I = annual heat index and is given by the equation:

$$I = \sum_{i=1}^{n}\left(\frac{T_{ai}}{5}\right)^{1.5}, \quad \text{for} \quad T_{ai} > 0°\text{C} \tag{6.2}$$

$$a = 0.49 + 0.0179I - 0.000077I^2 + 0.000000675I^3 \tag{6.3}$$

The unadjusted E'_{tp} from Equation (6.1) is for a standard month with 360 hours of daylight. The unadjusted value must be corrected for the varying length of day with latitude using the appropriate correction factor from Table 6.1.

Example 6.1

Given in Table 6.2 are climatological and environmental data for Salt Lake City, Utah. Calculate average E_{tp} for the month of May (14.9°C) using the Thornthwaite method. First, calculate the annual heat index I with Equation (6.2). Since the months of January and December have mean monthly temperatures less than 0°C, n = 10 and we use February through November to calculate the annual heat index:

$$I = [(1.1/5)^{1.5} + (4.8/5)^{1.5} + \ldots + (11.7/5)^{1.5} + (4.3/5)^{1.5}]$$

$$I = 50.05$$

Calculate the coefficient a using Equation (6.3):

$$a = 0.49 + 0.0179(50.05) - 0.000077(50.05)^2 + 0.000000675(50.05)^3$$

$$a = 1.28$$

Calculate unadjusted potential evapotranspiration E'_{tp} for May with Equation (6.1):

$$E'_{tp} = 1.6\left(\frac{10(14.9)}{50.05}\right)^{1.28} = 6.5 \text{ cm mo}^{-1}$$

The last step is to correct the unadjusted value using the appropriate factor from Table 6.1. For May at 40.7°N the factor is 1.20:

$$E_{tp} = 6.5(1.20) = 7.7 \text{ cm mo}^{-1}$$

Table 6.1. Factors for correcting unadjusted potental evapotranspiration by the Thornthwaite method (source: Dunne & Leopold 1978, used by permisson).

Lat.	Jan	Feb	Mar	Apr	May	Jun	Jul	Aug	Sep	Oct	Nov	Dec
60°N	0.54	0.67	0.97	1.19	1.33	1.56	1.55	1.33	1.07	0.84	0.58	0.48
50	0.71	0.84	0.98	1.14	1.28	1.36	1.33	1.21	1.06	0.90	0.76	0.68
40	0.80	0.89	0.99	1.10	1.20	1.25	1.23	1.15	1.04	0.93	0.83	0.78
30	0.87	0.93	1.00	1.07	1.14	1.17	1.16	1.11	1.03	0.96	0.89	0.85
20	0.92	0.96	1.00	1.05	1.09	1.11	1.10	1.07	1.02	0.98	0.93	0.91
10	0.97	0.98	1.00	1.03	1.05	1.06	1.05	1.04	1.02	0.99	0.97	0.96
0	1.00	1.00	1.00	1.00	1.00	1.00	1.00	1.00	1.00	1.00	1.00	1.00
10	1.05	1.04	1.02	0.99	0.97	0.96	0.97	0.98	1.00	1.03	1.05	1.06
20	1.10	1.07	1.02	0.98	0.93	0.91	0.92	0.96	1.00	1.05	1.09	1.11
30	1.16	1.11	1.03	0.96	0.89	0.85	0.87	0.93	1.00	1.07	1.14	1.17
40	1.23	1.15	1.04	0.93	0.83	0.78	0.80	0.89	0.99	1.10	1.20	1.25
50°S	1.33	1.19	1.05	0.89	0.75	0.68	0.70	0.82	0.97	1.13	1.27	1.36

Table 6.2. Normal monthly temperatures for Salt Lake City, UT.

	Minimum		Average		Maximum	
	°F	°C	°F	°C	°F	°C
Jan	19.7	–6.8	28.6	–1.9	37.4	3.0
Feb	24.4	–4.2	34.0	1.1	43.7	6.5
Mar	29.9	–1.2	40.7	4.8	51.5	10.8
Apr	37.2	2.9	49.2	9.6	61.1	16.2
May	45.2	7.3	58.8	14.9	72.4	22.4
Jun	53.3	11.8	68.3	20.2	83.3	28.5
Jul	61.8	16.6	77.5	25.3	93.2	34.0
Aug	59.7	15.4	74.8	23.8	90.0	32.2
Sep	50.0	10.0	65.0	18.3	80.0	26.7
Oct	39.3	4.1	53.0	11.7	66.7	19.3
Nov	29.2	–1.6	39.7	4.3	50.2	10.1
Dec	21.6	–5.8	30.3	–0.9	38.9	3.8

Latitude = 40.7°N; Station elevation = 1288 m.

6.2.3.2 *The Blaney-Criddle method*

H.F. Blaney and W.D. Criddle developed their method for calculating crop 'consumptive use' in the 1940s on the suggestion of geographer H.H. Barrows (White 1987). The method is based on correlations between crop consumptive-use data from the western United States, and monthly mean temperatures and the percentage of daytime hours (Blaney 1955). The original version of the Blaney-Criddle method has undergone numerous revisions with the SCS (1970) version one of the most popular. One of the more recent revisions of the Blaney-Criddle method was produced by the Food and Agricultural Organization (FAO) (Doorenbos & Pruitt 1977). The original Blaney-Criddle method, and the SCS modification, should only be used with data from the western United States. The FAO version is intended to be used internationally. The original Blaney-Criddle equation is:

$$E_{tp} = k\frac{T_a p}{100} \tag{6.4}$$

where E_{tp} = crop evapotranspiration (consumptive use) (in mo^{-1}), T_a = mean monthly air temperature (°F), k = crop consumptive use coefficient, p = monthly daytime hours given as a percent of the year.

Notice that the original method uses temperature in °F and calculates E_{tp} in inches per month. Table 6.3 gives k values for different crops measured throughout the western United States. Values of p by month and latitude are given in Table 6.4.

Table 6.3. Consumptive use coefficients for use with the original Blaney-Criddle method (source: Blaney 1959, Blaney et al. 1960)

Crop	Location	Mar	Apr	May	Jun	Jul	Aug	Sep	Oct	Nov
Alfalfa	CA, coastal	0.60	0.65	0.70	0.80	0.85	0.85	0.80	0.70	0.60
	CA, interior	0.65	0.70	0.80	0.90	1.10	1.00	0.85	0.80	0.70
	ND	–	0.84	0.89	1.00	0.86	0.78	0.72	–	–
	UT, St. George	–	0.88	1.15	1.24	0.97	0.87	0.81	–	–
	NM	0.70	0.75	0.80	0.90	1.00	1.00	0.80	0.70	0.65
Beans	NM	–	–	0.50	0.60	0.75	0.70	–	–	–
Corn	ND	–	–	0.47	0.63	0.78	0.79	0.70	–	–
	NM	–	–	0.50	0.70	0.80	0.80	0.70	–	–
Cotton	AZ	–	0.27	0.30	0.49	0.86	1.04	1.03	0.81	–
	NM	–	0.35	0.40	0.60	0.90	1.00	0.95	0.75	–
Citrus	AZ	0.57	0.60	0.60	0.64	0.64	0.68	0.68	0.65	0.62
Orchard	CA, coastal	–	0.40	0.42	0.52	0.55	0.55	0.55	0.50	0.45
Pasture	CA	–	–	0.84	0.84	0.77	0.82	1.09	0.70	–
Potatoes	ND	–	0.45	0.74	0.87	0.75	0.54	–	–	–
	SD	–	0.69	0.60	0.80	0.89	0.39	–	–	–
Small	ND	–	0.19	0.55	1.13	0.77	0.30	–	–	–
Grains	NM	–	0.40	0.50	0.90	0.80	–	–	–	–
Truck crops	CA, interior	0.19	0.26	0.38	0.55	0.71	0.82	0.69	0.37	0.35

Table 6.4. Percentage of daytime hours p for each month of the year for use with the Blaney-Criddle method (source: Chow 1964, used by permission).

Lat.	Jan	Feb	Mar	Apr	May	Jun	Jul	Aug	Sep	Oct	Nov	Dec
60°N	4.67	5.65	8.08	9.65	11.74	12.39	12.31	10.70	8.57	6.98	5.04	4.22
50	5.98	6.30	8.24	9.24	10.68	10.91	10.99	10.00	8.46	7.45	6.10	5.65
40	6.76	6.72	8.33	8.95	10.02	10.08	10.22	9.54	8.39	7.75	6.72	6.52
30	7.30	7.03	8.38	8.72	9.53	9.49	9.67	9.22	8.33	7.99	7.19	7.15
20	7.74	7.25	8.41	8.52	9.15	9.00	9.25	8.96	8.30	8.18	7.58	7.66
10	8.13	7.47	8.45	8.37	8.81	8.60	8.86	8.71	8.25	8.34	7.91	8.10
0	8.50	7.66	8.49	8.21	8.50	8.22	8.50	8.49	8.21	8.50	8.22	8.50
10	8.86	7.87	8.53	8.09	8.18	7.86	8.14	8.27	8.17	8.62	8.53	8.88
20	9.24	8.09	8.57	7.94	7.85	7.43	7.76	8.03	8.13	8.76	8.87	9.33
30	9.70	8.33	8.62	7.73	7.45	6.96	7.31	7.76	8.07	8.97	9.24	9.85
40°S	10.27	8.63	8.67	7.49	6.97	6.37	6.76	7.41	8.02	9.21	9.71	10.49

Example 6.2
Calculate the consumptive use for alfalfa in the vicinity of Salt Lake City using the Blaney-Criddle method. Alfalfa is a perennial crop. On average, alfalfa begins growing when the aver-

age air temperature reaches 50°F (10°C) and stops with the first frost. We will use the k values for St. George, however, they may not be representative of Salt Lake City farther to the north. The growing season for alfalfa is assumed to be April through September since coefficients have been determined for these months.

Month	T_a (°F)	p	k	E_{tp} (in.)	(cm)
April	49.2	8.95	0.88	3.9	9.8
May	58.8	10.02	1.15	6.8	17.2
June	68.3	10.08	1.24	8.5	21.7
July	77.5	10.22	0.97	7.7	19.5
Aug.	74.8	9.54	0.87	6.2	15.7
Sept.	65.0	8.39	0.81	4.4	11.2
Total				37.5	95.1

The Blaney-Criddle method calculates a value of 6.8 inches (17.2 cm) for the month of May. Compare this to the Thornthwaite method which yielded only 7.7 cm.

Reference crop evapotranspiration

Recently, the concept of potential evapotranspiration has been replaced by the concept of *reference crop evapotranspiration*. This evolution recognizes the fact that there really is not a single E_{tp} value, but that different crops transpire water at different potential rates. Alfalfa, for example, transpires about 15% more water than does short grass under the same climate and soil moisture conditions. Alfalfa and short grass are the two crops that have been used as reference crops. Reference crop evapotranspiration for alfalfa is designated E_{tr}, while reference crop evapotranspiration based on short grass is designated E_{to}. Alfalfa-based crop coefficients are calculated as:

$$k_c = \frac{E_t}{E_{tr}} \tag{6.5}$$

where k_c is the dimensionless crop coefficient for a particular crop at a particular stage of growth, and E_t is evapotranspiration for the same crop (Burman et al. 1980). Figure 6.4 is a generalized crop coefficient curve. The curve shows E_t increasing with emergence and rapid growth, peaking at full cover, and decreasing as the crop goes through maturation and senescence late in the growing season. The Jensen-Haise and the Penman methods are suitable for use with alfalfa-based crop coefficients. The analyst must be careful to use crop coefficients appropriate for the particular evapotranspiration formula. The Blaney-Criddle consumptive use crop coefficients in Table 6.3 cannot be used with any other method. The FAO version of the Blaney-Criddle method calculates reference crop evapotranspiration for grass (E_{to}), so grass-based crop coefficients must be used. The alfalfa-based coefficients given in Table 6.5 are appropriate for use in an arid, inter-mountain climate like that found throughout most of the western United States. The coefficients in Table 6.5 are called 'basal crop coefficients' because they assume the soil surface is dry. During and immediately following an irrigation the surface is wet and evapotranspiration

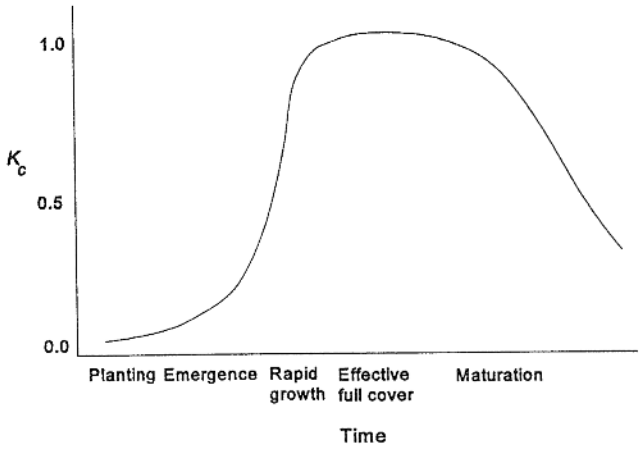

Figure 6.4. Generalized crop coefficient curve showing the change throughout the season.

Table 6.5. Alfalfa-based daily basal crop coefficients for use with the modified Jensen-Haise and Penman methods (source: Wright 1982, used by permission).

Time from planting to effective cover (%)										
Crop	10	20	30	40	50	60	70	80	90	100
Small grains	0.15	0.16	0.20	0.28	0.50	0.75	0.90	0.96	1.00	1.00
Beans	0.15	0.16	0.18	0.22	0.35	0.45	0.60	0.75	0.88	0.92
Sugar Beets	0.20	0.17	0.15	0.15	0.16	0.20	0.30	0.50	0.80	1.00
Corn	0.15	0.15	0.16	0.17	0.18	0.25	0.40	0.62	0.80	0.95
Winter Wheat	0.15	0.15	0.30	0.55	0.80	0.95	1.00	1.00	1.00	1.00
Days after effective cover										
Crop	10	20	30	40	50	60	70	80	90	100
Small grains	1.00	1.00	0.80	0.40	0.20	0.10	0.05	–	–	–
Beans	0.92	0.86	0.65	0.30	0.10	0.05	–	–	–	–
Sugar Beets	1.00	1.00	1.00	0.98	0.91	0.85	0.80	0.75	0.70	0.65
Corn	0.93	0.93	0.90	0.87	0.83	0.77	0.70	0.30	0.20	0.15
Winter Wheat	1.00	1.00	1.00	0.95	0.50	0.20	0.10	0.05	–	–
Time from new growth or harvest–to-harvest (%)										
Crop	10	20	30	40	50	60	70	80	90	100
Alfalfa (lst)	0.50	0.62	0.80	0.90	1.00	0.85	0.90	0.95	0.98	1.00
(2nd and 3rd)	0.30	0.40	0.70	0.90	0.95	1.00	1.00	0.98	0.95	0.95

exceeds the basal value until the surface drys out again. Burman et al. (1980) discuss methods for increasing k_c to account for wet-surface conditions.

6.2.3.3 *The modified Jensen-Haise method*

The original Jensen-Haise method was based on thousands of estimates of evapotranspiration made over several decades in the western United States. The original method used average monthly temperature and solar radiation as independent variables. The modified Jensen-Haise method presented here has an approximate vapor

pressure deficit term and corrects for elevation, and is recommended for estimating E_{tr} for periods of 5-days to a month. The Modified Jensen-Haise method is:

$$E_{tr} = C_T(T - T_x)Q_s \tag{6.6}$$

where E_{tr} has the same units as the solar radiation term Q_s, T is the average temperature (°C), and:

$$C_T = \frac{1}{C_1 + 7.3C_H} \tag{6.7}$$

$$C_1 = 38 - \frac{2E}{305} \tag{6.8}$$

$$C_H = \frac{50\,\text{mb}}{e_2 - e_1} \tag{6.9}$$

$$T_x = -2.5 - 0.14(e_2 - e_1) - \frac{E}{550} \tag{6.10}$$

In Equations (6.7)-(6.10), E is site elevation in meters, and e_1 and e_2 are the saturation vapor pressure (mb) for the mean monthly minimum and maximum air temperatures of the warmest month of the year, respectively.

Example 6.3

Calculate average E_{tr}, and E_t for alfalfa, for the month of May at Salt Lake City using the Jensen-Haise method.

From climatological records (1953-1975), the average daily global solar radiation for the month of May is 26,719 kJ m^{-2} d^{-1}. Multiply this value by 31 d mo^{-1} to get Q_s = 828,289 kJ m^{-2} mo^{-1}. Since Equation (6.6) yields E_{tr} in the same units as Q_s, convert kJ m^{-2} mo^{-1} into a depth of water equivalent. The result is Q_s = 34 cm mo^{-1} of water.

The warmest month is July. The mean minimum and maximum temperatures for July are 16.6 and 34.0°C, respectively. Using these values to get saturation vapor pressure, the components are:

$$C_1 = 38 - \frac{2(1288)}{305} = 29.55$$

$$C_H = \frac{50}{(53.19 - 18.89)} = 1.46$$

$$C_T = \frac{1}{29.55 + 7.3(1.46)} = 0.0249$$

$$T_x = -2.5 - 0.14(53.19 - 18.89) - \frac{1288}{550} = -9.64$$

$$E_{tr} = 0.0249(14.9 + 9.64)34 = 20.8 \text{ cm mo}^{-1}$$

The alfalfa-based crop coefficients are given for fractions of growth periods. For this example we assume the first-cutting growth period starts April 1 and ends at the first cutting on June 15 –

a total of 76 days. 10% of this interval is 7.6 days. For ease of calculation we alternate the lengths as 7 and 8 days. The first 10% of the growing period extends from April 1 to April 7 (7 days). The second 10% extends from April 8 to April 15 (8 days). The third from April 16 to April 22 (7 days), and so on (see below). An overall crop coefficient for May can be calculated as the weighted sum of the coefficients for the intervals as follows:

Percentage of growth period	Date	Crop coefficient from Table 6.5
0-10	April 1-April 7	0.50
11-20	April 8-April 15	0.62
21-30	April 16-April 22	0.80
31-40	April 23-April 30	0.90
41-50	May 1-May 7	1.00
51-60	May 8-May 15	0.85
61-70	May 16-May 22	0.90
71-80	May 23-May 30	0.95
81-90	May 31-June 6	0.98
91-100	June 7-June 15	1.00

$$k_c = 7/31(1.00) + 8/31(0.85) + 7/31(0.90) + 8/31(0.95) + 1/31(0.98)$$

$$k_c = 0.93$$

The average evapotranspiration for May is:

$$E_t = 0.93(20.8 \text{ cm mo}^{-1}) = 19.3 \text{ cm mo}^{-1}$$

6.2.3.4 *The Penman method*

The Penman equation estimates reference crop evapotranspiration for periods of one day to one month. When calibrated for local conditions this is considered one of the most accurate methods. As with the Jensen-Haise method it gives estimates of E_{tr} for use with alfalfa-based crop coefficients. The Penman equation is again:

$$E_{tr} = \frac{\Delta}{\Delta + \gamma} E_n + \frac{\gamma}{\Delta + \gamma} E_a \tag{6.11}$$

To estimate evapotranspiration for a particular crop at a particular point in the growing season, multiply E_{tr} calculated with Equation (6.11) by the crop coefficient from Table 6.5.

Example 6.4

Calculate average E_{tr}, and E_t for alfalfa, for the month of May at Salt Lake City by the Penman method.

Weighting factors

$$\Delta/(\Delta + \gamma) = 1.09/(1.09 + 0.66) = 0.62$$

$$\gamma/(\Delta + \gamma) = 0.66/(1.09 + 0.66) = 0.38$$

Energy component

Convert average daily solar radiation in kJ m^{-2} d^{-1} into cal cm^{-2} d^{-1}:

Q_s = 26,719 kJ m^{-2} d^{-1} = 638 cal cm^{-2} d^{-1}.

(Just for comparison, the average cloudiness for May at the Salt Lake station is 5.7%. Using this value with Equation (5.5) and I_o from Table 5.2 yields Q_s = 689 cal cm^{-2} d^{-1})

The albedo for alfalfa is taken as $\alpha = 0.22$, so that reflected solar radiation is:

$$Q_{rs} = 638(0.22) = 140 \text{ cal cm}^{-2} \text{ d}^{-1}$$

Net longwave radiation is calculated with Equation (5.10) as:

$$Q_{lw} = (1.17 \times 10^{-7})\,(288^4)\,(0.56 - 0.08\sqrt{8.31})\,(0.10 + 0.9(0.057))$$

$$Q_{lw} = 40 \text{ cal cm}^{-2} \text{ d}^{-1}$$

Net radiation is therefore:

$$Q_n = 638 - 140 - 40 = 458 \text{ cal cm}^{-2} \text{ d}^{-1}$$

Converting Q_n to depth of water equivalent (cm) by means of Equations (4.1) and (5.11):

$$E_n = 458/(589) = 0.78 \text{ cm d}^{-1}$$

Mass transfer/aerodynamic component

The average wind speed at Salt Lake City for the month of May is 15 km hr^{-1}, and the average relative humidity is 49%. Using these data, E_a is calculated with Equation (5.27) as:

$$E_a = [0.013 + 0.00016(360)]\,(16.96 - 8.31) = 0.61 \text{ cm d}^{-1}$$

Reference crop evapotranspiration is calculated as:

$$E_{tr} = 0.62(0.78) + 0.38(0.61) = 0.72 \text{ cm d}^{-1}$$

Finally, multiplying E_{tr} by 31 (days) and by the crop coefficient for May from Example 6.3, the average evapotranspiration for alfalfa for the month of May is:

$$E_t = 0.72(31)0.93 = 20.8 \text{ cm mo}^{-1}$$

In this example we calculated average daily E_{tr} and multiplied this value by 31 to get the monthly E_{tr}. This is the preferred approach as opposed to using monthly values directly in Equation (5.27), which is explicitly calibrated for daily wind speed.

Priestley-Taylor equation

For comparative purposes, the Priestley-Taylor equation gives:

$$E_{tr} = 1.3(0.62)(0.78) = 0.63 \text{ cm d}^{-1}$$

6.2.3.5 *The Penman-Monteith method*

One of the most physically-based equations for modeling transpiration is the Penman-Monteith equation (Monteith 1973). The equation incorporates stomatal resistance r_s and aerodynamic resistance r_a directly in the equation; hence, there is no need for empirical crop coefficients. The Penman-Monteith formula is:

$$E_t = \frac{\Delta(Q_n - G) + \rho c_p [(e_s - e_a)/r_a]}{L_v [\Delta + \gamma(1 + r_s / r_a)]} \tag{6.12}$$

where E_t = transpiration (kg m^{-2} s^{-1}), Q_n = net radiation (W m^{-2}), G = soil heat flux (W m^{-2}), ρ = air density (kg m^{-3}), c_p = specific heat of air at constant pressure (1005 J kg^{-1}), L_v = latent heat of vaporization (J kg^{-1}), e_a = vapor pressure (mb), e_s = satu-

ration vapor pressure (mb), r_s = stomatal resistance (s m^{-1}), r_a = aerodynamic resistance (s m^{-1}).

The dimensions of transpiration are mass per unit area per second. When estimating water loss to the nearest second it is necessary to account for the energy flux to and from the soil (G). This term was assumed to balance to zero for the daily version of the Penman formula (Eq. 6.11). While the Penman-Monteith equation is undoubtedly the most accurate, it is also the most demanding in terms of data requirements. The analyst must decide whether the level of accuracy provided is necessary, and whether it is worth the effort to collect the required input data. Kirkby et al. (1987) discuss methods for estimating the input requirements and provide a BASIC computer program for the Penman-Monteith equation.

6.3 MODELING EVAPOTRANSPIRATION UNDER LIMITED SOIL MOISTURE CONDITIONS

Crop coefficients are useful for irrigation water management, but they assume that soil moisture is adequate at all times. Crop coefficients are not useful for estimating evapotranspiration under conditions of variable soil moisture. Modeling actual evapotranspiration typically involves calculating potential evapotranspiration by one of the above equations and then modifying it by some function of soil moisture. The general relationship is:

$$E_t = E_{tp} f\left(\frac{AW}{AWC}\right) \tag{6.13}$$

where $f(\,)$ designates a functional relationship, AW is the available water held in the soil, and AWC is the total available water capacity of the soil, with the constraint that $AW \leq AWC$.

Soil moisture is discussed at length in the next chapter and for now we will use some simplified concepts. For a typical soil perhaps 30% of the volume is void space where water can be stored. If all the voids are filled with water the soil is saturated. Complete saturation may not occur because air can be trapped in some voids. If a soil is brought to the condition of saturation and then allowed to drain by gravity, water drains from the larger pore openings. After some period of time gravity drainage ceases. The amount of water held in the soil in equilibrium against the force of gravity is called the *field capacity* of the soil. At field capacity the tensional force of attraction between the soil and the water just exceeds the force of gravity. The approximate force boundary where this condition occurs is at a soil moisture tension of –0.33 bars. Water held at greater than –0.33 bars percolates downward under the force of gravity. Water held at a force less than –0.33 bars is held in the soil and is available for use by plants, since they can extract water from the soil down to a tension of approximately –15 bars. (Observe that when the term suction was used at the beginning of the chapter this force boundary was given as a positive number. Suction is conventionally taken to be the absolute value of tension.) As the soil dries, the water is held with stronger tensional force. If the soil dries to the level where the tensional force is less than the –15 bar limit, then plants can no longer extract moisture

and they wilt. The –15 bar limit is called the *permanent wilting point*. The maximum amount of water held in the soil between the –0.33 bar and –15 bar limits is the available water capacity (*AWC*). Said another way, the *AWC* is equal to the amount of water held in the soil between the field capacity (–0.33 bars) and the permanent wilting point (–15 bars). The *AWC* is determined per unit depth of soil. To find the total *AWC* for a particular soil, multiply the per unit depth value times the soil depth.

Soil moisture alone is not sufficient to describe the availability of water to plants. But our purpose here is to develop a basic understanding of how we might model evapotranspiration, and modeling necessarily involves some simplification of reality. Two approaches to modeling E_t as a function of soil moisture are described below.

6.3.1 *Modeling the soil as one-layer store*

One of the simplest approaches is to model the soil as a single store. With this approach the total *AWC* is first determined for the soil. At the beginning of each time interval evapotranspiration is calculated as a function of soil moisture as $E_t = E_{tp}(AW/AWC)$. At the end of each time step the *AW* is updated by subtracting E_t and adding any precipitation that may have recharged the soil moisture. For the next time step, E_t is calculated using the updated values of soil moisture. Example 6.5 demonstrates the one-store model.

Example 6.5

For this example assume the soil has an *AWC* = 12.0 cm and that the soil is at field capacity (*AW* = 12.0 cm) at the beginning of the calculations.

Time (days)	E_{tp} (cm)	P (cm)	*AW* begin (cm)	*AW/AWC*	E_t (cm)	*AW* end (cm)
1	0.70	0.0	12.00	1.00	0.70	11.30
2	0.70	0.0	11.30	0.94	0.66	10.64
3	0.70	0.0	10.64	0.89	0.62	10.02
4	0.70	0.0	10.02	0.83	0.58	9.44
5	0.70	0.0	9.44	0.79	0.55	8.89
6	0.70	0.0	8.89	0.74	0.52	8.37
7	0.70	2.5	8.37	0.70	0.49	10.38
8	0.70	0.0	10.38	0.87	0.61	9.77
9	0.70	0.0	9.77	0.81	0.57	9.20
10	0.70	0.0	9.20	0.77	0.54	8.67
Total	7.00				5.84	

At the end of each time period *AW* is updated by subtracting E_t for the period and adding any precipitation. It is assumed that all of the precipitation (2.5 cm) on day 7 went to recharge the soil. Figure 6.4 shows a graph of E_t calculated by the one layer model. Some example calculations are shown below.

Day 1: $E_t = 0.70(12.00/12.00) = 0.70$
$AW = 12.00 - 0.70 = 11.30$

Day 2: $E_t = 0.70(11.30/12.00) = 0.66$

$AW = 11.30 - 0.66 = 10.64$

Day 7: $E_t = 0.70(8.37/12.00) = 0.49$
$AW = 8.37 - 0.49 + 2.50 = 10.38$

6.3.2 *Modeling the soil as a two-layer store*

A slightly more complex approach is to divide the soil into two layers – an upper zone *UZ* and a lower zone *LZ* – where $UZ + LZ = AWC$. The *UZ* is typically assigned a smaller percentage of the *AWC* than the *LZ*. There are 3 rules for the two-layer approach:

1. Water is always extracted from the *UZ* at the potential rate;
2. Water is extracted from the lower zone at a rate proportional to the ratio *LZ/AWC*;
3. The *UZ* must be at field capacity before recharge to the *LZ* occurs.

By having a more dynamic *UZ*, we can model the condition where E_t continues for a period of time at the potential rate even as the soil dries. Example 6.6 demonstrates the two-store approach.

Example 6.6
In this example $AWC = 12.0$ cm as in the previous example, but it is divided so that $UZ = 2.5$ cm and the $LZ = 9.5$ cm. Assume the soil is at field capacity ($AW = 12.0$ cm) at the beginning of the calculations.

			Begin			End		
Time (days)	E_{tp} (cm)	P (cm)	*UZ* (cm)	*LZ* (cm)	E_t (cm)	*UZ* (cm)	*LZ* (cm)	*AW* (cm)
1	0.70	0.0	2.50	9.50	0.70	1.80	9.50	11.30
2	0.70	0.0	1.80	9.50	0.70	1.10	9.50	10.60
3	0.70	0.0	1.10	9.50	0.70	0.40	9.50	9.90
4	0.70	0.0	0.40	9.50	0.64	0.00	9.26	9.26
5	0.70	0.0	0.00	9.26	0.54	0.00	8.72	8.72
6	0.70	0.0	0.00	8.72	0.51	0.00	8.21	8.21
7	0.70	2.5	0.00	8.21	0.48	2.50	7.73	10.23
8	0.70	0.0	2.50	7.73	0.70	1.80	7.73	9.53
9	0.70	0.0	1.80	7.73	0.70	1.10	7.73	8.83
10	0.70	0.0	1.10	7.73	0.70	0.40	7.73	8.13
Total	7.00				6.37			

For the first three days, $E_t = E_{tp} = 0.70$ cm d^{-1}. On day 4 there is not enough moisture in the *UZ* to satisfy E_{tp}. In this case the remaining 0.40 cm of water are removed from the *UZ* and the balance is removed from the *LZ* at a rate proportional to *LZ/AWC*. The calculations for day 4 are:

Water removed from the $UZ = 0.40$ cm.

Water removed from the $LZ = 0.30(9.5/12.0) = 0.24$ cm

$E_t = (0.40 + 0.24) = 0.64$ cm

On day 7, E_t was calculated before the *UZ* was recharged by precipitation. This obviously produced a lower value than if E_t had been calculated after recharge occurred. This is a good example of how approximating a continuous process as a discrete process can create problems.

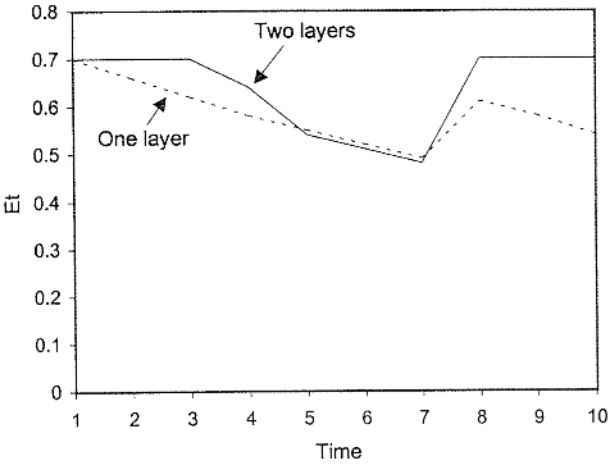

Figure 6.5. Actual evapotranspiration from the one-layer and two-layer models.

The two-layer model has a greater total E_t (6.37 cm) than the one-layer model (5.84 cm). This is due to the greater responsiveness of the *UZ* to the E_{tp} demand (see Fig. 6.5). Note that the one-layer model is a special case of the two-layer model where $UZ = 0$. By varying the capacity of the *UZ*, it is possible to reproduce the effect of any combination of soil texture and vegetation on evapotranspiration (see Fig. 6.1). It is worth noting that these models do not consider the actual physical processes involved. They may accurately reproduce the pattern of E_t but without the benefit of understanding the physical processes involved.

6.4 VEGETATION MODIFICATION

Considerable research has been done on how vegetation modification affects the basin-scale hydrologic cycle. Vegetation modification may be either structural changes such as clear cutting or patch cutting, or type conversion – replacing one type of vegetation with another. For structural changes the working, if overly simplistic, hypothesis is that removing the natural vegetation reduces evapotranspiration, which in turn increases soil moisture storage and runoff. Many of the early studies of vegetation modification were pragmatic and aimed at increasing water supply for various human uses.

The results from the accumulated experience are somewhat ambiguous. In cases where a large percentage of a drainage basin was clear cut, runoff increased for some time afterwards. In other cases where smaller areas were clear cut, or where patch cutting was used, removing the vegetation sometimes had minimal or no effect on runoff. The unpredictable nature of the response may be due to a number of factors. If the area is patch cut so that the cleared areas are small, the plants around the fringe may extend their roots into the clearing and tap the soil moisture. The plants along the boundary may also use advected energy from the clearing to increase evapotranspiration. If the area is only thinned, the remaining vegetation may utilize some of the percolating soil water (Turner 1991). The inconsistent results from such ex-

periments highlight our incomplete understanding of the subtle interaction among components of the hydrologic system.

Certain categories of vegetation type conversion produce predictable results. For example when shrubs and trees are replaced by grasses, evapotranspiration is reduced and runoff increases. This is primarily due to the change from deep-rooted to shallow-rooted plants; however, other factors may play a role including the change in aerodynamic roughness, stomatal resistance or plant albedo. Dunne & Leopold (1978) describe how widespread abandonment of farms in the southeast United States at the turn of the century, followed by secondary succession from weeds to the climax eastern deciduous forest, as been accompanied by increased interception and evapotranspiration and decreased runoff. There is also some evidence that changing from a deciduous forest to a needleleaf forest may increase evapotranspiration. Coniferous trees have lower albedos, intercept more water, and have a longer duration in leaf.

Changes in the water budget of a basin are only one aspect of vegetation manipulation. Clear cutting can have severe environmental consequences in terms of increased soil erosion and nutrient loss from the basin. Eroded soil causes sedimentation problems downstream and increases the turbidity of the water reducing the sunlight available for photosynthesis. Nutrients washed and leached from the hillslopes contribute to undesirable eutrophication of aquatic ecosystems downstream.

Deforestation was once considered a viable option for water supply augmentation, but today it must be viewed as largely unacceptable. The environmental costs simply outweigh the marginal benefits of increased water supply. With the increasing concern about the survival of forest ecosystems, other water management alternatives, especially those that manage the demand for water, should be viewed as preferable to deforestation to increase runoff and water supply.

SUMMARY

Evapotranspiration requires both water and energy. In well-watered ecosystems, actual evapotranspiration approaches the potential value for a continuous vegetative cover. Under these conditions evapotranspiration is limited by energy availability much like evaporation from a free water surface. In semiarid and arid environments lack of soil moisture, sparse vegetation cover, and shallow-rooted plants all cause the actual evapotranspiration rate to fall below the potential rate. In Chapter 9 we reexamine the difference between actual and potential evapotranspiration within the context of Thornthwaite's Water Balance procedure.

Estimating evapotranspiration has long been important for irrigation water management. Vegetation modification similarly has a long record of research activity, though many questions have yet to be resolved. Research on evapotranspiration has recently taken on new importance because of the growing concern over anthropogenically-forced climate change. Research is currently underway to understand the reciprocal influences between land surface processes and the atmosphere (NRC 1991). Evapotranspiration is a major process linking the land surface to the atmosphere through exchanges of water and energy. Of particular interest is how human activities can alter these natural processes. For example, how might tropical defor-

estation alter fluxes of water and energy, and how might these changes ultimately feedback to affect regional or global climate? Soil moisture was examined briefly in this chapter to help illustrate the factors that influence evapotranspiration. In the next chapter we focus on the properties and characteristics of water in the soil and their importance in water management.

PROBLEMS

6.1 Use the original Blaney-Criddle method to calculate monthly and seasonal consumptive use for corn and alfalfa near Deming, New Mexico. Assume the consumptive use for the period September 1 to September 15 is one-half of the total September value.

Crop	Growing season
Alfalfa	4/1 to 10/31
Grain corn	5/1 to 9/15

Mean monthly temperatures (°F) for Deming, NM

	Jan	Feb	Mar	Apr	May	Jun	Jul	Aug	Sep	Oct	Nov	Dec
T_a	40.6	45.1	50.7	59.1	67.4	77.5	80.4	78.6	72.8	62.0	48.8	42.0

6.2 Use the Thornthwaite method to calculate the monthly and seasonal potential evapotranspiration for alfalfa and corn near Deming, NM.

6.3 Recalculate Example 6.5 and Example 6.6 using the following E_{tp} sequence. Assume all other variables are the same as in the examples. Graph your results.

Time	E_{tp}
1	0.80
2	0.80
3	0.85
4	0.70
5	0.70
6	0.75
7	0.50
8	0.80
9	0.80
10	0.80

CHAPTER 7

Infiltration and soil moisture

Water on the Earth's surface may follow one of three paths: it may evaporate into the atmosphere, flow across the land surface towards stream channels as overland flow, or it may infiltrate into the ground (Fig. 1.2). Infiltration and surface runoff are inversely related; as one increases the other decreases. Overland flow is discussed in Chapter 10 under the topic of runoff. In this chapter we examine the process of infiltration and the storage and movement of water in the soil. Infiltration is the passage of water through the land surface into the soil. It involves the entrance of water into the soil, the storage of water within the soil mass, and the transmission of water through the soil by percolation (Linsley et al. 1982). Limitations in any one of these component processes can reduce infiltration at the surface. Two forces act to move water into the soil – gravity and capillary suction. The terms capillary suction and soil moisture tension were used synonymously in Chapter 6. Later in this chapter we address the issue of soil moisture terminology. Gravity pulls water down into the large (noncapillary) openings such as fractures, cracks and solution channels. Under the force of gravity water literally falls into the ground. Water is sucked into the soil by capillary forces. Capillary suction moves water vertically (up and down) as well as horizontally in the soil. Capillary suction is created through the mutual attraction between the water molecules, and the attraction between water and solid soil particles by hydrogen bonding. The strength of the force is largely a function of the radial distance between the water molecule and the surface of the soil particle. The closer a water molecule is to a soil particle, the stronger the bonding force. Dry soil has stronger capillary forces than wet soil because the water molecules are closer to the soil particles in the dry soil. The forces decrease with increasing soil moisture because additional water molecules are bonded at greater distances from the soil particles. Capillary forces are stronger in fine-textured clayey soils than in coarse-textured sandy soils because the fine-texture soils have very small interstices, so water is very close to the particle surfaces, and there is also more total surface area. Water only moves under the force of gravity if the gravitational force exceeds the tensional force. In Chapter 6 we saw the approximate tension boundary of –0.33 bars marked the threshold separating 'capillary water', water that is held in the soil, from 'gravity water', water that drains through the soil.

Infiltration (f) changes as a function of time and is a *rate* variable (LT^{-1}). An idealized curve of *infiltration capacity* (f_p) is shown in Figure 7.1. The infiltration capacity for a soil is the maximum rate of infiltration limited only by the properties of the soil. The relationship between infiltration and the infiltration capacity is

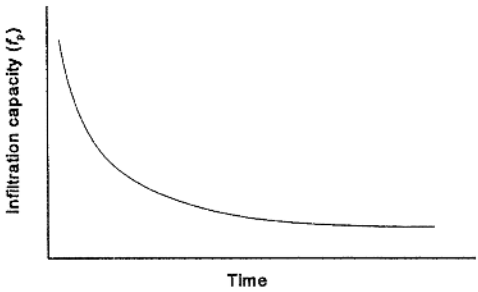

Figure 7.1. Stylized infiltration capacity curve. Infiltration capacity starts out high and decreases over time.

$0 \leq f \leq f_p$. The general shape of an infiltration capacity curve can be explained by the forces and processes at work. If the soil is initially dry when infiltration begins, the infiltration capacity is high since both strong capillary and gravity forces work to draw water into the soil. As the soil becomes wet, capillary forces decrease causing the rate of infiltration to decrease. Eventually, infiltration capacity approaches a low constant rate controlled primarily by gravity and the rate that water can percolate downward through the soil. Water is now only able to enter the soil as fast as space is made available by downward percolation.

7.1 FACTORS CONTROLLING INFILTRATION

The factors that influence infiltration are the physical and chemical properties of the soil, surface characteristics including vegetation and land use, antecedent moisture conditions, seasonal factors, topography and precipitation characteristics. Soil-related factors include all of the properties and characteristics that influence a soil's *permeability*. These include soil texture, structure, entrapped air and the presence of subsurface horizons of low permeability. Permeability is the ability of a material to transmit water and, like infiltration, has the dimensions of velocity (LT^{-1}). Another term to describe the permeability of earth materials is *hydraulic conductivity* (K). When the material is not saturated the term is *unsaturated* hydraulic conductivity, otherwise it is called the *saturated* hydraulic conductivity (K_s). Most soils most of the time are unsaturated. For a given material the unsaturated hydraulic conductivity is usually much lower than the saturated value. Coarse-texture sandy soils are more permeable than fine-texture clay soils and have a correspondingly greater infiltration capacity (Fig. 7.2). The small interstices in clay soils are difficult for water to move through because strong capillary forces hold the water in place.

Soil structure describes how individual soil particles combine to form larger aggregates. Structure is controlled by the amount and disposition of the clay particles in the soil. Clay particles are negatively charged colloidal minerals. In a soil they may group together (flocculate) to form larger aggregates and produce 'good' soil structure, or they may disperse (deflocculate) as individual particles throughout the soil creating 'poor' structure. Flocculated clays produce good structure because the large aggregates make the soil behave more like a coarse-texture soil. Whether clays flocculate or deflocculate depends on the type and quantity of cations in the soil. When sodium (Na^+) cations make up a significant proportion (10 to 20%) of the cations in

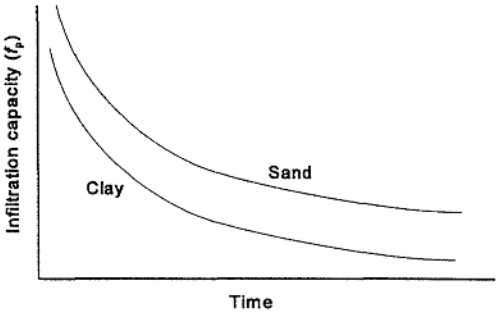

Figure 7.2. Stylized curves of infiltration capacity for a sand and a clay soil.

the soil, clays tend to deflocculate, creating poor structure and reducing infiltration capacity. This is one of the detrimental consequences of soil salinization. Mather (1984) quotes a study by Wiesner (1970) on the variation in infiltration capacity with soil texture and structure. In the experiment, course-texture sandy soils with good structure had infiltration capacities ranging from 2.0 to 2.5 cm hr^{-1}. Sandy loams and clay loams with good structure had capacities of 1.3 cm hr^{-1} and 0.75 cm hr^{-1}, respectively. With poor structure the infiltration rates were reduced anywhere from 20 to nearly 50%.

Vegetation and land use influence infiltration through the direct control on the entrance of water into the soil. Vegetated surfaces have greater infiltration capacities than nonvegetated surfaces (e.g. bare rock and compacted dirt roads). Exposed soils can be sealed by fine particles dislodged by raindrops. Human-created impermeable surfaces like streets, parking lots and driveways permit virtually no infiltration. As between different types of vegetation, forests and undisturbed pastures generally have the highest infiltration capacities, while infiltration on cropland is generally lower than most areas of continuous natural vegetation. Infiltration capacities under forests can be very high with values from 5 to 100 cm hr^{-1}. Such high capacities mean there is little or no surface runoff from undisturbed forested areas even under extreme rainfall events. Figure 7.3 shows *cumulative infiltration* (F) curves typical of three Piedmont soils (Holtan & Kirkpatrick 1950). The superior infiltration of natural vegetation versus cropland, and of vegetated versus nonvegetated soils is easily seen. Holtan & Musgrave (1947) give results from an experiment that isolated the differential effects of vegetation and soil (Table 7.1). The five soils in Table 7.1 are ranked by depth of the profile and organic matter content. The Muscatine soil has the deepest profile and the most organic matter; the Viola soil is relatively shallow with poor organic matter content. The results demonstrate consistent differences in infiltration capacity based on soil and vegetation cover. In every case infiltration was greater under the bluegrass pasture than under corn, and with good vegetation cover (bluegrass), infiltration decreased with decreasing soil depth. However, under the corn crop the role of soil depth is inconsistent. The conclusion is that deep soils that might normally be expected to have high infiltration rates may not under adverse land-cover conditions.

If antecedent soil moisture is high at the beginning of a rainfall, capillary forces and available void space in the soil are lower than if the same soil were initially dry (Fig. 7.4). This is one of the reason why the same soil can generate very different

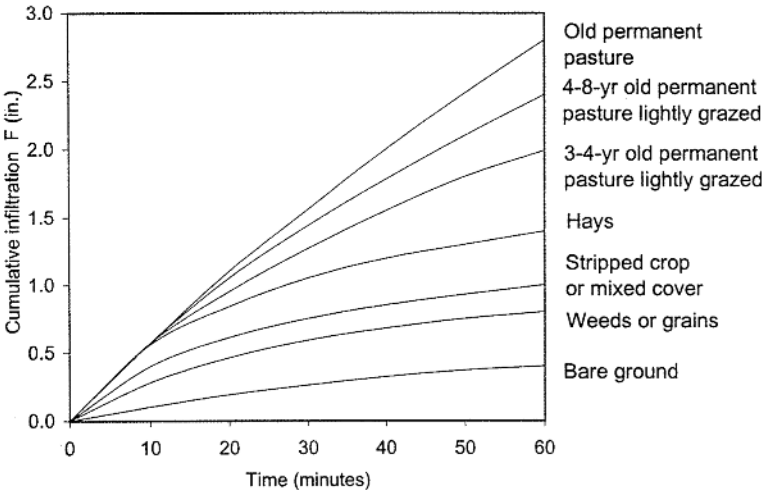

Figure 7.3. Cumulative infiltration curves from Cecil, Madison, and Durham soils (source: Holtan & Kirkpatrick 1950).

Table 7.1. Infiltration into soils of varying depth and organic matter content with contrasting vegetation covers (source: Holtan & Musgrave 1947).

Silt loam soils	Total infiltration in 5 hours (inches)	Total infiltration in 5 hours (inches)	Difference due to land use (inches)
	Bluegrass	Corn	
Muscatine	5.38	1.34	4.04
Tama	5.03	1.51	3.52
Berwick	3.48	1.21	2.27
Clinton	2.77	2.17	0.60
Viola	1.63	1.28	0.35

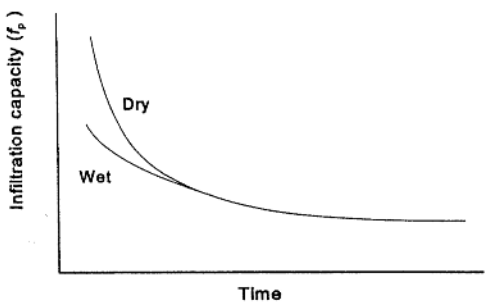

Figure 7.4. Infiltration capacity affected by different antecedent moisture conditions.

rates of runoff from similar storms. In continental climates with cold winters, the soil matrix freezes during the winter season largely preventing infiltration. This can create a potential flood hazard when the snowpack melts in the spring and the soil is still frozen. Vegetation is important here too because it influences the degree and pattern of soil freezing.

Topography modifies infiltration directly and indirectly. Slope angle directly affects infiltration because steep slopes promote rapid surface runoff giving the water less time to infiltrate. Indirectly, elevation and slope aspect influence vegetation, soil development and antecedent moisture conditions. South-facing slopes in the northern hemisphere are usually dryer and support a sparser vegetation cover than north-facing slopes. Finally, the role of precipitation must be considered. If the rate of water supply to the surface (rainfall intensity) i is less than the infiltration capacity f_p, then the actual infiltration rate equals the supply rate ($f = i$). Only when the supply rate exceeds the infiltration capacity can the actual infiltration rate equal the infiltration capacity. Other factors influencing infiltration have been identified including soil and water temperature and hydrophobic coatings on soil particles (Garstka 1978).

7.2 INFILTRATION RATE VERSUS CUMULATIVE INFILTRATION

Let us take a moment and distinguish between the infiltration rate f (LT^{-1}) and cumulative infiltration F (L). Doing so provides another example of the continuous variable versus discrete variable issue. It also provides an opportunity to demonstrate and apply important mathematical concepts to an actual physical process. If water is ponded on the soil surface infiltration is continuous, and the instantaneous rate of infiltration changes with time (Fig. 7.1). The total amount of water that infiltrates over some period depends upon the infiltration rate, and is also a function of time. Because infiltration is a continuous process, it is properly described using equations from calculus. As we saw with Equations (3.16) and (3.17), these two concepts – the instantaneous rate of change and the accumulated amount – are mathematical inverses:

$$f(t) = \frac{\mathrm{d}F(t)}{\mathrm{d}t} \tag{7.1}$$

and

$$F(t) = \int_0^t f(u)\mathrm{d}u \tag{7.2}$$

Equation (7.1) is a differential equation and here describes the instantaneous infiltration rate $f(t)$. It says the infiltration rate is the derivative of cumulative infiltration $F(t)$. In other words, the infiltration rate $f(t)$ is equal to the *slope* of the $F(t)$ curve at time t (Fig. 7.5b). The slope of the curve of F at time t is an infinitesimally small increment in infiltration dF divided by the infinitesimally small increment of time dt. Equation (7.2) says the cumulative infiltration $F(t)$ is the definite integral of the infiltration rate. In other words, $F(t)$ is equal to the area under the $f(t)$ curve (Fig. 7.5a). Example 7.1 demonstrates these concepts, but as was the case in Chapter 2 for the reservoir example, rather than using continuous variables and calculus we use discrete approximations and algebra.

Compare the continuous versus the discrete infiltration equations in Table 7.2. The delta Δ symbol and the sigma Σ symbol are essentially discrete analogs of the differentiation d symbol and the integral $\int$ symbol in the continuous equations.

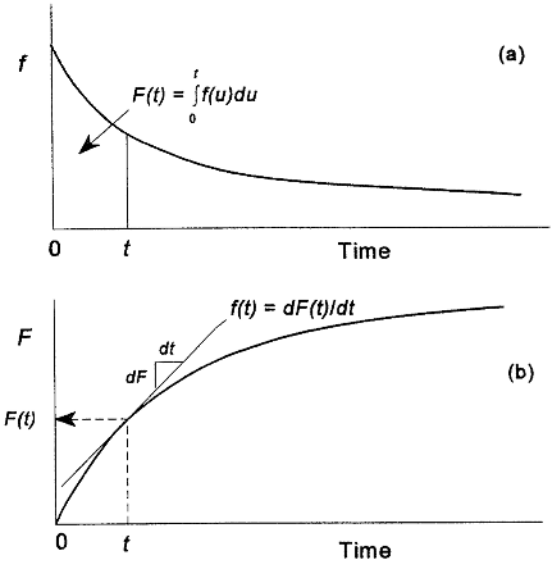

Figure 7.5. a) The infiltration rate curve $f(t)$. The area under the curve from time 0 to time t equals the cumulative infiltration $F(t)$. b) The cumulative infiltration curve $F(t)$. The derivative (slope) of the function $F(t)$ is the infiltration rate $f(t)$.

Table 7.2. Comparison between continuous and discrete equations for infiltration rate and cumulative infiltration.

Process	Continuous	Discrete
Infiltration rate	$f(t) = \frac{dF(t)}{dt}$	$f_t = \frac{\Delta F}{\Delta t}$
Cumulative infiltration	$F(t) = \int_0^t f(u)du$	$F_t = \Sigma f_t \Delta t$

Example 7.1

For this example data from the 'strip crop or mixed cover' curve in Figure 7.3 are used to explore the relationship between infiltration rate and cumulative infiltration. The continuous functions $f(t)$ and $F(t)$ are approximated using as discrete functions f_t and F_t, where the time step $\Delta t = 10$ min. $= 0.167$ hrs.

For the times 0, 10, 20, 30, 40, 50 and 60 min., the corresponding value of $F(t)$ is read from Figure 7.3 and placed in Table 7.3 (column 3). The discrete, linear approximation for the infiltration rate f_t is given by:

$$f = \Delta F / \Delta t = (F_t - F_{t-1}] / \Delta t$$

For example, the calculation of the infiltration rate for time interval 1 (from 0 to 10 min.) is:

$$f_1 = (0.40 - 0.00) \text{ inch} / 0.167 \text{ hr} = 2.40 \text{ in hr}^{-1}$$

The assumption is that this rate is constant over the 10-minute interval. The f_t values are plotted to produce an approximate infiltration rate curve as Figure 7.6.

Just as the continuous infiltration rate $f(t)$ can be linearly approximated by f_t, the cumulative infiltration $F(t)$ may too be approximated. For each time period the incremental cumulative infiltration is calculated as:

$$f_t \Delta t = (\Delta F / \Delta t) \Delta t = \Delta F$$

Table 7.3. Infiltration rate calculated from the 'stripped crop or mixed cover' curve in Figure 7.3.

t (period)	Time (minutes)	$F(t)$ (inch)	f_t (in hr^{-1})
0	0	0.00	–
	5	–	2.40
1	10	0.40	–
	15	–	1.26
2	20	0.61	–
	25	–	0.90
3	30	0.76	–
	35	–	0.54
4	40	0.85	–
	45	–	0.48
5	50	0.93	–
	55	–	0.42
6	60	1.00	–

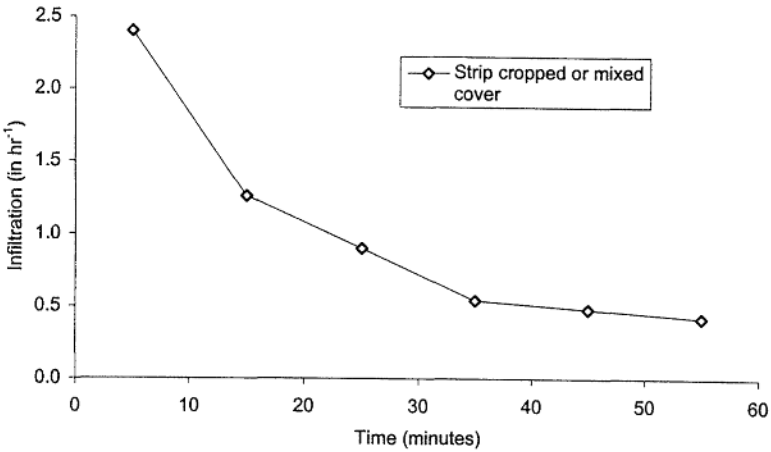

Figure 7.6. Approximated infiltration rate derived from the continuous 'stripped crop mixed cover' infiltration curve in Figure 7.3.

The cumulative infiltration F_t through time t is the sum of individual increments:

$$F_t = \sum_{i=0}^{t} f_i \Delta t$$

For example, the cumulative infiltration for time period 1 (from 0 to 10 min.) is:

$$F_1 = 2.40 \text{ in hr}^{-1} \times 0.167 \text{ hr} = 0.40 \text{ inch}$$

And the cumulative infiltration through time period 2 is:

$$F_2 = (1.26 \text{ in hr}^{-1} \times 0.167 \text{ hr}) + 0.40 \text{ inch} = 0.61 \text{ inch}$$

The linearly-approximated F_t values are the same as for the original $F(t)$ curve (Fig. 7.3 and Table 7.3), but are achieved in discrete steps rather than as a continuous accumulation of infiltrated water (Table 7.4).

Table 7.4. Cumulative infiltration calculated from the infiltration rate in Table 7.3.

t (period)	Time (minutes)	Average f_t (in hr^{-1})	ΔF (inch)	F_t
0	0	–	0.00	0.00
	5	2.40	–	–
1	10	–	0.40	0.40
	15	1.26	–	–
2	20	–	0.21	0.61
	25	0.90	–	–
3	30	–	0.15	0.76
	35	0.54	–	–
4	40	–	0.09	0.85
	45	0.48	–	–
5	50	–	0.08	0.93
	55	0.42	–	–
6	60	–	0.07	1.00

7.3 INFILTRATION MEASUREMENT AND ESTIMATION

Infiltration is temporally and spatially heterogeneous because all the factors that influence infiltration vary over time and space. Soil texture can change over a distance of a few meters horizontally and with depth in the soil. Vegetation changes with elevation, aspect, season and human activities. Antecedent moisture generally increases downslope, and changes with each passing storm and intervening period of drying. Given such variability it is impossible to know infiltration precisely even for a small area. Therefore, average infiltration values are often estimated based on soil properties and vegetation cover. For a specific project requiring detailed information, infiltration may be measured or estimated by one of the following methods.

7.3.1 *Infiltrometers*

Infiltration can be measured using a ring infiltrometer or a rainfall simulator. A single-ring infiltrometer is a cylinder 10 to 30 cm in diameter and varying in length from 45 to 60 cm. The tube is driven into the ground anywhere from 10 to 50 cm. Water is applied so that a constant head (depth) of water is maintained within the ring. The amount of water added at successive time periods to maintain a constant head gives a direct measurement of the rate and the amount of infiltration. The advantage of the device is that it is portable and easy to install, and so multiple measurements can be made in a short period of time. The main drawback is the mechanical disturbance of the soil adjacent to the tube wall. This causes measured infiltration to be up to 10 times the natural rate (Dunne & Leopold 1978). To minimize this edge problem double-ring infiltrometers have been developed. Since these devices may not give accurate measurements of infiltration capacity, they are best used to establish an index of relative infiltration between different sites.

7.3.2 *Rainfall simulators*

Moving up in scale, the rainfall simulator or sprinkler infiltrometer can be used to estimate infiltration for areas ranging from a few square meters to hundreds of square meters. A site is selected and a framework of overhead sprinklers installed. At the downslope-end of the site provision is made for collecting surface runoff. Sprinkler nozzles and water pressure are designed to simulated varying rainfall intensity, drop size and fall velocity. Using a continuity equation, the simulator allows infiltration to be determined as the difference between irrigation, runoff, water detained in flow across the plot, and water retained in surface depressions. These devices provide estimates of infiltration for larger areas than the ring infiltrometer, but they are expensive and difficult to set up in the field. Both ring infiltrometers and rainfall simulators permit spatial sampling and the mapping of isolines of (relative) infiltration over an area.

7.3.3 *Hydrograph analysis*

An approximate method for estimating infiltration for small drainage basins combines the analysis of rainfall hyetographs and stream hydrographs from a basin. The technique is also called the block method or the average infiltration method. The former name describes the method while the later describes the results. A complex storm consisting of multiple bursts (blocks) of rainfall is identified and at least three distinct rainfall bursts are selected. Total rainfall for each burst is calculated and converted into an average rainfall intensity by dividing by the rainfall duration. The corresponding storm runoff for each event is first converted into a uniform depth over the basin and then into an average runoff intensity using the same duration. Storm runoff is equal to the total runoff minus the baseflow. Average infiltration during each event is the difference between average rainfall intensity and the average runoff intensity (see Example 7.2).

Example 7.2

The data for this example are from the Swarr Run basin located in southeastern Lancaster County, Pennsylvania. The basin is 8.67 mi^{-2} in size. Basin land use is approximately 53% farmland, 10% forest and 37% urban. The urban land use is predominantly single-family homes, though a four-lane highway crosses the basin and some small industrial areas are present. The soils are predominantly silt loams. Figure 7.7a shows a storm sequence for a 40-hour period starting the evening of July 19 and ending in the early afternoon of July 21. Figure 7.7b shows the runoff generated from these rainfall bursts. Table 7.5 demonstrates the average infiltration method.

Plotted on Figure 7.7c are the average infiltration estimates. The points do not follow a smoothly decreasing curve. One reason could be that the length of time between the first and second rainfall events was long enough to allow the infiltration rate to recover somewhat, producing a higher rate at the beginning of the second storm. An equally likely explanation is the potential error in the measurement of precipitation. Precipitation measurements for Swarr Run are based on a single gage, so the spatial variability within individual storms is not well represented. The average infiltration method assumes rainfall to be spatially uniform over the basin, which it is not.

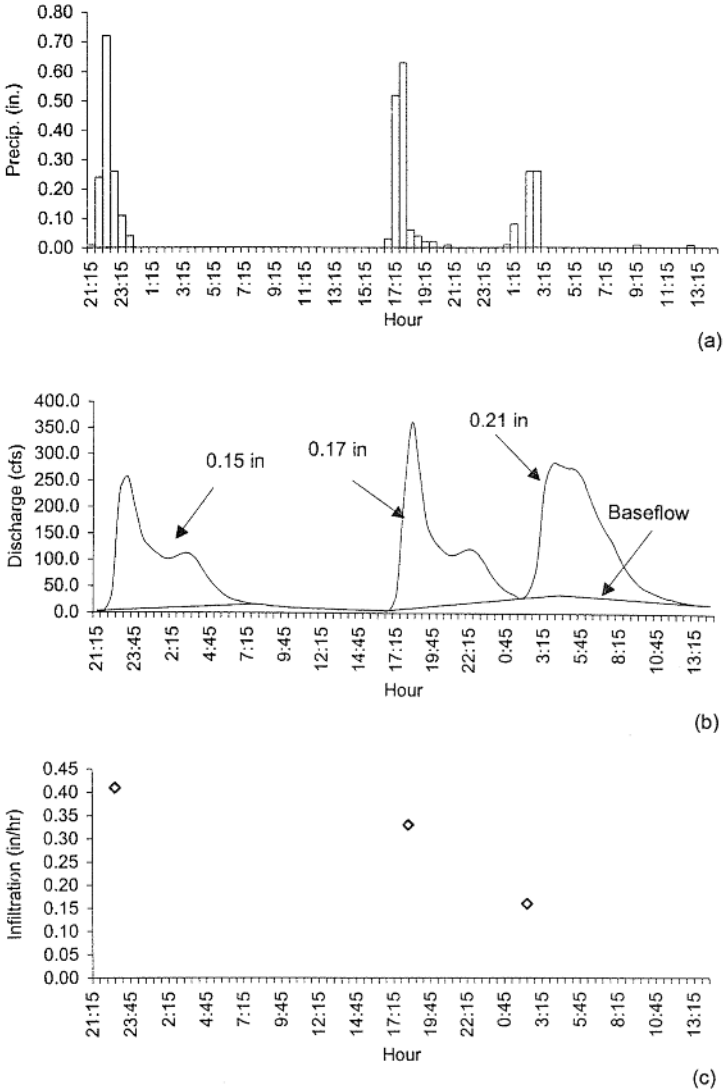

Figure 7.7. a) The hyetographs for the storm sequence for the period July 19-21 over the Swarr Run basin, b) The runoff hydrographs. The numbers represent the equivalent uniform depth of water over the basin, and c) The estimated point infiltration values.

Table 7.5. Data for the average infiltration method.

Event	Duration (hours)	Precipitation		Runoff		Infiltration (in hr^{-1})
		(inch)	(in hr^{-1})	(inch)	(in hr^{-1})	
1	3.0	1.38	0.46	0.15	0.05	0.41
2	3.5	1.32	0.38	0.17	0.05	0.33
3	2.5	0.61	0.24	0.21	0.08	0.16

7.4 INFILTRATION MODELS

Singh (1989) groups infiltration models into two groups: empirical and conceptual. Empirical equations model infiltration as a function of time, whereas conceptual models represent infiltration using physics of flow through porous media. It is beyond the scope of this book to do more than just introduce a couple of the more popular models.

7.4.1 *Horton's model*

One of the earliest and best-known empirical infiltration equations is from Horton (1939, 1940). Robert Horton was a luminary of modern hydrology and made significant contributions to the science of hydrology in the areas of infiltration, surface runoff generation, and drainage basin morphology. Horton's equation models the infiltration process as negative exponential function:

$$f_p = f_c + (f_o - f_c)e^{-kt} \tag{7.3}$$

where f_p = infiltration capacity, f_c = the equilibrium (constant) infiltration capacity, f_o = the initial infiltration capacity, e = is the base of the natural logs, k = a constant that depends on soil type (range 2-40), t = time from the beginning of rain.

Figure 7.8 graphically defines the terms in the Horton equation. For a given soil and initial conditions the only variable in the equation is time t, everything else is constant. The equation has two parts: a constant term f_c and a variable term $(f_o - f_c)e^{-kt}$. But even the variable part has a constant term $(f_o - f_c)$ set by the initial conditions. The product of $(f_o - f_c)$ and the exponential term (e^{-kt}) asymptotically approaches zero as time increases. Thus, f_p approaches f_c asymptotically over time. Figure 7.9 shows the effect of varying k. The larger k, the more rapidly infiltration approaches f_c. Horton's equation assumes infiltration equals the infiltration capacity when the supply rate exceeds the infiltration capacity, and that infiltration equals the supply rate when the supply rate is less than the infiltration capacity. Unfortunately, f_p in Equation (7.3) decreases solely as a function of time and not as a function of the actual amount of water that has infiltrated (F). For initial conditions $F = 0$ at $t = 0$, Equation (7.3) can be integrated to give the cumulative infiltration (see Table 7.6).

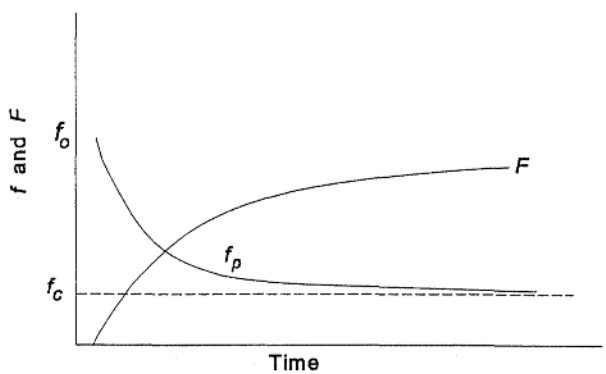

Figure 7.8. Diagrammatic representation of the components of the Horton infiltration equation.

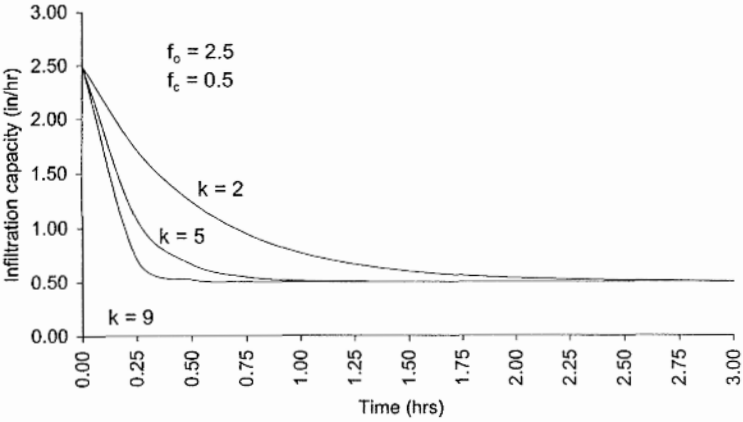

Figure 7.9. Graphs showing the effect on f_p of varying the parameter k in the Horton equation.

Table 7.6. Equations for infiltration rate f and cumulative infiltration F for the Horton and Philip equations.

Equation	Infiltration rate (f)	Cumulative infiltration (F)
Horton	$f_p = f_c + (f_o - f_c)e^{-kt}$	$F = f_c t + \frac{1}{k}(f_o - f_c)(1 - e^{-kt})$
Philip	$f_p = \frac{1}{2}St^{-1/2} + A$	$F = St^{1/2} + At$

Table 7.7. Values of f_o, f_c and k for use in the Horton infiltration equation (source: Rawls et al. 1976).

Soil type	f_o (in hr^{-1})	f_c (in hr^{-1})	k (hr^{-1})
Alpha loam	19.00	1.40	38.29
Carnegie sandy loam	14.77	1.77	19.64
Cowarts loamy sand	15.28	1.95	10.65
Dothan loamy sand	3.47	2.63	1.40
Fuquay pebbly loamy sand	6.24	2.42	4.70
Leefield loamy sand	11.34	1.73	7.70
Robertsdale loamy sand	12.41	1.18	21.75
Stilson loamy sand	8.11	1.55	6.55
Tooup sand	23.01	1.80	2,71
Tifton loamy sand	9.67	1.63	7.28

Singh (1989) discusses how to estimate the three parameters f_o, f_c, and k. Unfortunately, there has not been much work relating these parameters to readily measurable soil properties. Some experimentally-determined values for the parameters for the southeast coastal plain region are given in Table 7.7.

7.4.2 *Philip's model*

Philip's equation (Philip 1957) is one of the more accessible conceptual approaches

to modeling infiltration. The method is considered conceptual because the terms have direct physical interpretations. The basic model is given by the two-term equation:

$$f_p = \frac{1}{2} St^{-1/2} + A \tag{7.4}$$

where S is called the *sorptivity* or 'diffusion' term, and is a function of the capillary forces. A is the 'transmission' term, and is closely related to the saturated hydraulic conductivity (K_s) and the movement of water by gravity. Philip's equation thus incorporates the two forces that move water into and through the soil. For water moving horizontally in a soil, the transmission term is zero, and capillary forces alone draw water into the soil. For vertical downward flow, as $t \rightarrow 0$, $f_p \rightarrow St^{-1/2}$, and as $t \rightarrow \infty$, $f_p \rightarrow A$. Equation (7.4) is easily integrated to give cumulative infiltration (Table 7.6).

7.5 OTHER METHODS FOR ESTIMATING INFILTRATION

7.5.1 *The Φ index*

The Φ index is one of the simplest methods of estimating infiltration. The index represents the amount of precipitation retained by the basin divided by the duration of the storm. In other words, it is the average 'loss' rate. It is a loss rate because it includes depression storage and any other retentions as well as infiltration. In concept it is very similar to the average infiltration method described earlier. Being an average (constant) value the Φ index underestimates infiltration at the beginning of a storm when infiltration is high, and overestimates infiltration at the end of the storm when it is low. Example 7.3 shows how to calculate Φ two ways.

Example 7.3

Find the Φ index for the first storm event in Example 7.2. The first way to calculate Φ is to simply take the total storm rainfall, subtract the total runoff, and divide the remainder by the duration of the storm. The rainfall data for the first storm event by 30-minute intervals are given in Table 7.8.

The duration of the storm is 3 hours (hour 21:00 to hour 24:00). Total rainfall is 1.38 inches and the total runoff is 0.15 inches. This gives an approximation of $\Phi = (1.38 - 0.15) / 3 = 0.41$ in hr^{-1}. This is the same value we got for the average infiltration method in Example 7.2.

A second somewhat more detailed approach solves for Φ by trial and error using the following equation:

$$D_1(i_1 - \Phi) + D_2(i_2 - \Phi) + \ldots + D_n(i_n - \Phi) = Q_T$$

where D is the duration of the rainfall interval, i is the rainfall intensity in the interval, Q_T is the total runoff, and the subscripts represent the individual time intervals from Table 7.8. If Φ is greater than the incremental rainfall, that term is dropped from the calculation because negative values are not used. Since the rainfall durations are all 0.5 hours, inserting values from Table 7.8 into the equation and simplifying gives:

$$0.5[(0.32 - \Phi) + (0.66 - \Phi) + (1.28 - \Phi) + (0.32 - \Phi) + (0.14 - \Phi) + (0.04 - \Phi)] = 0.15$$

The value for Φ is found by trial and error. Let's first try the value $\Phi = 0.41$, which was calculated above. Using this value four terms drop out of the equation. The two remaining terms give

$0.5[(0.66 - 0.41) + (1.28 - 0.41)] = 0.64$ inches, which is greater than the observed runoff of 0.15 inches. Continued trial and error eventually produces a value of $0.5(1.28 - 0.98) = 0.15$ inches. The final value for the Φ index is $\Phi = 0.98$ in hr^{-1}.

The easiest way to find the Φ index using the second approach is with a spreadsheet program. Enter the equation into a cell in the spreadsheet and have Φ in the equation referenced as another cell. When you enter different values for Φ, the result is automatically recalculated and displayed in the equation cell. Remember to delete all terms from the equation where Φ is greater than the precipitation intensity.

Table 7.8. Precipitation data for the July 19, 1988 rainfall event over the Swarr Run Basin.

Interval	Time (hr)	Incremental precipitation up to the time indicated (inch)	Precipitation intensity (in hr^{-1})
1	21:30	0.16	0.32
2	22:00	0.33	0.66
3	22:30	0.64	1.28
4	23:00	0.16	0.32
5	23:30	0.07	0.14
6	24:00	0.02	0.04
Total		1.38	

7.5.2 *Soil classification*

Major soil groups in the United States have been assigned to one of four Hydrologic Soil Groups (HSG). Obtaining an estimate of infiltration capacity is as simple as identifying the soil type and the infiltration group to which that soil has been assigned. Table 7.9 lists the soil groups and the infiltration ranges associated with each group (Musgrave 1955). The SCS has a complete listing of soils in the United States by infiltration group (see SCS 1986). This information is also available in SCS county soil survey reports, along with other useful soil information.

7.6 PONDING TIME AND RUNOFF

Three possible situations exist between the interrelated processes of rainfall, infiltration and runoff. The different cases are based on the relative magnitudes of i, f_p and K_s. In the first case, when $i < K_s$, the rainfall intensity is less than the saturated hydraulic conductivity. There is no surface runoff in this situation since the water supply rate to the surface is less than the minimum value of infiltration capacity. In the second case $i > f_p$ and surface runoff occurs immediately. In the third case, $K_s < i < f_p$. Here all of the rainfall infiltrates at the beginning of the storm, since the infiltration capacity exceeds the rainfall intensity. But as infiltration capacity decreases through the storm, the rainfall rate eventually exceeds the infiltration capacity and runoff commences. The time from the beginning of rainfall until runoff commences is called the *ponding time*. This is represented on Figure 7.10 as the part of the curve from time $t = 0$ to $t = t_p$. The ponding time is important because it is the moment when overland flow begins. Some percentage of the initial runoff will be stored in surface depressions and irregularities as depression storage. In addition to calculating infiltration,

Table 7.9. Classification of soils into Hydrologic Soil Groups by infiltration capacity after prolonged wetting when planted to clean-tilled crops (source: Musgrave 1955 and other sources).

Soil group	Characteristics	Minimum infiltration capacity (mm hr^{-1})
A	Soils that are sandy, deep and well drained	8-12
B	Sandy loams, moderately deep and moderately well-drained soils	4-8
C	Clay loam soils, shallow sandy loams often with a low-permeability horizon impeding drainage	1-4
D	Heavy clay soils with high swelling potential, water-logged soils or shallow soils over an essentially impermeable layer	0-1

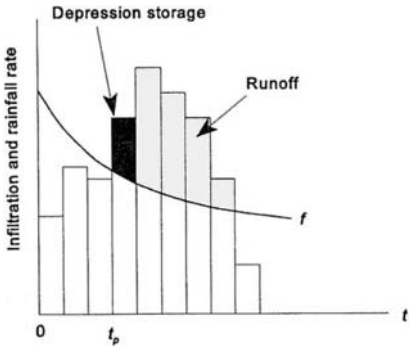

Figure 7.10. Graph showing a rainfall hyetograph and infiltration curve. The first increment of excess rainfall goes into depression storage. All rainfall below the infiltration curve is absorbed by the soil. Rainfall above the curve becomes runoff which starts at the ponding time.

infiltration equations can also be used to calculate the ponding time. Identifying areas that are likely to generate surface runoff is important in flood studies and also in water quality studies because these areas are potential sources of nonpoint source pollution.

7.7 SOIL WATER

Soil moisture is important in many ways. The most obvious is its importance to crop plants and vegetation. It is not surprising that much of the early research on soil moisture focused on agriculture. Many of the soil moisture terms and concepts used today reflect this agricultural legacy, e.g. field capacity and wilting point. The purpose of irrigation is to provide optimal soil moisture conditions for the crop. In the United States most of the irrigated cropland is in the West, but irrigated acreage has been increasing in eastern states where irrigation is used as a backup in times of drought. Soil conservation techniques to reduce soil erosion, such as contour plowing and terracing, affect soil moisture by slowing surface runoff and promoting infiltration.

Soil moisture and infiltration are important to society in other ways. More and more people are making their homes in rural areas beyond the reach of water and sewer facilities. They depend on well and septic systems to bring water into the

home and remove the wastes. Septic systems have two basic components. The waste stream leaving the house enters a holding tank where the heavier solid particles settle. The remaining liquid waste flows to a subsurface leach field. The wastewater percolates into the ground and is cleansed by a combination of natural biological decomposition and adsorption onto soil particles. The adequacy of a soil for a septic system is often the single most important factor in the development of rural areas. Most areas now require a 'perc' test to determine the saturated hydraulic conductivity and the soil's suitability for a septic system. Areas with saturated soils, poor drainage or shallow water tables are unsuitable as leach fields.

A major concern today is contamination of soil and groundwater by hazardous and toxic substances. Underground storage tanks, accidental spills, landfills, dump sites, and leach fields are all sources of contamination. Contaminants released at or near the ground surface migrate through the soil and may eventually reach groundwater. Understanding the migration of pollutants in the soil is a major area of research today.

7.7.1 *Porosity*

The amount of water stored in the soil is small from a global perspective; however, it is an active storage location with water cycling in and out of the soil on a time scale of days to months (Table 1.1). Water is stored within the void spaces in the soil mass, so the soil's porosity is the upper limit for storage capacity. Porosity n is the percentage of the soil volume that is void space and is defined as the volume of the voids V_v divided by the total volume of the material V_T:

$$n = \frac{V_v}{V_T} \tag{7.5}$$

Porosity for sand typically ranges between 25 and 45%. For silt, porosity may be 35 to 50%. Clay may have porosities from 40 to as high as 70%.

7.7.2 *Soil water potential*

Water is held in the soil by the force of attraction between the water and the soil particles. As we have seen, various terms are used to describe this force. We encountered capillary suction and soil moisture tension in this chapter and in Chapter 6. These are not the only terms used to describe soil moisture. This lack of agreement on terminology can be somewhat confusing. What makes matters worse is that some terms refer to a negative number while others refer to a positive number. Suction, for example, is a positive number, while tension is a negative number, and yet they are describing the same energy phenomena. From this point on we use soil water *potential* ψ to describe the potential energy with which water is held in the soil. As with soil water terminology, there are a variety of units for expressing soil water potential. Potential may be expressed as energy per unit volume of water, which has the dimensions of pressure ($ML^{-1}T^{-2}$), and the familiar units of millibars, bars or pascals. Another convenient way to express potential is to convert pressure into the equivalent height of a column of liquid water that exerts a given pressure at the bottom of

the column. This is called *head h*, and has the dimension of length (*L*). We will see this term again in the study of groundwater in Chapter 8.

Applying this terminology the two sources of energy acting on soil water are the *gravitational potential* ψ_z and the *pressure* or *matric potential* ψ_p. The gravitational potential is the potential energy due to the acceleration of gravity. It is equal to the weight of the water γ times its elevation z above some reference plane. The gravitational potential is significant only when the soil moisture level exceeds the field capacity, i.e. when $\psi_p > -0.33$ bars, otherwise the pressure potential dominates. The pressure potential is what we have previously called capillary suction or tension – it is the potential energy due to the attraction of water for soil particles. If we ignore some other very small potentials, we can assume that the sum of the gravitational potential and pressure potential equals the total soil moisture potential ψ:

$$\psi = \psi_z + \psi_p \tag{7.6}$$

The pressure potential changes continuously with water content. Viewed along a transect from the surface into the soil, pressure potential is negative in the unsaturated *zone of aeration* above the water table and positive below the water table in the *groundwater zone* (Fig. 7.11). The term groundwater zone is used here rather than *zone of saturation* because the *capillary fringe* and the *soil moisture zone* may be saturated even though pressure potential is negative. Some texts use the terms groundwater zone and zone of saturation synonymously. The *vadose zone* is defined as the region between the soil moisture zone and the capillary fringe and is normally unsaturated. Again, other books define the vadose zone differently, equating it to what we call the zone of aeration here. Soil moisture potential is defined to be zero at the water table, where pressure is equal to atmospheric pressure. Figure 7.12 shows an energy continuum from negative to positive potential, along with some frequently used terms. As a soil dries the potential decreases (becomes a larger negative number). Wetting the soil increases the potential. A wet soil has a greater potential than a dry soil and water moves from higher to lower potential energy. Water thus flows from wet to dry soil. This is the advantage of using the concept of potential energy in describing soil moisture; it applies to both unsaturated and saturated conditions. The terms tension and suction apply only to the unsaturated condition.

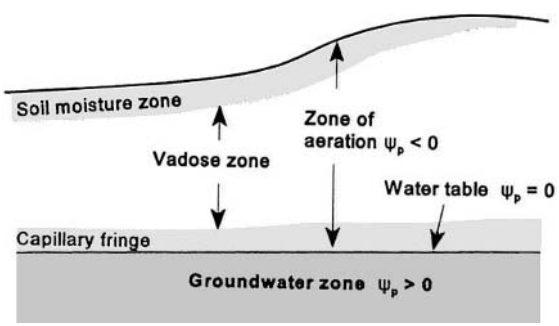

Figure 7.11. A cross-section through the ground showing the value of pressure potential at different locations. In the zone of aeration pressure potential is negative. Pressure potential is defined to be zero at the water table. In the groundwater zone pressure potential is positive.

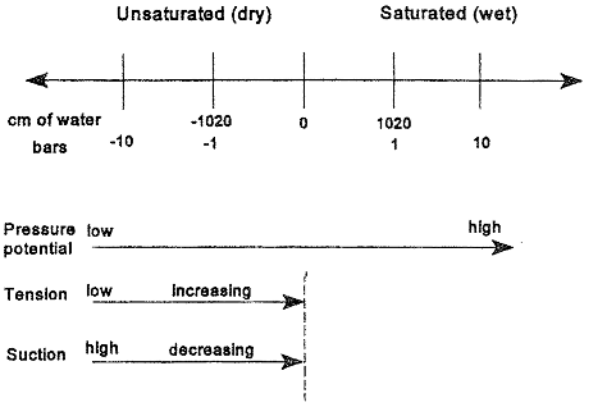

Figure 7.12. A continuum for soil moisture potential. Dry soil has a lower potential than wet soil. The term tension refers to a negative number, the same as potential; however, suction refers to a positive number. The terms tension and suction apply only in the zone of aeration.

7.7.3 *Soil water characteristic*

A graph showing the variation in soil water potential versus moisture content θ is called a *soil water characteristic* curve (Fig. 7.13). As the soil dries, the potential decreases in a nonlinear fashion. The abrupt change in the shape of the curve on the far right side at high potential corresponds to the 'air entry level.' This is the moisture level when air becomes continuous in the pore spaces and represents the top of the capillary fringe. Water content and potential are strongly related to soil texture through the effects of pore size and shape. The soil water characteristic can be used to estimate the amount of water $(\theta_2 - \theta_1)$ held between any two pressure limits $(\psi_2 - \psi_1)$. Figure 7.14 shows soil water characteristic curves for two different soils – the Plainfield Sand and Yolo Clay (Mein & Larson 1971 referenced in Singh 1989). The clay soil holds the same amount of water with greater force (lower potential) than does the sand. Said another way, at the same potential clay holds more water than does sand. One consequence of this is that water will migrate from a sandy layer to a clay layer if they both have the same initial moisture content. In reality soil moisture displays hysteresis (Fig. 7.15). This means the soil characteristic curve is different depending upon whether the soil was wetting or drying to reach the specific levels of moisture and potential. Because of hysteresis a drying soil contains more water at a given pressure potential than if the soil had reached that same potential by wetting. Hysteresis is often ignored in practice, but it obviously affects the estimate of water content held between any two values of ψ. Figure 7.16 shows median values for porosity, field capacity and wilting point for a range of soil texture. In Chapter 6 we defined available water capacity *AWC* as the total amount of water held in the soil between the –15 bar (wilting point) and –0.33 bar (field capacity) potentials. Figure 7.16 shows that the *AWC* for sand-texture soils is fairly low, around 6% by volume. Silt loams generally have the highest values in the range of 18%. SCS county-level soil surveys contain a wide variety of physical and chemical information about soils, including *AWC* per unit depth (inches of water per inch of soil) (Fig. 7.17). If soil survey data are not available, Figure 7.18 can give approximate values

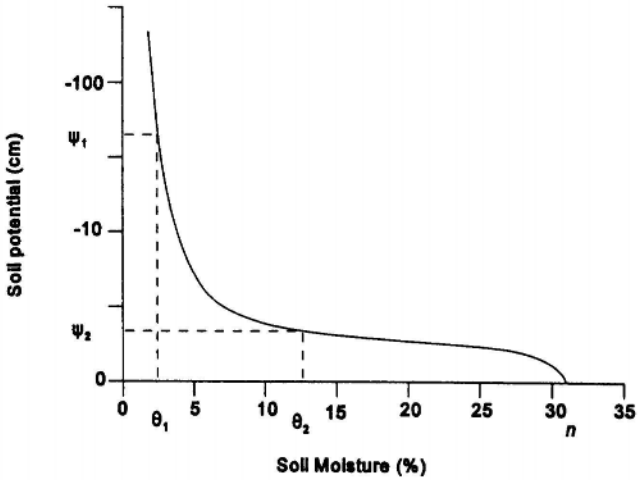

Figure 7.13. Soil moisture characteristic curve showing the relationship between soil moisture content θ and the potential ψ. As the soil dries the potential decreases and the water is held in the soil with greater force.

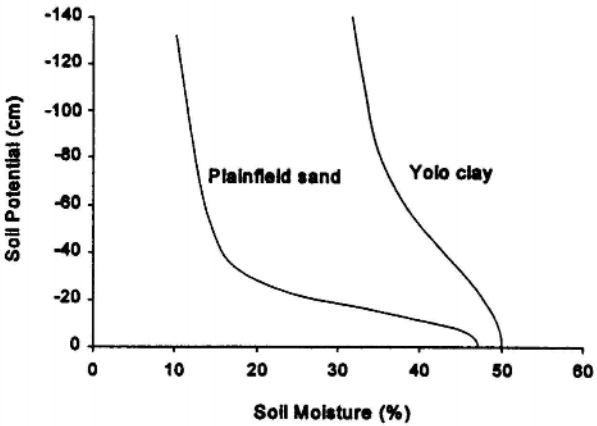

Figure 7.14. Soil moisture characteristic curves for a sand and a clay soil. At a given soil moisture level the potential is lower in clay than sand, and the water is held with greater force in the clay (after Mein & Larson 1977).

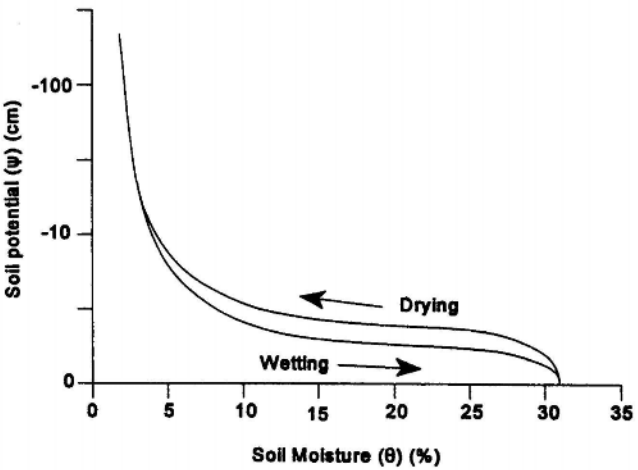

Figure 7.15. Hysteresis in a soil means the soil can have a different moisture content for a given soil potential depending upon whether the soil dried or wetted to reach the moisture level.

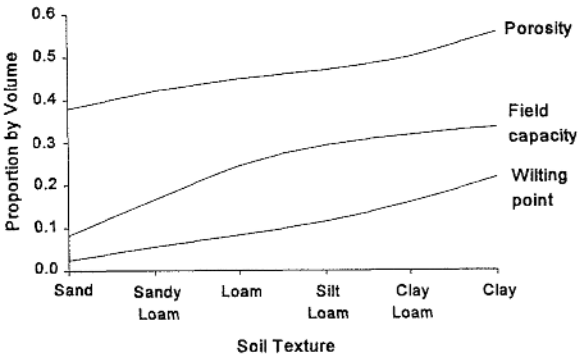

Figure 7.16. Median values for porosity, field capacity and wilting point for a range of soil texture (source: US Department of Agriculture 1955, Dunne & Leopold 1978).

Soil name and map symbol	Depth	Clay	Moist bulk density	Permeability	Available water capacity	Soil reaction	Shrink-swell potential	Erosion factors		Organic matter
								K	T	
	In	Pct	G/cm³	In/hr	In/in	pH				Pct
LdA, LdB, LdC----	0-9	15-25	1.20-1.40	0.6-2.0	0.16-0.20	5.1-7.8	Low----------	0.32	4	1-3
Letort	9-32	18-35	1.40-1.60	0.6-2.0	0.12-0.16	5.1-7.8	Low----------	0.28		
	32-62	18-35	1.40-1.60	0.6-2.0	0.08-0.12	5.6-7.8	Low----------	0.17		
Lg----------	0-10	10-18	1.20-1.40	2.0-6.0	0.14-0.18	5.6-7.3	Low----------	0.37	4	1-4
Linden	10-50	10-18	1.20-1.40	2.0-6.0	0.14-0.18	5.6-7.3	Low----------	0.37		
	50-60	5-25	1.20-1.40	6.0-20	0.05-0.08	5.6-7.3	Low----------	0.17		
Ln----------	0-10	15-27	1.20-1.40	0.6-2.0	0.20-0.26	5.1-7.3	Low----------	0.32	5	2-4
Lindside	10-50	18-35	1.20-1.40	0.2-2.0	0.17-0.22	5.1-7.3	Low----------	0.37		
	50-60	18-35	1.20-1.40	0.2-6.0	0.12-0.18	5.6-7.3	Low----------	0.32		
MaB, MaC, MaD----	0-10	10-25	1.20-1.40	0.6-2.0	0.17-0.21	4.5-7.3	Low----------	0.37	3	1-3
Manor	10-23	10-25	1.30-1.50	0.6-2.0	0.14-0.20	4.5-7.3	Low----------	0.32		
	23-60	5-20	1.25-1.50	0.6-6.0	0.10-0.17	4.5-7.3	Low----------	0.49		
MbB, MbD, MbF----	0-10	10-25	1.20-1.45	0.6-2.0	0.14-0.17	4.5-7.3	Low----------	0.32	3	---
Manor	10-23	10-25	1.30-1.50	0.6-2.0	0.14-0.20	4.5-7.3	Low----------	0.32		
	23-60	5-20	1.25-1.50	0.6-6.0	0.10-0.17	4.5-7.3	Low----------	0.49		
MdB----------	0-8	10-20	1.20-1.30	0.6-2.0	0.18-0.22	5.1-7.3	Low----------	0.37	4	1-2
Mount Lucas	8-30	17-32	1.30-1.60	0.06-0.6	0.12-0.16	5.1-7.3	Low----------	0.28		
	30-60	5-20	1.30-1.70	0.06-6.0	0.04-0.12	5.6-7.3	Low----------	0.28		
MeB----------	0-6	10-20	1.20-1.30	0.6-2.0	0.16-0.22	5.1-7.3	Low----------	0.28	3	---
Mount Lucas	6-30	17-32	1.30-1.60	0.06-0.6	0.12-0.16	5.1-7.3	Low----------	0.28		
	30-60	5-32	1.30-1.70	0.06-6.0	0.04-0.12	5.6-7.3	Low----------	0.28		
Nc, Nd----------	0-16	7-27	1.20-1.40	0.6-2.0	0.15-0.23	5.6-7.8	Low----------	0.43	5	1-4
Newark	16-32	18-35	1.20-1.45	0.6-2.0	0.18-0.23	5.6-7.8	Low----------	0.43		
	32-60	12-40	1.30-1.50	0.6-2.0	0.15-0.22	5.6-7.8	Low----------	0.43		
Ne----------	0-10	12-35	1.20-1.40	0.6-2.0	0.18-0.23	5.6-8.4	Low----------	0.43	5	2-4
Nolin	10-60	18-35	1.25-1.50	0.6-2.0	0.18-0.23	5.6-8.4	Low----------	0.43		
Pa----------	0-12	15-25	1.20-1.40	0.6-2.0	0.16-0.20	5.6-7.3	Low----------	0.43	3	2-4
Penlaw	12-29	20-35	1.40-1.60	0.6-2.0	0.16-0.20	5.6-7.3	Moderate-----	0.24		
	29-55	20-35	1.60-1.80	0.06-0.2	0.10-0.16	5.6-7.3	Moderate-----	0.24		
	55-60	15-50	1.40-1.60	0.06-0.6	0.12-0.16	5.6-7.3	Moderate-----	0.24		
PeC, PeD, PeE----	0-10	10-20	1.10-1.40	0.6-6.0	0.12-0.18	6.1-7.3	Low----------	0.43	3	1-3
Pequea	10-26	10-20	1.20-1.50	0.6-6.0	0.10-0.14	6.1-7.3	Low----------	0.28		
	26-52	10-20	1.20-1.50	0.6-6.0	0.06-0.12	7.4-8.4	Low----------	0.28		
	52	---	---	---	---	---	----------	----		
Qu*.										
Pits										
RaB----------	0-9	15-20	1.20-1.40	0.6-2.0	0.16-0.20	4.5-6.5	Low----------	0.43	3	1-3
Readington	9-33	18-35	1.40-1.60	0.6-2.0	0.08-0.14	4.5-6.5	Low----------	0.32		
	33-58	20-30	1.60-1.80	0.2-0.6	0.06-0.10	4.5-6.5	Low----------	0.32		
	58	---	---	---	---	---	----------	----		
RbB----------	0-9	15-20	1.20-1.40	0.6-2.0	0.14-0.18	4.5-6.5	Low----------	0.28	3	1-3
Readington	9-33	18-35	1.40-1.60	0.6-2.0	0.08-0.14	4.5-6.5	Low----------	0.32		
	33-58	20-30	1.60-1.80	0.2-0.6	0.06-0.10	5.1-6.5	Low----------	0.32		
	58	---	---	---	---	---	----------	----		
Rd----------	0-9	10-20	1.10-1.30	0.2-2.0	0.14-0.18	5.1-7.3	Low----------	0.43	4	2-4
Rowland	9-25	15-32	1.20-1.50	0.2-2.0	0.14-0.18	5.1-7.3	Low----------	0.28		
	25-42	15-32	1.20-1.50	0.2-2.0	0.12-0.16	5.1-7.3	Low----------	0.28		
	42-60	3-12	1.40-1.70	2.0-6.0	0.03-0.08	5.1-7.3	Low----------	0.17		
UaB, UaC, UaD----	0-10	10-20	1.20-1.40	0.6-2.0	0.10-0.18	3.6-7.3	Low----------	0.32	3	1-2
Ungers	10-46	17-27	1.30-1.50	0.6-2.0	0.10-0.14	3.6-7.3	Low----------	0.17		
	46-50	10-20	1.30-1.50	0.6-2.0	0.06-0.12	3.6-7.3	Low----------	0.17		
	50	---	---	---	---	---	----------	----		

Figure 7.17. A page from the Lancaste County soil survey showing some of the technical information available about soils (source: SCS 1985).

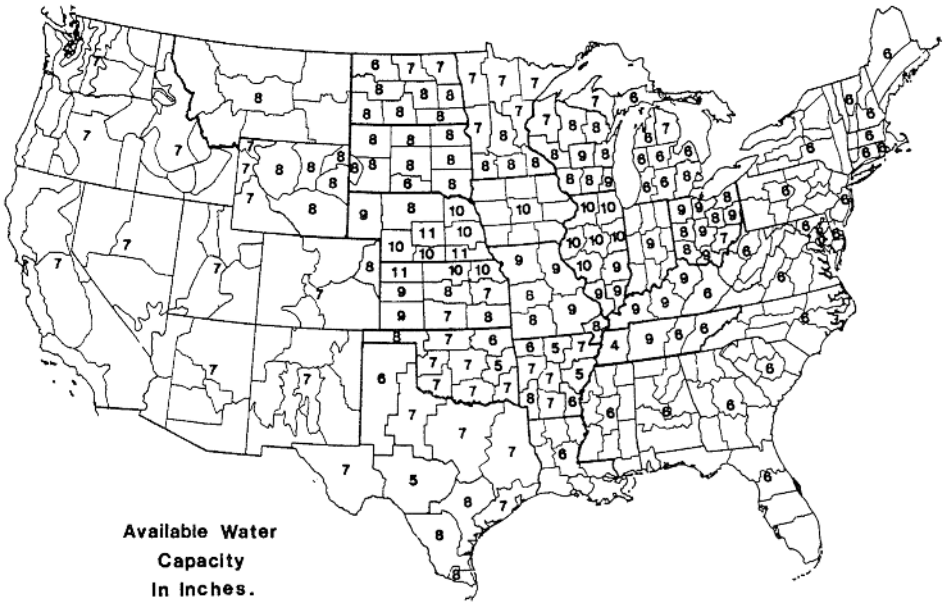

Figure 7.18. A map showing generalized estimates of available water capacity (*AWC*) (source: National Climatic Data Center, no date).

for total *AWC* throughout the United States. When using the SCS soil survey data, the total *AWC* for a soil is determined by multiplying the available water capacity per unit depth for each horizon (*awc*) by the depth of the horizon (*d*) and summing the total:

$$AWC = \sum_{i=1}^{n} awc_i(d_i) \tag{7.7}$$

For example, the median total *AWC* for the Letort soil group in Figure 7.17 would be calculated as:

$$AWC = 0.18(9) + 0.14(23) + 0.10(30) = 7.8 \text{ inches}$$

7.7.4 *Water movement in the soil*

When the upper-most layer of soil becomes saturated either from prolonged rainfall or by irrigation, water advances downward as a 'wetting front' shown in Figure 7.19. The front advances as the soil progressively reaches saturation at lower levels. The curves in Figure 7.19 show the position of the wetting front at sequential times *t*. After the cessation of water input, the soil water redistributes throughout the soil column by gravity percolation. The moisture content in the upper layers decreases while the moisture in the lower layers increases (Fig. 7.20). Subsequent evaporation from the surface further modifies the shape of the curve.

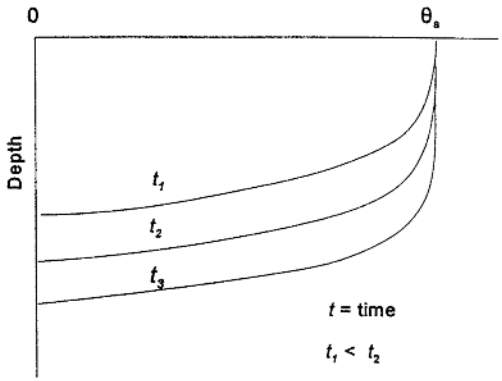

Figure 7.19. The downward movement of the wetting front over time with constant infiltration at the surface. The value θ_s represents the condition of saturation.

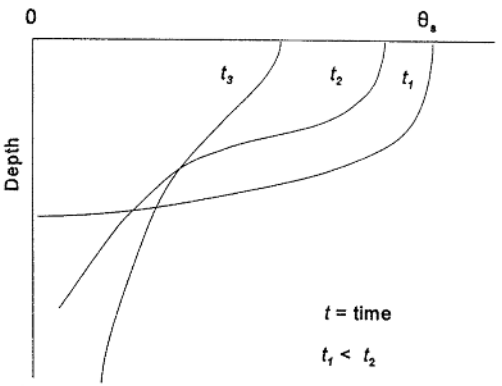

Figure 7.20. How the soil water redistributes by gravity after infiltration stops. Soil moisture decreases in the upper layers and increases in the deeper layers.

7.7.5 *Soil moisture measurement*

Soil moisture can be measure in the laboratory, in the field, or remotely using microwave sensors. The accepted standard for measuring soil moisture is the gravimetric method. A sample of soil is taken to the laboratory and weighed. The sample is then oven dried and weighed again to determine the amount of water lost. The water content is easily determined as the change in weight between the wet and dry sample. The main problem with the gravimetric method is that only a shallow soil layer can be sampled.

In the field neutron scattering is used to determine *in situ* water content. With this method a tube is installed in the ground and a high-energy neutron probe is lowered in the tube. Neutrons emitted into the soil from the energy source are slowed by collisions with hydrogen atoms present in water. The slowed neutrons randomly migrate back to the probe and are counted. The number of slowed neutrons counted per unit time yields and estimate of water content. The method requires calibration of the device and has high initial costs for the equipment and installation of the probe tubes. Tensiometers are inexpensive instruments for field measurement of soil potential. A tensiometer is a sealed, water-filled tube with a porous ceramic cup at the bottom. As the soil dries, water is drawn through the ceramic cup into the soil by the potential gradient between the soil and the saturated cup. This creates a vacuum inside the ten-

siometer which is measured with a gage or a manometer. Tensiometers can record potential only for fairly wet soil conditions. The maximum potential that a tensiometer can record is around –0.80 bars.

Using remote sensing technology for measuring of soil moisture has evolved rapidly in the last 10 years. The advantages of remote sensing included rapid measurements over large areas, as well as the ability to measure moisture to depths of a meter or more. Remote sensing methods will continue to play an important role in hydrologic research on land surface-atmospheric interactions.

SUMMARY

Water at the Earth's surface is partitioned by infiltration into soil water or surface runoff. Soil water is important to society in many ways from agriculture to rural subdivision planning. This chapter focused on infiltration and soil moisture but the direct and complementary relationship to runoff was recognized. Human activities dramatically alter the infiltration-runoff relationship. By creating impermeable surfaces in urban areas, cutting down forests, and tilling the soil, we set into motion a cascade of changes and feedbacks in the hydrologic system. For example, reduced infiltration in urban areas increases in the speed and the amount of surface runoff, causing changes in flood frequency, erosion and sediment transport downstream. The spread of urban surfaces can also reduce groundwater recharge, one of the topics of Chapter 8.

PROBLEMS

7.1 Use the average infiltration method to determine a basin-wide infiltration curve from the following data. Graph your infiltration curve.

Time	Total precipitation (cm)	Total runoff (cm)
8:00-9:30	2.3	0.2
11:00-11:40	0.5	0.3
1:00-1:50	0.4	0.2

7.2 Find the Φ index for the following set of data two ways as demonstrated in text Example 7.3. The easiest way to find the Φ index using the more complex formula is to use a spreadsheet program. Enter the equation into a cell in the spreadsheet and have the value for Φ in the equation be referenced in another cell. As you enter different values for Φ in its cell, the calculated result will automatically change. Remember to delete all terms from the equation where Φ is greater than the precipitation intensity.

Basin area = 3.5 mi^2
Total runoff volume = 112 ac–ft

Time	Accumulated precipitation (inch)
2:00-2:15	0.25
2:15-2:30	0.56
2:30-2:45	0.44
2:45-3:00	0.18
3:00-3:15	0.04

CHAPTER 8

Groundwater

Groundwater is a hydrologic subsystem that goes largely unobserved. We only see groundwater when it emerges at the surface as springs or seeps, occupying the bottom of a shallow well, or perhaps dripping down the walls and sitting in pools in underground caverns. The actual movement of water through the Earth is not directly observable. Groundwater is an important water resource. Groundwater accounts for nearly 25% of all freshwater used in the United States. In some western states more than 90% of all the water used is groundwater. Groundwater re-emerging in stream channels provides baseflow for perennial streams. In deserts, riparian vegetation tapping shallow groundwater adjacent to stream channels supports a ribbon of relatively lush habitat in an otherwise inhospitable environment.

Over the last two decades no other field in hydrology has undergone such a surge in interest as has the study of groundwater. The explosion in interest in this subfield of hydrology has been driven by growing concerns about groundwater quality and quantity. Underground storage tanks, septic systems, leachate from land fills and cropland have all caused groundwater pollution. In the mid 1980s the federal government got involved in groundwater management by encouraging states to develop wellhead protection programs to safeguard community water supply wells. In many areas groundwater pumping exceeds the rate of recharge to the aquifer, threatening the long-term sustainable use of the resource.

This chapter begins by examining the basic properties and characteristics of aquifers. Most of the chapter is devoted to understanding the physical characteristics of groundwater storage and flow, with a section touching on simulation modeling of groundwater flow (Section 8.9). At the end of the chapter (Section 8.12) is a brief look at major groundwater regions in the United States. In this chapter we do not discuss underground rivers and streams, even though such water is technically groundwater. This type of groundwater is limited in occurrence and its movement is governed by the forces that control open-channel flow rather than flow through porous media. By necessity this chapter is only an introduction to an extensive subfield in hydrology. The interested student can find detailed information on advanced topics in textbooks and journals devoted to groundwater.

8.1 GROUNDWATER DEFINED

What is groundwater? Like soil water it is subsurface water held in the interstices

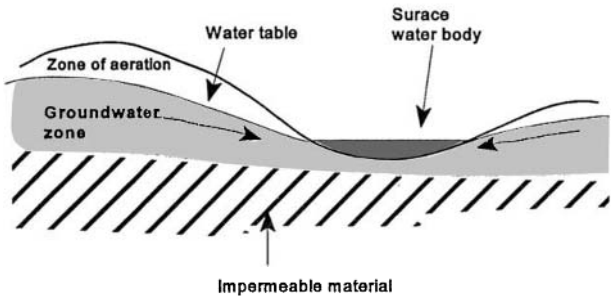

Figure 8.1. Cross-sectional diagram of the component zones of an unconfined aquifer. The extensive water table is open to recharge by precipitation. The water table intersects the ground and groundwater flows towards a surface (stream or lake) water body.

and fractures within earth materials. How is groundwater different from soil moisture? In Chapter 7 we defined soil water pressure potential along a continuum of potential energy (Figs 7.11 and 7.12). Soil moisture normally has negative pressure potential relative to atmospheric pressure. The pressure potential of the water table is zero, since the water table is at atmospheric pressure. Water below the water table has positive pressure potential. Groundwater is the water held in the interstices, cracks and fractures at positive pressure. Positive pressure only occurs in saturated material. Figure 8.1 is a schematic cross-section from the surface down to groundwater (see also Fig. 7.11) showing two major zones – the zone of aeration and the groundwater zone. The zone of aeration is normally unsaturated and includes the soil moisture zone, the vadose zone and the capillary fringe. The soil moisture zone may become saturated during prolonged rainfall, with irrigation, or when a deep snowpack melts in the spring. The capillary fringe develops immediately above the water table. The capillary fringe is created by water wicking up into the dryer (lower potential) material above the water table. The height of the capillary fringe depends upon the texture of the material. In silt and clay with strong capillary forces it can rise 100 cm above the water table; in coarse sand it is only about 12 cm. The capillary fringe is saturated close to the water table and the proportion of air in the pore spaces increases with distance away from the water table. The top of the capillary fringe is where air becomes continuous in the pore spaces. The water table marks the top of the groundwater zone. The groundwater zone is saturated and the water is under positive pressure potential. Groundwater flows into wells penetrating into the groundwater zone because the pressure inside the well is less than the pressure of the groundwater, and water flows from higher to lower potential.

8.2 AQUIFERS

An aquifer is a water-bearing layer of earth material sufficiently permeable to yield water to wells. The definition of an aquifer is qualified by the ability to yield water to wells. This qualification is necessary because material like clay may store large quantities of water, but is relatively impermeable, and so clays do not make good aq-

uifers. Low-permeability materials are called *aquitards*, since they slow the movement of water, and *aquicludes* if they are impermeable to water flow.

From a water management perspective the definition of an aquifer could be further modified to recognize different economic uses. In this case an aquifer is defined as a water-bearing layer of earth material sufficiently permeable to yield water to wells in economically useable quantities. For example, if a well could pump 10 gal min^{-1}, would this be an aquifer? The answer really depends on the use. If the well is for domestic use in and around a single-family home, the answer is yes, because a 10 gal min^{-1} well is normally sufficient for a single residence. If the economic use is to irrigate 640 acres of corn, then the answer would surely be no. A good agricultural well pumps hundreds-to-thousands of gallons of water per minute.

8.2.1 *Unconfined aquifers*

Aquifers are classified as *unconfined* or *confined*. Figure 8.1 is a cross-section of an unconfined aquifer. An unconfined aquifer has an extensive water table open to recharge by percolation from the surface. Unconfined aquifers are also called *water table* aquifers. The position of the water table reflects the amount of water in storage and it moves up and down depending upon the relative rates of recharge (input) and discharge (output) (see Eq. 1.1). Precipitation is the main source of natural recharge, but for some aquifers other types of recharge are important. In areas with irrigation agriculture, a significant fraction of the irrigation water applied to the fields may go to recharge groundwater. In fact excess irrigation water is purposefully applied to leach accumulated salts from the root zone. Along the South Platte River in Colorado, years of irrigation on the alluvial benches adjacent to the river converted the South Platte from an intermittent river that dried up in the summer to a perennial river. The recharge of groundwater by irrigation increased the amount of groundwater in storage to the point where it provided baseflow to the South Platte River all year. In other areas treated sewage effluent is spread over the ground, or is directly pumped into the ground. This practice accomplishes both advanced wastewater treatment and groundwater recharge at the same time.

Natural recharge is controlled by weather and climate. For example, in Southeastern Pennsylvania mean monthly precipitation is quite uniform, with every month receiving between 7 and 10 cm (3 and 4 in.). During the summer groundwater recharge is reduced because evapotranspiration returns most of the precipitation to the atmosphere. The coldest winter months of January and February also have limited recharge, as frozen soil reduces infiltration, and precipitation is stored on the surface as snow. Groundwater recharge occurs mainly in the fall and spring when precipitation is plentiful, evapotranspiration is low, and infiltration is unaffected by frozen soil. A dry spring or fall may have a disproportionately greater impact on groundwater recharge than a dry summer or winter.

Because unconfined aquifers have extensive water tables they are vulnerable to pollution. Any land use or activity occurring over the aquifer that releases pollutants could potentially contaminate the aquifer. The aquifer's vulnerability to pollution depends upon the depth to the water table and the rate of migration of pollutants through the vadose zone. Studies in southeastern Pennsylvania show that in areas

with fractured carbonate bedrock, nitrogen from fertilizers can reach groundwater within a matter of hours following a rainstorm (Hall & Risser 1993).

Urbanization can have a two-fold impact on groundwater quantity. The increase in water demand with population growth increases groundwater withdrawals. At the same time the increase in impermeable surface area can reduce recharge. Land use regulation for the protection of groundwater is a relatively new concept, but it is necessary in some areas to insure both the quality and quantity of the resource.

8.2.2 *Confined aquifers*

Confined aquifers are water-bearing layers of rock material sandwiched between impermeable aquicludes or semi-permeable aquitards (Fig. 8.2). These layers prohibit or inhibit vertical communication between water in the confined aquifer and water above or below. Recharge to a confined aquifer occurs in a spatially-restricted recharge area where the aquifer outcrops at the surface. When the confining layers are aquitards, recharge may occur through vertical seepage, in which case it is a 'leaky' confined aquifer. The defining characteristics of confined aquifers is that they do not have a water table, except in the recharge zone, and they are pressurized. The pressure condition in a confined aquifer is given by the *potentiometric or piezometric surface* (Fig. 8.2). The potentiometric surface surface is identified using a *piezometer*. A piezometer is a tube open only at the ends. A piezometer is different from a well which is perforated along its length allowing water to flow in laterally. If a piezometer is inserted into a confined aquifer water can only enter through the lower end. The height the water rises in the piezometer gives the location of the potentiometric surface at that location. If the potentiometric surface is above the ground surface, water flows to the surface without pumping. This is called a flowing *artesian* well, named for the province of Artois in northern France where the phenomena was first observed. We examine the pressure condition of unconfined and confined aquifers in Section 8.4.

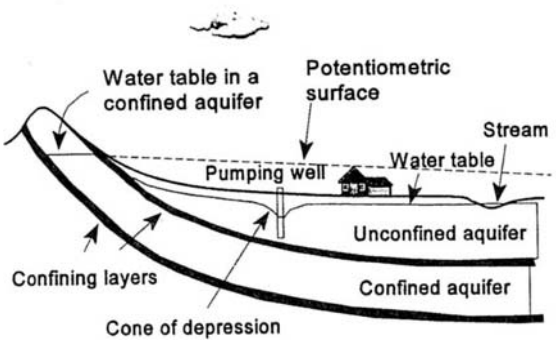

Figure 8.2. Cross-sectional diagram of a confined aquifer. The aquifer is confined between less permeable confining layers. The potentiometric surface defines the pressure condition within the confined aquifer. The potentiometric surface slopes in the direction of water flow because friction between the flowing water and the aquifer material reduces the potential energy of the water. This picture shows that a confined aquifer can occur beneath an unconfined aquifer.

This simple classification of aquifers is useful but somewhat misleading because the real world is always much more complex. It is possible for a largely unconfined aquifer to locally display confined conditions where isolated lenses of clay confine the flow. Fractured consolidated aquifers may be unconfined and yet display pressure conditions indicative of a confined aquifer because rapid water flow in fractures and solution channels creates increased hydraulic pressure.

8.3 PROPERTIES OF AQUIFER MATERIALS

The two primary properties of aquifer materials are porosity and permeability. Of the two, permeability is perhaps more important from a groundwater quantity perspective, because even with high porosity, low permeability can make water use uneconomical.

8.3.1 *Porosity and water storage*

The best aquifers are made of materials with both high porosity and high permeability. The greater the porosity the more available space to store water; the higher the permeability, the easier water flows to wells. The definition of porosity n was given in Equation (7.5). *Primary porosity* is the porosity attributable to the interstitial void spaces between individual rock particles (Fig. 8.3). *Secondary porosity* is created by fractures and solution channels within the solid rock mass. Aquifers can be composed of either unconsolidated or consolidated material. Unconsolidated sand and gravel in alluvial valleys and along coastal plains make excellent aquifers. Glacial outwash deposits can sometimes be high-yielding aquifers. Table 8.1 gives representative values for porosity for different materials. Generally speaking, uniform texture materials have higher porosities than well-graded materials. The reason is that in graded materials the smaller particles tend to fill in the void spaces between the larger particles.

Consolidated aquifers occur in sedimentary, igneous and metamorphic rocks. In sedimentary rocks the calcium and silica cement between the individual grains fills the interstitial spaces. In igneous and metamorphic rocks the interlocking crystalline structure largely precludes the formation of interstices.

Porosity in consolidated material is virtually all secondary porosity. Comparing

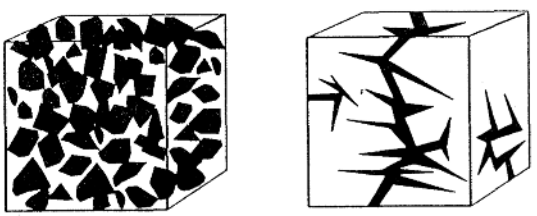

Figure 8.3. Primary porosity is composed of the interstices between individual grains. Secondary porosity is made up of the openings created by cracks and fractures in rock material.

Table 8.1. Representative values of porosity for unconsolidated and consolidated materials. (sources: Dunne & Leopold 1978, Davis 1969).

Materials	Porosity
Unconsolidated	
Clays	0.40-0.60
Silt	0.35-0.50
Loess	0.40-0.55
Fine sand	0.30-0.40
Coarse sand	0.25-0.30
Sand and gravel	0.10-0.30
Gravel	0.20-0.30
Glacial till	0.25-0.45
Consolidated	
Sedimentary rocks	0.05-0.30
Igneous rocks	0.01-0.05
Metamorphic rocks	0.01-0.05
Fractured and weathered igneous rock	0.02-0.10
Recent basalt	0.02-0.10
Vesicular lava	0.10-0.50

consolidated and unconsolidated materials, porosities are much higher for unconsolidated materials. The *storage coefficient S* is a measure of the volume of water that is released (or taken up, ignoring hysteresis) by a given volume of aquifer material. More specifically, it is the volume of water released or taken up per unit surface area of the aquifer per unit change in head (Fig. 8.4). For an unconfined aquifer the change in head is the change in the elevation of the water table. For a confined aquifer the change in head equals a change in the elevation of the potentiometric surface. The storage coefficient is expressed as a dimensionless fraction or percentage. For an unconfined aquifer the storage coefficient is also called the *specific yield.*

Example 8.1
Calculate the specific yield for the following hypothetical situation. A well pumps 3500 m^3 of water and causes the (horizontal) water table to drop 2 m over an area of 10,000 m^2. The storage coefficient is the volume of water released per unit volume of aquifer.

Volume of water released = 3500 m^3

Volume of aquifer = (2 m) (10,000 m^2) = 20,000 m^3

Storage coefficient = (3500 m^3) / (20,000 m^3) = 0.175

Fine-textured materials have specific yields much lower than their porosity because capillary forces in the small interstices do not easily release water. In coarse-textured materials the storage coefficient approximates the porosity (Fig. 8.5). Water is released from unconfined aquifers by the drainage of pore spaces. Confined aquifers remain saturated as water is released because there is no falling water table except at the recharge zone. Water is released from confined aquifers by compression of the aquifer, and in some cases by leakage from aquitards. Storage coefficients for

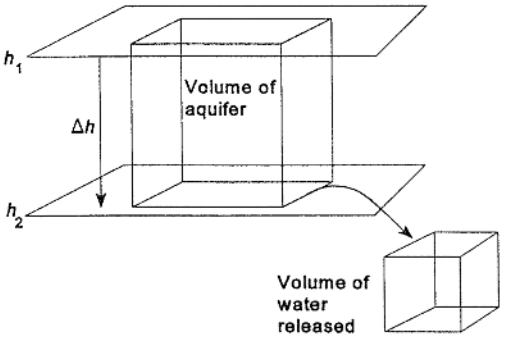

Figure 8.4. The storage coefficient equals the volume of water released per unit surface area of aquifer material per unit change in head.

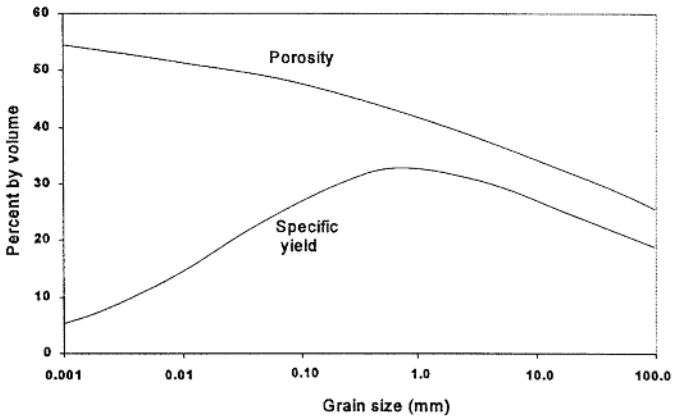

Figure 8.5. The curves show the relationship between the specific yield and porosity for materials in the Western United States. For fine-texture materials porosity is much higher than the specific yield. Fine-texture materials do not easily release the water held in storage. Coarse-texture materials have specific yields that come close to the porosity of the material (source: Davis & Dewiest 1966, used by permission).

confined aquifers can be two to four orders-of-magnitude smaller than for unconfined aquifers. Excessive over pumping and prolonged compression of confined aquifers can result in land subsidence and an irreversible loss of porosity. Dunne & Leopold (1978) relate a fascinating story about land subsidence in and around Venice, Italy caused by groundwater pumping. Even a few centimeters of subsidence can be potentially devastating to Venice because the city is at sea level. By the 1960s subsidence around Venice had reached 10 cm. It is believed that 85% of the subsidence is irreversible because the underlying layers of sand, silt and clay have been permanently compacted.

Hydrologically the term *safe yield* means the rate that water can be withdrawn from and aquifer without causing a long-term decline in the water table or potentiometric surface. Over the long term safe yield equals the average recharge rate. Some aquifers have little or no natural recharge. The Ogallala Aquifer underlying the High Plains in the central United States is an example. Pumping groundwater from the

Ogallala is analogous to pumping oil – once pumped, the water is gone. The proper management of finite groundwater resources like the Ogallala pose difficult questions for society. The major management issue revolves around how we value the future. Should we use the water today, or save it for our children? Safe yield under these conditions is very different than in the case of renewable groundwater. Here safe yield under the conditions of a finite resource might mean the rate of withdrawal that does not exhaust the supply before an alternative water source is developed. In some states, the aquifer is given an arbitrary lifetime and total withdrawals are adjusted to exhaust the supply over that time period.

8.3.2 *Hydraulic conductivity*

As we learned in Chapter 7, the term saturated hydraulic conductivity K_s describes the permeability of earth materials under saturated conditions. Since we will always be dealing with the condition of saturation when studying groundwater, we use the term hydraulic conductivity K and assume saturation. Hydraulic conductivity describes how easily water flows through an aquifer. The determination of K is done in the field using a pump test. The determination K is described in section 8.7. The dimensions of K are velocity (LT^{-1}), so a value of $K = 10$ m d^{-1} versus a value of $K = 0.001$ m d^{-1} means that water moves 10,000 time faster in the first aquifer than in the second. Figure 8.6 gives values of K for different materials and shows an astonishing 12 orders-of-magnitude range.

Hydraulic conductivity is a function of both the aquifer material and the water. That portion of K controlled by the properties of the aquifer material is the *intrinsic permeability*. Intrinsic permeability is related to porosity and to the size and shape of the voids spaces. The property of the water affecting K is the dynamic viscosity. As water temperature increases, the dynamic viscosity of water decreases. Hydraulic conductivity is inversely related to viscosity, and the relationship is linear – a doubling of viscosity reduces K by 50%.

Alluvial deposits are usually *anisotropic*. Anisotropy means that K is different in different directions within the material. For example, hydraulic conductivity in the

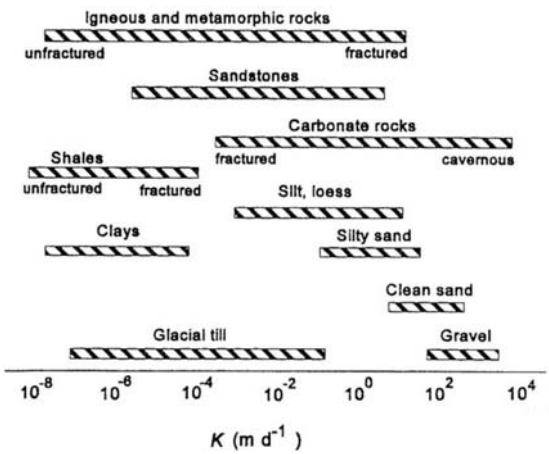

Figure 8.6. Ranges in hydraulic conductivity for different aquifer materials (source: Heath 1991).

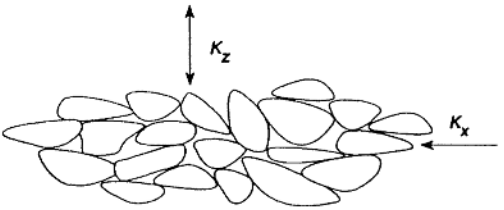

Figure 8.7. Diagrammatic representation of imbricated sediments (after Bouwer 1978).

vertical direction K_z may be ten to twenty times smaller than in the downstream direction K_x. When K is the same in all directions the aquifer is said to be *isotropic*. One cause of anisotropy is *imbrication* of the sediments. Individual particles are not spherical, and when they are deposited they preferentially lay on their flat side slightly overlapping particles in the direction of flow (Fig. 8.7). This overlapping orientation of sediments is imbrication. Another cause of anisotropy is layering of sediments with different K values. When K is different at different locations within an aquifer, the aquifer is *heterogeneous*. When K is the same throughout the aquifer it is *homogeneous*. Example 8.2 demonstrates the calculation of average K values for a layered anisotropic aquifer.

Example 8.2

This example demonstrates the effect on the hydraulic conductivity when the aquifer is composed of multiple layers, with each layer having a different K value. A two-layer aquifer as shown in Figure 8.8. Each layer is horizontal and assumed to be isotropic with its own value of K.

Without deriving the equations (see Bouwer 1978), the average hydraulic conductivity in the downstream direction K_x is calculated as the weighted arithmetic average of the individual layers:

$$K_x = \frac{K_1 z_1 + K_2 z_2}{Z} \tag{8.1}$$

where K_1 and K_2, and z_1 and z_2 are the hydraulic conductivity and thickness of layers 1 and 2, respectively, and $Z = z_1 + z_2$ is the overall thickness of the aquifer.

The calculation of the average hydraulic conductivity in the vertical direction K_z is:

$$K_z = \frac{Z}{\left(z_1 / K_1\right) + \left(z_2 / K_2\right)} \tag{8.2}$$

If the individual layers z_i are the same thickness, then Equations (8.1) and (8.2) can be generalized for n layers as:

$$K_x = \frac{K_1 + K_2 + \ldots + K_{n-1} + K_n}{n} \tag{8.3}$$

and

$$K_z = \frac{n}{\left(1/K_1\right) + \left(1/K_2\right) + \ldots \left(1/K_{n-1}\right) + \left(1/K_n\right)} \tag{8.4}$$

Equations (8.3) and (8.4) are the arithmetic mean (Eq. 3.3) and the harmonic mean (Eq. 3.5). The harmonic mean is always smaller than the arithmetic mean. Therefore, just by having different

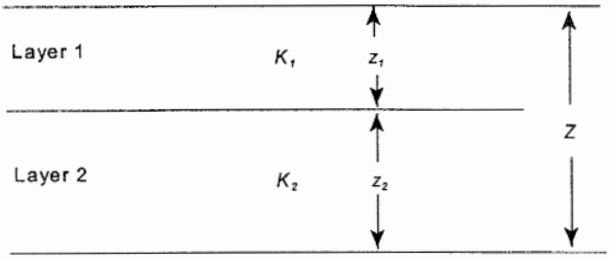

Figure 8.8. A two-layer aquifer. Each layer is isotropic and has a separate value of K (after Bouwer 1978).

layers of material with different hydraulic conductivities the average vertical hydraulic conductivity K_z will be less than the average horizontal hydraulic conductivity K_x.

8.4 GROUNDWATER HEAD

In Chapter 7 the total soil moisture potential (Eq. 7.6) equaled the gravitational potential plus the pressure potential. The total potential for groundwater is defined in identical fashion. The two sources of potential energy for a parcel of groundwater are the (positive) pressure potential energy ψ_p due to the depth of the parcel beneath the water surface, and the gravitational potential energy ψ_z, which is a function of the elevation of the water parcel relative to some arbitrary datum. Figure 8.9 shows two water parcels in an unconfined aquifer. Each parcel is at depth p beneath the water surface and at elevation z above the reference datum. The positive pressure potential energy of each parcel is:

$$\psi_p = \gamma V p \tag{8.5}$$

where γ = the weight density of water ($ML^{-2}T^{-2}$), V = volume of the parcel (L^3), and p = depth below the water table (L).

The units of weight density could be lbs ft^{-3} or N m^{-3}. Similarly, the gravitational potential energy of each parcel is equal to the elevation of the parcel times the weight of the parcel:

$$\psi_z = \gamma V z \tag{8.6}$$

The total potential energy ψ is thus:

$$\psi = \gamma V p + \gamma V z \tag{8.7}$$

Dividing each term by the weight of the parcel γV gives:

$$h = p + z \tag{8.8}$$

The total potential energy of a parcel is expressed in terms of head h, having the dimension of length (L). Equation (8.8) shows that the total head h at a point is composed of the *pressure head p* and the *elevation head z*. The pressure head is equal to the depth below the water table for an unconfined aquifer, and the depth below the potentiometric surface for a confined aquifer. Pressure head is measured with a piezometer. If the water is not moving or is flowing horizontally, then the height that

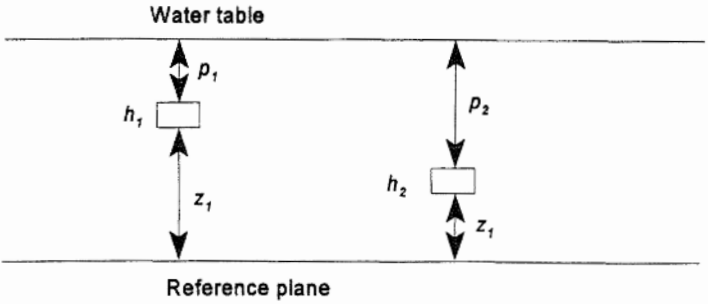

Figure 8.9. Two parcels of water in an unconfined aquifer. The total head h is equal to the pressure head p plus the elevation head z. The total head of parcel 1 is the same as the total head of parcel 2 and therefore the water table is horizontal.

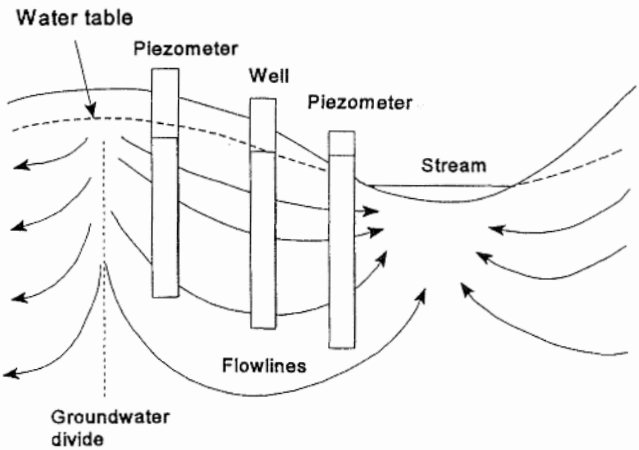

Figure 8.10. An unconfined aquifer with two piezometers and a well. The water level in the well indicates the position of the water table. The water level in the piezometers differs from the level in the well because of vertical flow.

water rises in a piezometer inserted into the aquifer equals the pressure head at that point. Vertical flow can alter the reading of a piezometer. If there is a downward component to the flow, then the piezometer will read lower than expected. Conversely, an upward flow causes the water level in the piezometer to be higher than expected. Figure 8.10 shows piezometers inserted into an unconfined aquifer. The piezometer near the top of the hill is inserted into groundwater flowing with a downward component. As a result the water level in the piezometer is lower than the water table. The water level in the piezometer at the bottom of the hill is higher than the water table because of the upward flow of the groundwater. Because water can enter a well laterally through the perforated casing, the static water level in a well is usually very close to the position of the water table.

8.4.1 *Hydraulic gradient*

It is the difference in h that causes groundwater to move because water flows from higher to lower head (potential energy). In Figure 8.9 both parcels have the same total head $h_1 = h_2$ even though their pressure and elevation heads are different. As a result, the water table is horizontal and there is no water movement. The *hydraulic gradient* is the change in h with distance x. Head changes continuously with distance, which is to say it is a continuous function of distance. Therefore it is appropriate to describe the hydraulic gradient using the derivative dh/dx from calculus. The derivative dh/dx gives the instantaneous rate of change of head with distance. But once again, when it comes to application we substitute a discrete linear approximation for the actual continuous function. The discrete approximation of the hydraulic gradient is denoted as $\Delta h/\Delta x$, where $\Delta h = \Delta h_2 - \Delta h_1$, and $\Delta x = \Delta x_2 - \Delta x_1$ is the distance between locations 1 and 2. Observe that since head decreases in the direction of flow $\Delta h/\Delta x$ is negative. (When there is no gradient, as in Fig. 8.9, $\Delta h/\Delta x = 0$.) Figure 8.11 is a sketch of groundwater where the hydraulic gradient is not zero. Two piezometers are inserted into the flow. The piezometers are inserted to the same depth so that they are on the same streamline. Streamlines are idealized flow paths for water molecules. In reality the individual water molecules follow a contorted path as they are forced over, under and around solid particles. In an isotropic aquifer flow lines are perpendicular to the hydraulic gradient. The head at location 1 is $h_1 = p_1 + z_1$ and the head at location 2 is $h_2 = p_2 + z_2$. From the diagram it is apparent that $h_1 > h_2$ so water flows from location 1 to location 2. Moving the arbitrary reference plane up or down has no effect on the relative magnitudes of h_1 and h_2. The change in head Δh between points 1 and 2 represents the conversion of potential energy into heat energy by friction as the water moves through the aquifer.

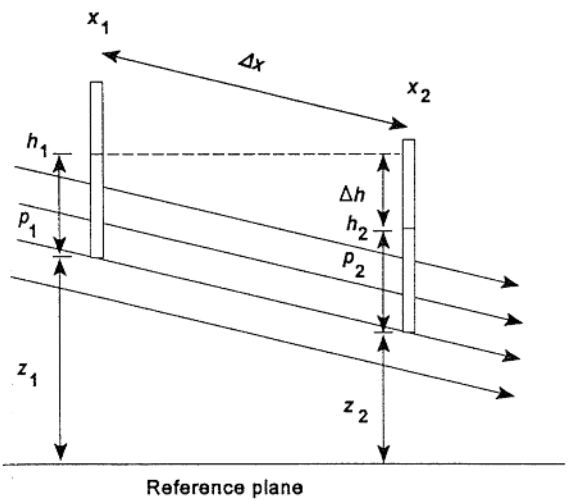

Figure 8.11. A cross-sectional view of a groundwater flow system. The streamlines of flow are idealized as straight lines. Two piezometers are inserted along the same streamline for the definition of terms used in calculating the hydraulic gradient (after Bouwer 1978).

8.4.2 *The three-point method*

The 'three point method' is a graphical technique for determining the local magnitude and direction of the hydraulic gradient. The magnitude of the hydraulic gradient is one of the variables controlling the velocity of groundwater flow. The direction of flow is important in cases of groundwater contamination. If there were an accidental spill and toxic chemicals were released into the groundwater, the direction of migration of the pollutants would be vital information for remedial action. Example 8.3 demonstrates the three-point method.

Example 8.3

The three-point method can be demonstrated as a series of 5 steps. The numerical values in this example are taken from Heath (1991). All values are in meters (m).

Step 1. Obtain head data for three wells (or piezometers) (Fig. 8.12a). The distance between the wells should ideally be governed by the requirements of problem at hand and the geology of the aquifer, but will most likely depend on data availability. Identify the well with the intermediate head (Well 2).

Step 2. Draw a straight line connecting the well with the highest head (Well 1) and the well with the lowest head (Well 3). Find the point on this line where the head is equal to the head at Well 2. This point can be found by using linear interpolation. Linear interpolation assumes that the incremental distance is in the same proportion to the incremental change in head, as the total distance is to the total change in head. Referring to Figure 8.12b, the unknown distance d_1 from Well 1 along the line to Well 3 using linear interpolation is:

$$\frac{h_1 - h_2}{d_1} = \frac{h_1 - h_3}{D} \tag{8.9}$$

where D is the total distance between Well 1 and Well 3. Equation (8.9) is easily solved for d_1. Inserting the data from Figure 8.12:

$$\frac{26.26 - 26.20}{d_1} = \frac{26.26 - 26.07}{215}$$

giving $d_1 = 68$ m from Well 1.

Step 3. Draw a straight line from Well 2 to the point located in Step 2. Since this line connects

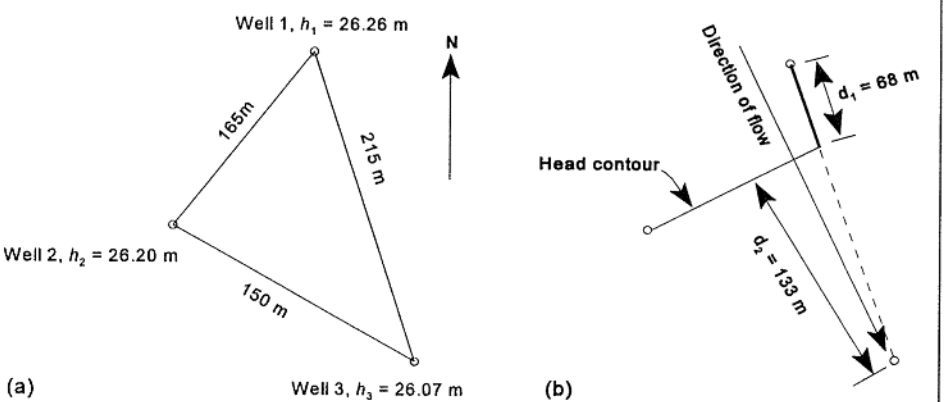

Figure 8.12. a) Heads and distances for the three wells, and b) How to determine the direction and magnitude of the hydraulic gradient.

two points of equal head ($h_2 = 26.20$ m), it represents a contour line of equal head. Contour lines of equal head are called *equipotential lines*.

Step 4. Draw a third line perpendicular to the equipotential line (drawn in Step 3) passing through either Well 1 or Well 3. Because groundwater flows perpendicular to equipotential lines, this line indicates the direction of flow, from higher to lower head.

Step 5. Measure and determine the distance d_2 along the path of groundwater flow. The hydraulic gradient is $(h_2 - h_3) / d_2$. Substituting values, the hydraulic gradient is (26.20 m – 26.07 m) / 133 m = 0.00097.

8.5 GROUNDWATER FLOW

Analyzing the flow paths for groundwater can get quite complex because groundwater can flow in all three directions x, y and z. As a result, we would need to consider the change in head in all three directions dh/dx, dh/dy and dh/dz. In developing a basic understanding of groundwater flow, we limit the discussion to very simple one-dimensional flow situations. Later we briefly consider two-dimensional flow. Analysis of three-dimensional flow is analytically difficult to say the least, and is only practical using groundwater simulation models. Flow dimensions are only one of many considerations in groundwater movement. Others factors include whether the aquifer is confined or unconfined, whether recharge is occurring or not, whether the groundwater system is steady, unsteady, uniform or nonuniform (see Table 1.3), and finally what types of flow boundaries exist around the aquifer? Combinations of these various factors create many different flow situations.

8.5.1 *Darcy's Law*

The French hydraulician Henri Darcy set forth the fundamental equation governing groundwater flow. Darcy's equation is the foundation of even the most sophisticated groundwater models. Based on experiments Darcy posited that the velocity of groundwater flow was directly proportional to the change in head and inversely proportional to the distance. For the continuous case Darcy's Law is:

$$v = -K\frac{dh}{dx} \tag{8.10}$$

The discrete linear approximation of Darcy's Law is:

$$v = -K\frac{h_2 - h_1}{x_2 - x_1} = -K\frac{\Delta h}{\Delta x} \tag{8.11}$$

where v is called the *Darcy velocity* and has dimensions (LT^{-1}). (Darcy velocity is also called the *specific discharge* in some texts.) Equations (8.10) and (8.11) are one-dimensional flow equations; in this case for flow in the x direction. The minus sign makes the Darcy velocity a positive number, since the hydraulic gradient is negative. Again, Equations (8.10) and (8.11) indicate that groundwater flows in the direction of decreasing head. If we always subtract the lower head value from the higher head value ($\Delta h = h_1 - h_2$) and substitute the length L between the two points for Δx (as in example 8.3), we will always have a positive value for the hydraulic gradient and we can ignore the minus sign:

$$v = K\frac{\Delta h}{L} \tag{8.12}$$

Groundwater flows at velocities very much slower than those of surface water. The Darcy velocity is the velocity as if the water were flowing through the entire cross-section of the aquifer (solids as well as voids), not just through the void spaces. As a result, the Darcy velocity is not the true *pore* or *macroscopic velocity* v_m of the water, because the water actually flows only through the voids in the porous media. The time-averaged macroscopic velocity can be determined as:

$$v_m = \frac{v}{n} \tag{8.13}$$

where n is the porosity of the material. The distinction between v and v_m is important in studies of contaminant transport. Theoretically, pollutants can travel at the macroscopic velocity, however, dispersion and other factors can cause pollutants to travel at velocities less than the macroscopic velocity. Contaminant transport is discussed in Section 8.10.2.

8.5.2 *Groundwater Discharge*

A very common problem is that of determining the quantity of water flowing through an aquifer. Variations of this basic problem include finding the baseflow to a stream or determining how much water might seep from an unlined irrigation ditch. The volumetric flow of water with time is called *discharge* (L^3T^{-1}). Discharge can be calculated as the Darcy velocity times the cross-sectional area that the water moves through:

$$Q = vA \tag{8.14}$$

Cross-sectional area A equals the average width w times the average depth y (see Eq. 2.1a). In an unconfined aquifer depth equals the saturated thickness of the aquifer. Substituting Equation (8.12) into Equation (8.14), gives the basic equation for calculating groundwater discharge:

$$Q = AK\frac{\Delta h}{L} \tag{8.15}$$

In some applications it's easier to calculate *discharge per unit width* q_w rather than the total discharge Q:

$$q_w = \frac{Q}{w} = yK\frac{\Delta h}{L} \tag{8.16}$$

The term *transmissivity* T is used in many groundwater studies. The transmissivity of an aquifer is equal to the hydraulic conductivity K times the saturated thickness y and has dimensions (L^2T^{-1}):

$$T = yK \tag{8.17}$$

Combining Equations (8.16) and (8.17) gives:

$$q_w = T\frac{\Delta h}{L} \tag{8.18}$$

Example 8.4
Assume an aquifer has the following characteristics:

$w = 1000$ m (width)

$y = 10$ m (depth)

$v = 0.1$ m d^{-1} (Darcy velocity)

$n = 0.4$ (porosity)

1. Calculate the volume of water flowing in the entire aquifer. Inserting these values directly into Equation (8.14):

   $Q = (10\text{ m})(1000\text{ m})(0.1\text{ m d}^{-1}) = 1000\text{ m}^3\text{ d}^{-1}$

2. Convert this discharge in m^3 d^{-1} into ft^3 d^{-1} and gal d^{-1}. There are 35.31 ft^3 m^{-3}, so conversion yields an equivalent discharge of 35,310 ft^3 d^{-1}. There are approximately 7.48 gal ft^{-3}, so conversion yields an equivalent discharge of 264,119 gal d^{-1}.
3. Find the macroscopic velocity of the water v_m.

   $v_m = v/n = 0.1\text{ m d}^{-1}/0.4 = 0.25\text{ m d}^{-1}$

4. Find the discharge per unit width of the aquifer q_w.

   $q_w = (1\text{ m})(10\text{ m})(0.1\text{ m d}^{-1}) = 1\text{ m}^3\text{ d}^{-1}$

5. What is the transmissivity of the aquifer?
   Transmissivity is $T = Ky$. The transmissivity cannot be calculated since we do not know the value of K for this problem.

The simplest models of groundwater flow are one-dimensional, steady, uniform flow systems. Recall from Chapter 1 that steady groundwater flow means flow does not change with time. In an unconfined aquifer this would mean the water table remains at a constant level. If the water table were rising or falling, this would indicate unsteady conditions. Uniform flow means that flow does not change with distance. Figure 8.11 shows uniform flow because the streamlines do not converge or diverge. Around a pumped well flow becomes nonuniform because streamlines converge near the well. If we make some simplifying assumptions we can solve many one-dimensional groundwater flow problems by direct application of Darcy's Law.

Figure 8.13 is a cross-sectional sketch of a stream-aquifer system. This is an *effluent* stream where groundwater provides baseflow to the stream. Effluent streams are also perennial streams. An *influent* stream is one where water seeps from the channel into the aquifer. Influent streams are found mainly in arid and semi-arid environments. Let us assume for Figure 8.13 that the flow is nearly horizontal and uniform with depth, the hydraulic gradient, which is very small, is equal to the slope of the water table, and the total head is equal to the saturated thickness of the aquifer. These assumptions are collectively called the *Dupuit-Forchheimer assumptions*. In Example 8.5 we use Darcy's Law to calculate the groundwater flow to the stream in Figure 8.13. Example 8.6 uses Darcy's Law to determine the height of water in a piezometer when vertical flow is present.

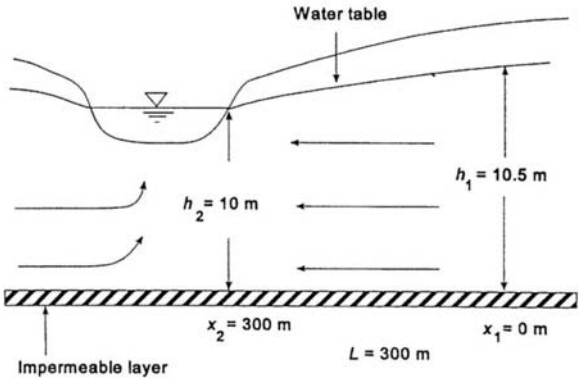

Figure 8.13. A simple stream–aquifer system. The aquifer is unconfined and provides baseflow to the stream.

Example 8.5

Use Darcy's Law to calculate the groundwater flow per unit length of channel from the aquifer to the stream in Figure 8.13. Assume that the Dupuit-Forchheimer assumptions are valid and that the aquifer is homogeneous and isotropic with $K = 3$ m d^{-1}.

First determine the hydraulic gradient along the water table streamline. Since the Dupuit-Forchheimer assumptions are valid, the hydraulic gradient is the same along any streamline. The advantage of using the water table is that the pressure head equals zero and disappears from the equation. Using Equation (8.12):

$$h_1 = p_1 + z_1 = 0 + 10.5 \text{ m} = 10.5 \text{ m}$$

$$h_2 = p_2 + z_2 = 0 + 10.0 \text{ m} = 10.0 \text{ m}$$

$$\Delta h = h_1 - h_2 = 0.5 \text{ m}$$

$$L = 300 \text{ m}$$

The hydraulic gradient is $\Delta h/L = 0.5$ m/300 m = 0.00167.
The velocity is $v = K(\Delta h/L) = 3.0(0.00167) = 0.005$ m d^{-1}.

Next, find the unit cross-sectional area A. Since we are determining q_w, the width $w = 1$ m. The depth of the aquifer varies from 10.5 to 10 m, and so we use an average depth of 10.25 m. The discharge, per meter of channel, from the right side is thus:

$$q_{wr} = (0.005 \text{ m d}^{-1})(10.25 \text{ m}^2) = 0.05125 \text{ m}^3 \text{ d}^{-1}$$

Assuming the conditions are identical on the left side of the channel, the discharge per meter of channel is:

$$q_w = 2(0.05125) = 0.102 \text{ m}^3 \text{ d}^{-1}$$

To find the total discharge Q from the aquifer to the stream simply multiply the q_w value by the total length of the channel in contact with the aquifer.

What is the transmissivity of this aquifer?

$$T = Ky = 3.0(10.25) = 30.75 \text{ m}^2 \text{ d}^{-1}$$

Example 8.6

This example taken from Bouwer (1978) demonstrates how vertical flow can affect the measurement of head in a piezometer (Fig. 8.10). A piezometer is inserted into an unconfined aquifer as shown in Figure 8.14. Assume there is a steady-state infiltration of 1.5 cm d^{-1} and that water leaks out the bottom of the aquifer at the same rate. The hydraulic conductivity is $K = 0.2$ m d^{-1}.

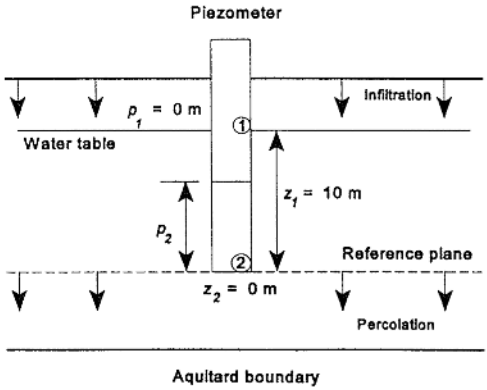

Figure 8.14. A piezometer in an aquifer with downward flow of 1.5 cm d^{-1}. The water level in the piezometer is lower than the water table.

Use Darcy's Law to find the height of water in the piezometer. Observe that the velocity is already given as $v = 1.5$ cm d^{-1}.

The reference plane is set at the bottom of the piezometer. Call this reference location 2 and the water table location 1. The total head at points 1 and 2 are:

$$h_1 = (p_1 + z_1) = (0 \text{ m} + 10 \text{ m}) = 10 \text{ m}$$

$$h_2 = (p_2 + z_2) = (p_2 + 0 \text{ m}) = p_2$$

The value of p_2 is what we are trying to find. Substitute all values into Darcy's equation:

$$v = K(h_1 - h_2) / L$$

$$0.015 \text{ m d}^{-1} = 0.2[(10 \text{ m}) - (p_2)] / 10 \text{ m}.$$

Solving for p_2 yields: $p_2 = 9.25$ m.

With a downward flow of 0.015 m d^{-1} (1.5 cm d^{-1}), the water level in the piezometer is 0.75 m below the water table.

Darcy's Law is used directly to solve many one-dimensional flow problems. When the Dupuit-Forchheimer assumptions are valid, you can use the Dupuit-Forchheimer equation:

$$q_w = \frac{K}{2L}\left(h_1^2 - h_2^2\right) \tag{8.19}$$

Using the values from Example 8.5 in Equation (8.19) the answer is:

$$q_w = \frac{3}{2(300)}\left(10.5^2 - 10.0^2\right) = 0.05125 \text{ m}^3 \text{ d}^{-1}$$

A related problem is finding h at any point between x_1 and x_2. The governing equation for one-dimensional, unconfined flow under Dupuit assumptions is:

$$\frac{K}{2}\frac{d^2h^2}{dx^2} = -R \tag{8.20}$$

Where $-R$ is the recharge rate. If we assume $R = 0$, then twice integrating Equation (8.20) gives:

$$h^2 = a_1 x + a_2 \tag{8.21}$$

where a_1 and a_2 are integration constants. Taking the square root of Equation (8.21):

$$h = \sqrt{a_1 x + a_2} \tag{8.22}$$

Equation (8.22) gives the value of h anywhere from x_1 to x_2 (see Example 8.7).

Example 8.7
Find the equation that gives the value of h at any location x for the aquifer in Figure 8.13. The values of the constants a_1 and a_2 can be determined by solving the equation $h^2 = a_1 x + a_2$ at the two boundary conditions. From Figure 8.13 we see that $x_1 = 0$ m and $h_1 = 10.5$ m, and $x_2 = 300$ m and $h_2 = 10.0$ m. Substituting the first boundary condition into Equation (8.22) and solving for a_2:

$$(10.5)^2 = a_1(0) + a_2$$

$$a_2 = (10.5)^2 = 110.25 \text{ m}$$

Using this value for a_2 with the conditions at the second boundary gives a value for a_1 of:

$$(10)^2 = a_1(300) + (10.5)^2$$

$$a_1 = -0.0342.$$

The value of h anywhere along the water table in Figure 8.13 can be determined as:

$$h = \sqrt{-0.0342x + 110.25}$$

For example, at $x = 50$ m from x_1, $h = 10.42$ m.

8.6 GROUNDWATER AND WELLS

A pumping well in an unconfined aquifer draws the water table down into a *cone of depression* (Fig. 8.15). The cone of depression forms as pumping lowers the water level in the well relative to the surrounding water table, which causes water to flow from the aquifer to the well, and dewaters the aquifer near the well. The cone of depression is maintained because a steeper hydraulic gradient is required as the area through which water flows to the well decreases. Groundwater flow becomes non-

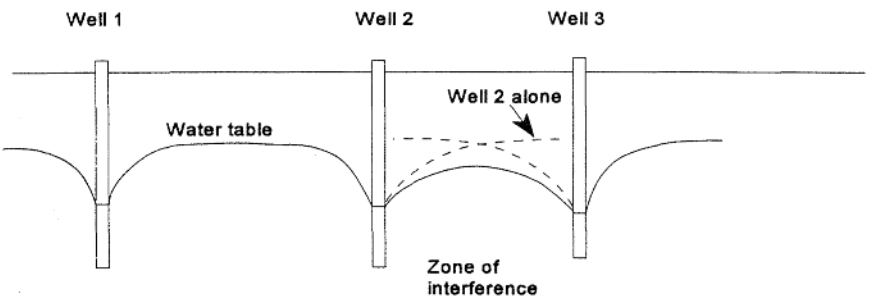

Figure 8.15. Three wells pumping in an unconfined aquifer with a cone of depression around each well. Where the cones of depression overlap (Well 2 and Well 3) well interference occurs.

uniform in the vicinity of the well. If under constant pumping the cone of depression stabilizes over time, the flow system is steady. If the cone of depression continues to deepen and spread radially from the well over time, this is unsteady flow. In a confined aquifer the cone of depression forms in the potentiometric surface, not in the water because the confined aquifer remains saturated.

If two or more wells are pumping from the same aquifer, their cones of depression may overlap resulting in well *interference*. In a confined aquifer the total drawdown in the zone of interference equals the algebraic sum of the drawdowns from each well separately as if it were the only pumping well; however, this additive solution only approximates the total drawdown in an unconfined aquifer. In an unconfined aquifer the total drawdown can exceed the sum of the individual drawdowns because of the increased hydraulic gradient that follows from the decrease in saturated thickness and transmissivity. A deep, large-capacity well can lower the water table below a shallower well (Fig. 8.16). This presents an interesting problem in groundwater management. Can or should the owner of the dry well receive compensation from the party that caused the injury? Whether the owner of the dry well receives compensation depends upon the prevailing state groundwater law and a consideration of the overall costs and benefits involved. Groundwater pumping causes other environmental impacts. The cone of depression from a well near an effluent stream may reverse the hydraulic gradient, causing the stream to become influent in this reach; in effect the well is 'stealing' water from the stream. A few states recognize the need for 'conjunctive management' of ground and surface water and have modified their water laws to more accurately reflect hydrology. The laws in many states still treat groundwater and surface water as separate systems. Groundwater pumping along coastlines causes the landward migration of the interface between the fresh groundwater under the land and the saline groundwater under the oceans. When this interface moves inland past a pumping well, the well begins pumping saltwater. Another impact of pumping is on the migration of pollutants. Pollutants in the groundwater migrate with the water towards a pumping well, and hundreds of private and public wells in the United States have been closed because of contamination. We already mentioned the problem of land surface subsidence from overpumping. Subsidence is

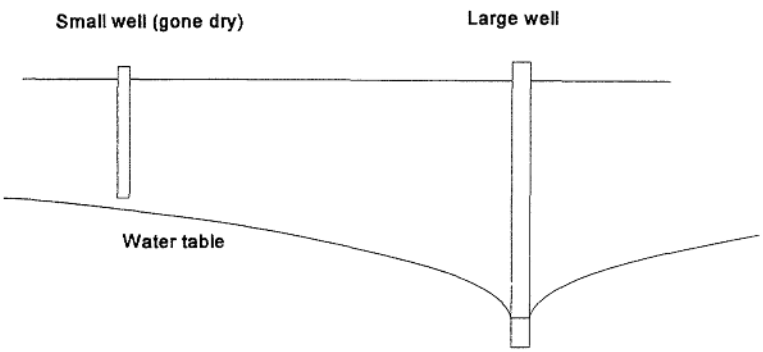

Figure 8.16. A large–capacity well draws the water table down below a shallow well. The shallow well has gone dry.

a problem in many major cities around the world from Mexico City to Bejing and London. Subsidence in some areas has been in excess of 8 m (25 ft).

Not all of the environmental impacts from groundwater pumping are necessarily negative. In the southwest United States the Tamarisk (*Tamarix chinensis*) or 'salt cedar' was released into riparian ecosystems. As with many species introduced into a foreign ecosystem the Tamarisk has out competed the indigenous species of cottonwood and willow that are major components of the native riparian ecosystem. From an ecological point of view Tamarisk is less desirable than the native species because it does not provide suitable habitat for wildlife. From a water resource perspective the plant is a water hog. The Tamarisk has a tremendous thirst and taps groundwater to satisfy its transpiration requirement. This results in the loss of large volumes of groundwater in a region where water is already extremely scarce. Various methods have been tried to control the spread of the Tamarisk including burning and bulldozing but all have been unsuccessful. One method of control that was discovered quite inadvertently has proven effective. In parts of Arizona, excessive groundwater pumping along the Salt River in the Phoenix area rapidly lowered the water table below the root zone of the plants. Without water the Tamarisk died. While this approach is unlikely to be used as a method of control, it did stop the Tamarisk in this part of Arizona (Graf 1985).

8.7 GROUNDWATER FLOW TO WELLS

When studying the flow of groundwater to a well an important distinction is between steady flow and unsteady flow (or transient) systems. Steady flow represents an equilibrium condition between discharge from the well and recharge to the aquifer. When this occurs the water table or potentiometric surface remains constant in position and shape over time. With unsteady flow the water table or potentiometric surface continues to lower and/or spread radially away from the well.

8.7.1 *Steady flow*

8.7.1.1 *Unconfined aquifer*

For this discussion the following assumptions apply: the aquifer is homogeneous and isotropic and of infinite extent, the well fully penetrates the aquifer, and water is released immediately from the aquifer as it is pumped. The diagram depicting this situation for a pumping well in an unconfined aquifer is shown in Figure 8.17. Distances r are measured radially away from the well. At each distance r_i there is a corresponding value of head h_i. The subscript w indicates values at the well.

To begin developing the equations describing steady flow imagine a pumping well surrounded by an imaginary cylinder at a radial distance r (Fig. 8.18). With steady-state conditions the volume of water flowing across the surface of the cylinder towards the well must equal the discharge Q from the well. The surface area of the cylinder is:

$$A = 2\pi rh \tag{8.23}$$

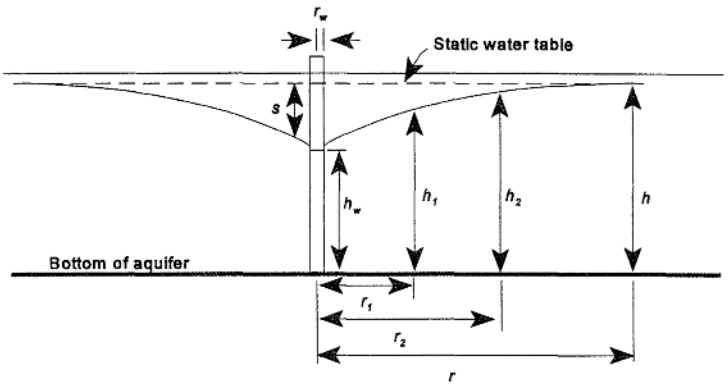

Figure 8.17. Steady-state flow conditions for a fully-penetrating pumping well in an unconfined aquifer.

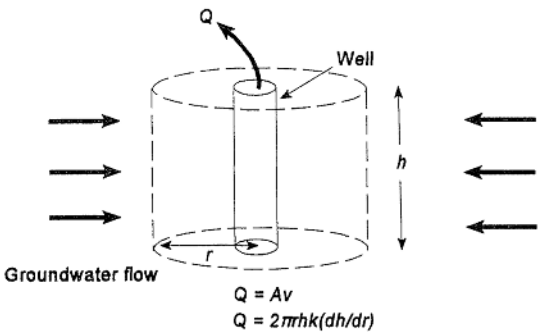

Figure 8.18. An imaginary cylinder of height h at radius r from a pumping well.

Using Equation (8.14) and the continuous version of Darcy's Law (Eq. 8.10), the flow across the cylinder is:

$$Q = (2\pi rh)K\frac{\mathrm{d}h}{\mathrm{d}r} \tag{8.24}$$

Equation (8.24) is a straightforward application of Darcy's Law to the radial flow of groundwater to a well. Separating the variables r and h and integrating between appropriate limits, we get:

$$Q = \frac{\pi K\left(h_2^2 - h_1^2\right)}{\ln\left(r_2 / r_1\right)} \tag{8.25}$$

where r_1, r_2, h_1 and h_2 are defined as in Figure 8.17. Equation (8.25) is Thiem's equation for steady flow in an unconfined aquifer. The units of Q are in the same units as r and h. The utility of the Thiem equation, however, is *not* in the calculation of Q. After all, we can measure Q directly with a flow meter. Thiem's equation is useful because it can be rearranged and solved for the hydraulic conductivity K. This is in fact how hydraulic conductivity is determined in the field using a pump test. To determine K, a well is pumped and head is measured at two observation wells along the cone of depression. Rather than measuring head we usually measure the draw-

down $s_i = (h - h_i)$, where h is the total head without pumping and h_i is the head at radial distance r_i (Fig. 8.17).

8.7.1.2 *Confined aquifer*

Thiem's equation for confined flow is similar to the unconfined equation. For the confined case head values h_i are measured from the bottom of the aquifer to the potentiometric surface as shown in Figure 8.19. Thiem's equation for a confined aquifer is:

$$Q = \frac{2\pi T\left(h_2 - h_1\right)}{\ln\left(r_2 / r_1\right)} \tag{8.26}$$

where T is the transmissivity (Eq. 8.17). Again, Equation (8.26) can be rearranged and solved for T. Equation (8.26) could be used to calculate the transmissivity for an *unconfined* aquifer by using y equal to the saturated thickness of the aquifer outside of the cone of depression.

8.7.2 *Unsteady flow*

8.7.2.1 *Confined aquifer: Theis solution – match point method*

Determining the hydraulic properties of an aquifer from a pump test under unsteady flow conditions is more complex. With unsteady flow the water table (unconfined aquifer) or potentiometric surface (confined aquifer) continues to decrease over time with pumping. C.V Theis (1935) was the first person to develop a method that included the time of pumping as a factor in the analysis of pump test data. The Theis solution was developed for confined aquifers under specific assumptions.

Theis assumptions for unsteady flow to a well in a confined aquifer:

– Water withdrawn from the well is derived entirely from aquifer storage and is released instantaneously with decline in head;

– The well fully penetrates and is open through the entire thickness of the aquifer;

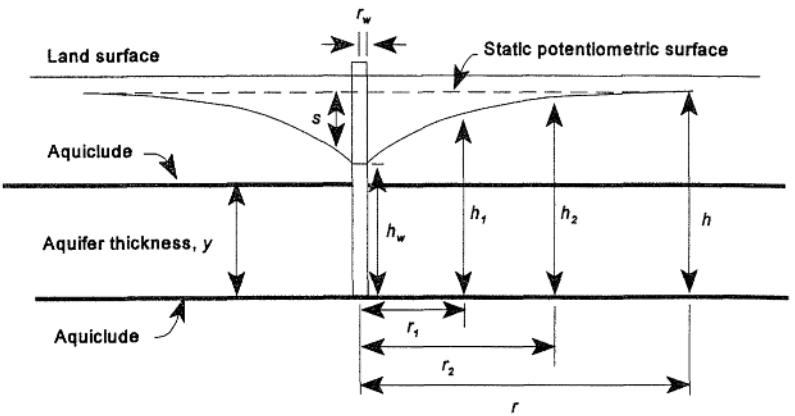

Figure 8.19. Steady-state flow conditions for a fully-penetrating pumping well in a confined aquifer.

– The well's radius is small so that water storage within the well is negligble in comparison to the pumping rate;

– Flow to the well is horizontal and laminar;

– The aquifer is horizontal, infinite in extent, uniform in thickness, homogenous and isotropic;

– The aquifer remains saturated during pumping.

The method may be used for unsteady flow in unconfined aquifers, if the assumptions are met.

Theis developed his procedure using heat-flow theory as an analogy for water flow through an aquifer. The two basic equations of the Theis method are:

$$s = \frac{Q}{4\pi T} \int_{u}^{\infty} \left(\frac{e^{-u}}{u} \right) du \tag{8.27}$$

and

$$u = \frac{r^2 S}{4Tt} \tag{8.28}$$

where s = drawdown ($s = h - h_i$) (see Fig. 8.19), T = transmissivity, S = storage coefficient, r = radial distance, and t = time since pumping began.

The improper integral in Equation (8.27) is called the well function $W(u)$, and its value is approximated using a series expansion as:

$$W(u) = \int_{u}^{\infty} \left(\frac{e^{-u}}{u} \right) du \approx -0.577216 - \ln u + u - \frac{u^2}{2 \times 2!} + \frac{u^3}{3 \times 3!} - \ldots \tag{8.29}$$

Table 8.2 gives $W(u)$ for values of u calculated from Equation (8.29). To use the

Table 8.2. Values of the well function $W(u)$ for different values of u.

u	1.0	2.0	3.0	4.0	5.0	6.0	7.0	8.0	9.0
$\times 1$	0.219	0.049	0.013	0.0038	0.00114	0.00036	0.00012	3.8E–05	1.2E–05
$\times 10^{-1}$	1.82	1.22	0.91	0.70	0.56	0.45	0.37	0.31	0.26
$\times 10^{-2}$	4.04	3.35	2.96	2.68	2.48	2.30	2.15	2.03	1.94
$\times 10^{-3}$	6.33	5.64	5.23	4.95	4.73	4.54	4.39	4.26	4.14
$\times 10^{-4}$	8.63	7.94	7.53	7.25	7.02	6.84	6.69	6.55	6.44
$\times 10^{-5}$	10.95	10.24	9.84	9.55	9.33	9.14	8.99	8.86	8.74
$\times 10^{-6}$	13.24	12.55	12.14	11.85	11.63	11.45	11.29	11.16	11.04
$\times 10^{-7}$	15.54	14.85	14.44	14.15	13.93	13.75	13.60	13.46	13.34
$\times 10^{-8}$	17.84	17.15	16.74	16.46	16.23	16.05	15.90	15.76	15.65
$\times 10^{-9}$	20.15	19.45	19.05	18.76	18.54	18.35	18.20	18.07	17.95
$\times 10^{-10}$	22.45	21.76	21.35	21.06	20.84	20.66	20.50	20.37	20.25
$\times 10^{-11}$	24.75	24.06	23.65	23.36	23.14	22.95	22.81	22.67	22.55
$\times 10^{-12}$	27.05	26.36	25.95	25.66	25.44	25.26	25.11	24.97	24.86
$\times 10^{-13}$	29.36	28.66	28.26	27.97	27.75	27.56	27.41	27.28	27.16
$\times 10^{-14}$	31.66	30.97	30.56	30.27	30.05	29.87	29.71	29.58	29.46
$\times 10^{-15}$	33.96	33.27	32.86	32.58	32.35	32.17	32.02	31.88	31.76

Theis method rewrite Equations (8.27) and (8.28) as Equations (8.30) and (8.31):

$$T = \frac{QW(u)}{4\pi s} \tag{8.30}$$

$$S = \frac{4Ttu}{r^2} \tag{8.31}$$

It is now a relatively simple matter of finding $W(u)$ and s and solving for transmissivity (T) with Equation (8.30), and then with T and u solving for S by means of Equation (8.31). Unfortunately it is not possible to solve these equations directly. To overcome this problem Theis devised a graphical method of solution which is called the *match point* method. Their are 5 steps to the match point method:

1. Plot on log-log paper values of drawdown (s) versus time (t).
2. Plot on log-log paper values of $1/u$ versus the well function $W(u)$.
3. Physically overlay the two graphs so that the two sets of plotted points correspond throughout some range of values.
4. Choose a common (match) point on the two graphs and read $1/u$, $W(u)$, s, and t from the corresponding axes.
5. With these values solve Equations (8.30) and (8.31).

Example 8.8

This example demonstrates the match point method for finding the transmissivity and the storage coefficient of an aquifer under unsteady flow conditions. A well is pumped at a constant $Q = 500$ gal min^{-1} and drawdown is measured at an observation well located $r = 400$ ft from the pumping well. Table 8.3 gives the results from the pumping test.

Step 1. Plot the pump test data from Table 8.3 on log-log paper (see Fig. 8.20).

Step 2. Plot values of $1/u$ versus $W(u)$ from Table 8.2 (see Fig. 8.21).

Step 3. Physically overlay the two graphs until the trends in the two sets of points correspond (Fig. 8.22).

Step 4. Choose a match point common to each graph and read the values of the variables from the corresponding axes. For the match point in Figure 8.22, $s = 1.65$ ft, $t = 25$ min., $1/u = 31$, $W(u) = 2.9$.

Step 5. Solve Equations (8.30) and (8.31) with these values. To make Equation (8.30) dimensionally homogeneous convert $Q = 500$ gal min^{-1} into $Q = 96{,}257$ ft^3 d^{-1}.

Table 8.3. Drawdown with time at the observation well. (Data from Lohman, 1972).

Time (min)	Drawdown (ft)	Time (min)	Drawdown (ft)	Time (min)	Drawdown (ft)
1.0	0.16	10	1.12	60	2.11
1.5	0.27	12	1.21	80	2.24
2.0	0.38	14	1.26	100	2.38
2.5	0.46	18	1.43	120	2.49
3.0	0.53	24	1.58	150	2.62
4.0	0.67	30	1.70	180	2.72
5.0	0.77	40	1.88	210	2.81
6.0	0.87	50	2.00	240	2.88
8.0	0.99				

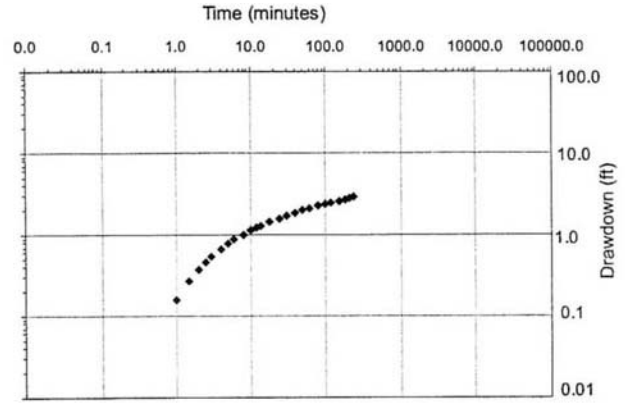

Figure 8.20. Graph of drawdown versus time (data taken from Table 8.3).

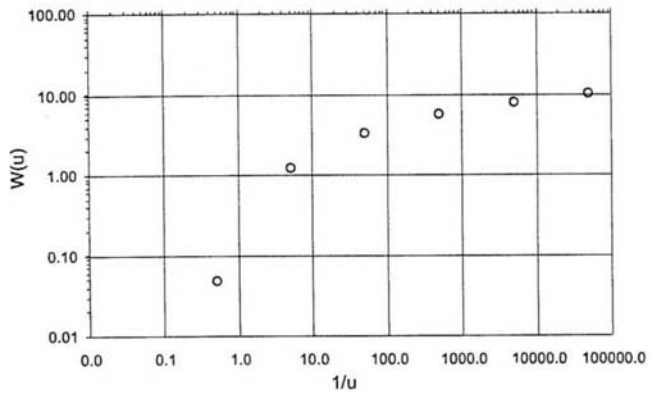

Figure 8.21. Graph of $1/u$ versus $W(u)$ using values from column three of Table 8.2.

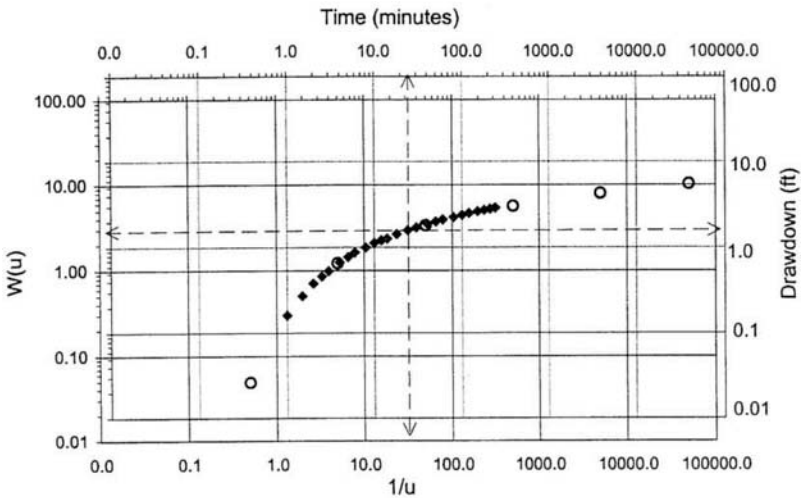

Figure 8.22. This graph is created by physically overlaying Figures 8.20 and 8.21. The graphs are aligned with their axes parallel and a 'match point' common to both plots is found. The values for solving the equations at the match point are read from the corresponding axes.

$$T = \frac{QW(u)}{4\pi s} = \frac{(96{,}257\text{ft}^3\text{d}^{-1})(2.9)}{(4)(3.1416)(1.65\text{ft})} = 13{,}463\text{ ft}^2\text{ d}^{-1}$$

and

$$S = \frac{4Ttu}{r^2} = \frac{(4)(13{,}463\text{ft}^2\text{d}^{-1})(0.01736\text{ d})(0.032)}{400^2\text{ ft}^2} = 0.00019$$

8.7.2.2 *Confined aquifer: Cooper-Jacob solution – time versus drawdown method*
The Cooper-Jacob (1946) method determines aquifer properties by plotting drawdown versus time on semi-log paper. When the variable u is small, say less than 0.03, then the terms following ln u in Equation (8.29) are very small and can be neglected. Copper and Jacob noted that when pumping times are large, u is small, and a plot of drawdown versus time quickly produces a straight line on semi-log paper. The straight line graph means the increase in drawdown is occurring at a steady rate. The equations for the Cooper-Jacob solution of Theis's equations are:

$$T = \frac{2.3Q}{(4\pi\Delta s)} \tag{8.32}$$

and

$$S = \frac{(2.25Tt_0)}{r^2} \tag{8.33}$$

where Δs is the drawdown during one log cycle, and t_0 is the initial time drawdown began at the steady rate, and is obtained by fitting a straight line to the plotted data and extending the line back to intercept the time axis. The steps in the Cooper-Jacob method are:

1. Plot the pump test data on semi-log paper. Plot drawdown on the arithmetic axis and time on the log axis.
2. Fit a straight line to the 'linear' portion of the graph, and extend the line back to intercept the time axis. The time value at the intercept is the value for t_0.
3. Determine the drawdown at the beginning and the end of one log cycle of time. The difference between these two drawdown values is Δs.
4. Use Equation (8.32) and (8.33) to solve for T and S.

Example 8.9 uses the same data from Example 8.8 to find T and S using the Cooper-Jacob method.

Example 8.9

Step 1. The drawdown versus time data from Table 8.3 are plotted on semi-log paper (Fig. 8.23).

Step 2. A straight line is fitted to the linear portion of the graph an extended back to intercept the time axis. This is the value for $t_0 = 0.00094$ days.

Step 3. Determine the drawdown over one log cycle. The drawdown at $t = 0.01$ days is $s_1 = 1.3$ ft, and the drawdown at $t = 0.10$ days $s_2 = 2.6$ ft, therefore $\Delta s = 1.3$ ft.

Step 4. Inserting these values into Equations (8.32) and (8.33):

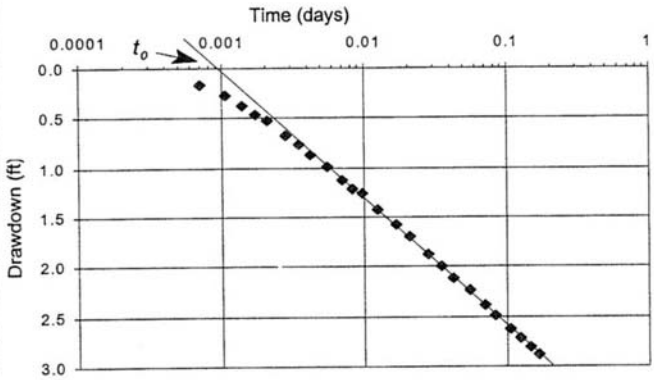

Figure 8.23. Plot of drawdown versus time on semi-log paper. The straight line fitted to the linear part of the graph intersects the time axis at t_0.

$$T = \frac{2.3Q}{4\pi\Delta s} = \frac{(2.3)\left(96{,}257\text{ft}^3\text{d}^{-1}\right)}{(4)(3.1416)(1.3\text{ft})} = 13{,}552\text{ft}^2\text{d}^{-1}$$

and

$$S = \frac{2.25Tt_0}{r^2} = \frac{(2.25)\left(13{,}552\text{ft}^2\text{d}^{-1}\right)(0.00094\,\text{d})}{400^2\,\text{d}^2} = 0.00018$$

8.7.2.3 *Unconfined aquifers*

As mentioned at the beginning of Section 8.7.2, the Theis solution was developed for confined aquifers. The technique can be used for unconfined aquifers if the basic assumptions are met. The value of S is now the specific yield, and T is the average height of the water table between two observation wells (Bouwer 1978).

8.8 TWO AND THREE DIMENSIONAL FLOW

Our discussion to this point has focused on one-dimensional steady flow in an isotropic, homogeneous aquifer. Two-dimensional steady flow becomes more complex mathematically, because the governing equation for flow is a two-dimensional, second-order, partial differential equation. There is a relatively simple graphical technique for analyzing two-dimensional flow called a *flow net*. A flow net is an orthogonal network of equipotential lines and flow lines, and is constructed subject to existing boundary conditions. Flow nets may be constructed either in planimetric view or in cross-section. A flow net is constructed by first mapping values of h in two dimensions, and then drawing equipotential contour lines at a spacing of Δx (Fig. 8.24). A second set of flow lines are drawn perpendicular to the equipotential lines at the same spacing. The area bounded by two flow lines and two equipotential lines thus approximates a square. The flow through any square between two flow lines is:

$$q = Ky\Delta w\frac{\Delta h}{\Delta x} \tag{8.34}$$

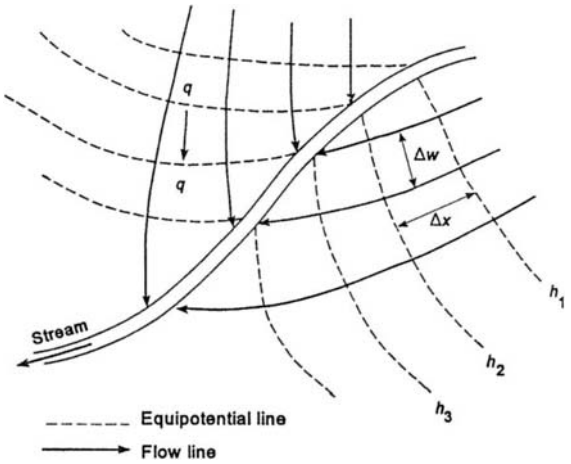

Figure 8.24. A planimetric view of a flow net. The flow net is constructed so that Δw and Δx are approximately equal.

where y is the aquifer thickness in the square and $\Delta h = h_1 - h_2$ is the contour interval between equipotential lines. However, since $\Delta x \approx \Delta w$, the flow through any square is simply:

$$q = Ky\Delta h \tag{8.35}$$

Groundwater flow through a square is computed from the hydraulic conductivity and the geometry of the flow net, that is by spacing the flow lines so that they equal the spacing of the equipotential lines. The flow net is only an approximate graphical solution of the differential equation governing two-dimensional flow. The governing equation for three-dimensional groundwater flow in an isotropic, homogeneous aquifer under steady-state conditions is:

$$\frac{\partial^2 h}{\partial x^2} + \frac{\partial^2 h}{\partial y^2} + \frac{\partial^2 h}{\partial z^2} = 0 \tag{8.36}$$

Equation (8.36) is the three-dimensional version of Laplace's equation. Laplace's equation is derived by combining Darcy's Law with a continuity equation for a unit volume of an aquifer. Laplace's equation says that water flows in response to the gradient in head (in all directions), and that the *net* change in the volume rate of flow in all directions, per unit volume of aquifer, equals zero. In other words, an increase in flow in any one direction must be accompanied by a decrease in flow in one or both of the other directions, because water can neither be created nor destroyed. Laplace's equation can only be solved for specified boundary conditions, and a major challenge for the hydrologist is to accurately define the boundary conditions. The general types of boundaries are:

1. A boundary where head is known,
2. A boundary where flow is known, or
3. Some combination of 1 and 2.

With the exception of flow nets, the only reasonable method for studying multi-dimensional groundwater flow is with the use of groundwater simulation models.

Simulation models are employed in the study of one, two and three-dimensional groundwater flow.

8.9 GROUNDWATER MODELS

The two basic approaches to numerical groundwater modeling are *finite difference* and the *finite element* models. The finite difference model is the simpler of the two and is briefly described here. A finite difference model divides space into discrete (finite) intervals. Instead of using calculus and differential equations, the model uses algebra and ordinary difference equations to approximate the equations of flow. For example, Figure 8.25 is a finite difference grid superimposed over an imaginary aquifer with *nodes* located at the intersection of the grid lines. Nodes represent locations where head h is either known, i.e. along a boundary, or is unknown and is to be calculated by the model. Distance is discretized into segments Δx and Δy. Following the discussion by Wang & Anderson (1983), Figure 8.26 is a two-dimensional finite

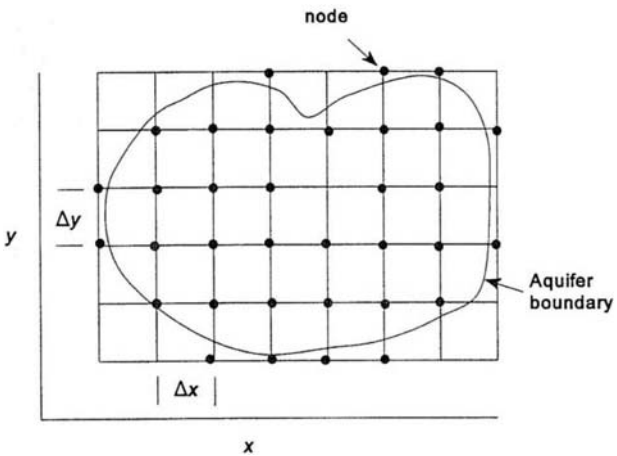

Figure 8.25. An imaginary aquifer with a finite difference grid superimposed. The intersection of the grid lines are nodes where head is either known or calculated by the model.

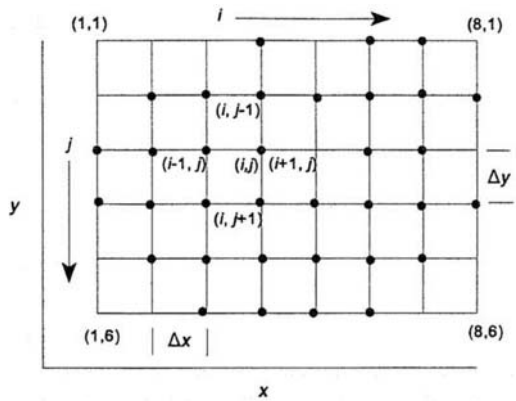

Figure 8.26. Numbering convention for the nodes in the finite difference grid shown in Figure 8.25.

difference grid showing the numbering convention for nodes. The rows are indexed with the letter j, which increases from top to bottom. Columns are indexed with the letter i and increase from left to right. This numbering convention inverts rows and columns when compared to standard matrix notation. The value of head at node (i, j) is designated $h_{i,j}$.

The two-dimensional form of Laplace's equations is:

$$\frac{\partial^2 h}{\partial x^2} + \frac{\partial^2 h}{\partial y^2} = 0 \tag{8.37}$$

The derivatives in Laplace's equation are approximated using finite differences between nodes. For example, an approximation for the first-order partial derivative of head in the x direction is:

$$\frac{\partial h}{\partial x} \approx \frac{h_{i+1,j} - h_{i,j}}{\Delta x} = \frac{\Delta h}{\Delta x} \tag{8.38}$$

This is precisely how the hydraulic gradient was approximated in Equation (8.11). The curly derivative symbol (∂) represents a partial derivative. A partial derivative is used when a variable (in this case h) changes in more than one direction at the same time. Partial derivatives are interpreted just like ordinary derivatives. The partial derivative in Equation (8.38) means the rate of change in head h, with respect to direction x, when the rates of change in head in all other directions are held constant. An approximation of the second-order partial derivative of h with respect to x is found by 'differencing' Equation (8.38):

$$\frac{\partial^2 h}{\partial x^2} \approx \frac{[(h_{i+1,j} - h_{i,j})/\Delta x] - [(h_{i,j} - h_{i-1,j})/\Delta x]}{\Delta x} \tag{8.39}$$

Since the $h_{i,j}$ term appears twice, Equation (8.39) simplifies to:

$$\frac{\partial^2 h}{\partial x^2} \approx \frac{h_{i-1,j} - 2h_{i,j} + h_{i+1,j}}{(\Delta x)^2} \tag{8.40}$$

and in a similar fashion for the y direction:

$$\frac{\partial^2 h}{\partial y^2} \approx \frac{h_{i,j-1} - 2h_{i,j} + h_{i,j+1}}{(\Delta y)^2} \tag{8.41}$$

Laplace's equation says add Equations (8.40) and (8.41) and set the result equal to zero. If the grid is square so that $\Delta x = \Delta y$, then the finite difference approximation of the two-dimensional Laplace's equation (Eq. 8.37) is:

$$h_{i-1,j} + h_{i+1,j} + h_{i,j-1} + h_{i,j+1} - 4h_{i,j} = 0 \tag{8.42}$$

Equation (8.41) in this or some other form is the basic equation for the finite difference solution for steady-state conditions, and is at the core of finite difference computer simulation models of groundwater flow (Wang & Anderson 1983). Equation (8.42) is written for each interior node in the grid where head is unknown. For n unknown interior nodes this generates a system of n equations. The equations are then

solved using known heads along the boundary to determine the unknown heads at the interior nodes. It should be pointed out that this model is based on the assumption of flow though porous media. When secondary porosity is important and groundwater flow occurs through fractures and channels, these types of models are insufficient.

The development of groundwater modeling followed first from a desire to understand and accurately describe groundwater *quantity*. The explosion in the use of models starting in the 1980s can be tied to a series of regulatory statutes passed in the 1970s and 1980s focusing on groundwater *quality* (NRC 1990). The Comprehensive Environmental Response, Compensation, and Liability Act (CERLCA) commonly known as 'Superfund,' the Resource Conservation and Recovery Act (RCRA), the Safe Drinking Water Act (SDWA), and the National Environmental Policy Act (NEPA) have increased the need for computer modeling and pushed the development of better models. Groundwater models have become quite sophisticated with the incorporation of subroutines to model the advection and diffusion of contaminants. It would be difficult, if not impossible, to carry out some of the requirements of these statutes without computer models.

The National Research Council (NRC 1990) evaluated the use of computer models in support of statutory requirements, as well as on their scientific basis. The NRC reached a number of conclusions and made a number of recommendations, two of which bear repeating.

One conclusion was: 'Properly applied models are useful tools to 1) assist in problem identification, 2) design remedial strategies, 3) conceptualize and study flow processes, 4) provide additional information for decision making, and 5) recognize limitations in data and guide collection of new data.' These are some of the most useful aspects and functions of models.

A recommendation was: 'The results of mathematical computer models may appear more certain than they really are; decision makers must be aware of the limitations.' Models are all based on assumptions of one form or another. Models are simplifications of reality, and the output from a model is only as good as the input data. This applies to all models not just groundwater models. Because the computer produces 'numbers' there may be a tendency to confuse these numbers with the truth.

8.10 GROUNDWATER QUALITY AND CONTAMINANT TRANSPORT

There are literally millions of potential sources of groundwater contamination in the United States. Contamination sources include landfills, hazardous waste sites, mining waste sites, injection wells, unplugged abandoned wells, underground and above ground storage tanks, pipelines, accidental spills, agricultural (farming and feedlot) operations, and on-lot septic systems. The list of potential contaminants is just as awesome and includes inorganic chemicals, organic chemicals and bacterial and viral pathogens. In general, when analyzing the migration of pollutants in groundwater we can consider two cases:

1. Multiphase flow where the contaminant does not dissolve appreciably in the groundwater, and
2. Flow systems where the contaminants are dissolved in the groundwater.

8.10.1 *Multiphase flow*

Immiscible organic liquids present an important example of multiphase flow where the fluids do not readily mix and dissolve in the groundwater. Immiscible liquids can be either less dense or more dense than the water. The portion of the liquid that is not dissolved is, by definition, not in the 'aqueous phase,' and is referred to as a 'light nonaqueous phase liquid' (LNAPL) if it is lighter than water, and a 'dense nonaqueous phase liquid' (DNAPL) if it is heavier than water. As with groundwater these fluids move in response to a difference in potential, but not necessarily the same potential gradient that controls the flow of water. It is possible for a DNAPL to actually flow in a direction opposite the flow of the groundwater.

If released near the surface both a LNAPL and a DNAPL will migrate vertically through the vadose zone. As the fluid moves downward it leaves a residual trail of contamination in the pore spaces on the surfaces of solid particles. If the amount of liquid released is small and the vadose zone large, it is possible that no liquid will reach the groundwater. When these liquids reach the top of the capillary fringe the differences in density begins to affect their transport. A LNAPL will accumulate near the water table and flow following the slope and direction of water table. Some of the liquid may mix with the groundwater and be carried along within the groundwater flow. Upon reaching the capillary fringe a DNAPL may begin to mound slightly but it continues to move downward eventually accumulating on the bottom of the aquifer. When it reaches the bottom it will flow in response to the direction and dip angle of the geologic unit. As with a LNAPL, there may be some mixing and transportation of the DNAPL with the groundwater.

8.10.2 *Dissolved contaminant transport*

Dissolved contaminants are carried along in the groundwater flow. The change in concentration of a contaminant with time and/or distance in the aquifer depends upon two groups of processes. One group are the *transport processes* that control the direction and speed of contaminant migration. The two most important transport processes are advection and dispersion. The other group are the *transformation processes*. Transformation processes include various chemical, biological and radioactive reactions that alter a contaminant as it migrates.

8.10.2.1 *Transport processes*

Advection is the single-most important process controlling contaminant transport. Advection is the transport of a contaminant as a consequence of the fact that the water in which it (the contaminant) is dissolved is moving. The moving groundwater carries the contaminant along. Equation (8.13) gives the time-averaged macroscopic velocity v_m of groundwater flow. In most cases it is acceptable to assume that dissolved pollutants travel in the same direction and with the same average velocity as the groundwater. Dispersion is a secondary transport process that modifies the direction and speed of advection. Dispersion is caused by both microscale (individual pore) variations and macroscale heterogeneities in the aquifer (Fig. 8.27). The time-averaged velocity v_m necessarily means that some water travels faster, while some travels slower, than the average, and contaminants in the faster flow move ahead of

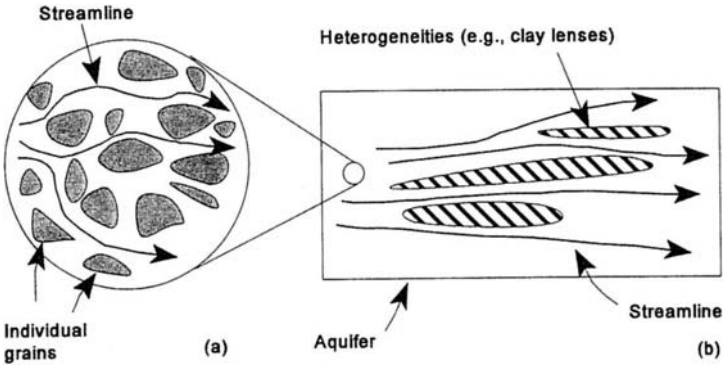

Figure 8.27. a) Microscale dispersion around individual grains of aquifer material, and b) Macroscale dispersion caused by heterogeneities in the aquifer.

contaminants in the slower flow streams. This is type of dispersion is termed *longitudinal dispersion* as it is in the same direction as the flow. Some groundwater will follow flow paths that diverge from the downstream direction. This results in contaminants spreading and mixing perpendicular to the downstream flow path. Dispersion perpendicular to the downstream flow is termed *transverse dispersion.* The net result of longitudinal and transverse dispersion is a lengthening and widening of the contaminant plume in the downstream direction, and an overall reduction in contaminant concentration when compared to advective transport alone.

8.10.2.2 *Transformation processes*

Contaminants in groundwater are subject to chemical, biological and radioactive transformation reactions as they migrate through the vadose zone and as they flow with the groundwater. In some cases a pollutant may be completely destroyed by the reaction, as with many organic pollutants and pathogenic organisms. In other cases the contaminant may be changed into new substances. In still other cases the aquifer may act as a 'sink' and sequester the material; however, the pollutant may be remobilized and come out of 'storage' if environmental conditions change in the aquifer. Table 8.4 is taken from the NRC (1990) report and lists the most important types of transformation reactions affecting groundwater pollutants. Understanding the effects of transformation reactions is made more complex by the fact that many reactions are interrelated. For example, microorganisms that accomplish biodegradation produce enzymes that can speed up other reactions such as redox reactions and hydrolysis. Another example is when changes in pH change the electrical charge on solid-particle surfaces causing differences in sorption processes (NRC 1990).

8.11 WELLHEAD PROTECTION

In 1986 Congress took a significant step in the management of groundwater resources. In 1986 Congress amended the Safe Drinking Water Act of 1974 to include a new section on state wellhead protection programs (WHPP) for public water supply

Table 8.4. Transformation reactions affecting contaminants in groundwater (source: NRC 1990).

Process	Definition	Impact on transport
Acid/base reactions	Reactions involving a transfer of protons (H^+)	Mainly an indirect control on contaminant transport by controlling the pH of the water. Important for contaminant reduction but may create undesirable daughter products
Biological transformation	Reactions involving the degradation of organic compounds by microorganisms and redox conditions	Can increase the solubility of metals in groundwater if adsorption is not increased
Complexation	Combination of cations and anions to form a more complex ion	Important process affecting contaminant concentration
Dissolution/precipitation	The process of adding or removing contaminants from solution by dissolving or precipitation solids	Precipitation is an important contaminant attenuation process. Contaminants may go back into solution if aquifer conditions change
Hydrolysis/substitution	Reaction of a halogenated organic compound with water or a component ion of water (hydrolysis) or with another anion (substitution)	May make an organic contaminant more susceptible to biodegradation and solution
Redox reactions	Reactions involving the transfer of electrons between elements with multiple oxidation states	An important group of reactions that can result in the precipitation of metals and their immobilization
Radioactive decay	Spontaneous decay of an unstable isotope of an element	A method of contaminant attenuation, especially when the half-life is less than or equal to the residence time in the flow system
Sorption	Partitioning of a contaminant between groundwater and mineral or organic aquifer material	Important in reducing contaminant concentration by sequestering contaminants on solid surfaces (Desorption may add contaminants to the groundwater)

wells. The program is voluntary though states establishing wellhead protection programs are eligible for federal grants to help implement the plans. The Environmental Protection Agency (EPA) has created guidelines for the development of WHPP plans and the identification of well head protection areas (WHPA) (EPA 1987, 1993).

Wellhead protection programs involve both management issues and technical issues. Some of the management issues include budgeting for the costs in both time and money needed to establish a program, developing guidelines and regulations that are understandable by the public and defensible in court, and participating in intergovernmental negotiation where aquifers cross jurisdictional boundaries. Wellhead protection programs will often involve the very sensitive issue of land use regulation. A successful WHPP must be supported by the public. It is imperative that the responsible government agencies cultivate public support by bringing the public into the decision-making process early and in a meaningful way. Technical issues include

identifying all potential sources of contamination for a water supply well, and choosing and implementing the method for WHPA delineation. Identifying contaminant sources can be a major undertaking simply because of the number of potential sources, and in most communities contaminant sources have never been cataloged and georeferenced. A geographic information system (GIS) is an excellent tool for storing, retrieving, and mapping contaminant-source information (GIS is discussed in Chapter 13). Delineation of a WHPA essentially involves 3 steps:

1. Determining the objectives of the WHPA,
2. Choosing a delineation criterion or criteria, and
3. Choosing a method for mapping the WHPA based on the criterion/criteria.

WHPA objectives. The EPA identified three general objectives for a WHPA: to provide a remedial action zone; to provide a zone for contaminant attenuation; or to provide a well-field management zone. A remedial action zone provides a buffer allowing cleanup of a pollutant before it reaches the well. An attenuation zone provides a buffer large enough so that contaminants are sufficiently degraded through transformation processes (Table 8.4) before reaching the well. A well-field management zone is the most general of the objectives and aims to restrict the types of land uses and activities that occur within the zone.

WHPA delineation criteria. The term *criteria* as used by the EPA refers to the '...conceptual standards that form the basis for WHPA delineation.' They are also the factors that are specifically referred to in the 1986 statute (EPA 1987). Five criteria on which to base a WHPA are – distance, drawdown, time of travel, flow boundaries and assimilative capacity of the aquifer. The choice of criteria is not solely a technical issue, however, since the best criteria from a technical point of view may not be the best from an administrative viewpoint.

WHPA delineation methods. Well head delineation methods are the procedures for translating the WHPA criteria into actual mappable boundaries. Table 8.5 gives six delineation methods listed roughly in order of increasing complexity and cost. The

Table 8.5. WHPA delineation methods (source: EPA 1987).

Method	Delineation criteria	Comments
Arbitrary fixed radii	Distance	Circle drawn around the well based on an arbitrary distance. Inexpensive and easy to apply. Does not use any pumping or aquifer-related data. May or may not provide sufficient protection but may be useful as a first step towards a more sophisticated WHPA
Calculated fixed radii	Time of travel (TOT)	Circle drawn around well based on a specified TOT. Requires data on pumping rate and aquifer characteristics. Requires limited technical expertise and is easy and relatively inexpensive to apply
Simplified variable shapes	TOT and flow boundaries (FB)	A representative 'standardized variable shape', generated by analytical methods using TOT and FB criteria, is oriented around the well according to groundwater flow patterns. The method is easily implemented once the standardized forms are generated. Since it accounts for the direction of flow it is a step up from the fixed radii method

Table 8.5. Continued.

Method	Delineation criteria	Comments
Analytical methods	TOT and FB	Flow equations are used to determine the zone of contribution (ZOC) to a pumping well. The WHPA is delineated based on the extent of the ZOC, modified by TOT and FB. Site-specific hydrogeologic data are required for each well. Requires modest technical expertise, and is one of the widely used methods
Hydrogeologic mapping	TOT and FB	Flow boundaries, TOT and aquifer properties are determined and mapped using geological, geophysical or dye tracing methods. The method is well suited to aquifers with near-surface flow boundaries and aquifers with high secondary porosity, where assumptions of flow through porous media are not valid. The method requires extensive geotechnical expertise and can be expensive if there is little existing data
Numerical flow/transport models	TOT, FB, and drawdown	Computer models are used to calculate TOT and drawdown; FB must be specified for the model. Computer models provide potentially high accuracy. The method is usually more expensive to develop than other methods because of the hydrogeologic data needed to parameterize the model and the level of technical expertise required

arbitrary fixed radii method draws a circle of specified radius around the well. The method uses distance as the sole criterion and does not consider groundwater processes, e.g. direction and velocity of flow, nor does it consider aquifer characteristics that affect assimilative capacity and contaminant transformation. However, the method is inexpensive and easy to apply and is certainly appropriate as a 'first step' towards a more comprehensive strategy. The calculated fixed radii method uses a time of travel (TOT) criterion to define the radius. Travel time to the well is specified based on one of the WHPA objectives. For a fixed pumping rate and aquifer properties, e.g. porosity, transmissivity, and storage coefficient, the radius is calculated as a function of the volume of water pumped in that period of time. In Florida a WHPA is delineated by the radius calculated from the following equation using a 5-year TOT:

$$Qt = n\pi hr^2 \tag{8.43}$$

and solving for the radius:

$$r = \sqrt{\frac{Qt}{\pi nh}} \tag{8.44}$$

where n is porosity and h the length of the well screen opening.

The remaining WHPA delineation methods listed in Table 8.5 all identify and distinguish the zone of influence (ZOI) from the zone of contribution (ZOC) to a pumping well. The zone of influence is same as the cone of depression described earlier. The zone of contribution is the area actually contributing water to the well. The ZOI and ZOC are *not* the same, except in the relatively rare circumstance where

the potentiometric surface (or water table) is perfectly horizontal. Figure 8.28 shows a pumping well in porous media. The ZOI is asymmetrical about the well extending further downgradient than it does upgradient. The ZOC extends upgradient to the groundwater divide and downgradient to the *stagnation point* or *null* point. The stagnation point is the point where the pull of gravity just equals the pull towards the pumping well. Water near the groundwater divide has not yet entered the ZOI. Water flowing laterally by the well will deviate toward the well when it enters the ZOI, but will continue downgradient where the natural hydraulic gradient is stronger than the gradient towards the well. Pollutants moving toward the well move faster on the upgradient side than on the downgradient side because of the differences in groundwater velocity. Let us call the macroscopic velocity due to the natural hydraulic gradient v_{nat} and the macroscopic velocity due to pumping v_p. From Equations (8.12 and 8.13) the natural groundwater velocity is $v_{nat} = K(\Delta h/Ln)$. The groundwater velocity due to pumping is:

$$v_p = \frac{Q}{2\pi rhn} \tag{8.45}$$

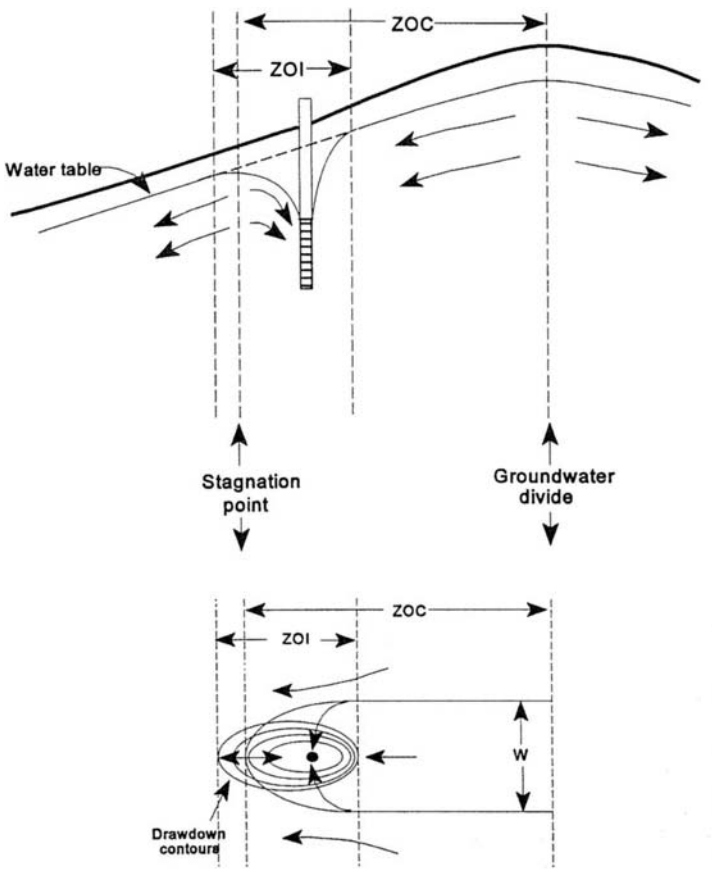

Figure 8.28. A cross-sectional view (a) and plan view (b) of a pumping well in an aquifer with a sloping water table showing the ZOI and the ZOC.

where r is the is the distance to the point of interest on the cone of depression, h is the saturated thickness at r, and n is the porosity (Kasenow 1995). The net upgradient velocity is the sum of the natural velocity and the pumping velocity:

$$v_{ug} = \frac{Q}{2\pi rhn} + k\frac{\Delta h}{Ln} \tag{8.46}$$

The net downgradient velocity is the difference between the natural velocity and the pumping velocity:

$$v_{dg} = \frac{Q}{2\pi rhn} - k\frac{\Delta h}{Ln} \tag{8.47}$$

A more conservative approach is to use the *effective porosity* n_e rather than n. The effective porosity is essentially equal to the specific yield (see Fig. 8.5). Assuming steady, uniform flow conditions the limits of the ZOC can be determined from the uniform flow equations (Todd 1980). The downgradient stagnation point where the pull towards the well just balances the gravitational pull downslope is calculated as:

$$r_{\text{stpt}} = \frac{Q}{2\pi hnv_{\text{nat}}} \tag{8.48}$$

where r_{stpt} = stagnation point downgradient from the well, Q = pumping rate, h = the effective saturated thickness of the aquifer zone, and v_{nat} = natural groundwater velocity.

The maximum width (W) of the ZOC at steady-state is:

$$W = 2\pi r_{\text{stpt}} \tag{8.49}$$

Again, a more conservative approach is to use n_e, the effective porosity, rather than n.

The simplified variable shapes delineation method uses Equations (8.48) and (8.49) and the location of flow boundaries to determine the WHPA. The remaining three delineation methods use analytical flow equations, geologic field mapping or numerical groundwater flow and/or contaminant transport models to determine the ZOC and WHPA. In areas where secondary porosity dominates flow conditions, aerial photography and detailed field mapping may also be required to identify groundwater flow paths and boundaries.

8.12 GROUNDWATER REGIONS IN THE UNITED STATES

Thomas (1952) identified 10 major groundwater regions in the United States (Fig. 8.29). The *Western Mountain Region* includes the Cascades, Sierra Nevada and Rocky Mountains, as well as smaller mountain ranges. Groundwater is found in the thin mantle of soil and fractured bedrock. The intermontane valleys may also contain water. One of the most productive aquifers in the country is found in this region in the Palouse Hills near Spokane, Washington. The *Alluvial Basins* occupy the areas between the major mountain ranges. Basins are found in Central and Southern California, in the Basin and Range Province of Nevada, as well as parts of Utah, Arizona

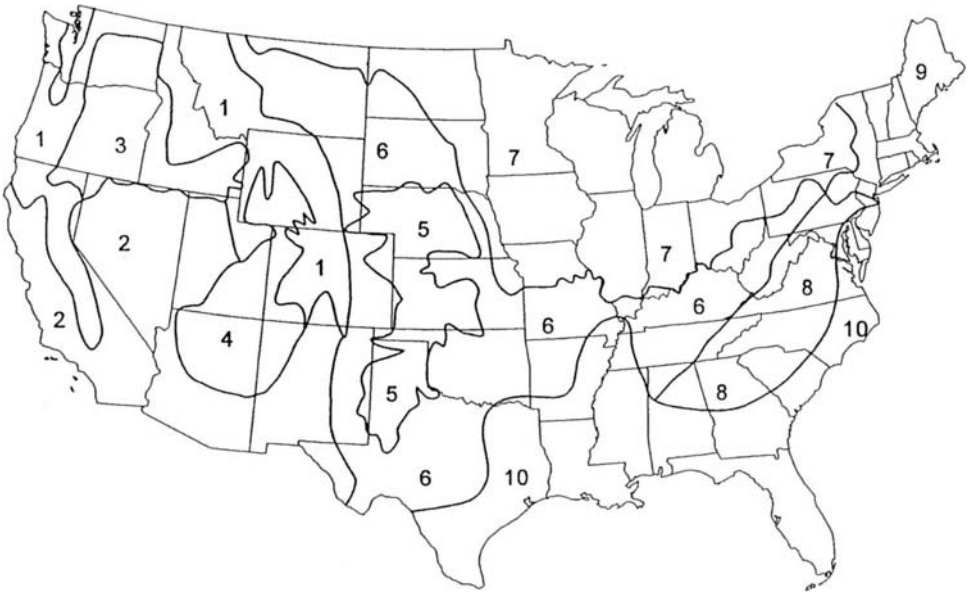

Figure 8.29. Groundwater regions in the continental United States (after Thomas 1952. Map redrawn from Gleick 1993 and AIPG 1983). 1. Western Mountains, 2. Alluvial Basins, 3. Columbia Plateau, 4. Colorado Plateau, 5. High Plains/Ogallala, 6. Unglaciated Central Region, 7. Glaciated Central Region, 8. Unglaciated Appalachians, 9. Glaciated Appalachians, 10. Atlantic and Gulf Coastal Plains.

and New Mexico. The eastern-most extent of this region is the Rio Grande Valley in New Mexico. Many of these basins have excellent aquifers and supply large quantities of water to irrigation and municipal wells. This is largely a desert environment so recharge is limited and well levels are falling in many areas. The *Columbia Plateau* is a large basaltic (lava) plateau covering parts of Idaho, Washington and Oregon. It is overlain and interbedded with alluvial material. The overall thickness of the basaltic flows exceeds 1000 m in places. The basalt can be an excellent aquifer where it is recharged by surface runoff and streams. The *Colorado Plateau* is composed of nearly-horizontal sedimentary rock layers. Sandstones, limestones and shales are the most common strata. Aquifers are generally not very productive yielding around 1 to 10 $m^3\ d^{-1}$. *The High Plains* or *Ogallala* aquifer underlies parts of seven states in the High Plains of the central United States. The aquifer consists of alluvium overlying sedimentary strata. The alluvium forms the stratigraphic unit referred to as the Ogallala. The aquifer has variable thickness, but is generally thickest in the north and is thinner in the south. The Ogallala has been pumped extensively for irrigation water over the last 50 years and well level are dropping throughout the aquifer. The Ogallala's recharge zone was destroyed in the geologic past, and, when combined with a dry climate, the result is very little natural recharge. Stretching in a great wedge from the Rocky Mountains to southern Illinois and then northeast to New York is the *Unglaciated Central Region*. This is a complex of plains and plateaus underlain by sedimentary rock, and wells here produce low to moderately low yields. Some of the

more productive wells have brackish water. The *Glaciated Central Region* is hydrogeologically similar to the unglaciated central region with one major difference – the area is overlain by glacial till reaching a thickness in some areas of 300 m. Till is unconsolidated, poorly-sorted debris deposited by glacial processes and makes good aquifer material many areas. From Alabama to Pennsylvania is an area of ancient, weathered crystalline rock forming the *Unglaciated Appalachian Region.* The weathered mantle of igneous and metamorphic rock produces small but reliable well yields. The valleys, with a bed of alluvium, tend to have slightly better yields. Some ridges like the Blue Ridge are hard and dense and produce very little water. Most of New England is contained within the *Glaciated Appalachian Region.* As before, the hydrogeology is similar to the Unglaciated Appalachian Region, with the main difference being the existence of a layer of till. The best wells are in the areas where the till is thickest. The last region is the *Atlantic and Gulf Coastal Plain.* The region extends down the Atlantic seaboard from Cape Cod to Florida, across to east Texas and up the Mississippi River. This is an area of unconsolidated to consolidated sedimentary material. The thickness of the sedimentary material may exceed 10,000 m near the coasts. The combination of unconsolidated material and high rainfall combine to create very productive aquifers in this area.

SUMMARY

The study of groundwater has always been constrained by our inability to directly observe the system. This places limits on the accuracy with which we can define groundwater processes. Groundwater is an important water resource for society. As our use of this resource continues to increase, and as various activities threaten groundwater quality, we need to improve our basic knowledge of groundwater systems. In this regard expansion of data collection and monitoring is essential. What we know about aquifers is often based on point measurements from a relatively few number of wells. Exactly what is going on between these points must largely be inferred. Numerical groundwater models have made the study of complex flow systems possible, but still the model parameters must be estimated from actual data. Groundwater quantity and quality have become some of the most important topics in hydrology today.

PROBLEMS

8.1 The points A, B and C on the map below show the relative geographic positions and heads of three wells. Determine the following.

a) Give the direction (in degrees from north) of groundwater flow. Assume geographic north is at the top of the map. (Show the direction of flow on your map with an arrow.)

b) Calculate the hydraulic gradient.

c) Calculate the specific discharge (q_w) per meter of aquifer. The aquifer is 45 m thick.
$K = 2.1$ m d^{-1} Map scale = 1:18,000

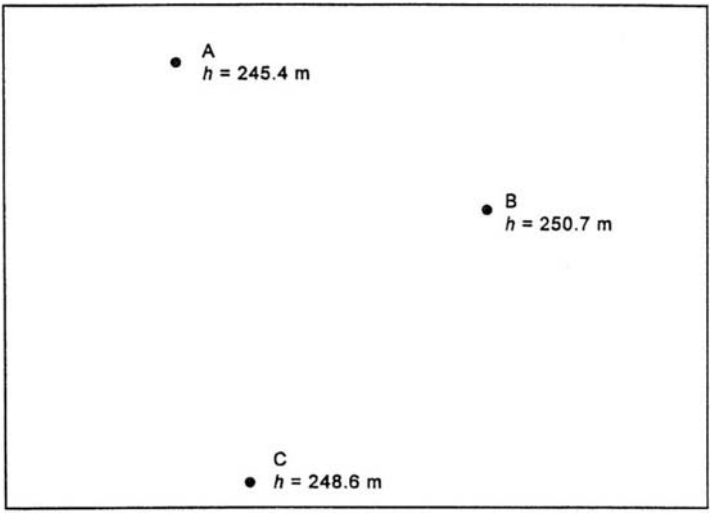

8.2 The figures below are a cross section and longitudinal section through an idealized montane valley. Two piezometers are installed in the center of the valley.

Width $w = 1700$ m
Saturated thickness $y = 24$ m
$L = 1102$ m
$K = 25$ m d^{-1}
$n = 40\%$
$z_1 = 103.7$ m
$z_2 = 102.0$ m
$p_1 = 20.2$ m
$p_2 = 19.5$ m

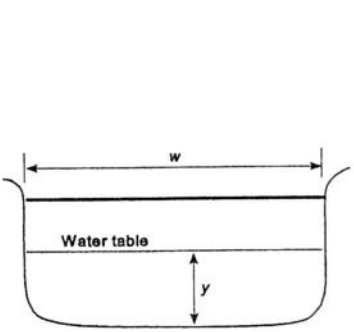

Cross-sectional view

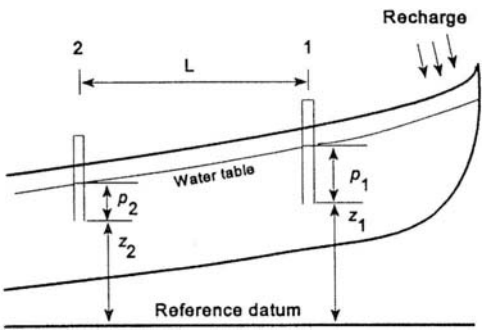

Longitudinal view

a) What is the total volume rate of groundwater flow (discharge) through the aquifer?
b) Assuming a pollutant travels as fast as the water, how long would it take a pollutant to travel from the head of the valley (recharge zone) to a point 5 km downstream?
c) For an average per capita water use of 500 liter/day, how large a population could be supported without overdrafting the aquifer?

8.3 The figure below is a cross-section diagram showing water seeping out of an unlined canal. Assume identical isotropic and homogeneous aquifer conditions on both sides of the canal. Assume also that the Dupuit-Forchheimer assumption apply.

$h_1 = 9.23$ m
$h_2 = 7.92$ m
$K = 0.65$ m d^{-1}

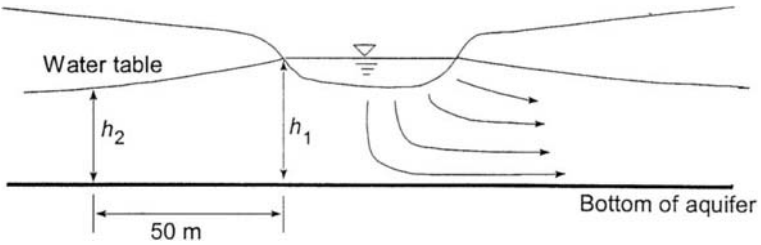

a) Use Darcy's law to find the volume of water seepage per meter of canal.
b) Use the Dupuit-Forchheimer equation to solve this problem.
c) If the canal is 4.6 miles long, how much water seeps from the entire canal?
d) Find the value of head at 13 m from location 1.

8.4 A 12-inch diameter well penetrates 90 ft below the static water table in an unconfined aquifer. After 24 hours of pumping at 1200 gal min^{-1} the water level in a test well at 310 ft is lowered 1.77 ft, and in a well 105 ft away the drawdown is 3.85 ft. What is the transmissivity (approximately) of the aquifer? (You should draw a diagram for this problem.)

8.5 The map below shows measured values of head (feet) at observation wells and along a stream channel (water surface elevation).
a) Draw a flow net. (Use a head contour interval of 10 ft.)
b) Assuming the saturated thickness of the aquifer is 20 ft and the hydraulic conductivity is $K = 2.9$ ft d^{-1} calculate q, the flow between two flow lines, and the total flow Q between points C and D along the channel.
c) On the lower graph draw the cross-sectional view of the water table from A to A'.

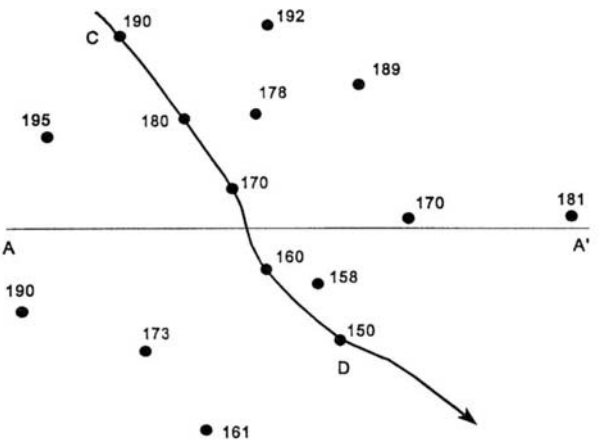

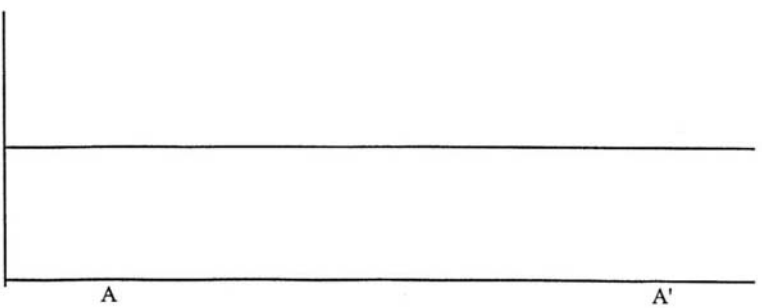

8.6 Given in the table are data (from Bouwer 1978) for drawdown versus time from a pump test. The drawdown data were observed at an observation well $r = 200$ m from a well pumping $Q = 1000\ m^3\ d^{-1}$. Find S and T using:

1. Theis match point method, and
2. Cooper-Jacob method

t (days)	s (m)
0.001	0.017
0.005	0.097
0.01	0.145
0.05	0.267
0.1	0.322
0.5	0.449
1.0	0.504
5	0.632
10	0.687

CHAPTER 9

The water balance

Through the 1940s and early 1950s C.W. Thornthwaite and J.R. Mather developed and refined a bookkeeping procedure they called 'The Water Balance' (Thornthwaite & Mather 1955). The procedure uses the discrete mass balance (Eq. 2.8), and a simplified hydrologic system where soil moisture is the only water store (Fig. 9.1). The water balance procedure has been widely used by geographers, hydrologists and climatologists in teaching, research and applied water-resources planning, particularly in agricultural applications. The water balance combines precipitation and evapotranspiration for specific time periods and evaluates the effects on soil moisture storage and runoff. The magnitudes of the inputs and outputs, and their variation through the year, are a function of the local climate. For example, in the United States the period of greatest potential evapotranspiration in the summer might coincide with either a dry season on the West Coast, or with a wet season in the Southeast. In desert climates potential evapotranspiration exceeds precipitation all year, while in an equatorial climate the opposite may be true. It is the ability to evaluate the impacts on soil moisture and runoff from the changing inputs and outputs which makes the water balance a useful tool.

9.1 COMPONENTS OF THE WATER BALANCE

Only two variables and one parameter are required to calculate a water balance. The simplicity of the data requirements is one a major advantage of the method. The two input variables are precipitation and temperature; the only parameter is the *AWC* of the soil. Since precipitation and temperature are fundamental elements of climate, the water balance is sometimes referred to as the 'climatic water balance'. Temperature is used for the calculation of potential evapotranspiration by Equation (6.1); however, potential evapotranspiration can be estimated by any of the methods discussed in Chapter 6.

A water balance can be calculated for any time interval Δt, with daily, weekly or monthly being the most common. We will limit our discussion to a monthly water balance. Two different types of water balances may be calculated – a continuous water balance or an average water balance. The continuous water balance begins on particular date and is calculated forward in time on intervals of Δt for as long as necessary. The continuous balance uses a time series of inputs to produce a time series of water balance outputs, and tracks the actual changing climate conditions and the

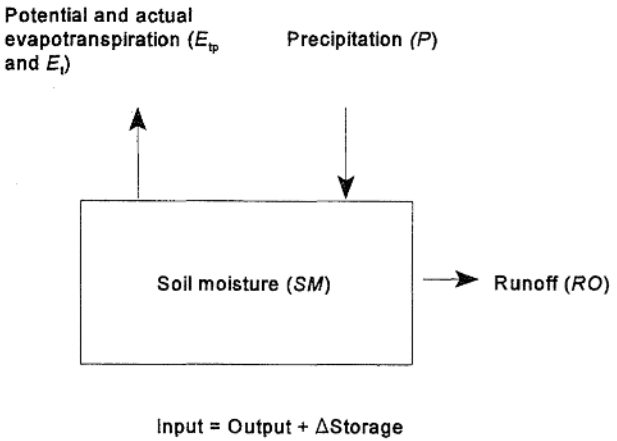

Figure 9.1. Simplified hydrologic system for the water balance procedure.

effects on runoff and soil moisture availability. The average water balance uses average values of precipitation and temperature and produces averages for the various water balance components. It does not track actual conditions, but rather describes the average conditions for a particular locale.

9.2 THE WATER BALANCE PROCEDURE

The water balance is based on the mass balance principle: *Input = Output + Change in storage.*

Using the water-balance terminology, the simplified mass balance is:

$$P = E_t + RO + \Delta SM \tag{9.1}$$

where P is precipitation, E_t is evapotranspiration, RO is runoff and ΔSM is the change in soil moisture storage. The procedure does not differentiate between surface runoff and groundwater runoff, though it is possible to differentiate runoff from snowmelt as opposed to runoff from rainfall using air temperature criteria. Physical runoff processes are not modeled in the water balance. Runoff is simply a volume of 'surplus' water; how the water actually flows out of the area is not considered. The water balance can be computed for any area having uniform climate and soil characteristics. This area could be a drainage basin, but need not be.

9.2.1 *Steps in calculating an average water balance*

a) Obtain climate data for the area of interest. In addition to the sources listed in Appendix C, many state universities, agricultural experiment stations and special water districts maintain local climatological records.

b) Determine the *AWC* of the soil as described in Chapter 7. It is helpful to know the level of soil moisture storage *SM* at the time when the water balance begins, but if it is not known the model will eventually converge on the correct value.

c) The 14 steps for calculating a water balance are given below. A sample water

balance is calculated in the next section. We will refer back to these steps as we proceed through the example.

1. Potential evapotranspiration (E_{tp}). Calculate E_{tp} by one of the accepted methods. If E_{tp} is estimated by a method other than the Thornthwaite equation additional data will be required.

2. Precipitation (P). Precipitation is obtained from climatological records in the same units as E_{tp}.

3. $P - E_{tp}$. Values of $P - E_{tp}$ can be positive or negative. Positive values indicate water is available for recharging soil moisture and/or for runoff. Negative values indicate the amount by which precipitation fails to supply the E_{tp} requirement. Most midlatitude locations have only one wet season $P - E_{tp} > 0$ and one dry season $P - E_{tp} < 0$.

4. Accumulated Potential Water Loss (*Acc. Pot. WL*). This value is the accumulated sum of the negative $P - E_{tp}$ values. In dry climates, successive approximations will be required to determine the value of this component.

5. Soil moisture storage (*SM*). Soil moisture storage is less than or equal to *AWC*. For months in which there is an *Acc. Pot WL*, you need to determine the amount of moisture remaining in the soil given that level of *Acc. Pot WL*. Soil moisture retention is determined using tables, graphs or equations. When $P - E_{tp}$ is positive and soil moisture storage is less than *AWC*, this positive value is added to the previous month's *SM* to determine current *SM*. Positive $P - E_{tp}$ values when the soil is at *AWC* represent excess rainfall available for runoff (see Step 11).

6. Change in soil moisture (ΔSM). This is either positive or negative but is only recorded when the *SM* is less than the *AWC*. This value is used in computing E_t in Step 7.

7. Actual evapotranspiration (E_t). The rules for calculating E_t are:

$$E_t = E_{tp} \text{ when } P > E_{tp}$$

$$E_t = P + |\Delta SM| \text{ when } P < E_{tp}$$

8. Moisture deficit (D). This is the difference between E_{tp} and E_t. This is an estimate of the amount of water that would have to be supplied by irrigation during the month to have E_t equal E_{tp}.

9. Moisture surplus (S). When the soil is at field capacity, precipitation in excess of E_{tp} is considered surplus and is available for runoff (*RO*). The model does not differentiate surface runoff from groundwater runoff.

10. Total available for runoff (*TARO*). This is not in the original water balance procedure but was added by Dunne & Leopold (1978) and is helpful for calculating runoff. *TARO* is equal to the present month's surplus plus any water detained *DT* in the basin from the previous month. *DT* is equal to one half of the *TARO* from the previous month. For month i:

$$TARO_i = (S_i + DT_{i-1}) = [S_i + 0.5(TARO_{i-1})]$$

11. Runoff (*RO*). Runoff *RO* is rainfall-generated runoff. A simplifying assumption is that only one-half of the total water available for runoff (*TARO*) in a given month actually runs off in that month. The other half is detained (*DT*) in the basin

and is added to the next month's surplus, and is available to run off the next month. The 'one half' rule can be changed to reflect the conditions in a particular basin. Changing the percentage of runoff changes *TARO* in Step 10.

12. Snow melt runoff (*SMRO*). To simplify the discussion, *SMRO* will not be considered here. For an explanation of the calculation of *SMRO* see Thornthwaite & Mather (1957).

13. Total runoff (*TOT RO*). This term is equal to rainfall runoff *RO* and snowmelt runoff *SMRO*:

$$TOT\,RO = (RO + SMRO)$$

Since we are not considering *SMRO*, total runoff equals rainfall runoff:

$$TOT\,RO = RO$$

14. Moisture detention (*DT*). This is the moisture detained in the basin during the current month and available for runoff next month (see Step 11):

$$DT = (TARO - RO)$$

9.2.2 *An example water balance calculation*

The best way to understand the water balance is to follow a worked example. The example here is a simplified average monthly water balance. The simplification is that runoff from melting snow will be ignored. For a more detailed description of the water balance procedure the reader should obtain the publication by Thornthwaite & Mather (1957). The example here is for Lexington, Kentucky. The Lexington station is at 38.08°N latitude and 298 m in elevation. The climate of Lexington is borderline between the humid subtropical climate found in the Southeast and the colder humid continental climate of the Midwest. Every month has ample precipitation, though the fall season is typically the driest time of year. For this example the *AWC* is assumed to be 230 mm (Fig. 7.18). All values are in millimeters of water.

Table 9.1 shows the first four steps (rows) of the water balance. Potential evapotranspiration was calculated using Thornthwaite's equation. Once P and E_{tp} are entered in rows 1 and 2 their difference is placed in row 3. Step 4 is to find the accumulated potential water loss (*Acc. Pot. WL*). This value is used in determining the current level of soil moisture storage. Completing the first 4 rows is straightforward. Row 5 is not quite so simple. The *AWC* of the soil is 230 mm, but the actual water content of the soil (*SM*) is unknown. As it turns out you can assume any value between $0 \leq SM \leq AWC$ and the procedure will eventually converge on the correct value. How long before convergence depends upon how close the initial estimate

Table 9.1. Water balance for Lexington, steps 1 to 4.

	Jan	Feb	Mar	Apr	May	Jun	Jul	Aug	Sep	Oct	Nov	Dec	Year
P	112	84	112	91	94	107	109	86	71	61	81	91	1099
E_{tp}	1	2	19	49	93	133	150	136	96	54	18	3	754
$P - E_{tp}$	111	82	93	42	1	–26	–41	–50	–25	7	63	88	
Acc. Pot. WL						–26	–67	–117	–142				

is to the correct value. Some suggested guides for estimating initial values for *SM* are to either assume $SM = AWC$ at the end of the wet season, or that $SM = 0$ at the end of the end of the dry season. The former is more appropriate for humid climates and the latter for dry climates. In arid and semi-arid climates *SM* may never reach *AWC*. But, regardless of the initial guess for *SM* the procedure eventually converges to the correct value. The terms 'wet season' and 'dry season' refer to periods defined by the relative magnitudes of precipitation and potential evapotranspiration. When precipitation exceeds potential evapotranspiration it is considered the wet season and vice versa for the dry season. For the Lexington example assume $SM = AWC$ at the end of the wet season in May. The rationale is that, even if soil moisture was completely exhausted at the end of the dry season in September ($SM = 0$), there is enough precipitation in excess of the potential evapotranspiration (row 3) in the following eight months to completely recharge soil moisture by May. In fact, there is enough excess precipitation to completely recharge the soil by December. To start the *SM* row insert 230 mm for May (Table 9.2). In June E_{tp} exceeds *P* by 26 mm. When $E_{tp} > P$ it is assumed that all the precipitation is vaporized and any additional moisture needed to satisfy the E_{tp} demand is taken from the soil. To determine how much water is withdrawn from the soil use either a graph such as Figure 9.2 or a soil moisture retention table appropriate for the *AWC*. For a given *Acc. Pot. WL* the table (or graph) gives the amount of water remaining in the soil. The soil moisture retention table for an *AWC* of 230 mm is given as Table 9.4. For an *Acc. Pot. WL* of –26 mm in June Table 9.4 gives 205 mm remaining in the soil, therefore the change in soil moisture storage

Table 9.2. Water balance for Lexington, steps 1 to 5.

	Jan	Feb	Mar	Apr	May	Jun	Jul	Aug	Sep	Oct	Nov	Dec	Year
P	112	84	112	91	94	107	109	86	71	61	81	91	1099
E_{tp}	1	2	19	49	93	133	150	136	96	54	18	3	754
$P - E_{tp}$	111	82	93	42	1	–26	–41	–50	–25	7	63	88	
Acc. Pot. WL						–26	–67	–117	–142				
SM	230	230	230	230	230	205	171	138	124	131	194	230	

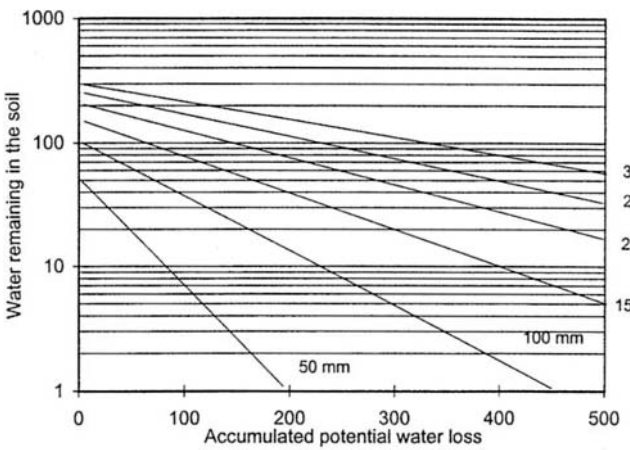

Figure 9.2. Soil moisture retention curves. The curves indicate the amount of water remaining in a soil having a specified *AWC* after experiencing the indicated accumulated potential water loss.

Table 9.3. Complete water balance for Lexington.

	Jan	Feb	Mar	Apr	May	Jun	Jul	Aug	Sep	Oct	Nov	Dec	Year
P	112	84	112	91	94	107	109	86	71	61	81	91	1099
E_{tp}	1	2	19	49	93	133	150	136	96	54	18	3	754
$P - E_{tp}$	111	82	93	42	1	–26	–41	–50	–25	7	63	88	
Acc. Pot. WL						–26	–67	–117	–142				
SM	230	230	230	230	230	205	171	138	124	131	194	230	
ΔSM	0	0	0	0	0	–25	–34	–33	–14	7	63	36	
E_t	1	2	19	49	93	132	143	119	85	54	18	3	718
D	0	0	0	0	0	1	7	17	11	0	0	0	36
S	111	82	93	42	1	0	0	0	0	0	0	52	381
TARO	137	151	168	126	64	32	16	8	4	2	1	53	
DT	69	75	84	63	32	16	8	4	2	1	1	26	
RO	68	76	84	63	32	16	8	4	2	1	0	27	381

Table 9.4. AWC = 230 mm. Moisture remaining in the soil (mm) after a given amount of *Acc. Pot WL*.

	0	1	2	3	4	5	6	7	8	9
0	230	229	228	227	226	225	224	223	222	221
10	220	219	218	217	216	215	215	214	213	212
20	211	210	209	208	207	206	205	205	204	203
30	202	201	200	199	198	198	197	196	195	194
40	193	192	192	191	190	189	188	187	187	186
50	185	184	183	183	182	181	180	180	179	178
60	177	176	176	175	174	173	172	171	171	170
70	170	169	168	167	167	166	165	165	164	163
80	162	162	161	160	160	159	158	158	157	156
90	156	155	154	154	153	152	152	151	150	150
100	149	148	148	147	146	146	145	144	144	143
110	143	142	141	141	140	139	139	138	138	137
120	136	136	135	135	134	134	133	132	132	131
130	131	130	130	129	128	128	127	127	126	126
140	125	125	124	124	123	122	122	121	121	120
150	120	119	119	118	118	117	117	116	116	115
160	115	114	114	113	113	112	112	111	111	110
170	110	109	109	108	108	107	107	107	106	106
180	105	105	104	104	103	103	102	102	102	101
190	101	100	100	99	99	99	98	98	97	97
200	96	96	96	95	95	94	94	94	93	93
210	92	92	91	91	91	90	90	90	89	89
220	88	88	88	87	87	86	86	86	85	85
230	85	84	84	84	83	83	82	82	82	81
240	81	81	80	80	80	79	79	79	78	78
250	78	77	77	77	76	76	76	75	75	75

from May to June is ΔS = –25 mm. Recall that as the soil dries it becomes more difficult to remove moisture so ΔS is slightly less (1 mm) than the *Acc. Pot WL*. In July the *Acc. Pot. WL* is –67 mm and 171 mm remain in the soil. This process for determining soil moisture storage continues for every month having an *Acc. Pot WL*, i.e.

thorough September. In October precipitation again exceeds evapotranspiration and the excess precipitation now goes to *recharge* soil moisture. Recharge continues until $SM = AWC$, after which any excess precipitation is available to run off. Tables 9.5-9.9 are soil moisture retention tables for a range of *AWC*s from 100 mm to 300 mm.

Table 9.3 gives the complete water balance for the Lexington example. As described above the change in soil moisture ΔSM (Step 6) is either positive, negative or zero. It is positive when moisture is recharging, negative when moisture is withdrawn from the soil, and zero when the soil moisture does not change from one month to the next. The calculation of actual evapotranspiration (Step 7) follows the logic developed in Chapter 6 where actual evapotranspiration is less-than-or-equal-to potential evapotranspiration, because as the soil dries the rate of actual evapotranspiration decreases. In our example, E_t for the month of July is equal to (109 + 34 = 143). The deficit D (Step 8) is simply the difference between potential and actual evapotranspiration. The deficit for July is (150 –143) = 7. The deficit is a rough approximation of the irrigation requirement. On the average, the annual irrigation requirement in Lexington is only 36 mm. There can only be a surplus S (Step 9) if there is excess precipitation and the soil is at *AWC*. If there is excess precipitation, but soil moisture is depleted, the excess goes to recharge soil moisture and is therefore not surplus (see October). Surplus water is available to run off. Steps 10-14 are all related to the calculation of runoff. The assumption is that only a portion of the water available to run off in a given month actually runs off in that month. The remainder is detained and runs off in subsequent months. 50% is a rule-of-thumb value for the percentage of water that runs off in a given month, but this percentage may be adjusted to match local conditions. The total amount of water available for runoff *TARO* in a given month (Step 10) is equal to the current month's surplus plus the detention *DT* from the previous month. For example, the runoff for March in Lexington using a 50% rule is 0.5 (93 + 75) = 84. When the runoff percentage is 50%, then *RO* and *DT* are identical.

9.2.3 *Graphing the water balance*

Figure 9.3 is the graph of the Lexington water balance. The curves are precipitation, potential evapotranspiration and actual evapotranspiration. The areas under and between the curves represent the deficit, soil moisture utilization ($-\Delta SM$), soil moisture recharge ($+\Delta SM$) and surplus. The curves clearly show for example how summer E_t equals the vertical sum of P and soil moisture utilization $-\Delta SM$, and how the deficit equals the unmet E_{tp}. In October when P once again exceeds E_{tp} the excess precipitation goes to recharge the soil ($+\Delta SM$). After the soil reaches *AWC* the excess becomes surplus and runoff commences.

For comparison, Figure 9.4 shows the average water balance for Wichita, Kansas. The *AWC* for Wichita is set at 180 mm (see Fig. 7.18). Wichita is located in the Great Plains where the climate is sub-humid to semi-arid. Precipitation is lower and potential evapotranspiration is higher than in Lexington. As a result the annual deficit is larger and the soil is considerably dryer in Wichita. Average soil moisture storage in September is 54 mm, only 30% of the *AWC*. The annual deficit averages 90

Table 9.5. *AWC* = 100 mm. Moisture remaining in the soil (mm) following a given amount of *Acc. Pot WL.*

	0	1	2	3	4	5	6	7	8	9
0	100	99	98	97	96	95	94	93	92	91
10	90	90	89	88	87	86	85	84	84	83
20	82	81	80	79	79	78	77	76	76	75
30	74	73	73	72	71	70	70	69	68	68
40	67	66	66	65	64	64	63	62	62	61
50	61	60	59	59	58	58	57	57	56	55
60	55	54	54	53	53	52	52	51	51	50
70	50	49	49	48	48	47	47	46	46	45
80	45	44	44	44	43	43	42	42	41	41
90	41	40	40	39	39	39	38	38	38	37
100	37	36	36	36	35	35	35	34	34	34
110	33	33	33	32	32	32	31	31	31	30
120	30	30	30	29	29	29	28	28	28	28
130	27	27	27	26	26	26	26	25	25	25
140	25	24	24	24	24	23	23	23	23	23
150	22	22	22	22	21	21	21	21	21	20
160	20	20	20	20	19	19	19	19	19	18
170	18	18	18	18	18	17	17	17	17	17
180	17	16	16	16	16	16	16	15	15	15
190	15	15	15	15	14	14	14	14	14	14
200	14	13	13	13	13	13	13	13	12	12
210	12	12	12	12	12	12	12	11	11	11
220	11	11	11	11	11	11	10	10	10	10
230	10	10	10	10	10	10	9	9	9	9
240	9	9	9	9	9	9	9	8	8	8
250	8	8	8	8	8	8	8	8	8	7
260	7	7	7	7	7	7	7	7	7	7
270	7	7	7	7	6	6	6	6	6	6
280	6	6	6	6	6	6	6	6	6	6
290	5	5	5	5	5	5	5	5	5	5
300	5	5	5	5	5	5	5	5	5	5
310	5	4	4	4	4	4	4	4	4	4
320	4	4	4	4	4	4	4	4	4	4
330	4	4	4	4	4	4	3	3	3	3
340	3	3	3	3	3	3	3	3	3	3
350	3	3	3	3	3	3	3	3	3	3
360	3	3	3	3	3	3	3	3	3	2
370	2	2	2	2	2	2	2	2	2	2
380	2	2	2	2	2	2	2	2	2	2
390	2	2	2	2	2	2	2	2	2	2
400	2	2	2	2	2	2	2	2	2	2
410	2	2	2	2	2	2	2	2	2	2
420	1	1	1	1	1	1	1	1	1	1
430	1	1	1	1	1	1	1	1	1	1
440	1	1	1	1	1	1	1	1	1	1
450	1	1	1	1	1	1	1	1	1	1
460	1	1	1	1	1	1	1	1	1	1
470	1	1	1	1	1	1	1	1	1	1
480	1	1	1	1	1	1	1	1	1	1
490	1	1	1	1	1	1	1	1	1	1

Table 9.6. *AWC* = 150 mm. Moisture remaining in the soil (mm) following a given amount of *Acc. Pot WL.*

	0	1	2	3	4	5	6	7	8	9
0	150	149	148	147	146	145	144	143	142	141
10	140	139	138	138	137	136	135	134	133	132
20	131	130	130	129	128	127	126	125	124	124
30	123	122	121	120	120	119	118	117	116	116
40	115	114	113	113	112	111	110	110	109	108
50	107	107	106	105	105	104	103	103	102	101
60	101	100	99	99	98	97	97	96	95	95
70	94	93	93	92	92	91	90	90	89	89
80	88	87	87	86	86	85	85	84	83	83
90	82	82	81	81	80	80	79	79	78	78
100	77	76	76	75	75	74	74	73	73	73
110	72	72	71	71	70	70	69	69	68	68
120	67	67	67	66	66	65	65	64	64	63
130	63	63	62	62	61	61	61	60	60	59
140	59	59	58	58	57	57	57	56	56	56
150	55	55	54	54	54	53	53	53	52	52
160	52	51	51	51	50	50	50	49	49	49
170	48	48	48	47	47	47	46	46	46	45
180	45	45	45	44	44	44	43	43	43	43
190	42	42	42	41	41	41	41	40	40	40
200	40	39	39	39	38	38	38	38	37	37
210	37	37	36	36	36	36	36	35	35	35
220	35	34	34	34	34	33	33	33	33	33
230	32	32	32	32	32	31	31	31	31	30
240	30	30	30	30	29	29	29	29	29	29
250	28	28	28	28	28	27	27	27	27	27
260	26	26	26	26	26	26	25	25	25	25
270	25	25	24	24	24	24	24	24	24	23
280	23	23	23	23	23	22	22	22	22	22
290	22	22	21	21	21	21	21	21	21	20
300	20	20	20	20	20	20	19	19	19	19
310	19	19	19	19	18	18	18	18	18	18
320	18	18	18	17	17	17	17	17	17	17
330	17	17	16	16	16	16	16	16	16	16
340	16	15	15	15	15	15	15	15	15	15
350	15	14	14	14	14	14	14	14	14	14
360	14	14	13	13	13	13	13	13	13	13
370	13	13	13	12	12	12	12	12	12	12
380	12	12	12	12	12	12	11	11	11	11
390	11	11	11	11	11	11	11	11	11	10
400	10	10	10	10	10	10	10	10	10	10
410	10	10	10	10	9	9	9	9	9	9
420	9	9	9	9	9	9	9	9	9	9
430	9	8	8	8	8	8	8	8	8	8
440	8	8	8	8	8	8	8	8	8	8
450	7	7	7	7	7	7	7	7	7	7
460	7	7	7	7	7	7	7	7	7	7
470	7	6	6	6	6	6	6	6	6	6
480	6	6	6	6	6	6	6	6	6	6
490	6	6	6	6	6	6	5	5	5	5

Table 9.7. *AWC* = 200 mm. Moisture remaining in the soil (mm) following a given amount of *Acc. Pot WL.*

	0	1	2	3	4	5	6	7	8	9
0	200	199	198	197	196	195	194	193	192	191
10	190	189	188	187	186	186	185	184	183	182
20	181	180	179	178	177	176	176	175	174	173
30	172	171	170	170	169	168	167	166	165	165
40	164	163	162	161	161	160	159	158	157	157
50	156	155	154	153	153	152	151	150	150	149
60	148	147	147	146	145	145	144	143	142	142
70	141	140	140	139	138	137	137	136	135	135
80	134	133	133	132	131	131	130	129	129	128
90	128	127	126	126	125	124	124	123	123	122
100	121	121	120	119	119	118	118	117	117	116
110	115	115	114	114	113	113	112	111	111	110
120	110	109	109	108	108	107	107	106	105	105
130	104	104	103	103	102	102	101	101	100	100
140	99	99	98	98	97	97	96	96	95	95
150	94	94	94	93	93	92	92	91	91	90
160	90	89	89	89	88	88	87	87	86	86
170	85	85	85	84	84	83	83	83	82	82
180	81	81	80	80	80	79	79	79	78	78
190	77	77	77	76	76	75	75	75	74	74
200	74	73	73	72	72	72	71	71	71	70
210	70	70	69	69	69	68	68	68	67	67
220	67	66	66	66	65	65	65	64	64	64
230	63	63	63	62	62	62	61	61	61	61
240	60	60	60	59	59	59	58	58	58	58
250	57	57	57	56	56	56	56	55	55	55
260	55	54	54	54	53	53	53	53	52	52
270	52	52	51	51	51	51	50	50	50	50
280	49	49	49	49	48	48	48	48	47	47
290	47	47	46	46	46	46	46	45	45	45
300	45	44	44	44	44	44	43	43	43	43
310	42	42	42	42	42	41	41	41	41	41
320	40	40	40	40	40	39	39	39	39	39
330	38	38	38	38	38	37	37	37	37	37
340	37	36	36	36	36	36	35	35	35	35
350	35	35	34	34	34	34	34	34	33	33
360	33	33	33	33	32	32	32	32	32	32
370	31	31	31	31	31	31	31	30	30	30
380	30	30	30	29	29	29	29	29	29	29
390	28	28	28	28	28	28	28	27	27	27
400	27	27	27	27	27	26	26	26	26	26
410	26	26	25	25	25	25	25	25	25	25
420	24	24	24	24	24	24	24	24	24	23
430	23	23	23	23	23	23	23	22	22	22
440	22	22	22	22	22	22	22	21	21	21
450	21	21	21	21	21	21	20	20	20	20
460	20	20	20	20	20	20	19	19	19	19
470	19	19	19	19	19	19	19	18	18	18
480	18	18	18	18	18	18	18	18	17	17
490	17	17	17	17	17	17	17	17	17	16

Table 9.8. *AWC* = 250 mm. Moisture remaining in the soil (mm) following a given amount of *Acc. Pot WL.*

	0	1	2	3	4	5	6	7	8	9
0	250	249	248	247	246	245	244	243	242	241
10	240	239	238	237	236	235	235	234	233	232
20	231	230	229	228	227	226	225	224	224	223
30	222	221	220	219	218	217	216	216	215	214
40	213	212	211	210	210	209	208	207	206	206
50	205	204	203	202	201	201	200	199	198	197
60	197	196	195	194	194	193	192	191	190	190
70	189	188	187	187	186	185	184	184	183	182
80	182	181	180	179	179	178	177	177	176	175
90	174	174	173	172	172	171	170	170	169	168
100	168	167	166	166	165	164	164	163	162	162
110	161	160	160	159	158	158	157	157	156	155
120	155	154	153	153	152	152	151	150	150	149
130	149	148	147	147	146	146	145	145	144	143
140	143	142	142	141	141	140	139	139	138	138
150	137	137	136	136	135	134	134	133	133	132
160	132	131	131	130	130	129	129	128	128	127
170	127	126	126	125	125	124	124	123	123	122
180	122	121	121	120	120	119	119	118	118	117
190	117	116	116	116	115	115	114	114	113	113
200	112	112	111	111	111	110	110	109	109	108
210	108	107	107	107	106	106	105	105	105	104
220	104	103	103	102	102	102	101	101	100	100
230	100	99	99	98	98	98	97	97	96	96
240	96	95	95	95	94	94	93	93	93	92
250	92	92	91	91	91	90	90	89	89	89
260	88	88	88	87	87	87	86	86	86	85
270	85	85	84	84	84	83	83	83	82	82
280	82	81	81	81	80	80	80	79	79	79
290	78	78	78	77	77	77	77	76	76	76
300	75	75	75	74	74	74	74	73	73	73
310	72	72	72	71	71	71	71	70	70	70
320	70	69	69	69	68	68	68	68	67	67
330	67	67	66	66	66	65	65	65	65	64
340	64	64	64	63	63	63	63	62	62	62
350	62	61	61	61	61	60	60	60	60	59
360	59	59	59	59	58	58	58	58	57	57
370	57	57	56	56	56	56	56	55	55	55
380	55	54	54	54	54	54	53	53	53	53
390	53	52	52	52	52	51	51	51	51	51
400	50	50	50	50	50	49	49	49	49	49
410	48	48	48	48	48	48	47	47	47	47
420	47	46	46	46	46	46	45	45	45	45
430	45	45	44	44	44	44	44	44	43	43
440	43	43	43	42	42	42	42	42	42	41
450	41	41	41	41	41	41	40	40	40	40
460	40	40	39	39	39	39	39	39	38	38
470	38	38	38	38	38	37	37	37	37	37
480	37	37	36	36	36	36	36	36	35	35
490	35	35	35	35	35	35	34	34	34	34

Table 9.9. *AWC* = 300 mm. Moisture remaining in the soil (mm) following a given amount of Acc. Pot WL.

	0	1	2	3	4	5	6	7	8	9
0	300	299	298	297	296	295	294	293	292	291
10	290	289	288	287	286	285	284	283	283	282
20	281	280	279	278	277	276	275	274	273	272
30	271	271	270	269	268	267	266	265	264	263
40	263	262	261	260	259	258	257	256	256	255
50	254	253	252	251	251	250	249	248	247	246
60	246	245	244	243	242	242	241	240	239	238
70	238	237	236	235	234	234	233	232	231	231
80	230	229	228	227	227	226	225	224	224	223
90	222	222	221	220	219	219	218	217	216	216
100	215	214	214	213	212	211	211	210	209	209
110	208	207	207	206	205	204	204	203	202	202
120	201	200	200	199	198	198	197	196	196	195
130	194	194	193	193	192	191	191	190	189	189
140	188	187	187	186	186	185	184	184	183	183
150	182	181	181	180	180	179	178	178	177	177
160	176	175	175	174	174	173	173	172	171	171
170	170	170	169	169	168	167	167	166	166	165
180	165	164	164	163	162	162	161	161	160	160
190	159	159	158	158	157	157	156	156	155	155
200	154	154	153	152	152	151	151	150	150	149
210	149	148	148	147	147	147	146	146	145	145
220	144	144	143	143	142	142	141	141	140	140
230	139	139	138	138	138	137	137	136	136	135
240	135	134	134	133	133	133	132	132	131	131
250	130	130	130	129	129	128	128	127	127	127
260	126	126	125	125	124	124	124	123	123	122
270	122	122	121	121	120	120	120	119	119	118
280	118	118	117	117	116	116	116	115	115	114
290	114	114	113	113	113	112	112	111	111	111
300	110	110	110	109	109	109	108	108	107	107
310	107	106	106	106	105	105	105	104	104	104
320	103	103	103	102	102	102	101	101	101	100
330	100	100	99	99	99	98	98	98	97	97
340	97	96	96	96	95	95	95	94	94	94
350	93	93	93	92	92	92	92	91	91	91
360	90	90	90	89	89	89	89	88	88	88
370	87	87	87	87	86	86	86	85	85	85
380	85	84	84	84	83	83	83	83	82	82
390	82	81	81	81	81	80	80	80	80	79
400	79	79	79	78	78	78	78	77	77	77
410	76	76	76	76	75	75	75	75	74	74
420	74	74	73	73	73	73	73	72	72	72
430	72	71	71	71	71	70	70	70	70	69
440	69	69	69	69	68	68	68	68	67	67
450	67	67	66	66	66	66	66	65	65	65
460	65	65	64	64	64	64	63	63	63	63
470	63	62	62	62	62	62	61	61	61	61
480	61	60	60	60	60	60	59	59	59	59
490	59	58	58	58	58	58	57	57	57	57

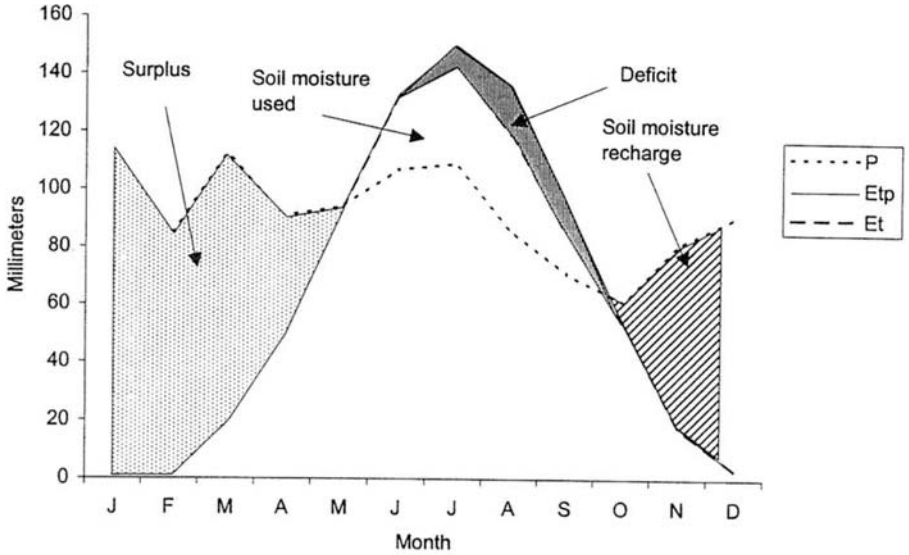

Figure 9.3. Average water balance for Lexington, Kentucky.

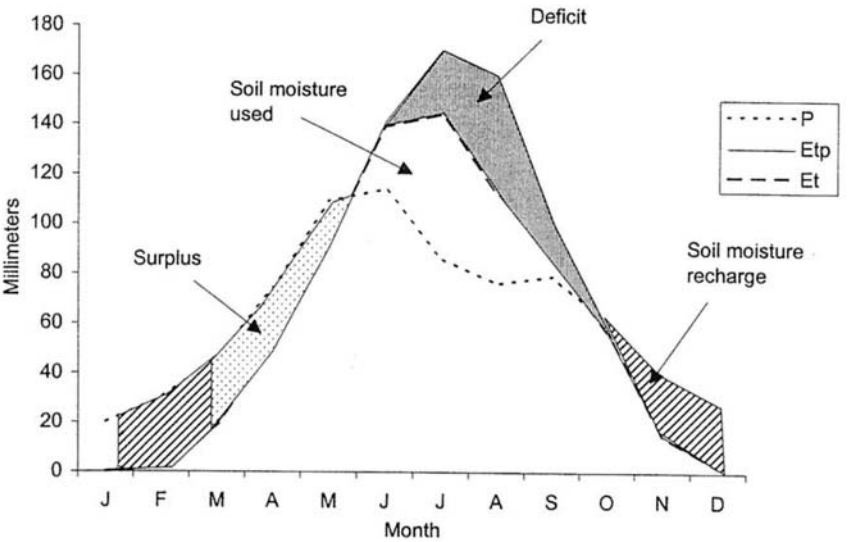

Figure 9.4. Average water balance for Wichita, Kansas.

mm, more than twice that of Lexington. Successful agriculture in this part of the country relies on supplemental irrigation water. There is enough precipitation in the spring in excess of potential evapotranspiration to allow the soil to reach and stay at field capacity for three months. In Lexington the soil is at field capacity for six months. Finally, Wichita averages only 40 mm of runoff compared to 381 mm in Lexington (Fig. 9.5).

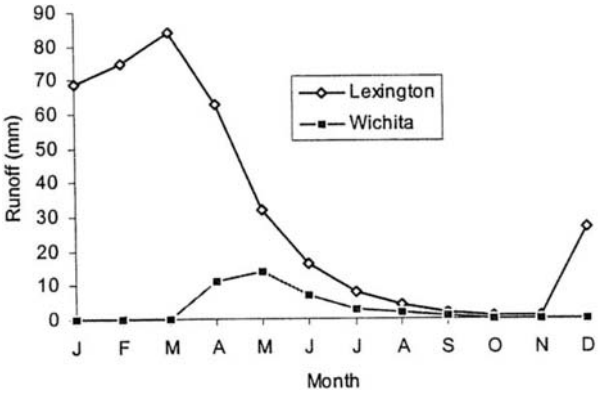

Figure 9.5. Computed runoff for Lexington and Wichita.

Water balances for even drier climates have larger deficits and lower soil moisture levels. Eventually, the point is reached where the soil moisture never reaches field capacity under normal conditions. As a result, irrigation becomes essential for agriculture in these areas. It is important to point out that the Thornthwaite equation tends to *underestimate* E_{tp} in dry climates. If another method were used to estimate E_{tp} the deficits would be even larger and the soil even dryer.

9.2.4 *Sensitivity of the water balance to* AWC

Since *AWC* is the only adjustable parameter, it is worth exploring the sensitivity of the water balance to this parameter. Figures 9.6 and 9.7 are the results of a sensitivity analysis for Lexington and Wichita. The analysis examines the changes in the annual total deficit and runoff with changes in the *AWC*. The axes of the graphs have been scaled relative to the values for the deficit and runoff when the soil is at *AWC*. At the Lexington station the deficit is sensitive to the *AWC*, however runoff is not. As the *AWC* increases, the deficit decreases and vice versa. Apparently the deficit decreases with increasing *AWC* because with more water stored in the soil it is easier to satisfy the evapotranspiration demand. In the drier Wichita climate, both the deficit and runoff are sensitive to *AWC*. In this case, as the *AWC* increases, what little excess precipitation there is can be absorbed by the soil; hence, runoff drops dramatically. That same water is now stored in the soil and goes to reduce the deficit.

It is useful to examine the sensitivity of a model to its parameters. In this case there is only one parameter; in sophisticated hydrologic simulation models there can be dozens of parameters that need estimating. Knowing which parameters the model is most sensitive to is a way of prioritizing the collection of data. If a model is not sensitive to a certain parameter, then you shouldn't waste limited time and resources collecting detailed information about that parameter.

9.3 APPLICATIONS OF THE WATER BALANCE

The water balance has been used for many types of environmental analyses. The deficit is an approximate measure of the irrigation water requirement so an average

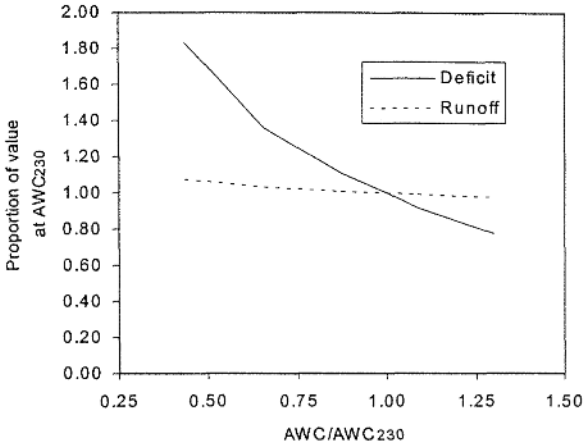

Figure 9.6. Sensitivity analysis of the deficit and runoff to changes in the *AWC* parameter for Lexington. The deficit is fairly sensitive to *AWC*, but runoff is not.

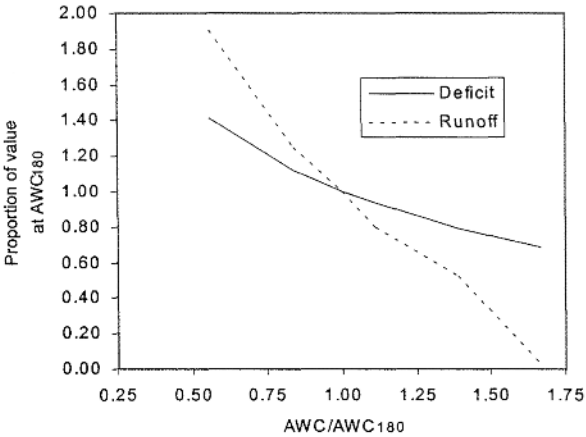

Figure 9.7. Sensitivity analysis of the deficit and runoff to changes in the *AWC* parameter for Wichita. In the drier climate of Wichita both the deficit and runoff were sensitive to *AWC*.

water balance indicates, on the average, when and how much irrigation water is required. If a continuous water balance were calculated, then the annual deficit for each year could be ranked and analyzed using a frequency analysis as in Example 4.5. You would then be able to estimate the probability of a getting deficit of a certain magnitude in any given year. You could also do a frequency analysis for individual monthly deficits as was shown in Figure 3.5. In a very different application, the US Environmental Protection Agency (1978) modified the water balance for use in evaluating the potential for leachate production from landfills. The author used the water balance in an examination of the possible impacts from climate change (Thompson 1992). He used a stochastic weather simulator model to simulate changing temperature and precipitation over a 50-year period. These variables were then used in a computer program of the water balance (Willmott 1977) to explore what might happen to runoff, the deficit, and soil moisture levels as temperature and precipitation change. Figure 9.8 shows the simulated impact on runoff in central Missouri given a 2.5°C increase in temperature and a 10% increase in precipitation.

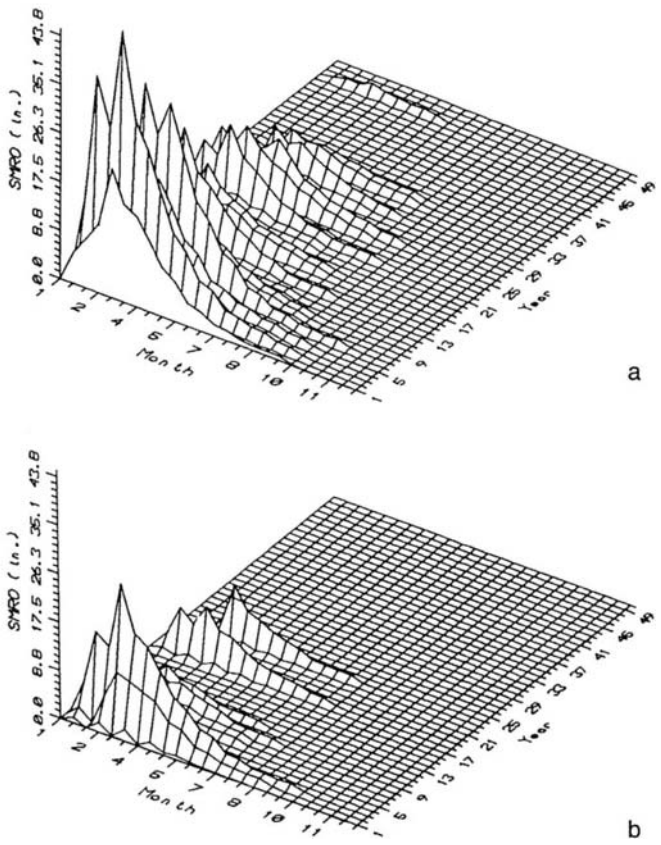

Figure 9.8. Simulated impact on snowmelt runoff in Missouri climate divisions 2 (a) and 3 (b) from a hypothetical increase in temperature of 2.5°C and a 10% increase in precipitation over 50 years (after Thompson 1992).

SUMMARY

The water balance procedure brings together many of the components of the hydrologic system into a single unified analysis. The procedure has minimal data requirements which makes it easy to apply. Even though it is not a sophisticated process-based model of the hydrologic system, it is useful in its ability to evaluate the time-varying moisture regime at any location. The fact that it can be used either on an average or continuous basis makes it applicable to a wide variety of environmental problems. One of the most important processes in the hydrologic system is runoff and stream flow. The water balance treats runoff only in a very generalized fashion. In Chapter 10 we examine runoff processes in more detail.

PROBLEMS

9.1 Calculate an average water balance using the climate data in Table 9.10. All data are in millimeters. Calculate the *AWC* using the soil data in Table 9.11. Round *AWC* to the nearest 50 millimeters for selecting the appropriate *AWC* table.

Graphing the water balance

a) Use the following scheme and graph the components of the water balance.
   P..... blue (or solid) line
   E_{tp}..... red (or dashed) line
   E_t..... green (or dotted) line
b) Color the appropriate areas under/between the lines using the following scheme.
   Water surplus region..... green
   Water deficit region..... red
   Soil moisture used..... yellow
   Soil moisture recharge..... blue

Table 9.10. Monthly evapotranspiration and precipitation data.

	Jan	Feb	Mar	Apr	May	Jun	Jul	Aug	Sep	Oct	Nov	Dec
E_{tp}	26	32	45	56	71	84	88	82	75	63	43	28
P	130	112	94	37	24	5	1	1	13	31	62	106

Table 9.11. Available water capacity per unit depth for three soil horizons.

Depth (inch)	AWC (in in^{-1})
0-10	0.15
11-24	0.10
25-36	0.09

CHAPTER 10

Basin morphometry and runoff

Water at the Earth's surface that neither infiltrates nor suffers evapotranspiration is destined to become surface runoff. The outline for this chapter is to first discuss some physical characteristics of the drainage basin that influence the magnitude and timing of runoff. Following this we examine the kinematic wave model for runoff, the timing of runoff from a basin, and basic runoff processes. Runoff is a continuum of water moving from the land surface into stream channels, and down the channels towards the basin outlet. Here we focus mainly on the land surface portion. Chapter 11 treats runoff after it reaches the channel and becomes streamflow. It is within the realm of runoff generation and channel flow that the disciplines of hydrology and fluvial geomorphology merge. Fluvial geomorphologists concern themselves with how moving water shapes the surface of the Earth through erosion, transport and deposition, and, conversely, how the Earth's surface modulates the flow of water. Some major water management issues surrounding runoff are flood hazard mitigation, erosion and sediment control, and water quality degradation from nonpoint sources of pollution. Nonpoint pollution sources are spatially extensive sources such as farmlands, city streets or deposition from the atmosphere. Understanding runoff processes and how human activities alter those processes is integral to managing society's vulnerability to flooding and water quality degradation.

10.1 BASIN MORPHOMETRY

Basin morphometry is the measurement and description of the geometric characteristics of the drainage basin. Some of the more readily observable characteristics include stream channel length, basin area and slope. The purpose here is to introduce a few morphometric properties that are germane to a discussion of runoff and channel flow.

10.1.1 *Stream ordering*

A stream channel network is a hierarchical system of tributaries feeding the master stream, or trunk channel, that exits the basin at the outlet. The channel network develops over geologic time scales, evolving characteristics that allow for the efficient movement of water and sediment through the basin. *Stream ordering* was first proposed by Horton (1945). It is a systematic procedure for ranking and numbering

stream channels by their relative position in the channel network. There are different methods for assigning an order number u to a stream channel, but they all start by assigning the lowest order to the smallest channels, and higher orders to the larger channels. The Strahler stream-ordering procedure (Strahler 1952) assigns the smallest initial tributaries an order of $u = 1$. When two channels of the *same* order join, the order of the channel segment below their junction is increased by one. For example, when two first-order tributaries meet they form a channel of order 2. When two second-order channels merge they form a 3rd-order segment and so on. Figure 10.1 shows a stream network and the ordering of channel segments by Strahler's method. With Strahler's method the order of a channel segment does not change after a junction with a segment of lower order. The *bifurcation ratio* R_b is the ratio of the number of streams of a given order N_u divided by the number of streams of the next higher order N_{u+1}:

$$R_b = \frac{N_u}{N_{u+1}} \tag{10.1}$$

Bifurcation ratios typically range between 3.0 and 5.0, except where the underlying geologic structure exerts a distorting influence. Researchers have found consistent relationships between stream order and physical properties of the stream such as mean length, mean gradient and the number of channel segments of a given order. Some of these relationships have been referred to as 'laws', though they are not true physical laws, but just strong statistical relationships. Horton's *Law of stream numbers* states that the number of streams of a given order forms an inverse geometric sequence with order:

$$N_u = R_b^{k-u} \tag{10.2}$$

where k is the order of the master stream (highest order) in the basin. Figure 10.2 is a

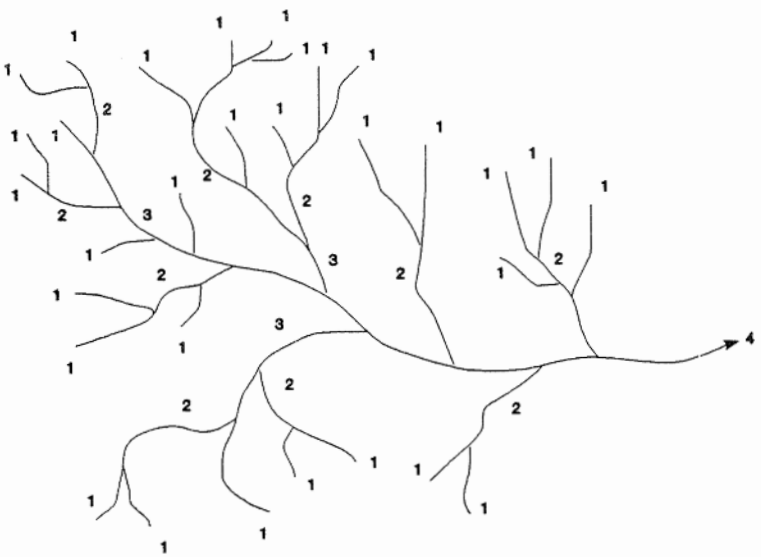

Figure 10.1. A stream network and stream orders using the Strahler method.

Order u	Number	Bifurcation Ratio
1	31	
		3.1
2	10	
		3.3
3	3	
		3
4	1	
	Average =	3.13

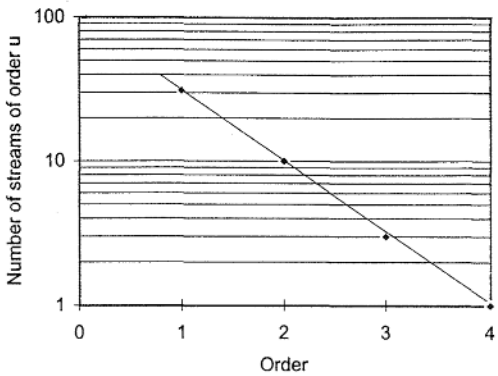

Figure 10.2. Bifurcation ratios for the streams in Figure 10.1 and the average bifurcation ratio for the basin. The number of streams of a given order u form and inverse geometric series with order.

plot of the number of streams versus order from Figure 10.1 and shows the inverse geometric relationship. The average bifurcation ratio for the entire basin in Figure 10.1 is 3.13 (Fig. 10.2). Stream ordering is scale dependent. The first-order streams are the smallest initial channels, that is those with no tributaries. But identifying first-order channels depends upon the scale of analysis. An acceptable working definition is that first-order streams are the initial blue-line channels identifiable on US Geological Survey quadrangle maps at a scale of 1:24,000. However, smaller channels not shown on the quadrangle maps can be identified in the field.

10.1.2 *Stream length*

Stream length is measured on a map using a chartometer. When estimating the length of a particular channel segment it is advisable to make a series of repeated measurements and calculate an average length. Horton found that stream lengths produced a direct geometric sequence with order – as order increases average stream length increases geometrically. This is Horton's *Law of stream lengths*.

Various measurements of stream length and basin length are important in the analysis of runoff and streamflow. The length of the watershed L_w is the maximum length along the main stream from the outlet (or gage) to the most distant ridge on the drainage divide. When measuring this distance on a topographic map the main channel is unambiguous near the mouth, but in the upper reaches of the basin a choice will likely have to be made as to which channel best represents the main channel. The choice will usually be between following the path that produces the longest total distance to the divide, or the path that is most directly in line with the downstream segment of next higher order. Another measure of stream length used in hydrograph analysis is the length along the main channel to a point nearest the centroid of the basin L_c. The centroid of the basin is the center of gravity of the basin when projected horizontally. Both of these measures are used in Chapter 11 in the development of synthetic unit hydrographs.

The total accumulated length of stream channels L_T is the sum of the lengths of all channel segments of all orders in the basin. L_T is used to calculate *drainage density*

D, the total accumulated length of all channel segments in a basin divided by the basin area (A):

$$D = \frac{L_T}{A} \tag{10.3}$$

All measurements in Equation (10.3) should be in the same units, e.g. miles per square mile. The dimensions of D are (L^{-1}). Measurements of drainage density in the United States range from values as low as 3 to 4 mi mi^2, to values as high as 1000 to 1300 mi mi^2 depending upon the climate and geology of the area (Schumm 1956). A way to think of drainage density is as a measure of the closeness of spacing of stream channels, which approximates the distance water must travel before reaching a stream channel. Water flowing over the ground surface as a nonchannelized, discontinuous sheet of water is called overland flow or *sheet flow*. Overland flow velocities range from tens to hundreds of meters per hour, with depths of flow between 1 and 10 mm. The length of the overland flow path can be an important control on the timing of runoff from a basin. Overland flow is normally the only source of water to first-order streams, and provides water to higher-order streams from interbasin areas. Figure 10.3 shows four first-order streams and their drainage areas. The interbasin areas between the first-order basins do not drain to the first-order streams but into the second-order stream.

Horton defined the *length of overland flow* L_g as the length of the flow path, projected to the horizontal, of nonchannel flow from a point on the drainage divide to a point on the adjacent stream channel (quoted in Strahler 1964). Since there are an infinite number of such point pairs, it is reasonable to compute an *average* length of overland flow $\bar{L}_g$ from a sample of such paired measurements. There is, however, a maximum length of overland flow in any basin. Since $\bar{L}_g$ is roughly half the distance between channels, an approximate value for $\bar{L}_g$ is:

$$\bar{L}_g \approx \frac{1}{2D} \tag{10.4}$$

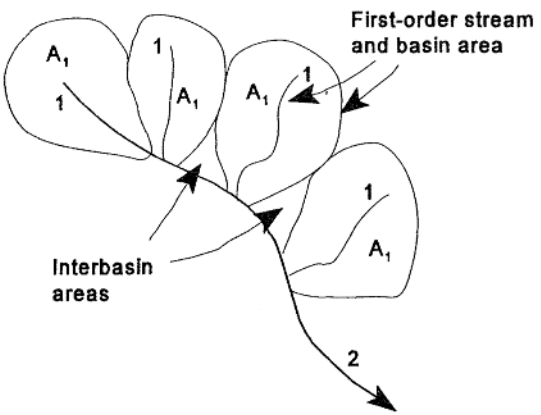

Figure 10.3. Interbasin areas between first-order stream basins (A_1). The interbasin areas drain directly to the second-order stream.

10.1.3 *Basin area*

Just as with stream channels there is a hierarchy for basin areas that contribute runoff to channels of different orders. A basin area of order A_u is the area contributing runoff to a stream of order u. A first-order drainage basin A_1 supplies runoff to a first-order stream segment (Fig. 10.3). The area of all the A_1 basins, plus any interbasin areas, constitute the area of the second-order basins A_2, and so on. The accumulated areas of all sub-basins of all orders is the total area of the basin A. Just as with stream numbers and stream lengths, Schumm (1956) proposed a *Law of basin areas*. The law states that average basin area forms a direct geometric sequence with basin order.

Strahler (1964) suggested that first-order streams and their contributing first-order basin areas are the 'unit cell', or building block of any watershed. Presumably runoff generation was one of the processes he had in mind in this construction of the basin. While this is reasonable conceptually, most physically-based simulation models take a more spatially abstract approach to modeling runoff generation. Physically-based simulation models usually define a fundamental runoff unit, but this spatial unit does not necessarily correspond to the areal dimensions of a first-order basin. Recent approaches to runoff modeling incorporate the idea of a representative elementary area (REA) for runoff generation (Wood et al. 1988). These areas are also called hydrologic response units (HRU) (Stuebe & Johnson 1990). The REA (HRU) is an area of a watershed within which physical conditions controlling runoff generation are spatially uniform. The REAs are the fundamental building block for catchment modeling (Sasowsky & Gardner 1991), but they may not, and probably do not, correspond to first-order basins.

Basin area is directly related to runoff volume. A plot of annual average discharge versus drainage area is shown in Figure 10.4 for the Potomac River basin. The relationship is exponential and can be described by an equation of the form:

$$\overline{Q} = kA^n \tag{10.5}$$

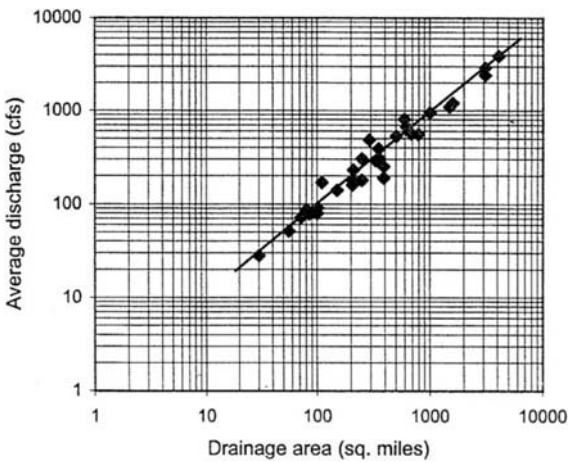

Figure 10.4. Regression relationship of average discharge to basin area for streams in the Potomac River basin (redrawn from Hack 1957).

where $\bar{Q}$ is average annual discharge, A is basin area, and k and n are empirically derived by fitting a regression line to the data.

Stream lengths and basin areas are functionally related to one another. From geometry the relationship should be a power function, since streams have length dimension (L) and basin area has dimension (L^2). We might expect stream length to be related as the square root of basin area, $L_w = A^{0.5}$. Hack (1957) plotted length versus area for basins in Virginia and Maryland and developed the equation:

$$L_w = 1.4A^{0.6} \tag{10.6}$$

where L_w is the length of the main channel in miles, and A is basin area in square miles. The power function relationship was confirmed, but the fact that the exponent is 0.6 and not 0.5 indicates that basins become longer and narrower as they increase in size.

10.1.4 *Basin relief and slope*

The last group of morphometric properties affecting runoff are those describing vertical differences within a basin. *Maximum basin relief* H_m is the difference in elevation between the highest point on the basin perimeter and the basin mouth. If there are a few extreme peaks along the perimeter this may not be the most representative measure of basin relief. In this case a mean perimeter elevation may be more appropriate, and could be used to calculate a measure of mean basin relief. Other measures of basin relief have been proposed, with some specifying the direction for measurement, such as along the longest dimension of the basin parallel to the principle drainage line (e.g. Schumm 1956).

Relief is a measure of the potential energy in a basin due to the difference in elevation (dz). Combining relief with the distance (dx) over which elevation changes gives ground surface slope or gradient:

$$S_o = -\frac{dz}{dx} = -\frac{\Delta z}{\Delta x} \tag{10.7}$$

where slope (S_o) has the dimension (LL^{-1}) or (1). The minus sign makes slope a positive number since elevation decreases with increasing distance downstream. Water moves down hill in response to the force of gravity, so the timing of runoff is inversely related to the slope – steeper slopes produce higher water velocities and shorter travel times. Other factors being equal, basins with steep slopes have shorter runoff response times than basins with gentler slopes. There may also be a direct relationship between the volume of surface runoff and slope. Steeper slopes shed water faster and so there is less time for infiltration and more surface runoff is generated.

A *longitudinal profile* is a plot of stream elevation with distance along the stream (Fig. 10.5). It is necessary to exaggerate the vertical scale of the plot for higher-order streams. Longitudinal profiles have a general concave-skyward appearance. The stream gradient in the headwaters is steeper than the gradient towards the mouth. The cause(s) of upward concavity is not completely understood though it is thought to be related to the downstream changes in discharge and the caliber (size) of the sediment load. A longitudinal profile is not going to be a smooth continuous change in eleva-

tion with distance as shown in Figure 10.5. Abrupt changes in gradient occur at stream junctions, knickpoints, and waterfalls. At stream junctions significant additions in discharge and/or sediment load occur. The stream adjusts to the new conditions by adjusting its gradient. It is common for gradient to decrease below a major junction and remain fairly uniform through the reach until the next major junction where it may decrease again. In hydrologic simulation models slope may be defined for individual subbasins and for individual reaches along the channel. The terms slope and gradient have so far been used without distinguishing between the slope of the water surface and the slope of the stream bed. At the basin scale differences between the two are trivial and can be ignored. At smaller scales, and especially when analyzing the hydraulics of open channel flow, the differences must be considered. The slope of the water surface can be greater than or less than the slope of the bed. The difference is important in detailed studies of the dynamics of open channel flow.

The sine, cosine and tangent functions are defined from geometry with reference to a right triangle as shown in Figure 10.6. In Figure 10.6 the slope is equal to the tangent of the angle θ:

$$\tan\theta = \frac{Z}{X} = S_o \tag{10.8}$$

The sine of angle θ is:

$$\sin\theta = \frac{Z}{K} \tag{10.9}$$

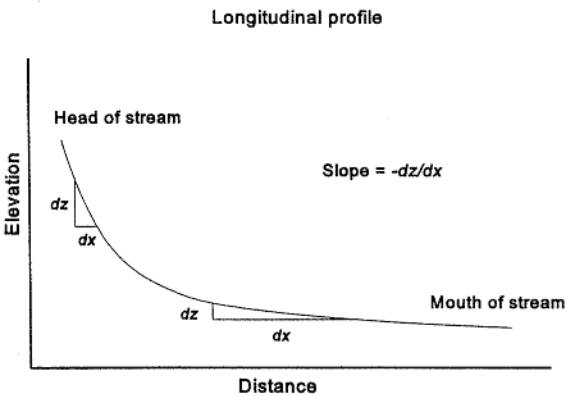

Figure 10.5. A generalized longitudinal profile of a stream. Channel slope (gradient) decreases from head to mouth.

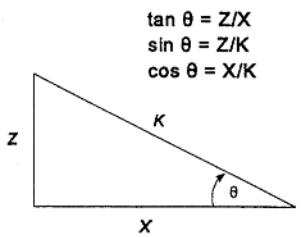

Figure 10.6. A right triangle showing the definition of sine, cosine and tangent.

Sine is used in the derivation of many basic flow equations because the fundamental force causing water to flow is the weight density (γ) of the water times the sine of the slope angle (θ). For very small values of θ, $\sin\theta \approx \tan\theta$, and it is common to substitute S_o for $\sin\theta$ in flow equations.

10.2 RUNOFF KINEMATICS

In physics *kinematics* is that part of mechanics that describes motion, while *dynamics* explains motion. Here we describe overland flow and channel flow by focusing on the kinematic wave model of runoff. A kinematic wave is a wave caused by an accumulation of water due to lateral inflows. With a kinematic wave there is no acceleration of the water. Zero acceleration means that the gravitational (driving) force equals the resisting forces due to friction from the bed and banks and within the water itself. The net force acting on the water is thus zero and a kinematic wave can be described using only a continuity equation and an equation of motion.

10.2.1 *Continuity*

On a hillslope lateral inflow is the excess precipitation (i_e) which accumulates downslope (Fig. 10.7). Excess precipitation is the difference between precipitation intensity at the surface (i) and infiltration (f), $i_e = (i - f)$. The situation depicted in Figure 10.7 assumes it has been raining long enough so that all flows are steady. Overland flow per unit width of channel q_o is:

$$q_o = VY = (i - f)L_o \cos\theta \tag{10.10}$$

where velocity (V) is measured parallel to the bed and depth (Y) is measured perpendicular to the bed.

The continuity equation governing the overland flow kinematic wave is:

$$i_e = \frac{\partial Y}{\partial t} + \frac{\partial q_o}{\partial x} \tag{10.11}$$

where $\partial Y/\partial t$ is the change in depth with time and $\partial q_o/\partial x$ is the change in discharge with distance. In words this equation says excess precipitation results in either a change in depth with time, a change in discharge downslope, or both. For instance, on a horizonal surface $\partial q/\partial x = 0$ and all of the excess precipitation would be accounted for as an increase in water depth with time.

Along a stream channel the lateral inflows are the spatially distributed sheet flows accumulating down the reach (Fig. 10.8). The basic kinematic wave equation for open channel flow is identical in form to Equation (10.11):

$$q_o = \frac{\partial A}{\partial t} + \frac{\partial Q}{\partial x} \tag{10.12}$$

where q_o is lateral inflow per unit length of channel, A is the cross-sectional area of the channel, and Q is discharge within the channel.

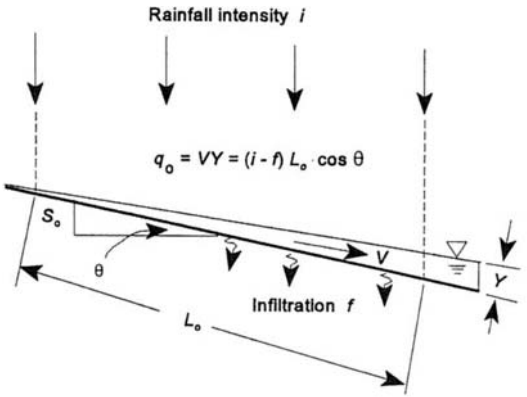

Figure 10.7. Steady flow on a uniform plane under rainfall (after Chow et al. 1988, used by permission).

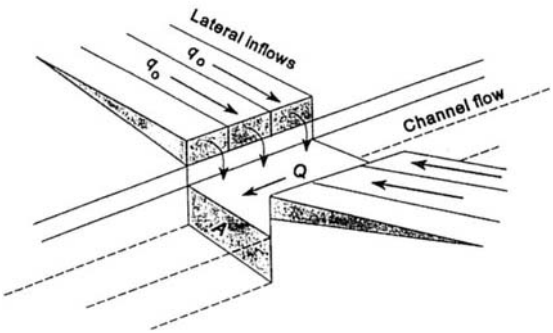

Figure 10.8. A cartoon representation of distributed lateral overland flows entering a channel.

10.2.2 *Motion: Laminar versus turbulent flow*

Flowing water is classified as laminar, transitional or turbulent. The classification is based on threshold values of the *Reynold's number* R. The Reynold's number is *proportional* the ratio of the turbulent forces in the water to the viscous forces. Turbulent forces are inertial forces due to swirling eddies in the flow. Viscous forces are created by the internal friction between water molecules and depends upon the water's temperature. Laminar flow can only occur at very low velocities and is characterized by water molecules moving/sliding in straight streamlines, essentially as layers, or 'laminae', with little or no vertical mixing. In turbulent flow water moves downstream in chaotic swirls, with turbulent eddies mixing the water vertically and laterally. Turbulent mixing diffuses momentum into the stream bed, so turbulence acts like a frictional force retarding the flow. Most open-channel flow is turbulent, and laminar flow, if it occurs at all, is confined to a very thin layer immediately above the stream bed. (Most groundwater flow through porous media is laminar, though it can be turbulent near a pumped well, and in large solution channels and fractures associated with secondary porosity.) The Reynold's number is calculated as:

$$R = \frac{\overline{Y}\,\overline{V}}{\nu} \tag{10.13}$$

where $\overline{Y}$ is the average depth, $\overline{V}$ is the average velocity and v is the kinematic viscosity (see Table A1). Flow is laminar for R < 500 and turbulent for R > 2000. For 500 < R < 2000 the flow is transitional between laminar and turbulent.

Overland flow is somewhat unique. It is often laminar because the velocities are low, but it differs from open channel flow in that flow obstructions (rocks, twigs, vegetation etc.) are large relative to the depth of flow, which is usually less than 1 cm. Even the impact of raindrops can cause significant turbulence in overland flow. Overland flow is sometimes called *mixed flow* because of these special conditions (Dingman 1984).

Different equations are used to calculate water velocity for overland flow and channel flow depending upon whether the flow is laminar or turbulent. Laminar overland flow moves considerably faster than turbulent overland flow because of the retarding effect of turbulence. For uniform laminar flow the average velocity is given by:

$$\overline{V} = (gS_o)\frac{\overline{Y}^2}{3\nu} \tag{10.14}$$

where g is the acceleration of gravity (9.81 m s^{-2} or 32.2 ft s^{-2}). The term (gS_o) represents the downstream driving force, while $\overline{Y}^2/3\nu$ is the 'conductivity' of the channel. For uniform turbulent flow the average velocity is based on Manning's equation for open channel flow (see Eq. 2.2):

$$\overline{V} = \frac{uS_o^{1/2}\overline{Y}^{2/3}}{n} \tag{10.15}$$

where n is Manning's roughness coefficient for overland flow (Table 10.1), u = 1.49 if units are in feet, and u = 1.0 for units in meters. The modification of Manning's

Table 10.1. Values of Manning's n for overland flow (source: Engman 1986, SCS 1986).

Land surface	n	Range
Concrete or asphalt	0.011	0.01-0.13
Bare sand	0.01	0.01-0.016
Graveled surface	0.02	0.012-0.03
Bare clay-loam (eroded)	0.02	0.012-0.03
Range land	0.13	0.01-0.32
Bluegrass sod	0.45	0.39-0.63
Short-grass prairie	0.15	0.10-0.20
Bermuda grass	0.41	0.30-0.48
Fallow (no residue)	0.05	
Cultivated soils:		
– Residue cover < 20%	0.06*	
– Residue cover > 20%	0.17*	
Dense grasses	0.24*	
Woods:		
– Light underbrush	0.40*	
– Dense underbrush	0.80*	

*From the SCS (1986), but some are based on values computed by Engman (1986).

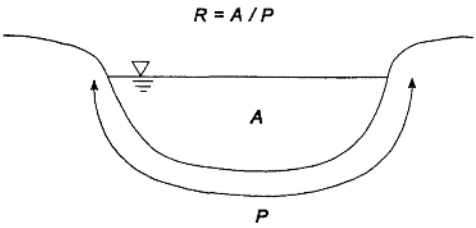

Figure 10.9. The hydraulic radius R is the cross-sectional area A divided by the wetted perimeter P.

equation for overland flow is the use of the average depth ($\bar{Y}$) instead of the hydraulic radius (R). The hydraulic radius is the cross-sectional area of a channel divided by the wetted perimeter ($R = A/P$) (Fig. 10.9). As a channel becomes wider and shallower, R approaches the average depth, and for wide, shallow sheet flows there is virtually no difference between the two measures.

In using Equation (10.14) or Equation (10.15) depth must be known. Depth can be determined by combining the continuity equation for flow per unit width (Eq. 10.10) with either Equation (10.14) for laminar or Equation (10.15) for turbulent flow. For the laminar case, substitute Equation (10.14) for V in Equation (10.10) to get:

$$\frac{gS_o Y^2}{3\nu} Y = (i - f)L_o \cos\theta \tag{10.16}$$

which is solved for Y as:

$$Y = \left(\frac{(i - f)L_o \cos\theta \, 3\nu}{gS_o} \right)^{1/3} \tag{10.17}$$

This equation slightly underestimates depth if it is raining, because the raindrop impacts increase the frictional resistance in the flow, which slows the water down, and which means the water must actually be deeper to have the q_o given by Equation (10.10.).

Combining the turbulent overland flow equation (Eq. 10.15) with the continuity equation (Eq. 10.10) gives the depth of turbulent overland flow as:

$$Y = \left(\frac{(i - f)L_o \cos\theta n}{uS_o^{1/2}} \right)^{3/5} \tag{10.18}$$

Example 10.1

Rain is falling at a rate of 2 in hr^{-1} on an impermeable concrete driveway. The driveway is 50 ft long, has a slope of 3%, a roughness of $n = 0.012$, and the water temperature is 50°F. Find q_o, average velocity, and flow depth assuming laminar conditions. First convert the rainfall intensity (i) from in hr^{-1} to ft s^{-1}.

$i = 2$ in $hr^{-1} = 4.63 \times 10^{-5}$ ft s^{-1}

$f = 0$

From equation (10.10):

$$q_o = (4.63 \times 10^{-5} \text{ ft s}^{-1})\,(50 \text{ ft})\,(0.999) = 0.0023 \text{ ft}^3 \text{ s}^{-1} \text{ per ft}$$

For the laminar case Equation (10.17) gives Y as:

$$Y = \left(\frac{(4.63 \times 10^{-5} \text{ ft s}^{-1})\,(50 \text{ ft})\,(0.999)\,3\,(1.409 \times 10^{-5} \text{ ft}^2 \text{ s}^{-1})}{32.2 \text{ ft s}^{-2}\,0.03} \right)^{1/3}$$

$$Y = 0.0047 \text{ ft} = 0.056 \text{ inches}$$

Laminar flow velocity can be found either from Equation (10.14), or simply as:

$$V = q_o / Y = 0.49 \text{ ft s}^{-1}$$

As mentioned above the depth is likely to be underestimated by this method because it neglects the frictional resistance from the impact of the rain drops. A somewhat more complex method for calculating Y that considers frictional resistance gives depth as $Y = 0.0063$ ft $= 0.076$ inches (see Chow et al. 1988 pp. 158–159).

A widely accepted compromise for calculating the average velocity of mixed overland flow is to simply use Manning's equation with a coefficient of 1.0 on the average depth term:

$$\overline{V} = \left(\frac{u}{n} \right) \overline{Y} S_o^{1/2} \tag{10.19}$$

A kinematic wave actually moves faster than the water itself. The term for the velocity of a wave relative to the velocity of the water is wave *celerity*. Theoretically, for water flowing in a wide rectangular channel the velocity of a kinematic wave (V_k) is 1.67 times the velocity of the water (V) itself. For different channel geometries the celerity is different, but is always greater than one unless significant overbank flow occurs (Dingman 1984).

10.3 TIMING OF RUNOFF

A critical variable in the analysis of runoff is the travel time of the water through the basin. This is especially true for urban-basin hydrology. The time it takes water to traverse a given distance depends upon the water's velocity:

$$\text{Time}\,(T) = \frac{\text{Distance}\,(L)}{\text{Velocity}\,(LT^{-1})} \tag{10.20}$$

10.3.1 *Time of concentration*

The *time of concentration* t_c is often defined as the time it takes a parcel of water to flow from the hydrologically most distant part of the basin to the point of interest. A more sophisticated analysis reveals that t_c is not the time it takes a parcel of water to move through the basin, but rather the time it takes a kinematic wave to move from the hydrologically most remote part of the basin to the point of interest.

There are various ways to estimate t_c. Kirpich (1940) developed a simple empirical formula for t_c using data from small agricultural watersheds:

$$t_c = \frac{L_w^{1.15}}{7700 H_m^{0.38}} \tag{10.21}$$

where t_c is in hours, L_w and H_m were defined previously and are measured in feet. Components of H_m related to waterfalls should be excluded, and it has been suggested that for overland flow across concrete or asphalt t_c be multiplied by 0.40.

A components-based approach to calculating t_c recognizes that t_c is equal to the sum of the travel times of the various flow components (Fig. 10.10). The overland flow travel time t_{of} is the time from the commencement of overland flow until the water (kinematic wave) reaches the channel. Water moving through the *i*th channel segment has a travel time t_i. The t_c for the basin is the sum of the travel times of the individual components:

$$t_c = t_{of} + t_1 + t_2 + \ldots + t_{n-1} + t_n \tag{10.22}$$

where the subscripts refer to the travel time through the *i*th channel segment and *n* is the number of segments. A third type of flow called *shallow concentrated flow* is sometimes identified for urban runoff situations. Shallow concentrated flow is transitional between overland flow and open-channel flow. The existence of different flow types should be confirmed by field inspection.

10.3.2 *Overland flow travel time*

An easy way to estimate t_{of} is by use of a diagram such as Figure 10.11. Figure 10.11 is a simplification of a more comprehensive diagram found in Dunne & Leopold (1978, p. 303) based on data from Rantz (1971). Travel time is a function of three variables: overland flow length L_o, the rational runoff coefficient C, and land surface slope S_o in percent. As an example, with a flow length of 200 ft, a slope of 0.5% and a runoff coefficient of 0.4, Figure 10.11 gives $t_{of} \approx 22.5$ min. This represents and average flow velocity of 0.148 ft s^{-1} (4.5 cm s^{-1}). The rational runoff coefficient C is:

$$C = \frac{\text{Runoff rate}}{\text{Rainfall rate}} \tag{10.23}$$

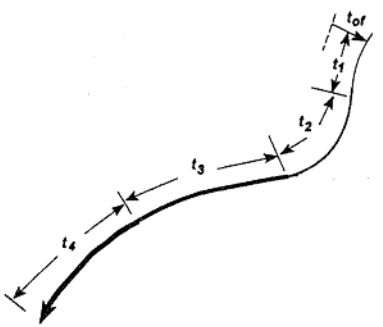

Figure 10.10. Individual component travel times for water flowing through a basin. The sum of the travel times for each component gives the time of concentration t_c for the basin.

The runoff coefficient incorporates all catchment losses and has been determined for different land uses (Table 10.2). The values of C in Table 10.2 are for rainfall recurrence intervals of 5 to 10 years. For greater return periods C values should be increased (see Rantz 1971), which results in the overland flow travel time decreasing with more intense rainfall.

The basic equation for overland flow travel time using the kinematic wave formula is:

$$t_{of} = \left(\frac{L_o}{\alpha i_e^{m-1}} \right)^{1/m} \tag{10.24}$$

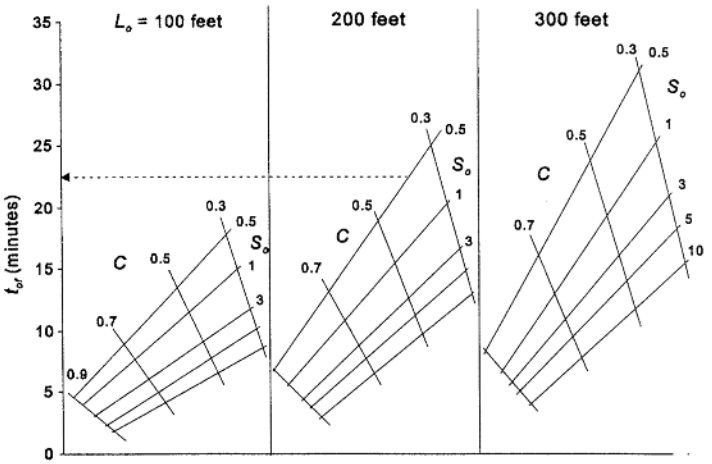

Figure 10.11. Overland flow travel time as a function of flow length (ft), slope (%) and the rational runoff coefficient (source: Modified from Dunne & Leopold 1978, data originally from Rantz 1971).

Table 10.2. Values of the rational runoff coefficient C for recurrence intervals of 5-10 years (source: Viessman & Welty 1985, Dunne & Leopold 1978).

Urban areas		Rural areas	
Land use	C	Land use	C
Business:		Sandy and gravelly soils:	
– Downtown areas	0.70-0.95	– Cultivated	0.40
– Neighborhood areas	0.50-0.70	– Pasture	0.35
Residential:		– Woodland	0.30
– Single family	0.30-0.50	Heavy clay soils or shallow	
– Multiunits, detached	0.40-0.60	soils over bedrock:	
– Multiunits, attached	0.60-0.75	– Cultivated	0.50
Residential (suburban)	0.25-0.40	– Pasture	0.45
Apartment dwelling areas	0.50-0.70	– Woodland	0.40
Industrial:			
– Light areas	0.50-0.80		
– Heavy areas	0.60-0.90		

Table 10.2. Continued.

Urban areas		Rural areas	
Land use	C	Land use	C
Parks, cemeteries	0.10-0.25		
Playgrounds	0.20-0.35		
Railroad yards	0.20-0.40		
Unimproved areas	0.10-0.30		
Streets:			
– Asphalt	0.70-0.95		
– Concrete	0.80-0.95		
– Brick	0.70-0.85		
Drives and walks	0.75-0.85		
Roofs	0.75-0.95		
Lawns, sand soil:			
– Flat, 2 %	0.05-0.10		
– Average, 2-7%	0.10-0.15		
– Steep, 7%	0.15-0.20		
Lawns, heavy soil:			
– Flat, 2%	0.13-0.17		
– Average, 2-7%	0.18-0.22		
– Steep, 7%	0.25-0.35		

where t_{of} is in seconds, and all units must be consistent, e.g. if L_o is in feet then rainfall is in ft s^{-1}. The values of m and α depend on whether the flow is laminar or turbulent. For laminar flow $m = 3$ and $\alpha = (gS_o/3\nu)$; for turbulent flow $m = 5/3$ and $\alpha = (uS_o^{0.5}/n)$. Use of Equation (10.24) is straightforward if rainfall excess i_e is known. In Chapter 11 we encounter a situation where rainfall intensity is not known *a priori*. Equation (10.23) can still be used but it must be solved iteratively.

The SCS (1986) developed a similar kinematic-flow-based equation for t_{of} simplified for use with their generalized precipitation intensity curves (Fig. 4.11). For flow lengths less than 300 ft the SCS equation is:

$$t_{of} = \frac{0.007(L_o n)^{0.8}}{(P_2)^{0.5} S_o^{0.4}} \tag{10.25}$$

where t_{of} is overland flow travel time in *hours*, P_2 is the 2-year, 24-hour rainfall in inches (Fig. 4.19), and L_o is measured in feet.

Example 10.2
This example calculates overland flow travel time t_{of} three different ways:
1. Using Figure 10.11,
2. Using Equation (10.24), and
3. Using Equation (10.25).

Location: The Texas-New Mexico border.
Surface: concrete
Overland flow length: 150 ft
Slope: 0.015
$i_e = 3$ in hr^{-1}

1. t_{of} using Figure 10.11
   $C = 0.90$ (Table 10.2)
   $L_o = 150$ ft
   $S_o = 0.015 = 1.5\%$
   From the graph of $L_o = 100$, $t_{of} \approx 3.75$ min.
   From the graph of $L_o = 200$, $t_{of} \approx 5.0$ min.
   Using an average of these two values gives $t_{of} \approx (3.75 + 5.0) / 2 = 4.38$ min.
2. t_{of} from Equation (10.24) assuming turbulent flow:
   $u_m = 1.49$
   $n = 0.012$ (Table 10.2)
   $i_e = 3$ in hr^{-1} = 0.0000694 ft s^{-1}

$$t_{of} = \frac{[150(0.012)]^{0.6}}{1.49^{0.6}\left(0.0000694^{0.4}\right)0.015^{0.3}} = 182\text{sec}.$$

   $t_{of} = 3.03$ min.
3. t_{of} using Equation (10.25)
   $P_{2,100} = 2.5$ inches (Fig. 4.20)

$$t_{of} = \frac{0.007[150(0.012)]^{0.8}}{\left(2.5^{0.5}\right)0.015^{0.4}} = 0.038\text{hours}$$

   $t_{of} = 2.28$ min.

10.3.3 *Channel travel time*

Travel time for water flowing in an open channel can be calculated using Manning's equation and substituting into Equation (10.20) with the length of the channel segment. Manning's n for channel flow in are given in Table 10.3 and are different from Manning's n for overland flow (Table 10.1). The overland flow n values are larger than the open channel values because obstructions are so much larger relative to the flow depth, resulting in greater relative roughness and friction. The total travel time for open-channel flow is the sum of the travel times through the individual segments (Eq. 10.22). Recognize that this is only an approximation of the channel travel time, because as noted earlier a kinematic wave usually travels faster than the average water velocity. The true travel time t_i for the ith channel segment is between:

Table 10.3. Values of Manning's n for open-channel flow (source: Chow 1959, US Dept. of Transportation 1961).

Channel type	n
Streams on plains:	
– Clean, straight, no riffles or pools	0.025-0.033
– Clean, winding, some pools and shoals	0.033-0.045
– Clean, winding, some stones and weeds	0.035-0.050
– Sluggish reaches, weedy, deep pools	0.050-0.080
–Very weedy, deep pools, heavy underbrush	0.075-0.150

Table 10.3. Continued.

Channel type	*n*
Mountain streams:	
– No vegetation in channel, steep banks vegetation along bank submerged at high stage:	
– Bottom: gravels, cobbles and few boulders	0.030-0.050
– Bottom: cobbles with large boulders	0.040-0.070
Floodplains:	
– Short-grass pasture	0.025-0.035
– Tall-grass pasture	0.030-0.050
Cultivated areas:	
– Fallow	0.020-0.040
– Manured row crops	0.025-0.045
– Manured field crops	0.030-0.050
Brush:	
– Scattered brush with weeds	0.035-0.070
– Light brush and tress	0.035-0.080
– Medium to dense brush	0.045-0.160
Trees:	
– Dense willows	0.110-0.120
– Heavy stand of timber	0.080-0.120
Concrete pipe	0.011-0.013
Concrete lined channel	0.013-0.022

$$\frac{L_i}{V_k} \le t_i \le \frac{L_i}{V}, \quad V_k = mV \tag{10.26}$$

where L_i is the length of the ith channel segment. The value of m depends on channel geometry. For wide rectangular channels $m = 5/3$. For square and triangular channels $m = 4/3$ (COE 1987).

10.4 RUNOFF PROCESSES

Runoff generation can be fairly simple or quite complex. The simplest case is runoff from an impermeable surface like a concrete driveway. There is virtually no infiltration and after depression storage is filled runoff commences. Runoff generation from natural areas is much more complex involving interactions between topography, depth to groundwater, precipitation duration and intensity, and infiltration characteristics modulated by soil and vegetation. Two basic types of runoff generation are *hortonian overland flow* and *saturation overland flow*.

10.4.1 *Hortonian overland flow*

The discussion of runoff throughout the chapter has implicitly emphasized overland flow generated by precipitation exceeding infiltration ($i > f$). This type of runoff is

called hortonian overland flow, named for Robert Horton who first described the phenomena. Hortonian overland flow commences at the ponding time and after depression storage is satisfied (Fig. 7.10). During a storm rainfall intensity increases and decreases with individual bursts of precipitation. Consequently hortonian flow may commence, then cease, and begin again. Under steady-state conditions the amount of basin area contributing surface runoff to the channel (a_c) is:

$$a_c\left(L^2\right) = \frac{\text{Stream discharge}\left(L^3T^{-1}\right)}{\text{Rainfall intensity}\left(\text{LT}^{-1}\right)} \tag{10.27}$$

The capacity for depression storage depends upon the physical characteristics of the surface and land use. Depression storage may range anywhere from 1 to 50 mm of precipitation. The lower values are associated with smoother urban surfaces like streets and parking lots. Plowed farm fields can have very large surface storage capacities. Table 10.4 gives some estimates for depression storage for different land surfaces. In the absence of better data, Kidd (1978) gives the following empirical equation for estimating depression storage in urbanized areas with large proportions of impervious area:

$$D_p = 0.0303S_o^{-0.49} \tag{10.28}$$

where D_p is depression storage in inches and slope is in percent.

Hortonian overland flow is generated from areas of thin or clayey soils, areas devoid of vegetation, areas subject to high rainfall intensities, urban areas and areas where soil compaction has reduced infiltration capacity such as construction sites and dirt roads. Hortonian overland flow is unlikely to occur from undisturbed forest or pasture lands because of their high infiltration capacities (Chapter 7). The smaller the basin the more homogeneous the physical characteristics are likely to be. If those characteristics promote hortonian overland flow, it may be possible for overland flow to commence over the entire basin at the same time. As the size of the watershed increases it becomes more heterogeneous and hortonian overland flow might be generated from some areas but not from others. Hortonian overland flow generated from only limited parts of the watershed has been called the *partial area* concept for runoff generation by Betson (1964).

Table 10.4. Typical depression and detention storage for various land surfaces (source: Sheaffer et al. 1982).

Land surface	Range (mm)	Recommended (mm)
Impervious:		
– Large paved areas	1.3-3.8	2.5
– Roofs, flat	2.5-7.5	2.5
– Roofs, Sloped	1.2-2.5	1.2
Pervious		
– Lawn grass	2.0-12.5	7.5
– Wooded areas and open fields	5.0-15.0	Determine by field inspection

10.4.2 *Saturation overland flow*

In areas with deep soils and high infiltration rates it is still possible to generate surface runoff by a totally different mechanism. Figure 10.12a is a cartoon of a hillslope in cross-section from the surface down to groundwater. The water table is closest to the surface at the foot of the slope and in the valley adjacent to the channel. Figure 10.12a shows the situation before the rain begins. In Figure 10.12b it has been raining for some time, and infiltration and percolation are recharging the groundwater where it is closest to the surface. This causes the water table to rise and intersect the land surface. Direct rainfall on this saturated ground becomes surface runoff. In addition, groundwater exfiltrating at the surface becomes surface runoff. Direct precipitation on saturated ground and exfiltration of groundwater combine to generate saturation overland flow. With this runoff process rainfall intensity need not exceed the infiltration capacity. Infiltration and percolation raise the water table and the soil is saturated from below. With time through the storm the water table intersects the land surface higher and higher upslope, thus the saturated area expands and more and more area contributes runoff (Fig. 10.13). Saturation overland flow is generated mainly near the foot of concave slopes, in low-lying swales between hills and from the areas immediately adjacent to stream channels. These areas usually have the water table nearest to the surface and generally have higher soil moisture levels than areas upslope. The fraction of the basin generating saturation overland flow may fluctuate between 5 and 30%. In the upslope regions it is possible to have significant amounts of interflow through the soil and upper vadose zone. Interflow occurs on fairly steep slopes with deep, permeable soils. The velocities for interflow are on the order of 1 to 10 m d^{-1}, which is in the realm of groundwater velocities. This subsurface stormflow may or may not contribute to downstream flooding depending upon travel time to the channel.

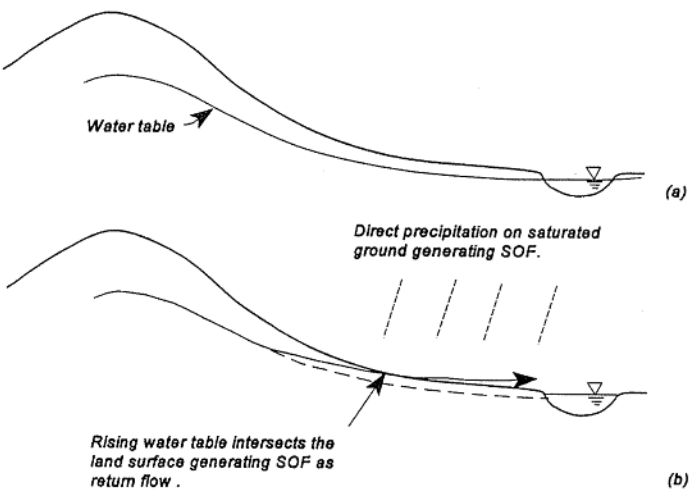

Figure 10.12. Cross-section through a hillslope from the surface to groundwater. a) Conditions before the storm, and b) Conditions some time during the storm. The water table has risen to intersect the surface at the foot of the slope. Direct precipitation on the saturated ground and exfiltration of groundwater combine to create saturation overland flow (SOF).

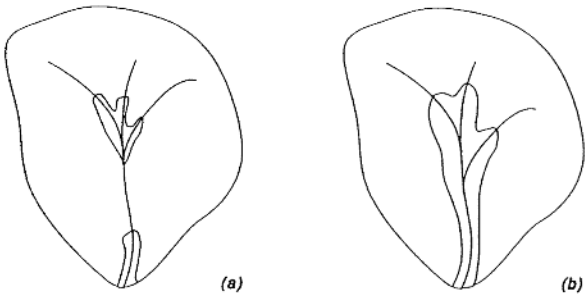

Figures 10.13. Planimetric views of how the saturated area expands during a storm. a) At the beginning of the storm showing the saturated ground restricted to limited areas near the channel, and b) Later in the storm, the rising water table intersects the land surface further upslope, expanding the saturated area away from the channel and up the basin.

This complex model of runoff generation including saturation overland flow generated from variable-size areas subject to saturation from below, interflow on convex hillslopes with deep, permeable soils, and hortonian overland flow from restricted areas with limited infiltration capacity is termed the *variable source concept* (Hewlett & Hibbert 1967).

In a recent study of hillslope runoff generation McDonnell et al. (1996) examined the volume and peak runoff from a hillslope in relation to both the surface and the subsurface bedrock topography. Their field site was a single hillslope in the Panola Mountian research watershed in Georgia. They were trying to determine the degree to which hillslope runoff is controlled by surface and/or subsurface topgraphy. They computed a surface and subsurface hillslope index ln (a/tan b) for points across the slope, where a is the upslope contributing area to a point, and tan b is the local slope angle (Bevens & Kirkby 1979). The pattern of the hillslope index indicates the propensity for a point on the slope to become saturated. They found that both volume and peak flows correlated much more strongly with subsurface flow paths (subsurface index pattern) than with the surface flow paths. They concluded that, 'these data provide compelling evidence that the bedrock surface controls downslope water movement at the hillslope scale'.

10.4.3 *Human activities affecting runoff*

Human activities can have a direct impact on the volume and timing of surface runoff. Changing land use from forest to crops or from natural surfaces to impermeable urban land uses reduces infiltration and increases runoff volume. In many cases transformed land surfaces may be hydraulically more efficient and the velocity of flow increases as well. The increased volume and velocity causes increased peak discharges downstream. The installation of gutters and storm sewers can change the timing of runoff as well. Travel times may increase where drainage structures convey water parallel to the elevation contours. Travel times decrease when these structures convey water downslope perpendicular to the contours. Many local governments have adopted ordinances requiring runoff detention or retention facilities in conjunction with land development. The objective is to control the increase in runoff so that

post development runoff is not significantly different than the predevelopment conditions. Some communities have even tried economic incentives to reduce surface runoff. The City of Boulder, Colorado taxes every parcel of land in the city according to the proportion of impermeable surface. Monies from the tax are used to improve the storm drainage system. Property owners can reduce their tax by either reducing the amount of impermeable surface or by providing on-site detention storage (Thompson 1982).

In agricultural areas various soil and water conservation methods are used to slow surface runoff and promote infiltration. Contour plowing, hillslope terraces, strip cropping and no-till and minimum-till cultivation are effective at reducing runoff and soil erosion, and encouraging infiltration and the deposition of sediment carried from upslope areas. While these practices are effective for soil and water conservation they are not as effective at reducing chemical pollutants carried along in the water.

SUMMARY

This chapter introduced aspects of drainage basin morphometry and their relationship to runoff. Surface runoff can be a fairly simple and straightforward process, as in the case of hortonian overland flow, or complex when soil, topography and groundwater combine to generate saturated overland flow. Surface runoff flows into stream channels and may result in flooding. Analysis of flood flows is a major field in hydrology and of great practical interest in water management. This is the topic of Chapter 11.

PROBLEMS

10.1 Use the figure below and calculate the average bifurcation ratio and plot your results.

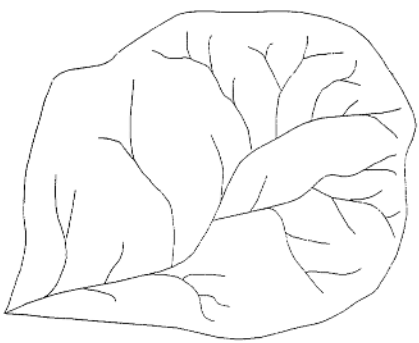

10.2 Calculate equilibrium overland flow q_o (ft^2s^{-1} per foot), the average velocity ($ft\ s^{-1}$), and the overland flow depth (feet) for both laminar and turbulent overland flow conditions.
- Surface: short grass prairie
- Rainfall intensity (i) = 3 in hr^{-1}
- Infiltration (f) = 1.1 in hr^{-1}
- Slope (S_o) = 5%
- Slope length (L_o) = 120 ft
- Water temperature = 59°F

CHAPTER 11

Streamflow and floods

In the watershed system the channel network serves as the pathway for outputs from the basin (Fig. 11.1). When precipitation input to a basin exceeds output, storage increases and runoff is generated. Runoff from hillslopes flows into channels causing stream discharge Q to increase. This can result in flooding when the discharge exceeds the capacity of the channel in a particular reach. Along steep mountain streams, desert arroyos, and in small basins given to hortonian overland flow, the rise in discharge can be extremely rapid leading to flash floods. On large rivers the rise is slower taking days or weeks to reach the peak discharge.

Flood mitigation and floodplain management are major water-resource issues. The Great Flood during the summer of 1993 along the Lower Missouri and Upper Mississippi Rivers, followed only a year and a half later by unprecedented flooding in California in 1995, caused tens of billions of dollars in damages. Perhaps more importantly it has caused a critical reappraisal of our strategies for manipulating the hydrologic system. Variables to consider in analyzing floods are the volume, peak discharge, flood height, duration of flooding, the area inundated for a given discharge, water velocity, and the potential for erosion and deposition of sediment. Many of these variables are interrelated. Flood height and the area inundated are both functions of the peak discharge and the cross-sectional area of the floodplain. In this chapter we examine some basic techniques for estimating runoff volume and peak discharge, and for analyzing flood hydrographs. Many methods for estimating future flood characteristics rely on historic flood data. In the United States the US Geological Survey (USGS) is the primary federal agency responsible for collecting streamflow data. The USGS publishes streamflow data for each state in a series entitled

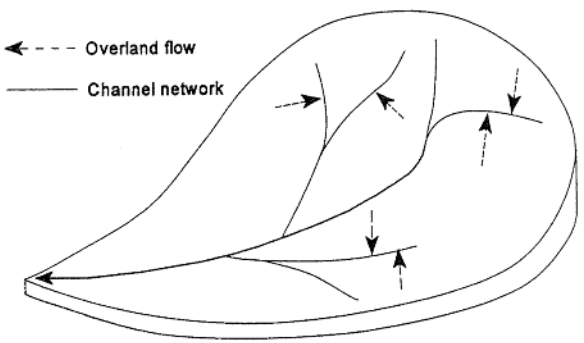

Figure 11.1. Runoff and streamflow output from the drainage basin system.

JUNIATA RIVER BASIN

01558000 LITTLE JUNIATA RIVER AT SPRUCE CREEK, PA

LOCATION.--Lat 40°36'45", long 78°08'27", Huntingdon County, Hydrologic Unit 02050302, on right bank on SR 4006, 150 ft downstream from Penn Central Railroad bridge, 0.5 mi northwest of village of Spruce Creek, and 0.5 mi upstream from Spruce Creek.
DRAINAGE AREA.--220 mi^2.
PERIOD OF RECORD.--June 1938 to current year. Prior to October 1938 monthly discharge only, published in WSP 1302.
GAGE.--Water-stage recorder. Datum of gage is 751.15 ft above sea level.
REMARKS.--Records good except those for estimated daily discharges, which are fair. Several measurements of water temperature were made during the year. National Weather Service satellite telemeter at station.
EXTREMES OUTSIDE PERIOD OF RECORD.--Flood of Mar. 18, 1936 reached a stage of 19.1 ft, from floodmarks 175 ft downstream, discharge, 39,800 ft^3/s, from rating curve extended as explained below.

DISCHARGE, CUBIC FEET PER SECOND, WATER YEAR OCTOBER 1992 TO SEPTEMBER 1993
DAILY MEAN VALUES

DAY	OCT	NOV	DEC	JAN	FEB	MAR	APR	MAY	JUN	JUL	AUG	SEP
1	e140	e105	293	2140	e230	e110	5130	913	258	106	83	71
2	e135	e200	275	1430	e200	e120	3550	746	185	351	81	71
3	e130	560	264	1100	e250	e200	2430	626	175	260	93	102
4	e130	260	237	895	251	410	1760	557	175	163	81	169
5	e125	221	247	1180	e210	584	1390	653	167	136	75	113
6	e120	265	221	922	e190	471	1170	523	160	124	73	87
7	e115	220	208	784	203	406	1020	454	149	115	74	79
8	e115	202	198	690	210	590	909	423	178	110	74	77
9	e120	190	186	601	204	826	845	398	485	107	71	77
10	e125	182	180	521	200	674	1280	379	281	102	73	80
11	e120	179	255	477	203	566	1240	368	204	98	187	80
12	e120	200	393	458	202	481	1090	353	181	98	224	75
13	e115	491	319	782	205	e430	932	370	168	105	115	72
14	e110	335	287	837	196	e350	794	325	159	98	96	71
15	e125	308	266	655	188	e300	699	303	153	93	85	70
16	e120	284	254	e560	186	e270	4340	284	149	89	82	72
17	e115	264	616	e450	205	e350	5230	271	142	86	84	74
18	e110	251	791	e400	176	e480	2410	274	138	84	99	80
19	e110	235	604	e360	139	419	1630	350	151	84	89	80
20	e110	219	731	e330	e120	e330	1300	279	142	86	85	72
21	e105	271	745	e300	e100	e400	1820	253	140	86	84	81
22	e105	428	636	e270	e92	509	2260	237	134	82	80	127
23	e105	473	601	e260	e170	626	1770	225	125	79	76	92
24	e105	411	587	e240	159	1380	1440	221	116	76	77	95
25	e105	506	471	e300	144	1520	1210	214	113	76	86	88
26	e105	445	439	e270	e130	1950	2910	203	112	78	76	194
27	e100	404	361	e240	e120	2290	2900	194	112	111	72	561
28	e100	370	e330	e220	e115	3740	1860	190	109	91	71	357
29	e100	340	e310	e200	---	3870	1400	190	107	133	71	207
30	e100	314	e300	e180	---	4730	1120	182	106	109	71	176
31	e100	---	e1200	e250	---	4170	---	207	---	93	70	---
TOTAL	3540	9133	12805	18302	4998	33552	57839	11165	4974	3509	2758	3650
MEAN	114	304	413	590	178	1082	1928	360	166	113	89.0	122
MAX	140	560	1200	2140	251	4730	5230	913	485	351	224	561
MIN	100	105	180	180	92	110	699	182	106	76	70	70
CFSM	.52	1.38	1.88	2.68	.81	4.92	8.76	1.64	.75	.51	.40	.55
IN.	.60	1.54	2.17	3.09	.85	5.67	9.78	1.89	.84	.59	.47	.62

STATISTICS OF MONTHLY MEAN DATA FOR WATER YEARS 1939 - 1993, BY WATER YEAR (WY)

MEAN	186	257	357	370	486	778	726	522	347	191	140	140
MAX	816	1092	997	991	1128	1609	1928	1239	2022	623	389	533
(WY)	1991	1951	1973	1949	1976	1979	1993	1978	1972	1956	1956	1975
MIN	64.7	71.3	73.2	90.5	138	261	228	150	104	70.4	56.9	64.3
(WY)	1964	1939	1966	1940	1963	1990	1946	1976	1965	1965	1966	1966

SUMMARY STATISTICS	**FOR 1992 CALENDAR YEAR**		**FOR 1993 WATER YEAR**		**WATER YEARS 1939 - 1993**	
ANNUAL TOTAL	106588		166225			
ANNUAL MEAN	291		455		374	
HIGHEST ANNUAL MEAN					630	1972
LOWEST ANNUAL MEAN					248	1966
HIGHEST DAILY MEAN	1410	Mar 27	5230	Apr 17	21100	Jun 23 1972
LOWEST DAILY MEAN	85	Aug 22-26	70	Aug 31	50	Sep 2 1966
ANNUAL SEVEN-DAY MINIMUM	86	Aug 21	71	Aug 27	51	Aug 28 1966
INSTANTANEOUS PEAK FLOW			7530	Apr 17	a28600	Jun 23 1972
INSTANTANEOUS PEAK STAGE			8.88	Apr 17	16.98	Jun 23 1972
INSTANTANEOUS LOW FLOW			69	Aug 10,31, Sep 15	45	Sep 26 1943b
ANNUAL RUNOFF (CFSM)	1.32		2.07		1.70	
ANNUAL RUNOFF (INCHES)	18.02		28.11		23.11	
10 PERCENT EXCEEDS	590		1090		811	
50 PERCENT EXCEEDS	201		203		220	
90 PERCENT EXCEEDS	105		81		83	

a From rating curve extended above 5,600 ft^3/s on basis of slope-area measurement at gage height 15.77 ft.
b Also Oct. 4, 1949.
e Estimated.

Figure 11.2. A page from the *Water Resources Data for Pennsylvania*, 1993 (USGS, 1993). At the top of the page is gage-related information. The main body of the table gives average daily discharges in cfs. At the bottom are various streamflow statistics for this basin.

Water Resources Data for (State). These reports are a continuation of the earlier *Water Supply Papers* that provided data for the entire United States. The reports also include limited data on groundwater levels, and since the 1970s have included water quality data as well. Figure 11.2 is a page from one such report. Information includes the location and elevation of the gage, the size of the basin above the gage, average daily discharge and peak discharge for the year. Other federal and state agencies collect or have collected water quantity or quality data. For example, there are numerous experimental watersheds operated by the US Department of Agriculture in conjunction with state universities. Appendix C contains a partial listing of sources of water-resources data.

11.1 FLOOD WAVES

Certain types of streamflow analyses require defining individual channel segments as the subsystem of interest. Inputs to the channel subsystem include direct precipitation, lateral overland flow and interflow, baseflow, and streamflow entering the channel segment from upstream Q_{in} (Fig. 11.3). Outputs from the segment are evaporation, infiltration, and downstream outflow from the reach Q_{out}. In many cases direct atmospheric inputs and outputs (channel precipitation and evaporation) are ignored, and bed infiltration is usually only important for influent streams in dry climates. Floods move down the channel as a wave of increasing and then decreasing discharge. In Chapter 10 we introduced the kinematic wave, which is a wave caused by an accumulation of water in the channel. With a kinematic wave the gravitational force equals the frictional force from the bed and banks, so there is negligible acceleration of the water. To an observer standing along the bank the passage of a kinematic wave appears as a steady, uniform rise and fall in the water surface. In Figure 11.4 the water rises from its level at time t_1 to a higher level at time t_2. With a kinematic wave, the water surface remains parallel to the bed.

The second major type of flood wave moving in a stream channel is a *dynamic* wave. Inertial forces and pressure forces are important in dynamic waves, but not in kinematic waves. To the observer the dynamic wave would have a sloping water surface as it approached and passed. Because the forces acting on the water are unequal within a dynamic wave, these waves are unsteady and nonuniform and involve acceleration of the water. The analysis of dynamic waves is complex and beyond our scope here.

Waves in stream channels are subject to two processes – *translation* and *attenuation* (Dunne & Leopold 1978). Translation is the downstream movement of the wave without changing the shape of the wave (Fig. 11.5a). Translation is the dominant process over short distances and in narrow stream valleys with steep channels. The second process is attenuation (Fig. 11.5b). Attenuation changes the shape of the wave by reducing the peak and extending the base. In Chapters 1 and 2 the input and output hydrographs for a hypothetical reservoir showed the attenuation effect of the reservoir. A flood wave moving in a channel is subject to storage and attenuation in the channel. Flood waves in most rivers are subject to both translation and attenuation as they move downstream (Fig. 11.5c). If the flood waters are high enough to flow over the banks on to the adjacent floodplain, storage and attenuation of

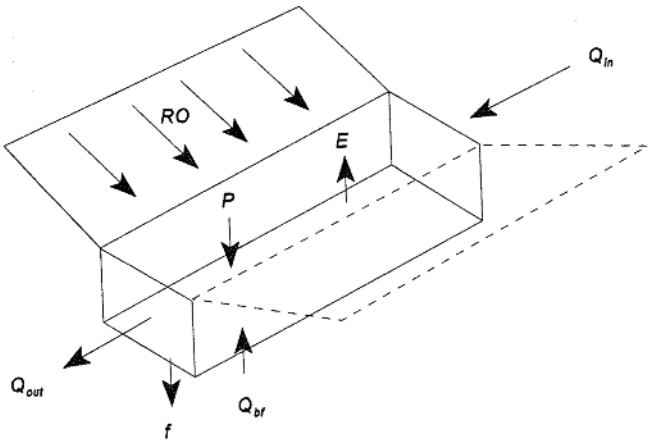

Figure 11.3. Diagrammatic representation of the inputs and outputs to a channel subsystem.

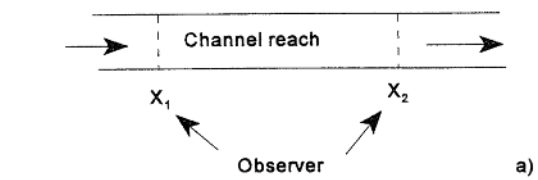

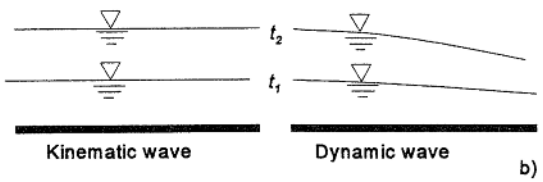

Figure 11.4. These figures show the passage of a kinematic wave as a uniform rise and fall of the water surface, and the passage of a dynamic wave observed as a sloping water surface (after Chow et al. 1988, used by permission).

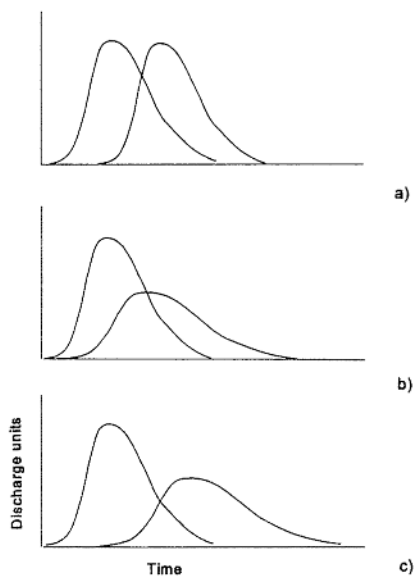

Figure 11.5. a) The process of translation of a flood wave in a channel, b) The flood wave is attenuated, and c) The combination of translation and attenuation of a flood wave moving down a channel (after Dunne & Leopold 1978).

the wave can be substantial. This of course is the crux of society's dilemma concerning the flood hazard. During periods of high flow the stream must use the floodplain to store the excess water; however, people have moved onto the floodplain and built levees to deny the stream access. Eventually a discharge will occur that exceeds the design criteria of the flood control structure. The Great Flood of 1993 damaged 1,082 of the 1,576 levees in the region (Myers & White 1993). Another problem is that constraining the flood within levees may protect the immediately-adjacent land but it increases flood heights downstream. Every time a major levee failed during the 1993 flood there was a noticeable drop (attenuation of the peak) in water surface elevation downstream.

11.1.1 *Hydrographs*

A hydrograph is a graph of stream discharge, or water surface elevation, versus time (Fig. 11.6). Later we discuss relating water surface elevation to discharge using a *rating curve*. (A graph of water level versus time in a well is also called a hydrograph.) A hydrograph is divided into a *rising limb*, a *crest segment*, and a *falling limb*, or *recession curve*. The rising limb is controlled by the rate of runoff into the stream, which in turn is related to the physical characteristics of the basin and the intensity-duration characteristics of the storm. The water draining from the basin comes from a varying combination of surface runoff, interflow and baseflow. Surface runoff drains away first since it reaches the channel most rapidly. Interflow drains away next and the lowermost segment of the recession curve is assumed to be comprised entirely of baseflow from groundwater. The point of inflection on the recession limb is assumed to indicate the time when surface runoff to the channel stops (Linsley et al. 1982). The falling limb is a *depletion curve* – a curve describing the drainage of water from storage. A general baseflow depletion curve can be modeled as an exponentially-decaying process, where discharge at time t+1 is proportional to discharge at time t one period earlier:

$$Q_{t+1} = kQ_t \tag{11.1}$$

The constant of proportionality is:

$$k = \frac{Q_{t+1}}{Q_t}, \quad k < 1.0 \tag{11.2}$$

Time t is not calendar or clock time, but an integer time step, i.e. 1, 2, 3, ..., n. The value of k depends upon the amount of actual time between the integer time steps. Discharge at any time step in the future, assuming continuous and uninterrupted depletion, is:

$$Q_t = Q_o k^t \tag{11.3}$$

where Q_o is the initial value of baseflow at $t = 0$. Example 11.1 explains how to determine the value of k.

Some methods of flood analysis use only the portion of the hydrograph generated by direct storm runoff, which requires the storm runoff be separated from the baseflow (Fig. 11.7). Baseflow can be added back in later to produce the total hydrograph

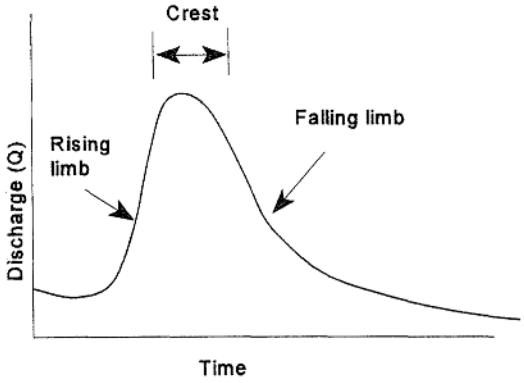

Figure 11.6. A stream hydrograph showing the three basic elements – the rising limb, crest segment and falling limb.

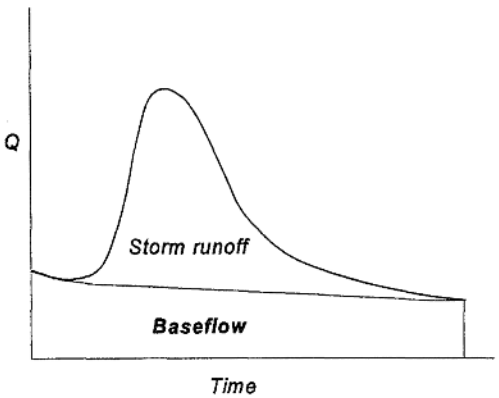

Figure 11.7. Hydrograph showing the two components of storm runoff and baseflow.

if necessary. Storm runoff is defined by the time of arrival of the water at the channel and not by the actual pathways the water travels to reach the channel. Storm runoff is sometimes called *quickflow* for this reason. Methods of separating storm runoff from baseflow are all arbitrary and have little physical foundation. The guiding principle is to be consistent and use the same separation method throughout the analysis.

Example 11.1
Find the value of the baseflow recession constant k using the data given in Table 11.1. An exponential depletion curve like Equation (11.1) plots as a straight line on semi-logarithmic graph paper. Plot discharge versus time step, with discharge on the log axis (Fig. 11.8). When the graph becomes straight the assumption is that all discharge is baseflow. The slope of the straight line is k (Eq. 11.2).

Table 11.1. Falling limb discharge data from Swarr Run, Pennsylvania. Data are from a storm that occurred on July 21, 1988.

Time step	Hour	Q (cfs)	Time step	Hour	Q (cfs)	Time step	Hour	Q (cfs)
1	5:15	275	8	8:45	81	15	12:15	24
2	5:45	258	9	9:15	63	16	12:45	22

Table 11.1. Continued.

Time step	Hour	Q (cfs)	Time step	Hour	Q (cfs)	Time step	Hour	Q (cfs)
3	6:15	222	10	9:45	50	17	13:15	20
4	6:45	187	11	10:15	43	18	13:45	19
5	7:15	159	12	10:45	37	19	14:15	18
6	7:45	137	13	11:15	31	20	14:45	17
7	8:15	107	14	11:45	28	21	15:15	16

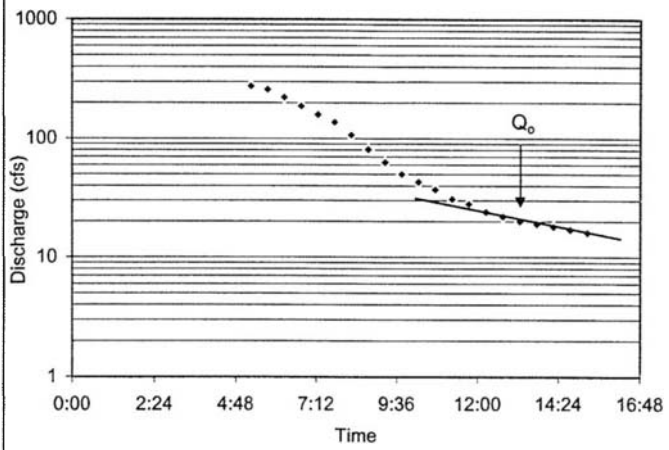

Figure 11.8. A plot of discharge versus time step from Table 11.1 for determining the baseflow recession constant k.

To find k, choose two sequential discharge values from the straight-line portion of the graph and use Equation (11.2). The graph clearly becomes straight at Time step 17 with a discharge of $Q_{17} = 20$ cfs. Using Time steps 17 and 18, $k = 19$ cfs/20 cfs = 0.95.

Equation (11.3) gives discharge n time periods later. The value of Q_o for Equation (11.3) is the first discharge value on the straight line, which is 20 cfs. For example, the discharge four time periods later is:

$$Q_{21} = Q_{17}k^4$$

$$Q_{21} = (20)\,(0.95)^4 = 16.3 \text{ cfs}$$

11.1.2 *Hydrograph separation*

Three different methods of separating baseflow are shown in Figure 11.9. Curve A is the simplest where a straight line is drawn from the point of rise to a point on the recession limb where storm runoff ends, and the recession curve is thought to be composed entirely of baseflow. As a guide, the point N on the recession limb can be approximated as:

$$N = A^{0.2} \tag{11.4}$$

where N is days after the peak, and A is basin area in square miles (Linsley et al. 1982). It is probably better to determine N by inspecting a number of hydrographs

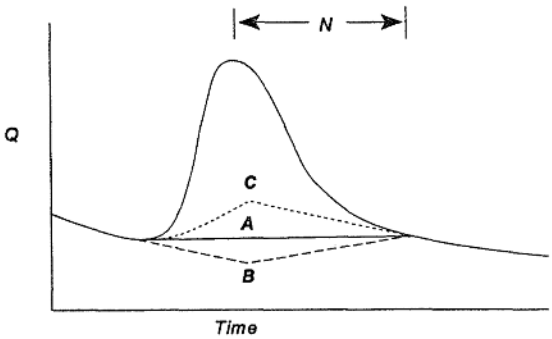

Figure 11.9. Three different methods of separating baseflow from storm runoff.

from the basin and using the method shown in Example 11.1. The method shown by curve *B* extends the prerise baseflow recession under the peak and then draws a straight line out to the baseflow recession curve as done for curve *A*. Curve *C* extends the baseflow recession on the falling limb backwards under the peak, and the segment from the point under the peak to the point of rise is sketched in. For curve *C* the extension of the baseflow recession curve backwards under the peak is accomplished using Equation (11.1) or Equation (11.3) and requires determining the value of the constant *k*.

11.2 RUNOFF VOLUME

Runoff volume (L^3) is an important flood variable because it determines the size requirements of storage facilities such as reservoirs, retention and detention basins. For example, if a new shopping center is built, this reduces infiltration and increases surface runoff. If the developer must detain the increased runoff on the site, this requires an estimate of the volume so the appropriate size detention facility can be constructed. On a larger scale, design and operation of flood control and water supply reservoirs require estimates of runoff volume. Runoff volume can be calculated from streamflow records; however, most rivers and streams do not have records and volume is estimated using other procedures.

11.2.1 *Infiltration-based approach*

In Chapter 7 we discussed infiltration. Runoff Q is the residual of the mass balance:

$$Q = P - F - D_p - E_t \tag{11.5}$$

Whether depression storage D_p and evapotranspiration E_t are significant depends upon the particular circumstances. For very short, intense storms evapotranspiration is negligible. For heavy rainfall over highly urbanized areas with steep slopes, the errors from ignoring depression storage may be inconsequential. Any of the infiltration formulas can be used to calculate F. The procedure can be tedious by hand, though spreadshees make the computations much easier (see Bedient & Huber 1992).

One of the simplest infiltration-based methods for calculating runoff volume uses the Φ index. Recall the Φ index is an average loss rate due to the combined processes of infiltration, depression storage and evapotranspiration. The Φ index is subtracted from the incremental precipitation to get an estimate of the incremental runoff for each time period. Summing the runoff increments gives the total runoff. Developing the Φ index required streamflow records, so this method is applicable to gaged basins (see Example 11.2).

Example 11.2
Use Φ = 0.98 in hr^{-1} from Example 7.3 to determine the incremental and total runoff from the following hypothetical storm (Table 11.2). Precipitation is measured at 15-minute intervals.

Table 11.2. Hypothetical runoff calculations using Φ = 0.98 in hr^{-1}.

Minutes	Precipitation (in)	Precipitation intensity (i) (in hr^{-1})	$i - \Phi$ (in hr^{-1})	Runoff (in)
15	0.15	0.60	–	0.00
30	0.27	1.08	0.10	0.03
45	0.40	1.60	0.62	0.16
60	0.25	1.00	0.02	0.01
75	0.18	0.72	–	0.00
90	0.05	0.20	–	0.00
Total	1.30			0.20

Being a constant the Φ index underestimates actual infiltration at the beginning of the storm and overestimates it at the end of the storm.

11.2.2 *SCS curve number method*

One of the most popular techniques for estimating the volume of runoff is the SCS curve number technique. The popularity of the method is due to its simplicity, not its accuracy. The method was originally conceived for estimating average runoff using average precipitation data, but it is now routinely applied to estimate runoff from individual storms (McCuen 1982). The method starts with the following assumption:

$$\frac{F}{S} = \frac{Q}{P - I_a} \tag{11.6}$$

where F is the actual retention (infiltration), S is the potential maximum storage in the basin, P is precipitation, Q is runoff, and I_a is the initial abstraction (depression storage). From the continuity equation (Eq. 11.5) and ignoring evapotranspiration:

$$F = (P - I_a) - Q \tag{11.7}$$

Substituting Equation (11.7) into Equation (11.6) yields:

$$\frac{(P-I_a)-Q}{S}=\frac{Q}{(P-I_a)} \tag{11.8}$$

Rearranging Equation (11.8) and solving for Q gives:

$$Q=\frac{(P-I_a)^2}{(P-I_a)+S} \tag{11.9}$$

Equation (11.9) gives runoff in terms of two unknowns, S and I_a. Experiments by the SCS have indicated that $I_a \approx 0.2(S)$, but I_a is an adjustable parameter of the method. Using $I_a = 0.2$ and substituting into Equation (11.9):

$$Q=\frac{(P-0.2S)^2}{(P+0.8S)} \tag{11.10}$$

Equation (11.10) is the basic equation for calculating runoff, and has one unknown, S. Further empirical study has determined:

$$S=\frac{1000}{CN}-10 \tag{11.11}$$

where CN is the curve number. Figure 11.10 is Equation (11.10) graphed for different values of P and CN. Knowing the curve number and total precipitation, runoff is calculated using Equation (11.10) or Figure 11.10. The SCS method is thus centered around determining the appropriate curve number. Curve numbers are a function of

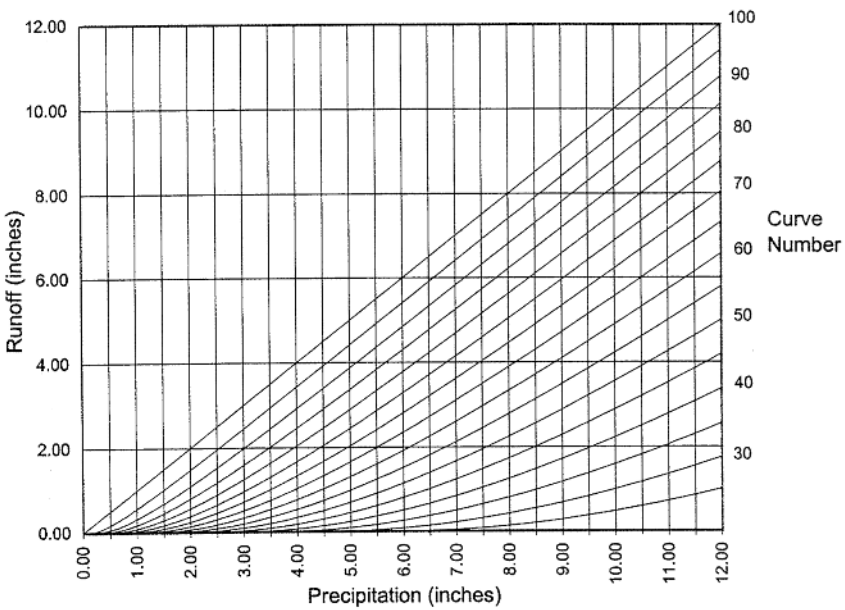

Figure 11.10. Runoff volume as a function of SCS curve number and total precipitation.

soil type, vegetation, land use, cultivation practice and antecedent moisture conditions. In Chapter 7 the four hydrologic soil groups (HSG) were described in Table 7.9. Table 11.3 gives *CN*s for agricultural land, Table 11.4 gives *CN*s for arid and range land, and Table 11.5 gives *CN*s for urban areas. The curve numbers in Tables 11.3-11.5 are for average antecedent moisture conditions, which is antecedent moisture condition II. Tables 11.6 and 11.7 give *CN*s for dryer (condition I) and wetter antecedent conditions (condition III). The composite curve numbers for urban areas in Table 11.5 were developed using average percentages of impervious area. Also, it

Table 11.3. *CN* values for cultivated agricultural land (source: SCS 1986).

Land cover	Treatment[1]	Hydrologic condition[2]	*CN* by soil group			
			A	B	C	D
Fallow	Bare soil	–	77	86	91	94
	Crop residue	Poor	76	85	90	93
		Good	74	83	88	90
Row crops	Straight row	Poor	72	81	88	91
		Good	67	78	85	89
	Straight row and crop residue	Poor	71	80	87	90
		Good	64	75	82	85
	Contoured	Poor	70	79	84	88
		Good	65	75	82	86
	Contoured and crop residue	Poor	69	78	83	87
		Good	64	74	81	85
	Contoured and terraced	Poor	66	74	80	82
		Good	62	71	78	81
	Contoured, terraced and crop residue	Poor	65	73	79	81
		Good	61	70	77	80
Small grain	Straight row	Poor	65	76	84	88
		Good	63	75	83	87
	Straight row and crop residue	Poor	64	75	83	86
		Good	60	72	80	84
	Contoured	Poor	63	74	82	85
		Good	61	73	81	84
	Contoured and crop residue	Poor	62	73	81	84
		Good	60	72	80	83
	Contoured and terraced	Poor	61	72	79	82
		Good	59	70	78	81
	Contoured, terraced and crop residue	Poor	60	71	78	81
		Good	58	69	77	80
Close seeded legumes or rotation meadow	Straight row	Poor	66	77	85	89
		Good	58	72	81	85
	Contoured	Poor	64	75	83	85
		Good	55	69	78	83
	Contoured and terraced	Poor	63	73	80	83
		Good	51	67	76	80

[1]Residue on at least 5% of the surface throughout the year.

[2]Hydrologic condition refers to factors that affect infiltration including density and canopy of vegetation, amount of year-round cover, amount of grass cover, percent of residue on the surface, and the degree of surface roughness. *Good* = factors encourage average or better than average infiltration. *Poor* = infiltration is impaired and runoff is increased.

Table 11.3. Continued.

Land cover	Hydrologic condition	*CN* by soil group			
		A	B	C	D
Pasture, grassland, or range: continuous grazing[1]	Poor	68	79	86	89
	Fair	49	69	79	84
	Good	39	61	74	80
Meadow: continuous grass protected from grazing and mowed for hay	–	30	58	71	78
Brush: brush-weed-grass mixture with brush the major element[2]	Poor	48	67	77	83
	Fair	35	56	70	77
	Good	30	48	65	73
Woods-grass combination (orchards and tree farms)	Poor	57	73	82	86
	Fair	43	65	76	82
	Good	32	58	72	79
Woods[3]	Poor	45	66	77	83
	Fair	36	60	73	79
	Good	30	55	70	77

[1]*Poor* = less than 50% ground cover or heavily grazed. *Fair* = 50 to 75% ground cover and not heavily grazed. *Good* = greater than 75% ground cover and lightly grazed.
[2]*Poor* = less than 50% ground cover. *Fair* = 50 to 75% ground cover. *Good* = greater than 75% ground cover.
[3]*Poor* = heavy grazing or burning, forest litter destroyed. *Fair* = some forest litter, some grazing, no burning. *Good* = good litter and brush undergrowth, no grazing or burning.

Table 11.4. *CN* values for arid and semi-arid rangeland (source: SCS 1986).

Land cover	Hydrologic condition[1]	*CN* by soil group			
		A	B	C	D
Herbaceous: mixture of grass weeds, and low-growing brush, with brush the minor element	Poor	80	87	93	–
	Fair	71	81	89	–
	Good	62	74	85	–
Oak-aspen: mountain brush mixture of oak brush, aspen, mountain mahogany and other bush	Poor	66	74	79	–
	Fair	48	57	63	–
	Good	30	41	48	–
Pinyon-juniper with grass understory	Poor	75	85	89	–
	Fair	58	73	80	–
	Good	41	61	71	–
Sagebrush with grass understory	Poor	67	80	85	–
	Fair	51	63	70	–
	Good	35	47	55	–
Desert shrub: bushes include saltbush greasewood, creosote, blackbrush, bursage, palo verde, mesquite and cactus	Poor	63	77	85	88
	Fair	55	72	81	86
	Good	49	68	79	84

[1]*Poor* = less than 30% ground cover (litter and brush overstory). *Fair* = 30 to 70% ground cover. *Good* = greater than 70% ground cover.

Table 11.5. *CN* values for urban areas (source: SCS 1986).

Land cover and hydrologic condition	Average impervious area in %	*CN* by soil group			
		A	B	C	D
Open space (lawns, parks, golf courses, cemeteries):					
– Poor condition (grass cover < 50 %)		68	79	86	89
– Fair condition (grass cover 50% to 75%)		49	69	79	84
– Good condition (grass cover > 75%)		39	61	74	80
Impervious areas:					
– Paved parking lots, roofs, driveways		98	98	98	98
– Streets and roads:					
– Paved; curbs and storm sewers		98	98	98	98
– Paved open ditch		83	89	92	93
– Gravel		76	85	89	91
– Dirt		72	82	87	89
Western desert urban areas:					
– Natural desert landscaping (pervious areas)		63	77	85	88
– Artificial desert landscaping (impervious weed barrier, desert shrub with 1- to 2-inch sand or gravel mulch)		96	96	96	96
Urban districts:					
– Commercial and business	85	89	92	94	95
– Industrial	72	81	88	91	93
Residential:					
– 1/8 acre or less townhouses	65	77	85	90	92
– 1/4 acre	38	61	75	83	87
– 1/3 acre	30	57	72	81	86
– 1/2 acre	25	54	70	80	85
– 1 acre	20	51	68	79	84
– 2 acres	12	46	65	77	82

Table 11.6. Rainfall limits for estimating antecedent moisture conditions (source: SCS 1972).

Antecedent moisture condition class	5-Day total antecedent rainfall (inches)	
	Dormant season	Growing season
I	Less than 0.5	Less than 1.4
II	0.5-1.1	1.4 -2.1
III	Over 1.1	Over 2.1

is assumed that the impervious area is directly connected to the drainage system. This means that water draining from an impervious area drains directly to the street. Unconnected impervious areas drain across a pervious surface, such as when runoff from a roof is directed onto a lawn. If the assumptions regarding the average impervious area, or if impervious areas are not directly connected to the drainage system, then the curve numbers should be modified using procedures outlined by the SCS (1986). Runoff often occurs from a mixture of land uses in which case a weighted curve number is calculated. The weights are the proportional areas of the different land uses.

Table 11.7. *CN* conversion from antecedent moisture class II to *CN* for antecedent moisture classes I and III (source: SCS 1972).

CN for antecedent moisture class	*CN* for antecedent moisture classes	
II	I	III
100	100	100
95	87	98
90	78	96
85	70	94
80	63	91
75	56	88
70	51	85
65	45	82
60	40	78
55	35	74
50	31	71
45	26	65
40	22	60
35	18	55
30	15	50

Example 11.3

Calculate the runoff from a 1200 acre basin from a storm producing 4.5 inches of precipitation. Land use in the basin is 1000 acres of row crops planted in straight rows in good hydrologic condition, a 170-acre residential development with 1-acre lots, and 30 acres of paved country roads. The entire basin is underlain by HSG *B*. Assume antecedent moisture condition II.

A good way to approach this problem is to set up Table 11.8 to organize the information.

Once the individual curve numbers for each cover type are found, the overall weighted *CN* for the basin is calculated using the fractional areas as weights:

$$CN = \frac{1000}{1200}(78) + \frac{170}{1200}(68) + \frac{30}{1200}(89) = 77$$

With a $CN = 77$ use either Equations (11.10) and (11.11) or Figure 11.10. The answer is $Q = 2.2$ inches of runoff.

Table 11.8. Data for determining CN for Example 11.3.

Cover	Area (acres)	HSG	Treatment	Condition	Moisture class	*CN*
Row crop	1000	B	Straight row	Good	II	78
Residential 1-acre lots	170	B	–	–	II	68
Paved roads open ditch	30	B	–	–	II	89

Recall that the SCS method only calculates runoff volume. The timing of the runoff and the shape of the hydrograph are unknown. The SCS has computerized the curve number procedure in the latest version of *TR55 Urban Hydrology for Small Watersheds* (SCS 1986). The computer program also determines the time of concentration and calculates approximate hydrographs. An obvious advantage of the curve number approach is that it does not require the use of historical streamflow data and can be used for determining runoff from ungaged basins. This makes the procedure ideal for predicting hydrologic consequences of future land development.

11.3 PEAK RUNOFF

The previous discussion dealt with estimating the volume of runoff. In many flood studies the critical variable is not volume, but peak discharge – the highest point on the hydrograph. For example, in sizing culverts and other crossing structures, designating floodplain boundaries, or deciding how high to build a levee, it is peak discharge which is important. The two methods for estimating peak discharge discussed in this section are the *rational method* and *flood frequency analysis*. The rational method is for use on small areas and does not require historical records. Frequency analysis can be applied to any stream with a suitable discharge record. Frequency analysis adds the dimension of probability, the likelihood of a given peak discharge occurring.

11.3.1 *The rational method*

The concept if not the origin of the rational method is attributed to the Irish engineer Mulvaney (1851). As a general rule, the rational method should only be used on watersheds less than 0.5 mi^2 (320 acres). This method is widely used in the design of storm sewers. The rational method has a number of assumptions:

1. The storm has uniform intensity and covers the entire basin,
2. The rate of runoff is at a maximum when the storm equals or exceeds the time of concentration t_c of the basin, and
3. Runoff is generated as hortonian overland flow.

In addition there should not be any lakes in the basin. These assumptions are more likely to obtain when analyzing small urban catchments. The second assumption is important because only when the entire basin is contributing runoff to the outlet can the peak discharge Q_{pk} occur. The upper part of Figure 11.11 depicts a uniform-intensity rain falling onto a strip of land. We saw that runoff increases downslope as the upstream contributing area increases (Fig. 10.7). In the lower part of Figure 11.11 are the rainfall hyetograph and the runoff hydrograph. After depression storage D_p is satisfied, runoff commences. As the contributing area at the outlet increases the hydrograph rises. In Figure 11.11 the initial runoff volumes at the outlet contributed by the areas A_1 and A_2 are shaded. At the time of concentration t_c, when the entire basin is contributing runoff to the outlet, the hydrograph reaches the maximum, steady-state equilibrium flow Q_e. Observe that if the duration of the storm t exactly equals the time of concentration t_c, the hydrograph would just reach its peak and then begin recession. This is why t_c is so important for the rational method. If the storm duration

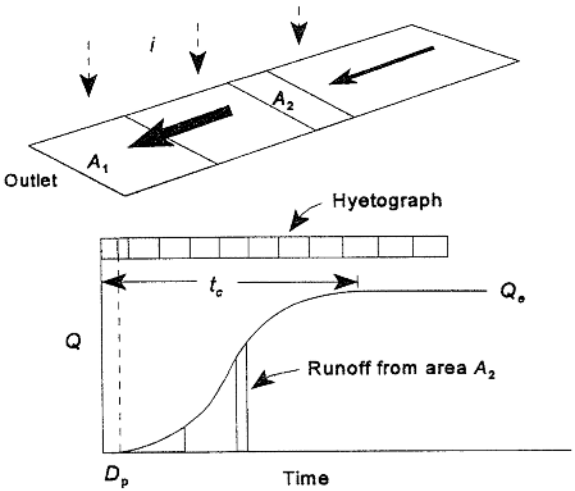

Figure 11.11. A uniform intensity rain (i) onto a strip of land, the rainfall hyetograph, and the runoff hydrograph at the downstream outlet. The hydrograph rises as the upstream area contributing runoff at the outlet increases. For example, the area A_2 contributes the incremental runoff volume shaded under the hydrograph. At the time of concentration t_c the whole area is contributing runoff and the hydrograph reaches its peak.

is shorter than the time of concentration, the hydrograph does not reach its peak because the whole basin is not contributing runoff. If a storm with a duration longer than t_c is used, then rainfall intensity, and peak flow, will be too low.

This is where the use of the kinematic wave equation for overland flow travel time (Eq. 10.24) becomes something of a chicken and the egg problem. We need t_{of} to find t_c for the basin (Eq. (10.22)).so we can choose the correct storm duration t and the corresponding rainfall intensity i. But t_{of} is itself a function of i, which is what we are trying to fine in the first place. One solution is to solve Equation (10.24) iteratively until $t \approx t_c$. First, choose an initial value for t. The initial value can be totally arbitrary or Kirpich's formula might be used to generate a first guess. For this duration read the corresponding i from the appropriate IDF curve (e.g., Fig. 4.18). Using this value of i, solve Equations (10.24) and (10.22) and compare t and t_c. This procedure is repeated until $t \approx t_c$. The formula for the rational method is:

$$Q = kCiA \tag{11.12}$$

where Q = peak discharge, C = rational runoff coefficient (Table 10.2), i = rainfall intensity, A = basin area, and k = conversion coefficient.

The value of k depends upon the system of units. For customary English units k = 1.008 and is usually ignored. Discharge Q is in cubic feet per second when i is in inches per hour and A is in acres. For i in millimeters per hour and A in square kilometers, k = 0.278 and Q is in cubic meters per second. The values of the runoff coefficient C given in Table 10.2 are for rainfall intensities having return periods of 5 to 10 years. For larger, less frequent storms, the greater depth of water on the surface drowns out surface irregularities and increases the amount of runoff. The value for C

should be increased for larger, less-frequent events. Rantz (1971) has provided adjusted C values for 25-year and 100-years events. More recently Aron (1994) has sought to develop a relationship between SCS curve numbers and rational runoff coefficients. His procedure makes the runoff coefficients a function of the soil-land cover complex and precipitation, whereas the values in Table 10.2 are a function only of land use.

Example 11.4

Calculate the peak discharge for a 10-year rainfall from a 200-acre basin outside Chicago, Illinois. The following information was derived from aerial photographs, topographic maps and soil surveys:

Land use: 160 acres single-family residential lots
40 acres of woodland on sandy soils
Basin length: $L_w = 2{,}300$ ft
Basin relief: $H_m = 12$ ft

We need t_c for the basin. The two major options are Kirpich's formula (Eq. 10.21) or the component-based travel time approach (Eq. 10.22). Because we do not have detailed channel geometry and roughness measurements we cannot use Manning's equation and the component-based approach. Using Kirpich's formula:

$$t_c = (2300)^{1.15} / 7700(12^{0.38}) = 0.37 \text{ hrs}$$

From the 10-year IDF curve for Chicago, $i = 3.8$ in hr^{-1} for $t = 22$ min. Calculate a weighted rational runoff coefficient using the same approach as in Example 11.3,

Single-family residential, $C = 0.40$
Woodland on sandy soil, $C = 0.30$

The weighted C is:

$$C = (160/200)0.40 + (40/200)0.30 = 0.38$$

Peak discharge is:

$$Q = CiA = 0.38(3.8)200 = 289 \text{ cfs}$$

The 10-year IDF curve for Chicago was derived as demonstrated in Example 4.7.

11.4 FLOOD FREQUENCY ANALYSIS

Flood frequency analysis determines the exceedence probability of an annual maximum peak discharge using historic streamflow data. The data for a frequency analysis are the annual maximum or partial duration series (see Chapter 2). The distribution of annual peak discharges is usually positively skewed. In this section the following five theoretical probability distributions are examined:

1. The normal distribution,
2. The log-normal distribution,
3. The Extreme Value I (Gumbel I) distribution,
4. The Pearson Type III distribution, and
5. The log-Pearson Type III distribution.

These five distributions are fit to the data in Table 11.9 using a combination of graphical, parametric, and frequency-factor techniques. Three of the five distribu-

Table 11.9. Annual maximum discharges for the San Gabriel River at Georgetown, Texas (1935-1973) (source: Chow et al. 1988, used by permission).

Year	Q	Year	Q	Year	Q
1935	25100	1948	14000	1961	22800
1936	32400	1949	6600	1962	4040
1937	16300	1950	5080	1963	858
1938	24800	1951	5350	1964	13800
1939	903	1952	11000	1965	26700
1940	34500	1953	14300	1966	5480
1941	30000	1954	24200	1967	1900
1942	18600	1955	12400	1968	21800
1943	7800	1956	5660	1969	20700
1944	37500	1957	155000	1970	11200
1945	10300	1958	21800	1971	9640
1946	8000	1959	3080	1972	4790
1947	21000	1960	71500	1973	18100

tions have dedicated graph paper which makes graphical fitting easy. All five can be fit using frequency factors (Eq. (3.21)). The Extreme Value I distribution is easily fit using the parameters of the distribution and the cumulative distribution function (CDF).

The choice of which probability distribution to use depends upon the goodness-of-fit, convenience, and comparability. Goodness-of-fit should be the most important criterion, but convenience is always a consideration. It is easy to fit the normal distribution to a set of data; however, if the fit is poor, how useful are the results? Comparability is sometimes an issue. As mentioned earlier it was recommended that federal agencies use the log-Pearson Type III distribution for flood frequency analysis.

Flood frequency analysis starts with the same five steps as outlined for precipitation frequency analysis in Chapter 4. The data were ranked and assigned sample frequencies F_s using the Weibull plotting position formula (see Table 11.10). The largest discharge for the period of record is 155,000 cfs which occurred in 1957. This is an extremely large discharge; so large in fact that it may be an 'outlier'. Outliers are data that do not seem to come from the same distribution as the rest of the data. The treatment of extremely large or small outliers poses a problem in frequency analysis. Should outliers be included or excluded from the analysis? Using the method of the Water Resources Council (1981) the 1957 discharge was classified a high outlier and was excluded from the analysis. The assumption is that this discharge has a return period much larger than that assigned by the plotting position formula, and including it in the analysis would distort the results. The second largest event and the two smallest discharges were also screened according to the WRC procedure. All three discharges came close but did not satisfy the outlier criterion, and are therefore included in the analysis.

The Weibull plotting position formula was used to assign the sample frequency estimates. There are other plotting position formulas, and for different probability distributions different formulas may be better. Cunnane (1978) suggested that Gringorten's (1963) formula is better for the Extreme Value I distribution. Gringorten's plotting position formula is:

Table 11.10. Ranked annual maximum discharges for the San Gabriel River at Georgetown, Texas (1935-1973).

Year	Rank	F_s	T (years)	Discharge (cfs)	Log_{10} discharge
1957				155000	5.1903
1960	1	0.026	39.00	71500	4.8543
1944	2	0.051	19.50	37500	4.5740
1940	3	0.077	13.00	34500	4.5378
1936	4	0.103	9.75	32400	4.5105
1941	5	0.128	7.80	30000	4.4771
1965	6	0.154	6.50	26700	4.4265
1935	7	0.179	5.57	25100	4.3997
1938	8	0.205	4.88	24800	4.3945
⋮	⋮	⋮	⋮	⋮	⋮
1966	30	0.769	1.30	5480	3.7388
1951	31	0.795	1.26	5350	3.7284
1950	32	0.821	1.22	5080	3.7059
1972	33	0.846	1.18	4790	3.6803
1962	34	0.872	1.15	4040	3.6064
1959	35	0.897	1.11	3080	3.4886
1967	36	0.923	1.08	1900	3.2788
1939	37	0.949	1.05	903	2.9557
1963	38	0.974	1.03	858	2.9335
Mean				16,421	4.0547
Standard deviation				13,521	0.4287
Coefficient of variation				0.823	0.1057
Skewness				1.934	–0.886
Skewness for lognormal distribution				3.028	

$$P(X \geq x) = \frac{m - 0.44}{n + 0.12} \tag{11.13}$$

In the following sections the San Gabriel River data are fit to each of the five theoretical distributions, and the Q_5, Q_{50} and Q_{100} discharges are estimated.

11.4.1 *The normal distribution*

Figure 11.12 shows the San Gabriel River data plotted on arithmetic normal probability paper. The theoretical normal distribution with a mean of 16,421 cfs and a standard deviation of 13,521 is plotted as the straight line. The fit is not very good because the theoretical distribution plots largely above the sample data.

This is because the normal distribution is for data with zero skewness. The theoretical distribution line is pulled upward by the positively-skewed data. A goodness-of-fit test could be performed to test the hypothesis that the sample data come from this distribution. The normal distribution can also be fit using frequency factors and Equation (3.21). The frequency factors are the Z scores from Table 3.3. For the 5, 50, 100-year return periods, the corresponding Z scores are 0.842, 2.054 and 2.326. For

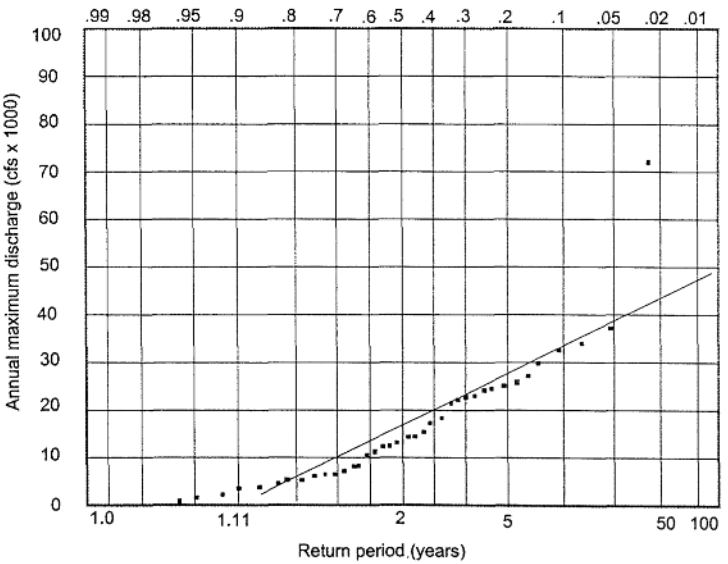

Figure 11.12. Sample frequencies and theoretical flood frequency curve for the San Gabriel River fitted to the normal distribution.

example, $T = 100$ is equivalent to an annual average exceedence probability of $p = 0.01$, so find the Z score that falls above 0.99 in the body of Table 3.3, which is $Z = 2.326$. The annual peak discharges for the three return periods from the normal distribution are:

$$Q_5 = 16{,}421 + 0.842(13{,}521) = 27{,}806 \text{ cfs}$$
$$Q_{50} = 16{,}421 + 2.054(13{,}521) = 44{,}193 \text{ cfs}$$
$$Q_{100} = 16{,}421 + 2.326(13{,}521) = 47{,}871 \text{ cfs}$$

11.4.2 *The lognormal distribution*

The lognormal distribution is based on the theory that the logarithms of the original data (y) are normally distributed even when the original data (x) are skewed. Any base can be used for the transformation $y = \log x$. The parameters of the lognormal distribution are given in Table 3.4 and are estimated by the statistics $\bar{y}$ and s_y. Chow (1964) gives moment-based estimators for the parameters, but using Equations (3.3) and (3.7) amounts to a maximum-likelihood estimation procedure. The San Gabriel River data are plotted on lognormal graph paper in Figure 11.13. Again, plotting the data directly on lognormal paper graphically fits the data to the distribution. Alternatively, you can plot the logarithmically-transformed data (y) on arithmetic normal probability paper as discussed in Chapter 2. Logarithmic transformation reduces skewness but does not necessarily eliminate it (see Table 11.10). Skewness for the lognormal distribution should not be calculated with Equation (3.9) but with the following equation from Chow (1964):

$$C_s = 3CV + CV^3 \tag{11.14}$$

where CV is the coefficient of variation. The theoretical lognormal distribution is the straight line graphed on Figure 11.13. The sample data fit the distribution fairly well for return periods $T > 1.6$ years. The fit deteriorates badly for more frequent events, but arguably it is the fit to the less frequent events which is more important. An adjustment that might improve the fit is to use a different plotting position formula such as Equation (11.13). Fitting the data to the lognormal distribution with frequency factors follows the same procedure as with the normal distribution. The lognormal frequency factors are given in Table 11.11 and are a function of the skewness and

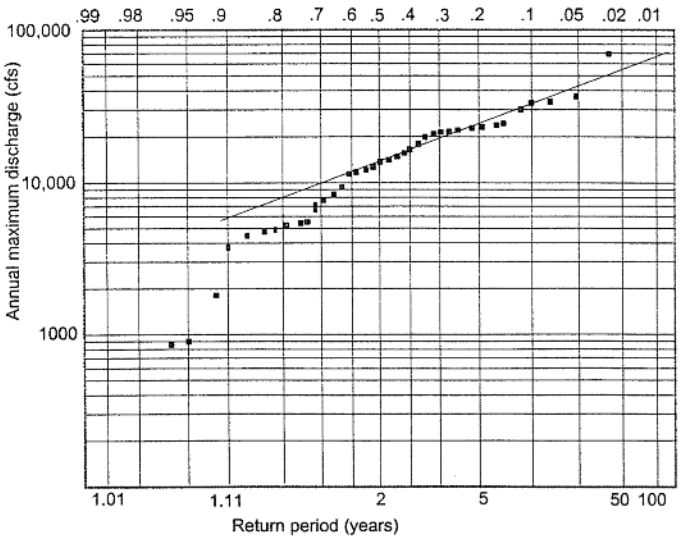

Figure 11.13. Sample frequencies and theoretical flood frequency curve for the San Gabriel River fitted to the lognormal distribution.

Table 11.11. Frequency factors K for the lognormal distribution (source: Chow 1964, used by permission).

C_s	CV	Return period (years)						
		1.01	1.05	1.25	2	5	20	100
		Exceedence probability						
		0.99	0.95	0.80	0.50	0.20	0.05	0.01
		−	−	−	−	+	+	+
0.0	0.000	2.33	1.65	0.84	0.00	0.84	1.64	2.33
0.1	0.033	2.25	1.62	0.85	0.02	0.84	1.67	2.40
0.2	0.067	2.18	1.59	0.85	0.03	0.83	1.70	2.48
0.3	0.100	2.11	1.56	0.85	0.05	0.82	1.72	2.55
0.4	0.136	2.04	1.52	0.85	0.07	0.81	1.75	2.63
0.5	0.166	1.97	1.49	0.86	0.08	0.80	1.77	2.70
0.6	0.197	1.91	1.46	0.85	0.10	0.79	1.79	2.77
0.7	0.230	1.85	1.43	0.85	0.11	0.78	1.81	2.84
0.8	0.262	1.79	1.40	0.84	0.13	0.77	1.82	2.90
0.9	0.292	1.74	1.37	0.84	0.14	0.76	1.84	2.97
1.0	0.324	1.68	1.34	0.83	0.15	0.74	1.85	3.04
1.1	0.351	1.63	1.31	0.83	0.16	0.73	1.86	3.09
1.2	0.381	1.58	1.29	0.82	0.17	0.72	1.87	3.15

Table 11.11. Continued.

C_s	CV	Return period (years) 1.01	1.05	1.25	2	5	20	100
		Exceedence probability 0.99	0.95	0.80	0.50	0.20	0.05	0.01
		−	−	−	−	+	+	+
1.3	0.409	1.54	1.26	0.82	0.18	0.71	1.88	3.21
1.4	0.436	1.50	1.23	0.81	0.19	0.69	1.88	3.26
1.5	0.462	1.46	1.21	0.81	0.20	0.68	1.89	3.30
1.6	0.490	1.42	1.19	0.80	0.21	0.67	1.89	3.35
1.7	0.517	1.38	1.16	0.79	0.22	0.65	1.89	3.40
1.8	0.544	1.34	1.14	0.78	0.22	0.64	1.89	3.44
1.9	0.570	1.31	1.12	0.78	0.23	0.63	1.89	3.48
2.0	0.596	1.28	1.10	0.77	0.24	0.61	1.89	3.52
2.1	0.620	1.25	1.08	0.76	0.24	0.60	1.89	3.55
2.2	0.643	1.22	1.06	0.76	0.25	0.59	1.89	3.59
2.3	0.667	1.20	1.04	0.75	0.25	0.58	1.88	3.62
2.4	0.691	1.17	1.02	0.74	0.26	0.57	1.88	3.65
2.5	0.713	1.15	1.00	0.74	0.26	0.56	1.88	3.67
2.6	0.734	1.12	0.99	0.73	0.26	0.55	1.87	3.70
2.7	0.755	1.10	0.97	0.72	0.27	0.54	1.87	3.72
2.8	0.776	1.08	0.96	0.72	0.27	0.53	1.86	3.74
2.9	0.796	1.06	0.95	0.71	0.27	0.52	1.86	3.76
3.0	0.918	1.04	0.93	0.70	0.28	0.51	1.85	3.78
3.2	0.857	1.01	0.90	0.69	0.28	0.49	1.84	3.81
3.4	0.895	0.98	0.88	0.68	0.29	0.47	1.82	3.84
3.6	0.930	0.95	0.86	0.67	0.29	0.46	1.81	3.87
3.8	0.966	0.92	0.84	0.66	0.29	0.44	1.80	3.89
4.0	1.000	0.90	0.82	0.65	0.29	0.42	1.78	3.91
4.5	1.081	0.84	0.78	0.63	0.30	0.39	1.75	3.94
5.0	1.155	0.80	0.74	0.60	0.30	0.36	1.71	3.96

the exceedence probability. Frequency factors in columns 1-4 are negative. Observe that for zero skewness the lognormal frequency factors are normal distribution Z scores. The estimated 5- and 100-year annual peak discharges using the lognormal distribution are:

$$Q_5 = 16{,}421 + 0.51(13{,}521) = 23{,}317 \text{ cfs}$$
$$Q_{100} = 16{,}421 + 3.78(13{,}521) = 67{,}530 \text{ cfs}$$

The Q_{50} discharge was not calculated using frequency factors, since interpolation of frequency factors between return periods is not recommended. Instead, the $Q_{50} = 54{,}500$ cfs discharge is read directly from the theoretical line plotted on Figure 11.13.

11.4.3 *The Extreme Value I distribution*

The Extreme Value I distribution is also called the Gumbel I distribution in recognition of Gumbel's work on the statistical theory of extreme values (Gumbel 1958).

The Gumbel I distribution is for use with positively skewed data. There is an Extreme Value III distribution (Gumbel III) for use with negatively skewed data. The Gumbel III distribution is used for the frequency analysis of droughts. The Gumbel I distribution can be fitted all three ways – graphically, using frequency factors, and by use of parameters and the CDF. One characteristic that makes the distribution easy to use is that skewness is constant, $C_s = 1.1396$. Figure 11.14 is the graphical fit of the data by plotting on Gumbel I graph paper. The data fit the Gumbel I distribution fairly well. The frequency factors for the Gumbel I distribution are given in Table 11.12. The factors are a function of sample size n and exceedence probability. For the three return periods the Gumbel-estimated discharges are:

$$Q_5 = 16{,}421 + 0.843(13{,}521) = 27{,}819 \text{ cfs}$$
$$Q_{50} = 16{,}421 + 2.957(13{,}521) = 56{,}403 \text{ cfs}$$
$$Q_{100} = 16{,}421 + 3.572(13{,}521) = 64{,}718 \text{ cfs}$$

Whereas interpolation of frequency factor values between return periods is not recommended, interpolation within a given return-period column is acceptable. The Gumbel I distribution is one of the easiest to fit using the distribution's parameters. The CDF for the Gumbel I distribution is a double negative exponential function:

$$F(x) = P(X \le x) = e^{-e^{-[(u+x)/\alpha]}} \tag{11.15}$$

where the parameters u and α are:

$$u = 0.5772\alpha - \mu \tag{11.16}$$

and

$$\alpha = \frac{\sqrt{6}}{\pi}\sigma = 0.7797\sigma \tag{11.17}$$

We can use these equations to calculate the exceedence probability for any peak discharge.

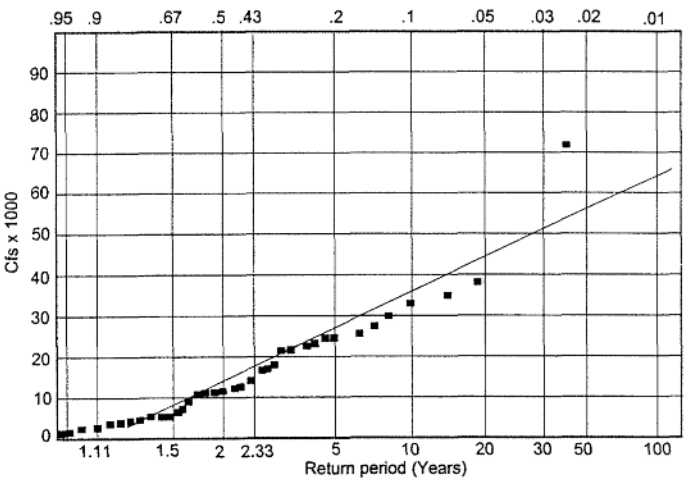

Figure 11.14. Sample frequencies and theoretical flood frequency curve for the San Gabriel River fitted to the Extreme Value 1 (Gumbel 1) distribution.

Table 11.12. Frequency factors K for the Gumbel Extreme Value I distribution (source: Hann 1977).

n	Return period (years)						
	5	10	15	20	25	50	100
	Exceedence probability						
	0.20	0.10	0.067	0.05	0.04	0.02	0.01
15	0.967	1.703	2.117	2.410	2.632	3.321	4.005
20	0.919	1.625	2.023	2.302	2.517	3.179	3.836
25	0.888	1.575	1.963	2.235	2.444	3.088	3.729
30	0.866	1.541	1.922	2.188	2.393	3.026	3.653
35	0.851	1.516	1.891	2.152	2.354	2.979	3.598
40	0.838	1.495	1.866	2.126	2.326	2.943	3.554
45	0.829	1.478	1.847	2.104	2.303	2.913	3.520
50	0.820	1.466	1.831	2.086	2.283	2.889	3.491
55	0.813	1.455	1.818	2.071	2.267	2.869	3.467
60	0.807	1.446	1.806	2.059	2.253	2.852	3.446
65	0.801	1.437	1.796	2.048	2.241	2.837	3.429
70	0.797	1.430	1.788	2.038	2.230	2.824	3.413
75	0.792	1.423	1.780	2.029	2.220	2.812	3.400
80	0.788	1.417	1.773	2.020	2.212	2.802	3.387
85	0.785	1.413	1.767	2.013	2.205	2.793	3.376
90	0.782	1.409	1.762	2.007	2.198	2.785	3.367
95	0.780	1.405	1.757	2.002	2.193	2.777	3.357
100	0.779	1.401	1.752	1.998	2.187	2.770	3.349
∞	0.719	1.305	1.635	1.866	2.044	2.592	3.137

Example 11.5

Find the return period T of an annual peak discharge of 40,000 cfs.

The sample mean $\bar{x}$ = 16,421 is used for μ in Equation (11.16), and s = 13,521 for σ in Equation (11.17). These give estimates of α = 10,542.3 and u = –10,335.9. Using these values and a value of x = 40,000 in Equation (11.15) gives the nonexceedence probability:

$$F(x) = P(X \leq x) = e^{-e^{\frac{(-10335.9+40000)}{10542.3}}} = 0.9418$$

The exceedence probability is (1 – 0.9418) = 0.058. The return period is the inverse of the exceedence probability for a final answer of T = 17.2 years. In other words, $Q_{17.2}$ = 40,000 cfs by the Gumbel I distribution.

If the mean is used for x in Equation (11.15) the result is $P(X \leq \bar{x})$ = 0.57, which is as exceedence probability of 0.43 or a return period of T = 2.33 years. For the Gumbel I distribution the arithmetic mean plots at $P(X \geq \bar{x})$ = 0.43 and *not* at 0.5 (see Fig. 11.14). The term $Q_{2.33}$ or 'mean annual flood' is frequently encountered in flood studies. The term takes its name from the statistical properties of the Gumbel I distribution.

11.4.4 *The Pearson Type III distribution*

The Pearson Type III distribution can be used either with the original data or with logarithmically transformed data. In the former case the distribution is simply the

Pearson Type III, in the latter it is the log-Pearson Type III. Fitting the Pearson Type III distribution is usually done with frequency factors because there is no dedicated graph paper, and using the CDF is too cumbersome. The frequency factors for the Pearson Type III are a function of the coefficient of skewness C_s and the return period T (Table 11.13). For samples with $n \leq 50$ Equation (3.10) in Chapter 3 can be used to adjust the sample skewness. The adjusted skewness for the San Gabriel River data is $C_s' = 2.36$. With this skewness the frequency factors are interpolated from Table 11.13 and the Pearson III estimates for the three discharges are:

$$Q_5 = 16{,}421 + 0.544(13{,}521) = 23{,}776 \text{ cfs}$$
$$Q_{50} = 16{,}421 + 3.01(13{,}521) = 57{,}119 \text{ cfs}$$
$$Q_{100} = 16{,}421 + 3.781(13{,}521) = 67{,}544 \text{ cfs}$$

These discharge values can be plotted on lognormal or semi-log graph paper, but will describe a curve, not a straight line.

Table 11.13. Frequency factors K for the Pearson III distribution (Water Resources Council 1981).

Skew	Return period (years)						
Cs	2	5	10	25	50	100	200
	Exceedence probability						
	0.50	0.20	0.10	0.04	0.02	0.01	0.005
3.0	–0.396	0.420	1.180	2.278	3.152	4.051	4.970
2.9	–0.390	0.440	1.195	2.277	3.134	4.013	4.909
2.8	–0.384	0.460	1.210	2.275	3.114	3.973	4.847
2.7	–0.376	0.479	1.224	2.272	3.093	3.932	4.783
2.6	–0.368	0.499	1.238	2.267	3.071	3.889	4.718
2.5	–0.360	0.518	1.250	2.262	3.048	3.845	4.652
2.4	–0.351	0.537	1.262	2.256	3.023	3.800	4.584
2.3	–0.341	0.555	1.274	2.248	2.997	3.753	4.515
2.2	–0.330	0.574	1.284	2.240	2.970	3.705	4.444
2.1	–0.319	0.592	1.294	2.230	2.942	3.656	4.372
2.0	–0.307	0.609	1.302	2.219	2.912	3.605	4.298
1.9	–0.294	0.627	1.310	2.207	2.881	3.553	4.223
1.8	–0.282	0.643	1.318	2.193	2.848	3.499	4.147
1.7	–0.268	0.660	1.324	2.179	2.815	3.444	4.069
1.6	–0.254	0.675	1.329	2.163	2.780	3.388	3.990
1.5	–0.240	0.690	1.333	2.146	2.743	3.330	3.910
1.4	–0.225	0.705	1.337	2.128	2.706	3.271	3.828
1.3	–0.210	0.719	1.339	2.108	2.666	3.211	3.745
1.2	–0.195	0.732	1.340	2.087	2.626	3.149	3.661
1.1	–0.180	0.745	1.341	2.066	2.585	3.087	3.575
1.0	–0.164	0.758	1.340	2.043	2.542	3.022	3.489
0.9	–0.148	0.769	1.339	2.018	2.498	2.957	3.401
0.8	–0.132	0.780	1.336	1.993	2.453	2.891	3.312
0.7	–0.116	0.790	1.333	1.967	2.407	2.824	3.223
0.6	–0.099	0.800	1.328	1.939	2.359	2.755	3.132
0.5	–0.083	0.808	1.323	1.910	2.311	2.686	3.041
0.4	–0.066	0.816	1.317	1.880	2.261	2.615	2.949

Table 11.13. Continued.

Skew	Return period (years)						
Cs	2	5	10	25	50	100	200
	Exceedence probability						
	0.50	0.20	0.10	0.04	0.02	0.01	0.005
0.3	–0.050	0.824	1.309	1.849	2.211	2.544	2.856
0.2	–0.033	0.830	1.301	1.818	2.159	2.472	2.763
0.1	–0.017	0.836	1.292	1.785	2.107	2.400	2.670
0.0	0.000	0.842	1.282	1.751	2.054	2.326	2.576
–0.1	0.017	0.846	1.270	1.716	2.000	2.252	2.482
–0.2	0.033	0.850	1.258	1.680	1.945	2.178	2.388
–0.3	0.050	0.853	1.245	1.643	1.890	2.104	2.294
–0.4	0.066	0.855	1.231	1.606	1.834	2.029	2.201
–0.5	0.083	0.856	1.216	1.567	1.777	1.955	2.108
–0.6	0.099	0.857	1.200	1.528	1.720	1.880	2.016
–0.7	0.116	0.857	1.183	1.488	1.663	1.806	1.926
–0.8	0.132	0.856	1.166	1.448	1.606	1.733	1.837
–0.9	0.148	0.854	1.147	1.407	1.549	1.660	1.749
–1.0	0.164	0.852	1.128	1.366	1.492	1.588	1.664
–1.1	0.180	0.848	1.107	1.324	1.435	1.518	1.581
–1.2	0.195	0.844	1.086	1.282	1.379	1.449	1.501
–1.3	0.210	0.838	1.064	1.240	1.324	1.383	1.424
–1.4	0.225	0.832	1.041	1.198	1.270	1.318	1.351
–1.5	0.240	0.825	1.018	1.157	1.217	1.256	1.282
–1.6	0.254	0.817	0.994	1.116	1.166	1.197	1.216
–1.7	0.268	0.808	0.970	1.075	1.116	1.140	1.155
–1.8	0.282	0.799	0.945	1.035	1.069	1.087	1.097
–1.9	0.292	0.788	0.920	0.996	1.023	1.037	1.044
–2.0	0.307	0.777	0.895	0.959	0.980	0.990	0.995
–2.1	0.319	0.765	0.869	0.923	0.939	0.946	0.949
–2.2	0.330	0.752	0.844	0.888	0.900	0.905	0.907
–2.3	0.341	0.739	0.819	0.855	0.864	0.867	0.869
–2.4	0.351	0.725	0.795	0.823	0.830	0.832	0.833
–2.5	0.360	0.711	0.771	0.793	0.798	0.799	0.800
–2.6	0.368	0.696	0.747	0.764	0.768	0.769	0.769
–2.7	0.376	0.681	0.724	0.738	0.740	0.740	0.741
–2.8	0.384	0.666	0.702	0.712	0.714	0.714	0.714
–2.9	0.390	0.651	0.681	0.683	0.689	0.690	0.690
–3.0	0.396	0.636	0.666	0.666	0.666	0.667	0.667

11.4.5 *The log-Pearson Type III distribution*

The log-Pearson Type III distribution has the distinction of being recommended for use by federal agencies in the United States. The procedure is identical to the Pearson Type III analysis except we work with the logs of the original data. The issue of determining skewness again presents a problem. There are generally three choices for skewness. You can use the sample estimated value (–0.886); however, there is still the uncertainty associated with the small sample size (n = 38). The skewness adjustment (Eq. 3.10) used in the previous section is not applicable to the skewness

of the logarithms of the original data. A second approach is to use a generalized skewness value taken from a map published by the Water Resources Council (WRC) (1981). Isolines of skewness for the logarithms of annual maximum streamflow are shown in Figure 11.15. For the San Gabriel River the map value for skewness is –0.28. A third alternative is a procedure developed by the WRC (1981) that combines the sample-estimated skewness and the map skewness value into a single weighted skewness C_{sw}. The details of the WRC's procedure are not described here, but the method was used to calculate a weighted skewness value of $C_{sw} = -0.63$. Frequency factors were chosen from Table 11.13 based on this weighted skewness. Using the mean and standard deviation of the logs (Table 11.10) in the frequency-factor equation (Eq. 3.21), the logs of the annual peak discharges are:

$$\log Q_5 = 4.0547 + 0.857(0.4287) = 4.4221$$
$$\log Q_{50} = 4.0547 + 1.70(0.4287) = 4.7835$$
$$\log Q_{100} = 4.0547 + 1.86(0.4287) = 4.8521$$

To find discharge, take the antilog of these values:

$$Q_5 = 10^{4.4221} = 26{,}430 \text{ cfs}$$
$$Q_{50} = 10^{4.7835} = 60{,}744 \text{ cfs}$$
$$Q_{100} = 10^{4.8521} = 71{,}138 \text{ cfs}$$

Again, there is no dedicated graph paper for the log-Pearson III distribution and the results can be plotted on lognormal or semi-log paper.

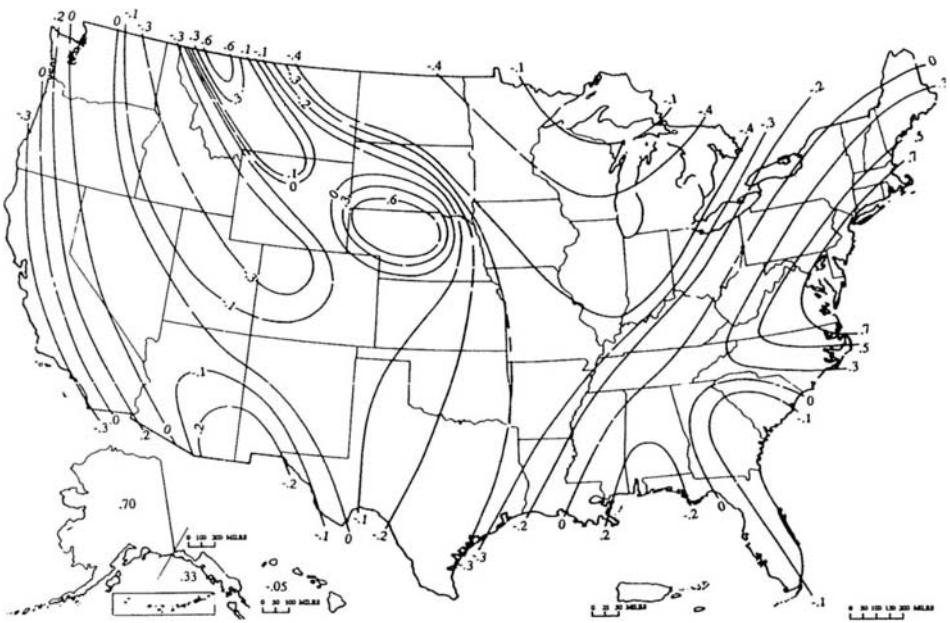

Figure 11.15. Generalized skewness coefficients of annual maximum streamflow (source: Water Resources Council 1981).

11.4.6 *Confidence limits*

Flood frequency estimates are statistically-based and are necessarily accompanied by uncertainty. Some researchers suggest placing confidence limits around the estimates. There are different ways to determine confidence limits depending upon the distribution (Kite 1977). The approach developed by Beard (1962) for the Gumbel I and lognormal distributions is described here.

The confidence limit formula is:

$$Q_{T,\alpha} = Q_T + \Delta Q \tag{11.18}$$

where

$$\Delta Q = sc_{T,\alpha} \tag{11.19}$$

In Equation (11.19) s is the standard deviation and $c_{T,\alpha}$ a coefficient that depends upon the return period T and significance level α. Values of $c_{T,\alpha}$ for $\alpha = 0.05$ are given in Table 11.14. A significance level of $\alpha = 0.05$ corresponds to a 90% confidence interval because there are both upper and lower confidence limits. If confidence limits are placed on all discharges, confidence intervals can be drawn as lines on either side of the theoretical distribution line. Figure 11.16 shows confidence interval around a flood frequency curve.

Table 11.14. Coefficient's for calculating the 90% confidence limits on annual peak discharge values calculated by the lognormal or Gumbel I distribution. (source: Beard 1968).

Confidence limit	Return period (years)						
	Years of record	1000	100	10	2	1.1	1.01
Upper	5	4.41	3.41	2.12	0.95	0.76	1.00
	10	2.11	1.65	1.07	0.58	0.57	0.76
	15	1.52	1.19	0.79	0.46	0.48	0.65
	20	1.23	0.97	0.64	0.39	0.42	0.58
	30	0.93	0.74	0.50	0.31	0.35	0.49
	40	0.77	0.61	0.42	0.27	0.31	0.43
	50	0.67	0.54	0.36	0.24	0.28	0.39
	70	0.55	0.44	0.30	0.20	0.24	0.34
	100	0.45	0.36	0.25	0.17	0.21	0.29
Lower	5	–1.22	–1.00	–0.76	–0.95	–2.12	–3.41
	10	–0.94	–0.76	–0.57	–0.58	–1.07	–1.65
	15	–0.80	–0.65	–0.48	–0.46	–0.79	–1.19
	20	–0.71	–0.58	–0.42	–0.39	–0.64	–0.97
	30	–0.60	–0.49	–0.35	–0.31	–0.50	–0.74
	40	–0.53	–0.43	–0.31	–0.27	–0.42	–0.61
	50	–0.49	–0.39	–0.28	–0.24	–0.36	–0.54
	70	–0.42	–0.34	–0.24	–0.20	–0.30	–0.44
	100	–0.37	–0.29	–0.21	–0.17	–0.25	–0.36

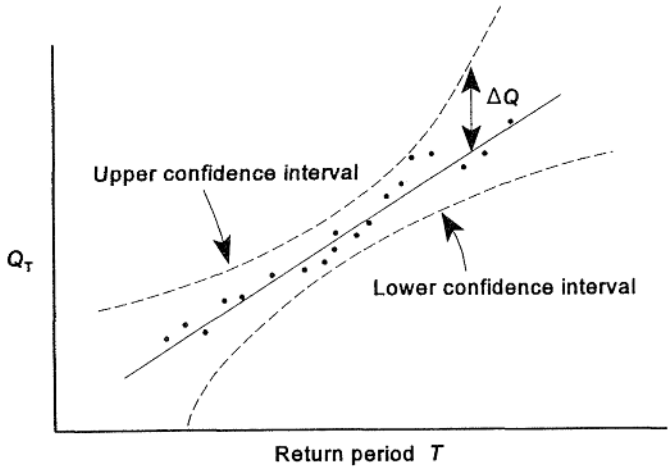

Figure 11.16. Confidence intervals around a flood frequency curve.

Example 11.6
Determine the 90% confidence limit around the Q_{100} discharge calculated by the Gumbel I distribution. The 100-year discharge is $Q_{100} = 64{,}718$. Interpolating in Table 11.14, the 90% upper confidence limit coefficient is $c^{U}_{100,0.05} = 0.64$ and the lower limit coefficient is $c^{L}_{100,0.05} = -0.44$.

The upper and lower discharge increments ΔQ are:

$$\Delta Q^{U} = 13{,}521(0.64) = 8653 \text{ cfs}$$
$$\Delta Q^{L} = 13{,}521(-0.44) = -5949 \text{ cfs}$$

The upper and lower 90% confidence limits are:

$$Q^{U}_{100,0.05} = 64{,}718 + 8653 = 73{,}371 \text{ cfs}$$
$$Q^{L}_{100,0.05} = 64{,}718 - 5949 = 58{,}769 \text{ cfs}$$

We should expect that 9 times out of 10 the actual Q_{100} discharge will fall within these confidence limits.

11.4.7 *Mixed distributions*

Precipitation generating mechanisms may be different at different times of the year. In the Southeast, tropical storms, hurricanes and air mass convection are all responsible for heavy rainfall in the summer and fall. In the Rocky Mountains, the upper Midwest, and the Northeast spring floods are generated by melting snow, while convective thunderstorms produce flooding in the summer season. The flood of record throughout much of Pennsylvania resulted from Hurricane Agnes in 1972. Different physical mechanisms for generating intense precipitation events may have different underlying probability distributions (Faiers et al. 1994). The annual maximum series assumes the data are homogeneous in time – that they come from the same distribu-

tion – when in fact different physical mechanisms with different distributions create a heterogeneous series. These distributions are 'mixed distributions'. Mixed distributions can also result from nonstationary data such as caused by a shift in climate. Improved estimates of flood frequency might be obtained by separating the flood peaks by their causal mechanism(s) and analyzing them separately. Methods for analyzing mixed distributions are beyond the scope this book but the problem exists and should be recognized.

11.5 REGIONAL ANALYSIS

Advancements in computers and statistical software packages have made complex multivariate analyses simple. This has improved our ability to develop regional multivariate regression equations that predict peak discharge from a variety of independent variables. The general form of the relationship is:

$$Q_T = aX_1^{b_1} X_2^{b_2} \ldots X_n^{b_n} \tag{11.20}$$

which is transformed into the standard linear regression equation form by taking the log of Equation (11.20):

$$\log Q_T = \log a + b_1 \log x_1 + b_2 \log x_2 + \ldots + b_n \log x_n \tag{11.21}$$

where a is the intercept, and b_i is the regression coefficient on the independent variable X_i. The independent variables are either climate or basin characteristics. One distinct advantage of regional analysis is the ability to estimate flood frequencies for ungaged basins. Waltmeyer (1986) undertook a regional flood frequency analysis for ungaged streams in New Mexico. He divided the state into eight physiographic regions, and developed regression equations for return periods of 2, 5, 10, 25, 50, and 100 years. Some example equations are given in Table 11.15.

In Table 11.15 Q is in cfs, A is drainage basin area in square miles and E is mean basin elevation in feet. The *standard error of estimate* (*SEE*) is the standard deviation of the (normal) distribution of the residuals about the regression line. For example, a *SEE* of 74% means about 68% of all values used to develop the regression equation are within 74% of the estimated values.

Table 11.15. Equations for regional flood frequency analysis in New Mexico. (source: Waltmeyer 1986).

Region	Equation	Average standard eror of estimate (%)
Northwest Plateau	$Q_{10} = 336A^{0.44}$	78
	$Q_{100} = 1090A^{0.37}$	74
Southeast Mountains	$Q_{10} = 34500A^{0.61}(E/1000)^{-2.55}$	53
	$Q_{100} = 257000A^{0.65}(E/1000)^{-3.02}$	59

11.6 THE UNIT HYDROGRAPH

The methods for flood analysis discussed so far have calculated either the volume of runoff or the hydrograph peak. The *unit hydrograph* is a method for deriving the complete runoff hydrograph – rising limb, falling limb, peak discharge, and the time base (duration). The unit hydrograph requires streamflow data so the technique is appropriate for gaged basins. In the next section we discuss generating 'synthetic' unit hydrographs for ungaged basins. Unit hydrograph analysis is applicable to basins less than 2000 mi^2 in area. An important assumption of the method is that the basin is a linear response system. In other words, for a given precipitation input there is a given discharge output, and if the input is doubled, the output is doubled and so on. Some hydrologists make the additional assumption that rainfall be uniform over the basin in both time and space. This assumption becomes more heroic as basin size increases. Other researchers state just that the rainfall pattern should be characteristic of storms over the basin (Dunne & Leopold 1978).

The concept of the unit hydrograph begins by recognizing that the factors controlling runoff can be considered as transient or permanent. The major transient factors are related to the storm, such as intensity, duration, and direction of movement. Infiltration and evaporation are also transient in time and space. Permanent factors include channel characteristics such as slope and roughness, and basin factors such as shape, size, relief and aspect. The unit hydrograph theory assumes that differences in runoff from a given basin are due mainly to differences in the transient factors. For a given basin similar storms should produce similar hydrographs, since the permanent factors do not change.

The unit hydrograph is defined as *the hydrograph from 1 unit of runoff from a storm of unit duration*. In conventional English units the unit of runoff is 1 inch, in metric units it is 1 cm. The unit duration storm can be of any length t. In practice this usually means choosing a storm duration that is typical for the basin. When we speak of the t-hour unit hydrograph, we are referring to the duration of the storm hyetograph that generated the hydrograph. The terminology can get a bit confusing and Figure 11.17 schematically shows the three different hydrographs involved. If the

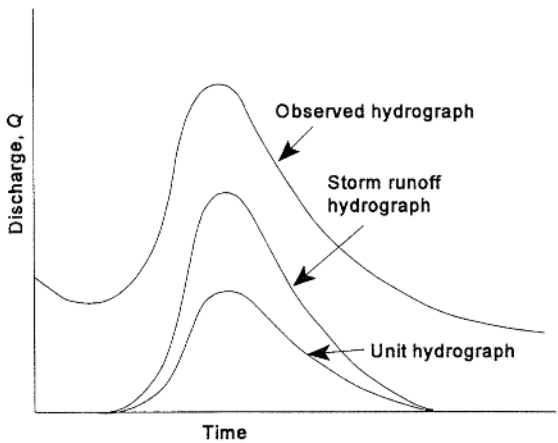

Figure 11.17. The observed hydrograph, the storm runoff hydrograph and the derived unit hydrograph.

unit hydrograph is the hydrograph from 1 unit of runoff, then the linear-system assumption means that 2 units of runoff would produce a hydrograph with ordinates twice as high as the ordinates of the unit hydrograph. In other words, once we have the t-hour unit hydrograph, we can reproduce a runoff hydrograph for any t-hour duration storm by multiplying the unit hydrograph ordinates by the runoff depth. The derivation of a unit hydrograph involves just three steps:

1. Obtain the storm runoff hydrograph by separating the baseflow from the observed hydrograph,
2. Determine the uniform depth of runoff over the basin,
3. Divide the storm runoff hydrograph ordinates by the runoff depth from Step 2.

Example 11.7 demonstrates the procedure.

Example 11.7

Derive the 3-hour unit hydrograph for a hypothetical basin with an area of 2.0 mi^2. Remember the 3-hour duration refers to the storm, not the hydrograph (Table 11.16).

Step 1. Subtract the baseflow from the observed hydrograph to get the storm runoff hydrograph ordinates.

Step 2. Determine the uniform depth of runoff from the basin:

$$\text{Depth} = \frac{\text{Volume}}{\text{Area}}$$

$$\text{Depth} = \frac{\left(2067\ \text{ft}^3\text{s}^{-1}\right)\left(3600\ \text{s hr}^{-1}\right)\left(2\ \text{hr}\right)}{\left(2\ \text{mi}^2\right)\left(640\ \text{acres mi}^{-2}\right)\left(43{,}560\ \text{ft}^2\text{acre}^{-1}\right)} = 0.267\ \text{ft}$$

Converting the answer to inches gives a uniform depth of 3.20 inches of runoff. Observe that we multiplied cfs in the numerator by 2 hours. This is the time interval for the hydrograph observations (columns 1 and 2).

Table 11.16. Example derivation of a unit hydrograph. All values are in cfs.

Time (hour)	Time interval	Observed H.G.	Baseflow	Runoff H.G.	Unit H.G.
3:00	0	15	15	0	0
5:00	2	160	15	145	45
7:00	4	350	15	335	105
9:00	6	435	16	419	131
11:00	8	320	16	304	95
13:00	10	250	16	234	73
15:00	12	200	17	183	57
17:00	14	155	17	138	43
19:00	16	125	18	107	33
21:00	18	98	18	80	25
23:00	20	74	19	55	17
1:00	22	55	19	36	11
3:00	24	40	19	21	7
5:00	26	30	20	10	3
7:00	28	22	22	0	0
				Σ 2067	Σ 645

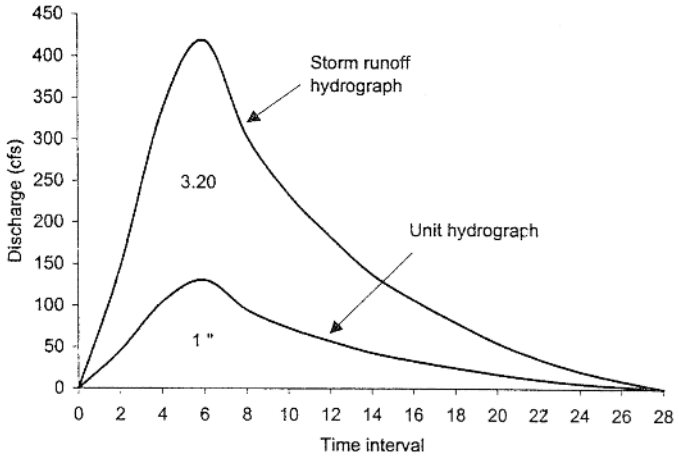

Figure 11.18. Hypothetical storm runoff hydrograph and derived 3-hour unit hydrograph.

Step 3. Derive the 3-hour unit hydrograph ordinates by dividing each ordinate of the storm runoff hydrograph by the runoff depth (3.2 inches). The storm runoff hydrograph and the 3-hour unit hydrograph are drawn in Figure 11.18. The area under the storm runoff hydrograph equals 3.20 inches, while the area under the unit hydrograph equals 1 inch.

Example 11.8

Determine the total flood hydrograph from a 3-hour storm that produced 2.3 inches of runoff from the same basin as in Example 11.7. Assume a constant 15 cfs baseflow.

The storm runoff hydrograph is generated by multiplying the runoff depth (2.3 inches) times the unit hydrograph ordinates. The total hydrograph is the sum of the storm runoff hydrograph and baseflow.

Using the unit hydrograph we estimate that a 3-hour storm producing 2.3 inches of runoff would have a time base of 28 hours, and would produce a peak discharge of 316 cfs occurring about 6 hours from the time of initial rise of the hydrograph (Table 11.17).

Table 11.17. Creation of a total storm hydrograph from a unit hydrograph.

Time interval	Unit H.G.	Storm runoff H.G.	Baseflow	Total storm H.G.
0	0	0	15	15
2	45	104	15	119
4	105	242	15	257
6	131	301	15	316
8	95	219	15	234
10	73	168	15	183
12	57	131	15	146
14	43	99	15	114
16	33	76	15	91
18	25	58	15	73
20	17	39	15	54
22	11	25	15	40
24	7	16	15	31
26	3	7	15	22
28	0	0	15	15

It is advisable to identify several storms of approximately t-hours duration, derive the unit hydrograph for each storm, and develop an average t-hour unit hydrograph. As a rule, storm durations of + or –25% of the nominal duration are acceptable. Once the t-hour unit hydrograph is derived it can be used to estimate hydrographs for any storm with a duration of approximately t hours.

11.6.1 *Alternate duration unit hydrographs*

A t-hour duration unit hydrograph is derived for a t-hour duration storm. The question then is, 'what about storms of other durations?' There are basically two ways to handle this question. You can develop a separate unit hydrograph for each storm duration following the procedure above. In practice this means developing unit hydrographs for all storm durations common for the basin. Another approach is to derive alternate duration unit hydrographs by either adding multiple unit hydrographs together, or using an S-curve approach.

11.6.1.1 *Adding multiple unit hydrographs*

If the alternate duration t' is an integer multiple of the original duration t, that is if $(t'/t) = n$, where n is an integer, you can add together n t-hour unit hydrographs that are lagged t hours with respect to the each other, and then adjust the total runoff volume to equal 1 unit. This approach derives unit hydrographs of durations that are greater than the initial duration. Example 11.9 demonstrates the procedure.

Example 11.9

In this example we derive the $t' = 4$-hour unit hydrograph from an original $t = 2$-hour unit hydrograph. The alternate duration is an integer multiple of the original duration (4/2)=2. Table 11.18 shows the calculations and Figure 11.19 a graphical representation of the derivation. When two 2-hour unit hydrographs are lagged and added you have a hydrograph of 2 inches of runoff in 4 hours. This 4-hour hydrograph is not a unit hydrograph. Divide the 4-hour hydrograph ordinates by 2 to get the 4-hour unit hydrograph. The 4-hour unit hydrograph has a longer time to the peak discharge, a lower peak discharge, and a longer time base T_b.

Table 11.18. Conversion of a 2-hour unit hydrograph to a 4-hour unit hydrograph.

1 Time	2 t-hr U.H.	3 t-hr U.H. lagged t hrs	4 columns 2 + 3	5 t'-hr U.H. column 4 × (t/t')
0	0		0	0
1	200		200	100
2	400	0	400	200
3	600	200	800	400
4	500	400	900	450
5	400	600	1000	500
6	300	500	800	400
7	200	400	600	300
8	100	300	400	200
9	0	200	200	100
10		100	100	50
11		0	0	0

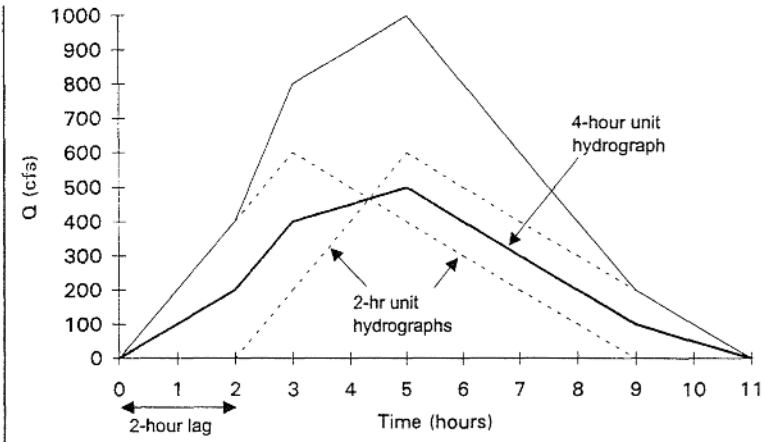

Figure 11.19. Two 2-hour unit hydrographs (dashed line) are added to produce the 4-hour hydrograph. The 4-hour hydrograph ordinates are divided by 2 to get the 4-hour unit hydrograph.

11.6.1.2 *S-curve method*

The *S*-curve or *summation* curve provides a more flexible method for deriving unit hydrographs of alternate durations. It can be used to derive longer or shorter durations, and the durations do not have to be integer multiples. If you sum an infinite number of t-hour unit hydrographs that are lagged t hours with respect to each other, an *S*-curve is the result (Fig. 11.20). This is the same curve we saw in Figure 11.11. The *S*-curve is the hydrograph from an infinitely long rain generating runoff at the rate of $1/t$ units per hour. The equilibrium flow Q_e in English units (cfs) is $Q_e = (645.3\ A/t)$, where A is in square miles. Actually, only T_b/t runoff increments need be summed to generate an *S*-curve, where T_b is the time base of the hydrograph (Fig. 11.20). To develop the alternate duration t' unit hydrograph, take two *S*-curves and lag them t' hours with respect to each other. The area between the two *S*-curves equals the volume of runoff in t' hours. Adjust the ordinates by the ratio t/t' and you have the alternate duration unit hydrograph (see Example 11.10).

Example 11.8 showed that a unit hydrograph can be used to create the total flood hydrograph. We can now combine flood analysis procedures. For example, the SCS

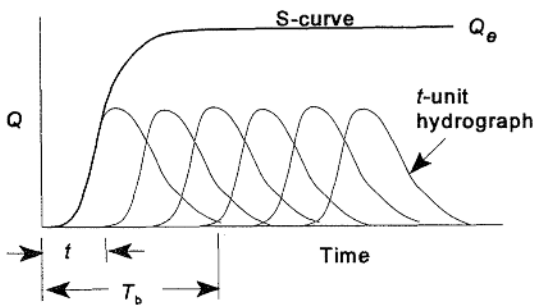

Figure 11.20. Development of the *S*-curve from the summation of n t-hour duration unit hydrographs each lagged t hours.

Example 11.10

Derive the $t' = 4$-hour unit hydrograph from an original $t = 2$-hour unit hydrograph. This is the same problem as in Example 11.9. The hydrographs are integer multiples but need not be for the *S*-curve method. Assume a basin area of 4.18 mi^2.

1. Develop the *S*-curve: Table 11.19 shows the complete derivation of the *S*-curve and the alternate duration unit hydrograph. Column 1 is the time intervals on which the runoff hydrograph observations are based. Column 2 are the 2-hour unit hydrograph ordinates. Column 3 is called the *S*-curve additions (Linsley et al. 1982). The values in column 3 are generated as follows. Starting with the first row, add column 2 and column 3. Place their sum in column 4. Now also place this sum in column 3 but lagged down by t hours. Continuing this procedure creates the *S*-curve in column 4.

2. Derive the alternate duration unit hydrograph: Now with the *S*-curve (column 4) we derive the alternate duration unit hydrograph. Lag the *S*-curve into column 5 by the alternate duration t'. The zero in row 5 of column 5 is the same zero from row 1 in column 4. Column 6 is column 5

Table 11.19. S-curve derivation of a 4-hour unit hydrograph from a 2-hour unit hydrograph.

1 Time (hrs)	2 t-hr U.H. (cfs)	3 *S*-curve additions (lag. col. 2 by t-hrs)	4 *S*-curve (col. 2 +3)	5 Lagged *S*-curve (lag. col. 4 by t')	6 Column (col. 4 – 5)	7 t'-hr U.H. col. 6 × (t/t')
0	0	0	0	0	0	0
1	200	0	200	0	200	100
2	400	0	400	0	400	200
3	600	200	800	0	800	400
4	500	400	900	0	900	450
5	400	800	1200	200	1000	500
6	300	900	1200	400	800	400
7	200	1200	1400	800	600	300
8	100	1200	1300	900	400	200
9	0	1400	1400	1200	200	100
10		1300	1300	1200	100	50
11		1400	1400	1400	0	0
Total	2700		$Q_e = 645.3(4.18)/2$			2700
			$Q_e = 1349$			

subtracted from column 4. We have now lagged and subtracted two *S*-curves. The last step is to adjust the values in column 6 by the ratio $t/t' = 2/4$. Multiply the values in column 6 by 0.5 and place the result in column 7. Column 7 is the alternate duration 4-hour unit hydrograph. Compare the values in column 7 with the values in Exercise 11.9.

Note that the *S*-curve began to oscillate between 1300 and 1400 cfs at hour 7. The *S*-curve can oscillate for different reasons. If we calculate the theoretical equilibrium flow we get, $Q_e = 645.3(4.18)/2 = 1349$ cfs. If we want we could substitute this value for oscillating values. As a check on your procedure, the sum of the ordinates in column 2 and column 7 should be the same, since they both represent 1 inch of runoff.

curve number method can be used to generate runoff depth and the unit hydrograph procedure to create the flood hydrograph. This is one way to use the unit hydrograph. Another way to use the unit hydrograph is *convolution* and is explained in Section 11.6.2.

11.6.2 *Unit hydrograph convolution*

Convolution is the process of generating the storm runoff hydrograph from multiperiod rainfall. The unit hydrograph ordinates are multiplied times the rainfall excess from each burst of rainfall, lagged, and then summed to produce the storm hydrograph. The general convolution equation is:

$$Q_n = P_1U_n + P_2U_{n-1} + P_3U_{n-2} + \ldots + P_{n-1}U_2 + P_nU_1 \tag{11.22}$$

or

$$Q_n = \sum_{i=1}^{n} P_iU_{n-i+1} \tag{11.23}$$

where Q_n is the storm runoff ordinate, P_i is the precipitation excess, and U_{n-i+1} is the unit hydrograph ordinate. The unit hydrograph duration and the precipitation measurement interval must be the same. The technique is illustrated in Example 11.11.

Example 11.11

This example demonstrates the convolution of rainfall excess into runoff using a unit hydrograph. The rainfall excess hyetograph and the ordinates for the 1-hour unit hydrograph are shown graphically in Figure 11.21.

Recall that precipitation data are pulse data, so the first value (0.25 in.) is the accumulated precipitation up through hour 1. Discharge data are sample data – discharge at an instant in time. The rainfall intervals match the unit hydrograph duration (1 hour).

In the same manner that we used the unit hydrograph in Example 11.8, calculate the storm runoff hydrograph from the first increment of excess precipitation ($P_1 = 0.25$ inch) by multiplying each unit hydrograph ordinate by 0.25 inch. Do the same for the increments P_2 and P_3; however, the runoff from P_2 is lagged 1 hour behind P_1, and P_3 is lagged 1 hour behind P_2. Table 11.20 and Figure 11.22 show the storm runoff hydrographs generated from each precipitation increment. For example, the first three discharges are:

$$Q_1 = P_1U_1 = 0.25(50) = 12.5$$
$$Q_2 = P_1U_2 + P_2U_1 = 0.25(100) + 0.50(50) = 50$$
$$Q_3 = P_1U_3 + P_2U_2 + P_3U_1 = 0.25(75) + 0.50(100) + 0.10(50) = 73.75$$

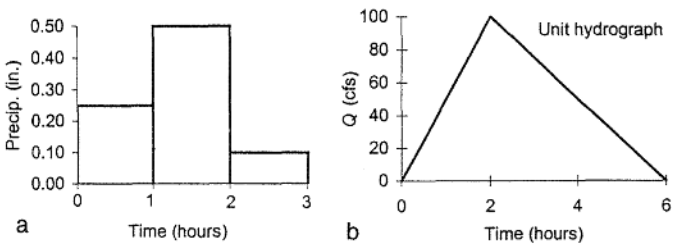

Figure 11.21. a) Rainfall excess hyetograph, and b) 1-hour unit hydrograph.

Table 11.20. Convolution of precipitation into runoff

Unit hydrograph ordinates (U)	P_1 0.25	P_2 0.50	P_3 0.10	Q
0	0.00			0.00
50	12.50	0.00		12.50

Table 11.20. Continued.

Unit hydrograph	P1 0.25	P2 0.50	P3 0.10	Q
100	25.00	25.00	0.00	50.00
75	18.75	50.00	5.00	73.75
50	12.50	37.50	10.00	60.00
25	6.25	25.00	7.50	38.75
0	0.00	12.50	5.00	17.50
		0.0	2.50	2.50
			0.00	0.00

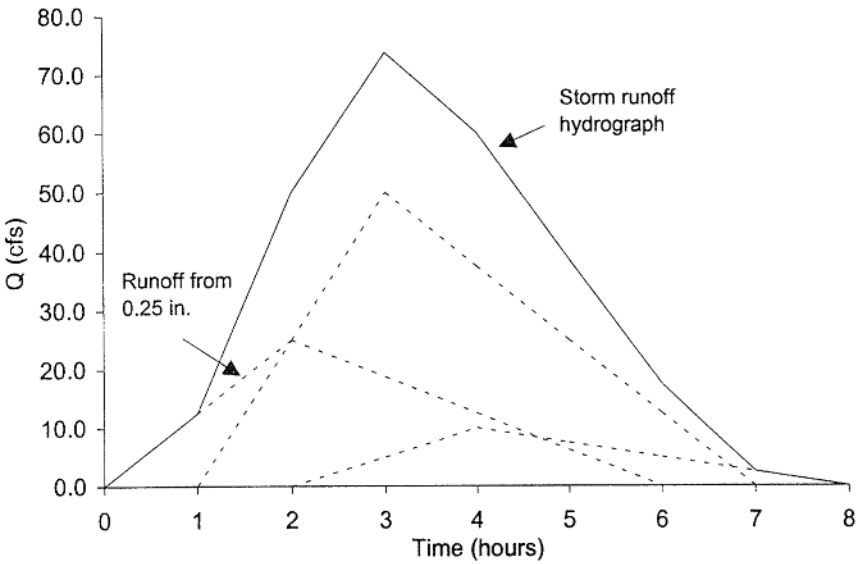

Figure 11.22. Convolution of increments excess precipitation into increments of runoff and the storm runoff hydrograph.

11.7 SYNTHETIC UNIT HYDROGRAPHS

The unit hydrograph is one of the most popular methods for flood analysis but requires streamflow data. Since most streams do not have records, researchers have devised procedures for developing synthetic unit hydrographs. The procedure is to determine three characteristics of the synthetic unit hydrograph – the time to peak t_p, the peak flow Q_{pk} and the time base T_b. The time to peak is defined as the time from the center of mass of precipitation to the hydrograph peak (Fig. 11.23). With these three elements a synthetic unit hydrograph can be sketched and the shape of the hydrograph is refined until the area under the curve equals 1 unit of runoff. Two widely

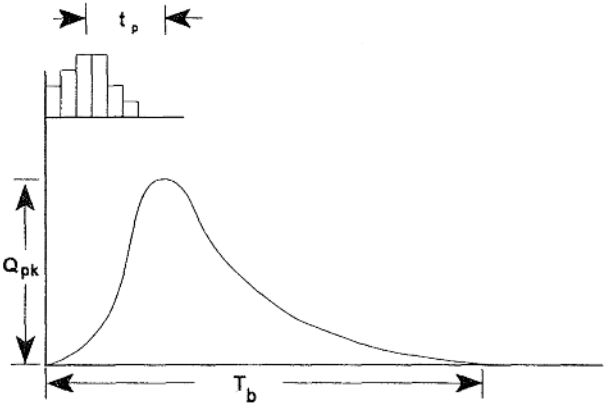

Figure 11.23. Component elements of a unit hydrograph. The time to peak t_p is the time from the center of mass of precipitation to the hydrograph peak.

used procedures are the SCS's triangular unit hydrograph and Snyder's synthetic unit hydrograph.

11.7.1 *SCS triangular synthetic unit hydrograph*

The SCS method is most appropriate for basins less than 100 mi^2. The SCS procedure starts with the assumption that a hydrograph can be approximated as a triangle as in Figure 11.24. The total runoff R is equal to the area under the hydrograph, or from the formula for the area of a triangle:

$$R = (R_1 + R_2) = \left(\frac{Q_{pk} T_1}{2} + \frac{Q_{pk} T_2}{2} \right) \tag{11.24}$$

Runoff R (inches) has two unknowns, T_1 and T_2. From experiments on small agricultural watersheds it has been found that $T_2 \approx 1.67T_1$. Further empirical study has also determined a relationship between the time to peak and the time of concentration as $t_p = 0.6t_c$. From Figure 11.24 $T_1 = (0.5t + t_p)$. Substituting these empirical relationships, solving for Q_{pk}, and converting runoff from inches to cfs yields:

$$Q_{pk} = \frac{484AR}{0.5t + 0.6t_c} \tag{11.25}$$

where Q_{pk} is in cfs, A is basin area in square miles, and storm duration t and time of concentration t_c are in hours. Notice that for the unit hydrograph R = 1. The other two elements required for the synthetic unit hydrograph are:

$$T_1 = 0.5t + 0.6t_c \tag{11.26}$$

$$T_b = 1.34t + 1.6t_c \tag{11.27}$$

Equations (11.25)-(11.27) define the three elements of the triangular unit hydrograph.

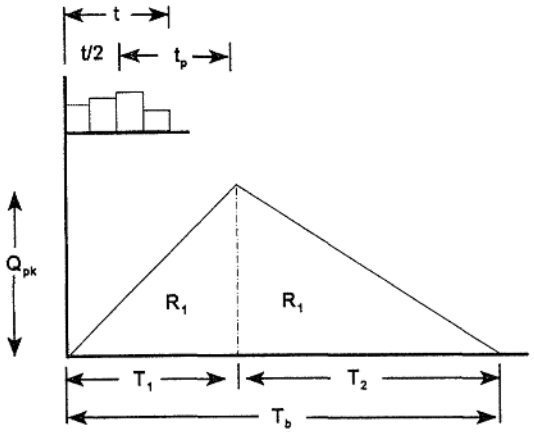

Figure 11.24. SCS triangular unit hydrograph where t is the duration of the storm, T_b is the time base of the unit hydrograph, t_p is the time to peak, Q_{pk} is the peak flow, and R is the volume of storm runoff (inches).

Example 11.12

Construct a 3/4-hour triangular unit hydrograph for a 6 mi^2 basin having a time of concentration t_c = 1 hour.

From Equation (11.25), the peak discharge is:

$$Q_{pk} = \frac{484 \times 6 \times 1.0}{0.5 \times 0.75 + 0.6 \times 1.0} = 2{,}978 \text{ cfs}$$

From Equation (11.26):

$$T_1 = (0.5 \times 0.75) + (0.6 \times 1.0) = 0.975 \text{ hrs}$$

And finally the time base from Equation (11.27):

$$T_b = (1.34 \times 0.75) + (1.6 \times 1.0) = 2.6 \text{ hrs}$$

The graph of the triangular unit hydrograph is shown as Figure 11.25.

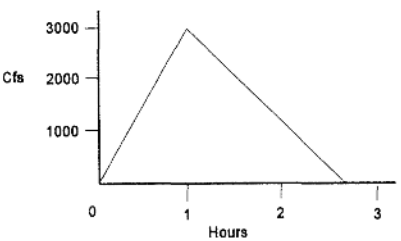

Figure 11.25. 3/4-hour SCS triangular unit hydrograph.

11.7.2 *Snyder's synthetic unit hydrograph*

Snyder (1938) developed a synthetic unit hydrograph procedure based on physiographic data from Appalachian watersheds ranging from 10 to 10,000 mi^2. The equation for the time to peak is:

$$t_p = C_t \left(L_w L_c \right)^{0.3} \tag{11.28}$$

where t_p is in hours, L_w and L_c were defined in Chapter 10 and are measured in miles, and C_t is a coefficient ranging from 1.8 to 2.2 depending upon channel slope. Steeper slopes have lower C_t values. Values for C_t outside of the Appalachian region have varied from less than 1 to as high as 10. The formula for peak discharge is:

$$Q_{pk} = \frac{640\, C_p A}{t_p} \tag{11.29}$$

where Q_{pk} is in cfs, A is basin area in square miles, and the coefficient C_p varies from 0.56 to 0.69. The C_p coefficient is small when C_t is large and vice versa. The C_p coefficient can be combined with the conversion constant (640) and Equation (11.29) rewritten as:

$$Q_{pk} = \frac{C_p A}{t_p} \tag{11.30}$$

where C_p varies from 358 to 441.

The last element defining the synthetic unit hydrograph is the time base T_b. Snyder's equation for the time base is:

$$T_b = (72 + 3t_p) \tag{11.31}$$

where T_b is in hours. Equation (11.31) is acceptable for large basins where the time base is measured in days, but not small basins where the time base is measure in hours. An alternative equation for small basins was developed by Taylor & Schwartz (1952):

$$T_b = 5(t_p + 0.5t) \tag{11.32}$$

However, for small basins it may be better to use the SCS triangular unit hydrograph. Snyder's synthetic unit hydrograph procedure assumes a 'standard duration storm' which Snyder defined as:

$$t = 0.18t_p \tag{11.33}$$

where t is in hours. For any alternate duration (t') different from the standard duration an alternate time to peak is calculated using:

$$t'_p = t_p + 0.25(t' - t) \tag{11.34}$$

This alternate time to peak is used to calculate Q_{pk} (Eq. 11.30) and T_b (Eqs 11.31 or 11.32). Use of the Snyder unit hydrograph depends upon determining representative values for the coefficients C_t and C_p. These can be determined by solving Equations (11.28) and (11.30) using data from gaged basins in the same region. Based on data from 20 basins in the North and Middle Atlantic states Taylor & Schwartz (1952) found $C_t = 0.6\sqrt{S}$ where S is basin slope. When graphing the synthetic unit hydrograph recall that the area under the curve is a unit volume of runoff. Two equations from the US army Corps of Engineers (1959) provide guidance in sketching the synthetic unit hydrograph:

$$W_{75} = \frac{440A}{Q_{pk}^{1.08}} \tag{11.35}$$

$$W_{50} = \frac{770A}{Q_{pk}^{1.08}} \tag{11.36}$$

where W_{50} and W_{75} represent the hydrograph's width (hours) at 50% and 75% of the peak discharge, respectively, A is basin area (mi^2), and Q_{pk} is in cfs. Figure 11.26 is a sketch of a synthetic unit hydrograph.

11.7.3 *Variations on Snyder's method*

Numerous empirical studies have developed relationships between t_p and basin geometry for synthetic unit hydrographs. The general form of the regression relationship is:

$$t_p = a\left(\frac{L_w L_c}{\sqrt{S}}\right)^b \tag{11.37}$$

where a and b are empirically determined and S is watershed slope (see Table 11.21).

And an alternative formula for peak discharge is:

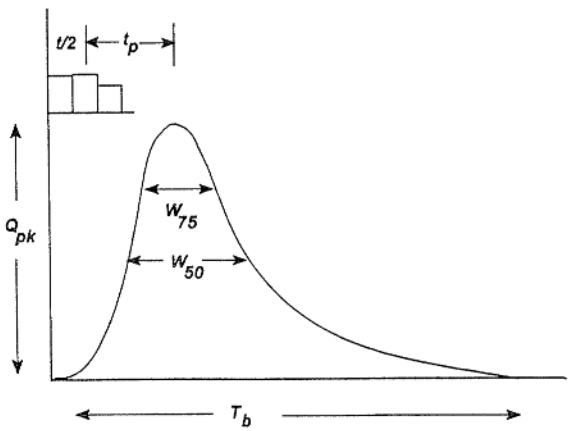

Figure 11.26. A sketch defining the elements of a synthetic unit hydrograph and the runoff-generating hyetograph.

Table 11.21. Empirically determined values for the coefficient a and exponent b in Equation (11.37) (source: Sheaffer et al. 1982).

Location	English units		Metric units	
	a	b	a	b
Tulsa, Oklahoma[1]				
Rural basins	1.42	0.39	0.1842	0.39

Table 11.21. Continued.

Location	English units		Metric units	
	a	*b*	*a*	*b*
Urban basins:				
– 50% urbanized	0.92	0.39	0.1193	0.39
– 100% urbanized	0.59	0.39	0.0765	0.39
Southern California[2]				
Mountains	1.20	0.38	0.1642	0.38
Foothills	0.72	0.38	0.0985	0.38

[1]US Army Corps of Engineers (1979). [2]RCFCWCD (1963). English units: S = ft mi^{-1}, L_w = mi, L_c = mi. Metric units: S = m m^{-1}, L_w = km, L_c = km.

$$Q_{pk} = cAt_p^{-0.92} \tag{11.38}$$

where Q_{pk} = cfs (cms), c = 380 (4.137), and A = mi^2 (km^2).

11.8 FLOW ROUTING

The beginning of the chapter qualitatively described how hydrographs suffer a reduction in peak and a lengthening of the time base due to storage as the flood wave passes through a reservoir or a channel reach (Fig. 11.5). Flow routing procedures quantitatively determine a downstream (output) hydrograph given an upstream (input) hydrograph. Two general classifications of flow routing are *hydrologic* routing and *hydraulic* routing. Hydrologic routing is the simpler of the two and calculates the downstream hydrograph as a function of time. Hydraulic routing is more complex with the water routed through a channel as a function of both time and space. Spatial changes in variables that effect the hydrograph are variations in channel shape, roughness and depth. In the next sections we examine only the simpler hydrologic routing.

11.8.1 *Reservoir routing*

Hydrologic routing of a flood wave through a reservoir is referred to as level-pool routing when it is assumed that the surface of the reservoir pool is horizontal. This is most likely true in deep, wide reservoirs. One method of level-pool routing is the 'storage-indication' or 'Puls' method. Assuming that the outflow from the reservoir is through an uncontrolled spillway, that is no human intervention, outflow is a function of the height of the water level above the spillway (Fig. 11.27). Calibrated equations for determining outflow for different spillway designs are available. For example, discharge over a rectangular, sharp-crested weir is:

$$Q = 3.33\,LH^{1.5} \tag{11.39}$$

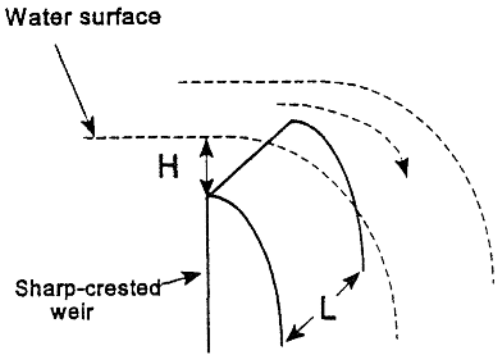

Figure 11.27. Water flow over a sharp-crested weir where H is the height of the water surface above the crest and L the length of the spillway.

where Q is discharge in cfs, L is the length (ft) of the rectangular outlet, and H is the height (ft) of the water surface above the bottom of the outlet (Dunne & Leopold 1978). The amount of water stored in a reservoir is also a function of the water surface elevation – the greater the pool elevation the greater the volume of water in storage. If outflow is a function of elevation, and storage is also a function of elevation, then outflow can be directly related to storage by a 'storage-outflow function.' The storage-indication method requires constructing a graphical relationship between the storage-outflow function and outflow. The storage-outflow function is based on the discrete continuity equation (Eq. 2.8) rewritten here as Equation (11.40). The only unknown in Equation (11.40) is Q_2, outflow at the end of the time period.

$$\Delta S = \left(S_2 - S_1\right) = \frac{\left(I_1 + I_2\right)}{2}\Delta t - \frac{\left(Q_1 + Q_2\right)}{2}\Delta t \tag{11.40}$$

For the storage indication method Equation (11.40) is rewritten as:

$$\left(\frac{S_2}{\Delta t} + \frac{Q_2}{2}\right) = \left(\frac{S_1}{\Delta t} - \frac{Q_1}{2}\right) + \left(\frac{I_1 + I_2}{2}\right) \tag{11.41}$$

The storage-outflow functions are the two terms on either side of the equal sign in Equation (11.41). Figure 11.28 shows the procedure for reservoir routing using the storage indication method. Start with the initial outflow Q_1 on the abscissa and read from the lower storage-outflow curve the corresponding ordinate value of $(S_1/\Delta t - Q_1/2)$. Calculate the average inflow $(I_1 + I_2)/2$ and solve for $(S_2/\Delta t + Q_2/2)$ using Equation (11.41). Now with $(S_2/\Delta t + Q_2/2)$ as the new ordinate value read across to the upper storage-outflow curve and down to the corresponding outflow Q_2 on the abscissa. This is the routed outflow at the end of the period. The procedure is repeated using Q_2 as Q_1 for the next period.

The availability of computer programs obviates the need for a detailed discussion of the graphical procedure. Box 1 is an example of a very simple BASIC program for reservoir routing using a modified storage indication method (Golding 1981). In running the program you are asked to input the name of the impoundment, the storage-outflow relationship for the impoundment and the time step. The program then routes the inflow hydrograph, which is input as DATA statements (lines 870–930). Initial

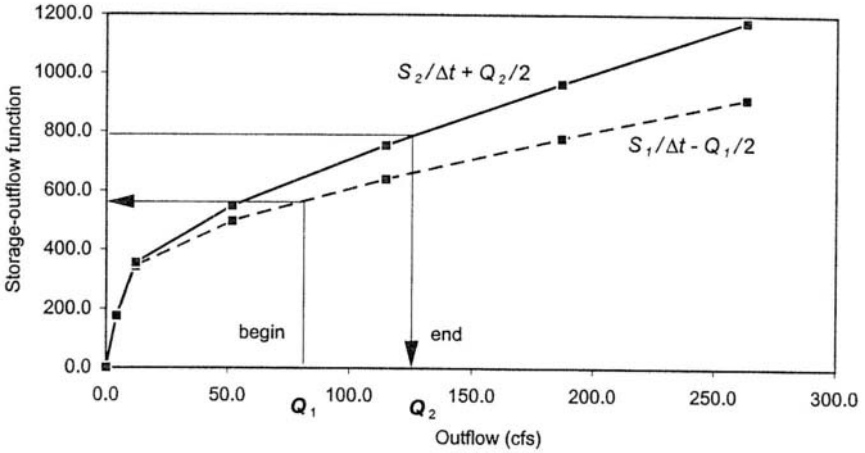

Figure 11.28. Reservoir routing by the storage indication method. See text for an explanation of the procedure.

BOX 1 RESERVOIR ROUTING PROGRAM

```
100 CLS:PRINT "FLOOD ROUTING PROGRAM"
110 REM PROGRAM WRITTEN BY B.L. GOLDING, 1981
120 PRINT "----------"
130 PRINT
140 INPUT "NAME OF IMPOUNDMENT";N$
160 DIM T1(60,2)
170 T2=0
180 PRINT
190 PRINT "SEPARATE DATA ITEMS REQUESTED WITH COMMAS "
200 PRINT "ENTER A VALUE OF -1, -1 TO END DATA ENTRY"
210 PRINT "ENTER  OUTFLOW (cfs),  STORAGE (ac-ft)"
220 INPUT Q,S1
230 T2=T2+1
240 T1(T2,1)=Q
250 T1(T2,2)=S1
260 IF Q<>-1 THEN 210
270 IF S1<>-1 THEN 210
280 T2=T2-1
290 PRINT
300 PRINT "INPUT TIME INCREMENT (hrs)
310 INPUT T
320 CLS
330 PRINT "OUTFLOW (cfs)   STORAGE (ac-ft)
340 PRINT "----------"
350 PRINT
360 FOR I=1 TO T2
370 PRINT USING "########.#"; T1(I,1), T1(I,2)
380 NEXT I
390 PRINT
400 FOR J=1 TO T2
410 T1(J,2)=T1(J,2)*12.1/T
420 T1(J,2)=T1(J,2)+T1(J,1)/2
430 NEXT J
440 PRINT
450 PRINT "OUTFLOW (cfs)   S/T+Q/2"
460 PRINT "----------"
470 PRINT
480 FOR R=1 TO T2
490 PRINT USING "########.#"; T1(R,1),T1(R,2)
500 NEXT R
510 T9=0
520 V1=0
530 I1=0
540 S6=0
550 Q=0
560 Q6=0
565 GOSUB 1050
570 PRINT
580 PRINT "T (hrs)   INFLOW (cfs)   OUTFLOW (cfs)"
590 PRINT "----------  ----------  ----------"
600 PRINT
610 READ I2
620 IF I2=-1 THEN 960
630 I3=(I1+I2)/2
640 R=S6+I3
650 S2=R-Q6
660 FOR U=1 TO T2
670 IF S2<T1(U,2) THEN 690
680 NEXT U
690 M=(T1(U,1)-T1(U-1,1))/(T1(U,2)-T1(U-1,2))
700 B=T1(U,1)-M*T1(U,2)
710 Q1=M*S2+B
720 I1=I2
730 Q3=Q1
740 Q6=Q1
750 S6=S2
760 V=I2-Q3
770 IF Q3>=I1 THEN 800
780 V1=V1+V
790 REM ROUND OFF
800 Q3=INT(Q3*10+0.5)/10
810 REM ROUND OFF
820 I2=INT(I2*10+0.5)/10
830 PRINT USING "########.#"; T9,I2,Q3
840 REM--INFLOW HYDROGRAPH IS CONTAINED IN THE DATA
850 REM--STATEMENTS BELOW.  CHANGE THESE STATEMENTS
860 REM--TO REFLECT YOUR DATA.
870 DATA 0,1.3,5.6,10.5,14.5
880 DATA 17.7,20.6,24,38.6
890 DATA 137.1,259.4,267
900 DATA 199.4,141.5,101
910 DATA 75.6,58.2,46.7,38.4
920 DATA 32.2,28.5,26,24.4
930 DATA 23.4,22.6,18,-1
940 T9=T9+T
950 GOTO 610
960 PRINT
970 V2=V1*T*(3600/43560)
980 REM ROUND OFF
990 V2=INT(V2*10+0.5)/10
1000 PRINT "VOLUME STORED =";
1005 PRINT USING "######.#"; V2;:PRINT "(ac-ft)"
1010 END
1050 PRINT:PRINT TAB(20)"<PRESS ANY KEY TO CONTINUE>"
1060 Q$=INKEY$
1070 IF Q$="" THEN 1060
1080 CLS
1090 RETURN
```

inflow (I_1), outflow (Q_1) and storage (S_1) are assumed to be zero. Golding (1981) describes the program's components in detail. Example 11.13 is a run of the program with the data provided by Golding (1981).

Example 11.13

This example demonstrates reservoir routing with the program in Box 1 using data from Brad Creek Reservoir given by Golding (1981, used by permission). The program produces the following output.

```
FLOOD ROUTING PROGRAM

NAME OF IMPOUNDMENT? BRAD CREEK RESERVOIR

NOTE: SEPARATE DATA ITEMS REQUESTED WITH COMMAS
NOTE: ENTER A VALUE OF -1, -1 TO END DATA ENTRY

ENTER OUTFLOW (cfs), STORAGE (ac-ft)? 0,0
ENTER OUTFLOW (cfs), STORAGE (ac-ft)? 4.24,14.4
ENTER OUTFLOW (cfs), STORAGE (ac-ft)? 12,28.8
ENTER OUTFLOW (cfs), STORAGE (ac-ft)? 51.71,43.2
ENTER OUTFLOW (cfs), STORAGE (ac-ft)? 114.67,57.6
ENTER OUTFLOW (cfs), STORAGE (ac-ft)? 186.81,72
ENTER OUTFLOW (cfs), STORAGE (ac-ft)? 263.19,86.4
ENTER OUTFLOW (cfs), STORAGE (ac-ft)? -1,-1

INPUT TIME INCREMENT (hrs)? 1
```

OUTFLOW (cfs)	STORAGE (ac-ft)
0.0	0.0
4.2	14.4
12.0	28.8
51.7	43.2
114.7	57.6
186.8	72.0
263.2	86.4

OUTFLOW (cfs)	S/T+Q/2
0.0	0.0
4.2	176.4
12.0	354.5
51.7	548.6
114.7	754.3
186.8	964.6
263.2	1177.0

T (hrs)	INFLOW (cfs)	OUTFLOW (cfs)
1.0	0.0	0.0
2.0	1.3	0.0
3.0	5.6	0.3
4.0	14.5	0.6
5.0	17.7	1.0
6.0	20.6	1.4
7.0	24.0	1.9
8.0	38.6	2.6
9.0	137.1	5.0
10.0	259.4	18.6
11.0	267.0	77.0
12.0	199.4	126.1
13.0	141.5	141.3
14.0	101.0	134.4
15.0	75.6	118.6
16.0	58.2	102.4
17.0	46.7	87.1
18.0	38.4	73.5

19.0	32.2	61.8
20.0	28.5	52.2
21.0	26.0	46.9
22.0	24.4	42.5
23.0	23.4	38.7
24.0	22.6	35.5
25.0	18.0	32.4

VOLUME STORED = 62.9 (ac–ft)

Figure 11.29 shows the inflow and routed outflow hydrographs from the program. As shown in Figure 1.4, storage increases as long as inflow exceeds outflow. The program calculates the maximum volume stored, which for this example is 62.9 ac–ft. The peak of the outflow hydrograph occurs on the recession limb of the inflow hydrograph, after which time storage decreases.

Figure 11.28 was created using the same Brad Creek Reservoir data. The beginning value Q_1 = 77 and the ending value Q_2 = 126 on Figure 11.28 correspond to the routed outflows at time intervals 11.0 and 12.0, respectively, from the computer program.

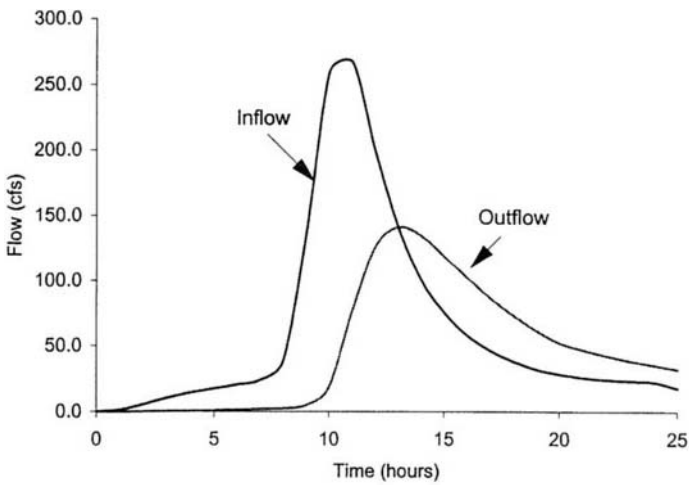

Figure 11.29. Inflow and routed outflow hydrographs for the reservoir routing example.

11.8.2 *Muskingum channel routing*

Routing a flood wave through a channel reach is more complex than level-pool reservoir routing. In reservoir routing storage and outflow are uniquely related. However, for a flood wave moving through a channel reach the slope of the water surface is not parallel to the channel bed (Fig. 11.30). On the rising limb the water-surface is steeper than the channel slope, but on the recession limb it is not as steep. This means that for the same outflow at say point A in Figure 11.30, the amount of water in storage is different on the rising limb and the falling limb because storage depends upon both the rate of inflow and the rate of outflow. This creates hysteresis in the relationship between storage and outflow; for a given outflow there is more water stored in the rising limb of the wave because inflow exceeds outflow than there is on the falling limb when outflow exceeds inflow. The Muskingum channel routing procedure was developed by McCarthy (1938) working for the Army Corps of Engi-

neers. The Muskingum method divides channel storage into *prism* storage and *wedge* storage (Fig. 11.31). Prism storage describes the steady-state discharge of water through the reach, i.e. when inflow is equal to outflow. Wedge storage accounts for the nonsteady effects of the flood wave. Wedge storage is positive on the rising limb and negative on the falling limb. Prism storage is defined as:

$$S_p = KQ \tag{11.42}$$

where S_p is prism storage (L^3), K is a time constant (T), and Q is outflow (L^3T^{-1}). Wedge storage depends on the relative magnitudes of inflow and outflow and is defined as:

$$S_w = Kx\left(I - Q\right) \tag{11.43}$$

Combining Equations (11.42) and (11.43) gives total storage as:

$$S = K\left[xI + \left(1 - x\right)Q\right] \tag{11.44}$$

Equation (11.44) says storage is linearly related to the weighted difference between inflow and outflow. The constant K is loosely interpreted as the travel time of the

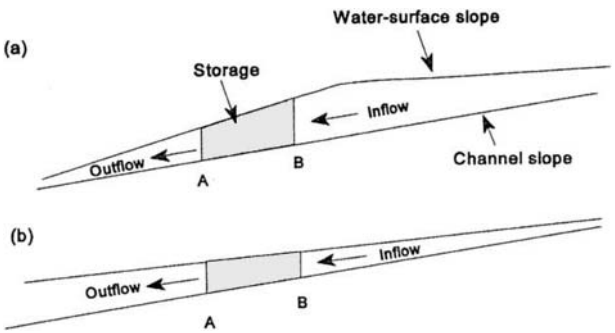

Figure 11.30. a) The water surface profile as the flood wave enters reach A-B, and b) The profile as the wave exits the reach. The discharge at point A is the same in both figures; however, channel storage is greater in *a* than in *b* because inflow exceeds outflow in the former whereas outflow exceeds inflow in the latter (after Dunne & Leopold 1978).

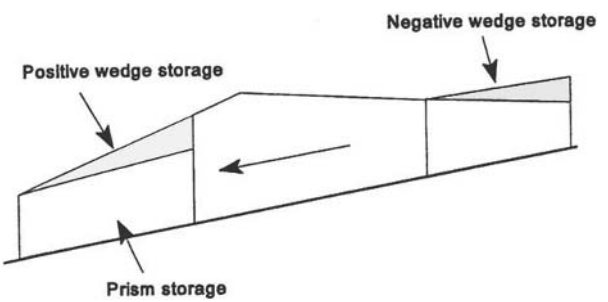

Figure 11.31. The concept of prism and wedge storage used in Muskingum channel routing to account for unsteady discharge accompanying a flood wave.

flood wave through the reach. Interpretation of the parameter x is more controversial but it controls the attenuation of the flood wave by weighting the relative influence of inflow and outflow on storage. Theoretically x can vary from ($0 \leq x \leq 1.0$), though some researchers suggest the more restricted range of ($0 \leq x \leq 0.5$). For $x = 0.5$, inflow and outflow have equal influence and there is no attenuation, the flood wave is simply translated through the reach. A value of $x = 0.0$ means inflow has no effect on storage and we have a pure reservoir effect where storage is a function of outflow alone. In most rivers x is between 0.1 and 0.3 indicating that both attenuation and translation occur in the channel. The Muskingum procedure requires determining x and K using measured inflow and outflow hydrographs. Once these parameters are determined any inflow hydrograph may be routed through the reach. The procedure for finding K and x is discussed in section 11.8.3.

In developing the Muskingum method the change in storage between two successive times steps is written:

$$S_2 - S_1 = K\left[x\left(I_2 - I_1\right) + (1-x)\left(Q_2 - Q_1\right)\right] \tag{11.45}$$

Combining Equation (11.45) with Equation (11.40) and solving for the unknown outflow Q_2 gives:

$$Q_2 = C_0 I_2 + C_1 I_1 + C_2 Q_1 \tag{11.46}$$

where

$$C_0 = -\frac{Kx - 0.5\Delta t}{C_3} \tag{11.47a}$$

$$C_1 = \frac{Kx + 0.5\Delta t}{C_3} \tag{11.47b}$$

$$C_2 = \frac{K - Kx - 0.5\Delta t}{C_3} \tag{11.47c}$$

$$C_3 = K - Kx + 0.5\Delta t \tag{11.47d}$$

Equation (11.46) is the Muskingum routing equation. As a check, $C_0 + C_1 + C_2 = 1.0$. It is commonly assumed that K and x are constant for the reach and for the range of discharges expected. Also, it is apparent that the coefficients C_0, C_1, and C_2 are appropriate only for the time step Δt. The choice of Δt is arbitrary but it should be much smaller than K. Local inflows and seepage losses can be accommodated by adding or subtracting the volumes from the outflow hydrograph.

11.8.3 *Determining K and x*

The procedure for determining the routing parameters is based on Equation (11.44). Values of storage S are plotted against $[xI + (1 - x)Q]$ for different values of x. Because of hysteresis the plot forms a loop. Figure 11.32 shows two hypothetical plots for different values of the parameter x. The objective is to select a value for x that

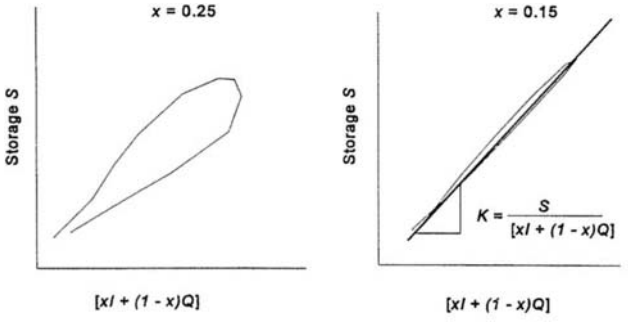

Figure 11.32. Hypothetical examples of how the hysteresis loop closes as the value of x is changed.

produces a loop closest to a single line. The value of K from rearranging Equation (11.44) is:

$$K = \frac{S}{[xI + (1-x)Q]} \tag{11.49}$$

K is the slope of the straight line drawn through the graph with the tightest loop.

This method for finding K and x is somewhat subjective and time consuming. Wu et al. (1985) developed an efficient procedure for determining optimal values for these parameters using a statistical t-test. As with reservoir routing the Muskingum method is easily programmed for a computer or implemented in a spreadsheet program. Example 11.14 demonstrates the Muskingum method and was generated in a spreadsheet program.

Example 11.14

The inflow and outflow data for this example were taken from Chow (1964). In Table 11.22 column 1 is the time step Δt. Since flows are measure in cfs, the time step is converted from 1 day into 86,400 seconds for subsequent calculations. Column 2 contains the inflow hydrograph ordinates, column 3 calculates the average inflow over the time interval, column 4 is the conversion of flow into volume by multiplying the average inflow (column 3) by 86400 seconds. Column 5 is the cumulative inflow. Columns 6-9 are the same steps applied to the outflow hydrograph. Column 10 is total storage, which equals cumulative inflow (column 5) minus cumulative outflow (column 9).

Table 11.23 shows the calculation of the weighted inflow-outflow function for $x = 0.11$ using inflows and outflows from Table 11.22. To find K plot the weighted inflow-outflow function against storage as shown in Figure 11.33. The slope of the straight line fitted to the loop is K and is estimated to be:

$$K = \frac{19{,}800{,}000 \text{ ft}^3}{100 \text{ ft}^3\text{s}^{-1}} = 198{,}000 \text{ s} = 2.29 \text{ days}$$

For the same data Chow (1964) obtained $x = 0.15$, $K = 2.3$ days, while Wu et al. (1985) obtained $x = 0.08$ and $K = 2.24$ days using their optimization procedure.

The values of x and K are substituted into Equations (11.47a)-(11.47d):

$$C_0 = -\frac{198{,}000(0.11) - 0.5(86400)}{198{,}000 - 198{,}000(0.11) + 0.5(86400)} = 0.098$$

Table 11.22. Calculation of storage using Equation (11.40).

1 Time (days)	2 I (cfs)	3 $(I_1 + I_2)/2$ (cfs)	4 $\Delta t(I_1 + I_2)/2$ (cu. ft.)	5 $\Sigma[\Delta t(I_1 + I_2)/2]$ (cu. ft.)	6 Q (cfs)	7 $(Q_1 + Q_2)/2$ (cfs)	8 $\Delta t(Q_1 + Q_2)/2$ (cu. ft.)	9 $\Sigma[\Delta t(Q_1 + Q_2)/2]$ (cu. ft.)	10 S (cu. ft.)
1	93			0	85			0	0
2	137	115	9936000	9936000	93	89	7689600	7689600	2246400
3	208	173	14904000	24840000	118	106	9115200	16804800	8035200
4	320	264	22809600	47649600	165	142	12225600	29030400	18619200
5	442	381	32918400	80568000	239	202	17452800	46483200	34084800
6	540	491	42422400	122990400	331	285	24624000	71107200	51883200
7	630	585	50544000	173534400	425	378	32659200	103766400	69768000
8	678	654	56505600	230040000	512	469	40478400	144244800	85795200
9	691	685	59140800	289180800	580	546	47174400	191419200	97761600
10	692	692	59745600	348926400	624	602	52012800	243432000	105494400
11	684	688	59443200	408369600	651	638	55080000	298512000	109857600
12	671	678	58536000	466905600	663	657	56764800	355276800	111628800
13	657	664	57369600	524275200	668	666	57499200	412776000	111499200
14	638	648	55944000	580219200	662	665	57456000	470232000	109987200
15	609	624	53870400	634089600	649	656	56635200	526867200	107222400
16	577	593	51235200	685324800	630	640	55252800	582120000	103204800
17	534	556	47995200	733320000	604	617	53308800	635428800	97891200
18	484	509	43977600	777297600	571	588	50760000	686188800	91108800
19	426	455	39312000	816609600	530	551	47563200	733752000	82857600
20	366	396	34214400	850824000	482	506	43718400	777470400	73353600
21	298	332	28684800	879508800	430	456	39398400	816868800	62640000
22	235	267	23025600	902534400	371	401	34603200	851472000	51062400
23	183	209	18057600	920592000	314	343	29592000	881064000	39528000

Table 11.23. Calculation of the weighted inflow-outflow function for $x = 0.11$.

Time (day)	xI (cfs)	$(1-x)Q$ (cfs)	$xI + (1-x)Q$ (cfs)	S (cu.ft)
1	10	76	86	0
2	15	83	98	2246400
3	23	105	128	8035200
4	35	147	182	18619200
5	49	213	261	34084800
6	59	295	354	51883200
7	69	378	448	69768000
8	75	456	530	85795200
9	76	516	592	97761600
10	76	555	631	105494400
11	75	579	655	109857600
12	74	590	664	111628800
13	72	595	667	111499200
14	70	589	659	109987200
15	67	578	645	107222400
16	63	561	624	103204800
17	59	538	596	97891200
18	53	508	561	91108800
19	47	472	519	82857600
20	40	429	469	73353600
21	33	383	415	62640000
22	26	330	356	51062400
23	20	279	300	39528000

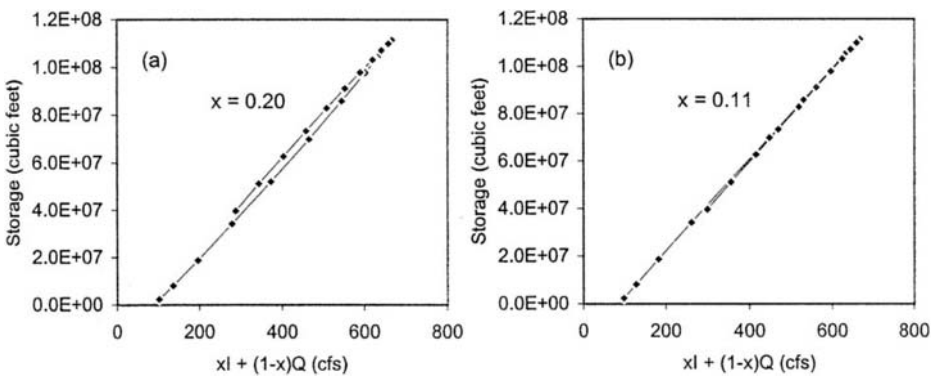

Figure 11.33. Plot of storage versus the weighted inflow-outflow function. Graph *a* is for $x = 0.20$ and graph *b* is for $x = 0.11$. Graph *b* is the tighter loop and yields a slope of $K = 198{,}000$ seconds (2.29 days).

$$C_1 = \frac{198{,}000(0.11) + 0.5(86400)}{198{,}000 - 198{,}000(0.11) + 0.5(86400)} = 0.296$$

$$C_2 = \frac{198{,}000 - 198{,}000(0.11) - 0.5(86400)}{198{,}000 - 198{,}000(0.11) + 0.5(86400)} = 0.606$$

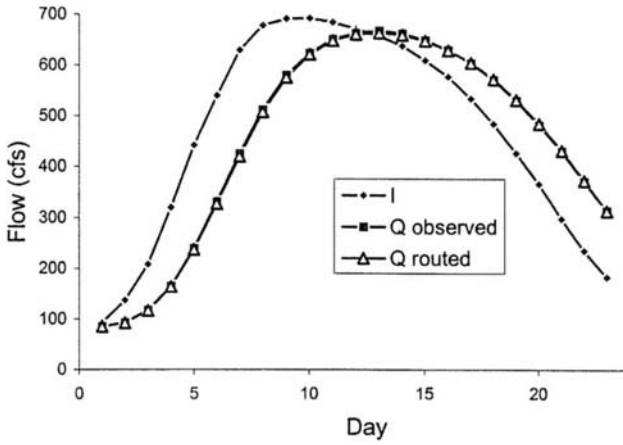

Figure 11.34. Observed inflow and outflow, and routed outflow.

Any inflow hydrograph can now be routed using Equation (11.46) as:

$$Q_2 = 0.098(I_2) + 0.296(I_1) + 0.606(Q_1)$$

For example, the routed outflow on day 2 is $Q_2 = 0.098(137) + 0.296(93) + 0.606(85) = 92.5$ cfs, which is close to the observed value of 93 cfs. Figure 11.34 shows the observed inflow and outflow hydrographs and the entire routed outflow hydrograph for comparison.

11.9 STREAMFLOW MEASUREMENT

River *stage* is the elevation of the stream surface above some arbitrary datum. The datum may be sea level but more often is an elevation just below the point of zero discharge. River stage is measured with *staff gages, recording gages, or crest-stage gages*. A staff gage is a scale mounted vertically on a pier, piling, or other structure extending into the channel. This is the cheapest method for measuring stage but requires an observer manually make the observation of stage during the period of runoff. Recording gages use an intake tube to admit water into a stilling well that suppresses water surface fluctuations from turbulence and waves. The water level in the stilling well is recorded on a continuous strip chart, punched tape, or more recently as a real-time signal sent via satellite to a data storage and retrieval center. Real-time monitoring of river stage has become an integral part of flood warning systems in certain communities that are susceptible to flash flooding. Crest stage gages record only the hydrograph peak. The US Geological Survey uses a tube containing ground cork. The cork adheres to the side of the tube marking the highest water elevation reached in the tube.

Stream velocity is measured with a current meter. Current meters may use conical cups rotating around a vertical axis (perpendicular to the flow) or propellers that rotate on an axis horizontal to the flow. The number of revolutions per second is converted into an estimate of water velocity. Current meters are expensive and can cost hundreds of dollars. For *very* general estimates of stream velocity a floating object can be timed as it travels through a measured length of channel.

Stream velocity (V) varies throughout the channel. On a straight channel it is generally lowest near the bed and banks due to friction (Fig. 11.35). The highest velocity tends to occur in the center of the channel at or near the surface. On a meandering channel the zone of maximum velocity migrates towards the outside of the meander. In longitudinal cross-section the idealized velocity profile is parabolic in shape (Fig. 11.36). It is recommended that the mean velocity in the vertical be calculated as the average of the velocity measured at two-tenths and eight-tenths the total depth (y) from the surface. Alternatively, the velocity at six-tenths the total depth is a good approximation of the vertically integrated mean velocity. The US Geological Survey has detailed procedures for making measurements of streamflow stage and discharge (Rantz 1982).

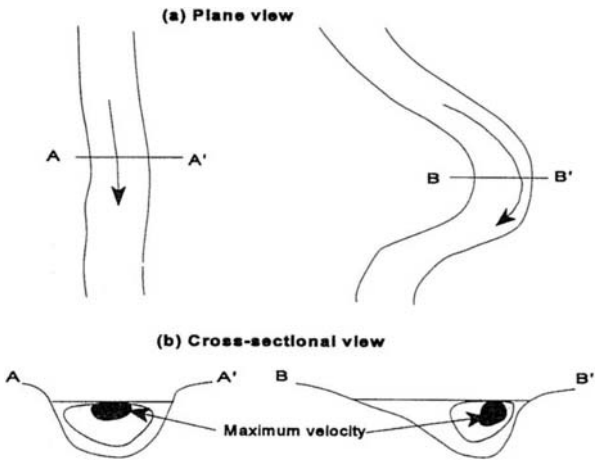

Figure 11.35. The illustrative figures in (a) are plane views of a straight channel and a meandering channel. The figures in (b) are cross-sectional views of the channels showing the distribution of water velocity. The highest velocity zones are shaded the darkest.

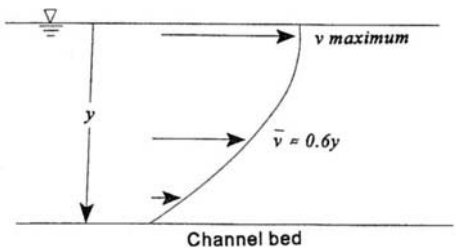

Figure 11.36. Idealized longitudinal cross-section showing velocity distribution in a stream. The maximum velocity occurs at or near the surface, while velocity decreases to zero at the bed. The velocity at 0.6 times the depth (y) approximates the mean velocity in the vertical. Depth is measured from the surface downward.

11.9.1 *Stage-discharge relations*

Routine measurements of streamflow are obtained through the use *rating curves*. A rating curve is a relationship between river stage and river discharge. Rating curves are developed through the simultaneous measurement of stage and discharge. Once the rating curve is defined, discharge is determined directly from measurements of stage. This obviously makes estimating discharge much easier. For most rivers a simple curve of stage versus discharge is satisfactory (Linsley et al. 1982). The best location for establishing a rating curve is where the channel cross-section is stable and not subject to variation in shape during high flows or affected by backwater. On streams with alluvial channels floods can scour the bed and banks changing the rating curve. Near tributary junctions high flows on one channel my cause backwater effects on the other. Gaging stations should be located far enough upstream to be beyond the influence of backwater. Linsley et al. (1982) discuss methods for correcting for these conditions of 'shifting control'. Figure 11.37 is an example of a rating curve for Swarr Run.

SUMMARY

This chapter has introduced some basic concepts and techniques used to analyze streamflows and flood discharges. Some of the techniques provide only limited information on runoff volume or peak discharge, while others provide additional information on flood frequency or hydrograph shape. These are important topics for water management. Society continues occupy floodplains and to suffer losses from riverine flooding. In the first half of the 1990s monetary damages from floods have run into the tens of billions of dollars, not to mention loss of life. Virtually every activity from agriculture to residential home construction modifies the hydrologic cycle

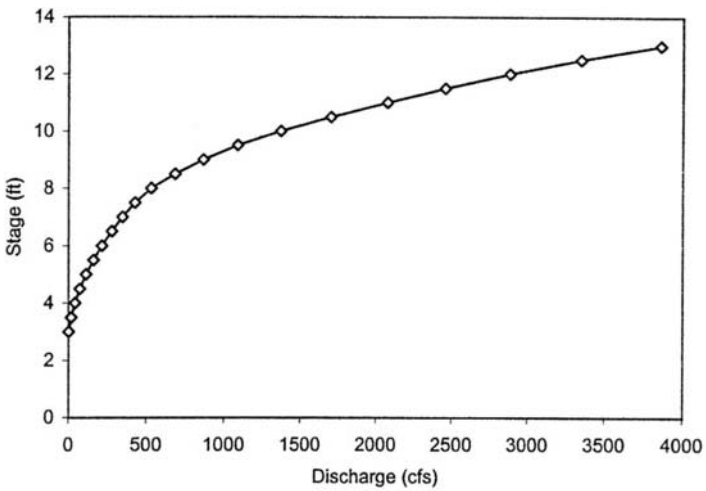

Figure 11.37. Rating curve for Swarr Run.

in some manner. By changing infiltration, runoff increases, and groundwater recharge is reduced. The result may be an increased downstream flood risk or the long-term impairment of the groundwater supply. As we move into the next century we must be more conscious of how our activities alter the natural environment. This chapter has focused on streamflow and flooding. Chapter 12 examines the opposite phenomena – drought.

PROBLEMS

11.1 Determine the runoff (in inches) from the 100-year, 6-hr storm in July occurring over a 120-acre field in southern Lancaster County, PA. The previous 5 days had 1.6 inches of rain. The field is planted to corn in straight rows and the hydrologic condition is poor. The soil is moderately well drained with average infiltration capacity. What is the volume of runoff in acre-feet? Clearly state all parameter values you use.

11.2 If a developer purchases 45 acres of the field in problem 1 and constructs a mixed development consisting of a 12-acre shopping center, an 18-acre residential subdivision ($^1/_4$ acre lots) and 15 acres of paved roads with curbs and sewers. Calculate the runoff from the entire field assuming the same conditions as in Problem 11.1. What was the increased volume (acre-feet) of runoff due to urbanization? If the county requires the developer to store this excess runoff in a detention basin, how deep would the basin have to be if the developer only has 25,000 ft^2 of space on which to build the basin?

11.3. Calculate the peak runoff from the 5-year storm for a basin near Oklahoma City, OK with the following characteristics. (Example 4.7 demonstrated how to interpolate IDF precipitation values.)
Basin area – 342 acres
Basin length – 4040 ft
Basin relief – 21 ft
Land use
– Single family residential ($^1/_8$ acre lots) – 239.4 acres
– Park in fair condition – 17.1 acres
– Native pasture in fair condition on loamy soil – 85.5 acres

11.4 The following data are the annual maximum discharges (m^3s^{-1}) for the Derwent River at Long-bridge Weir. Use the log-Pearson type III method and the Gumbel I method to fill in the tables below. Use natural logs.

269 258 228 180 167 144 143 143 142 126 124 117 115 110 109 108 106 102 102 99 98 95 87 85 81 77 68

The adjusted skewness of the natural logs is $C_s = 1.069$.

a) log-Pearson III

Return period T	Probability of exceedence	Frequency factor k	Q_T
100			
50			
25			
10			

b) Gumbel I

Return period T	Probability of exceedence	Frequency factor k	Q_T
100			
50			
25			
10			

c) Use the Gumbel I CDF to estimate:
$P(Q > 100\ m^3\ s^{-1})$ = _____, T = _____
$P(Q > 250\ m^3\ s^{-1})$ = _____, T = _____

11.5 Given below are the ranked annual maximum discharges ($m^3\ s^{-1}$) for the Derwent River at Longbridge Weir. Plot the data on arithmetic Gumbel paper (below) using the Gringorten plotting position formula to assign sample frequency estimates. Draw the theoretical (Gumbel I) flood frequency curve.

269 258 228 180 167 144 143 143 142 126 124 117 115 110 109 108 106 102 102 99 98 95 87 85 81 77 68

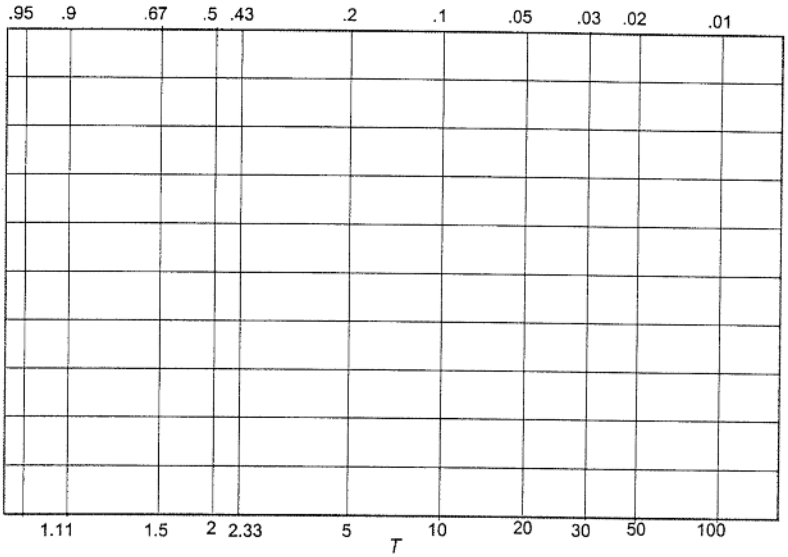

a) Estimate Q_{10} and Q_{100}.
Q_{10} _____ $m^3\ s^{-1}$
Q_{100} _____ $m^3\ s^{-1}$
b) Place 90% confidence limits around the two discharges.
Q_{10} upper _____ $m^3\ s^{-1}$
Q_{10} lower _____ $m^3\ s^{-1}$
Q_{100} upper _____ $m^3\ s^{-1}$
Q_{100} lower _____ $m^3\ s^{-1}$

11.6 This exercise has two parts. First you use the World Wide Web (WWW) to retrieve annual maximum series discharge data from the USGS website. Second, you'll do a spreadsheet-based flood frequency analysis with the data.

PART 1: Downloading data from the WWW
Log onto the WWW and go to the USGS homepage. The address (URL) for the USGS homepage is: http:// www.water.usgs.gov.
The formats of the web pages change over time so I'll only describe where you want to go, rather than what you might see on the pages.
Click on the **Water Data** hypertext.

This should bring up a map of the US with a listing of the states below.
Click on either the **state** of Pennsylvania (on the map), or **PA** in the name listing at the bottom of the page.
Click on the **Counties** hypertext.
Click on **Lancaster County**.

On the screen should be a list of the stream gages in Lancaster County. You want gage 01576500, the Conestoga River at Lancaster, PA. There are four types of data available for the gage:

1. A map of the region surrounding the gage
2. Historical Streamflow Daily Values
3. Current Conditions Data
4. Peak Flow Data.

You can investigate the different data sites later, but for this exercise click on the **Peak Flow Data**.

You now decide what dates to retrieve, what data to retrieve, and data output format.
Dates to retireve: Retrieve the record of peak flows from1929 to 1993. Retrieve them by water year.
Data to retrieve: Retrieve only the annual peaks. (This is the annual maximum series. All peaks above a base is a partial duration series.)
Output format: Tab-delimited text data file, YYYY.MM.DD format.
Click on **Retrieve**. You should now see the data as a text page. The top of the page provides gage-related information such as station name, station number, latitude and longitude etc. The actual data are listed below, ranked by year.
Finally, using the menu bar at the top of your window click on **File/Save** and save the data to your disk.

PART 2: Flood frequency analysis
Once you have the data saved on disk, open the text file and copy just the data (year and discharge) into a new spreadsheet. (I assume you're using the EXCEL® spreadsheet program). Now do a flood frequency analysis two ways. First, do a sample frequency analysis, and, second, a frequency analysis using the log-Pearson Type III method.

Sample frequency analysis
First set up your spreadsheet. At the top of the spreadsheet enter your name and the station data as shown in the box below.

Name _____	
Station name _____	Station (gage) number _____
Latitude _____	Longitude _____
State _____ Hydrologic unit _____	Drainage area _____
Length of record _____ years	

Now create a sample frequency analysis table similar to Table 11.10 in the text. Be sure when you rank the discharge data you carry the year along with it. If your ranking is correct the largest discharge is 50,300 cfs which occurred on June 23, 1972. This flood-of-record was caused by Hurricane Agnes. This discharge is nearly twice the second-ranked discharge (25,300 cfs). Using the WRC's high-outlier analysis (see text) the 1972 discharge should be classified a high outlier and excluded from the analysis. Eliminate this value from your table and adjust the record length (n). Use the spreadsheets's built-in functions to calculate the mean, standard deviation, and skewness.

Log-Pearson III frequency analysis

If you compare the sample skewness with the generalized skewness value on the map (Fig. 11.15) you'll see a noticeable difference. For this exercise use the map skewness value of 0.60.

Calculate Q_{10}, Q_{25}, Q_{50}, and Q_{100} using the log-Pearson III method. Use base 10 for the logs. Set up your four Q_T equations just like the examples in the book.

Finally, compare your sample frequency analysis discharges and the log-Pearson III discharges. A good way to compare them is by plotting the two sets of discharges (Q) versus return period (T). (Note you only need to plot the sample discharges which have return periods that are close to the log-Pearson III return periods).

11.7 Given below are the observed flows from a storm of 3 hours duration on a basin with an area of 122 mi^2. Assume a constant base flow of 600 cfs.

a) Derive the unit hydrograph.

b) What would be the peak flow of a 3-hr storm that yielded 3.7 inches of runoff?

Hour	Day 1	Day 2	Day 3
3 am	600	4600	1700
6 am	600	4000	1500
9 am	6000	3500	1300
noon	9500	3100	1100
3 pm	8000	2700	900
6 pm	7000	2400	800
9 pm	6100	2100	700
midnight	5300	1900	600

11.8 The following data are from a 3-hr unit hydrograph. Derive the 6-hr unit hydrograph by the S-curve method. The basin is 122 mi^2 in area.

Hour	UHO	Hour	UHO
3	0	3	769
6	2308	6	641
9	3803	9	556
12	3162	12	470
3	2735	3	385
6	2350	6	299
9	2008	9	214
12	1709	12	128
3	1453	3	85
6	1239	6	43
9	1068	9	0
12	897		

11.9 For the same basin and storm (near Oklahoma City) as in Problem 11.3 calculate the runoff (inches) using the SCS curve number method. Assume an average 'II' moisture condition and hydrologic soil group C.

Land use

– Single family residential (1/8 acre lots) – 239.4 acres

– Park in fair condition – 17.1 acres

– Native pasture in fair condition on loamy soil – 85.5 acres

11.10 Use the SCS triangular synthetic unit hydrograph to create the storm runoff hydrograph for Problem 11.9

11.11 Develop a 3-hour synthetic unit hydrograph using Snyder's method and the data below.

$C_t = 2.0$
$C_p = 397$
$A = 139$ mi^2
$L_w = 16$ mi
$L_c = 6$ mi
Use the T_b formula for small basins and plot the hydrograph using the COE plotting guideline equations.

11.12 Use the observed inflow and outflow data below to calculate the Muskingum parameters x and K. Then route the inflow hydrograph by the Muskingum method. Compare your routed outflow hydrograph to the observed outflow hydrograph.

Inflow and outflow data (source: Linsley et al. 1982).

Time (hrs)	Inflow (cfs)	Outflow (cfs)
0	56	70
6	66	66
12	250	102
18	550	185
24	595	265
30	420	335
36	295	370
42	210	368
48	147	310
54	100	245
60	74	200
66	60	165
72	51	132
78	46	100

CHAPTER 12

Drought and water supply

12.1 DEFINING DROUGHT

Drought (pronounced as in 'out') is often described as a creeping phenomena. Unlike a flood – you know when a flood starts, when it ends, and where it has been – drought is more difficult to define in time and space. It may take weeks or months of persistent dryness before a drought is finally acknowledged, and it may take a similar period of sustained wetness to bring the drought to an end. Just defining drought has been a major challenge in studying it as a hydrologic phenomena. There are many underlying problems in developing a suitable definition of drought. First, a drought may not affect all components of the hydrologic system simultaneously. It is possible for soil moisture levels to be abnormally low, while streamflow and lake levels are near normal. A farmer may have to adjust for low soil moisture levels, while the manager and customers of an urban water supply systems see no immediate problem. Another problem is that drought is not an absolute condition but rather a relative lack of moisture. A particular level of water deficit must be evaluated in terms of the expectation for water at that time and place. An increase in demand can lead to drought conditions just as surely as a decrease in water supply.

Dracup et al. (1980) suggest that the first step in defining drought be the clear identification of the subject of primary interest. The term *agricultural drought* obviously refers to drought affecting agriculture and focuses on soil moisture availability. *Hydrologic drought* focuses on water supply and might use an index of streamflow and/or reservoir storage. *Meteorological drought* refers to a period of below normal precipitation and above normal temperature. Some human activities defy such straight-forward identification of the hydrologic component of primary interest. Irrigation agriculture is a good example. Being a type of agriculture soil moisture is obviously important, but because it is irrigated, streamflow, reservoir storage or groundwater levels are also of primary importance. Human manipulation of the hydrologic cycle further complicates the picture by shifting drought impacts in time and space. Irrigation agriculture along the east slope of the Rocky Mountains in Colorado depends upon snowfall from the previous winter. A drought during the winter can cause economic hardship six months to a year later even if weather patterns have returned to normal. Much of northern California and the Pacific Northwest suffered a 6-year drought from 1987 to 1993. Southern California suffered as well because of the direct hydrological dependence of southern California on water supply from the north. The California Aqueduct, a major component of the California State Water

Plan, transfers water some 600 miles south from Shasta Reservoir in northern California to cities, industries, and irrigated farms in southern California.

Most drought definitions incorporate the idea that drought is an extended period of time during which water availability is significantly below *normal*. The time period may be weeks, months or even years depending upon the particular circumstance. What is significantly below also depends upon the situation because some activities are more sensitive to moisture deficits than others. Even the same activity may be more sensitive to drought at different times. A corn crop is extremely sensitive to soil moisture deficits at certain times in the growing season. Inadequate moisture for only a short period near maturation can reduce yields dramatically compared to the same level of moisture stress at earlier or later times in the season.

More comprehensive definitions of drought expand the concept of departure from normal and recognize that human societies are adapted to the average, or normally expected, moisture availability at that location. As Hounam et al. (1975) put it:

'... a pastoralist, raising fat lambs on improved pastures with a uniformly distributed rainfall averaging, say, 1000 mm a year, might be troubled by the relative 'dryness' in a year producing only 750 mm, irrespective of its temporal distribution. To another pastoralist in semi-arid country normally receiving 300 mm a year, this total 750 mm would represent a record wet year, bringing with it the troubles associated with excessive moisture.... The agriculturalist or pastoralist, especially in the drier regions, has assessed the nature of the local rainfall and, through years of long and sometimes bitter experience, has learnt to adapt his operation to rainfall characteristics of the area.'

Human manipulation of the hydrologic cycle through interbasin water diversions, water storage or groundwater pumping may complicate the situation but the fundamental concept remains valid.

One last comment on drought definitions is to recognize that drought is a stochastic hydrologic phenomena. The term stochastic means that successive observations of the hydrologic variable are dependent in time. Once a drought becomes established, it tends to persist. A good definition incorporates this stochastic character.

There are many ways to quantitatively define and analyze the phenomena of drought. First is by using a *runs* approach. A runs approach defines and describes drought using properties of a stochastic time series. Drought *indices* are a second way to define and describe drought. Some indices are extremely simple; some quite complex. An example of a simple index is to define a threshold value for a hydrologic variable and some duration of time when water availability is below that threshold. An example would be, say, less than 80% of normal precipitation in a 2-month period. The Palmer Drought Severity Index (PDSI) is a more complex index based on a water balance. The runs approach and the PDSI are discussed at length below. A third way to study drought is by *frequency analysis* similar to that used for floods in Chapter 11. Frequency analysis does not define droughts, it only assigns recurrence intervals to drought events that are defined by some other method. Drought frequency analysis can be applied to low streamflows exactly as was done for high streamflows. The *annual minimum streamflow series* is composed of the lowest streamflows for each year. The flows can be ranked and plotted on probability paper. The Gumbel Type III probability distribution (also called the Weibull distribution) fits annual minimum series data fairly well. In some cases the planner may need to

Table 12.1. Advantages and limitations of different method of analyzing drought.

Approach	Capable of defining drought characteristics (occurrence, length, etc.)	Capable of describing stochastic properties	Capable of describing frequency properties (e.g. return period)
Runs	Yes	Yes	No
Simple index	Yes	No	Yes, when combined with frequency analysis
PDSI	Yes	Yes	No
Frequency analysis	No	No	Yes
Markov chain	No	Yes	Yes

know the probability of discharge periods of various lengths, such as the driest 5-day period. Discharges for different intervals can be defined and subjected to the same type of frequency analysis.

A fourth approach to studying drought is by means of a Markov chain. A Markov chain describes probability characteristics of a stochastic process. As with frequency analysis a Markov chain does not define drought; rather, some type of index is first used to define the occurrence of a drought. A Markov chain can then be used to describe certain probability characteristics. Table 12.1 lists some of the advantages and disadvantages of these four approaches to studying drought.

12.2 RUNS ANALYSIS OF DROUGHT

A runs analysis of drought is based on the theory of runs for discrete variables, though the theory is applicable to continuous variables as well (Yevjevich 1972). The theory of runs is founded on the concept of two processes crossing each other. By hydrologic process we mean a stationary, stochastic time series for any hydrologic variable. A monthly precipitation time series would represent a precipitation process. Stationary means the parameters of the distribution (mean and variance) do not change with time. When applied to drought, runs theory quantitatively describes how a hydrologic process crosses above and below some critical threshold value. A threshold value is called a *truncation level*. Prior to analysis the original data should be transformed into either percentages of the mean, departures from the mean, or standardized Z-scores. Standardized Z-scores have the added advantage of being dimensionless, so that Z-scores of precipitation, say, can be directly compared to Z-scores of streamflow. The numerator in Equation 3.18 gives departures from the mean, while the entire equation transforms data into Z-scores.

Figure 12.1 is an illustrative time series for a discrete hydrologic variable x. The increments for time (t) could be weeks, months or years depending upon the situation. The truncation level x_o is the value of x for which negative departures are defined. Only negative departures are used to analyze drought, but analogous properties exist for positive departures. A negative departure $(x - x_o) < 0$ represents a drought. The truncation level can be set anywhere. Setting it slightly below the mean for x recognizes that small departures from the mean are still within the range of what is considered 'normal'. A downcrossing occurs when at time t–1, $(x - x_o) > 0$ and at

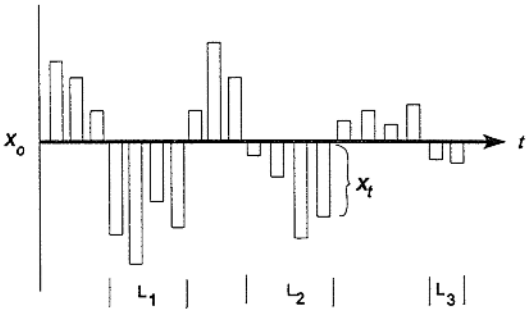

Figure 12.1. Runs properties for a discrete variable x. The truncation value x_o is used to define negative departures. L_i is the negative run length and defines drought duration for event i.

time t, $(x - x_o) < 0$. This marks the beginning of a drought as defined by that truncation level. For any drought event i the negative run length L_i is defined as a consecutive sequence of negative deviations preceded and succeeded by a positive deviation. Run length defines the *duration* of a drought episode. In Figure 12.1 there are three drought episodes. The first and second episodes are each four time periods long, while the third episode is two periods long. The sum of the negative deviations in run length i is called the run sum S_i and measures drought *magnitude*. Magnitude measures the cumulative water deficiency for a given drought episode. The ratio S_i / L_i measures the average drought *intensity*. And lastly, drought *severity* at time t is given by the magnitude of an individual negative deviation x_t. A runs-based definition is applicable to any hydrologic subsystem, e.g. precipitation, soil moisture or streamflow, and quantifies drought characteristics such as duration, magnitude, intensity and severity.

12.2.1 *Analysis of Oklahoma climate division 4*

Figure 12.2 is a time series of Z-transformed monthly precipitation data. The data are from Oklahoma climate division 4, located in west central Oklahoma along the border with Texas. The data are for the period 1929 to 1940, a total of 144 monthly observations. The data were fit to the gamma distribution, and Z-scores were calculated using the (gamma) mean and standard deviation (Table 3.4). Researchers at the National Climate Data Center (NCDC) use the categories in Table 12.2 to classify Z-transformed precipitation and temperature data. The classification shows that departures slightly more or less than one-half of one standard deviation are still considered normal. The greater the departure the more abnormal (wet or dry) environmental conditions are. The two lower boundaries (Z = –0.524 and Z = –1.28) are drawn as dashed lines on Figure 12.2. We can use each of these boundaries separately as a truncation level to demonstrate the analysis of *precipitation drought* by the runs approach in Example 12.1.

Example 12.1
The standardized precipitation data from Oklahoma climate division 4 are analyzed in this example by the runs method. The Z-scores for the 3-month drought in 1933, and the 3- and 2-month droughts in 1936 are given in Table 12.3. The results of the runs analysis are given in Table 12.4.

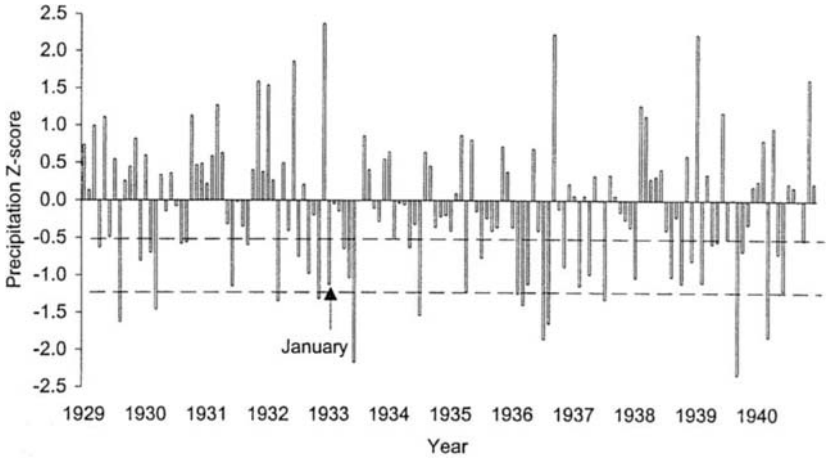

Figure 12.2. Time series of Z-transformed precipitation data for Oklahoma climate division 4, 1929-1940.

Table 12.2. Classification categories for Z-transformed precipitation and temperature data (source: NOAA/NCDC 1990).

Z-score	Classification
$1.282 < Z$	Much above
$0.524 < Z \leq 1.282$	Above
$-0.524 \leq Z \leq 0.524$	Normal
$-1.282 \leq Z < -0.524$	Below
$Z < -1.282$	Much below

Table 12.3. Z-scores for three precipitation drought events in Oklahoma climate division 4.

Year	Month	Z-score
1933	April	–0.65
	May	–1.04
	June	–2.17
1936	February	–1.25
	March	–1.40
	April	–1.12
1936	July	–1.86
	August	–1.65

Table 12.4. Runs analysis for the precipitation data from Oklahoma climate division 4.

	Truncation level x_o	
	–0.524	–1.282
Total number of drought months	43	12
Total number of drought events	32	11

Table 12.4. Continued.

	Truncation level x_o	
	–0.524	–1.282
1933 Drought		
Length *L*	3	1
Magnitude *S*	–3.86	–2.17
Intensity *S/L*	–1.28	–2.17
1936 February-April drought		
Length	3	1
Magnitude	–3.77	–1.40
Intensity	–1.26	–1.40
1936 July-August drought		
Length	2	2
Magnitude	–3.51	–3.51
Intensity	–1.76	–1.76

For the first truncation level x_o = –0.524 there are 32 separate precipitation droughts totalling 43 months, or about 30% of the 12-year period. Individual droughts lasted anywhere from 1 to 3 months. The two most severe drought months occurred in September 1939 and June 1933, with *Z*-scores of –2.34 and –2.17, respectively (see Fig. 12.2). There are two droughts with a duration of 3-months; one occurred from April to June in 1933, and the other from February to April in 1936. The magnitude of the 1933 event is $S = (-0.65 - 1.04 - 2.17) = -3.86$, while the magnitude of the 1936 event is $S = -3.77$. The average intensity for these droughts are –1.28 and –1.26, respectively (Table 12.4). There was a second drought in July and August of 1936. This event was shorter but more intense, lasting two months and having a magnitude of –3.51 and an intensity of –1.76.

For the lower truncation level $x_o = -1.282$ there are only 11 precipitation droughts totalling 12 months, or 8.3% of the period. The longest drought is now the 2-month event in the summer of 1936 (Fig. 12.2). The magnitude and intensity are the same as before. Setting the truncation level lower generally means that fewer, more intense droughts will be identified.

The runs approach quantifies drought occurrence, length, magnitude, intensity and severity, but the precise value of these characteristics depends upon the truncation level. The choice of truncation level is, however, completely arbitrary; there is no 'natural' way to decided where the truncation level should be set. This is perhaps the most notable drawback of the runs approach. The effect this has on drought analysis is illustrated by close inspection of Figure 12.2. The first six months of 1933 had negative precipitation departures. If the truncation level were set near 0, there would be a single 6-month drought at the beginning of 1933. Instead, with a truncation level of –0.524 there are two droughts, the 1-month January drought, and the 3-month drought of April to June. This is an important limitation of the runs approach: the identification and characteristics of a drought depend entirely on the truncation level, and the truncation level is arbitrarily chosen. Another problem is that the runs approach analyzes only one variable at a time. This poses a problem for the analysis of meteorological drought which usually occurs as a joint occurrence of below normal precipitation and above normal temperatures.

12.3 PALMER DROUGHT SEVERITY INDEX (PDSI)

The most widely used index of drought in the United States is the PDSI (Palmer, 1965). The PDSI ranges between +6.0 (extremely wet) and –6.0 (extreme drought) (Table 12.5). The index is calculated on a monthly basis, and is based on a weighted water balance. Human alterations of the water balance, e.g. reservoir storage, are not considered. The PDSI is a meteorological drought index. This means that the first month the weather begins to change from dry (wet) to near normal or wet (dry) conditions, the drought (wet spell) ends despite the fact that other components of the hydrological system such as soil moisture, rivers or lakes may be below or above their normal state (Karl 1983). This is why the NCDC now calculates a modified version of the index called the Palmer Hydrological Drought Index (PHDI). The PHDI is less sensitive to variations in weather and is thought to more accurately reflect hydrological conditions.

The popularity of the PDSI is due to its ability to capture the persistent nature of droughts while providing a single quantitative index of existing environmental conditions. Also, the PDSI is a standardized index which means it is directly comparable between different climatic regions at different times of the year. A PDSI value of –1.5 in September in Arizona is directly comparable to –1.5 in Florida in June. The PDSI reflects departures from climatic conditions that are normal or expected for that location at that particular time of the year.

The calculation of the PDSI uses a water balance similar to that of Thornthwaite & Mather (1955), except Palmer employed the two-layer soil model (Chapter 6) to calculate actual evapotranspiration. The PDSI procedure calculates potential evapotranspiration by the Thornthwaite method (Eq. 6.1). This is a good example of where the simpler temperature-based Thornthwaite equation is preferred over more data-intensive methods. In the discussion that follows actual evapotranspiration is designated as *ET* and potential evapotranspiration as *PE*, as these were the symbols used by Palmer. The PDSI water balance is:

$$P = ET + R + RO + L \tag{12.1}$$

where P is precipitation, ET is actual evapotranspiration, R is soil water recharge, RO is runoff, and L is the water loss from the soil. The change in soil moisture storage is

Table 12.5. Categories for wet spells and droughts using the PDSI (source: Palmer 1965).

PDSI	Classification
≥ 4.00	Extremely wet
3.00 to 3.99	Very wet
2.00 to 2.99	Moderately wet
1.00 to 1.99	Slightly wet
0.50 to 0.99	Incipient wet spell
0.49 to –0.49	Near normal
–0.50 to –0.99	Incipient drought
–1.00 to –1.99	Mild drought
–2.00 to –2.99	Moderate drought
–3.00 to –3.99	Severe drought
≤ –4.00	Extreme drought

calculated as $\Delta S = (R - L)$. The relationship between actual and potential evapotranspiration was described in Chapter 6. What Palmer did, and this really is the essence of his innovative approach, was to extend the actual-potential relationship to the remaining three variables on the right side of Equation (12.1) by defining new potential values. He thus defined potential recharge (*PR*), potential runoff (*PRO*), and potential soil water loss (*PL*). For example, *PR* is defined as the unused water storage capacity of the soil:

$$PR = (AWC - S) \tag{12.2}$$

where *AWC* is the available water capacity and *S* is the amount of water in both layers of the soil at the beginning of the month. The next step is to quantify these actual-potential relationships as parameters using long-term averages. For each month (t = 1 to 12) the normal relationships between the actual and the potential value are parameterized as:

$$\alpha = \left(\overline{ET} / \overline{PE}\right) \tag{12.3}$$

$$\beta = \left(\overline{R} / \overline{PR}\right) \tag{12.4}$$

$$\gamma = \left(\overline{RO} / \overline{PRO}\right) \tag{12.5}$$

$$\delta = \left(\overline{L} / \overline{PL}\right) \tag{12.6}$$

The overbar quantities are monthly means calculated for the period of record. For example, if the average *ET* for June at some location is 3.5 inches, and the average *PE* for June is 6 inches, then the normal relationship between the two is $\alpha = \overline{ET} / \overline{PE}$ = 3.5/6.0 = 0.583. This type of calculation is done for every month for each parameter yielding 48 parameter values at each location. If a particular June were warmer than normal and had, say, *PE* = 7.0 inches, then *ET* should be adjusted by α so that *ET* bears its normal relation to the climatic demand for moisture (Palmer 1965). For this example the adjustment gives *ET* = 0.583(7.0) = 4.08 inches. Palmer called this adjusted value *Climatically Appropriate For Existing Conditions (CAFEC)*, and designated it with a circumflex hat symbol $\hat{ET}$.

Palmer defined a new water balance equation, identical in form to Equation (12.1), composed of *CAFEC* components:

$$\hat{P} = \hat{ET} + \hat{R} + \hat{RO} + \hat{L} \tag{12.7}$$

The *CAFEC* quantities on the right side are defined by:

$$\hat{ET} = \alpha PE \tag{12.8}$$

$$\hat{R} = \beta PR \tag{12.9}$$

$$\hat{RO} = \gamma PRO \tag{12.10}$$

$$\hat{L} = \delta PL \tag{12.11}$$

Equation (12.7) calculates a *CAFEC* precipitation value $\hat{P}$ that is appropriate for the existing climatic conditions. The difference between the observed precipitation P and the *CAFEC* precipitation $\hat{P}$ is a moisture departure from normal:

$$d = P - \hat{P} \tag{12.12}$$

Since the PDSI is a standardized index directly comparable for any month at any location, the d's are weighted by another parameter K such that:

$$Z = dK \tag{12.13}$$

Z is called the 'moisture anomaly index' and is the heart of the PDSI. There is a K value for each month, and as with *CAFEC* parameters, the K's are determined from climate records before calculation of the PDSIs begin. K is the parameter that standardizes the moisture departures (d) by month and location. The equation for K was developed empirically as a function of the average of the absolute values of the moisture departures for the entire period of record, and the average water supply ($\bar{P}+\bar{L}$) and water demand ($\overline{PE}+\bar{R}+\overline{RO}$) at the location. The value of Z from Equation (12.13) is used to calculate the monthly PDSI such that:

$$PDSI_t = 0.897\,PDSI_{t-1} + 0.333Z_t \tag{12.14}$$

The stochastic nature of the PDSI is clearly seen in Equation (12.14) where the value of the PDSI for the current month t depends on the value of the PDSI in the previous month t–1. Palmer could have stopped here, but he further refined the index to make it a truly meteorological drought index. The details of this further refinement are somewhat complex and not relevant to the current discussion. The 'unrefined' index given by Equation (12.14) is the 'new' Palmer Hydrological Drought Index (PHDI) mentioned earlier.

Palmer conceived of meteorological drought as a departure of precipitation from what the established economy in a region has come to expect as normal. According to Palmer (1965):

'A drought period may now be defined as an interval of time, generally on the order of months to years in duration, during which the actual moisture supply at the given place rather consistently falls short of the climatically expected or climatically appropriate moisture supply... the problem here is to develop a method for computing the amount of precipitation that should have occurred in a given area during a given period of time in order for the 'weather' during the period to have been normal – normal in the sense that the moisture supply during the period satisfied the average or climatically expected percentage of the absolute moisture requirements during the period. In other words, the question is how much precipitation should have occurred during a given period to have kept the water resources of the area commensurate with their established use?'

12.3.1 *Analysis of Oklahoma climate division 4*

Figure 12.3 and Table 12.6 show the PDSIs for the same 12-year period in Oklahoma climate division 4 as analyzed previously for precipitation. From 1929 to 1933 environmental conditions oscillated between mild wetness and mild drought. The year

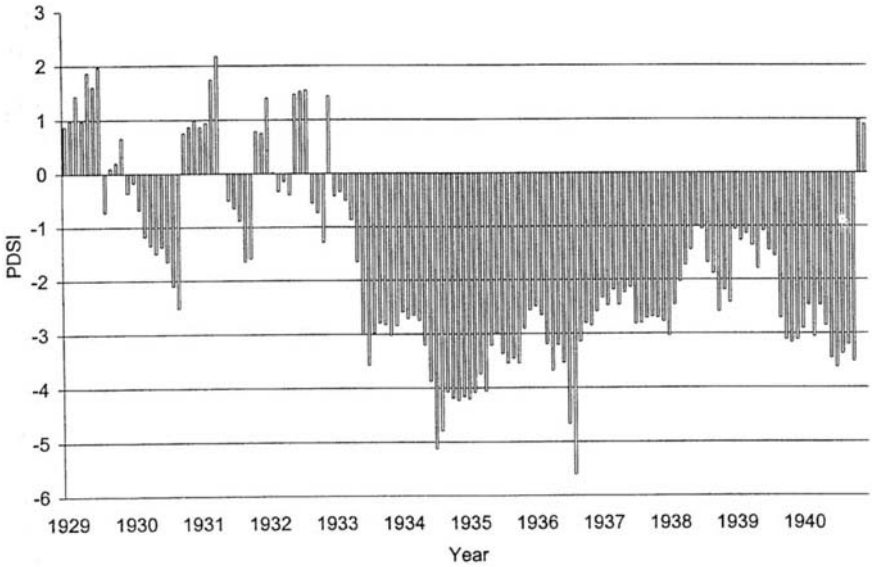

Figure 12.3. PDSI (1929-1940) for climate division 4 in Oklahoma. Data from Table 12.6 (source: NOAA/NCDC 1990).

Table 12.6. PDSI values for Oklahoma climate division 4 (source: NOAA/NCDC 1990).

	Jan	Feb	Mar	Apr	May	Jun	Jul	Aug	Sep	Oct	Nov	Dec
1929	0.88	0.99	1.44	0.97	1.87	1.61	1.97	–0.72	0.10	0.20	0.66	–0.36
1930	–0.17	–0.67	–1.17	–1.34	–1.49	–1.36	–1.64	–2.10	–2.51	0.75	0.87	0.99
1931	0.87	0.94	1.74	2.18	0.01	–0.50	–0.65	–0.88	–1.64	–1.58	0.79	0.75
1932	1.41	0.02	0.33	–0.14	–0.40	1.47	1.53	1.55	–0.55	–0.73	–1.28	1.44
1933	–0.42	–0.34	–0.50	–0.86	–1.65	–3.00	–3.57	–2.97	–2.79	–2.82	–3.02	–2.84
1934	–2.58	–2.71	–2.65	–2.74	–3.20	–3.87	–5.12	–4.79	–4.07	–4.19	–4.23	–4.16
1935	–4.20	–4.08	–3.74	–4.06	–3.21	–2.99	–3.36	–3.54	–3.45	–3.54	–2.90	–2.56
1936	–2.49	–2.65	–3.19	–3.68	–3.20	–3.53	–4.66	–5.60	–3.14	–2.80	–2.84	–2.58
1937	–2.33	–2.47	–2.18	–2.46	–2.23	–2.13	–2.81	–2.80	–2.71	–2.68	–2.70	–2.77
1938	–3.03	–2.46	–2.03	–1.72	–1.43	–1.00	–1.04	–1.67	–1.88	–2.59	–2.19	–2.42
1939	–1.05	–1.26	–1.13	–1.35	–1.79	–1.08	–1.44	–1.55	–2.71	–3.11	–3.16	–3.11
1940	–2.90	–2.47	–3.05	–2.47	–2.85	–3.45	–3.62	–3.37	–3.20	–3.51	0.98	0.90

1933 began with near normal conditions that turned into incipient drought by the spring. Conditions deteriorated significantly and the drought became severe (PDSI = –3.0) by June. For the next 58 months, from June 1933 to April 1938, drought conditions ranged between moderate and extreme, with the years 1934 and 1936 having the two most extreme months. The drought ended abruptly in November of 1940 when conditions turned wetter than normal. The pattern of drought defined by the PDSI is quite different than that defined by the runs analysis of precipitation alone. If we use PDSI = –0.50 as the threshold for defining drought occurrence, there are only five drought events. The first event in 1929 lasted only one month. The second and third droughts occurred in 1930 and 1931 and lasted eight and five months, respec-

tively. The fourth is a 3-month event at the end of 1932. The fifth and final drought was truly a great drought lasting 92 months from March 1933 to November 1940. The most severe drought months as defined by the PDSI usually, but not always, correspond with severe precipitation deficits (Fig. 12.2). The most extreme period in 1936 (Fig. 12.3) correlates with the precipitation deficit during seven of the first eight months of that year. By contrast the PDSI shows extreme drought in 1934, whereas the runs analysis showed only two months qualifying as drought months. An even greater discrepancy exists in 1939. The single-driest month in terms of precipitation over the 12-year period had only a modest impact on the PDSI. The reason of course is that the PDSI is based on a water balance that integrates the effects of various hydrologic components.

Figure 12.4 is the Palmer Hydrological Drought Index (PHDI) for Oklahoma climate division 4 for the same period and it bears a strong resemblance to Figure 12.3. The years 1929 to early 1933 are characterized by alternating periods of wetness and dryness followed by the great drought beginning in June of 1933. The PHDI indicates only four separate drought episodes (PHDI < –0.50) rather than five as indicated by the PDSI. One way to compare the PDSI and PHDI is by subtracting one index from the other (Fig. 12.5). Negative values on Figure 12.5 represent times when the PDSI < PHDI while positive values when the PDSI > PHDI. When their difference (either positive or negative) is small it means the two indices are approximately the same. When the difference between the two is large their assessment of environmental conditions is contradictory. The meteorological PDSI is the more sensitive of the two and it leads the change to a new environmental state. As an example, the PHDI recorded incipient to slightly wet conditions all throughout 1929. The PDSI on the other hand was more variable. It too indicated wet conditions in the first half of 1929 but changed to drought in July and then to near normal conditions for

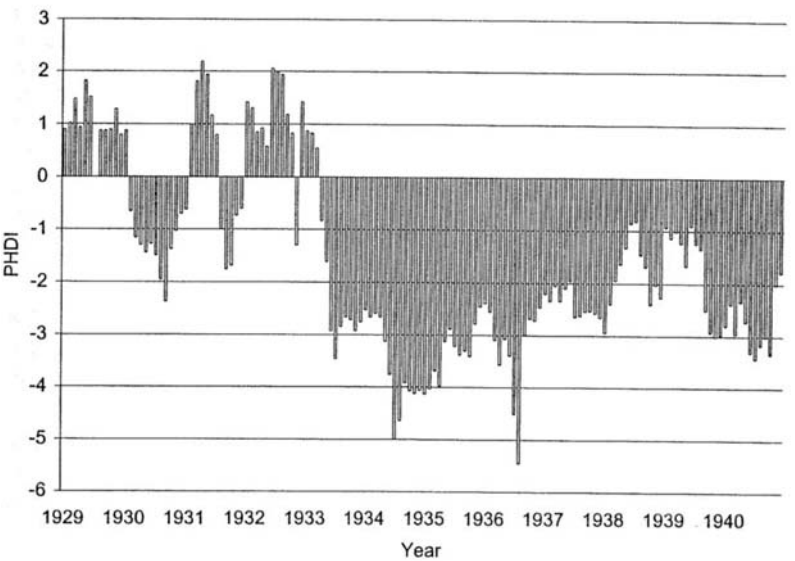

Figure 12.4. PHDI (1929-1940) for climate division 4 in Oklahoma (source: NOAA/NCDC 1990).

most of the remaining months. The result is seen on Figure 12.5 as large negative differences in the latter half of 1929. All through the great drought of the 1930s the two indices register nearly identical conditions, though the PDSI is always a little lower (more severe) than the PHDI. To put the drought of the 1930s in western Oklahoma into perspective Figure 12.6 shows the PHDI for the period 1895 to 1989. The drought of the 1950s was shorter but more intense than the 1930s. Figure 12.7

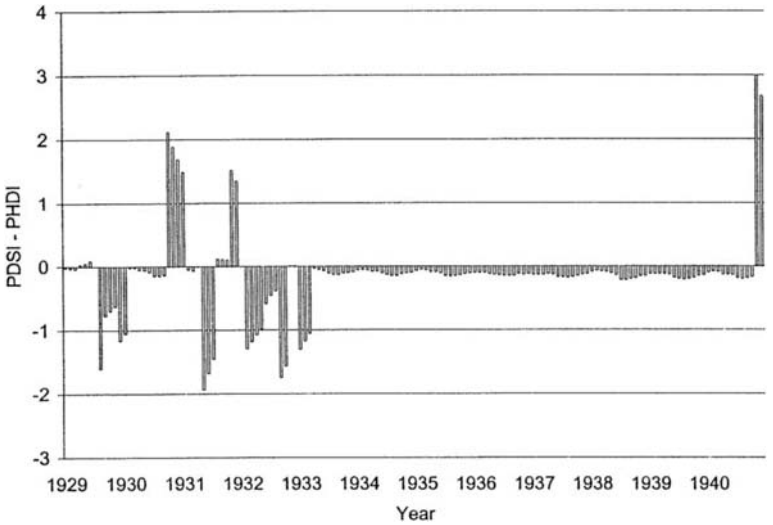

Figure 12.5. Differences between the PDSI and the PHDI for climate division 4 in Oklahoma.

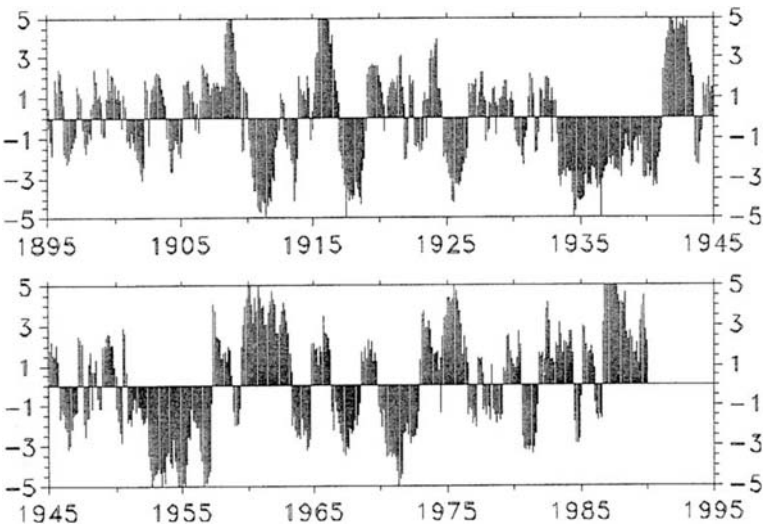

Figure 12.6. PHDI for Oklahoma climate division 4 from 1895 to 1989 (source: NOAA/NCDC 1990).

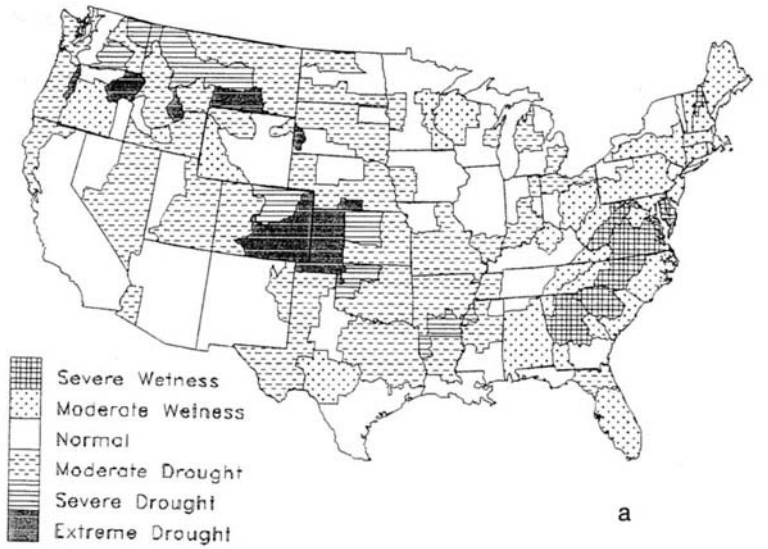

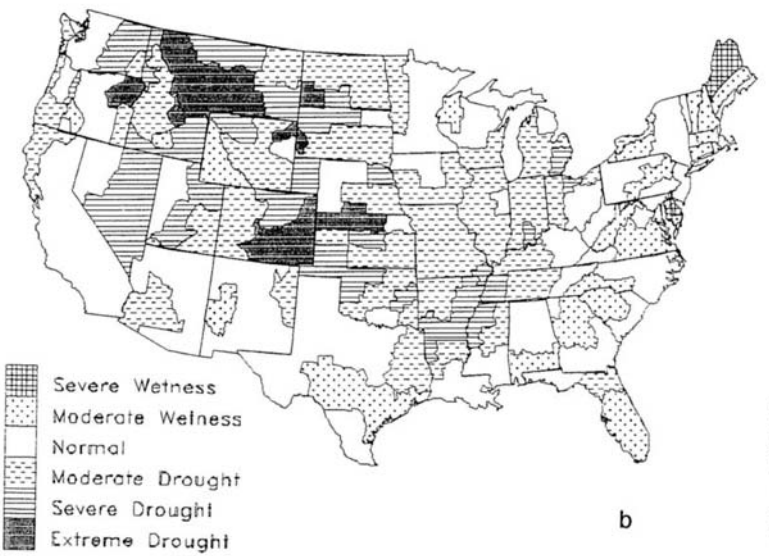

Figure 12.7. PHDI for April (a) and May (b) 1936 (source: NOAA/NCDC 1990).

shows the spatial pattern of drought for a 4-month period in 1936 across the United States. The decade of the 1930s saw some of the most devastating droughts in the recorded history of the Great Plains. Drought conditions waxed and waned throughout most of the decade, though in a few unfortunate areas on the central and northern plains the drought was nearly continuous for the entire decade. It is worth noting that since the PDSI (PHDI) is a stochastic time series it can be analyzed using the runs approach. The various PDSI categories are set as thresholds for the calculation of drought duration, magnitude, intensity and severity.

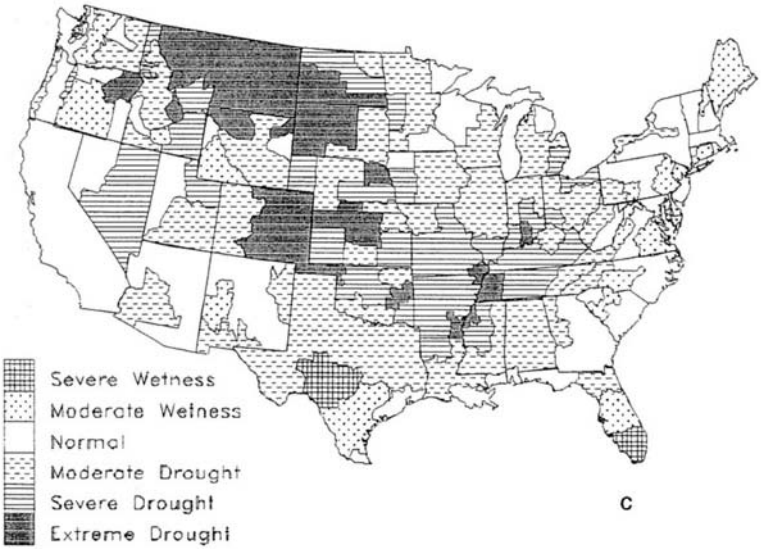

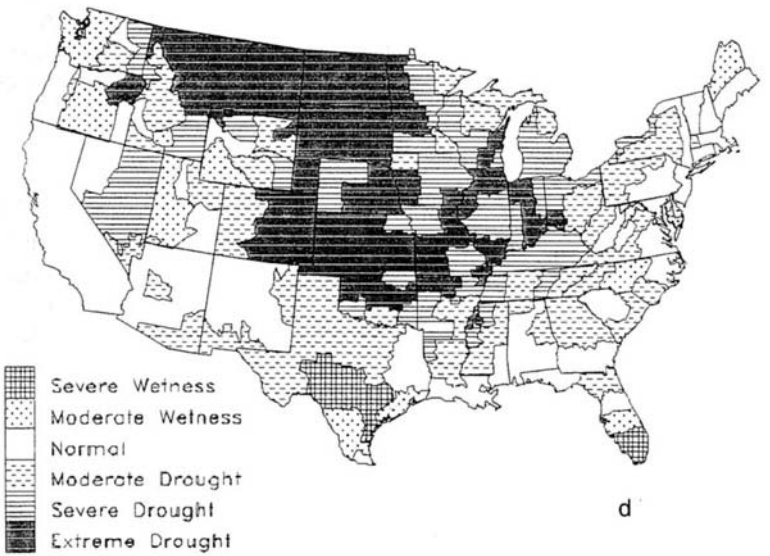

Figure 12.7. Continued. PHDI for June (c) and July (d) 1936 (source: NOAA/NCDC 1990).

12.4 MARKOV CHAIN MODEL OF DROUGHT

A Markov chain is a mathematical technique used for modeling discrete stochastic processes. The term Markov chain connotes that the model describes a sequence, or chain, of observations. The time dependency in the stochastic process can be incorporated using either serial correlation coefficients or *state transition probabilities*. Here we describe a Markov chain that uses state transition probabilities. Later in the section on water supply we introduce a Markov streamflow model that utilizes a se-

rial correlation coefficient. Markov chains are classified by the number of 'lags' (previous time steps) that are used to generate the conditions at the current time step *t*. A lag-1 Markov chain uses only the immediately-preceding time step *t*–1 in modeling current conditions. A lag-2 Markov chain uses the previous two time steps, and so on. The lag-1 Markov model is by far the most common and is the only one discussed here.

A lag-1 Markov chain says that the probability of the environment being in a certain 'state' at time *t* depends upon the state of the environment at the previous time interval *t*–1. The probability of having a drought (state) this month depends on whether drought conditions existed last month. It is unlikely (low probability) that the environment would change from extreme drought this month to extremely wet next month. It is more likely (higher probability) to go from extreme drought this month to some other drought state next month. The future development of the lag-1 Markov chain depends only upon the present state; the past history of the process or how the present state was reached is irrelevant. However, proportions of past states are necessarily included in the current state; hence the Markov chain does possess some memory (Thompson 1990). The PDSI could be modeled as a lag-1 Markov chain having the eleven states listed in Table 12.5.

The degree of dependence between states can be expressed as a state transition probability. The state transition probability P_{ij} is the probability of moving from the current state *i* to the future state *j* in the next time step. State transition probabilities are *conditional probabilities*. That is to say the probability of having state *j* in the next time step is conditioned on the fact that the environment is currently in state *i*. Figure 12.8 shows a three-step time sequence. At each step *t* the environment is in one of three possible states – drought (D), normal (N), or wet (W). The state transition probabilities for the drought state are $P_{D,D} = 0.6$, $P_{D,N} = 0.2$, and $P_{D,W} = 0.2$. In other words, if the environment is currently in a drought state there is a 60% chance of remaining in a drought in the next period, a 20% chance of changing from drought to normal, and a 20% chance of changing from drought to wet conditions. There are similar state transition probabilities for the normal and wet states. The state transition probabilities sum to 1.0 because the environment must move into one of the three

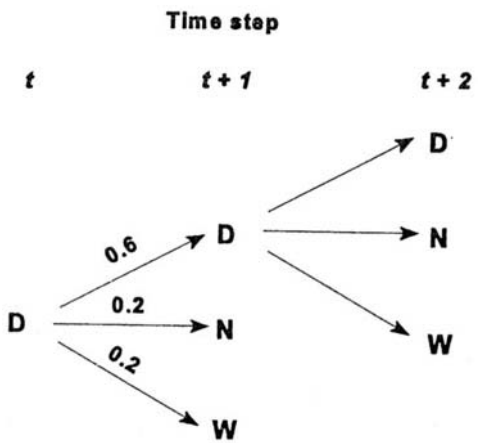

Figure 12.8. Diagrammatic representation of a three-state environment and the state transition probabilities between states. The state transition probabilities must sum to 1.0 because the environment must move to one of the three states at the next time step. See text for further discussion.

states in the next time step. State transition probabilities are determined empirically by analyzing a time series (see Example 12.2).

Example 12.2
This is an example demonstrating how to calculate state transition probabilities. Assume there are three possible states for the environment – drought (D), normal (N), and wet (W) – and we observe the following time series for the environment:

time (t)	1	2	3	4	5	6	7	8	9	10	11	12	13	14	15
state (S)	W	W	D	D	D	N	N	W	N	N	D	D	W	W	W

With 15 time steps there are only 14 state transitions. The environment at the last time step does not transition into a future state.

At each time the environment is in one and only one state. With three states there are a total of nine possible combinations of transitions between states. The state transition probabilities are calculated in groups of three corresponding to each of the three possible initial states. For a given initial state i, the transition probabilities are calculated as the observed relative frequencies of each transition from state i to state j. For example, for an initial drought state (D), count the number of transitions to each of the three possible subsequent states:

$$P_{D,D} = 3/5 = 0.60$$

$$P_{D,N} = 1/5 = 0.20$$

$$P_{D,W} = 1/5 = 0.20$$

The denominator is 5 because there were only 5 transitions that started with an initial state D. According to the Law of Total Probability (Chapter 3) the sum of the state transition probabilities must equal 1. In a similar manner the state transition probabilities for the initial states N and W are calculated as:

$$P_{N,W} = 1/4 = 0.25$$

$$P_{N,N} = 2/4 = 0.50$$

$$P_{N,D} = 1/4 = 0.25$$

and

$$P_{W,W} = 3/5 = 0.60$$

$$P_{W,N} = 1/5 = 0.20$$

$$P_{W,D} = 1/5 = 0.20$$

The denominator for the last group is 5 and not 6 because the last W state at $t = 15$ does not transition into a future state.

The state transition probabilities can be arranged as a *transition probability matrix* $\underline{P}$. The transition probability matrix for the example presented in Figure 12.8 and Example 12.2 is shown as Table 12.7.

If the transition probability matrix is multiplied against itself again and again, the individual state transition probabilities P_{ij} approach equilibrium (constant) values. These equilibrium probabilities P_i^* comprise a new matrix called the n-step *equilibrium matrix* $\underline{P^n}$. Each row in the equilibrium matrix is identical (Table 12.8).

Table 12.7. Transition probability matrix $\underline{P}$ for data in Figure 12.8

		Future State j		
		D	N	W
Current State i	D	0.60	0.20	0.20
	N	0.25	0.50	0.25
	W	0.20	0.20	0.60

Table 12.8. Equilibrium matrix $\underline{P^n}$ produced by powering matrix $\underline{P}$ in Table 12.7.

		State j		
		D	N	W
State i	D	0.357	0.286	0.357
	N	0.357	0.286	0.357
	W	0.357	0.286	0.357

Each element in the equilibrium matrix represents the equilibrium probability of being in that state after a large (n) number of time steps. In other words, the equilibrium probabilities represent the percentage of time, on average, that the process is in that state. Looking at Table 12.8 the environment is in a drought state $P_D^* = 35.7\%$ of the time, in the normal state $P_N^* = 28.6\%$, and in a wet state $P_W^* = 35.7\%$ of the time. Naturally, the equilibrium probabilities must also sum to 1.0.

The equilibrium probabilities in Table 12.8 could also be calculated as the relative frequency of any state over the entire time period. Referring to the time series in Example 12.2, there are 5 drought states out of a total of 14 transitions. The equilibrium probability for the drought state is therefore 5/14 = 0.357.

12.4.1 *Interrelating the Markov chain and runs theory*

From the theory of runs the expected number $E(N)$ of downcrossings (droughts) is equal to the probability of a downcrossing P_D at any time t multiplied by the length of the time period (L):

$$E(N) = P_D(L) \tag{12.15}$$

Also from runs theory, the expected length $E(L)$ of a downcrossing is equal to the probability that the process is below the threshold value divided by the probability of a downcrossing:

$$E(L) = \left(P_D^*\right) / \left(P_D\right) \tag{12.16}$$

This is where Markov analysis and runs theory can be combined. The probability of a downcrossing can be estimated using state transition and equilibrium probabilities, and the expected length of a drought can be determined using equilibrium probabilities and the probability of a downcrossing. Example 12.3 demonstrates the technique for the time series in Example 12.2.

Example 12.3
To find the expected number of droughts in a given period we need to first find the probability of a drought occurring at any time. For the data in Example 12.2 droughts can occurs two ways: either by having the environment in a wet state and changing to a drought state, or by being in a normal state and changing to drought. Thus the probability of a drought occurring can be estimated as the sum of the equilibrium probability for a each state times the state transition probability from that state to drought.

Expected number of droughts
Taking first the wet state:
- Equilibrium probability $P_W^* = 0.357$
- State transition probability $(P_{W,D}) = 0.20$

And, for the normal state:
- Equilibrium probability $P_N^* = 0.286$
- State transition probability $(P_{N,D}) = 0.25$.

The probability of a drought (downcrossing) at any time is:

$$P_D = (0.357 \times 0.2) + (0.286 \times 0.25) = 0.143$$

The expected number of droughts in the interval is therefore:

$$E(N) = 0.143 \times 14 = 2.0$$

Indeed, the time series in Example 12.2 shows two droughts.

The expected length of an individual drought

$$E(L) = 0.357/0.143 = 2.5$$

Again we see from the time series that one drought is 3 time periods long and the other 2 periods long. Their average length is $(3 + 2)/2 = 2.5$ periods.

The author combined runs analysis, Markov chain analysis, and the PDSI in a study of drought in the central United States from 1895 to 1988 (Thompson 1990). The transition probability matrix for Missouri climate division 4 (southwest Missouri) is given as Table 12.9. The number of PDSI states was reduced from eleven to

Table 12.9. Transition probability matrix for Missouri climate division 4 (source: Thompson 1990, used by permission).

	State *j*								
		ED	SD	MD	MLD	N	SW	MW	VW	EW
State *i*	ED	0.825	0.11			0.063				
	SD	0.323	0.516	0.097		0.65				
	MD	0.011	0.087	0.620	0.098	0.141	0.430			
	MLD			0.178	0.580	0.190	0.052			
	N			0.003	0.160	0.688	0.129	0.013	0.008	
	SW					0.228	0.503	0.234	0.035	
	MW				0.08	0.161	0.186	0.508	0.127	0.008
	VW					0.132		0.191	0.559	0.118
	EW					0.188			0.375	0.438

ED = extreme drought, SD = severe drought, MD = moderate drought, MLD = mild drought, N = normal, SW = slightly wet, MW = moderately wet, VW = very wet, and EW = extremely wet.

nine by combining the incipient wet and dry categories with the normal category. The main diagonal of the state transition matrix ($i = j$) is a measure of the persistence of any state. In southwestern Missouri extreme drought is the most persistent state with a state transition probability of $P_{ED,ED} = 0.825$. Once extreme drought becomes established it is very difficult to break. On the other hand extreme wet spells are only about half as persistent (0.438). The persistence for drought in general, that is going from a drought state to any other drought state, was found to be 0.254. Once drought becomes established there is about a one-in-four chance of it continuing in some form into the next month. Not all elements of the matrix are filled, which means it is impossible to go from certain states to other states, such as extreme wetness to extreme drought, in one month. The equilibrium matrix for southwestern Missouri is shown in Table 12.10.

Normal conditions prevailed about 34.8% of the time, while drought in some form or another occurred 31.8% of the time. Severe drought was the least common drought category. The expected number and length of droughts in this climate division are shown in Table 12.11. The expected (average) drought in southwestern Missouri is just short of a year (11.5 months), while the average observed drought lasted 10.4 months.

Figure 12.9 shows the persistence of extreme drought, defined as the value of the state transition probabilities ($P_{ED,ED}$), in a five-state region in the central United States. Extreme drought tends to be most persistent in the northern part of the region, especially along the Nebraska-Kansas boarder where probabilities exceed 90%. It is interesting that the pattern for severe drought persistence (not shown) is the reverse of Figure 12.9, with the higher probabilities clustering in the south. Figure 12.10 shows the pattern of extreme drought equilibrium probabilities. Again there is a core region of high values in Nebraska and Kansas. The climate divisions in this core region spent anywhere from 10.1 to 12% of the 94-year period in the condition of extreme drought. As was the case for persistence, the climate divisions with the highest equilibrium probabilities for severe drought (not shown) tend to be located mostly in the south, though the pattern is more variable. Another difference between extreme and severe droughts is that the highest equilibrium probabilities for severe drought did not exceed 10%.

Table 12.10. Equilibrium probability matrix for Missouri climate division 4 (source: Thompson 1990, used by permission).

State j								
ED	SD	MD	MLD	N	SW	MW	VW	EW
0.056	0.027	0.081	0.154	0.348	0.153	0.106	0.061	0.014

Table 12.11. Comparison of the expected and the observed number and length of droughts in Missouri climate division 4 (source: Thompson 1990, used by permission).

	Number	Length (months)
Expected	8.9	11.5
Observed	9.0	10.4

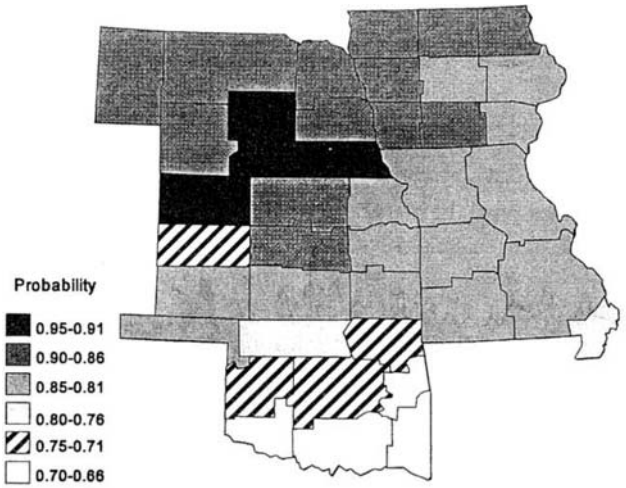

Figure 12.9. State transition probabilities from extreme drought to extreme drought by climate divisions in the central United States. This is a measure of the persistence of extreme drought (based on Thompson 1990, used by permission).

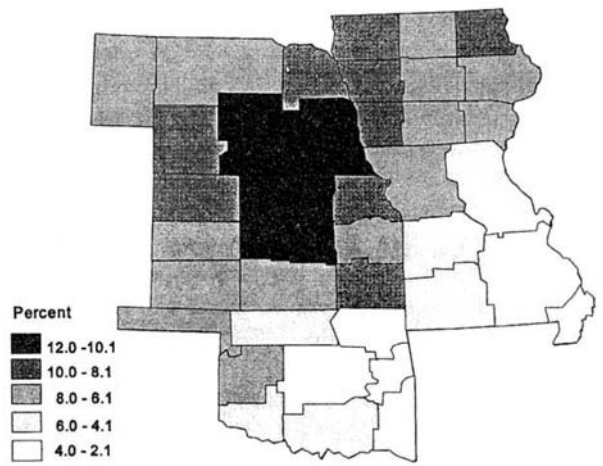

Figure 12.10. Equilibrium probabilities (percent) for extreme drought by climate division in the central United States. This is a measure of the percent of time the division experienced extreme drought (based on Thompson 1990, used by permission).

The strong persistence of drought in the central plains has been investigated by a number of researchers (Karl & Koscielny 1982, Diaz 1983). Their conclusion is that droughts are in fact more persistent in the interior plains compared to the coastal regions of the United States, and this is not an artifact of the PDSI calculation (Karl 1983). The reasons for the greater persistence and duration in the interior are not known but the role of feedback processes forced by land surface conditions, especially soil moisture and its effect on the partitioning of radiation, appear to be important (Oglesby & Erickson 1989).

12.5 WATER SUPPLY

Perhaps the single most important purpose of water-resources planning is the provi-

sion of adequate water supply. Whether for drinking, cooking, cleaning in the home, or for growing crops and manufacturing products water is essential to modern society. The basic objective of water supply management is to provide enough water of acceptable quality when and where it is needed. Failure to meet any of these constraints – quantity, quality, time or space – can cause severe hardship. For most of our history the emphasis has been on managing the supply. As population increased, new industries developed, or new land brought under irrigation, we met the increased demand for water by searching out new sources of supply. Alternatives for increasing supply include dams to impound water in reservoirs, interbasin diversion projects, groundwater mining, desalinization of salt and brackish water, and weather modification. If and when more water was needed the traditional response was to go find more. This attitude is expressed most recently in the reallocation of water between existing uses. In the western United States cities are looking to irrigated agriculture as a new source of supply. Cities can buy water rights in emerging water markets and transfer the water for use in their ever expanding suburbs. In the 1970s thinking began to change and water managers began speaking of demand management. Since water management is an issue of both supply and demand, rather than searching for increasingly scarce and more expensive supplies, managers began to take a critical look at current patterns of use and how demand might be reduced. Ways to reduce demand include raising prices, universal metering, changing antiquated laws that encourage waste, leak detection, and a host of water conservation methods. A wide variety of water conservation alternatives exist for cities, industry and agriculture. Low flow shower heads and water-displacement devices in toilet reservoirs can significantly reduce water use in the home. In January, 1994 federal legislation became effective requiring all new toilets to have a capacity of 1.6 gallons per flush, down from the 3.5 or even 5.0 gallon capacity of older models. Industrial conservation through recycling is one of the primary reasons that total water withdrawals in the United States actually *decreased* in the late 1980s after decades of explosive growth. An important reason for the increase in industrial recycling, however, was not a concern for water conservation *per se*, but the National Pollution Discharge Elimination Permits System (NPDES) of the federal Clean Water Act. In order to reduce their pollution discharges industries have turned to recycling. This is a good example of the systematic inter-relationship between water quantity and water quality. The following sections examine some methods for estimating and evaluating water supply, with a focus on supply from surface-water sources. The relationship to drought should be obvious – drought has always been one of the primary concerns for water supply planning. The USGS currently provides a monthly National Water Conditions Report. The report, including color graphics, can be accessed through the Internet. The World Wide Web address on the Internet is: http://water.usgs.gov/nwc/.

12.5.1 *Streamflow characteristics*

In Chapter 11 we studied hydrographs for individual floods. The continuous hydrograph for a stream shows the variation in discharge over time. Figure 12.11 is the hydrograph of mean monthly discharge for the Yadkin River at Patterson, NC from 1940 through 1955. The Yadkin River is included in the USGS Hydroclimatic Data

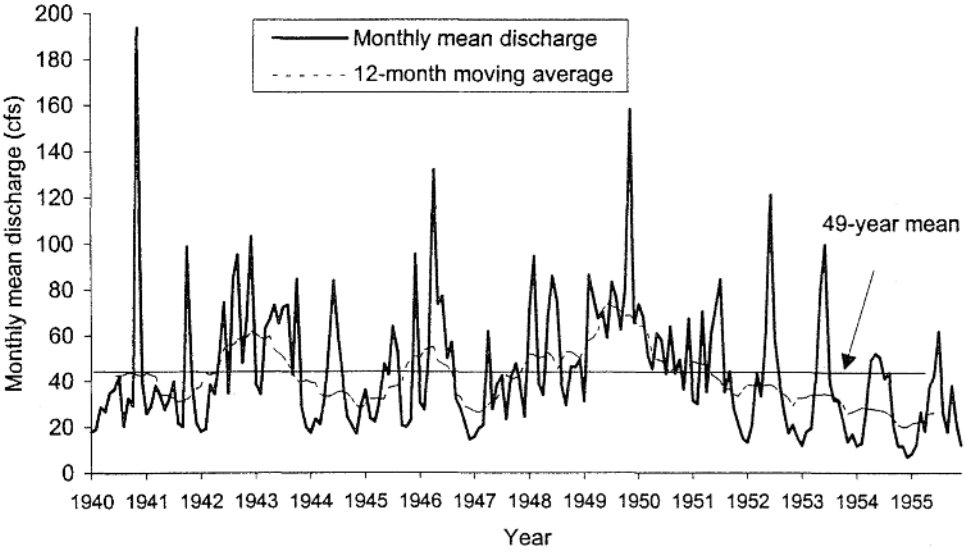

Figure 12.11. Mean monthly discharge for the Yadkin River at Patterson, NC from 1940-1955.

Network (HCDN) (Slack & Landwehr 1992). The HCDN is composed of gaging stations having good- to high-quality records, and, most importantly, their drainage basins have suffered little or no human alteration. The primary purpose of the HCDN is to assess the changes in streamflow that may be related to changing climate. Monthly mean discharge of the Yadkin River varied from a high of 195 cfs in August 1940 to a low of 6.9 cfs in September 1954. These two values happen to be the highest and lowest average monthly discharge for the entire 49-year record. The range in daily mean discharge is much greater with a maximum of 2130 cfs and a minimum of 5.3 cfs. In addition to the monthly mean discharges the 49-year mean (straight line) and the 12-month moving average (dashed line) of the monthly means are plotted on Figure 12.11. The moving average 'smooths' the data and helps elucidate possible trends. Through the 1940s there were wet periods and dry periods, indicated by the moving average rising slightly above and falling below the 49-year mean. The wettest period began in 1948 and continued into 1950. By 1951 below normal-low flows dominated and it appears that a hydrologic drought was under way during the first half of the decade of the 1950s.

A *flow duration curve* is another useful way to present discharge information for water planning. Figure 12.12 is the flow duration curve for the Yadkin River constructed from the average daily flows from the 49-year record. The flow duration curve shows the percentage of time discharge was below a certain level. 25% of the time mean daily discharge on the Yadkin River has been less than 22 cfs, and 50% of the time it has been less than 38 cfs. Flow duration curves are used in planning for water supply, navigation, hydropower, water quality and maintenance (low) flows for aquatic habitat.

It was mentioned at the beginning of the section on drought that frequency analysis is one method of analyzing drought. Table 12.12 shows the results of a frequency

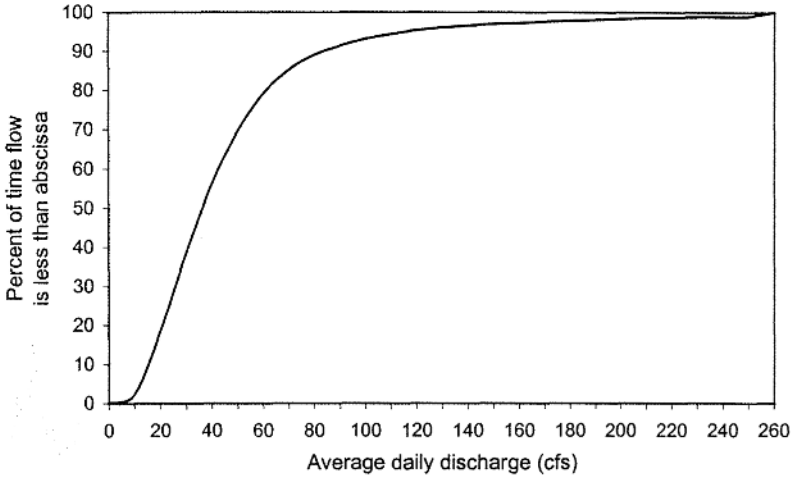

Figure 12.12. Flow duration curve for the Yadkin River at Patterson NC from 1940-1988.

Table 12.12. Low-flow frequency analysis of annual minimum mean daily flows for the Yadkin River, NC (data from Slack & Landwehr 1992).

Year	Q (cfs)	Rank	$m/(n+1)$	T	Number of consecutive days	Date of occurrence
1954	5.3	1	0.02	50.0	1	September 30
1956	5.3	2	0.04	25.0	1	September 17
1988	5.5	3	0.06	16.7	1	August 19
1955	6.0	4	0.08	12.5	1	October 01
1981	7.5	5	0.10	10.0	1	August 29
1982	7.6	6	0.12	8.3	1	October 09
1986	7.6	7	0.14	7.1	1	August 02
1941	9.0	8	0.16	6.3	1	June 22
1953	9.7	9	0.18	5.6	2	
1940	10	10	0.20	5.0	1	May 18
1944	10	11	0.22	4.5	1	August 25
1947	10	12	0.24	4.2	5	
1964	10	13	0.26	3.8	1	December 16
1987	10	14	0.28	3.6	3	
1942	11	15	0.30	3.3	1	October 26
1945	11	16	0.32	3.1	1	July 12
1946	11	17	0.34	2.9	4	
1952	11	18	0.36	2.8	20	
1957	11	19	0.38	2.6	7	
1968	11	20	0.40	2.5	5	
1969	11	21	0.42	2.4	3	
1951	12	22	0.44	2.3	3	
1963	12	23	0.46	2.2	5	
1985	12	24	0.48	2.1	7	
1959	14	25	0.50	2.0	3	
1984	14	26	0.52	1.9	4	
1966	15	27	0.54	1.9	3	
1976	15	28	0.56	1.8	1	September 09
1979	15	29	0.58	1.7	5	
1983	15	30	0.60	1.7	1	September 19

Table 12.12. Continued.

Year	Q (cfs)	Rank	$m/(n+1)$	T	Number of consecutive days	Date of occurrence
1943	16	31	0.62	1.6	2	
1980	16	32	0.64	1.6	3	
1948	17	33	0.66	1.5	9	
1967	17	34	0.68	1.5	3	
1970	17	35	0.70	1.4	5	
1977	17	36	0.72	1.4	5	
1965	18	37	0.74	1.4	1	September 22
1972	18	38	0.76	1.3	9	
1973	18	39	0.78	1.3	1	October 16
1978	18	40	0.80	1.3	2	
1971	19	41	0.82	1.2	1	September 10
1958	21	42	0.84	1.2	2	
1962	22	43	0.86	1.2	1	September 13
1950	24	44	0.88	1.1	4	
1961	24	45	0.90	1.1	1	December 22
1949	25	46	0.92	1.1	7	
1975	25	47	0.94	1.1	4	
1974	27	48	0.96	1.0	4	
1960	29	49	0.98	1.0	2	

analysis of the annual minimum series of daily mean flows on the Yadkin River. A minimum mean daily flow of 5.3 cfs can be expected to occur, on the average, once every 25 to 50 years. Three of the lowest mean daily flows on record occurred in the mid-1950s (Fig. 12.11). Table 12.12 also gives the number of consecutive days the low flow was observed that year. The year 1952 ranks 18th with a mean flow of 11 cfs, but this discharge lasted for 20 days! This certainly could have had a more severe impact than a lower flow that lasted for a shorter period of time. For low flows that lasted only one day, the date of occurrence is given in Table 12.12. Low flows on the Yadkin River are most prevalent during the late summer and fall.

12.5.2 *Estimating water storage requirements*

Stream discharge varies on many time scales. Depending upon the size of the stream, discharge can go up and down in a matter of hours or days following individual storms. Discharge varies on a seasonal basis in response to the balance between precipitation and evapotranspiration, and on an annual basis following wet spells and droughts. On large streams where demand is a small fraction of the supply there is rarely a problem in meeting the demand. In cases where demand is a significant fraction of the supply the challenge to make sure there is enough water to carry over through the critical dry period(s). This requires providing reservoir storage to capture water during periods of high flow for use during times of low flow. A basic problem for water supply planning and management is estimating the amount of storage necessary to meet a given demand. The water *yield* is the amount of water that can be obtained from a source. Reservoir storage increases the yield by capturing the high flows for use at a later time. Assuming no water losses by seepage and evaporation,

the maximum yield over time from a stream equals the mean annual streamflow. However, storing water in reservoirs inevitably causes losses by seepage and evaporation and reduces the maximum yield below the mean annual discharge. Two methods for estimating reservoir storage are the *mass curve* and the *sequent-peak* method.

12.5.2.1 *Mass curve*

One of the earliest methods devised for estimating reservoir storage is a *mass curve*. A mass curve is a curve of the cumulative discharge for a river. The slope of the mass curve at any point equals the discharge rate (Fig. 12.13). If demand is constant over some time period, the cumulative demand curve is a straight line with a slope equal to the demand. The amount of reservoir storage for a given demand is found by drawing a line with a slope equal to the demand curve tangent to the high points of the mass curve. The required storage is the maximum difference between the cumulative demand curve and the mass curve. It is important that the period chosen for the analysis include a critical period of low flow. The critical dry period might be the single driest year (month) or a run of several dry years (months). A sequence of several dry years (months) is preferable since water supply failure is more likely to occur during a run of dry years (months). Data for a hypothetical mass curve is given in Table 12.13 and plotted on Figure 12.13. In column 2 are the mean annual discharges (Q), column 3 the cumulative discharge (mass curve), and column 4 the demand (D), which is a constant 3000 cfs. Demand is composed of reservoir releases and losses by seepage and evaporation. The required storage capacity for this level of demand and this streamflow record is 2700 cfs (Fig. 12.13). To convert storage in units of flow (L^3T^{-1}) into a volume, multiply by time (T).

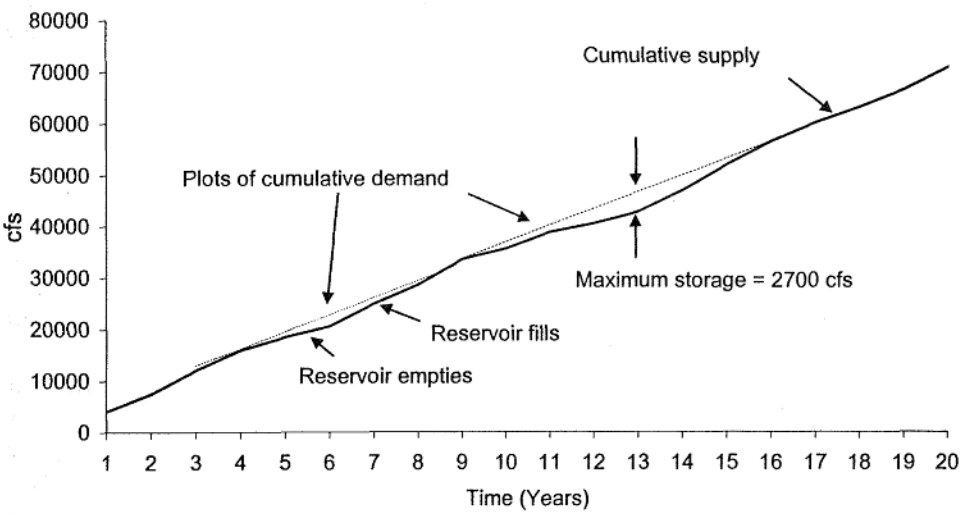

Figure 12.13. Hypothetical mass curve showing the determination of storage as the maximum difference between the cumulative supply (mass) curve and the cumulative demand curve. The cumulative demand is drawn tangent to the supply curve with a slope equal to the demand.

Table 12.13. Data for the mass curve shown in Figure 12.13.

Time	Q (cfs)	ΣQ	D (cfs)	Time	Q (cfs)	ΣQ	D (cfs)
1	4000	4000	3000	14	3480	47080	3000
2	3380	7380	3000	15	5050	52130	3000
3	4610	11990	3000	16	4500	56630	3000
4	3940	15930	3000	17	3650	60280	3000
5	2480	18410	3000	18	3050	63330	3000
6	2750	20560	3000	19	3370	66700	3000
7	3760	24930	3000	20	4380	71080	3000
8	3650	28580	3000	21	2220	73300	3000
9	4900	33480	3000	22	2810	76110	3000
10	2080	35560	3000	23	3250	79360	3000
11	3210	38770	3000	24	3560	82920	3000
12	1710	40480	3000	25	2940	85860	3000
13	2300	42780	3000				

12.5.2.2 *Sequent-peak method*

The sequent-peak method is an alternative way to estimate reservoir storage. The sequent-peak procedure gives the same result as the mass curve method but it is somewhat easier to use. With the sequent-peak method the cumulative difference between supply and demand is calculated and plotted. A horizontal line is drawn from each peak to the next higher (sequent) peak. The maximum difference between any horizontal line (peak) and the intervening valley on the curve is the maximum required storage capacity. The method is shown in Table 12.14 and Figure 12.14.

12.5.2.3 *Stochastic streamflow simulation*

The problem of short streamflow records plagues the estimation of reservoir storage just as it increased the uncertainty in the estimation of flood peaks. It is unlikely that a relatively short streamflow record will contain the lowest-flow sequence that is possible for that stream. There may have been a drought many centuries ago, or one yet to come in the future, that was or will be more severe than anything in the his-

Table 12.14. Sequent peak analysis of the same data as in Table 12.13.

Time	Q	D	$Q-D$	$\Sigma(Q-D)$	Time	Q	D	$Q-D$	$\Sigma(Q-D)$
1	4000	3000	1000	1000	14	3480	3000	1300	5080
2	3380	3000	380	1380	15	5050	3000	2050	7130
3	4610	3000	1610	2990	16	4500	3000	1500	8630
4	3940	3000	940	3930	17	3650	3000	650	9280
5	2480	3000	–520	3410	18	3050	3000	50	9330
6	2750	3000	–850	2560	19	3370	3000	370	9700
7	3760	3000	1370	3930	20	4380	3000	1380	11080
8	3650	3000	650	4580	21	2220	3000	–780	10300
9	4900	3000	1900	6480	22	2810	3000	–190	10110
10	2080	3000	–920	5560	23	3250	3000	250	10360
11	3210	3000	210	5770	24	3560	3000	560	10920
12	1710	3000	–1290	4480	25	2940	3000	–60	10860
13	2300	3000	–700	3780					

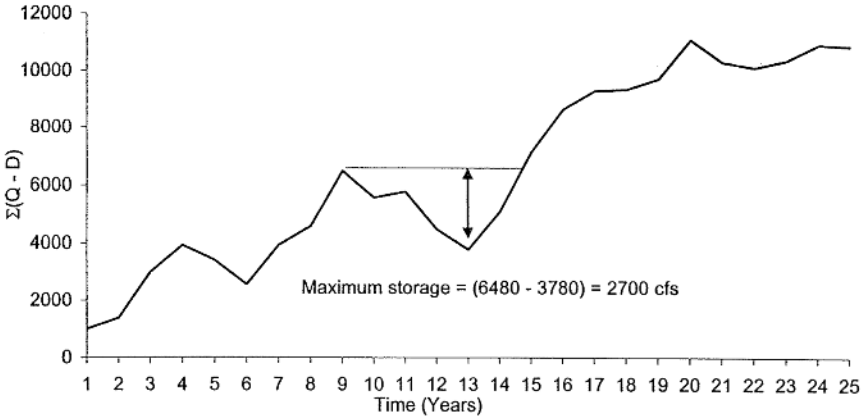

Figure 12.14. Hypothetical sequent-peak graph. Storage is equal to the maximum difference between the horizontal line and the curve of the cumulative difference between supply and demand.

torical record. One way to address this problem is by simulating streamflow. Streamflows generated by abstract mathematical models are referred to as 'synthetic' streamflows. The stochastic model used here is a lag-1 Markov model for annual streamflow. The Markov model described here is also called an autoregressive (AR) model. Autoregressive simply refers to the stochastic characteristic of persistence. Since the Markov model is a lag-1 model it is denoted as an AR(1) model. More complex stochastic models for simulating seasonal streamflows can be constructed. A major assumption with this model is that the process (streamflow) is stationary. The lag-1 Markov model for annual average streamflow is:

$$Q_t = \overline{Q} + r\left(Q_{t-1} - \overline{Q}\right) + e_t s\left(1 - r^2\right)^{0.5} \tag{12.17}$$

where Q_t is discharge in year t, $\overline{Q}$ is the mean annual discharge, s is the standard deviation of the annual discharges, and r is the serial correlation coefficient between discharge Q_{t-1} and Q_t. The three parameters are estimated from historical streamflow records. The last component of the model is the random variate e_t. The model states that streamflow in the current year t depends upon the long-term average streamflow, the previous year's streamflow, the correlation between streamflows from one year to the next, and a random component. The second term on the right-hand side of Equation (12.17) models the persistence between flows. The third term generates random variations in the model. The random variate e_t has a mean of 0 and a standard deviation of 1, and is chosen from an appropriate probability distribution. Many investigators have found that the normal distribution is most satisfactory, in which case the random variate is taken from a standard normal distribution. Tables of random standard normal deviates are available in many statistics textbooks (e.g. Haan 1977). Computer programs are also available for generating random variates from different distributions. There is no way to choose the probability distribution *a priori*, and short historical records may not clearly define the underlying distribution. Any disparity between the assumed distribution and the true natural process is perpetuated in the simulated flow sequence creating an operational bias. The Markov

model reproduces annual streamflows having the same mean and variation as found in the historical sample. The accuracy of the model is limited by the accuracy of the estimated parameters. Whether the lag-1 dependence structure is adequate in replicating the long-term persistence in the natural process is subject to debate (Linsley et al. 1982). Once the parameters are estimated, synthetic streamflow sequences (called traces) of length n can be generated. Given the uncertainty regarding the characteristics of the long-term persistence it is recommended that n not exceed 100 years. This type of stochastic model does not attempt to replicate the actual pattern of historical flows, it simply generates statistically similar flows – flows that are statistically possible. Figure 12.15 shows mean annual flows for the Yadkin River and a synthetically generated trace. The parameters of the model for the Yadkin River are $\bar{Q}$ = 48.9 cfs, s = 14.9 cfs, and r = 0.305. The model requires an initial discharge for Q_{t-1} to begin the simulation. The initial discharge was set equal to 43.9 cfs, the observed discharge for 1940. The trace in Figure 12.15 has a higher peak and a lower minimum than any found in the historical record.

Box 2 is a BASIC computer program to generate synthetic streamflows using Equation (12.17). The random variate is generated for a standard normal distribution in a two-step procedure. First, a random number between 0 and 1 is generated by the computer (line 170). This random number is then used to produce a standard normal variates using a subroutine (line 1000) that approximates an inverse transformation of the normal distribution (Ruckdeschel 1981). The inverse transformation is the procedure of finding the corresponding Z-score for a given probability. The procedure is the exact opposite (inverse) of what we did in Chapter 3.

12.5.2.4 *Frequency estimation of storage requirements*

Using the historical streamflow record we could calculate only one estimate of reservoir storage for a given demand. The synthetic streamflow generation model allows

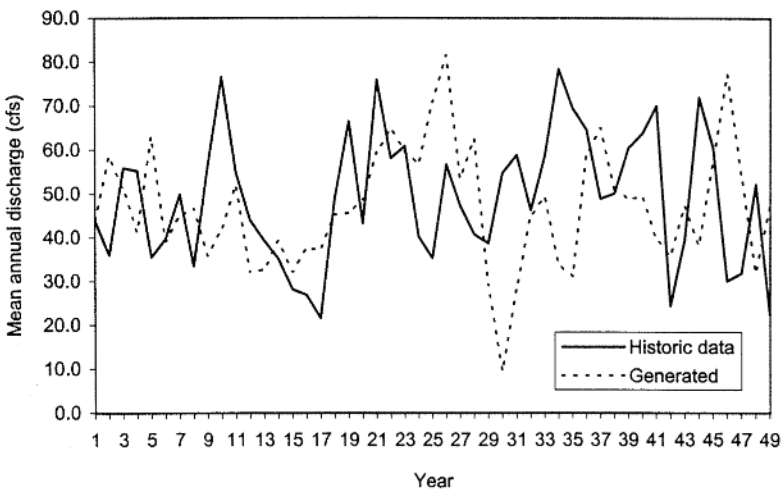

Figure 12.15. Graphs of the historical mean annual discharge and a synthetically-generated trace for the Yadkin River.

BOX 2 MARKOV STREAMFLOW SIMULATION PROGRAM

```
10 REM PROGRAM TO SIMULATE STREAMFLOW USING A LAG 1 MARKOV MODEL
20 REM
30 REM MAIN PROGRAM WRITTEN BY STEPHEN A. THOMPSON, 1995.
40 REM NORMAL VARIATE GENERATION IS BASED ON A SUBROUTINE FROM RUCKDESCHEL, 1981 (SEE BELOW).
50 COLOR 14,1:CLS
60 DIM Q(500)
70 PRINT "FOR THE HISTORIC DATA SERIES ENTER FOLLOWING:": PRINT
80 INPUT "THE MEAN"; QBAR: PRINT
90 INPUT "THE STANDARD DEVIATION"; SD: PRINT
100 INPUT "THE LAG-1 SERIAL CORRELATION COEFFICIENT"; RHO: PRINT
110 INPUT "A STARTING FLOW VALUE TO 'SEED' THE MODEL"; Q(1): PRINT
120 INPUT "HOW MANY YEARS DO YOU WANT TO SIMULATE"; N
130 CLS
140 RANDOMIZE TIMER
150 PRINT "TIME"; TAB(15); "Q"
160 FOR I = 2 TO N
170 Y = RND(I)
180 IF Y > .5 THEN Y = 1 - Y: FLAG = 1
190 GOSUB 1000
200 Ei = X
210 IF FLAG = 1 THEN Ei = -1 * Ei: FLAG = 0
220 Q(I) = QBAR + RHO * (Q(I - 1) - QBAR) + Ei * SD * SQR((1 - RHO * RHO))
230 PRINT I; TAB(10); : PRINT USING "#####.#"; Q(I)
240 NEXT
250 PRINT:PRINT "NORMAL END OF PROGRAM":END
260 REM
1000 REM ***** INVERSE NORMAL DISTRIBUTION SUBROUTINE *******
1010 REM
1020 REM CALCULATES AND APPROXIMATION TO THE INTEGRAL OF THE NORMAL
1030 REM DISTRIBUTION FUNCTION FROM X TO INFINITY
1040 REM USING A RATIONAL POLYNOMIAL.
1050 REM THE INPUT IS Y; THE RESULT IS RETURNED IN X
1060 REM ACCURACY IS BETTER THAN 0.0005 IN THE RANGE 0<Y<0.5.
1070 REM FROM RUCKDESCHEL (1981), BASIC SCIENTIFIC SUBROUTINES VOL. II,
1080 REM BYTE/MCGRAW-HILL, PAGE 164-166.
1090 C0 = 2.515517
1100 C1 = 0.802853
1110 C2 = 0.010328
1120 D1 = 1.432788
1130 D2 = 0.189269
1140 D3 = 0.001308
1150 IF Y = 0 THEN X = 1
1160 IF Y = 0 THEN RETURN
1170 Z = SQR(-LOG(Y * Y))
1180 X = 1 + D1 * Z + D2 * Z * Z + D3 * Z * Z * Z
1190 X = (C0 + C1 * Z + C2 * Z * Z) / X
1200 X = Z - X
1210 RETURN
```

us to generate multiple streamflow traces, and for each trace a value of reservoir storage can be calculated. These values for reservoir storage can then be ranked and assigned exceedence probabilities. Example 12.4 demonstrates the procedure.

Example 12.4

For this example the hypothetical discharge data from Table 12.14 are taken to represent the 'historical' data, and the mean, standard deviation and serial correlation coefficient were calculated. Twenty traces were generated, with each trace 50 years in length. If we include the historical streamflow sequence we have a total of 21 separate streamflow sequences for the frequency analysis (Table 12.15).

For each trace the storage capacity needed to meet the demand of 3000 cfs was determined by the sequent-peak procedure. The storage values were then ranked and assigned sample frequency

Table 12.15. Frequency analysis of reservoir storage for a demand of 3000 cfs.

Rank	Storage	F
1	6558	0.05
2	6505	0.09
3	6115	0.14
4	5859	0.18
5	5482	0.23
6	5294	0.27
7	5028	0.32
8	4938	0.36
9	4804	0.41
10	4350	0.45
11	4312	0.50
12	4302	0.55
13	3854	0.59
14	3156	0.64
15	2700	0.68
16	2531	0.73
17	2473	0.77
18	2374	0.82
19	2184	0.86
20	1482	0.91
21	1179	0.95

estimates (exceedence probabilities) using the Weibull formula $F_s = m/(n+1)$. The original storage requirement of 2700 cfs from Figure 12.14 would be exceeded 68% of the time. In fact, 50% of the time more than 4312 cfs of storage is needed. It is up to the decision makers to choose the amount of storage to be provided based on the cost of building storage and the amount of risk they are willing to accept. The risk is that the reservoir will go dry.

The required storage capacity increases as the demand increases. Figure 12.16 shows the results of a series of simulations of storage capacity with increasing demand. In this particular example no storage was required until demand exceeded 75% of the mean annual streamflow. After that the amount of storage increased dramatically. The amount of storage also increases as streamflow variability increases. This is one reason the storage capacity for water supply systems in the western United States is greater than for systems in the East. To produce the same yield, reservoirs in the West need to be larger because of the greater variability in discharge. Figure 12.17 shows a simulated example of how increasing streamflow variability increases the required storage for a given demand. It should be pointed out that the simulations that produced Figures 12.16 and 12.17 were run with line 140 of the model deleted (see Box 2). Line 140 instructs the computer to use a different random number every time to 'seed' the random number generator. With line 140 deleted, the computer generates the same sequence every time, in which case the sequences are not really random at all.

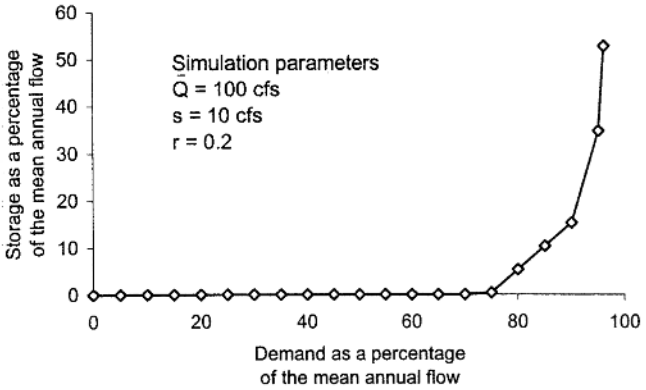

Figure 12.16. Results of a series of simulations that show the effect of increasing demand on the amount of storage required to meet that demand. For each simulation the mean is 100 cfs, the standard deviation 10 cfs and the serial correlation coefficient 0.2.

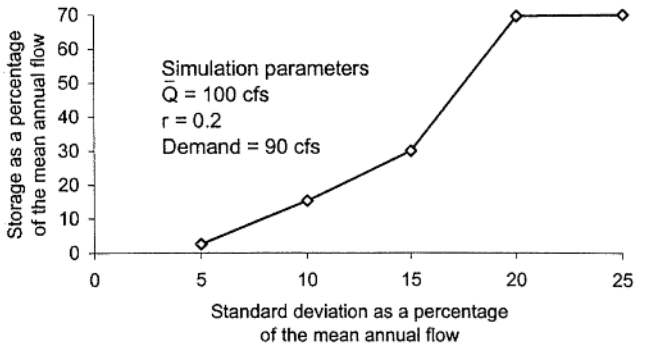

Figure 12.17. Results of a series of simulations that show how increasing streamflow variability increases the amount of storage required to meet a given demand. For each simulation the mean is 100 cfs, the serial correlation coefficient 0.2 and the demand 90 cfs.

SUMMARY

In this chapter we defined and analyzed drought using a variety of approaches. Drought is a difficult phenomena to study because it is a relative rather than absolute phenomena, and it effects both the input and the output variables of the hydrologic system. The runs approach provides a convenient means of defining drought characteristics. The most widely used method for defining and analyzing drought, at least in the United States, is the Palmer Drought Severity Index or the closely related Palmer Hydrological Drought Index. For more limited purposes a narrowly-tailored drought index might be used. Frequency analysis can be used, but it requires that droughts first be defined by some other means.

One of the most important impacts from drought is reduced water supply. Water supply managers must plan for this contingency and provide adequate water storage

to carry the system through the drought period. Mass curves and the sequent-peak method calculate storage for a given streamflow and demand regime. Stochastic simulation models can be extremely useful in extending limited streamflow records. Models are now indispensable in all areas of hydrology from the study of groundwater to surface water, and for issues of water quantity to water quality. Chapter 13 examines hydrologic models and Geographical Information Systems as applied to hydrology and water management.

PROBLEMS

12.1 Set the truncation level at –1.00 and calculate drought duration, intensity, severity and magnitude for the droughts contained within the PDSI record of Table 12.6.

12.2 Find the state transition probability matrix $\underline{P}$ for the time series below. Use three environmental states – drought, normal and wet.

Time	1	2	3	4	5	6	7	8	9	10	11	12	13	14	15	16	17	18	19	20	21	22
State	W	W	N	N	N	D	D	D	N	N	D	D	D	D	N	N	N	W	W	N	N	W

12.3 Calculate the reservoir storage required to meet a demand of 200 cfs given the following time series of mean annual streamflows.

Year	Flow (cfs)	Year	Flow (cfs)
1	140	11	250
2	190	12	235
3	230	13	170
4	250	14	155
5	200	15	175
6	270	16	190
7	340	17	260
8	215	18	250
9	275	19	240
10	320	20	310

12.4 Use the Markov streamflow model to generate a synthetic streamflow trace for the data in Problem 12.3. The serial correlation coefficient for the data is $r = 0.36$.

CHAPTER 13

Hydrologic models and geographic information systems

Computer modeling has become indispensable for understanding and predicting the behavior of hydrologic systems, while Geographical Information Systems (GIS) are revolutionizing the storage, retrieval and analysis of spatial data. Each by itself is a powerful tool for water resources planning and management but some of the most promising advances merge the two into a unified resource-analysis system. In this chapter we first discuss hydrologic simulation models and then GIS. Two hydrologic models HEC-1 and AGNPS are described in detail. In section 13.2.2 we look at some applications where the models and GIS have been combined to address water resource problems.

13.1 HYDROLOGIC MODELS

Why use models? Kirkby et al. (1987) identify three distinct uses of models. Models are used in teaching; they illustrate how complex physical systems work. Models are used in research and have redefined traditional research practice by substituting computer experimentation for traditional field experimentation. Lastly, models are used in forecasting and predication. Government agencies routinely use models to forecast weather conditions, snowmelt runoff and stream discharge.

Some have argued that we may depend too much on computer models and that more time should be spent in the field. There is certainly a danger in becoming too reliant on any tool, and one of the dangers of models is that we may believe their output is true. The output from a model is only as good as the input data and the equations used to represent the physical processes. If the data are of low quality, the output will be poor no matter how sophisticated the model – garbage in, garbage out. If the model's structure poorly approximates the operation of the real system, the output will always be poor no matter how good the input data. A good model run with good data can provide useful information. In some cases, without models there would be no way to begin to understand the subtle interactions within complex real-world systems.

13.1.1 *Types of models*

There are different types of hydrologic models. Two types of models are *scale* models and *mathematical* or *computer* models. A scale model is a miniaturized replica of

a real physical system and is composed of materials similar to those found in the real system. An example of a scale model is the Corps of Engineers' model of the Mississippi River system near Vicksburg, Mississippi. The model covers many acres and replicates in detail the channel network and the control structures that have been built on the river. The model allows the engineers to simulate high flows, low flows and the intricacies of contaminant transport. One reason for using scale models is that the operation and dynamics of the real system are too complex to simulate on a computer. Another group of scale models becoming popular among the public at large are the small aquarium style models of unconfined aquifers. The models are made of alternating layers of sand and clay with a small pump acting as a well. Food coloring is added to simulate the release of a pollutant. These models are showing up in elementary schools and at local government planning meetings where wellhead protection programs are being discussed. The purpose of these models is to improve the public's understanding of groundwater flow and contaminant transport.

Mathematical models simulate the operation of real systems using mathematical equations. Penman's equation for estimating evaporation is a model of the evaporation process. While individual equations can be solved readily by hand, more complex hydrologic models link many equations in sequence and/or repetitively solve the same set of equations. In this case it is much more efficient to program the equations for solution by a computer. Since the mathematical models discussed here are all computer models the two are considered synonymous from now on. The focus in this chapter is primarily on computer *simulation models*. Simulation models replicate, with varying degrees of complexity and resolution, the time and/or space movement of mass, energy and momentum. There are other types of mathematical models used in water resource management. *Optimization models* are an example. An optimization model does not attempt to replicate the movement of mass, energy or momentum. The purpose of an optimization model is to maximize (minimize) some attribute of a water resource management system. In the parlance of optimization modeling, the goal is to maximize (minimize) some *objective function*. For example, suppose there are two wastewater treatment plants discharging treated wastewater into a stream. This water resource management system involves the natural river system having certain water quantity and quality characteristics, and the human system composed of storm sewers and waste treatment plants. An optimization model is not concerned with *how* the water flows through this system, but only with optimizing some characteristic of the system. In this case the objective function might be to minimize the total cost of wastewater treatment subject to the constraint that water quality meets certain criteria downstream of the plants. The model is a set of equations – the objective function and the *constraint* equations. The constraint equations limit (constrain) the values of certain variables within the model. Optimization models can be either *linear* or *nonlinear*. The linear models are easier to solve and are more common.

13.1.2 *Deterministic versus stochastic simulation models*

The Markov streamflow model in Chapter 12 is a stochastic simulation model. For the same model parameters and initial flow the model produces a different sequence of streamflows each time it is run. For a given input a stochastic model does not pro-

duce the same output. Also, the stochastic model does not, and can not, replicate the actual historical sequence of flows used to estimate the model parameters. With a *deterministic* simulation model, once the parameters are set, the same input data produce the same output every time. For example, if you use the same data in Penman's equation you always get the same result. However, even the parameters of a deterministic model are based on a sample of data, and different samples can produce different values for the parameters. In this sense even a deterministic model produces 'random' outputs; the outputs belong to a random distribution of possible outputs. Our focus in this chapter is exclusively on deterministic simulation models.

13.1.3 *Classifying deterministic models*

The internal complexity of deterministic simulation models is sometimes described as being analogous to a box having different shades of grey. The structure and operation of a 'white box' model is built from the knowledge of the variables in the real system and the relationships between those variables (Kirkby et al. 1987). Equations ('transfer functions') simulate as closely as possible the functioning of the real hydrologic components and processes. The white box model converts inputs (e.g. precipitation) into outputs (e.g. streamflow) using explicit transfer functions. The term white box implies that the operation of the system is well understood, as if a light were illuminating the internal components of the model. At the other end of the spectrum are 'black box' models. Black box models convert inputs into outputs but the system is treated as a single unit with no attempt to understand its operation. The unit hydrograph is a black box model that converts rainfall into a hydrograph but without any consideration or illumination of the hydrologic processes at work in the drainage basin. Empirical regression equations such as those developed for regional flood frequency analysis are another example of black box models. The Markov streamflow simulation model is also a black box.

Simulation models have different characteristics, and they have been categorized according to one or more of these attributes (Table 13.1). There are models that simulate surface water flow, models that simulate groundwater flow, and models that simulate combined surface and groundwater flow systems. Some models simulate only water quantity, while others simulate water quality; however, most water quality models necessarily simulate water quantity as well. Another distinction between models is the number of spatial dimensions incorporated in the model – one, two or three dimensions. In Chapter 8 spatial dimensions were discussed for groundwater models. Still another difference between models is the degree of spatial heterogeneity allowed within the model. *Lumped parameter* models are spatially

Table 13.1. Some characteristics used to categorize hydrologic simulation models.

Surface water, groundwater, both surface and groundwater
Water quantity versus water quality
One, two or three spatial dimensions
Event-based versus continuous simulation
Lumped parameter versus distributed parameter
Deterministic versus stochastic

homogeneous, while *distributed parameter* models are more heterogeneous. An example of a lumped parameter model would be a model of a drainage basin that allows only a single (average) value for infiltration over the entire basin. A distributed parameter model would allow infiltration to vary at different locations throughout the basin. Some models offer a compromise; for each subbasin the parameter is a constant, but the model allows the drainage basin to be divided into an unlimited number of subbasins. While a distributed parameter model has the potential to be more accurate, it requires more time and effort in data collection and parameter estimation. In modeling we once again face the inescapable tradeoff between accuracy and effort. Still another characteristic is whether the model is *event-based* or a *continuous* simulation model. An example of an event-based, surface water quantity model is a *rainfall-runoff* model. The purpose of a rainfall-runoff model is to simulate a stream hydrograph (output) from a given precipitation hyetograph (input). Event-based means the model simulates individual storms lasting from a few minutes to a few days. This type of model does not simulate the entire hydrologic cycle. Certain processes and components like evapotranspiration, soil moisture, and subsurface flows (interflow and groundwater) are either ignored completely or they are 'parameterized', which means they are not modeled explicitly. A continuous simulation model replicates the entire hydrologic system (Fig. 1.2), and continuously updates components and processes at each time step. For example, at each time step a continuous model would update soil moisture storage by simulating gains through infiltration and losses from evapotranspiration and deep percolation. This type of model is used to simulate the operation of a drainage basin over many years. The water balance within the Palmer Drought Severity Index program is a continuous model.

An example of an event-based, rainfall-runoff model is HEC-1 from the Corps of Engineers. (HEC stands for Hydrologic Engineering Center at Davis, California.) One reason for the model's popularity is the capability of mixing and matching different modeling options, and the wide variety of options available.

13.1.4 *Steps in using a computer model*

13.1.4.1 *Model identification and selection*

The assumption is that there exists a model capable of doing what it is that you want to do. If this is not the case, then you may have to build your own model. Given the explosive growth in availability off-the-shelf models it is unlikely you will need to build your own model. There are literally dozens of models available, with new ones being developed, and old ones being modified all the time. This surge in model building also means it is difficult to find an up-to-date listing of the different models and their capabilities. The Office of Technology Assessment (1982) comparatively evaluated different water resource models. More recently the NRC (1990) evaluated approaches to groundwater modeling, though not the performance of individual models. Dzurik (1990) lists dozens of surface water models for analyzing both water quality and quantity. He gives the common acronym for the model, who developed the model, and the types of water resource problems that the model is appropriate for. A good reference for streamflow models is the text *Hydrologic Systems: Watershed Modeling, Volume II* (Singh 1989). He devotes two entire chapters to models; one chapter for event-based models and one for continuous models.

Many federal and some state agencies have developed their own simulation model(s) including the US Geological Survey, the Soil Conservation Service (now called the Natural Resources Conservation Service), the US Forest Service, the Environmental Protection Agency, the National Weather Service, the Corps of Engineers, and the US Fish and Wildlife Service. A number of major state universities have developed hydrologic simulation models including Ohio State, Penn State, and Colorado State University. In addition there are three major modeling centers in the United States: The Center for Water Quality Modeling of the US Environmental Protection Agency in Athens, Georgia, the Hydrologic Engineering Center of the Corps of Engineers in Davis California, and the International Groundwater Modeling Center of the Holcomb Research Institute in Indianapolis, Indiana (Dzurik 1990).

Choosing which model to use depends upon your needs and upon the model's capabilities. If you want to simulate the hydrograph from a storm of a certain intensity and duration to help determine floodplain boundaries, then an event-based model is adequate. If the problem is to simulate the long-term transport and fate of pesticides applied to farm fields, then a continuous water quality model simulating both surface and groundwater flow may be required. The characteristics of the model determine what kind of input data are needed to run the model. There are two types of input data – data for estimating model *parameters*, and the data used to drive the simulation. Parameters are values that either describe physical characteristics of the hydrologic system, set initial conditions for components, or act as rate constants for processes. For a surface water model the input data to drive the simulation is precipitation, but it might include air temperature, solar radiation and wind speed if the model simulates evaportranspiration. Depending upon the model and problem at hand the time interval for the input data could be minutes, days, or even years in the case of some groundwater simulations.

A final consideration in choosing a model is how difficult it is to use. On the one hand difficulty is related to the amount of data needed to run the model. On the other it depends on the availability and quality of the documentation that explains the operation and use of the model. Good documentation will explain the model's structure, what the model's major assumptions are, and how to obtain data for estimating the parameters. A good model that is poorly documented can be very difficult to use. In the following discussion surface water models are used as examples but the same procedures apply to any model.

13.1.4.2 *Model calibration and verification*

The process of setting parameter values is called model calibration. Verification is assessing the accuracy of the model's output, and it could lead to further (re)calibration. Model calibration and verification may thus be an iterative procedure. Figure 13.1 shows the steps in calibration and verification. There are two basic types of model parameters – *physical* parameters and *process* parameters. Physical parameters describe the model's physical structure such as soil depth, channel length and basin area. Process parameters set initial conditions for components and flow rates, and might include initial soil moisture storage, the limiting infiltration rate f_c, or the rate of baseflow prior to storm-generated runoff.

Once an appropriate model is selected data must be collected to estimate the parameters. The values for most physical parameters are usually determined fairly

easily. For other parameter, especially process parameters, determining the best value can be more difficult. Finding the best value for a parameter is called parameter optimization. Two things to keep in mind are that data collection involves sampling so you want to be sure to get a representative sample, and that a model may be more sensitive to certain parameters than to others. If the model has many parameters, before embarking on an expensive data collection program it is advisable to do a *sensitivity analysis*. Sensitivity analysis means running the model with different values for the parameter and comparing the effect on the model's output. If the output does not change much as the parameter's value changes, then the model is not very sensitive to that parameter. You should not spend a lot of time collecting data for a parameter that has only a small influence on the model's performance. Given the limits on time and money you should concentrate on getting the best data for the parameters the model is most sensitive to.

Model calibration and optimization involves setting the process parameters and comparing the output to a set of observed data (Fig. 13.1). The objective is to minimize the error (difference) between the observed and the predicted values. Optimal parameter values will minimize this error. Once the model is calibrated it must still be verified for accuracy. Verification involves running the model again but with a different set of data. If the model is well calibrated it should produce acceptable output using any set of input data, not just the data on which it was calibrated. This is why verification uses a different set of data than that used for calibration. If the verification run is unacceptable, you may need to go back to the calibration stage.

13.1.4.3 *Types of error measurement*

There are different ways to measure the error between the observed data and simulated output. The most common measure of error E_1 is the sum of the squares of difference between the individual observed values of the variable and the corresponding predicted values:

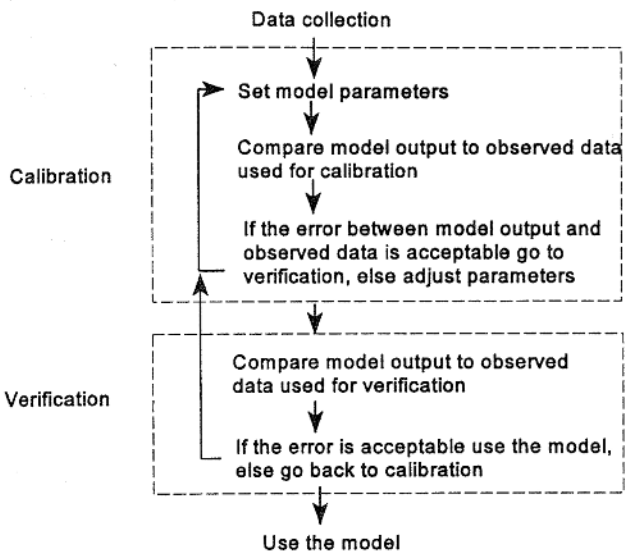

Figure 13.1. Steps in model calibration and verification. The verification procedure may lead to further calibration.

$$E_1 = \sum_{i=1}^{n} (O_i - P_i)^2 \tag{13.1}$$

where O_i is the observed value for the variable at time i and P_i is the corresponding predicted value. Squaring makes all of the differences positive, which is the same approach used in calculating the standard deviation. One problem with this measure of error is that small differences in the *timing* of observed and predicted values can cause E_1 to be large. Two other measures of error used in streamflow modeling are:

$$E_2 \left(\sum_{i=1}^{n} O_i - \sum_{i=1}^{n} P_i \right)^2 \tag{13.2}$$

and

$$E_3 = (O_{pk} - P_{pk})^2 \tag{13.3}$$

E_2 compares the volumes of runoff, while E_3 compares peak discharges. The objective of the simulation exercise dictates which measure of error is most appropriate.

Another way to express the error between individual observed and predicted values is the Root Mean Square Error (RMSE):

$$\text{RMSE} = \sqrt{\frac{\sum_{i=1}^{n} (O_i - P_i)^2}{n}} \tag{13.4}$$

The HEC-1 model uses a weighted RMSE that emphasizes the accurate reproduction of peak flows rather than low flows (COE 1987a).

The previous error formulas all give results that reflect the magnitudes of the observed and predicted values. This makes it difficult to compare, in a relative way, the error between different problems or different models. Willmott (1982) proposed a measure called the 'index of agreement.' The index of agreement d is a descriptive measure of error that allows direct comparison of the relative error. The index is bounded by 0 and 1. The closer the index is to 1 the better the agreement (smaller the differences) between the observed and predicted values. The index of agreement is calculated as:

$$d = 1 - \left[\sum_{i=1}^{n} (P_i - O_i)^2 / \sum_{i=1}^{n} \left(|P_i'| + |O_i'| \right)^2 \right] \tag{13.5}$$

where

$$P_i' = P_i - \overline{O} \tag{13.6}$$

and

$$O_i' = O_i - \overline{O} \tag{13.7}$$

Example 13.1

Figure 13.2 shows hypothetical observed and predicted hydrograph ordinates in cubic meters per second (cms). The arrow on the figure graphically depicts the error at time period 5. Table 13.2 gives the observed hydrograph ordinates in column 2 and the predicted hydrograph ordinates in column 3. Column 4 is the difference between the observed and predicted values ($O - P$), and column 5 the square of these differences.

The five measures of error are:

$$E_1 = \Sigma(O - P)^2 = 8050 \text{ cms}^2$$

$$E_2 = (1753 - 1655)^2 = 98^2 = 9604 \text{ cms}^2$$

$$E_2 = (255 - 270)^2 = (-15)^2 = 225 \text{ cms}^2$$

$$\text{RMSE} = (8050/15)^{0.5} = 23.2 \text{ cms}$$

$$d = 0.97$$

The average error measured by the RMSE is 23.2 cms, and the index of agreement $d = 0.97$ shows that the predicted hydrograph is quite close to the observed.

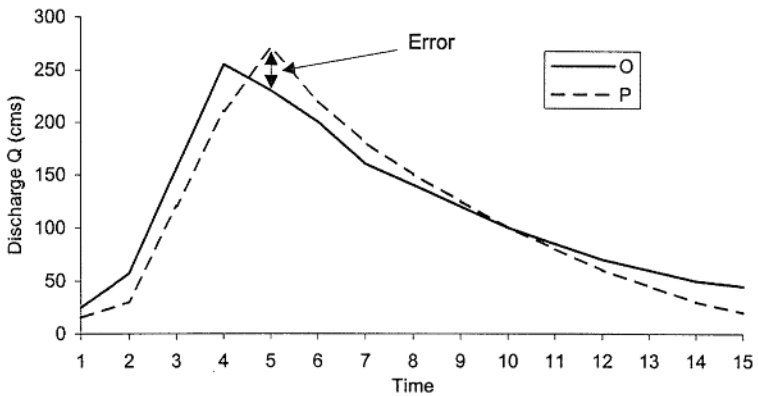

Figure 13.2. Hypothetical observed and predicted hydrographs for demonstration of error calculations.

Table 13.2. Hypothetical observed (O) and predicted (P) hydrograph ordinates (cms).

Time	O	P	$O - P$	$(O - P)^2$
1	25	20	5	25
2	57	35	22	484
3	56	150	6	36
4	255	220	35	1225
5	230	270	–40	1600
6	200	240	–40	1600
7	160	180	–20	400
8	140	150	–10	100
9	120	125	–5	25
10	100	100	0	0
11	85	80	5	25
12	70	60	10	100

Table 13.2. Continued.

Time	O	P	$O-P$	$(O-P)^2$
13	60	45	15	225
14	50	30	20	400
15	45	20	25	625
Total	Σ 1753	Σ 1655		Σ 8050

13.1.5 *The HEC-1 simulation model*

The HEC-1 model is an event-based, surface water, water quantity simulation model. Both mainframe and PC-computer versions of HEC-1 are available. HEC-1 does not have a single model structure. Different options can be selected and combined for modeling different hydrologic processes. In essence you create your own custom model by mixing and matching model options. For example, infiltration can be simulated five different ways, and runoff hydrographs can be generated using a unit hydrograph, synthetic unit hydrographs, or a kinematic wave. In addition to the basic rainfall-runoff component HEC-1 has automatic parameter optimization, it can simulate the operation of pumps and water diversions in and out of the basin, it performs reservoir routing, and can even do economic analysis and optimization. The output from HEC-1 can be input directly into the HEC-2 model. HEC-2 calculates water surface profiles and elevations for floodplain delineation. In the discussion below we only consider the Rainfall-Runoff (RR) part of the model.

13.1.6 *Model components*

13.1.6.1 *Stream network development*

Using topographic maps, aerial photos, soil surveys, field measurements and any other source of geographic information, the stream network is divided into an interconnected set of components. The basic RR components are subbasin runoff components and channel routing components. Figure 13.3 shows a drainage basin divided into three subbasins, A, B, and C. Figure 13.4 is a schematic diagram of the basin components. The four-steps for developing the schematic diagram are as follows (COE 1987a):

1. Delineate the basin boundary using geographic data. In urban areas municipal drainage maps will be needed to identify drainage via storm sewers.

2. Divide the basin into subbasins. There is no limit to the number of subbasins. Two considerations that control the degree of basin segmentation are: 1) the purpose of the study, and 2) the hydrometeorological variability throughout the basin. The purpose of the study dictates where information is needed and hence subbasin boundaries and outlets. Since HEC-1 is a lumped parameter model, average values for model parameters are used for the entire subbasin area. Subbasins should try to define areas that have similar hydrologic and hydraulic properties.

3. Each subbasin is represented by a combination of model components. The basic RR components are subbasin runoff components and channel routing components. (Other model components include reservoirs, pumps, and diversion facilities).

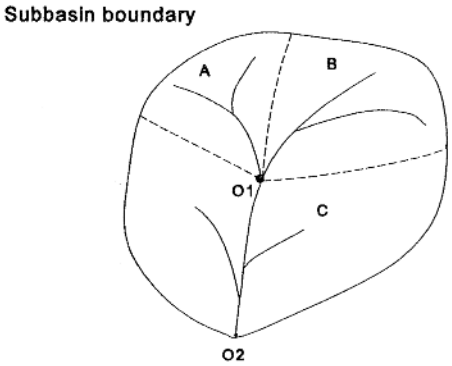

Figure 13.3. Sample drainage basin subdivided into three subbasins.

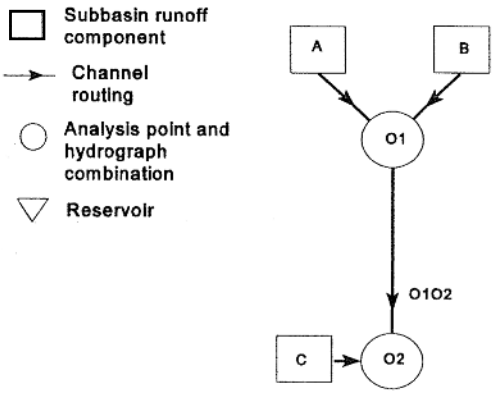

Figure 13.4. Schematic diagram of the basin showing linked model components.

4. The subbasins and their components are linked together completing the interconnected basin system.

In Figure 13.3 the outlet for the upper subbasins A and B is at O1, and runoff from the two subbasins is combined at this point. The combined runoff flows down the channel to the basin outlet O2. At the basin outlet the runoff from subbasin C is added to the runoff from A and B. HEC-1 has different options for generating land surface runoff and routing it to the subbasin or basin outlet. The circles on Figure 13.4 are points for hydrograph combination and output analysis. HEC-1 can be instructed to produce graphics (hydrographs) and tabular data about the simulation at analysis points.

13.1.6.2 *Land surface runoff*

Modeling land surface runoff from a subbasin begins with a precipitation hyetograph. The model assumes evapotranspiration for an individual storm is insignificant. HEC-1 accepts precipitation input either in the form of recording-gage data or total storm precipitation. The model can even generate hypothetical hyetographs for design storms. HEC-1 can weight individual gages to determine the areal average precipitation for a subbasin as done in Chapter 4. Infiltration and surface detention are subtracted from precipitation using one of four available 'loss' options (Table 13.3). Both precipitation and infiltration are assumed to be uniform (lumped) over

Table 13.3. Options available for rainfall runoff simulation in HEC-1.

Precipitation	Infiltration and detention (losses)	Runoff
Historical storms	Initial and uniform loss	Unit hydrograph supplied by user
– Basin average precipitation	(ϕ index)	(this can be synthetic)
– Weighted precipitation gages	Exponential loss rate	Synthetic unit hydrographs
Synthetic storms	SCS curve number	Clark unit hydrograph
– Standard project storm		Synder unit hydrograph
– Probable maximum storm	Holtan loss rate	SCS dimensionless unit hydrograph
– From depth-area-duration data		Kinematic wave
Snowfall and snowmelt		
– Degree-day method		
– Energy-budget method		

the subbasin. Excess precipitation is convoluted into runoff and routed to the subbasin outlet using either a unit hydrograph (black box) or the kinematic wave (white box) runoff option. The unit hydrograph options produce the runoff hydrograph at the subbasin outlet. Referring to Figures 13.3 and 13.4, runoff hydrographs are generated for both subbasins A and B at their mutual outlet O1. You must tell the model to combine the two runoff hydrographs at that point.

The kinematic wave runoff option generates runoff distributed laterally along the length of the channel. The kinematic wave is a more physically-based modeling approach. Lateral inflows to the channel accumulate to create the runoff hydrograph at point O1. Again, HEC must be told to combine the runoff from the two subbasins. You could generate runoff from one subbasin using a unit hydrograph and from the other basin using a kinematic wave. The kinematic wave option is described further below. Note that if a unit hydrograph is used there is no 'routing' of flow down the channel; the hydrograph is generated at the outlet.

Baseflow is computed similar to the approach in Example 11.1. Prior to the hydrograph rise baseflow is computed using a specified starting value and recession constant ($1/k$). On the recession limb a new (higher) starting value for baseflow is specified. Once the computed hydrograph value equals this value, baseflow recession begins again.

13.1.7 *Kinematic wave*

The kinematic wave runoff option is composed of three basic elements – overland flow elements, collector channels, and the main channel (Fig. 13.5). Runoff from overland flow elements enters either collector channels or the main channel. The HEC-1 version of the kinematic wave was adapted from the Massachusetts Institute of Technology (MIT) catchment model (Harley 1975, Feldman 1981).

13.1.7.1 *Overland flow element*

An overland flow element is modeled as a wide rectangular channel of unit width

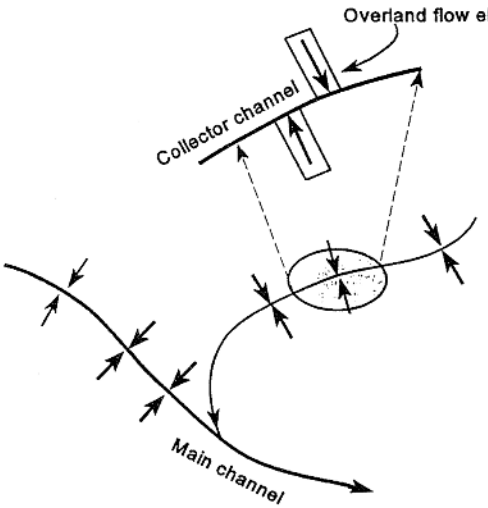

Figure 13.5. Relationship between kinematic wave flow elements. Overland flow elements feed into channels. Smaller collector channels feed into the main channel.

(COE 1987a). For computational purposes rainfall excess is the lateral inflow to this 'channel'. An overland flow element is described by four physical parameters: typical overland flow length, slope, roughness, and the percentage of the basin represented by this element (COE 1987a). Roughness is defined with Manning's n for overland flow (Table 10.1). If the land use in the subbasin is fairly homogenous only a single typical overland flow element is needed. If the basin is more heterogeneous, HEC-1 allows two separate overland flow elements to be defined for each subbasin, e.g. for different land uses like urban and agricultural. The proportion of the subbasin represented by the different element(s) must sum to 100%.

The HEC-1 model simulates runoff as hortonian overland flow. It does not simulate the process of saturation overland flow described in Section 10.4.2. There are models that simulate both runoff generation mechanisms. TOPMODEL (Bevin & Kirkby 1979, Bevin et al. 1984) is an example of such a model. In this regard TOPMODEL is a more physically-based model than is HEC-1.

13.1.7.2 *Channel elements*

Channel elements are defined using the following physical parameters: reach length, slope, roughness, shape, width or diameter, and side slope. Figure 13.6 shows the dimensional components for a rectangular and trapezoidal cross section. HEC-1 can model circular, square, and triangular shapes as well. The total overland flow in a subbasin is uniformly distributed as lateral inflow along the entire length of the channel reach. The last channel segment in a subbasin is designated the main channel. Any intermediate channels between the overland flow elements and the main channel are designated collectors. The use of collector channels is optional. Channel flow is then routed downstream. For influent streams HEC-1 can simulate channel infiltration.

13.1.7.3 *Element combination*

Overland flow elements feed runoff into channel elements (collector and/or main) and the channels convey the water to the subbasin outlet. As an example, if we were

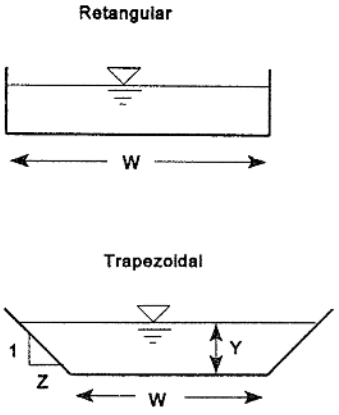

Figure 13.6. Dimensional components for two channel shapes (source: COE 1987a).

modeling an urban area we might use two representative overland flow elements – one for residential areas and one for commercial land uses. Overland flow from the individual lots enters gutters and small storm drains (collectors). The collectors then convey the water to the main stream draining the watershed.

13.1.7.4 *Channel routing*

HEC-1 offers five different routing options including the Muskingum, modified Puls, and kinematic wave. The Muskingum method requires that you know the Muskingum K and x parameters. This means discharge data above and below the reach must be available. The kinematic wave routing is based on physical channel characteristics that can be measured in the field. The storage-outflow routing methods require data for the parameters that define the storage characteristics of the reach. None of the routing procedures considers backwater effects.

13.1.8 *Input data file and schematic model structure*

How does HEC-1 know that subbasin A in Figure 13.4 is higher up in the basin than subbasin C? *The topology of the subbasins and channel reaches is defined by the sequence of the records listed in the input data file.* Therefore, you would list the commands to calculate surface runoff in subbasins A and B in the input file before the commands to calculate runoff in subbasin C. Other records must also follow a certain order. For example, you need to give the precipitation data before the commands for runoff calculation.

13.1.8.1 *File format*

HEC-1 has two general types of data records. First are the *input control records*. Input control records control diagnostic analyses and the format of input data. Input control records have an asterisk in column 1 followed by a command. The input control record *DIAGRAM tells the program to draw a schematic diagram of the basin similar to Figure 13.4. This is a useful check to see that the topology of the basin is correct. The second type of input records are the *simulation control records* (Table 13.4). Simulation control records begin with a unique two-letter code followed by

Table 13.4. Examples of HEC-1 simulation control records (source: COE 1987a).

Data category	Record identification	Description
Job initialization	IT	Job time control
	IM	Data in metric units
	IO	General output control for program
	IN	Time control for input data arrays
Optimization	OU	Optimize unit hydrograph and loss rate parameters
Job step control	KK	Stream station identification (identifies separate elements)
	KM	Alphanumeric message (used to insert comments in a program)
Hydrograph transformation	HC	Combine hydrographs
	HQ/HS	Stage/discharge rating curve
Hydrograph data	QO	Observed hydrograph values (used for parameter optimization)
	QI	Direct input hydrograph
Basin data	BA	Basin area
	BF	Baseflow characteristics
Precipitation data	PB	Basin-average total precipitation
	PI	Incremental precipitation time series (from a recording gage)
	PG	Gage storm total precipitation
	PR	Recording gages to be weighted
	PT	Storm total gages to be weighted
	PW	Weightings for precipitation gages
Loss rate data	LU	Initial and uniform loss rates
	LS	SCS curve number
Unit hydrograph data	UI	Direct input unit hydrograph
	US	Snyder synthetic unit hydrograph
	UD	SCS dimensionless synthetic unit hydrograph
	UK	Kinematic overland flow
	RK	Kinematic wave channel (collector, main)
Routing data	RL	Channel loss rate
	RM	Muskingum parameters
	RK	Kinematic wave
End of job	ZZ	Required to end job (this is the last statement in the data file and nothing, not even blank spaces, should come after this)

either data, parameter values, or text. HEC-1 allows both fixed-field (*FIXED) and free-field (*FREE) data formats for the input file. Fixed format is easier for debugging and is described here. The input file is created using a text editor or a word processor that can save files in text (ASCII) format. The computer screen is divided horizontally into 80 columns (spaces). The columns are grouped into 10 *fields*, with each field 8 columns wide (Fig. 13.7). Input data in fixed format are right justified in the fields. When entering data *do not* use a capital letter 'O' for a zero '0' because computers know the difference. Table 13.4 lists a few of HECs 110 different commands, and Example 13.2 shows two examples of the full specification for a record.

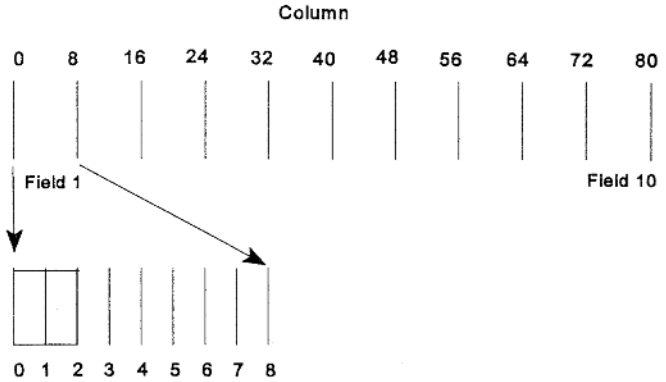

Figure 13.7. Diagram showing 80 columns grouped into 10 fixed-length fields. The first two columns are reserved for simulation control record codes. Input control records have an asterisk * in column 1 followed by a text command.

At this point the best way to further understand the model is to study a simple simulation example.

Example 13.2
This example shows the full input structure for two simulation control records, the IT and the LS records.

IT The IT record is required for all jobs and controls the time interval, starting date and time, and length of hydrographs calculated by the program.

Field	Program variable	Value	Description
Col 1+2 ID	IT		Record identification.
1	NMIN	+	Integer number of minutes in tabulation interval. The minimum is one minute.
2	IDATE[a]	+	Day, month, and year of the beginning of the first time interval, e.g., 20MAR80 for March 20, 1980.
3	ITIME[a]	+	Integer number for hours and minute of the beginning of the first time interval, e.g., 1545 for 3:45 p.m.
4	NQ	+	Integer number of hydrograph ordinates to be computed (300 max) If end date and time are specified in Fields 5 and 6, NQ will be computed from the beginning and end dates and times.
5	NDDATE	+	Day, month, and year of last ordinate (used to compute NQ).
6	NDTIME	+	Integer number for time of last ordinate (used to compute NQ).

[a]IDATE and ITIME are the time of initial flow conditions. No runoff calculations are made from precipitation preceding this time.

Example usage of the IT record: `IT 30 20MAR80 815 35`

With fixed-field input the data are right justified in the 8-column fields. For example, the NQ (35) variable is right-justified in Field 4. Fields 5 and 6 are left blank if NQ is specified. If NDDATE and NDTIME were specified, then Field 4 would be left blank.

LS The LS record is the SCS curve number loss rate option.

Field	Program variable	Value	Description
Col 1+2 ID	LS		Record identification.
1	STRTL	+	Initial rainfall abstraction in inches (mm) for snow-free ground. For an optimization job (OU record) this variable is fixed at the given value.
		0	Initial abstraction is computed as $0.2 \times (1000 - 10 \times \text{CRVNBR})/\text{CRVNBR}$. For an optimization job, initial abstraction varies with CRVNBR.
		–1	For optimization only (OU record previously supplied), program will assume a starting value and then optimize.
		–	Same as (–1) above but program uses this value (after sign change) as the starting point for optimization.
2	CRVNBR	0, +	SCS curve number for snow-free ground. If this is an optimization job (OU record previously supplied), this variable will be fixed at this value and not optimized.
		–	Same as (-1) above but program uses this value (after sign change) as the starting point for optimization.
3	RTIMO[a]	+	Percent of drainage basin that is impervious. No losses are computed for this portion of the basin.
4-6			Specify loss rate variables similar to Fields 1-3 for second kinematic subbasin if used.

[a]This factor should only be used for directly connected impervious areas not already accounted for in the curve number land use.

Example usage of the LS record: `LS  0  65`

In this example placing a 0 in Field 1 means use the'standard' value for the initial abstraction (I_a). The curve number is 65 in Field 2. There is no optimization. Field 3 is left blank because the curve number fully accounts for the basin land use.

13.1.9 *Example simulation using HEC-1*

The Swarr Run basin in Lancaster County, Pennsylvania is used for this example. The USGS in conjunction with the Lancaster County Planning Commission installed a stream gage and recording precipitation gage on Swarr Run, just upstream of its junction with the Little Conestoga River. The Swarr Run basin was gaged from 1986 to 1989. The data were gathered to support the development of urban runoff control regulations pursuant to a state law passed in 1978. Table 13.5 lists geographic information about the basin.

For this example the basin will not be divided into subbasins. The purpose of this example is to demonstrate the input file structure for HEC-1, not to achieve the best possible output. The following options are used: a single recording precipitation gage, the SCS loss rate option, and the SCS dimensionless unit hydrograph. The input file for this simulation is given in Table 13.6.

Table 13.5. Geographic data for the Swarr Run drainage basin, Lancaster County, PA.

Land use data:	Area (mi^2)	Percent of basin
Urban – Single family residential and roads	1.87	21.6
Forested	0.74	8.5
Agricultural	6.06	69.9
Total	8.67	100.0
Soil data	HSG	
Bedington silt loam (3-8% slopes)	B	
Bedington silt loam (8-3% slopes)	B	
Duffield silt loam (3-8% slopes)	B	
Morphometric data		
Main channel length (L_w)	30,000 ft	
Maximum basin relief (H_m)	225 ft	
Gage elevation	315 ft (above sea level)	

Table 13.6. Input file for HEC-1 simulation of Swarr Run.

```
ID SWARR RUN SIMULATION
ID S.A. THOMPSON
*DIAGRAM
IT    10 19JUL88     2045          20JUL88   1500
IO     0       2
PGLANDIS       0
IN     5 19JUL88     2115
PI   .01     .03      .08     .04      .01     .05     .03     .08     .05     .11
PI   .19     .16      .13     .05      .05     .06     .05     .03     .02     .03
PI   .01     .02      .02     .02      .01     .01     .01     .01     .00     .01
PI   .00     .00      .00     .00      .00     .00     .00     .00     .00     .00
PI   .00     .01
KK SWARR
KM   CALCULATE RUNOFF FROM BASIN
KM   SCS LOSS RATE AND SCS HYDROGRAPH
BA  8.67
BF   2.4      21     1.15
PRLANDIS
PW     1
PTLANDIS
PW     1
LS     0      73
UD  1.64
KK  GAGE
KM  COMPARE COMPUTED AND OBSERVED HYDROGRAPHS AT OUTLET
IN    15 19JUL88     2045
QO   2.4     2.4      3.0     3.4      4.0      15      37     141     230     258
QO   258     237      199     165      143     131     123     117     111     106
QO   102     101      103     107      110     112     112     109     102      92
QO    80      69       59      50       44      38      32      28      25      23
QO    21      19       18      17       16      16      15      14      13      13
QO    12      12       11      11      9.9     9.5     9.5     9.1     8.8     8.4
QO   8.4     8.1      8.1     7.7      7.7     7.4     7.1     7.1     6.9     6.6
ZZ
```

13.1.9.1 *Discussion of input file (Table 13.6)*

The IT record indicates that the simulation begins at 2045 (8:45 p.m.) on July 19, 1988, and hydrographs will be calculated every 10 minutes. The last hydrograph ordinate will be calculated at 1500 (3:00 p.m.) on July 20, 1988. Since the beginning and ending times of the simulation are specified, HEC-1 determines the number of hydrograph ordinates (NQ). The IO card with a 0 in Field 1 and a 2 in Field 2 tells HEC-1 to print all output and plot all hydrographs. The PG record with a 0 in Field 2 means calculate total storm precipitation from the following PI (incremental precipitation) records. The precipitation gage name is LANDIS. The IN record controls the time interval for the following PI data. The precipitation data are measured on a 5-minute interval (Field 1) starting at 2115 (9:15 p.m.) on July 19, 1988. The data in the PI records are 5-minute incremental precipitation in inches. Note that the storm must be continuous from beginning to end. This means if there was no recorded precipitation during a particular time interval, that time interval must still be included in the input data series with a value of 0.0.

The KK record identifies the entire basin (SWARR) as the first station for which computations are to be made. If the basin were subdivided this would be the first (upper-most) subbasin. The KM record is a message line inserted to help clarify the program. Text following a KM message is not restricted to fields. BA is the basin area in square miles. (If this were a subbasin BA would be the subbasin's area.) BF is the baseflow record. Field 1 is baseflow in cfs at the start of the simulation before runoff begins, 21 is the value for baseflow on the recession limb in cfs, and 1.15 is the inverse of the baseflow recession constant ($1/k$). In this case the recession constant $k = 0.87$ (see Example 11.1). The PR, PW and PT records tell HEC-1 to use the precipitation data from the LANDIS gage. The LS record is the SCS curve number loss rate (see Example 13.2). The fields indicate use of the standard initial abstraction, and the weighted curve number for the entire basin is 73. The weighted curve number was determined before hand from the data in Table 13.5. The UD record calculates the runoff hydrograph using the SCS synthetic dimensionless unit hydrograph. Field 2 in the UD record is the TLAG variable, which is the time to peak in hours. HEC determines this variable as TLAG = $0.6t_c$, where t_c is the time of concentration of the basin. In other words TLAG is what we called t_p in Chapter 11 in the discussion of the SCS synthetic triangular unit hydrograph. The time of concentration estimated by Equation (10.22) is $t_c = 2.73$ hours, giving TLAG=1.64 hours. (Eq. 10.21 gives $t_c = 2.33$ hours.)

The KK record identifies the stream gage (GAGE) at the basin outlet as the analysis point for hydrograph computation. The IN record controls the time interval for the observed hydrograph data, which are entered in the QO records. These data are used for model calibration and optimization. The final ZZ record ends the job. The plot of the observed and simulated hydrographs for this simulation are graphed in Figure 13.8.

Inspection of Figure 13.8 and Table 13.7 show that this simulation not very good. The simulated peak flow is too low and it comes more than an hour after the observed peak. The simulated runoff volume (depth) is also too low. Table 13.7 gives the various quantitative measures of error. Three parameters that might be recalibrated to improve the predicted hydrograph are TLAG (time to peak), STRTL (initial abstraction), which might be reduced, or CRVNBR (curve number) which might be

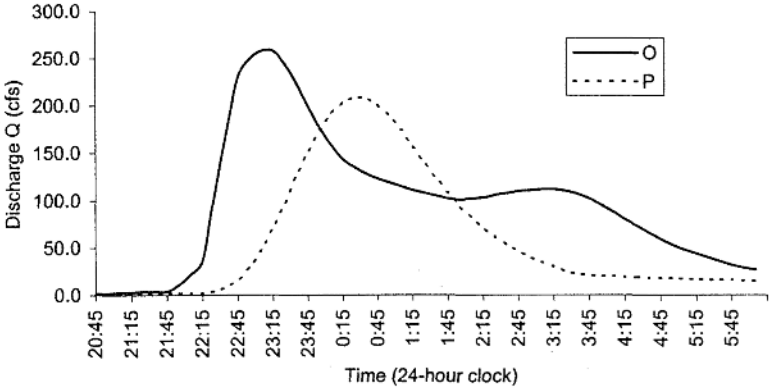

Figure 13.8. Observed and predicted hydrographs for the HEC-1 simulation using the input file in Table 13.6.

Table 13.7. Comparison of observed and predicted hydrographs from Swarr Run simulation (Fig. 13.8).

	Observed	Predicted
Time to peak (hrs)	2.33	3.67
Runoff depth (in)	0.185	0.117
Error measures:		
E_1	355,334 cfs^2	
E_2	4,562,496 cfs^2	
E_3	2401 cfs^2	
RMSE	79 cfs	
HEC weighted *RMS*	84 cfs	
d	0.66	

increased to generate more runoff. HEC-1 can automatically optimize STRTL and CRVNBR if requested. Alternatively we could try different loss and runoff options, or the basin could be divided into subbasins.

13.1.10 *Agricultural nonpoint source pollution model (AGNPS)*

The AGNPS simulation model (Young et al. 1989) is a PC-based computer program that provides basic information on water quality for classifying nonpoint source pollution problems in agricultural watersheds (Young et al. 1987). The model is a single event, distributed-parameter model that predicts runoff volume and peak flow, sediment yield from upland areas and channel erosion, nitrogen (N), phosphorous (P), and chemical oxygen demand (COD). Runoff is calculated using the SCS curve number method. The model is very 'user friendly' with pulldown menus, excellent graphic and tabular output displays, and good documentation.

The watershed is segmented into squares called 'cells' (Fig. 13.9) and parameters are set for each cell. Cells can be any size but should be chosen so that parameter

values are representative for the entire cell. Some suggested guidelines for cell sizes are 10-acre cells for watersheds less than 2000 acres and 40-acre cells for watersheds greater than 2000 acres (Young et al. 1987). The maximum number of cells allowed in AGNPS version 5.0 is 1900. The model allows an original initial cell to be subdivided into smaller subcells. This procedure of cell division can be carried out three times resulting in cells 1/64th the size of the original (Young et al. 1990). The first subdivision creates level-1 cells, the second subdivision creates level-2 cells, and the third level-3 cells. New parameter values can be assigned to the subdivided cells. Cell division is useful for detailed modeling of sensitive areas such as buffer strips along watercourses. The topology of the basin is established by first consecutively numbering the cells from 1 to the number of cells, starting in the northwest quadrant of the watershed and continuing west to east southward (Fig. 13.10). Next the drainage direction for each cell is defined. Drainage direction is the direction of water flow from the cell and can be in one of eight possible directions (Fig. 13.11). Cells

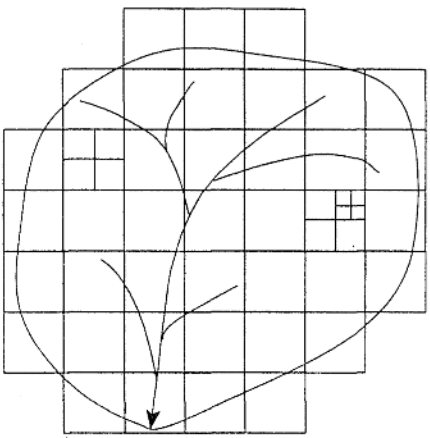

Figure 13.9. Drainage basin subdivided into cells. The cell on the right side has been subdivided two times (level 2). The cell in the upper left has been subdivided once (level 1). Three levels of subdivision are allowed for each cell.

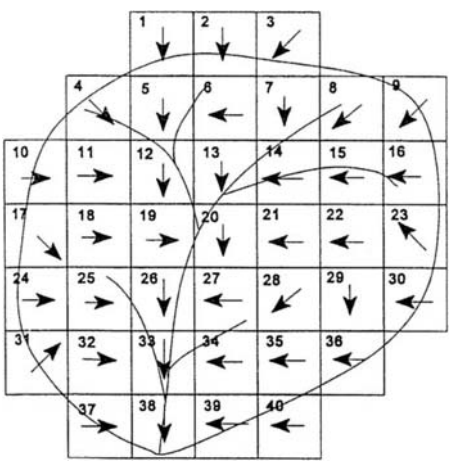

Figure 13.10. Cell numbering convention and drainage direction.

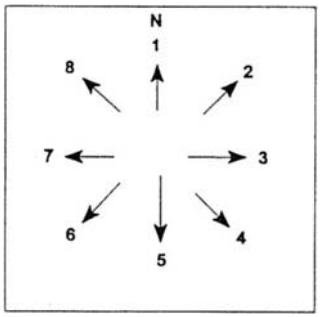

Figure 13.11. Possible drainage paths from a cell and the corresponding path identification number.

can be identified as sink holes, in which case there is no outflow from that cell, otherwise each cell must receive flow from one or more upper cells and send flow out to a lower cell.

13.1.10.1 *Data for the model*

The data for the model can be categorized as whole watershed data and cell data. Data for the whole watershed include the number of cells, the size of a cell, storm data (total precipitation), and basin name and other simulation identification information. Cell data include the SCS curve number, land slope and shape, field slope length, surface roughness, soil texture, channel characteristics, data on nutrient application and availability, as well as factors used to calculate soil erosion using the in the Universal Soil Loss Equation (USLE) (Wischmeier & Smith 1978). Individual cells can also be identified as being a point source for pollution, e.g. a feedlot.

The authors performed a sensitivity analysis and found the cell variables most significantly affecting sediment yield and sediment-associated nutrient yields were land slope, the soil erodibility factor (K), storm energy intensity (EI), the cropping factor (C), and the curve number. The soil erodibility factor, storm energy intensity, and the cropping factor are all components of the ULSE. The curve number also strongly affected the water-soluble nutrient yield. Care should be taken in estimating these parameters as accurately as possible (Young et al. 1987).

13.2 GEOGRAPHIC INFORMATION SYSTEMS (GIS)

Geographic Information Systems are computer-based systems for storing, retrieving, manipulating and displaying spatial data. Spatial data are *georeferenced*, that is their geographic position is known. All of the environmental data we work with in hydrology can be assigned geographic coordinates and analyzed with a GIS. In its simplest use GIS computerizes traditional cartographic activities. We can enter into the computer the geographic coordinates of drainage basin features and have the GIS draw maps of the basin. GIS can also do simple arithmetic such as calculating basin area or the proportion of the basin underlain by different types of soil. But one of the most powerful applications of GIS is the creation of new information. For example, a GIS could combine data on soil, slope, and land use and classify areas in a basin by their soil-erosion potential (Fig. 13.12). Resource analysts and managers traditionally did

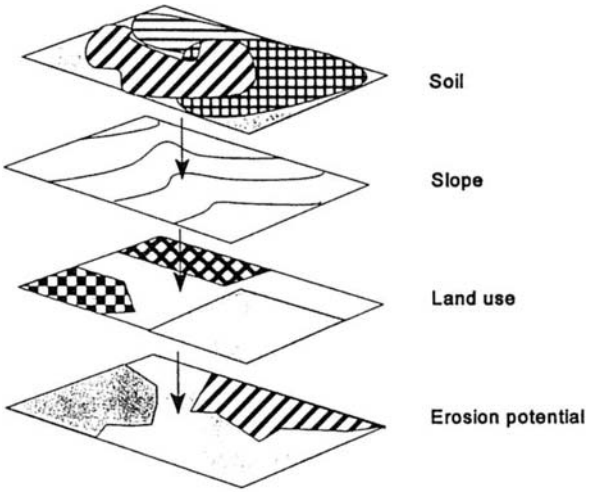

Figure 13.12. Schematic representation of how a GIS can combine different types of environmental data to derive new information. Here data on soil, slope and land use are combined to create a map of erosion potential.

this type of derivative analysis using a base map and transparent overlays of the different variables. Now it can be done more accurately and much faster using GIS. Geographic information systems contain a wide variety of analytical functions for manipulating spatial data. They can perform addition, subtraction, multiplication, and division; they can do statistical analysis including spatial correlation and regression; calculate distances and areas, and even do mathematical interpolation.

13.2.1 *Types of GIS*

There are two types of GIS – vector and raster – and each type has certain advantages and disadvantages. For both types of GIS space is defined using some geographic coordinate system. The coordinate system may be an arbitrary X, Y system, but it is better to use an actual geographic coordinate system like latitude/longitude or a state plane coordinate system. The difference between vector and raster systems is in how they represent and store spatial data.

13.2.1.1 *Vector GIS*

A vector GIS defines and describes spatial data as either a *point*, a *line*, or a *polygon* (area). A point feature is located and defined by a single set of spatial coordinates (Fig. 13.13). A water supply well, a precipitation gage, or an underground storage tank are examples of features that are represented as points, and are georeferenced with a single latitude/longitude coordinate pair. A line feature is composed of two or more points. In the language of GIS the points that make up a line are called *nodes* and the line between the nodes is an *arc*. At a minimum a line must have two nodes – a starting node and an ending node. Each node is assigned a separate coordinate. A river, a road, or a sewer line would be represented as a line feature. A polygon feature is an enclosed area. A polygon is made up of lines (arcs) with the characteristic that the starting node is the same as the ending node. A drainage basin, a soil polygon, or a particular land use would be represented as a polygon. The GIS knows where things are (absolute location) based on the feature's coordinates. The GIS also

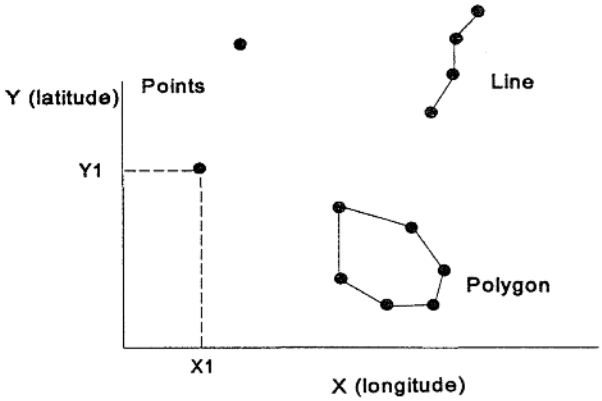

Figure 13.13. Representation of spatial features in a vector GIS. Spatial data are represented as either a point, a line, or a polygon.

knows the topology of the area (relative location); topology is the spatial relationship between features. The GIS knows, for example, that one polygon is north of another polygon, or that one arc is west of another arc.

Once features are defined in a vector GIS, any amount of information can be assigned to that feature. This related information is stored in a separate database. Take as an example a point representing a water supply well. Related information that could be stored about the well include the owner, when it was drilled, the depth, the diameter of the casing, and the aquifer in which it was completed. For a polygon feature representing a distinct type of soil related information might include texture, depth, pH, underlying bedrock, or hydrologic soil group (HSG). This is one of the advantages of a vector GIS. The geographic features – point, line, or polygon – are defined once and then any amount of related information can be assigned to that feature. This is why databases associated with vector GIS are referred to as relational databases. The combination of a georeferenced feature and the related database about that features constitutes a *coverage*. So for example there could be a 'well coverage' or a 'soil coverage' or a 'stream coverage.'

13.2.1.2 *Raster GIS*

A raster (grid) GIS divides space into a uniform grid and each cell of the grid is georeferenced to the coordinate system (Fig. 13.14). Environmental data are stored in the individual cells. Therefore, in a raster system georeferencing and data storage are combined within the cells. Data are stored in what are called *layers* rather than coverages, and a layer in a raster GIS typically contains only one type of information. As an example, suppose you wanted to store information about soil depth, soil pH, and soil texture. For the 'soil depth layer' each cell in the grid would be given a quantitative value equal to the thickness of the soil at that cell location. Since a cell can contain only one value, you need separate layers for pH and texture. In this example three separate and complete layers are needed to store the three different types of soil information. By contrast, a vector system would have one 'soil coverage' composed of the soil polygons and a related database containing all the information (thickness, pH, texture) for each polygon. This is one of the major drawbacks of the raster GIS; it requires a separate layer for each type of data and thus consumes large amounts of

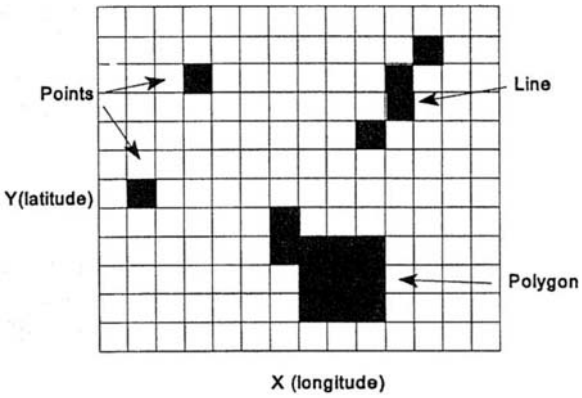

Figure 13.14. Representation of spatial features in a raster GIS. The cells produce a blocky representation of point, line, and polygon features compared to the vector system in Figure 13.13.

storage space on the computer. Another disadvantage is that the smallest mappable unit is the size of an individual cell. If the cell size is, say, 100 m by 100 m, and you are mapping well locations, an individual well occupies an entire 100-meter-square cell. This is why raster systems produce a 'blocky' representation of spatial features. However, there are advantages to the raster GIS. The uniform grid structure makes mathematical manipulation of data much more efficient. Another advantage is that digital remotely sensed data from satellites and aerial photography are, or can be, stored in raster format. This makes it easy to bring remotely sensed data directly into a raster GIS, and remote sensing has become an important means of gathering environmental data.

13.2.2 *GIS applications to hydrology*

GIS applications in hydrology and water resource fall into two main categories – informational and analytical. Informational uses include data storage, retrieval, and display. Water related features like well locations, stream channels, reservoirs, and sewer lines can be stored within a GIS. Resource mangers and planners can readily use this information to support comprehensive land and water planning activities. For example, the USGS operates a National Water Use Information Program. It collects data on water use by state, region, and type of use, and publishes this information in national water use reports (e.g. Solley et al. 1993). GIS is being used to restructure the availability of this water use data (Juracek & Kenny 1993).

The author participated in a local county-level plan for wellhead protection. A vector GIS was used to store all the information on potential groundwater contamination sources, including above- and underground storage tanks, other hazardous chemical use and storage locations, graveyards, landfills and much more. The GIS was also used to develop wellhead protection areas around municipal water supply wells. The GIS will be valuable in other ways. Lending institutions will be able to find out if a particular parcel of land has hazardous materials used or stored upon it, or if it is located near a site that uses or stores hazardous waste.

Analytical uses of GIS are all related to modeling. GIS supports modeling primarily by storing, reformatting, and generating data used for parameterizing simula-

tion models. GIS is also used to assist automated procedures for deriving morphometric drainage basin characteristics. GIS-assisted model parameterization is the most common use and new parameterization techniques now so tightly integrate GIS with simulation models that it is difficult to say where one program begins and the other ends. Morphometric basin characteristics are needed as model parameters as well, but the two uses of GIS are discussed separately here.

13.2.2.1 *Model parameterization*

Geographic information systems are excellently suited for organizing data for model parameterization. Simulation models, whether of the lumped-parameter or distributed-parameter type, require data on soils, land use, slope, and basin boundaries. GIS can efficiently store and retrieve this information. Using a GIS for model parameterization may require writing a computer program that reads the GIS's files and reformats the data for use by the simulation model.

The gridded structure of AGNPS makes it well suited for use with a raster GIS, and a number of researchers have explored integrating the two (Mitchell 1993, Chansheng et al. 1993). Newer versions of AGNPS have a built-in option of writing simulation results into a 'GIS-format' file. This creates a two-way connection between the GIS and the simulation model – GIS is first used to parameterize the model, and then the model's results are sent back to the GIS for further analysis and graphic display. Srinivasan and Arnold (1994) integrated a raster GIS with a continuous time, distributed-parameter, basin-wide, water quality model. They used GRASS (Geographic Resource Analysis Support System) which is a public domain raster GIS developed by the US Army Corps of Engineers (COE 1987b). The simulation model is called SWAT (Soil and Water Assessment Tool) and is a modification of still another model called SWRBB (Arnold et al. 1990).

With advances in computer technology and GIS, two-dimensional, physically-based, distributed-parameter models are becoming more and more popular among hydrologists. Some of the more recent models operate on watersheds discretized into square (raster) elements. These models are being designed expressly for the purpose of fully utilizing raster GIS and radar-derived rainfall data from the NEXRAD doppler radars. The CASC2D model is one of these new breed of models and has been directly linked to the GRASS GIS (Julien et al. 1995).

Orzol & McGrath (1993), Richards et al. (1993) and Hinaman (1993) used a vector GIS to parameterize the USGS's groundwater flow model MODFLOW. They used the GIS to process the input data into a standard gridded format required by MODFLOW. The GIS facilitates modeling by allowing graphic display of data sets, and easy editing of parameters during calibration and verification. The model results are brought back into the GIS for display and analysis.

GIS is used not just to parameterize models, but as a hydrologic model itself. Stuebe & Johnson (1990) automated the SCS curve number method for the GRASS GIS. First they manually digitized SCS soil survey sheets to create a hydrologic soil group layer. Next they created a landcover layer using vegetation data from the LANDSAT satellite, and land use data from existing aerial photography. These layers were combined using GRASS to create hydrologic response units (HRU), and the GIS calculated and assigned curve numbers to each HRU. In addition they had the GIS automatically delineate watershed boundaries using Digital Elevation Model

(DEM) data. A DEM is a file containing digital elevation data. A Digital Line Graph (DLG) file contains digital representations of linear features (lines and polygons) including stream channels, roads and political boundaries. They compared the GIS-generated runoff estimates to manual runoff calculations in six watersheds. The watersheds had land use/land cover varying from farmland to forest. The GIS-generated runoff estimates were similar in four of the six watersheds (Table 13.8). The mean difference in these four basins was 9.5%. In two basins (basin 3 and 7 in Table 13.8) the mean error was 30.5%. The authors feel that most of the error in these two watersheds resulted from the automated watershed delineation procedure. DEM data contain subtle elevation errors which can influence watershed boundary delineation in areas with flat terrain. A one-meter error in the DEM data may be sufficient to route water in a different direction in flat areas, whereas a similar one-meter error in a region of steep slopes has minimal effect on the direction of runoff. Since runoff volume is sensitive to the contributing area, errors in basin delineation cause errors in runoff estimation. Table 13.8 shows that basin areas for watersheds 3 and 7 are underestimated by the GIS-delineation method.

Table 13.8. Area and runoff values for study watersheds (source: Stuebe & Johnson 1990, used by permission).

	Area (acres)			Runoff (acre-feet)		
Basin ID No.	Manual	GIS	Difference %	Manual	GIS	Difference %
2	900.64	904.02	0.4	30.25	35.03	15.8
3	696.30	434.33	37.6	47.93	34.35	28.3
4	329.76	362.50	9.9	32.01	33.09	3.3
5	1778.85	1753.55	1.4	147.05	148.39	0.9
6	455.04	471.91	3.7	32.49	38.38	18.1
7	254.20	184.14	27.6	29.93	20.11	32.8

13.2.2.2 *Derivation of morphometric properties of a drainage basin*

As an example of an automated procedure for deriving morphometric basin characteristics, the USGS developed a Basin Characteristics System (BCS) (Eash 1994). The BCS was developed as part of a regional study relating flood magnitude and frequency to drainage basin characteristics (Eash 1993). The BCS is a four-step procedure. The first step is to create four digital base maps – a drainage-divide map, a basin length map, a drainage network map, and a elevation-contour map. The first two are created manually by digitizing topographic maps; the third and fourth maps are created automatically by a vector GIS using 1:250,000-scale DEM and 1:100,000 DLG data. The second step in the BCS uses custom computer programs to assign attributes to points, lines, and polygons in three of the base maps. For example, Strahler stream orders are assigned to each channel segment in the drainage network map. The third step uses more custom software to quantify 24 morphometric basin characteristics including measurements of area, length, shape, and relief. The fourth step digitally quantifies precipitation data for the flood estimation analysis. All of the data are stored in the GIS. Compared to manual methods of measurement, the BCS

significantly reduced the time needed to derive these morphometric characteristics. Comparison tests indicated the BCS measurements were not significantly different from their manual counterparts for 11 of the 12 primary drainage basin characteristics. The BCS did significantly underestimate basin slope (Eash 1994).

Other researchers have developed custom computer programs for automatically deriving morphometric basin characteristics. These programs may or may not explicitly involve the use of a GIS. Tachikawa et al. (1994) developed a Basin Geomorphic Information System (BGIS) that uses DEM and DLG data. The BGIS represents the basin landscape as a set of contiguous non-overlapping triangular facets (Fig. 13.15). Modeling the land surface as a set of triangular facets is called a Triangular Irregular Network (TIN), and some commercially-available GIS programs have routines for creating TINs from DEM files. The BGIS further identifies the direction of water flow, the channel network, and the contributing basin area to each channel segment. Problems can occur with automated systems where basins have complicated topography and the grid spacing on which the triangles are created is too coarse, or in areas of low relief where the vertical resolution of the DEM is a significant fraction of the local relief. Many raster GIS programs have routines for creating three-dimensional surface layers and drainage pathways using DEM and DLG files.

Martz & Garbrecht (1993a, b) created a computer program that automatically extracts basin characteristics using DEM data. When compared to values generated by hand the automated procedure was very good at replicating the channel network structure, channel lengths, and drainage areas. The difference between the manual and computer-generated values is generally less than 2%. The largest difference between the two methods occurred in determining channel slopes. The computer-generated slopes were consistently less than the manually-generated values by 4.7 to 26.6%.

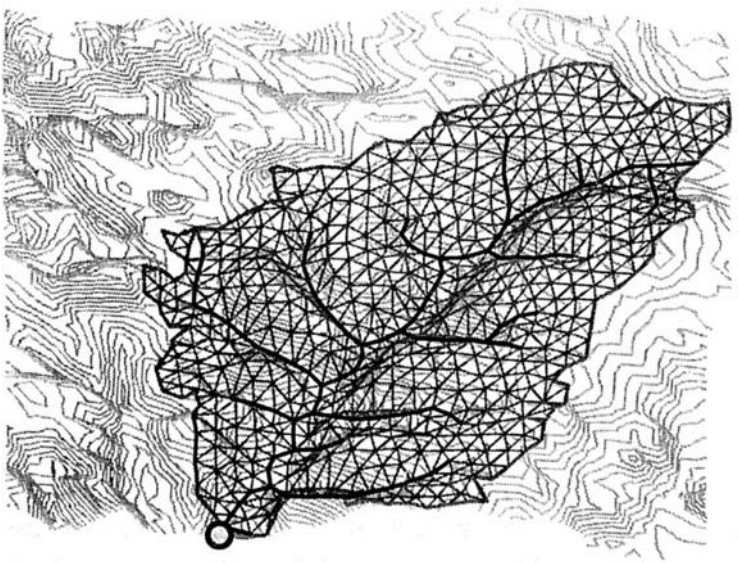

Figure 13.15. Schematic representation of a basin using a Triangular Irregular Network (TIN) structure.

SUMMARY

The use of computer simulation models has become routine and even mandatory in many hydrologic studies. Simulation models allow experimentation on hydrologic systems in a way not before possible. It is now common to do 'What if?' type planning studies. If a shopping center is built how will the change in land use affect the timing and amount of runoff. If a storm of a certain magnitude and duration passed over the basin what would be the resulting peak flow at some point downstream? Or, what if a certain type of pollutant got into the groundwater? How long would it take to reach a water supply well? All of these questions can be explored in the computer. The quality of the simulation depends on the model, the input data, and how well the model is calibrated.

Geographic information systems are revolutionizing the handling of spatial data. Their biggest impacts on hydrology and water-resource planning are in the handling of water related information and improving our use of models. Together they are a powerful tool for integrated resource analysis.

This Page Intentionally Left Blank

Appendices

APPENDIX A: UNIT CONVERSIONS AND EQUIVALENTS

Length

multiply	by	to get
feet	30.48	centimeters
feet	0.3048	meters
miles	1.6093	kilometers
miles	63360	inches
miles	5280	feet
kilometers	0.6214	miles
kilometers	1000	meters
meters	100	centimeters
meters	39.37	inches

Volume

multiply	by	to get
ft^3	7.481	gallons
ft^3	0.02832	m^3
acre-feet	43560	ft^3
acre-feet	1233.62	m^3
m^3	264.2	gallons

Area

multiply	by	to get
acres	43560	ft^2
acres	4047	m^2
acres	0.4047	hectares
mi^2	640	acres
mi^2	2.590	km^2

Pressure

multiply	by	to get
feet of water	0.02950	atmospheres
feet of water	62.43	pounds per ft^2
bars	2.089×10^{-3}	pounds per ft^2
bars	0.987	atmospheres
bars	1000	millibars
millibars	100	pascals

Temperature

$°C = 5/9(°F - 32)$
$°F = 9/5(°C) + 32$
$°K = °C + 273$

Velocity

multiply	by	to get
meters per second	3.6	kilometers per hour
meters per second	2.237	miles per hour
feet per second	0.6818	miles per hour
feet per second	0.3048	meters per second

Energy and power

multiply	by	to get
Joules	0.2389	calories

Discharge

multiply	by	to get
cubic meters per second (cms)	35.31	cubic feet per second (cfs)

Table A1. Physical properties of water as a function of temperature.

		Mass density (ρ)	Weight density (γ)	Dynamic viscosity (μ)	Kinematic viscosity (υ)
°C	°F	kg m^{-3}	Nm^{-3}	Pa · s	$m^2 s^{-1}$
0	32	999.870	9799.00	0.001787	1.787E-06
5	41	999.970	9799.98	0.001519	1.518E-06
10	50	999.730	9797.63	0.001307	1.307E-06
15	59	999.130	9791.75	0.001139	1.399E-06
20	68	998.230	9782.93	0.001002	1.004E-06
25	77	997.070	9771.56	0.000891	8.930E-07
30	86	995.671	9757.84	0.000798	8.009E-07
		slugs ft^{-3}	lb ft^{-3}	lb s ft^{-2}	$ft^2 s^{-1}$
0	32	1.9397	62.4600	3.735E-05	1.926E-05
5	41	1.93989	62.4662	3.175E-05	1.637E-05
10	50	1.93943	62.4513	2.732E-05	1.409E-05
15	59	1.93826	62.4138	2.381E-05	1.229E-05
20	68	1.93652	62.3576	2.094E-05	1.082E-05
25	77	1.93427	62.2851	1.861E-05	9.624E-06
30	86	1.93155	62.1977	1.667E-05	8.632E-06

Important equivalents
1 Watt = 1 Joule per second,
1 Watt per m^2 = 0.001433 calories per cm^2 per minute,
1 langley = 1 calorie per cm^2 per minute,
1 cfs for 1 day = 1.98 acre-feet,
1 cfs = 2447 m^3 per day,
1 gallon per minute = 0.002228 cfs,
1 inch of runoff per hour from 1 acre = 1.008 cfs,
1 inch of runoff per hour from 1 mi^2 = 645.3 cfs,
1 inch of runoff from 1 mi^2 = 2,323,200 ft^3 = 53.33 acre-feet.

APPENDIX B: ANNUAL MAXIMUM SERIES TO PARTIAL-DURATION SERIES CONVERSION FACTORS (SOURCE: DUNNE & LEOPOLD 1978)

Recurrence interval	*Conversion factor*
2	1.13
5	1.04
10	1.01
20	1.00

To use the conversion factors, multiply the *T*-year quantity determined from the annual maximum series by the conversion factor to get the *T*-year quantity for the partial duration series. For example, if the 5-year, 6-hour precipitation given by the annual maximum series is 130 mm, the 5-year, 6-hour precipitation for the partial duration series is 130 × 1.04 = 135 mm.

APPENDIX C: SOURCES OF WATER-RELATED INFORMATION IN THE UNITED STATES

Precipitation data	*Internet/WWW address*
National Weather Service	
Climatological Data (state)	
Local Climatological Data	
National Climatic Data Center, Asheville, North Carolina	http://www.ncdc.noaa.gov
USDA agricultural experiment stations	http://hydrolab.arsusda.gov/arswater.html
Water Data	
US Geological Survey	http://water.usgs.gov
Water Supply Papers	
Water Resources Data (by state)	
Hydroclimatic Data Network	
Water Data Storage and Retrieval (WATSTOR)	
US Environmental Protection Agency	http://www.epa.gov/waterhome/programs.html
Storage and Retrieval System (STORET)	
Water Body System (WBS)	

Water-related journals

Water Resources Research
Journal of the American Water Resources Association (formerly Water Resources Bulletin)
Groundwater
Journal of Hydrology
Bulletin of the American Meteorological Society
Monthly Weather Review
Physical Geography

This Page Intentionally Left Blank

References

American Institute of Professional Geologists (AIPG) 1983. *Ground Water Issues and Answers*, Arvada, Colorado.

Aron, Gert 1994. Rational C related to return period and SCS curve number. Paper presented at the annual meeting of the Pennsylvania Section of the American Water Resources Association, October, 1994, Carlisle, Pennsylvania.

Arnold, J.G., J.R. Williams, A.D. Nicks & N.B. Sammons 1990. *SWRBB – A Basin Scale Simulation Model for Soil and Water Resources Management*, Texas A&M Press, College Station, Texas.

Bedient, P.B. & W.C. Huber 1992. *Hydrology and Floodplain Analysis*, Addison-Wesley Publishing Company, Reading, Pennsylvania.

Bennett, R.J. & R.J. Chorley 1978. *Environmental Systems: Philosophy, Analysis and Control*, Methuen, London.

Benton, G.S. & M.A. Estoque 1954. Water vapor transfer over the North American continent, *Journal of Meteorology*, 11: 462-477.

Betson, R.P. 1964. What is watershed runoff? *Journal of Geophysical Research*, 69(8): 1541-1552.

Beven, K.J. & M.J. Kirkby 1979. A physically-based variable contributing area model of basin hydrology, *Hydrology Science Bulletin*, 24: 43-69.

Beven, K.J., M.J. Kirkby, N. Schonfield & A.F. Tagg 1984. Testing a physically-based flood forecasting model (TOPMODEL) for three UK catchments, *Journal of Hydrology*, 69: 119-143.

Black, J.N., C.W. Bonython & J.A. Prescott 1954. Solar radiation and the duration of sunshine, *Quarterly Journal, Royal Meteorological Society* 80: 231-235.

Blaney, H.F. 1955. Climate as an index of irrigation needs, *Water, The Yearbook of Agriculture 1955*, US Department of Agriculture, Yearbook of Agriculture 1955, USGPO, Washington, DC.

Blaney, H.F. 1959. Monthly consumptive use requirements for irrigated crops, *Proceedings of the American Society of Civil Engineers, Journal of Irrigation and Drainage Division*, 84(IR1): 1-12.

Blaney, H.F., H.R. Haise & M.E. Jensen 1960. Monthly consumptive use by irrigated crops in the western United States, *Provisional Supplement to SCS TP-96*, US Soil Conservation Service, USGPO, Washington, DC.

Bosen, J.F. 1960. A formula for approximation of the saturation vapor pressure over water, *Monthly Weather Review*, 88(8): 275.

Bouwer, H. 1978. *Groundwater Hydrology*, McGraw-Hill, New York.

Brutsaert, W. 1982. *Evaporation into the Atmosphere*, D. Reidel, Dordrecht, Holland.

Chang, J. 1968. *Climate and Agriculture: An Ecological Survey*, Aldine Publishing Company, Chicago.

Chansheng, A., J.F. Riggs & Y.T. Kang 1993. Integration of geographic information systems and a computer model to evaluate impacts of agricultural runoff on water quality, *Water Resources Bulletin*, 29(6): 891-900.

Chen, D. & W. Brutsaert 1994. Diagnostics of land surface spatial variability and water vapor flux, *EOS, Transactions of the American Geophysical Union*, 75(16): 172 (supplement).

Chow, V.T. 1951. A generalized formula for hydrologic frequency analysis, *Transactions of the American Geophysical Union*, 32(2): 231-237.
Chow, V.T. 1959. *Open Channel Hydraulics*, McGraw-Hill, New York.
Chow, V.T. (ed.) 1964. *Handbook of Applied Hydrology*, McGraw-Hill, New York.
Chow, V.T., D.R. Maidment & L.W. Mays 1988. *Applied Hydrology*, McGraw-Hill, New York.
Christopherson, R.W. 1992. *Geosystems: An Introduction to Physical Geography*, Macmillian Publishing Co., New York.
Cooper, H.H. Jr. & C.E. Jacob 1946. A generalized graphical method for evaluating formation constants and summarizing well-field history. *Transactions of the American Geophysical Union*, 27(4): 526-534.
Cunnane, C. 1978. Unbiased plotting positions – a review, *Journal of Hydrology*, 37: 205-222.
Davis, S.N. 1969. Porosity and permeability of natural materials, in R.J.M. DeWiest (ed.), *Flow Through Porous Media*, Academic Press, New York.
Davis, S.N. & R.J.M. DeWiest, 1966. *Hydrogeology*, John Wiley and Sons, New York.
Diaz, H.F. 1983. Some aspects of major dry and wet periods in the contiguous United States, 1985-1981, *Journal of Climate and Applied Meteorology*, 22: 3-16.
Dingman, S.L. 1984. *Fluvial Hydrology*, W.H. Freeman and Company, New York.
Doorenbos, J. & W.O Pruitt 1977. *Crop Water Requirements*, FAO Irrigation and Drainage Paper 24 (revised), UN Food and Agricultural Organization (FAO), Rome.
Dracup, J.A., K.S. Lee & E.G. Paulson Jr. 1980. On the definition of droughts, *Water Resources Research*, 16(2): 297-302.
Dunne, T. & L.B. Leopold 1978. *Water in Environmental Planning*, W.H. Freeman and Company, New York.
Eash, D.A. 1993. Estimating Design Food Discharges for Streams in Iowa Using Drainage-Basin and Channel Geometry Characteristics, US Geological Survey Water-Resources Investigations Report 93-4062, 96 pp.
Eash, D.A. 1994. A geographic information system procedure to quantify drainage basin characteristics, *Water Resources Bulletin*, 30(1): 1-8.
Engman, E.T. 1986. Roughness coefficients for routing surface runoff, *Journal of Irrigation and Drainage Engineering*, 112(1): 39-53.
Faiers, G.E., B.D. Keim & K.K. Hirschboeck 1994. A synoptic evaluation of frequencies and intensities of extreme three- and 24-hour rainfall in Louisiana, *The Professional Geographer*, 46(2): 157-163.
Farnsworth, R.K., E.S. Thompson & E.L. Peck 1982. Evaporation Atlas for the Contiguous 48 United States, NOAA Technical Report NWS 33, USGPO, Washington, DC.
Feldman, A.D. 1981. *HEC Models for Water Resources System Simulation: Theory and Experience*, Advances in Hydroscience, Vol. 12, Academic Press, New York.
Frohlich, C. 1977. Contemporary measures of the solar constant, in O.R. White (ed.), *The Solar Output and its Variations*, Colorado Associated University Press.
Graf, W.L. 1985. *The Colorado River: Instability and Basin Management*, Resource publications in geography, the Association of American Geographers.
Gardner, J.S. 1977. *Physical Geography*, Harper's College Press, New York.
Garstka, W.U. 1978. *Water Resources and the National Welfare*, Water Resources Publications, Fort Collins, Colorado.
Gilman, C.S. 1964. Rainfall, in V.T. Chow (ed.), *Handbook of Applied Hydrology*, Section 9: 1-68, McGraw-Hill, New York.
Golding, B.L. 1981. Flood routing program, *Civil Engineering – ASCE*, June 1981, pp. 74-75.
Gringorten, I.I. 1963. A plotting rule for extreme value probability paper, *Journal of Geophysical Research*, 68(3): 813-814.
Groisman, P. & D.R. Legates 1994. The accuracy of United States precipitation measurement, *Bulletin of the American Meteorological Society*, 75(2): 215-227.
Gumbel, E.J. 1958. *Statistics of Extreme Values*, Columbia University Press, New York.
Haan C.T. 1977. *Statistical Methods in Hydrology*, The Iowa State University Press, Ames, Iowa.

Hack, J.T. 1957. Studies of longitudinal stream profiles in Virginia and Maryland, US Geological Survey Professional Paper 294-B, USGPO, Washington, D.C.

Hall, R.C. & D.R. Risser 1993. Effects of agricultural nutrient management on nitrogen fate and transport in Lancaster County, Pennsylvania, *Water Resources Bulletin*, 29(1): 55-76.

Harbeck, G.E. & others 1951. Utility of Selected Western Lakes and Reservoirs for Water-Loss Studies, Technical Report, US Geological Survey Circular, 103.

Harley, B.M. 1975. *MITCAT catchment simulation model, Description and user manual*, Version 6, Resource Analysis Corporation, Massachusetts.

Hatfield, J.L., R.J. Reginato & S.B. Idso 1983. Comparison of long-wave radiation calculation methods over the United States, *Water Resources Research*, 19(1): 285-288.

Heath, R.C. 1991. *Basic Ground-Water Hydrology*, US Geological Survey Water Supply Paper 2220, USGPO, Washington, DC.

Henderson-Sellers, A. & P.J. Robinson 1986. *Contemporary Climatology*, Longman Scientific & Technical and copublished by John Wiley & Sons, New York.

Hersfield, D.M. 1961. Rainfall-Frequency Atlas of the United States for Durations from 30 Minutes to 24 Hours and Return Periods from 1 to 100 Years. US Weather Bureau Technical Paper 40.

Hewlett, J.D. & A.R. Hibbert 1967. Factors affecting the response of small watersheds to precipitation in humid areas, in W.E. Sopper & H.W. Lull (eds), *Proceedings of International Symposium on Forest Hydrology*, Pergamon Press, Oxford.

Hinaman, K.C. 1993. Use of a geographic information system to assemble input-data sets for a finite-difference model of ground-water flow, *Water Resources Bulletin*, 29(3): 401-405.

Holtan, H.N. & M.H. Kirkpatrick Jr. 1950. Rainfall, infiltration and hydraulics of flow in run-off computation, *Transactions of the American Geophysical Union*, 20: 771-779.

Holtan, N.H. & G.W. Musgrave 1947. Soil water and its disposal under corn and under bluegrass, *US Department of Agriculture Soil Conservation Service*, TP-68.

Horton, R.E. 1939. Analysis of runoff-plat experiments with varying infiltration capacity, *Transactions of the American Geophysical Union*, 20: 693-711.

Horton, R.E. 1940. An approach towards a physical interpretation of infiltration capacity, *Proceedings of the Soil Science Society of America*, 5: 399-417.

Horton, R.E. 1945. Erosional development of streams and their drainage basins: Hydrophysical approach to quantitative morphology, *Bulletin of the Geological Society of America*, 56: 275-370.

Hounam, C.E., J.J. Burgos, M.S. Kalik, W.C. Palmer & J. Rodda 1975. Drought and Agriculture, Technical Note No. 138, World Meteorological Organization.

Hugget, R.J. 1980. *Systems Analysis in Geography*, Oxford University Press, New York.

Julien, P.Y., B. Saghafian & F.L. Ogden 1995. Raster-based hydrologic modeling of spatially-varied surface runoff, *Water Resources Bulletin*, 31(3): 523-536.

Juracek, K.E. & J.F. Kenny 1993. Management and analysis of water use data using a geographic information system, *Water Resources Bulletin*, 29(6): 973-979.

Karl, T.R. 1983. Some spatial characteristics of drought duration in the United States, *Journal of Climate and Applied Meteorology*, 22(8): 1356-1366.

Karl, T.R. & A.J. Koscielny 1982. Drought in the United States: 1895-1981. *Journal of Climatology*, 2: 313-329.

Kasenow, M. 1995. *Introduction to Aquifer Analysis*, Wm. C. Brown Publishers, Dubuque, Iowa.

Kidd, C.H.R. 1978. *Rainfall-Runoff Processes over Urban Surfaces*, Proceedings of the International Workshop held at the Institute of Hydrology, Wallingford, Oxford, UK.

Kirkby, M.J. 1969. Infiltration, throughflow and overland flow, in R.J. Chorley (ed.), *Introduction to Fluvial Processes*, Metheun and Co., Ltd., Bungay, Suffolk, UK.

Kirkby, M.J., P.S. Naden, T.P. Burt & D.P. Butcher 1987. *Computer Simulation in Physical Geography*, John Wiley & Sons, Chichester, UK.

Kirpich, Z.P. 1940. Time of concentration of small agricultural watersheds, *Civil Engineering*, 10(6): 362.

Kite, G.W. 1977. *Frequency and Risk Analysis in Hydrology*, Water Resources Publications, Littleton, Colorado.

Kohler, M.A., T.J. Nordenson & D.R. Baker 1959. Evaporation Maps for the United States, *US Weather Bureau Technical Paper 37*, USGPO, Washington, DC.

Kottegota, N.T. 1980. *Stochastic Water Resources Technology*, John Wiley & Sons, New York.

Lilliefors, H.W. 1967. On the Kolmogorov-Smirnov test for normality with mean and variance unknown, *Journal of the American Statistical Association*, 62: 400.

Linsley, R.K. *Hydrology for Engineers* (3rd ed.), McGraw-Hill, New York

Linsley, R.K., M.A. Kohler & J.L.H. Paulhus 1982. *Hydrology for Engineers* (4th ed.), McGraw-Hill, New York.

Lohman, S.W. 1972. *Ground-water Hydraulics*, US Geological Survey, Professional Paper, 708, USGPO., Washington, DC.

Mather, J.R. 1984. *Water Resources: Distribution, Use and Management*, John Wiley & Sons, New York.

Martz. L.W. & J. Garbrecht 1993a. Automated extraction of drainage network and watershed data from digital elevation models, *Water Resources Bulletin*, 29(6): 901-908.

Martz. L.W. & J. Garbrecht 1993b. Network and subwatershed parameters extracted from digital elevation models: The Bill's Creek experience, *Water Resources Bulletin*, 29(6): 909-916.

McCabe, J.A. 1962. *Floods in Kentucky – Magnitude and Frequency*, Information Circular 9, Kentucky Geological Survey, Lexington, Kentucky.

McCarthy, G.T. 1938. *The Unit Hydrograph and Flood Routing*. Unpublished manuscript presented at a conference of the North Atlantic Division, June 24, US Army Corps of Engineers.

McCuen, R.M. 1982. *A Guide to Hydrologic Analysis Using SCS Methods*, Prentice Hall, Englewood Cliffs, New Jersey.

McDonnell, J.J., J. Freer, R. Hooper, C. Kendall, D. Burns, K. Beven & J. Peters 1996. New method developed for studying flow on hillslopes, *EOS, Transactions of the American Geophysical Union*, 77(47): 465 and 472.

Mein, R.G. & C.L. Larson 1971. Modeling the infiltration component of the rainfall-runoff process. *WRRC Bulletin* 43, Water Resources Research Institute, University of Minnesota, Minneapolis, Minnesota.

Miller, D.H. 1977. *Water at the Surface of the Earth*, Academic Press, New York.

Microsoft EXCEL, Microsoft Corporation, USA.

Mitchell, J.K., B.A. Engel, R. Srinivasan & S.S.Y. Wang 1993. Validation of AGNPS for small watersheds using an integrated AGNPS/GIS system, *Water Resources Bulletin*, 29(5): 833-842.

Monteith, J.L. 1973. *Principles of Environmental Physics*, Edward Arnold, London.

Myers, M.F. & G.F. White 1993. The challenge of the Mississippi flood. *Environment*, 35(10): 6-9, 25-35.

Mulvaney, T.J. 1851. On the use of self-registering rain and flood gauges, *Transactions, Institute of Civil Engineers (Ireland)*, 4(2): 18.

Musgrave, G.W. 1955. How much of the rain enters the soil?, *Water, The Yearbook of Agriculture*, US Department of Agriculture, Yearbook of Agriculture 1955, USGPO, Washington, DC.

National Oceanic and Atmospheric Administration (NOAA) 1973. *Precipitation-Frequency Atlas of the Western United States*, Atlas 2, Vols. I-XI, Silver Spring, US Department of Commerce, Maryland.

National Oceanic and Atmospheric Administration (NOAA) & National Climate Data Center (NCDC) 1990. *National Climate Information Disc, Vol. 1, 48 State-Divisional Year-Month Departures, 1985 to 1989*. US Department of Commerce, CD-ROM.

National Research Council 1990. *Ground Water Models: Scientific and Regulatory Applications*, National Academy Press, Washington, DC.

National Research Council 1991. *Opportunities in the Hydrologic Sciences*, National Academy Press, Washington, DC.

Oglesby, R.J. & D.J. Erickson III 1989. Soil moisture and the persistence of North American drought, *Journal of Climate*, 2: 1362-1380.

Office of Technology Assessment 1982. *Use of Models for Water Resources Management, Planning, and Policy*, USGPO, Washington, DC.

Orzol, L.L. & T.S. McGrath 1993. Summary of modifications of the US Geological Survey Modular, Finite-Difference, Ground-Water Flow Model to read and write geographic information system files, *Water Resources Bulletin*, 29(5): 843-846.

Panofsky, H.A. & G.W. Briar 1968. *Some Applications of Statistics to Meteorology*. Pennsylvania State University Press: University Park, Pennsylvania.

Palmer, W.C. 1965. *Meteorological Drought*, US Weather Bureau, Research Paper 45. Washington, DC.

Philip, J.R. 1957. The theory of infiltration: The infiltration equation and its solution, *Soil Science*, 83(5): 345-357.

Penman, H.L. 1948. Natural evaporation from open water, bare soil, and grass, *Proceedings of the Royal Society of London*, 139(A): 120-146.

Priestley, C.H.B. & R.J. Taylor 1972. On the assessment of surface heat flux and evaporation using large scale parameters, *Monthly Weather Review*, 100: 31-92.

Rantz, S.E. 1971. Suggested criteria for hydrologic design of storm drainage facilities in the San Francisco Bay Region, California, US Geological Survey Open File Report, Menlo Park, California.

Rantz, S.E. & others 1982. *Measurement and Computation of Streamflow: Vol. 1. Measurement of Stage and Discharge, and Measurement and Computation of Streamflow: Vol. 2. Computation of Discharge*, US Geological Survey Water Supply Paper 2175, USGPO, Washington, DC.

Rawls, W., P. Yates & L. Asmussen 1976. *Calibration of selected infiltration equations for the Georgia Coastal Plain*, Agricultural Research Service, ARS-S-113, US Department of Agriculture, Washington, DC.

Richards, C.J., H. Roaza & R.M. Roaza 1993. Integrating geographic information systems and MODFLOW for ground water resource assessments, *Water Resources Bulletin*, 29(5): 847-853.

Riverside County Flood Control and Water Conservation District (RCFCWCD) 1963. *The Application of Synthetic Unit Hydrographs to Drainage Basins in the Riverside County Flood Control and Water Conservation District*, Riverside, CA.

Ruckdeschel, F.R. 1981. *BASIC Scientific Subroutines Vol. II*, Byte/McGraw-Hill, Peterborough, New Hampshire.

Sasowsky, K.C. & T.W. Gardner 1991. Watershed configuration and geographic information system parameterization for SPUR model hydrologic simulations, *Water Resources Bulletin*, 27(1): 7-18.

Schumm, S.A. 1956. Evolution of drainage systems and slopes in badlands at Perth Amboy, New Jersey, *Bulletin of the Geological Society of America*, 67: 597-646.

Sheaffer, J.R., K.R. Wright, W.C. Taggart & R.M. Wright 1982. *Urban Storm Drainage Management*, Marcel Dekker, New York.

Singh, V.P. 1988. *Hydrologic Systems: Rainfall-Runoff Modelling, Vol. I*, Prentice Hall, Englewood Cliffs, New Jersey.

Singh, V.P. 1989. *Hydrologic Systems: Watershed Modelling, Vol. II*, Prentice Hall, Englewood Cliffs, New Jersey.

Skaggs, R.W., D.E. Miller & R.H. Brooks 1980. Soil Water, Part 1 – Properties, in M.E. Jensen (ed.) *Design and Operation of Farm Irrigation Systems*, The American Society of Agricultural Engineers, St. Joseph, Michigan.

Slack, J.R. & J.M. Landwehr 1992. Hydroclimatic Data Network (HCDN): A US Geological Survey Streamflow Data Set for the United States for the Study of Climate Variations, *1874-1988*. US Geological Survey, Open File Report 92-129, and accompanying CD-ROM, Reston, Virginia.

Snyder, F.F. 1938. Synthetic unit hydrographs. *Transactions of the American Geophysical Union*, 19: 447-454.

Srinivasan, R. & J.G. Arnold 1994. Integration of a basin-scale water quality model with GIS, *Water Resources Bulletin*, 30(3): 453-462.

Solley, W.B., R.R. Pierce & H.A. Perlman 1993. *Estimated Use of Water in the United States in 1990*, US Geological Survey Circular 1081, USGPO, Washington, DC.

Strahler, A.N. 1952. Hypsometric (area-altitude) analysis of erosional topography, *Bulletin of the Geological Society of America*, 63: 1117-1142.

Strahler A.N. 1964. Quantitive geomorphology of drainage basins and channel networks, in V.T. Chow (ed.), Handbook of Applied Hydrology, 4-II: 4-39-4-76, McGraw-Hill, New York.

Stuebe, M.M. & D.M. Johnson 1990. Runoff volume estimation using GIS techniques. *Water Resources Bulletin*, 26(4): 611-620.

Tachikawa, Y., M. Shiiba & T. Takasao 1994. Development of a basin geomorphic information system using a TIN-DEM data structure, *Water Resources Bulletin*, 30(1): 9-17.

Taylor, A.B. & H.E. Schwarz 1952. Unit hydrograph lag and peak flow related to basin characteristics, *Transactions of the American Geophysical Union*, 33: 235-246.

Theis, C.V. 1935. The relation between the lowering of the piezometric surface and the rate and duration of discharge of a well using ground-water storage, *Transactions of the American Geophysical Union*, 16: 519-514.

Thomas, H.E. 1952. Ground-water regions of the United States – Their storage facilities, *Physical and Economic Foundations of Natural Resources*, Vol. 3.

Thompson, S.A. 1982. Reduction in urban runoff through economic incentives: Boulder Colorado, *Water Resources Bulletin*, 18(1): 125-127.

Thompson, S.A. 1990. A Markov and runs analysis of drought in the central United States, *Physical Geography*, 11(3): 191-205.

Thompson, S.A. 1992. Simulation of the climate change impacts on the water balance in the central United States, *Physical Geography*, 13(1): 31-52.

Thornthwaite, C.W. 1948. An approach towards a rational classification of climate, *Geographical Review*, 38: 55-94.

Thornthwaite, C.W. & J.R. Mather 1955. *The Water Balance*, Publications in Climatology, Vol. VIII(1), Centerton, New Jersey: Drexel Institute of Technology, Laboratory of Climatology.

Thornthwaite, C.W. & J.R. Mather 1957. *Instructions and Tables for Computing Potential Evapotranspiration and the Water Balance*, Publications in Climatology, Vol. X(3), Drexel Institute of Technology, Laboratory of Climatology, Centerton, New Jersey.

Todd, D.K. 1980. *Groundwater Hydrology,* 2nd ed., John Wiley & Sons, New York.

Turner, K.M. 1991. Annual evapotranspiration of native vegetation in a mediterranean climate, *Water Resources Bulletin*, 27(1): 1-6.

US Army Corps of Engineers 1959. *Flood Hydrograph Analysis and Computations*, Engineering and Design Manuals, EM 1110-2-1405, USGPO, Washington, DC.

US Army Corps of Engineers 1977. *Snyder's synthetic unit hydrograph coefficients, Central and Northeastern Oklahoma*, Tulsa District, Tulsa, OK.

US Army Corps of Engineers (COE) 1987a. *HEC-1 Flood Hydrograph Package Users Manual*, The Hydrologic Engineering Center, Davis, California.

US Army Corps of Engineers (COE) 1987b. *GRASS Reference Manual*, USA CERL, Champaign, Illinois.

US Department of Agriculture, Soil Conservation Service 1970. Irrigation Water Requirements, Technical Release No. 21, USGPO, Washington, DC.

US Department of Agriculture, Soil Conservation Service 1985. *Soil Survey of Lancaster County, Pennsylvania.*

US Department of Agriculture 1955. *Water: The Yearbook of Agriculture 1955*, USGPO, Washington, DC.

US Department of Agriculture, Soil Conservation Service 1972. *Hydrology*, Section 4, *National Engineering Handbook*, USGPO, Washington, DC.

US Department of Agriculture, Soil Conservation Service 1986. *Technical Release 55, Urban Hydrology for Small Watershed*, National Technical Information Service, Springfield, Virginia.

US Environmental Protection Agency 1978. *Use of the Water Balance Method for Predicting Leachate Generation from Solid Waste Disposal Sites*, EPA 530/SW-168, Washington, DC.

US Environmental Protection Agency 1987 and 1993, *Guidelines for Delineation of Wellhead Protection Areas*, USGPO, Washington, DC. Available from US Department of Commerce, National Technical Information Service, Springfield, Virginia.

US Department of Interior, US Geological Survey (USGS), *Water Resources Data, Pennsylvania, Water Year 1993,* Vol. 2, Susquehanna and Potomac River Basins. Available from the National Technical Information Service, Springfield, Virginia.

US National Weather Service (NWS) 1972. *National Weather Service River Forecast System. Forecast Procedures*. NOAA Technical Memorandum, NWS HYDRO.

US Water Resources Council (WRC) 1981. *Guidelines for Determining Flood Flow Frequency*, Bulletin 17B. Available from the Office of Water Data Coordination, US Geological Survey, Reston, Virginia.

US Weather Bureau 1957. Rainfall intensity-frequency regime: Part IV, Northeastern United States, *Technical Paper 38*, USGPO, Washington, DC.

Viessman, W. Jr. & C. Welty 1985. *Water Management: Technology and Institutions*, Harper & Row Publishers, New York.

Waltmeyer, S.D. 1986. *Techniques for Estimating Flood-Flow Frequency for Unregulated Streams in New Mexico*, US Geological Survey Report 86-4104, Albuquerque, New Mexico.

Wang, H.F. & M.P. Anderson 1983. *Introduction to Groundwater Modeling*, W.H. Freeman and Company, New York.

White, G.F. 1987. Personal communication.

Wiesner, C.J. 1970. *Climate, Irrigation and Agriculture*, Angus & Robertson, Sydney, Australia.

Willmott, C.J. 1977. *WATBUG: A FORTRAN IV Alogrithm for Calculating the Climatic Water Budget*, Publications in Climatology, Vol. XXX(2), C.W. Thornthwaite Associates Laboratory of Climatology, Elmer, New Jersey.

Willmot, C.J. 1982. Some comments on the evaluation of model performance, *Bulletin of the American Meteorological Society*, 63(11), 1309-1313.

Wischmeier, W.H. & D.D. Smith 1978. *Predicting rainfall erosion losses*, US Department of Agriculture, Agricultural Handbook, 537, 58 p.

Wood, E.F., M. Sivapalan, K. Beven & L. Band 1988. Effects of spatial variability and scale with implications to hydrologic modeling, *Journal of Hydrology*, 29: 29-47.

Wright, J.L. 1982. New evapotranspiration crop coefficients, *Journal of the Irrigation and Drainage Division*, American Society of Civil Engineers, 108(IR1): 57-74.

Wu, J.S., E.L. King & M. Wang 1985. Optimal identification of Muskingum routing coefficients, *Water Resources Bulletin*, 21(3): 417-421.

Yevjevich, V. 1972. *Stochastic Processes in Hydrology*, Water Resources Publications, Colorado State University, Fort Collins, Colorado.

Young, R.A., C.A. Onstad, D.D. Bosch & W.P. Anderson 1987. *AGNPS, Agricultural Non-Point-Source Pollution Model*. A Watershed Analysis Tool. US Department of Agriculture, Agricultural Research Service, Conservation Report 35, National Technical Information Service, Springfield, Virginia.

Young, R.A., C.A. Onstad, D.D. Bosch & W.P. Anderson 1989. AGNPS: A Nonpoint Source Pollution Model for Evaluation Agricultural Watersheds, *Journal of Soil and Water Conservation*, 44(2): 168-173.

This Page Intentionally Left Blank

Subject index

ϕ index 133, 234
Accumulated potential water loss 190, 191
Actual evapotranspiration 102
Adiabatic process 51
AGNPS model 336
Albedo 84
Anisotropy 151
Annual maximum series 17, 242
Annual minimum series 309
Antecedent soil 236
Aquiclude 146
Aquifer 145
  confined aquifer 147
  unconfined aquifer 146
Arithmetic mean 26
Artesian well 147
Atmospheric stability 52
Autocorrelation 25
Autoregressive (AR) model 312
Available water capacity 115, 141, 189
Average infiltration method 129

Baseflow 3, 230
Basin morphometry 205
Basin area 219
Basin relief 210
Bifurcation ratio 206
Blackbody 88
Blaney-Criddle method 108

Capillary suction and tension 121
Channel travel time 220
Channel waves 228
Coefficient of variation 28
Combination approach 97
Condensation nuclei 50
Cone of depression 162
Confidence limits 253
Contaminant transport 175
Contaminant transformation 177
Continuity equation 5
Correlation 18
Cooper-Jacob method 170
Closed system 5
Cumulative distribution function 32
Cumulative frequency function 32
Cumulative infiltration 123, 125
Curve numbers 235

Darcy's Law 157
Data
  classified 30
  complete duration series 16
  continuous 12
  discrete 12
  extreme value series 16
  level of measurement 15
  observation 25
  outliers 243
  partial duration series 16
  precision 11
  Système International 10
Dependent variable 25
Depression storage 3, 134, 222
Deterministic model 319
Dew point temperature 47
Differential equation 5
Digital elevation model (DEM) 342
Digital line graph (DLG) 343
Dimensions 10
Double-mass analysis 63
Drainage basin 3
Drainage density 207
Drought 286
  Markov chain 299
  Palmer Drought Severity Index 292
  runs approach 288
Dry adiabatic lapse rate 51

Dupuit-Forchheimer assumptions159
Dynamic wave 228
Dynamic equilibrium 5

Electromagnetic radiation 83
Emissivity 88
Energy flux 85
Environmental lapse rate 51
Equipotential lines 157, 171
Error measurement 323
Evaporation 82
Evaporation equations
  combination equations 97
  mass transfer/aerodynamic approach 95
Evaporation pan 91
Evapotranspiration 102
Exceedence probability 65
Extreme Value I distribution 247

Field capacity 115
Finite difference model 173
Flood frequency analysis 242
Flood waves 228
Flow duration curve 307
Flow net 171
Flow routing 268
Frequency analysis 65, 173, 313
Frequency factors 38, 246, 249, 250
Fronts 49

Gamma distribution 39, 66
Geographic Information System (GIS) 338
  applications to hydrology 341
  raster 340
  vector 339
Geometric mean 27
Goodness of fit test 40, 68
Graphing data 17
Graphical interpolation 75
GRASS (GIS) 342
Gravitational potential 137, 153
Groundwater 144
Groundwater flow to wells 164
Groundwater modeling 173
Groundwater regions 182
Groundwater velocity
  darcy velocity 157
  macroscopic velocity 158
Groundwater zone 137, 145
Gumbel I distribution 247

Harmonic mean 27, 152
Head 137, 153
HEC-1 model 326
Histogram 30
Horton's infiltration equation 131
Hortonian overland flow 221
Humidity 48
Hydraulic conductivity 134, 151
Hydraulic gradient 155
Hydraulic radius 215
Hydrograph 230
Hydrograph analysis of infiltration 129
Hydrograph separation 232
Hydrologic data series 16
Hydrologic models 318
Hydrologic response units 209
Hydrologic Soil Groups 134, 236
Hydrology 1
Hyetograph 54
Hygroscopic particles 50
Hysteresis 138, 272

Imbrication 152
Independent variable 25
Infiltration capacity 121
Infiltration models
  ϕ index 133
  Horton's equation 131
  Philip's equation 132
Infiltrometer 128
Insolation 83
Integration 6, 125
Intensity duration frequency (IDF) 69
Interflow 3
Intrinsic permeability 151
Isotropy 152

Jensen-Haise method 111

Kinematic wave 212, 228, 328
Kolmogorov-Smirnov test 40, 68

Laminar flow 213
Laplace's equation 172
Latent heat 45
Law of basin areas 209
Law of stream lengths 207
Law of stream numbers 206
Law of Total Probability 34
Lifting condensation level 52
Lifting mechanisms 49
Log-Pearson Type III distribution 251
Logarithmic data transformation 19
Logarithmic wind velocity profile 58
Lognormal distribution 245

Longitudinal profile 210
Longwave energy 84
Lysimeter 105

Manning's equation 11, 214
Manning's roughness coefficient
  channel flow 220
  overland flow 214
Markov chain and drought analysis 299
Markov streamflow simulation 312
Mass curve 310
Mass transfer/aerodynamic method 95
Maximum basin relief 210
Mean annual flood 249
Mean annual precipitation for US 54
Median 26
Missing (precipitation) data 59
Mixed distributions 254
Mode 27
Modeling 7, 318
Model calibration 322
Modeling evapotranspiration 115
Multiphase flow 176
Muskingum channel routing 272

Net allwave radiation 84
Non-steady 7
Non-uniform 7
Normal precipitation 53
Normal distribution 34, 244

Open system 5
Overland flow 208
Overland flow length 208
Overland flow travel time 217
Overland flow velocity 214

Palmer Drought Severity Index 292
Pan coefficient 92
Parameter estimation and modeling 322
Partial area concept 223
Peak flow 240
Pearson Type III distribution 249
Penman equation 98, 113
Penman-Monteith equation 114
Permanent wilting point 103
Permeability 122, 145
Piezometer 153
Philip's equation 132
Plotting position formulas
  Gringorten 244
  Weibull 65
Ponding time 134

Population 26
Porosity 136, 148
Potential evapotranspiration 102
Potentiometric surface 147
Precipitable water 48
Precipitation gage 53
Precipitation measurement 53
Pressure potential 137, 153
Probability density function 32
Probability distributions 38
  use defined 25
  fitting 38
  flood frequency analysis 242
  precipitation analysis 66
Psychometric constant 98

Rainfall simulator 129
Rational method 240
Recurrence interval 65
Reference crop evapotranspiration 110
Regional flood frequency analysis 255
Relative frequency function 31
Reservoir routing 268
Reservoir storage calculation 309
  mass curve 310
  sequent-peak 311
Return period 65
Reynold's number R 213
Risk 76
Routing 268
Runoff volume 233
Runs analysis of drought 288

Safe yield 150
Saturated adiabatic lapse rate 52
Saturation overland flow 223
Saturation vapor pressure 47
SCS precipitation intensity curves 55
SNOTEL 57
SCS curve number 234
Sensitivity analysis 201, 323
Sequent-peak method 323
Serial correlation 25, 312
Simulation models 311, 319
Skewness 28, 242, 252
Slope 210
Soil structure 122
Soil water 135
Soil water characteristic 138
Soil water potential 136
Solar energy 83
Solar constant 85
Space-time domain 7

Spatial averaging precipitation data 61
Specific humidity 47
Specific yield 149
Stability 52
Stage-discharge relations 280
Stagnation point 181
Standard deviation 28
Standard normal distribution 36
State transition probability 299
Steady 5
Stefan's Law 86
Streamflow measurement 278
Stochastic 26
Stochastic streamflow simulation 311
Storage coefficient 149
Stream length 207
Stream ordering 205
Stream velocity 220, 278
Synthetic unit hydrograph 263
Systems 3

Theis match point method 166
Thiem equation 165
Thiessen polygon 61
Thornthwaite method 106
Thornthwaite-Holzman equation 96
Thornthwaite Water Balance 188
Three point method 156
Time of concentration 216
Time series 25
  homogeneous 41, 63
  persistence 64, 313
  stationary 41
  stochastic 26
Transmissivity 158
Triangular Irregular Network (TIN) 344
Turbulent flow 213

Uniform 7
Unit hydrograph 256
  convolution 262
  S-curve method 260
Universal Soil Loss Equation 388

Vadose zone 137, 145
Vapor pressure 46
Vapor pressure deficit 90
Variable source concept 224
Variance 27
Vegetation modification 118
Velocity
  channel 220
  overland flow 214
  stream cross section 278

Water balance
  evaporation measurement 94
  evapotranspiration measurement 105
  Thornthwaite 188
Water supply 305
Water table 3, 137, 145
Weather modification 50
Well flow 164
  steady, uniform flow 164
  unsteady flow 166
Well interference 163
Wellhead protection 177
Wetting front 141

Yield from reservoirs 309

Z scores 35, 288
Zone of contribution 180
Zone of influence 180